

Quaternary Glaciation in the Pindus Mountains, Northwest Greece



Philip D. Hughes

Darwin College, University of Cambridge

March 2004

This dissertation is submitted for the degree of Doctor of Philosophy

This dissertation is the result of my own work and includes nothing which is the outcome of work done in collaboration except where specifically indicated in the text.

This thesis is no more than 80,000 words in length.

Abstract

Geomorphological and geological evidence for former Quaternary glaciation has been mapped in the Pindus Mountains of northwest Greece. The dynamics and chronology of glaciation in this area has been established through sedimentological analysis, soil analysis and Uranium-series dating. Four glacial events are recorded in the sedimentological and geomorphological records. The most extensive recorded glaciation pre-dates 350,000 years BP and was characterised by extensive valley glaciers and ice-fields. A second glaciation occurred prior to the last interglacial, before *ca.* 127,000 years BP, and was characterised by glaciers that reached mid-valley positions. The height of the last glacial stage in Greece (30-20,000 ¹⁴C years BP) is recorded by small cirque glacier moraines and relict periglacial rock glaciers. Evidence for a fourth glacial phase is recorded only in the highest cirques of Mount Smolikas (2637 m a.s.l.), the highest peak in the Pindus Mountains. This phase of glaciation is likely to have occurred during the Late-glacial Substage (14-10,000 ¹⁴C years BP). All of the glaciers during the different glacial stages were reconstructed and used alongside periglacial rock glaciers to determine palaeoclimate. During the glacial maximum of the last glacial stage, mean annual temperatures were *ca.* 8-9°C lower than at present and mean annual precipitation greater than 2000 mm - similar to modern values. Earlier glacial maxima are likely to have been colder but with mean annual precipitation still greater than 2000 mm. Maximum glacier extent in the Pindus Mountains is likely to have preceded the most severe arid phase of glacial cycles indicated in the pollen record and also global glacial maxima. This was because of the small size of the former Pindus glaciers and their rapid response to climate change, as well as the increased prevalence of aridity around the global glacial maxima. The glacial sequence in the Pindus Mountains represents the best-dated and longest recognised record of glaciation in the Mediterranean region and provides a stratigraphical framework for Quaternary cold-stage climates in Greece.

Acknowledgements

I would like to thank Phil Gibbard and Jamie Woodward for supporting this project and providing invaluable comments on the manuscript. They have both been key to this project and I appreciate the freedom they have allowed and their persistent encouragement. This project was largely funded by a University of Cambridge Domestic Research Studentship and grants from the Natural Environment Research Council, Darwin College, Cambridge European Trust, Quaternary Research Association, British Geomorphological Research Group, Department of Geography at the University of Cambridge and the Cambridge Philosophical Society. This project was made much more enjoyable by all in the Quaternary Palaeoenvironments Group in Cambridge, who provided morale boosting, general banter, tea and the occasional stronger refreshment. Especial thanks go to Steve Boreham and Chris Rolfe for providing endless support and putting work my way. Also, thank you to Charles Turner for providing maps and advice about Epirus. In Greece, appreciation must be given to Mrs. Gouris in Tsepelovo for looking after me on all those visits. Also, I would like to thank everyone who came out with me to the hills: Roger, Mum, Laurence Totelin and Jamie Woodward. At the Open University Uranium-Series Facility, I am thankful to Mabs Gilmour and Peter van Calsteren who let me loose in their new laboratories and made me feel at home, and to Jo Rhodes for processing some of my samples. My time in Milton Keynes was one of the best of the three years and a welcome change to familiar surroundings in Cambridge. I would also like to thank Doug Benn, Colin Ballantyne, Ian Fairchild, Mike Hambrey, Chris Jeans, Alan Pentecost, Peter Rowe, Chronis Tzedakis and Ian Willis for lots of crucial advice and information. Rich Betts must also be thanked for his unfailing support and camaraderie ever since those Exeter days. Also, thanks to George Speller for all those beers especially those near-completion Irish Guinnesses. Most of all, I wish to thank my parents and family for their support over the years and Laurence Totelin for being supportive and understanding, especially during the last six months of this thesis.

1.1 Contents

List of Figures	x
List of Tables	xv
Chapter One. Introduction	1
1.1 The Quaternary and glacial theory.....	1
1.2 Stratigraphy and the division of Quaternary time.....	2
1.3 Glacial Greece and its strategic significance in Quaternary studies.....	5
1.4 Aims and objectives of this research.....	7
Chapter Two. Background	8
2.1 The study area	8
2.2 Modern climate.....	11
2.3 Geology.....	13
2.4 Glaciation in the Mediterranean.....	15
2.4.1 The Balkans.....	16
2.4.2 The Italian Appenines.....	19
2.4.3 Corsica.....	22
2.4.4 The Alpes Maritimes.....	23
2.4.5 The Pyrenees and the Iberian peninsula.....	25
2.4.6 The Atlas Mountains.....	28
2.4.7 The eastern Mediterranean (Turkey and Lebanon).....	30
2.4.8 Greece.....	33
2.4.9 Towards an understanding of Mediterranean glacial history.....	37
2.5 Quaternary palaeoenvironments in Greece.....	38
Chapter Three. Methods – geomorphology and Sedimentology	45

3.1	Geomorphological Mapping.....	45
3.1.1	Ice-marginal moraines.....	45
3.1.2	Hummocky moraine.....	46
3.1.3	Fluted moraine.....	47
3.1.4	Drift limits.....	47
3.1.5	Perched boulders and boulder limits.....	48
3.1.6	Erosional forms.....	49
3.1.7	Glaciofluvial features.....	50
3.1.8	Periglacial features.....	51
3.1.9	Rock glaciers.....	51
3.1.10	Rock-slope failure deposits.....	54
3.1.11	Pronival (or protalus) ramparts.....	54
3.1.12	Symbols used in the geomorphological maps.....	55
3.2	Sedimentological Investigation.....	55
3.2.1	Section Logging.....	55
3.2.2	Clast Analysis.....	57
3.2.2.1	Clast fabric.....	58
3.2.2.2	Clast form and clast size.....	60
3.2.2.3	Clast surface features.....	63
3.2.2.4	Clast lithology.....	63
3.2.3	Fine-Fraction Particle-Size (< 2 mm).....	63
3.2.4	Carbonate Content.....	64
3.3	Morpho-lithostratigraphy.....	64

Chapter Four. Geomorphological and sedimentological evidence – Mount Tymphi..... 69

4.1	The Tsepelovo area.....	69
4.1.1	The Tsepelovo village area and the Laccorponi valley.....	69
4.1.2	Laccos Tselon.....	84
4.1.4	Morphostratigraphical summary of the Tsepelovo area.....	86
4.2	The Skamnelli area.....	88
4.2.1	The lower Skamnelli area.....	88

4.2.2	Vourtapa valley.....	95
4.2.3	Vrichos valley.....	96
4.2.4	Tsioumako valley.....	101
4.2.5	Morpho-lithostratigraphical summary of the Skamnelli area.....	103
4.3	The Vrisochori area.....	104
4.3.1	Maghoula valley.....	104
4.3.2	Morpho-lithostratigraphical summary of the Vrisochori area.....	107
4.4	The Iliochori area.....	108
4.4.1	Kriopotamos valley.....	108
4.4.2	Dimitrios cirque.....	109
4.4.3	Laccos cirque.....	111
4.4.4	Plaghia valley.....	111
4.4.6	Morpho-lithostratigraphical summary of the Iliochori area.....	112
4.5	Neraidhovrisi valley.....	113
4.6	Stani Katsanou valley.....	113
4.6.1	Aghia Triada and Stani Katsanou.....	113
4.6.2	Tsouka Rossa cirques.....	114
4.6.3	Karteros cirque.....	115
4.6.4	Morpho-lithostratigraphical summary of the Stani Katsanou valley.....	115
4.7	Mighia valley.....	117
4.7.1	Morpho-lithostratigraphical summary of the Mighia valley.....	118
4.8	Amarandos valley.....	119
4.8.1	Morpho-lithostratigraphical summary of the Amarandos valley.....	119
4.9	Megas Laccos valley.....	120
4.9.1	Morpho-lithostratigraphical summary of the Megas Laccos valley.....	125
4.10	Stani Grava.....	127
4.10.1	Morpho-lithostratigraphical summary of the Stani Grava area.....	128
4.11	Ghaidhouro valley.....	129
4.12	Raidhovoli valley.....	129
4.12.1	Morpho-lithostratigraphical summary of the Raidhovoli valley.....	132
4.13	Laccos Radenas.....	134
4.14	Spirokapa.....	135
1)	Mount Tymphi summits - geomorphological notes.....	137
4.16	Possible glacial evidence in outlying areas.....	138
4.17	Summary of Mount Tymphi.....	139

Chapter Five.	Geomorphological and sedimentological evidence - Mount Smolikas and Vasilitsa.....	140
5.1	The Vadulakkos valley and cirques.....	140
5.1.1	The lower Vadulakkos valley.....	140
5.1.2	Cirque 1.....	150
5.1.3	Cirque 2.....	150
5.1.4	Cirque 3.....	150
5.1.5	Cirque 4.....	152
5.1.6	Morpho-lithostratigraphical summary of the Vadulakkos valley.....	153
5.2	Northwestern Cirque.....	154
5.3	The Konkutino valley and cirques.....	156
5.3.1	Konkutino valley.....	156
5.3.2	Bogdoni cirque.....	156
5.3.3	Moasa northeastern cirque.....	157
5.3.4	Moasa southeastern cirque.....	158
5.3.5	Morpho-lithostratigraphical summary of the Konkutino valley.....	159
5.4	The Samarina Area.....	160
5.5	Northeastern slopes of Mount Vasilitsa.....	164
5.5.1	Morpho-lithostratigraphical summary of northeastern Mount Vasilitsa.....	164
5.6	Eastern slopes of Mount Vasilitsa.....	166
5.7	Differences between the Mount Smolikas/Vasilitsa glacial deposits and those on Mount Tymphi.....	166
5.8	Summary of Mount Smolikas and Vasilitsa.....	168
Chapter Six.	Chronology.....	169
6.1	Geochronology.....	169
6.1.1	U-series dating - theory.....	170
6.1.2	Secondary cements.....	172
6.1.2.1	Composition.....	172

6.1.2.2	Vadose zone cements.....	173
6.1.2.3	Phreatic zone cements.....	174
6.1.2.4	Mode of formation.....	175
6.1.2.5	Interpreting glacial sequences using U-series dates on cements.....	177
6.1.4	Uranium-series dating – methods.....	177
6.1.5	Uranium-series – results.....	179
6.1.5.1	Laccos Radenas Formation.....	180
6.1.5.2	Megas Laccos Formation.....	182
6.1.5.3	Tsepelovo Formation.....	183
6.1.5.4	Skamneli Formation.....	184
6.1.5.5	Raidhovoli Formation.....	186
6.1.5.6	The significance of the cement ages.....	187
6.2	Soil development as a relative age technique.....	191
6.2.1	Analysis of soil properties - methods.....	193
6.2.1.1	Rubification.....	193
6.2.1.2	Structure.....	194
6.2.1.3	Texture.....	194
6.2.1.4	Clay content.....	194
6.2.1.5	Organic content and melanization.....	195
6.2.1.6	Iron oxide content.....	195
6.2.1.7	Magnetic susceptibility.....	195
6.2.1.8	pH.....	195
6.2.2	Analysis of soil properties - results.....	196
6.2.2.1	Voidomatis Member soil.....	197
6.2.2.2	Maghoula Member soil.....	200
6.2.2.3	Kato Radza Member soil.....	201
6.2.2.4	Other soils.....	202
6.2.3	Soils – summary and significance.....	202
6.3	Defining a common inter-valley chronostratigraphy.....	204
6.3.1	Inter-valley correlations.....	207
6.3.2	Defining the chronostratigraphy with reference to a parastratotype.....	212
6.3.3	Missing Glacial Stages.....	215
	Chapter Seven. Glacier Reconstruction.....	217

7.1	Methods of glacier reconstruction.....	217
7.1.1	Glacier shape.....	217
7.1.2	Glacier surface contours.....	217
7.1.3	Glacier area.....	218
7.1.4	Ice-divides.....	218
7.1.5	Equilibrium Line Altitude (ELA).....	219
7.1.5.1	Maximum elevation of lateral moraines.....	219
7.1.5.2	Toe-to-headwall altitude ratio (THAR).....	220
7.1.5.3	Toe-to-summit altitude method (TSAM).....	220
7.1.5.4	Area-weighted mean altitude.....	220
7.1.5.5	Accumulation area ratio.....	221
7.1.5.6	Balance ratio.....	222
7.1.6	The method of ELA reconstruction applied here.....	223
7.1.7	Testing the glacier reconstructions using glaciological theory.....	224
7.1.8	Problems and limitations in glacier reconstruction.....	226
7.2	Skamnellian Stage glaciers.....	227
7.2.1	Mount Tymphi.....	229
7.2.1.1	Group A glaciers.....	230
7.2.1.2	Group B glaciers.....	231
7.2.1.3	Group C Glaciers.....	232
7.2.1.4	Group D glaciers.....	236
7.2.2	Mount Smolikas.....	240
7.2.3	Mount Vasilitsa.....	243
7.3	Vlasian Stage glaciers.....	244
7.3.1	Mount Tymphi.....	245
7.3.1.1	Group A glaciers.....	245
7.3.1.2	Group B glaciers.....	248
7.3.1.3	Group C Glaciers.....	249
7.3.1.4	Group D glaciers.....	251
7.3.1.5	Testing the glacier reconstructions.....	251
7.3.2	Mount Smolikas.....	253
7.3.3	Mount Vasilitsa.....	256
7.4	Tymphian Stage glaciers and rock glaciers.....	258
7.4.1	Mount Tymphi.....	259

7.4.2	Mount Smolikas.....	260
7.4.3	Mount Vasilitsa.....	263
7.5	Smolikasian Substage glaciers and rock glaciers.....	263
7.6	Glacier reconstruction - summary.....	265

Chapter Eight. Palaeoclimatic Reconstruction and Discussion.....268

8.1	Glaciers and climate.....	268
8.2	Rock glaciers and climate.....	270
8.3	Palaeoclimate during the Tymphian Stage.....	271
8.3.1	Local controls on glacier development.....	271
8.3.2	Palaeotemperature reconstruction.....	274
8.3.3	Palaeoprecipitation.....	275
8.3.4	Palaeoprecipitation - the importance of annual palaeotemperature range.....	276
8.3.5	The Smolikasian Substage.....	279
8.3.6	Limitations on the palaeoclimate reconstructions.....	282
8.4	Palaeoclimate during the Vlasian Stage.....	283
8.4.1	Local controls on glacier development.....	283
8.4.2	Palaeotemperature and palaeoprecipitation reconstruction.....	285
8.5	Palaeoclimate during the Skamnellian Stage.....	287
8.5.1	Local controls on glacier development.....	287
8.5.2	Palaeotemperatures and palaeoprecipitation.....	290
8.6	Climate during 'missing' glacial stages.....	291
8.7	Glacial Greece - discussion.....	293
8.7.1	Tymphian Stage.....	293
8.7.1.1	Smolikasian Substage.....	299
8.7.2	Vlasian Stage.....	300
8.7.3	Skamnellian Stage.....	301
8.8	Glacial climates in the Mediterranean.....	302

Chapter Nine. Conclusions..... 304

References.	307
Appendix 1.	U-series method for Thermal Ionisation Mass Spectrometry	332
Appendix 2.	Iron oxide extraction from soils	339
Appendix 3.	Soil data	340
Appendix 4.	Publications	342

List of Figures

Note: Figure captions listed here may be shortened versions of that which appears in the text.

1

Figure 1.1	Location map showing the North Pindus field area and long lacustrine and fluvial sites in Greece.....	5
Figure 1.2	Summary arboreal pollen (AP)/ non-arboreal pollen (NAP) percentages plotted against depth for Ioannina 249 and Tenaghi Philippon	6
Figure 2.1	Location map of Mount Smolikas, Mount Vasilitsa and Mount Tymphi...	9
Figure 2.2	Typical landscape of Mount Tymphi	10
Figure 2.3	Typical landscape of Mount Smolikas	10
Figure 2.4	Modern precipitation distribution on Mount Tymphi, Mount Smolikas and Mount Vasilitsa.....	13
Figure 2.5	Geological maps of the Mount Tymphi area (A.) Mount Smolikas (B.) and Mount Vasilitsa (C.).....	14
Figure 2.6	Distribution of Pleistocene glacial features in the Mediterranean region recognised by Messerli (1967).....	16
Figure 2.7	Location map showing some of the glaciated mountains of Greece, the Balkans, Italy and Corsica.....	17
Figure 2.8	The Triglav glacier, Slovenia, showing extent in 1967 and 1850.....	18
Figure 2.9	Location map showing some of the glaciated mountains of the Alpes Maritimes, the Pyrenees and the Iberian peninsula.....	24
Figure 2.10	Location map of the North African Atlas.....	28
Figure 2.11	The Eastern Mediterranean mountains including glaciated areas of Turkey and the Lebanon.....	31
Figure 2.12	Glacial geomorphological map of Mount Tymphi produced by Palmentola <i>et al.</i> (1992).....	34
Figure 2.13	Glacial geomorphological map of Mount Smolikas produced by Boenzi <i>et al.</i> (1992).....	35
Figure 2.14	Geomorphological map of the Mount Olympus area.....	36
Figure 2.15	Fluvial sediment sources based on a geochemical fingerprint technique in the Voidomatis basin.....	42
Figure 3.1	A perched rock in Scotland.....	48
Figure 3.2	Some types of geomorphological evidence used to delimit the extent	

	of local cirque or valley glaciers: a) limit of hummocky moraine; b) end moraine; c) boulder limit, and; d) drift limit.....	49
Figure 3.3	The formation of debris rockglaciers is illustrated in frame A. and the formation of talus rock glaciers in frame B.....	53
Figure 3.4	Key to geomorphological maps.....	56
Figure 3.5	Key to lithological logs.....	57
Figure 3.6	An example of a stereographic equal-area projection of clast orientation.....	59
Figure 3.7	Fabric shape represented on an equilateral ternary diagram.....	60
Figure 3.8	Clast shape data plotted on ternary diagrams and roundness data plotted as histograms.....	61
Figure 3.9	Clast images for visual determination of roundness.....	62
Figure 3.10	The hierarchical stratigraphical framework based on two simple valleys.....	67
Figure 4.1	Geomorphological map of the Lower Tsepelovo area and the the Laccorponi valley.....	70
Figure 4.2	Section photograph of the Voidomatis sedimentary sequence (section Va).....	71
Figure 4.3	Lithological log of the sediments at section Va on the banks of the Voidomatis.....	72
Figure 4.4	Clast analyses from the Voidomatis section (Va).....	73
Figure 4.5	Section Vb on the Tsepelovo Bypass.....	74
Figure 4.6	Clast analysis results for the Tsepelovo bypass till (section Vb).....	75
Figure 4.7	The percentage of total striated clasts in each roundness division (section Vb).....	76
Figure 4.8	The Tsepelovo buried soil.....	76
Figure 4.9	Sediment log from section Vc on the road from Skamnelli to Tsepelovo.....	79
Figure 4.10	Schematic sketch of the Tsepelovo-Skamnelli road section (Vc).....	80
Figure 4.11	Photograph of the Tsepelovo-Skamnelli road section (Vc).....	80
Figure 4.12	Clast analyses from units Vc 1 (A.), Vc 3 (B.) and Vc 6 (C.) in the section Vc on the road from Tsepelovo to Skamnelli.....	81
Figure 4.13	Geomorphological map of the Laccos Megalon Litharion and Laccos Tselon areas.....	85
Figure 4.14	The ridge of Vlasi between the Laccorponi and Vourtapa valleys on Mount Tymphi.....	87

Figure 4.15	Geomorphological map of the Skamnelli area.....	89
Figure 4.16	Lithological log of the sediments at section Ska, south of Skamnelli.....	90
Figure 4.17	Diamicton deposits under a house in Skamnelli village viewed from the main road.....	91
Figure 4.18	Section Ska, south of Skamnelli.....	91
Figure 4.19	Lithological log of the sediments at section SKb, south of Skamnelli.....	93
Figure 4.20	Clast analysis from Unit SKb1.....	93
Figure 4.21	The Vourtapa valley moraines (Vourtapa Member) viewed from the southern ridge of Vlasi	95
Figure 4.22	The pronival ramparts representing the Tsoukoula Member of the Skamnelli Formation	97
Figure 4.23	A weathered diamicton, section VR, in the lower Vrichos valley.....	97
Figure 4.24	Clast analysis results for the Vrichos diamicton, section VR.....	98
Figure 4.25	Aerial photograph of the Skamnelli area.....	100
Figure 4.26	Limestone pavement situated in the Tsioumako valley.....	102
Figure 4.27	The moraines of the Corifula Member, in the upper Tsiomako valley.....	102
Figure 4.28	Geomorphological map of the Vrisochori and Iliochoi area.....	105
Figure 4.29	The type area of the Vrisochori Member.....	106
Figure 4.30	Satellite image of the Vrisochori area.....	107
Figure 4.31	Clast analysis results from the Kriopotamos diamicton in section KR.....	109
Figure 4.32	A pronival rampart in the Dimitrios cirque (Dimitrios Member).....	110
Figure 4.33	The pronival rampart of the Dimitrios cirque (Dimitrios Member) taken from the proximal slope of the outer moraines (Tsouknidhes Member).....	110
Figure 4.34	Geomorphological map of the Vrisochori area.....	114
Figure 4.35	The Tsouka Rossa rock glacier viewed from the Tsouka Rossa col to the south near to peak 2377 m a.s.l.....	116
Figure 4.36	The Tsouka Rossa rockglacier viewed from within the cirque.....	116
Figure 4.37	Geomorphological map of the Tymphi plateau area.....	121
Figure 4.38	A matrix-supported diamicton containing subrounded clasts in the upper Megas Laccos valley.....	122
Figure 4.39	The upper Megas Laccos gorge.....	124
Figure 4.40	The lower Megas Laccos Gorge.....	124
Figure 4.41	Aerial photograph showing the upper Megas Laccos gorge and part of the south Tymphi Plateau.....	126
Figure 4.42	A perched rock on pavement inside of the Stani Grava moraines.....	127
Figure 4.43	Matrix-supported diamicton in a section cut through ridges at the northern end of the Raidhovoli valley.....	130

Figure 4.44	Moraine ridges impounding the lake of Xeroloutsas.....	130
Figure 4.45	Limestone pavements and the Catsantoni cirque behind.....	133
Figure 4.46	Boulder accumulations on the southeastern slopes of Ploskos.....	133
Figure 4.47	Geomorphological map of the Astraka area.....	135
Figure 4.48	Moraines in the Laccos Radenas valley, south of Astraka (2436 m a.s.l.).....	136
Figure 4.49	Shattered rocks on the southeast ridge of Astraka.....	137
Figure 5.1	Geomorphological map of the northern Mount Smolikas area.....	141
Figure 5.2	The Smolikas Vadulakkos moraines viewed from the north.....	142
Figure 5.3	The Vadulakkos section on the Aghia Paraskevi - Fourka road.....	142
Figure 5.4	Sediment log of the Smolikas Vadulakkos sediments (section SM).....	144
Figure 5.5	Clast analyses from the Smolikas Vadulakkos section (SM).....	145
Figure 5.6	Schematic diagram showing the down-valley profile of the Vadulakkos moraines and associated units.....	149
Figure 5.7	The arête dividing the Northwestern Cirque from Cirque 2 on Mount Smolikas.....	151
Figure 5.8	Moraines in Cirque 2 on Mount Smolikas.....	151
Figure 5.9	The summit ridge of Mount Smolikas looking east from the main summit (2637 m a.s.l.).....	155
Figure 5.10	Remnants of the weathered pre-glacial plateau surface to the north of the eastern Smolikas peak (2575 m a.s.l.).....	155
Figure 5.11	Geomorphological map of the eastern Smolikas area.....	157
Figure 5.12	The northeastern cirque of Moasa (2610 m a.s.l.) containing the lake Galanos Limni.....	159
Figure 5.13	Geomorphological map of the Samarina area.....	162
Figure 5.14	The Samarina moraines.....	162
Figure 5.15	Sample site SA on the crest of a moraine ridge.....	163
Figure 5.16	Clast analyses from a lateral moraine of the Samarina glacier (sample site SA).....	164
Figure 5.17	Geomorphological map of the Mount Vasilitsa area.....	163
Figure 5.18	A section through the Smixi Member.....	167
Figure 5.19	A moraine impounding a lake to the east of Mount Vasilitsa	167
Figure 6.1	Variation of $^{234}\text{U}/^{238}\text{U}$ and $^{230}\text{Th}/^{234}\text{U}$ activity ratios with time in a closed system with no initial ^{230}Th	171
Figure 6.2	XRD traces for cement samples.....	173
Figure 6.3	Vadose zone cement within the weathered glacial deposits of the	

	Vrichos Member on Mount Tymphi formed by the localised percolation of calcium-rich waters in the vadose zone.....	174
Figure 6.4	Phreatic zone cement within till of the Voidomatis Member.....	175
Figure 6.5	Mature profile of a Mediterranean alfisol in Greece.....	191
Figure 6.6	A flow diagram showing the various steps in deriving the Harden soil profile development index.....	196
Figure 6.7	Variations in iron oxide content, magnetic susceptibility, % organic content, % clay content and % calcium carbonate content down-profile of the Voidomatis buried soil.....	198
Figure 6.8	Inter-valley correlation of morpho-lithostratigraphical units on Mount Tymphi.....	209
Figure 6.9	Inter-valley correlation of morpho-lithostratigraphical units on Mount Smolikas.....	210
Figure 6.11	Correlations between formations on Mount Smolikas, Mount Vasilitsa and Mount Tymphi.....	211
Figure 7.1	Hypothetical glacier reconstruction showing different shaped glaciers and ice-divides.....	219
Figure 7.2	Graphical test for the accumulation area ratios (AAR) on three groups of reconstructed glaciers in the Ruwenzori Mountains of Central Africa.....	224
Figure 7.3	Standard deviation of the glacier surface altitudes at varying accumulation area ratios.....	228
Figure 7.4	The Group A glaciers of Mount Tymphi during the Skamnellian Stage....	231
Figure 7.5	The Group B glaciers of Mount Tymphi during the Skamnellian Stage....	233
Figure 7.6	The Stani Grava (1.) and Tsepelovo (2.) glaciers of Mount Tymphi during the Skamnellian Stage.....	234
Figure 7.7	The Skamnelli (1.) and Tsioumako (2.) glaciers of Mount Tymphi during the Skamnellian Stage.....	235
Figure 7.8	The source areas of the Tsepelovo and Skamnelli glaciers in the Laccos Tselon and Megalon Litharion cirques during the Skamnellian Stage.....	236
Figure 7.9	The easternmost Group D glaciers of Mount Tymphi during the Skamnellian Stage.....	238
Figure 7.10	The westernmost Group D glaciers of Mount Tymphi during the Skamnellian Stage.....	239
Figure 7.11	The Vadulakkos glacier of Mount Smolikas during the Skamnellian Stage.....	241
Figure 7.12	The Samarina glacier of Mount Smolikas during the Skamnellian Stage..	242
Figure 7.13	The Smixi glacier of Mount Vasilitsa during the Skamnellian Stage.....	242

Figure 7.14	Standard deviation of the Vlasian Stage glacier surface altitudes at varying accumulation area ratios.....	244
Figure 7.15	The Group A glaciers during the glacial maximum of the Vlasian Stage..	247
Figure 7.16	The Group B glaciers during the glacial maximum of the Vlasian Stage..	248
Figure 7.17	The western Group C glaciers during the glacial maximum of the Vlasian Stage.....	249
Figure 7.18	The easternmost Group C glaciers during the glacial maximum of the Vlasian Stage.....	250
Figure 7.19	The Xeroloutsa glacier (Group D). Glaciers are contoured at 50 m Intervals.....	251
Figure 7.20	Basal shear stress plotted against glacier surface altitude along centre-glacier profiles.....	252
Figure 7.21	The Vadulakkos glacier during the glacial maximum of the Vlasian Stage.....	254
Figure 7.22	The Konkutino (1.) and the Bogdoni (2.) glaciers during the Vlasian Stage glacial maximum.....	255
Figure 7.23	Basal shear stress plotted against glacier surface altitude along the centre-glacier profile of the Vadulakkos glacier.....	256
Figure 7.24	The Vasilitsa glaciers during the glacial maximum of the Vlasian Stage..	257
Figure 7.25	Standard deviation of the Tymphian Stage glacier surface altitudes at varying accumulation area ratios.....	259
Figure 7.26	The Mount Tymphi glaciers and rock glaciers during the glacial maximum of the Tymphian Stage.....	261
Figure 7.27	The Smolikas glaciers during the glacial maximum of the Tymphian Stage.....	262
Figure 7.28	The single Vasilitsa cirque glacier during the glacial maximum of the Tymphian Stage.....	263
Figure 7.29	The glaciers and rock glacier of Mount Smolikas during the Smolikasian Substage (Late-glacial Substage) of the Tymphian Stage.....	264
Figure 7.30	Summary of the glacier extent on Mount Tymphi during the Middle to Late Pleistocene.....	266
Figure 7.31	Summary of the glacier extent on Mount Smolikas during the Middle to Late Pleistocene.....	267
Figure 7.32	Summary of the glacier extent on Mount Vasilitsa during the Middle to Late Pleistocene.....	267
Figure 8.1	Annual total precipitation and the free-atmospheric temperature observed at the ELAs for 70 glaciers worldwide.....	269

Figure 8.2	Rock glacier - permafrost relationship based on modern rock glaciers in the Alps.....	270
Figure 8.3	Map of the Mediterranean showing the dominant air circulation paths during the last glacial period.....	272
Figure 8.4	The northeast-facing cliffs of Goura (2466 m a.s.l.) at the head of the Maghoula valley.....	273
Figure 8.5	Mean monthly temperatures distributed over the year using the modern mean monthly temperatures at Ioannina.....	278
Figure 8.6	Mean monthly temperature distribution at 2174 m a.s.l on Mount Tymphi during the Tymphian Stage based on a 2300 mm annual precipitation.....	279
Figure 8.7	The relationship between mean summer temperatures and precipitation during the glacial maximum of the Vlasian Stage relative to Tymphian Stage values.....	286
Figure 8.8	Gamila peak (2497 m a.s.l.) and the upper parts of the Amarendos valley..	289
Figure 8.9	Snow patches during July 2001 in a doline field on the unglaciated southern slopes of Goura (2466 m a.s.l.).....	289
Figure 8.10	The relationship between mean summer temperatures and precipitation during the glacial maximum of the Skamnellian Stage relative to Tymphian Stage values.....	291
Figure 8.11	The relationship between mean summer temperatures and precipitation during the different glacial stages relative to the Tymphian Stage glacial maximum.....	293
Figure 8.12	Reconstructed mean annual temperature depression (°C) for southern Europe during the LGM as deduced from pollen modelling.....	294
Figure 8.13	Events between 30,000 and 20,000 ¹⁴ C years in the Pindus Mountains of northwest Greece as deduced from a variety of geological and geomorphological records.....	297

List of Tables

Table 1.1	A simplified stratigraphy of the Middle-Late Pleistocene and Holocene of northern Europe and the Alps and correlations with the marine record.....	3
Table 2.1	Climate table for Ioannina (484 m a.s.l.) for the period 1961-1990.....	12
Table 2.2	Extrapolated mean monthly temperatures at 2000 m a.s.l. based on the Ioannina data.....	12
Table 4.1	Morpho-lithostratigraphical summary of the Tsepelovo area.....	87
Table 4.2	Morpho-lithostratigraphical summary of the Skamnelli area.....	104
Table 4.3	Morpho-lithostratigraphical summary of the Vrisochori area.....	108
Table 4.4	Morpho-lithostratigraphical summary of the Iliochori area.....	112
Table 4.5	Morpho-lithostratigraphical summary of the Stani Katsanou valley.....	117
Table 4.6	Morpho-lithostratigraphical summary of the Mighia valley.....	118
Table 4.7	Morpho-lithostratigraphical summary of the Amarandos valley.....	120
Table 4.8	Morpho-lithostratigraphical summary of the Megas Laccos valley.....	125
Table 4.9	Morpho-lithostratigraphical summary of the Stani Grava area.....	128
Table 4.10	Morpho-lithostratigraphical summary of the Raidhovoli valley.....	134
Table 5.1	Morpho-lithostratigraphy of the Vadulakkos valley.....	154
Table 5.2	Morpho-lithostratigraphy of the Konkutino valley.....	160
Table 5.3	Morpho-lithostratigraphy of the northeastern valley of Mount Vasilitsa...	166
Table 6.1	Uranium-series dates from cemented units in the Laccos Radenas Formation.....	179
Table 6.2	Uranium-series TIMS data.....	180
Table 6.3	Uranium-series dates from cemented units in the Megas Laccos Formation.....	182
Table 6.4	Uranium-series dates from cemented units in the Tsepelovo Formation...	184
Table 6.5	Uranium-series dates from cemented units in the Skamnelli Formation....	186

Table 6.6	Uranium-series dates from cemented units in the Raidhovoli Formation...	187
Table 6.7	Cement ages and the pollen stratigraphical record at Ioannina and correlations with the marine isotope record.....	188
Table 6.8	Maturity indicators for the B horizon of Quaternary soils in Greece as defined by van Andel (1998).....	192
Table 6.9	Harden index values for the Voidomatis soil profile.....	199
Table 6.10	Horizon characteristics from the Maghoula Member soil.....	201
Table 6.11	Horizon characteristics from the Kato Radza Member soil.....	202
Table 6.12	Conventional hierarchy of chronostratigraphical and geochronological units in the Quaternary.....	205
Table 6.13	The pollen stratigraphical sequences at Ioannina (cores IN 249 and 284) and Tenaghi Philippon.....	207
Table 6.14	Chronostratigraphical table showing the relationship between the fragmentary glacial sequence in the Pindus Mountains and the continuous parasequence in the Ioannina 249 and 284 cores.....	213
Table 7.1	Shape factor (F) for parabolic valley profiles derived from the ratio between the half width of the glacier to its maximum thickness (W).....	225
Table 7.2	Areas and equilibrium line altitudes of the glaciers of the Skamnellian Stage.....	229
Table 7.3	The glacier characteristics during the Skamnellian Stage on Mount Smolikas.....	240
Table 7.4	Glacier areas and ELAs for the Vlasian glaciers of Mount Tymphi.....	246
Table 7.5	Glacier areas and ELAs for the Vlasian glaciers of Mount Smolikas.....	253
Table 7.6	Glacier areas and ELAs for the Vlasian glaciers of Mount Vasilitsa.....	257
Table 7.7	The Tymphian Stage glaciers of Mount Tymphi.....	259
Table 7.8	The Tymphian Stage rock glaciers of Mount Tymphi.....	260
Table 7.9	The Tymphian Stage glaciers of Mount Smolikas.....	260
Table 7.10	The last glaciers of Mount Smolikas.....	265
Table 7.11	The rock glacier in the Northwestern cirque of Mount Smolikas.....	265
Table 8.1	Palaeoclimatic combinations reconstructed at the mean ELA of the last cirque glaciers on Mount Tymphi (2174 m a.s.l.).....	278
Table 8.2	Palaeoclimatic combinations reconstructed at the highest ELA of the last cirque glaciers on Mount Smolikas (2475 m a.s.l.).....	281

Chapter One

Introduction

Our understanding of Quaternary climate change and the glacial history of the Earth has been evolving for over 200 years. However, even today, knowledge of the detailed extent and chronology of former glaciations is limited in many mountain areas, especially in the Mediterranean region, south of the former large ice sheets of the Alps and northern Europe. This chapter reviews the early history of glacial studies and the record of Quaternary climatic change in both the oceans and on land. The key issues which are identified within this discussion provide the main research questions and the basis for the investigation of the glacial and periglacial deposits of northwest Greece, the primary focus of this research.

1.1 The Quaternary and glacial theory

The Quaternary Period is characterised by fluctuating climatic phases between cold 'glacial' and warm 'interglacial' phases over the past 2.6 million years (Shackleton *et al.* 1990). The Quaternary Period is traditionally subdivided into two Epochs: the Pleistocene and the Holocene, the latter being the present interglacial and the former representing multiple glacial-interglacial cycles. The term 'Quaternary' was first introduced by G. Arduino (1714-1795) who distinguished four separate stages or 'orders' in the geological column arranged one above the other (Schneer 1969). These four 'orders' were Primary, Secondary, Tertiary and Quaternary. The term 'Quaternary' was later applied by Desnoyers in 1829 (Lowe and Walker 1997) and the term 'Pleistocene', a subdivision of the latter, was first used by Forbes (1846) to describe the period in which 'ice-age' deposits formed.

The concept of former glacial or 'ice-age' climates, whereby glaciers assumed a much greater extent than currently observed, was mooted in the early 19th Century, most influentially by Louis Agassiz (1840). However, the concept of previously more extensive glacial phases was suggested even earlier by geologists such as Hutton (1795), Esmark (1824) and De Charpentier (1834) who had all come to the same conclusions as Agassiz (1840), though none held such an influential position.

Glacial theory, chiefly championed by Agassiz (1840), overcame debate and challenges from Diluvialists such as Buckland (1823) and others such as Lyell (1840) who favoured the drift theory. Diluvialists believed large erratic blocks to be the result of the Biblical Flood. However, the religious Diluvial concept of Buckland (1823) was only a

minority view with theories such as the 'Rollstein' or mudflow theory winning broader favour. The 'Rollstein' theory, advocated by scholars such as von Buch (1815) and von Humboldt (1845), whilst favouring a flood hypothesis, envisaged less spiritual a flood, and suggested that the erratic blocks had been spread by enormous water masses from the Alps and Scandanavian mountains – what they called the 'Petridelaunic Flood' (Ehlers 1996). Drift theory, proposed by Lyell (1840), involved movement of debris by icebergs within a cold sea. However, whilst briefly supported by scholars such as Darwin, drift theory managed only brief favour in Britain though retained popularity for many years in many parts of northern Europe (Ehlers 1996). In Britain, the glacial theory was promoted when Agassiz visited Scotland, and presented his ideas at the annual meeting of the British Society for the Advancement of Science in Glasgow in September 1840. It was on this visit that Agassiz convinced Buckland and it soon followed that other scholars such as Lyell converted to the glacial theory. Buckland subsequently worked to promote the development of glacial theory in Britain and by his death in 1856, glacial theory was firmly entrenched here (*cf.* Lyell 1863) as well as in the United States (*cf.* Dana 1863). Elsewhere in Europe, glacial theory was accepted particularly late. In Germany, for example, it was only in 1879 that glacial theory became fully established with Albrecht Penck's article on '*The erratic-bearing formation of North Germany*' (Ehlers 1996). The acceptance of glacial theory led to the observation of former glacial deposits throughout Europe and as far south as the mountains of the Mediterranean region. Here, glacial features were first described in the Pyrenees by Penck (1885), in the Lebanon by Diener (1886), on the Balkan peninsula by Cvijic (1898) and in Greece by Niculescu (1915).

1.2 Stratigraphy and the division of Quaternary time

Stratigraphical subdivision of the Quaternary is largely based on climate (Ehlers 1996). The earliest attempts at subdividing the Quaternary into glacial and interglacial stages were based on glacial and glaciofluvial deposits in the northern Alpine Foreland by Penck & Brückner (1909). They recognised four glaciations within the Quaternary – the Günz, Mindel, Riss and Würm. More recent studies, especially those of sediments in the marine realm, have shown that at least 50 glacial-interglacial cycles can be recognised since the beginning of the Quaternary 2.6 million years ago, and around ten glacial and interglacial stages during the past 800,000 years (Imbrie *et al.* 1984). The ocean-floor record was the key to this discovery since these sediments have built-up undisturbed throughout the Quaternary. Isotopic stratigraphy based on $^{18}\text{O}/^{16}\text{O}$ content in foraminifera tests has

Timescale (years BP)	Marine Isotope Stage	Alpine Stratigraphy	Northern Europe Stratigraphy	
0				
11,500		Holocene	Holocene	<i>Interglacial</i>
2 3 4		Würmian	Weichselian	<i>Glacial</i>
5d/5a				
115,000	5e	Riss/Würm	Eemian	<i>Interglacial</i>
130,000				
6 7 8 9 10		Rissian	Saalian Complex	<i>Glacial</i>
350,000				
430,000	11	Mindel/Riss	Holsteinian	<i>Interglacial</i>
	12	Mindel	Elsterian	<i>Glacial</i>

Table 1.1 A simplified stratigraphy of the Middle-Late Pleistocene and Holocene of northern Europe and the Alps and correlations with the marine record. Boundary ages are from Lowe and Walker (1997, Table 1.1).

enabled a continuous record of glacial-interglacial climates to be established covering the entire Quaternary, since the marine oxygen isotope balance is controlled by fluctuations in land ice volume (Shackleton and Opdyke 1973). This record can be replicated in cores taken from oceans in different parts of the world and therefore provides a record of global ice volume (Lowe and Walker 1997, p. 151).

On land, the Quaternary record is usually much more fragmented, hence the discovery of only four glacial phases in the Alpine record by Penck & Brückner (1909). This poses considerable problems for correlating between terrestrial sequences as well as problems for correlating with the continuous marine record. Table 1.1 shows a simplified stratigraphy of the Alps and northern Europe and correlation with the marine isotope record. However, the correlations shown in Table 1.1 are by no means certain, especially before the last interglacial where correlations are frequently speculative (Lowe and Walker 1997, p.9). This is largely because of the fragmentary nature of the terrestrial records and the frequent lack of geochronological control since many terrestrial sediments are not or cannot yet be dated. These problems are compounded by the complexity of some stratigraphical units. For example, the Saalian Stage in northern Europe, correlative with the Rissian Stage in the Alps, is characterised in its lower part by a repeated series of

warm-cold climatic oscillations, and the warm phases can attain a temperate interglacial character (Litt and Turner 1993). Moreover, at least two major glacial advances, the Drenthe and the Warthe glaciations which are separated by an interstadial, characterise the Upper Saalian Complex (Litt and Turner 1993). This complexity has considerable influence on direct correlations with other terrestrial records such as that in the Alps, and more especially that of the marine isotope record.

However, in some circumstances, such as in lacustrine basins well beyond former ice sheet limits, long continuous sequences spanning all, or part of, the Quaternary can provide a proxy for glacial-interglacial climates based on biostratigraphical evidence, such as pollen stratigraphy. Several such sequences exist in southern Europe (e.g. Tzedakis *et al.* 1997, Allen *et al.* 1999) and provide key reference points for comparing the terrestrial biotic signal with the global ice volume signal in the marine isotopic sequence. They also highlight key differences between these two signals, as well as the problems of correlating records from different proxies and from different terrestrial geographical regions (Tzedakis 2003). However, these long sequences are restricted in their capacity for reconstructing glacial climates because the main proxies from many long sequences are largely biological indicators such as pollen, ostracods or biogenic silica (*cf.* Tzedakis *et al.* 2002, Allen *et al.* 1999). Glacial phases are characterised by low-diversity biotic assemblages, which limits palaeoenvironmental, and more particularly, palaeoclimatic precision. For example, abundance of arboreal tree pollen is a blunt tool for determining former palaeoclimates, especially since such indicators correspond to a whole range of possible climatic combinations (*cf.* Prentice *et al.* 1992). Therefore, whilst these records provide unrivalled temporal span and resolution of biotic change, they are limited in recording precise climate change.

The record of glacial stages, based on true glacial and periglacial deposits, can provide unequivocal evidence of cold-stage climates. However, glacial and periglacial deposits are by nature discontinuous and suffer the disadvantage of representing only small periods of time in the Quaternary record. Despite this limitation, they have the potential to provide excellent glacial stage palaeoclimatic precision based on comparisons with modern glacier-climate and periglacial landform-climate relationships (*cf.* Sissons 1974, 1980, Ballantyne 1989, Hughes *et al.* 2003). The glacial and periglacial record, combined with other proxies such as pollen and lake level evidence, therefore help to resolve our understanding of Quaternary environments and provide key input data for palaeoclimatic models.

1.3 Glacial Greece and its strategic significance in Quaternary studies

Greece represents a key area for Quaternary research. For example, its location, outside of the former ice-sheets of the Alps and northern Europe, has been pivotal to the concept botanical refugia through glacial-interglacial cycles (*cf.* Willis 1992c, Tzedakis 1993). Furthermore, the presence of humans in Palaeolithic Greece has also been the focus of intensive research (*cf.* Bailey *et al.* 1984, Bailey 1997). The glacial and periglacial records, however, have received sparse attention relative to other studies.

In the mountains of Greece, the situation is typical of the wider Mediterranean in that the presence of former glaciers and relict periglacial features has long been recognised (*cf.* Messerli 1967). However, the detailed chronology and palaeoclimatic significance of these features has yet to be fully realised. In addition, the Pindus Mountains represent one of the most southerly glaciated regions of Europe, at the limit of former glaciation and thus may be expected to provide a sensitive record of environmental change (Bailey and Gamble 1990, Woodward *et al.* 2004). Furthermore, the glacial and periglacial record in the Greek mountains holds added potential because of the proximity to recently investigated long continuous lacustrine sequences within tectonic basins and karstic hollows (*poljes*). They include sites such as Ioannina (Tzedakis 1994), Tenaghi Philippon (Wijmstra 1969,

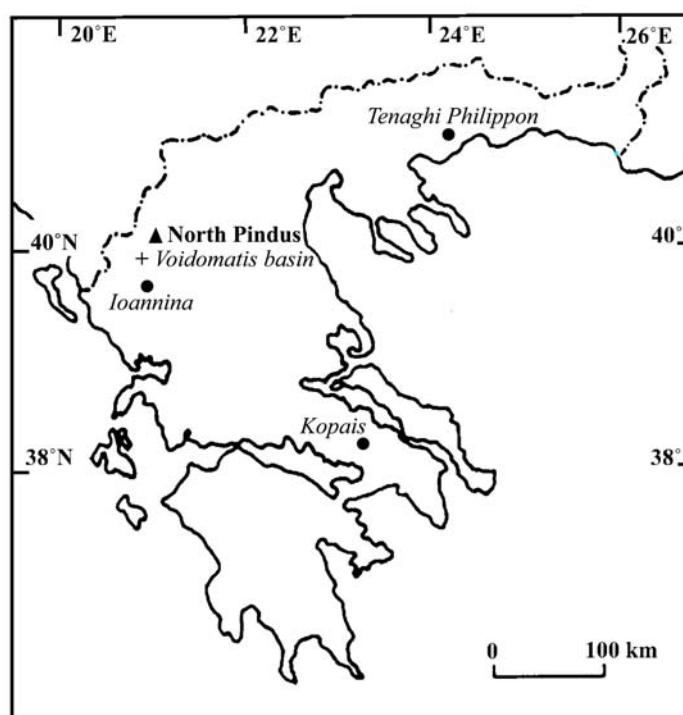


Figure 1.1 Location map showing the North Pindus field area and long lacustrine and fluvial sites in Greece.

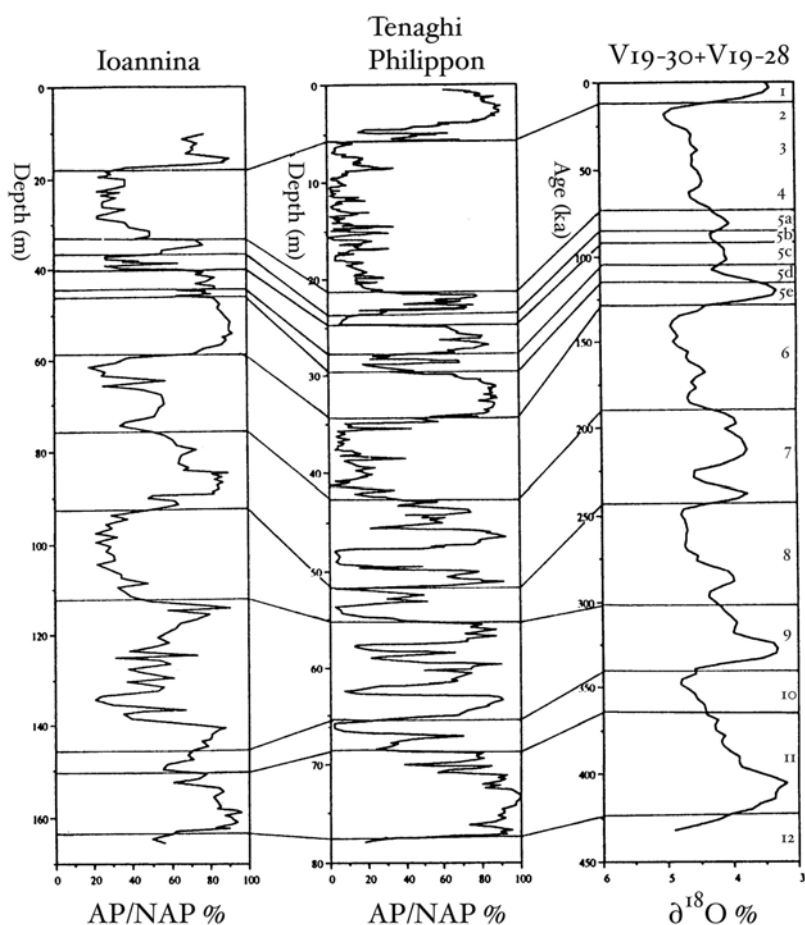


Figure 1.2 Summary arboreal pollen (AP)/ non-aboral pollen (NAP) percentages plotted against depth for Ioannina 249 and Tenaghi Philippon and correlated with the marine oxygen isotope record of V19-30 for the interval 0-340,000 years BP (Shackleton and Pisias 1985) and V19-28 for 340-432,000 years BP (Ninkovich & Shackleton 1975) (from Tzedakis 1993).

Wijmstra and Smit 1976, Wijmstra and Groenhart 1983, van der Wiel and Wijmstra 1987a, 1987b) and Kopais (Okuda *et al.* 2001, Tzedakis *et al.* 1999) (Fig. 1.1). These sites, apparently providing continuous records for up to 1 million years, have been shown to broadly correlate with the global marine record (Fig. 1.2). In addition to these long lacustrine sequences, fluvial deposits, such as those in the Voidomatis basin of the northern Pindus Mountains (Fig 1.1), record aggradation and incision over the last glacial-interglacial cycle, and potentially longer (Lewin *et al.* 1991, Woodward *et al.* 1992, Hamlin *et al.* 2000). Together, these records provide a unique palaeoenvironmental tapestry with which the glacial and periglacial record can be compared, providing a multiple record of palaeoenvironments for Greece and the eastern Mediterranean region.

Whilst long lacustrine terrestrial sequences provide continuous Quaternary records, as noted earlier, they provide limited data regarding palaeoenvironments during glacial intervals. The reasons for this are two-fold. Firstly, long lacustrine sequences have often employed pollen stratigraphy as the main tool. In isolation, pollen analysis is weak in

resolving glacial palaeoclimates since low arboreal pollen percentages of total pollen counts, the principal determinant of glacial climates in pollen stratigraphy, are not unequivocal in terms of climate. Determining the precise nature of palaeoclimate from the pollen record is therefore open to multiple interpretations (*cf.* Prentice *et al.* 1992).

The fluvial record from regions such as the Voidomatis basin in the northern Pindus (Fig 1.1), whilst providing interesting evidence for glacial stage river regimes and catchment characteristics (Lewin *et al.* 1991, Woodward *et al.* 1992, Hamlin *et al.* 2000), cannot resolve the limitations of the long biological records. However, the glacial and periglacial records offer the potential to do this, because of their sensitive physical relationship with climate. The glacial and periglacial records therefore have the potential, in conjunction with the valuable existing evidence provided by the deep lacustrine and fluvial records, to significantly improve our understanding of cold-stage environments in Greece.

1.4 Aims and objectives of this research

The major questions to be addressed based on the preceding discussion are:

- What was the extent of glaciation and periglacial features in the northern Pindus Mountains?
- How many phases of glaciation and major periglacial activity can be identified in the geomorphological and stratigraphical record?
- What is the chronology of this glacial/periglacial sequence?
- How does the glacial/periglacial sequence relate to other sequences in Greece, the Mediterranean and wider global climate change?
- What does the glacial/periglacial record reveal about glacial stage climates in Greece?

These questions can be addressed via the principal methods of this research to provide:

- a comprehensive mapping and interpretation of glacial sediments and landforms on three key mountains in northwest Greece;
- an understanding of the chronology and sequence of glaciation during the Quaternary;
- a correlation of the glacial sequence with nearby fluvial and long lacustrine sequences and the development of a regionally applicable chronostratigraphy;
- a reconstruction of the former glaciers during different glacial phases;
- and palaeoclimatic reconstructions for different glacial phases based on modern glacier- and periglacial-climate relationships.

The background to the research area in northwest Greece is the focus of Chapter Two.

Chapter Two

Background

2.1 The study area

The research centres on the mountains of Tymphi (2497 m a.s.l.), Smolikas (2637 m a.s.l.) and Vasilitsa (2248 m a.s.l.) in Epirus, northwest Greece, all of which provide the watershed of the Aoos river basin (Figure 2.1). Mount Tymphi is a complex mountain consisting of multiple summits over 2000 m a.s.l., several of which exceed 2400 m a.s.l. Mount Smolikas lies *ca.* 12 km to the northeast, across the valley of the Aoos and is the second highest mountain in Greece with over 25 km² of high ground over 2000 m a.s.l. Mount Vasilitsa lies to the east of both Tymphi and Smolikas and stands solitary above the villages of Distrato and Smixi.

The lower slopes of Mount Tymphi are covered with holly oak (*Quercus coccifera*) and hornbeam (*Carpinus orientalis*), intermediate heights are cloaked with beech forest (*Fagus sylvatica*) and black pine forest (*Pinus nigra*) whilst at the tree line (*ca.* 2000 m a.s.l.) Bosnian pine forest (*Pinus leucodermis*) can be found. However, much of the lower southern slopes of Tymphi near Skamnelli and Tsepelovo, as well as much of the gentle southern plateau consist of pasture and open grasslands, the result of both grazing and altitude. Surfaced roads skirt the lower areas of Mount Tymphi and bulldozed tracks penetrate the higher valley areas, especially above Tsepelovo and Skamnelli and in the slopes above Vrisochori (Fig. 2.1). Elsewhere on Tymphi, access can be made via small footpaths, though much of the field area is pathless, open terrain (Fig. 2.2).

On Mount Smolikas, black pine (*Pinus nigra*) forest dominates due to the high concentration of magnesium in the ophiolite bedrock (World Wildlife Fund 2003). Here, the extensive forests and lack of tracks make access particularly difficult (Fig. 2.3), although poorly-surfaced roads do encircle the massif. These factors, and the generally more inclement weather on Mount Smolikas (no doubt a function of its greater altitude), make for more difficult operation in this area compared with Mount Tymphi. Conversely, Mount Vasilitsa is easy to access since a ski development has been established on the northern flank, along with good access roads from Distrato to the west and Smixi to the east.

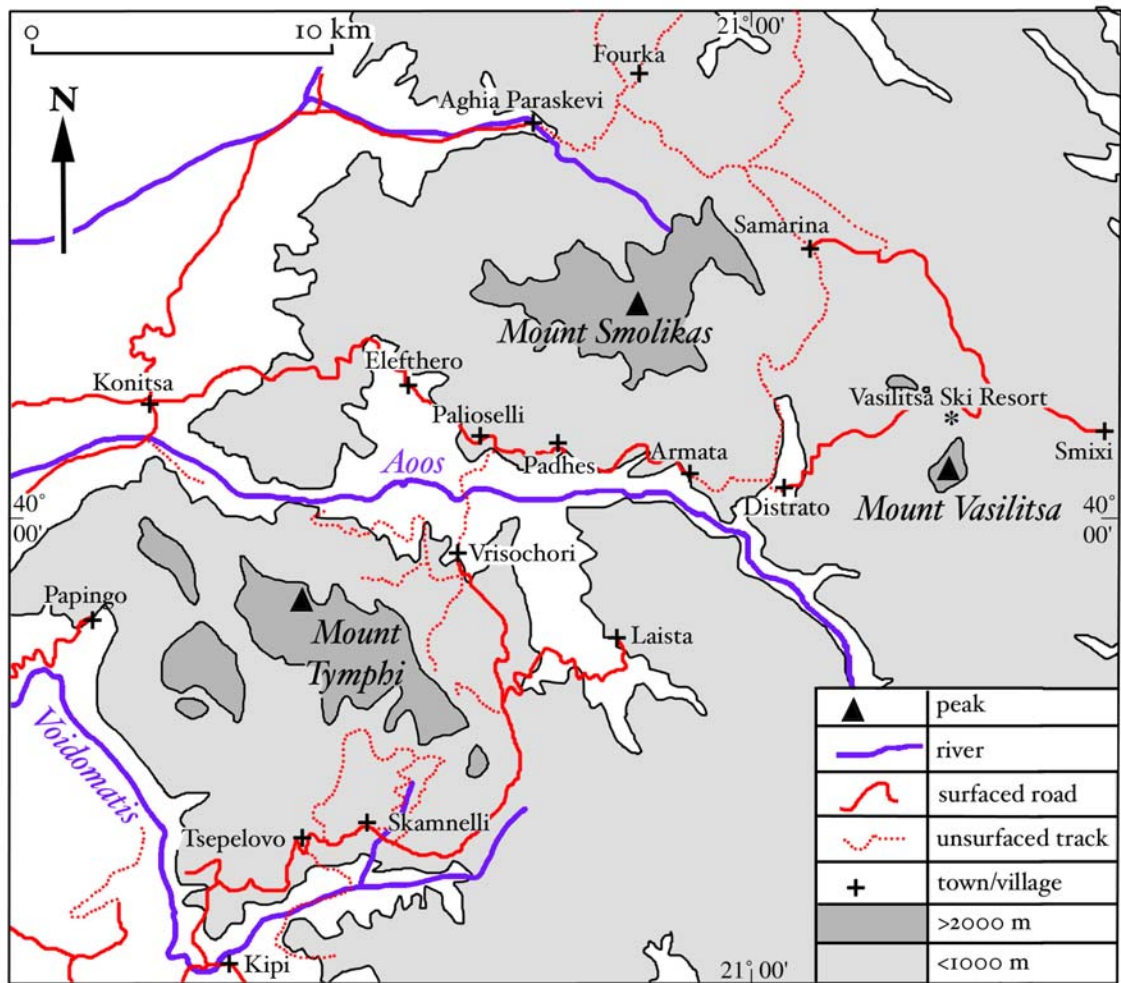
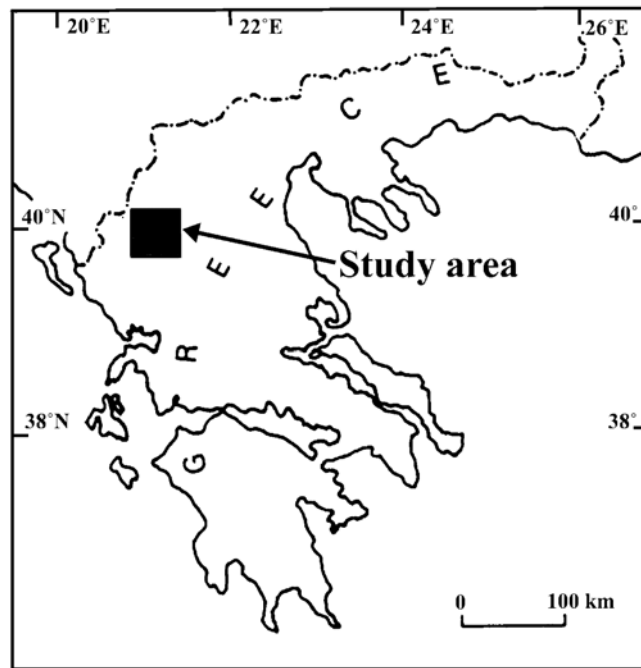


Figure 2.1 Location map of Mount Smolikas, Mount Vasilitsa and Mount Tymphi.



Figure 2.2 Typical landscape of Mount Tymphi (July 2001).



Figure 2.3 Typical landscape of Mount Smolikas (July 2001).

On all three mountains, brown bear (*Ursus arctos*), wolf (*Canis lupus*) and Balkan chamois (*Rupicapra rupicapra*) can be found. In fact, every species of large mammal found in mainland Greece, with the exception of the red deer (*Cervus elaphus*) has habitats in this area. This fact, combined with the presence of rare birds such as the Griffon vulture (*Gyps fulvus*) and the Golden eagle (*Aquila chrysaetos*), as well as impressive geomorphological features such as the Vikos Gorge, led to creation in 1973 of the Aooos-Vikos National Park on Mount Tymphi.

2.2 Modern climate

The climate of Epirus is transitional between that of central Europe and the Mediterranean, and local variations in climate are considerable, largely a result of relief. At Ioannina (39°40'N, 20°51'E, 484 m a.s.l.), for the the period 1961-1990, mean annual temperature was 14.3°C with mean January and July temperatures 4.6°C and 24.8° respectively. The mean annual precipitation was 1078 mm with 16.1% of this falling in December and 2.1% falling in August (World Meteorological Organisation 1998) (Table 2.1).

In the higher mountains, January and July temperatures of around minus 5°C and +15°C are typical (Furlan 1977) and consequently much of the winter precipitation falls as snow, patches of which persist until July. This is illustrated in Table 2.2 where the Ioannina climate data has been been extrapolated to 2000 m a.s.l. However, the threshold for permafrost conditions and the -2°C mean annual isotherm (*cf.* Haeberli 1982, 1985) is presently well above the highest peaks, at over 3000 m a.s.l.

Precipitation is also greater in the mountains although the study area, whilst containing the highest mountain of the Pindus range, is not the wettest. This exists in southeastern Epirus around Mount Tzoumerka (2363 m a.s.l.) where, even at the mid-altitude station of Theodoriana 960 m a.s.l., the mean precipitation is 2550 mm (Fotiadi *et al.* 1999). At Skamnelli (1180 m a.s.l.), on Mount Tymphi, mean annual precipitation is 1721 mm (Fotiadi *et al.* 1999). Figure 2.4 shows the precipitation values at various other sites in the study area. The Skamnelli value of 1721 mm is the highest registered mean annual precipitation on Mount Tymphi, although precipitation at the highest elevations (>2000 m a.s.l.) are likely to be higher, probably well over 2000 mm (Furlan 1977). On Mount Smolikas, the highest registered precipitation is at Fourka (1350 m a.s.l.) but again, the precipitation on the higher slopes are likely to be far higher. However, the fact that Skamnelli, on Mount Tymphi, receives more precipitation than the higher village of Fourka, on Mount Smolikas, suggests that Mount Tymphi receives more precipitation at a given altitude than Mount Smolikas. This is probably due to the fact that Mount Smolikas

is situated more inland than Mount Tymphi - a key factor in determining precipitation levels in northwest Greece (Fotiadi *et al.* 1999). On this basis, Vasilitsa would be expected to be the driest of the mountains and this is supported by the mean annual precipitation value at Distrato of 1045 mm - the lowest recorded in the area (Fig. 2.4).

Month	Mean Temperature (°C)	Precipitation (mm)	% of total precipitation
J	4.6	130.5	12.2
F	6.1	115.5	10.8
M	8.9	98.2	9.2
A	12.6	76.0	7.1
M	17.4	66.9	6.3
J	21.7	46.8	4.4
J	24.8	28.5	2.7
A	24.2	28.4	2.7
S	20.3	54.9	5.1
O	14.9	95.5	8.9
N	9.7	154.5	14.5
D	5.8	172.3	16.1
Mean annual temperature/ Total annual precipitation	14.3	1068	

Table 2.1 Climate table for Ioannina (484 m a.s.l.) for the period 1961-1990 (from World Meteorological Organisation 1998)

Month	Mean Temperature (°C)
J	-4.5
F	-3
M	-0.2
A	3.5
M	8.3
J	12.6
J	15.7
A	15.1
S	11.2
O	5.8
N	0.6
D	-3.3
Mean annual temperature	6.4

Table 2.2 Extrapolated mean monthly temperatures at 2000 m a.s.l. based on the Ioannina data using a standard atmospheric lapse rate of 0.6 per 100 m.

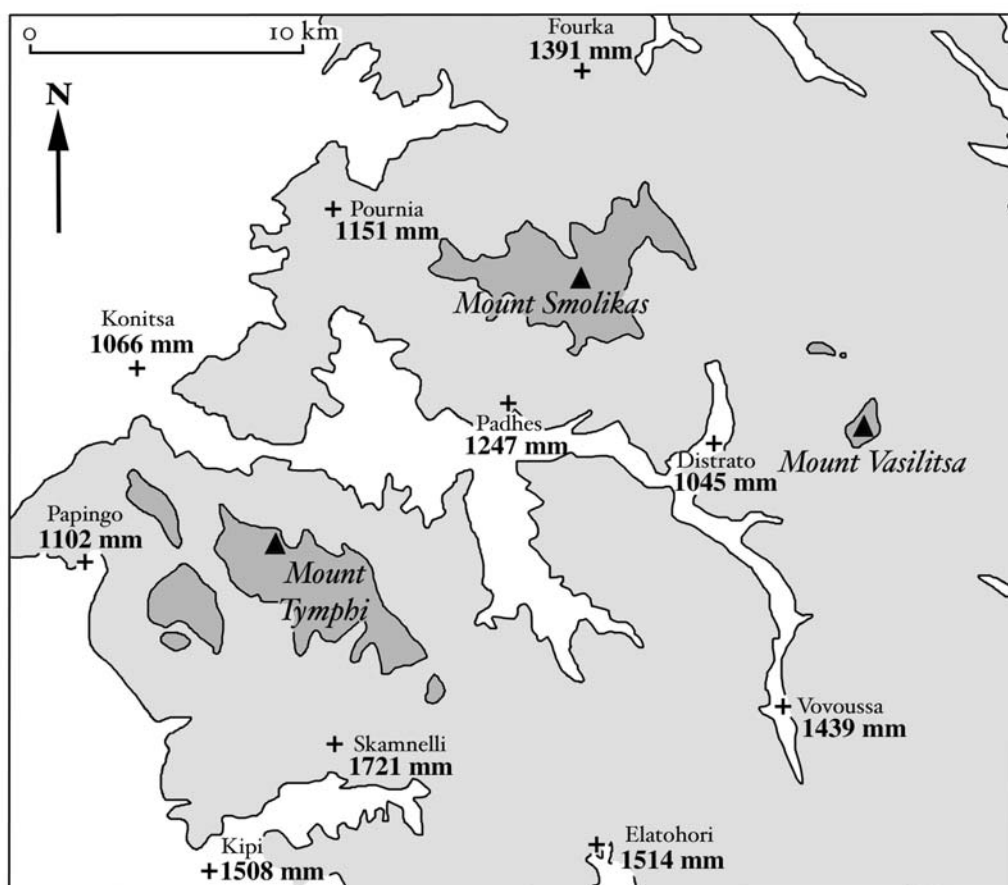


Figure 2.4 Modern precipitation distribution on Mount Tymphi, Mount Smolikas and Mount Vasilitsa (after Fotiadi *et al.* 1999).

2.3 Geology

The mountains of Epirus are part of the Pindus chain, which was formed by the Pindus thrust from mid-Eocene until Oligocene times (Clews 1989). The mountains are today part of a seismically active region and have been throughout the Quaternary. Regional uplift in Epirus is estimated at *ca.* 40 - 80 m in 100,000 years (King and Bailey 1985), although the net gain in height of the Pindus mountains is probably somewhat less due to erosion. Geological maps are provided in Figure 2.5.

Mount Tymphi represents a series of uplifted fault blocks and faulted escarpments and is formed largely in Palaeocene-Eocene limestone, with some exposures of Senonian-Jurassic dolomites and limestones on the northern scarp and in the Vikos Gorge to the south (IGME 1970, 1983). The limestones are pure, resistant, crystalline rocks typical of the wider Epirus region (Smith and Moores 1974) and karstic features are evident throughout the area. Dolines, pavements, vertical shafts and extensive cave systems are well-developed

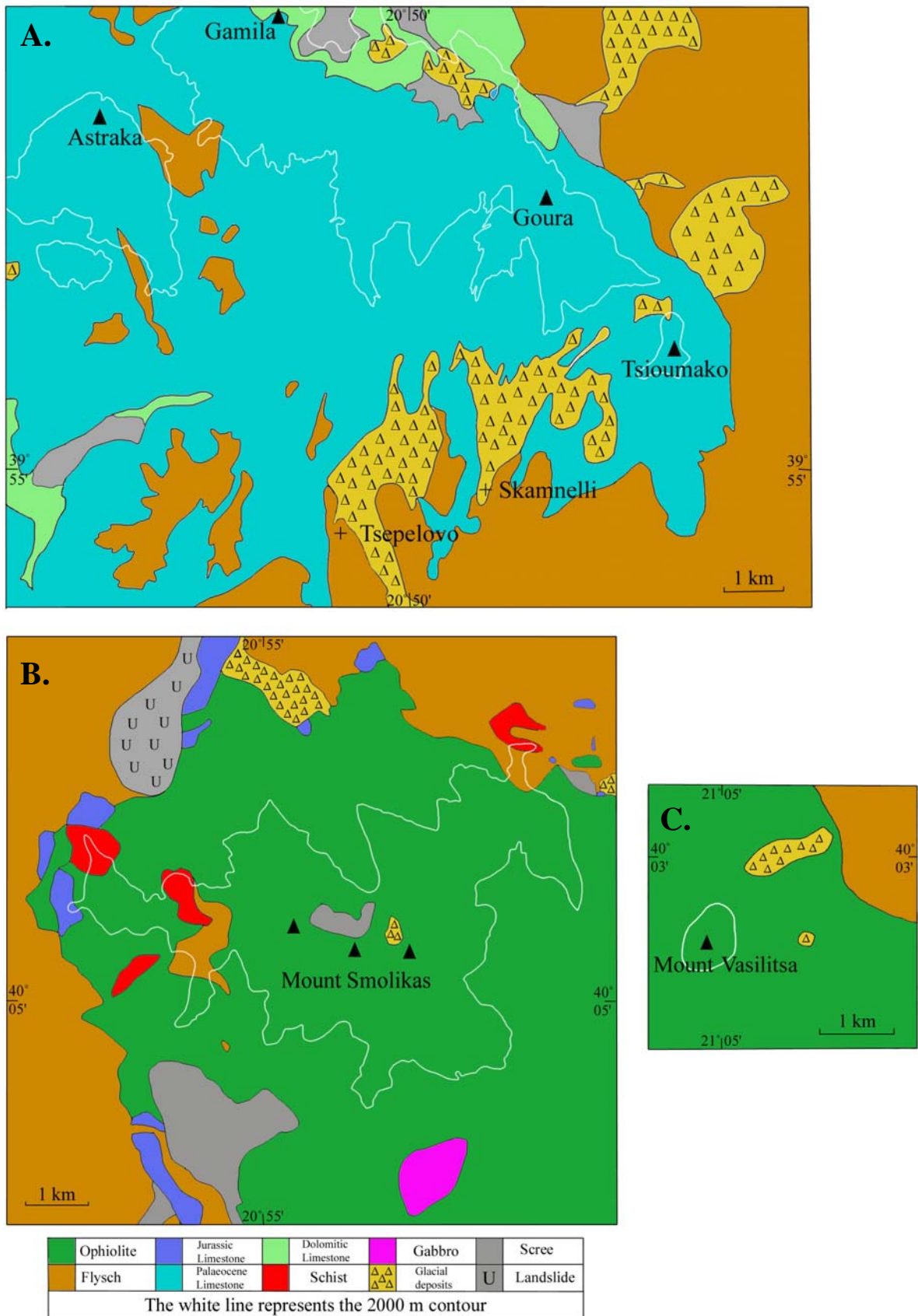


Figure 2.5 Geological maps of the Mount Tymphi area (A.) Mount Smolikas (B.) and Mount Vasilitsa (C.) (after IGME 1970, 1983, 1987).

all over the mountain and it is here on Mount Tymphi that the deepest known cave in Greece occurs - the Epos chasm, 442 m deep. Elsewhere, deep caverns abound with the Provetina, Tripa Tis Nifis and Tsepelovo Spiara reaching depths of 389, 299 and 228 m respectively (Waltham 1978). The lower slopes are dominated by younger flysch rocks (Late Eocene to Miocene) which consist of thin beds of graded sandstones (10-20 cm) intercalated with softer, fissile siltstones (Lewin *et al.* 1991). Glacial deposits are also marked on IGME geological maps in numerous valleys and cirques (Fig. 2.3) extending down to below 1000 m a.s.l.

The geology of Mount Smolikas and Mount Vasilitsa is completely different to that of Mount Tymphi since these mountains are formed in ultrabasic and basic ophiolitic rocks which include lithologies such as serpentinite, dunite and harzburgites (IGME 1983, 1987). These ophiolite rocks are sometimes termed serpentinites and are dark rocks - often composed of dark green to brown magnesium- and iron-rich olivine minerals. Jurassic limestones also occur in places, as do Jurassic schists, and both are found mainly at the overthrust nappe of the ophiolitic complex. Glacial deposits are also marked on the IGME geological maps of this area. However, it is often the case that where glacial deposits are present they are not marked on the IGME geological maps. Therefore, whilst the IGME geological maps provide valuable reconnaissance material, they are limited in the information they convey regarding the timing, accurate extent and dynamics of Quaternary glaciation.

2.4 Glaciation in the Mediterranean

The Quaternary Period, and in particular the Pleistocene Epoch, has been characterised by the occurrence of widespread glaciation. However, the common conception is of vast ice sheets over northern Europe and the Alps with little appreciation of the extent and chronology of Quaternary glaciers in the mountains of the Mediterranean. Much of the initial work regarding former glaciers of the Mediterranean mountains was published before 1970, and the classic review by Bruno Messerli (1967) probably represents the most comprehensive account of Mediterranean Quaternary glacial features ever published. This and other studies were largely reconnaissance work upon which much of the later investigation has been based. However, even today, few studies exist that have established a clear chronology for the glacial deposits of the Mediterranean and many workers often

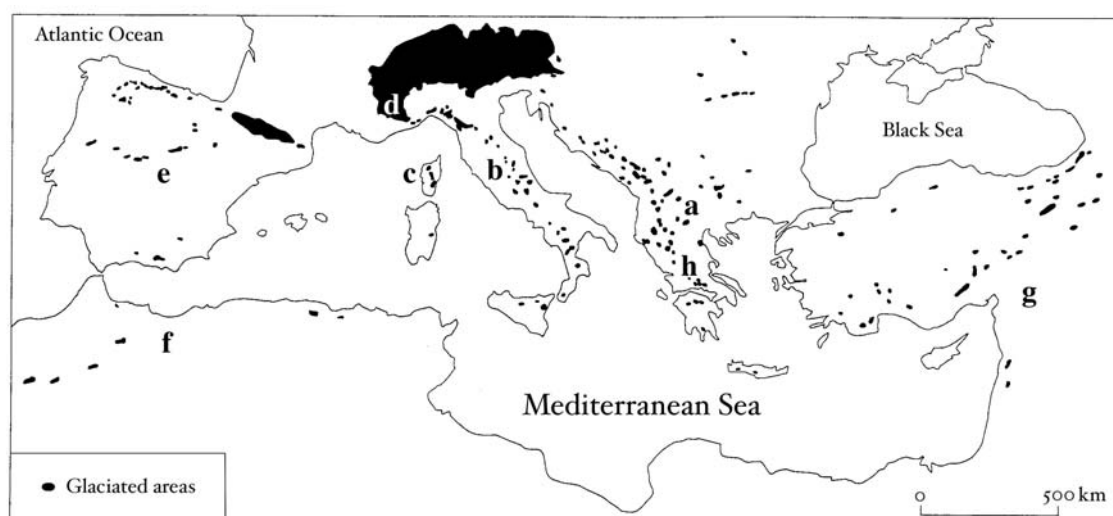


Figure 2.6 Distribution of Pleistocene glacial features in the Mediterranean region recognised by Messerli (1967). The areas discussed are labelled a: The Balkans; b: The Italian Apennines; c: Corsica; d: The Alpes Maritimes; e: The Pyrenees and the Iberian Peninsula; f: The Atlas Mountains; and g: The Eastern Mediterranean (Turkey and The Lebanon).

correlate preserved glacial features with the Last Glacial Maximum (LGM) of the Late Würmian.

In the following section, evidence for glaciation in the mountains of the Mediterranean is reviewed, concluding with the peninsula of Greece. The review is divided into mountain areas or physically-distinct regions rather than countries and covers all areas bordering the Mediterranean Sea including western Iberia and eastern Anatolia (Fig. 2.6).

2.4.1 The Balkans

The Balkan peninsula is particularly mountainous and evidence of former glaciation has been noted in the mountains of Albania, all of the former Yugoslavian republics and Bulgaria (Fig. 2.7). Unfortunately, in none of these areas have the glacial deposits been dated, and there is no sedimentological analysis presented in the literature. Therefore, any attempt to reconstruct the glacial chronology in this region remains entirely speculative. Nevertheless, the existing evidence represents an important record of the extent of Pleistocene glaciation in these areas.

Evidence for glaciation in southern Albania was first presented by Herbert Louis (1926) on the mountains of Nëmerçka (2495 m a.s.l.), on the Epirus border, and Mali i Lunxheriës (2200 m a.s.l.), southwest of Gjirokastër. Further north, in northern and eastern Albania, glacial features were noted as early as 1900 by Cvijic (1900). More recently,



Figure 2.7 Location map showing some of the glaciated mountains of Greece, the Balkans, Italy and Corsica.

Menkovic and Markovic (2004) used satellite images and small-scale topographical and geological maps to deduce evidence of glaciation in the Korab mountains (2753 m a.s.l.) and the Koritnik mountains (2394 m a.s.l.) in eastern Albania, and on the Prokletije mountains (2692 m a.s.l.) in the north Albanian Alps. In the latter area, Palmentola *et al.* (1995) noted the presence of relict rock glaciers above 1700 m a.s.l., inside of more extensive glacial features. They suggested that these rock glaciers may be of Late-glacial age because they believed the more extensive glacial features formed during the Last Glacial Maximum (LGM) of the Late Würmian. However, there are no radiometric dates to support such an assumption in this area, and the chronology of glaciation is unresolved.

The significance of glaciation in the Balkan Mountains is particularly evident on the Sara Mountains (2747 m a.s.l.), on the border of Serbia (Kosovo) and Macedonia. Here, a plateau-type ice cap covered an area of 30-35 km². The most widespread glaciation during

the Pleistocene occurred around the watershed between the Lepenec and Prizrenska Bistrica rivers as well as in the extreme southwestern part of the Sara Mountains (Menkovic and Markovic 2004).

Elsewhere in the former republics of Yugoslavia, evidence of glaciation was first mapped by Cvijic (1900) as part of his wider research of glaciation in the Balkans. More recently, reviews of the glaciation in the mountains have been presented for Montenegro by Menkovic and Markovic (2004), for Slovenia by Bavec and Verbic (2004) and for the Croatian Adriatic and Coastal Dinarides by Marjanac and Marjanac (2004). In Montenegro, on Mount Durmitor (2530 m a.s.l.), Alpine-type valley glaciers fed a high plateau glacier limited by deep canyons incised by the Piva and Tara rivers. Further west, near the Adriatic coast, Mount Orjen (1895 m a.s.l.) is characterised by glacio-karst landscapes. In fact, much of the northern Balkans and, as a consequence of the action of cold glacial meltwater, the uplands of Montenegro display the most intensive karstification anywhere in the Balkans (Menkovic and Markovic 2004). Further north, in Slovenia, a small glacier exists today on Triglav (2863 m a.s.l.), the highest mountain of the Julian Alps. This glacier has rapidly retreated through the 20th century (Sifrer 1963, Messerli 1967) (Fig. 2.8) and is now less than 4 hectares in area (Gams 2004).

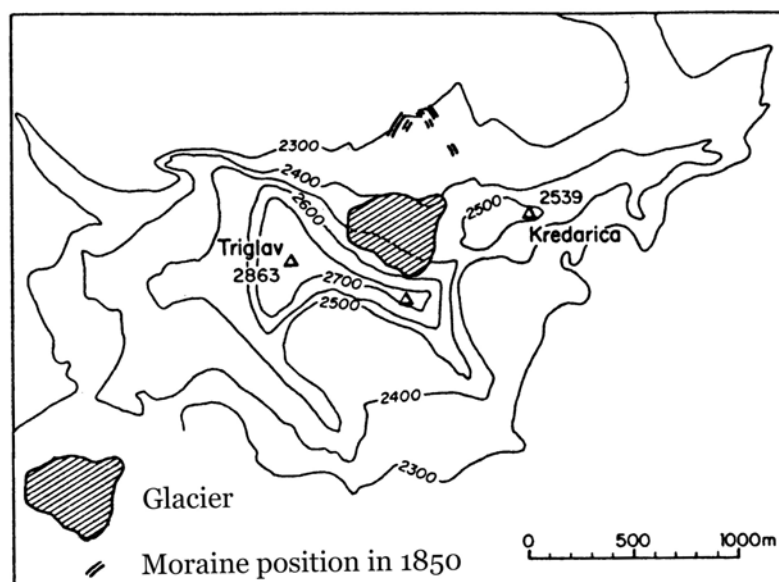


Figure 2.8 The Triglav glacier, Slovenia, showing extent in 1967 and 1850 (Adapted from Messerli 1967).

Early reports of relict glacial features in the Bulgarian mountains include those of Cvijic (1898, 1900) and later studies by Louis (1930). Glacial deposits were noted on all of the high mountains of the Pirin (2925 m a.s.l.) and the Rila (2920 m a.s.l.) ranges. Pleistocene snow lines in these areas are estimated at *ca.* 2200-2300 m a.s.l. (Messerli 1967). At Lake Dalgoto (2312 m a.s.l.), a glacial lake in the northern Pirin Mountains, an open xerophytic herb vegetation with *Artemisia* and *Chenopodiaceae* was widely developed around the lake during the Younger Dryas Chronozone (11,000-10,000 ¹⁴C yr BP). This indicates that climate was cold and possibly arid during this period (Stefanova and Ammann 2003). However, whilst the bottom of the core is dated to the Younger Dryas, there is no evidence of a marked climatic oscillation during the Late-glacial Substage (14-10,000 ¹⁴C years BP). The evidence would seem to suggest that open xerophytic herb vegetation existed throughout the Late-glacial following cirque glacier retreat. More significantly, it also suggests that no glacier ice occupied this cirque at the altitude of Lake Dalgoto (2312 m a.s.l.) during the Younger Dryas Chronozone.

2.4.2 The Italian Appenines

The Appenine mountains of Italy rise to 2912 m a.s.l. in the Gran Sasso at Corno Grande (Fig. 2.7). The Calderone glacier, Europe's southernmost modern glacier, occurs on this mountain and covers only a few hectares, well below the regional snow line, with its snout at *ca.* 2700 m a.s.l. The glacier survives due to the very steep cirque walls and a northeast exposure. During the Little Ice Age between AD 1550-1850, it is thought that the Calderone glacier reached as low as 2500 m a.s.l. (Gellatly *et al.* 1994) and five phases of Late Holocene neoglacial expansion have been recognised by Giraudi (2003, 2004). The glacial deposits of Italy are relatively well-studied, in comparison to those in the Balkans, and are therefore key to understanding the relationship between the deposits of Greece and the wider Mediterranean. The most widespread and best preserved relict glacial features are usually attributed to the Late Würmian Substage, although older, more extensive glacial deposits are thought to be of Middle Pleistocene age.

The Gran Sasso massif of the Central Appenines represents the best available glacial chronological sequence in Italy. Giraudi and Frezzotti (1997) mapped a series of moraines and rock glaciers and derived an age of $22,680 \pm 630$ ¹⁴C years BP from the base of lacustrine deposits in a basin formed by the glacial damming of the ice-free Coppone Valley. This led Giraudi and Frezzotti (1997) to assume that the lacustrine sedimentation began after the period of moraine formation, during the Campo Imperatore Stadial, equivalent to Last Glacial Maximum (LGM) of Marine Isotope Stage (MIS) 2. However, it

must be noted that the ^{14}C date represents a minimum age of glaciation, especially since the lacustrine sequence rested on gravels and not bedrock.

In the Coppone Valley, rock glaciers are thought to have formed contemporaneously with the main Campo Imperatore glacier, the fronts of which reached down to 1660 m a.s.l. Using these rock glaciers as indicators of the limit of discontinuous permafrost, Giraudi and Frezzotti (1997) concluded that mean annual temperatures were 7.3-8.3°C lower than present-day values. Also, they extrapolated this temperature reduction to the ELA (equilibrium line altitude) of the valley glaciers in the Campo Imperatore valley and, due to the well established relationship between accumulation and precipitation at the ELA of modern glaciers (*cf.* Ohmura *et al.* 1992), inferred that snowfall was the same as today. This is an interesting finding since it contradicts evidence from the pollen record at long lacustrine sequences in Italy such as at Lago Grande di Monticchio, where the evidence suggests a very arid LGM (Allen *et al.* 2000). However, Giraudi and Frezzotti (1997) do stress that similar snowfall compared with today may not imply similar rainfall during the summer season.

A series of recessional moraines and rock glaciers in the Gran Sasso are thought to correspond with periods of glacier stabilisation or re-advance between 20 and 10,000 ^{14}C years BP. They have been named the Fontari Stadial, which started after $17,840 \pm 200$ ^{14}C years BP and ended *ca.* 16,000 ^{14}C years BP and the Mount Aquila Stadial, corresponding with the Younger Dryas Chronozone between 11,000 and 10,000 ^{14}C years BP. During the Mount Aquila Stadial, glacier ELAs are reconstructed at *ca.* 2300 m a.s.l. This ELA altitude compares with that of 2450 m estimated for the Italian Alps in northern Italy (Porter and Orombelli 1982) and implies either greater accumulation or lower temperatures in the Gran Sasso massif. Rock glaciers in this massif, with fronts between 1850 and 1950 m a.s.l., have also been correlated with the glacier readvance of the Mount Aquila Stadial. Rock glaciers, ascribed to the Mount Aquila Stadial and the Younger Dryas Chronozone, have been described elsewhere in the Italian Appenines, such as on Mount Velino and Mount Maiella where they occur down to 1910 m a.s.l. (Dramis and Kotarba 1994). In the latter area, some high rock glaciers, with fronts above 2600 m a.s.l., contain ice and may be active today. This would imply that the modern limit of discontinuous permafrost occurs at around 2600 m a.s.l. in central Italy (Dramis and Kotarba 1994).

The occurrence of a climatic deterioration during the Younger Dryas has also been demonstrated in lacustrine sediments by Lowe (1992) in the Appennino Parmense (2165 m a.s.l.). Both the lithostratigraphy and pollen stratigraphy provide evidence for a climatic oscillation in lake sediments inside extensive valley glacier moraines but outside cirque

moraines. Inside the cirque moraines, no climatic oscillation comparable to the Younger Dryas is recorded in the pollen and lithostratigraphy. This led Lowe (1992) to suggest that the cirque moraines formed during the Younger Dryas and that the more extensive valley glacier moraines formed during the LGM of the Late Würmian. However, the snow line altitude of the supposed Younger Dryas glacier is estimated at *ca.* 1650 m a.s.l. This is far lower than in the Gran Sasso, further south, where snow lines were placed at *ca.* 2300 m a.s.l. and where rock glaciers occurred no lower than 1850 m a.s.l. It is also considerably lower than in the Italian Alps further north where the Younger Dryas snow line is estimated at *ca.* 2450 m a.s.l. (Porter and Orombelli 1982). This is acknowledged by Lowe (1992) who left open the possibility that these cirque moraines may in fact be older in age, which would seem highly probable given the snow line reconstructions elsewhere in Italy.

Glacial deposits also extend outside of the limits of glacial deposits dated to the Late Würmian Substage. For example, glacial deposits exist outside of the Campo Imperatore moraines dated by Giraudi and Frezzotti (1997), although they are less well preserved and are strongly eroded, smoothed and reduced in size (Kotarba *et al.* 2001). Calcite cements within these moraines have been dated, using Uranium-series, to at least $135,000 \pm 10,000$ years BP, and probably formed during the last interglacial. The moraines are therefore presumed to have formed during the preceding glacial, equivalent to the Rissian Stage in the Alps (Kotarba *et al.* 2001). It is therefore clear that two major glacial advances are recorded in the Gran Sasso area, with readvances also recorded during the Late-glacial. However, it is quite possible that the outermost glacial deposits dated by Kotarba *et al.* (2001) pre-date the Rissian Stage since the calcite date represents a minimum age. In addition, it would be useful to have Uranium-series dates from calcite cements in the higher Campo Imperatore moraines to verify the Late Würmian age suggested by the radiocarbon dates obtained by Giraudi and Frezzotti (1997).

Glacial deposits, which extend much lower than moraines assigned to the Late Würmian, have been noted in many other areas of the Italian Appennines. As in the Gran Sasso, they are often partially cemented and show a strong pink alteration colour. However, they are often fragmentary and incomplete and, unlike in the Gran Sasso, no radiometric dating has established their age. Glacial deposits of this type can be found in the northern Appennines on Mount Navert (Federici 1977) and in the central Appennines in several localities on Mount Velino (2487 m a.s.l.) (Cassoli *et al.* 1986, Giraudi 1998) and Mount Greco (2283 m a.s.l.) in Abruzzo (Cinque *et al.* 1990) (Fig. 2.5). In the southern Appennines erosional evidence suggests extensive glaciation before the most recent Würmian glaciers. For example, on Mount Matese (2050 m), some cirques are located at altitudes lower than

the snow line associated with the accepted Late Würmian glacial deposits (Palmentola and Acquafredda 1983).

In addition to the dated moraines in the Gran Sasso, a key area for determining the age of these older deposits is the Campo Velice in the Velino massif (Giraudi 1998) (Fig 2.5). Here, moraines are overlain by aeolian deposits containing a Mousterian culture chert artefact. In central Italy, humans of the Mousterian culture were present from at least the last interglacial (*ca.* 130-115,000 years BP) until *ca.* 58,000 years BP (equivalent to MIS 5e to the end of MIS 4), implying that the underlying till must have formed before this time. Giraudi (1998, 2003, 2004) suggests that the till was deposited during one of the cold stages preceding the last interglacial of MIS 5e. Due to the fairly good preservation of these moraines, Giraudi (1998, 2003, 2004) suggests that they may have formed during an interval probably equivalent to the Rissian glaciation of the Alps. This is corroborated by the dated Uranium-series dates obtained in the Gran Sasso massif (Kotarba *et al.* 2001). However, whether they relate to the glaciation immediately preceding the last interglacial or earlier is unknown since these are minimum ages. Jaurand (1994, 1998) has suggested that a moraine on Mount Navert in the northern Apennines could be of even greater antiquity and may have formed before the late Middle Pleistocene, although no dating is presented. This is important since it would imply that three glacial stages are recorded in the Italian Apennines.

2.4.3 Corsica

The mountains of the island of Corsica rise to 2710 m a.s.l. at Monte Cinto (Fig 2.5). Glacial deposits were first documented by Pumpelly (1859) and the most recent studies are those of Heybrock (1954), Letsch (1956), Conchon (1986) and Hewitt (2001). Conchon recognised four sets of glacial deposits. The youngest deposits are characterised by cirque moraines. On the basis of a lake sequence inside of moraine limits, Reille (1975) showed that one moraine of this phase is older than the Late Würmian Allerød Interstadial. Two sets of valley moraines exist in lower areas, both of which have been attributed to valley glaciation during the Würmian with fronts at altitudes of 1700-1800 m a.s.l. and 700-1100 m a.s.l. Also, Conchon (1986) suggests that weathered glaciofluvial deposits beyond the lowest valley moraines may be of pre-Würmian age.

Conchon (1986) concluded that glaciers had existed at least four times during the Quaternary. The oldest deposits were presumed to be pre-Würmian, two valley glacier phases were presumed to belong to the Würmian and small cirque glaciers to the Late-glacial. However, other chronologies have equal validity based on the data presented by

Conchon (1986). For example, why should the cirque moraines not belong to the glacial maximum of the Würmian Stage? In this scenario it is possible that the valley glacier deposits are of Rissian age and the outermost weathered glaciofluvial deposits of a Middle Pleistocene age. A number of alternative chronologies can be envisaged fitting the data presented by Conchon (1986). As with elsewhere in the Mediterranean, it would appear that many workers feel drawn to a classic Würmian glacial sequence, with little conclusive evidence to support such deductions.

2.4.4 The Alpes Maritimes

The Alpes Maritimes are important in studies of Mediterranean glaciation since the most extensive modern glaciers of the Mediterranean are found here. The highest peak, Argentera (3297 m a.s.l.), is situated less than 50 km from the Mediterranean coast at Monte Carlo (Fig. 2.9) and supports six glaciers with a present day ELA of *ca.* 2800 m a.s.l. (Finsinger and Ribolini 2001). The lower discontinuous permafrost boundary is estimated at *ca.* 2600 m a.s.l. (Ribolini 2001) and represents the threshold for permafrost creep – important in rock glacier formation.

During the Würmian Stage, the Alpes Maritimes were covered by ice contiguous with the Alpine ice sheet which covered an area of *ca.* 126,000 km² (Ehlers 1996). The classic Alpine Quaternary stratigraphy is based largely on the morphostratigraphy of glacial gravel spreads, terraces and moraines (Ehlers 1996) and was first established by Penck and Brückner (1909) in the northern Alpine foreland. Their model of four glaciations, Günz-Mindel-Riss-Würm, was widely applied through the 20th Century and is still used today in reference to the Middle to Late Pleistocene glaciations (Table 1.1). However, the classic sequence of Günz-Mindel-Riss-Würm glaciations is seriously in doubt, and revision of the Alpine glacial stratigraphy was far from complete during the 1990s (Ehlers 1996) and remains so today.

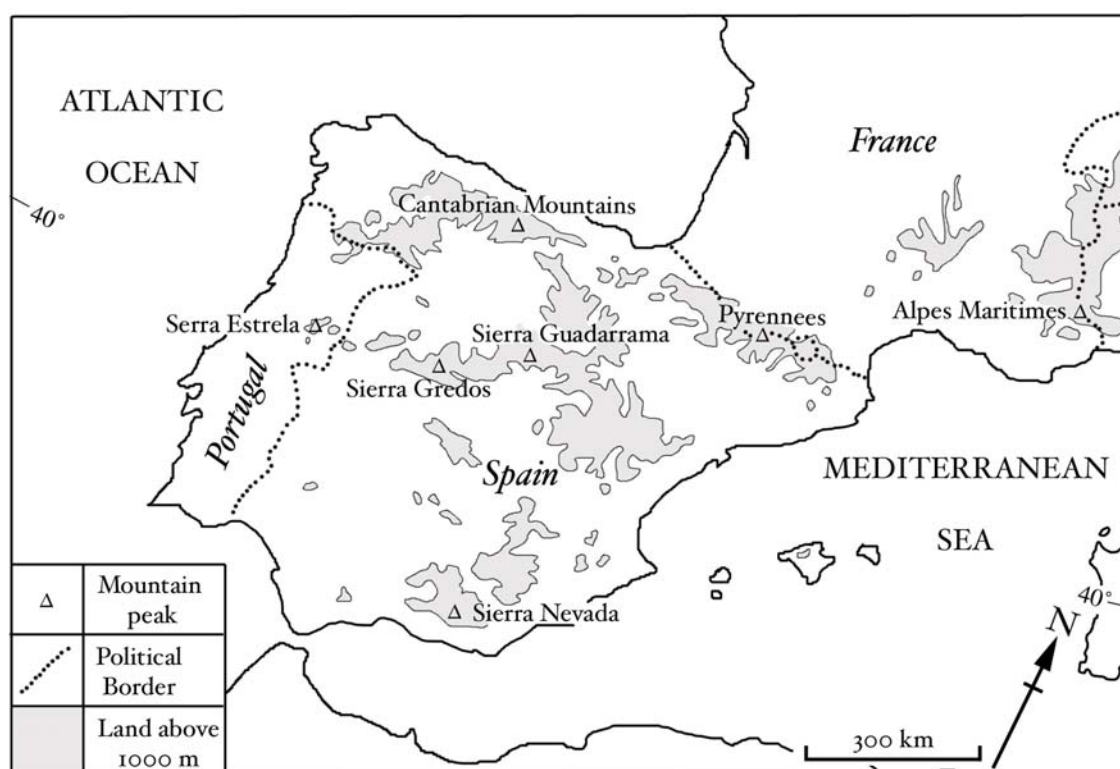


Figure 2.9 Location map showing some of the glaciated mountains of the Alpes Maritimes, the Pyrenees and the Iberian peninsula..

In the Alpes Maritimes, the glacial geomorphology has been described by Ribolini (1996). The valleys of the area are deeply scoured, and large moraines were deposited in the lower parts of the valleys. Little attention has been given to recognising different glacial phases, and most of the moraines are assumed to be of Würmian age. The Würmian glacial maximum in the Alps occurred between 28,000 and 20,000 ± 1,800 ¹⁴C years BP in the northern Alpine foreland (Ivy-Ochs 1996, Florineth and Schlüchter 2000) and between 24,000 and 17,700 ± 360 ¹⁴C years BP in the southern Alpine forelands (Orombelli 1974, Fliri 1989). It is therefore reasonable to assume that the glacial maximum in the Alpes Maritimes occurred during the Late Würmian, and lacustrine sediments at Lac Long Inférieur in a glaciated cirque (2090 m a.s.l.) have been dated to 14,190 ± 130 ¹⁴C years BP, indicating that ice had retreated by this time. However, during the Late-glacial Substage there is evidence for glacial advance during the Older and Younger Dryas Chronozones according to Fisinger and Ribolini (2001).

During the Younger Dryas, glaciers are thought to have had a mean ELA of 2500 m a.s.l. and the lower discontinuous permafrost boundary, corresponding with the occurrence of rock glacier fronts, occurred between 2300 and 2400 m a.s.l. (Fisinger and Ribolini

2001). Based on this evidence, Fisinger and Ribolini (2001) calculate that mean annual temperatures were *ca.* 4°C lower than present-day values and that precipitation was 50% lower. The reconstructed glacier ELAs and altitude of the lower discontinuous boundary for the Younger Dryas compare with altitudes of *ca.* 2300 m and 1850 m a.s.l. for glacier ELAs and lowest rock glaciers fronts during the same period further south in the Italian Apennines (Dramis and Kotarba 1994, Giraudi and Frezzotti 1997). Whilst the glacier ELAs are relatively close, the positions of the discontinuous permafrost boundary differ by over 450 m a.s.l. Given that the lower discontinuous boundary generally corresponds to the -2°C mean annual isotherm (Belloni *et al.* 1988, Carton *et al.* 1988, Brazier *et al.* 1998) and assuming a standard lapse rate of 0.6°C per 100 m, this implies that mean annual temperatures during the Younger Dryas were at least 2.5°C higher in the Alpes Maritimes compared with the Gran Sasso. This is perhaps contrary to what one would expect given that the Alpes Maritimes are nearly 2° further north, and, therefore, caution must be given to such correlations until conclusive dating is available.

2.4.5 The Pyrenees and the Iberian peninsula

The Pyrenees were extensively glaciated during the Quaternary, a fact recognised in the early 19th Century by Penck (1885), and today small glaciers still exist on the highest peaks such as Pico de Aneto (3404 m a.s.l.) and Monte Perdido (3352 m a.s.l.). Evidence of former Quaternary glaciation is also present in many other major mountain regions of Spain and Portugal, including the Sierra Nevada, the Sierra Gredos, the Sierra Guaderrama (Messerli 1967) and the Cantabrian Mountains (Smart 1986, Gale and Hoare 1997, Jiménez-Sánchez and Farias 2002) in Spain, and the Serra Estrela (Daveau 1971) in Portugal (Fig. 2.9).

In the Spanish Pyrenees, most glacial deposits are thought to have formed during the last glaciation, although some isolated glacial deposits have been attributed to previous glaciations. However, the chronology of glaciation in the Spanish Pyrenees is based on very little dating. Correlations have often been made on the basis of morphostratigraphical comparison, and even the maximum extent of the last glaciation remains one of the most significant problems of Pyrenean Quaternary geology (García-Ruiz *et al.* 2003). Nevertheless, there is evidence that the maximum extent of ice during the last glacial stage occurred earlier than for the major ice sheets of Britain and Scandinavia, which reached their maximum between 21 and 18,000 ¹⁴C years BP (Sibrava *et al.* 1986). Sedimentological and palynological analyses and an accelerator mass spectrometry ¹⁴C chronology based on minimum ages from glacial lake sediments suggest that the maximum

extent of glaciation during the last glacial phase occurred before 30,000 ^{14}C years BP (García-Ruiz *et al.* 2003). This is corroborated using a similar technique at Tramacastilla, where the onset of deglaciation is dated at older than 29,400 ^{14}C years BP.

In the Spanish Pyrenees, the snow line during the ice maximum of the Würmian Stage was *ca.* 1900 m a.s.l. (García-Ruiz *et al.* 2000). Subsequent retreat was characterised by a phase of upper valley glaciers between 16,000 and 15,000 years BP and then by a phase of cirque glaciation between 14,000 and 13,000 years BP (Bordonau 1992). The last stage of Pleistocene glaciation is represented by large moraines and rock glaciers close to the cirque backwalls and may date from the Younger Dryas between 11,000 and 10,000 ^{14}C years BP (Serrat 1979).

In the French Pyrenees, small glaciers exist today on peaks such as Vignemale (3296 m a.s.l.) near Caunterets. Glacial deposits as low as 950 m a.s.l. indicate much greater ice extent during former Pleistocene glacial phases (Calvet 2004). Quaternary glacial events have also been recognised from U-series dating of speleothems in the Niaux-Lombart-Sabart Caves of Ariège. Here, Bakalowicz *et al.* (1984) recognised the existence of two major glacial phases, one between 20,000 and 90,000 years BP and another between 200,000 and 250,000 years BP, corresponding to part of the Würmian (MIS 2-4) and the early Rissian or Saalian Complex (MIS 8). Two, more subdued, glacial phases are recorded between 130,000 and 175,000 years BP and between 290,000 and 350,000 years BP, both corresponding with the earliest and late Rissian or Saalian Stages respectively (MIS 6 and 10). It is thought that during the last glaciation, the glacial maximum occurred before 38,000 ^{14}C years BP in the French Pyrenees (Hérail *et al.* 1986, Jalut *et al.* 1992), similar to findings in the Spanish Pyrenees. The chronology of the last glaciation in the French Pyrenees is based on sedimentological and palynological studies and radiocarbon dating of lacustrine sediments near to former glacier margins. Radiocarbon dates from basal lake sediments inside of moraine limits indicate that deglaciation began before 38,400 ^{14}C years BP at Biscaye, and before 34,000 ^{14}C years BP at Lourdes and Monges. However, relatively little dating exists across both the French and Spanish Pyrenees, and inter-site correlation is largely based on morphostratigraphical position. The Würmian glaciation appears to have removed much of the older deposits but in parts traces of older, more extensive, glacial deposits do exist and probably relate to the Rissian or earlier glaciations (Calvet 2003).

In the Picos de Europa of the Cantabrian Mountains, the glacio-karst system is particularly well-developed and the development of glaciers would have been aided by snow accumulation in doline hollows (Smart 1986). More recent work by Gale and Hoare

(1997) demonstrates that five glacial phases can be distinguished. Speleothem dates have been employed to determine long-term rates of fluvial incision in parts of the Picos de Europa, yielding consistent rates of 0.3 metres per 1,000 years (Smart 1986). Gale and Hoare (1997) used this rate to estimate the time elapsed since the most extensive phase of glaciation where fluvial action has incised into a glaciated U-shaped valley. They derived a minimum age of 850,000 years for the glacial valley and argued that this provides evidence of Early Pleistocene glaciation in the Picos de Europa. However, this is not a firm basis for reconstructing a glacial chronology since it is likely that rates of incision have varied tremendously over climatic cycles due to variations in water discharge, sediment supply, changes in sea-level and tectonic uplift. Whilst no certain age can be given to this glacial phase, it is suggested that the long-term preservation of landforms in the Picos de Europa may be because of the karstic nature of the bedrock. Surface runoff is negligible and thus surface processes are relatively unimportant (Gale and Hoare 1997). This is an important factor and is applicable to Mount Tymphi in Greece and other Mediterranean mountain areas, where the limestone bedrock is highly karstic and surface runoff particularly low.

In the Sierra Nevada of Andalucia, the southernmost modern glacier in Europe existed until recently. Ice was observed in the Corral Veleta up until the beginning of the 20th century and, according to Messerli (1967), this glacier was "the sensation of Sierra Nevada". Messerli (1967) recognised three distinct phases of glaciation in this area. He was of the opinion that the uppermost moraines, formed by glaciers with a snow line of between 2700 and 3000 m a.s.l., existed during the Würmian Late-glacial Substage. Valley glaciers up to 9.5 km long with snow lines between 2300 and 2400 m a.s.l. are thought to have formed during the Late Würmian glacial maximum. However, the oldest, most extensive glacial deposits extend up to 4 km from the end moraines of the Würmian glaciers with a snow line around 200 m lower. Messerli (1967) considered these deposits to belong to the Rissian Stage, although, as with elsewhere in Spain, neither relative nor radiometric dating is available to confirm this hypothesis.

In the Serra da Estrela, Portugal, glacial features were described by Daveau (1971). A plateau ice-cap fed diffluent glaciers, the longest of which was 13 km long. Daveau (1971) distinguishes a series of stages: a) a short-lived advance; b) a long period of stabilisation and the development of well-developed lateral moraines and; c) kame terraces and a series of stages of recession, marked by successive loops of frontal moraines. The maximum extent of glaciation is attributed to the Würmian Stage by Daveau (1971), although it is possible that the multiple sets of moraines correspond to different glaciations rather than representing glacier recession during the same glacial stage.

2.4.6 The Atlas Mountains

Quaternary glacial and periglacial features are in evidence on the High and Middle Atlas of Morocco and the available literature has recently been reviewed by Hughes *et al.* (2004). The highest mountains exist in the High Atlas, including Jbel Toubkal (4165 m a.s.l.), Irhil M'Goun (4071 m a.s.l.) and Jbel Ayachi (3751 m a.s.l.) (Fig. 2.10). Glacial features such as cirques, troughs, *roche moutonnée*, *riegels* and moraines have been noted in all of these massifs (Dresch 1941, 1949, Heybrock 1953, Mensching 1953, Wiche 1953, Awad 1963, Beaudet 1971). In the Toubkal area, glacial incision has resulted in a web of arêtes around the highest peaks, as well as deep troughs. The glacial features of the Irhil M'Goun area were mapped by Wiche (1953). Here, cirques and associated moraines are in evidence on the northern slopes of both the highest peak of Irhil M'Goun (4071 m a.s.l.) and on nearby Jbel Ouaougoulzat (3770 m a.s.l.).

Periglacial features are widespread in the High Atlas, and solifluction lobes, *rasentrappen*, *thufurs*, polygons, stone stripes and *felsenmeer* are active today above *ca.* 2000 m a.s.l. (Couvreur 1966). Rock glaciers, almost certainly relict since they form in areas of discontinuous permafrost, are observed on Irhil M'Goun and on nearby Jbel Ouaougoulzat (Wiche 1953). On the latter mountain, these features form below cirque

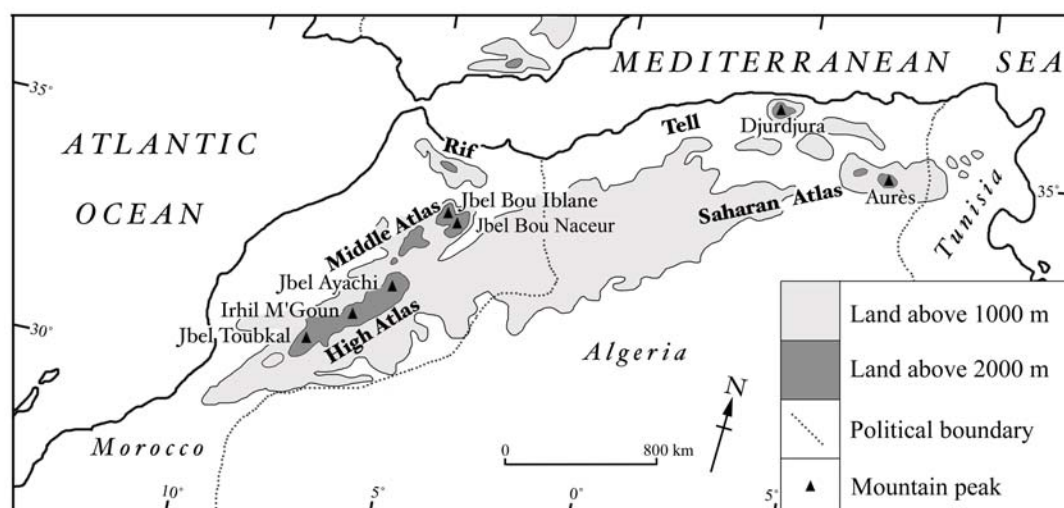


Figure 2.10 Location map of the North African Atlas.

moraines and it is likely that they represent debris rock glaciers, as defined by Barsch (1996), whereby they are supplied debris from the cirque glacier moraines above. Frosts are frequent, even in modern times, where in winter minimum temperatures at 2000 m a.s.l. are often in the range 0 to -10°C and can fall to as low as -20°C (Robinson and Williams 1992). Blockfields are widespread on Jbel Toubkal and extensive talus slopes supply the lower valleys with huge amounts of debris as a result of frost-shattering. For example, the valley containing Lac D'Infi (2312 m a.s.l.), to the east of Toubkal, is choked with debris derived from periglacial weathering in the surrounding catchment.

Even today, in some sheltered cirques on Toubkal, snow fields are perennial, although the true snow line lies slightly above the highest peaks, probably at *ca.* 4200 m a.s.l. (Messerli 1967). However, during the Pleistocene cold stages, snow lines must have descended to lower altitudes. Dresch (1941) reconstructed former Pleistocene cold stage snow lines for the High Atlas at 3600-3700 m a.s.l. Later literature places the lowest Pleistocene snow line slightly lower. For example, Mensching (1953) places the snow line at 3400-3500m a.s.l. and Awad (1963) at 3300-3400 m a.s.l.

The Middle Atlas lie to the north-east of the High Atlas in central Morocco. Here, the highest peaks include Jbel Bou Iblane (3340 m a.s.l.) and Jbel Naceur (3310 m a.s.l.), both of which show evidence of former glaciation (Dresch and Raynal 1953, Raynal *et al.* 1953, Awad 1963, Beudet 1971). According to Awad (1963), the most remarkable collection of glacial troughs in the Atlas Mountains are to be found on the southern and eastern slopes of Jbel Bou Iblane. Terminal and lateral moraines are widely preserved and extend down to *ca.* 2400-2500 m a.s.l. (Raynal *et al.* 1953). Here in the Middle Atlas, the former regional snow line is estimated at *ca.* 2800 m a.s.l. during the most extensive glacial phase (Awad 1963). Further north, the Rif mountains are thought to have lain beneath the regional snow line although, according to Mensching (1960), there is evidence for former perennial snow patches and rock glaciers on the highest mountain Tidirhin-Kette (2456 m a.s.l.).

Periglacial features are widely observed in the Middle Atlas. Stone polygons, solifluction features and rock glaciers are described on Bou Iblane and Jbel Bou-Naceur by numerous workers (Raynal 1952, Dresch and Raynal 1953, Awad 1963). According to Awad (1963), rock glaciers are especially abundant between 2100 and 2500 m a.s.l. in the eastern valleys of the Bou-Naceur massif. He is of the opinion that these features formed during the penultimate phase of glaciation since they form directly below cirque moraines. However, given the more recent ideas of Barsch (1996) whereby debris rock glaciers exist contemporaneously with cirque glaciers which supply debris from above it is perhaps more

probable that these rock glaciers belong to the last glacial phase. It is also unlikely that such features would have been preserved directly below glaciers during a subsequent glacial phase in the path of meltwater outflow.

Glacial and periglacial features have also been noted in the Djurdjura massif of the Algerian Tell (Barbier and Cailleux 1950, Büdel 1952, Tihay 1972, 1973) and in the Aurès massif of the Saharan Atlas (Ballais 1983). In the Djurdjura massif (2308 m a.s.l.), cirques, U-shaped valleys and terminal moraines are all in evidence according to Barbier and Cailleux (1950). They note the transition between glacially-smoothed limestone pavements on the upper slopes and sub-aerially eroded karstic forms on the lower slopes. Glacial deposits extend to exceptionally low altitudes for this latitude, reaching as low as 750 m a.s.l. on the northern slopes, and 1270 m a.s.l. on the west. The formation of glaciers was probably aided by snow accumulation in dolines and even today snow lies in dolines throughout the summer above 2000 m a.s.l. This probably arises from high precipitation of this area, which exceeds 1500 mm, and largely falls during the winter months. The snow line here, during the most extensive glacial phase, was as low as 1900 m a.s.l., although Büdel (cited in Messerli 1967) puts the snow line slightly higher at 2100 m a.s.l. As is the case today, this probably results from the influence of maritime air masses from the nearby western Mediterranean.

South-east of the Djurdjura massif, in the Aurès massif of the Saharan Atlas, Ballais (1983) noted the presence of glacial moraines on Jbel Ahmar Khaddou (2017 m a.s.l.) and Jbel Mahmel (2321 m a.s.l.) above 1600 m a.s.l. and in the latter area, two phases of glaciation are evident. However, no glacial deposits were noted on the highest peak, Jbel Chélia (2326 m a.s.l.). It would appear that conditions in this region were marginal to glaciation, and glaciers only formed in exceptional topographical localities. This is no doubt due to the proximity of the arid Sahara region and low precipitation levels compared with the Djurdjura massif.

2.4.7 The eastern Mediterranean (Turkey and Lebanon)

Evidence of former glaciation in the mountains of Lebanon was first noted by Diener (1886) on the mountains of the Jbel Liban, particularly on the highest peak Qornetes Saouda (3088 m a.s.l.) and on Mount Hermon (2814 m a.s.l.) in the southern Anti-Lebanon (Fig 2.11). On Qornetes Saouda, moraines occur down to 2500 m a.s.l. and there is possible evidence of a lower, more extensive glaciation. In all areas, the snow line altitude at the time when the major moraines were formed was *ca.* 2500 m a.s.l. (Messerli 1967).

Evidence of Quaternary glaciation can be found in high mountains of the Taurus and Pontic Mountains of Turkey. The Taurus Mountains are in southern Turkey and extend from Bey Daglari (3086 m a.s.l.) in the southwest Turkey to Cilo Dagi (4168 m a.s.l.) in Kurdistan (Fig 2.11). The Taurus Mountains include some of the highest peaks in Turkey and two thirds of the modern glaciers are found here (Ciner 2004). The presence of glaciers in the Taurus Mountains was noted in the 19th century by Ainsworth (1842) and Palgrave (1872). More recently, the extent of modern glaciation in Turkey was reviewed by Kurter and Sungur (1980). Most modern glaciers occur in the eastern part of the Taurus, in Kurdistan. Here, at least 20 modern glaciers exist, and the Resko valley glacier on Mount Cilo covers an area of 8 km² (Ciner 2004). On Mount Ararat (5165 m a.s.l.), near the border with Armenia, a modern ice cap exists. Here, the modern snow line is *ca.* 4300 m a.s.l., whilst in the main range of the eastern Taurus, in Kurdistan to the south, the modern snow line is between 3400 and 3600 m a.s.l. During the Pleistocene, snow lines are estimated to have been as low as 2800 m a.s.l. (Messerli 1967), well below the altitude of the highest mountains.

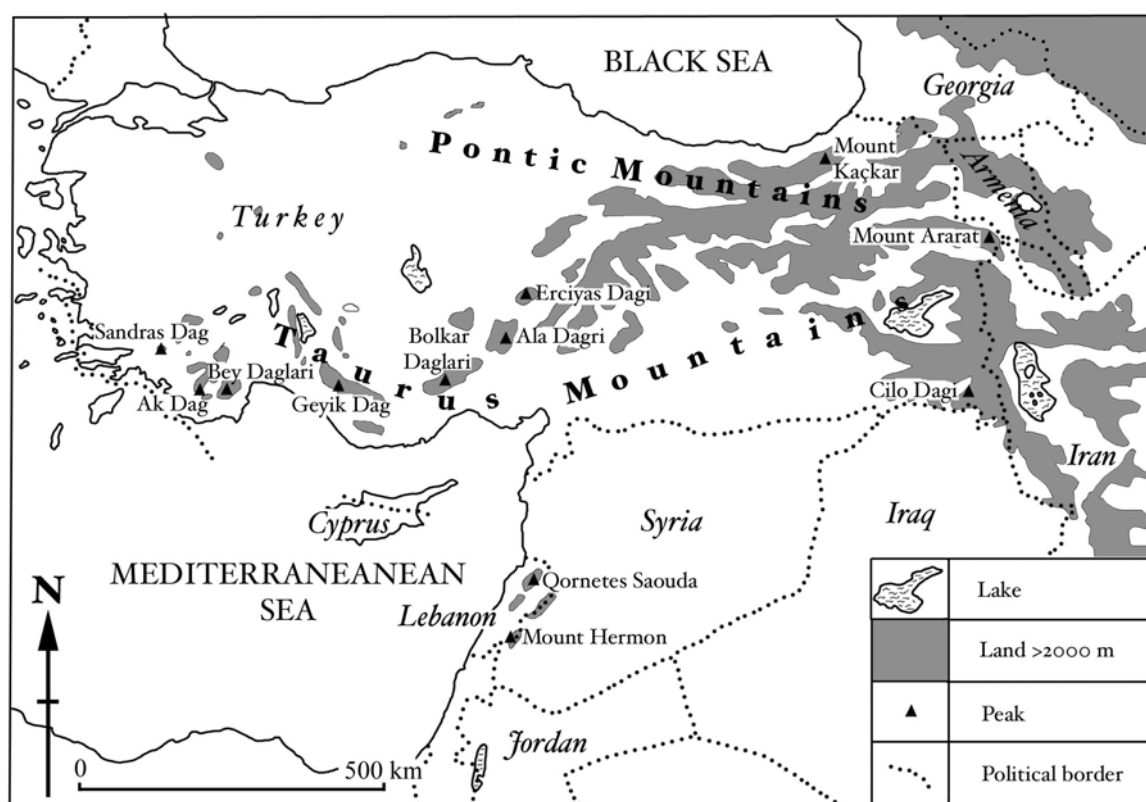


Figure 2.11 The Eastern Mediterranean mountains including glaciated areas of Turkey and the Lebanon.

Evidence of extensive Pleistocene glaciation in the Kurdistan region is described by Wright (1962) and on Ararat by Blumenthal (1958). On Mount Ararat, Blumenthal (1958) calculated a snow line altitude of 3000 m a.s.l. for the most extensive glaciation of the Pleistocene. However, moraines are not well-preserved on Mount Ararat. Blumenthal (1958) suggests that this is due to the lack of confining ridges to control valley glaciers, insufficient debris load to form moraines and volcanic eruptions that later covered the pre-existing moraines.

In the central Taurus, modern glaciers are smaller and less extensive than in the east, although a 1 km long glacier, the Lolut glacier, exists on Ala Daglari (3910 m a.s.l.) as well as smaller cirque glaciers on Bolkar Daglari (3585 m a.s.l.). Pleistocene glaciers appear to have extended down to 2100 m a.s.l. in this area, and terminal and lateral moraines clearly delimit the extent of these former glaciers (Ciner 2004). In the Namars and Susam valleys, on Geyik Dag (2890 m a.s.l.), chaotic knob-and-kettle topography is interpreted as glacially-deposited hummocky moraines by Ciner (1999). U-shaped valleys and cirques, as well as the widespread distribution of diamicton containing striated and bullet-shaped clasts, support the interpretation that this area was glaciated during the Pleistocene. Glacial deposits are also preserved on the volcano Erciyas Dagi (3916 m a.s.l.) and glaciers existed here as recently as 1902 with rock glaciers forming below, although by 1962 the glaciers had melted. Moraines in the lower parts of the mountain indicate that glaciers once reached lengths of 5 km and are assumed to have formed during the Würmian Stage. In addition, erratics have been found 2 km beyond these glacial limits suggesting a snow line of *ca.* 2200 m a.s.l. during the most extensive glacial phases (Messerli 1967).

The western Taurus do not support any modern glaciers, although glacial landforms are well preserved. Cirque moraines are evident on Bey Daglari (3086 m a.s.l.) and Ak Dag (3073 m a.s.l.) and may represent former Holocene glaciers since in many areas glaciers have been retreating in recent times (Ciner 2004). Moraines are also evident in the lower valleys down to 2000 m a.s.l., indicating the presence of valley glaciers at one time in this area. Messerli (1967) estimates former Pleistocene snow lines at around 2500 m a.s.l. on Ak Dag. In the Sandras Dag (2294 m a.s.l.), near Denizli, however, snow lines appear to have been 200-300 m lower (Messerli 1967). This is perhaps due to the western position of this mountain and higher precipitation from air masses coming off the Aegean Sea.

The Pontic Mountains border the Black Sea in Northern Turkey. On the highest peak, Mount Kaçkar (3932 m a.s.l.) five glaciers exist on its northern flank (Ciner 2004). The modern snow line in these mountains is above 3000 m a.s.l., whilst during the last

glaciation it is thought to have been at *ca.* 2600 m a.s.l. U-shaped valleys, moraines, *roches moutonnées* and glacial lakes are preserved in many areas of the Pontic Mountains. However, most of the landforms, as with elsewhere in Turkey, have not been studied in detail and their exact age has not been established (Ciner 2004).

2.4.8 Greece

Evidence of glaciation in the mountains of Greece was reported by Niculescu (1915) who noted the moraines on Mount Smolikas. Other early research included glacial studies on Mounts Oeta and Oxya (Mistardis 1952) and Mount Parnassus (Pechoux 1970) in the Sterea Ellas, as well as in the mountains of Epirus (Sestini 1933, Mercer 1963). An early review of glaciation in the Pindus Mountains, as well on Mount Olympus to the east, was provided by Messerli (1967). He noted the extensive glacial moraines on Mount Tymphi and Smolikas, as well as throughout the Pindus chain. More recently, glacial investigations have been published on the hills of the Peloponnese (Mastronuzzi *et al.* 1994), Mount Olympus (Smith *et al.* 1997), Mount Smolikas (Boenzi *et al.* 1992) and Mount Tymphi (Palmentola *et al.* 1990a, Smith *et al.* 2000, Woodward *et al.* 2004) (Fig. 2.5).

In the 1962 Cambridge caving expedition to the Pindus Mountains, Mercer (1963) noted that moraines and the "work of frost action in periglacial times, on the edge of small local ice caps" was in evidence all over the Pindus Mountains, northeast of Ioannina. More recently, on Mount Tymphi, Palmentola *et al.* (1990a) mapped the position of major moraine systems. However, the work was essentially morphological and no details regarding the glacial sedimentology are presented (Fig. 2.12). Therefore, whilst useful, the work of Palmentola *et al.* (1990a) can only be regarded as reconnaissance. Palmentola *et al.* (1990a) identified five sets of moraines at different altitudes and assumed that all of the moraines were formed during the Late Würmian. However, Woodward *et al.* (2004) have provided U-series dates from cemented tills in the Tsepelovo and Skamnelli areas and derive very a different chronology. Woodward *et al.* (2004) showed that the major moraine systems near Tsepelovo and Skamnelli formed at least 60,000 years prior to the global last glacial maximum, and one till unit exceeded 350,000 years in age. The use of U-series dating as a tool in dating the cemented tills of Tymphi represented a breakthrough in

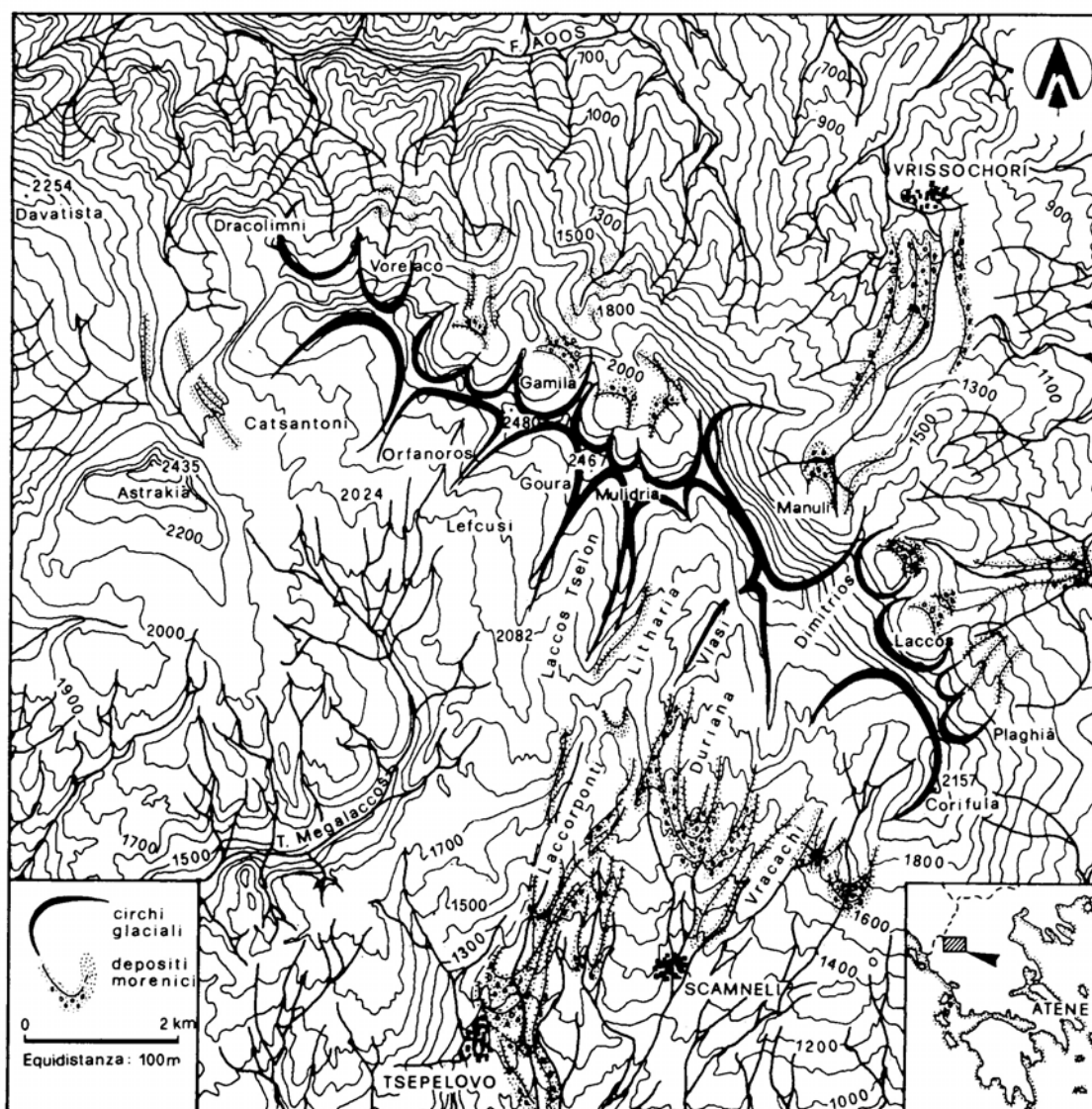


Figure 2.12 Glacial geomorphological map of Mount Tymphi produced by Palmentola *et al.* (1990a).

establishing the geochronology of glacial deposits in Greece and provided the platform on which this thesis is based.

On Mount Smolikas, the initial work of Niculescu (1915) recognised at least two phases of glaciation. The highest glaciation was restricted to the highest cirques on the northern and north eastern slopes of the mountain. A more extensive phase of glaciation was also noted in the Vadulakkos valley. The distribution of glacial features on Mount Smolikas was reiterated in the work of Boenzi *et al.* (1992). However, they identified six sets of glacial moraines and assumed, in the absence of direct dating, that all of these formed during the Late Würmian (Fig. 2.13).

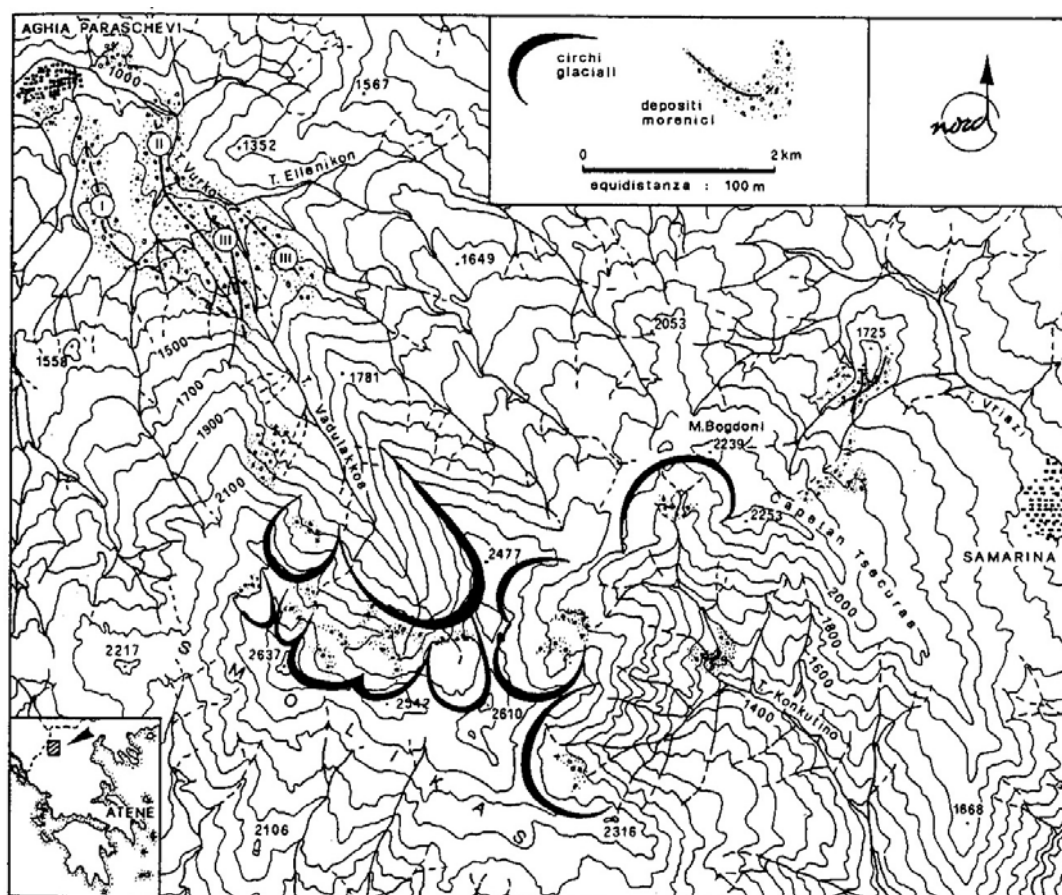


Figure 2.13 Glacial geomorphological map of Mount Smolikas produced by Boenzi *et al.* (1992).

The glacial history of Mount Olympus (2917 m a.s.l.), the highest mountain in Greece, has most recently been investigated by Smith *et al.* (1997). Olympus is usually regarded as separate from the Pindus chain and lies to the east, on the coast of the Aegean Sea (Fig. 2.7). Smith *et al.* (1997) argued that earlier research (*e.g.* Messerli 1967, Faugères 1969) had underestimated the extent of glaciation on Olympus and they recognised at least three phases of glaciation. The maximum glaciation was characterised by an upland ice cap, extensive valley glaciation and piedmont lobes in the surrounding lowlands. A second glaciation involved the development of upland ice and valley glaciers that did not reach the piedmont. A third, and most recent, glaciation was restricted to valley heads (no upland ice) and glaciers that extended to mid-valley positions (Fig 2.14).

The chronology of glaciations on Mount Olympus has been deduced by correlating soils on glacial deposits with dated soils in the Larissa basin (Demitrack 1986, van Andel *et al.* 1990). The basis for correlation was the pedogenic maturity of the soils quantified using profile development indices. Smith *et al.* (1997) tentatively placed the oldest most extensive glaciation, where glaciers extended as low as 100 m over the eastern

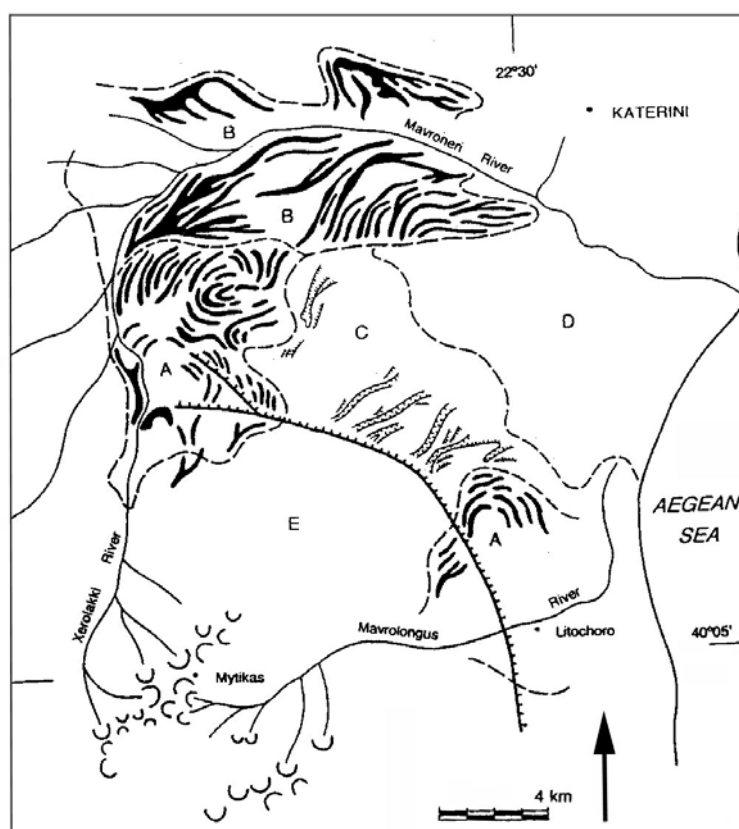


Figure 2.14 Geomorphological map of the Mount Olympus area. Dashed lines - geomorphological boundaries; heavy barbed line – Mount Olympus boundary fault; semi-circles – cirques; irregular heavy dark lines – end moraines; A – piedmont glacial deposits of Mount Olympus provenance; B – piedmont glacial deposits of Mount Piera provenance; C – modern alluvial deposits; D – dissected (terraced) alluvial fan deposits; E – valley and upland glacial deposits (from Smith *et al.* 1997).

piedmont, before 200,000 years BP, and suggest that this glaciation may have occurred during the early Rissian Stage and MIS 8. A second glaciation involved production of upland ice and valley glaciers which did not reach the piedmont, and Smith *et al.* (1997) correlate this phase with the late Rissian Stage and MIS 6. The ELA of glaciers during this phase is estimated at 1000-1030 m a.s.l. A third phase of glaciation was restricted to valley heads, and glaciers extended to only mid-valley positions where ELAs were *ca.* 2200 m a.s.l. This phase is correlated with part of the Würmian Stage (MIS 4 to 2). A further set of moraines are found in the highest cirques (above 2200 m a.s.l.) and Smith *et al.* (1997) suggested that these may be Neoglacial, although it is possible that these deposits represent Late-glacial moraines.

Additional data has been provided by cosmogenic dating of boulders on the most extensive glacial deposits by Manz (1988 as cited in Woodward *et al.* 2004). However, the dates obtained, 43-56,000 years BP, are at odds with the chronological model of Smith *et al.* (1997) who place these glacial deposits in the early Rissian Stage (MIS 8) before 200,000 years BP. It is evident, therefore, that the glacial chronology of Mount Olympus

lacks a firm consistent basis. Even if Manz's work is disregarded, the chronological model of Smith *et al.* (1997) can only be regarded as tentative, as indeed the authors themselves acknowledge. Nevertheless, the proposed chronology is consistent with the U-series dates of Woodward *et al.* (2003), from Mount Tymphi, in that the most extensive glacial phases pre-date the Würmian Stage.

The work of Smith *et al.* (1997) on Mount Olympus, suggesting that glaciers came as low as 100 m a.s.l. in the form of piedmont lobes, is a radical revision of the early work of Faugères (1969) and Messerli (1967). These workers concluded that glaciers on Mount Olympus did not descend to altitudes lower than 1600 m a.s.l., and Faugères (1969) interpreted many of the lowest piedmont deposits as fluvial deposits and alluvial fans. If the interpretations of Smith *et al.* (1997) are correct, this has important implications regarding the extent of glaciation in the Pindus Mountains to the west. Whilst there is evidence of glaciation as low as 850 m a.s.l. on Mount Tymphi (Woodward *et al.* 2004), nowhere in Greece are glacial deposits recorded as low as on Mount Olympus. Comparison of snow lines elsewhere in Greece with those reconstructed for Mount Olympus is difficult since ELA reconstructions presented in Smith *et al.* (1997) are very unclear and contradictory. For example, they state in their introduction that former snow lines during the most extensive glacial phase were *ca.* 1900 m a.s.l. In their conclusions, however, they state that snow lines during the maximum glacial phase were depressed by 3000 m compared with the modern estimate. Given that they accept that the present snow line is at *ca.* 3500 m a.s.l., this implies that the former snow line was at 500 m a.s.l. Similarly, they conclude that during another glacial phase attributed to the Rissian Stage and MIS 6, snow lines were depressed by *ca.* 2500 m at 1000-1030 m a.s.l. These issues and the fact that the chronology of glacial sequence of Olympus is very poorly constrained limits the value of the data presented by Smith *et al.* (1997). Nevertheless, the Olympus sequence represents one of the most important comparative sequences available and is a key area in understanding the glacial history of Greece.

2.4.9 Towards an understanding of Mediterranean glacial history

It is clear that during Pleistocene cold stages glaciers developed throughout the high mountains of the Mediterranean. However, many of the glaciers and their snow line altitudes cannot be easily compared because of a problem of chronology. Also, variation in the method of snow line reconstruction between studies poses problems of comparison. Many workers have correlated glacial deposits over large areas to the last glacial phase, *i.e.* during the Würmian Stage, without any means of dating. For example, Boenzi and

Palmentola (1997) correlated glacial deposits in Italy, Albania and Greece assuming that the outer limits of well-preserved moraines were all formed during the Würmian Stage and inner moraines were formed during overall retreat during the Late-glacial period. Messerli (1967) did the same for well-preserved moraines throughout the Mediterranean and such work, whilst having unquestioned merit as reconnaissance geomorphological investigations, cannot be accepted as chronological bases for glacial stratigraphy in the Mediterranean region. Nevertheless, all of the data described in the previous section, whilst often not having a firm chronology, is both useful and very relevant when comparing former glaciers of Mounts Tymphi, Smolikas and Vasilitsa with other glaciated areas of the Mediterranean. Eventually, once a firm glacial chronology is established for numerous key areas, a pan-Mediterranean glacial chronology can be established bringing with it important data regarding spatial and temporal variations in glacial Mediterranean climates. This study aims to contribute to that goal.

2.5 Quaternary palaeoenvironments in Greece

The glacial and periglacial record represents only one aspect of Pleistocene cold-stage environments in Greece. The glacial and periglacial sequence in the mountains of Greece can be correlated and compared with other proxy data, such as that derived from lacustrine and fluvial sediments.

Continuous long lacustrine sequences at Ioannina (Tzedakis 1993, 1994, Tzedakis *et al.* 2002), Tenaghi Philippon (Wijmstra 1969, Wijmstra and Smit 1976, Wijmstra and Groenhart 1983, van der Wiel and Wijmstra 1987a, 1987b) and Kopais (Okuda *et al.* 2001) extend as far back as the Middle and Early Pleistocene. Because of their continuity, these sequences provide some of the most important information regarding past environments in Greece. A location map is provided in Chapter One, Figure 1.1.

Tenaghi Philippon is a fault-formed basin lying *ca.* 300 km to the east of Mount Smolikas, near to the town of Kavalla. Two boreholes, 120 and 280m deep, through clay, marl and peat deposits were analysed for pollen at various depths in Wijmstra (1969), Wijmstra and Smit (1976), van der Wiel and Wijmstra (1987a, 1987b). The Quaternary pollen stratigraphy is known for this basin down to the onset of the Jaramillo magnetic Event at *ca.* 900,000 years BP, equivalent to MIS 48. Glacial stages are represented by *Artemisia*-*Chenopodiaceae* steppic assemblages and a noticeable absence of arboreal pollen. This probably reflects aridity during glacial phases, a situation promoted by the position of Tenaghi Philippon to the east of the Pindus mountains in the lee of prevailing westerlies.

The Kopais basin is a large karstic basin or *polje* and was filled with a seasonal lake *ca.* 20 km long until drained in the 19th century. A 120 m long sediment core was removed by Okuda *et al.* (2001) which covered the Middle to Late Pleistocene. Pollen analyses showed that glacial stages consisted of open steppe with *Artemisia* and Chenopodiaceae associated with Compositae (Tubiflorae) and other herbs and a notable absence of tree pollen. As at Tenaghi Philippon, this probably reflects the position of Kopais in the rain shadow of the Pindus Mountains. Tzedakis (1999) also analysed pollen from a 60 m core from Kopais. The sediments in this core spanned from the last interglacial to the early Holocene and the pollen stratigraphy bears strong similarities to other records in Greece, but also revealed the presence of high frequency oscillations with higher amplitudes than previously seen at other sites (Tzedakis 1999).

The Ioannina plain is a karstic basin or *polje*, sealed during the Late Pliocene-Early Pleistocene by fluvial deposition, and is situated less than 25 km from Mount Tymphi. Lacustrine deposition has occurred continuously right up to the present day where it still occurs in Lake Pamvotis. The pollen stratigraphy of a borehole down to 163 m is thought to represent a record of approximately the last 423,000 years (Tzedakis 1993, 1994). Two adjacent cores, I249 and I284 have been analysed for pollen at differing resolutions. The core I249 was used in Tzedakis (1993, 1994) and has been supplanted for the last glacial cycle by core I284, where pollen analysis has been done at a much higher resolution (Galanidou *et al.* 2000, Tzedakis *et al.* 2002). Ioannina differs from Tenaghi Philippon and Kopais in that there is a permanence of tree taxa such as *Quercus*, *Abies*, *Pinus*, *Ulmus*, and *Corylus* recorded throughout glacial-interglacial cycles. This reflects the local position of Ioannina, at mid altitude (484 m a.s.l.) in the heart of the Pindus Mountains, where precipitation levels are among the highest in Greece. Lower areas would have been too dry and higher altitudes probably too cold to support such assemblages.

The pollen records of Tenaghi Philippon and Ioannina, as well as other long lacustrine records in southern Europe, have been correlated with the global marine isotope sequence (Tzedakis *et al.* 1997). They therefore provide a stepping-stone with which to correlate the glacial sequence and that of the marine realm (Chapter One, Fig. 1.2). This is especially useful at Ioannina, which is less than 25 km from Mount Tymphi, and it is likely that a particularly close link exists between the long pollen record and the glacial sequence on this mountain.

The climate in Northwest Greece and the wider Mediterranean at the Last Glacial Maximum (LGM) during the Late Würmian Substage has been the subject of much debate (Bailey *et al.* 1983, Prentice *et al.* 1992). Pollen evidence for this period suggests that in

much of the Balkans the predominant vegetation consisted of an *Artemisia-Chenopodiaceae* steppe which is thought to represent rather drier climatic conditions than present (Bottema, 1974, van Zeist and Bottema 1991, Tzedakis 1993, Willis 1994). However, elevated lake beach deposits, dated to $20,800 \pm 810$ and $20,200 \pm 480$ ^{14}C years BP at the Kastritsa rockshelter near Lake Pamvotis (Ioannina), have been used to suggest a higher lake level at this time and a pluvial LGM (*cf.* Higgs *et al.* 1967, Bailey *et al.* 1983). Prentice *et al.* (1992) attempted to reconcile this conflict using a combined water-balance and biome model. They proposed an increase in *seasonality* with a prolonged summer drought inhibiting tree growth and stormier and wetter winters producing high lake levels. However, more recently Galanidou *et al.* (2000) have suggested that evidence of higher lake levels at Ioannina may be purely an artefact of tectonic uplift of the Kastritsa ridge – an idea first proposed by King and Bailey (1985). They also provide a revised chronology of the deposits used in the model of Prentice *et al.* (1992), showing that they are not of LGM age, as previously thought, but formed during a period of intermediate rather than extreme conditions *prior* to the LGM.

The most severe temperature depression in the region occurred at *ca.* 22-20,000 ^{14}C years BP, coeval with Heinrich Event 2 in the North Atlantic (Galanidou *et al.* 2000). This is prior to the time of maximum global ice volume at *ca.* $18,000 \pm 1,000$ ^{14}C years BP. Ostracoda evidence during the coldest phase indicate a distinct lowering of lake-levels during this period (Frogley 1997). The case for a higher lake stand at Ioannina during the LGM is therefore open to question and is also at odds with evidence from other lakes in Greece. At Lake Xinias, for example, Digerfeldt *et al.* (2000) found evidence of a low lake level from *ca.* 32,000 BP through to *ca.* 15,000 BP, in accordance with the pollen evidence for arid steppe vegetation. Similarly, at Lake Kopais, Okuda *et al.* (2001) propose that the lake level was low during the full-glacial period on the basis of the presence of lignite lenses, indicative of swamp development and therefore lower lake levels, throughout the core horizons dated to this period. More recently, estimates of LGM temperatures and precipitation for the Ioannina region have been provided by Tzedakis *et al.* (2002) using data from a nested global General Circulation Model developed by E.J. Barron and D. Pollard . At 21,000 years BP, the model suggests that mean January and July temperatures were 10°C and 7°C lower than present respectively and also precipitation values *ca.* 545 mm lower.

In the Voidomatis basin, which drains the southern slopes of Mount Tymphi, fluvial sediments record phases of aggradation and incision through the Würmian Stage and possibly earlier. Much of the work on these deposits was initiated as part of the Klithi

Project (Bailey 1997) and results are presented by Woodward (1990), Lewin *et al.* (1991), Woodward *et al.* (1992), (1994), (1995), Macklin *et al.* (1997), Hamlin (2000) and Hamlin *et al.* (2000). Rockshelter sediments in the Voidomatis basin have also provided information regarding past environments and these have also been worked on by Woodward and co-workers (Woodward 1990, 1997a, 1997b, Woodward and Goldberg 2001, Woodward and Bailey 2000, Woodward *et al.* 2001).

Several periods of fluvial aggradation in the Voidomatis basin have been interpreted as representing cold phase climate. Lewin *et al.* (1991) suggested that major periods of alluviation were associated with glaciation and subsequent deglaciation during the Late Würmian. Using soil weathering profiles to differentiate between sediment units, Woodward *et al.* (1994) recognised two phases of glaciation recorded in fluvial aggradational units. Subsequent analysis of gravel lithologies and fine sediment 'fingerprinting' has shown that during at least four phases, aggradation has occurred with sediments predominately sourced from glaciated headwaters (Hamlin *et al.* 2000). This led Hamlin *et al.* (2000) to conclude that increased sediment supply was due to cold-climate processes. The cessation of the four phases of aggradation have been dated to approximately $113,000 \pm 6,000$, $80,000 \pm 7,000$, $55,000 \pm 4,000$ and $25,000 \pm 2,500$ years BP through the U-series dating of calcite cements (Fig. 2.15). It is important to recognise that increased sediment supply due to cold-stage processes could have been the result of periglacial or paraglacial processes and particularly the re-working of pre-existing glacial deposits. Therefore, the aggradational units do not necessarily reflect contemporaneous glaciation.

Across the Mediterranean, Late Pleistocene river alluviation phases generally occurred during cool, dry stadials when steppe vegetation replaced forest or wooded steppe biomes (Macklin *et al.* 2002). Parts of the Early Würmian (MIS 5d-5a) are thought to have been periods of pronounced landscape change in many Mediterranean catchments. The

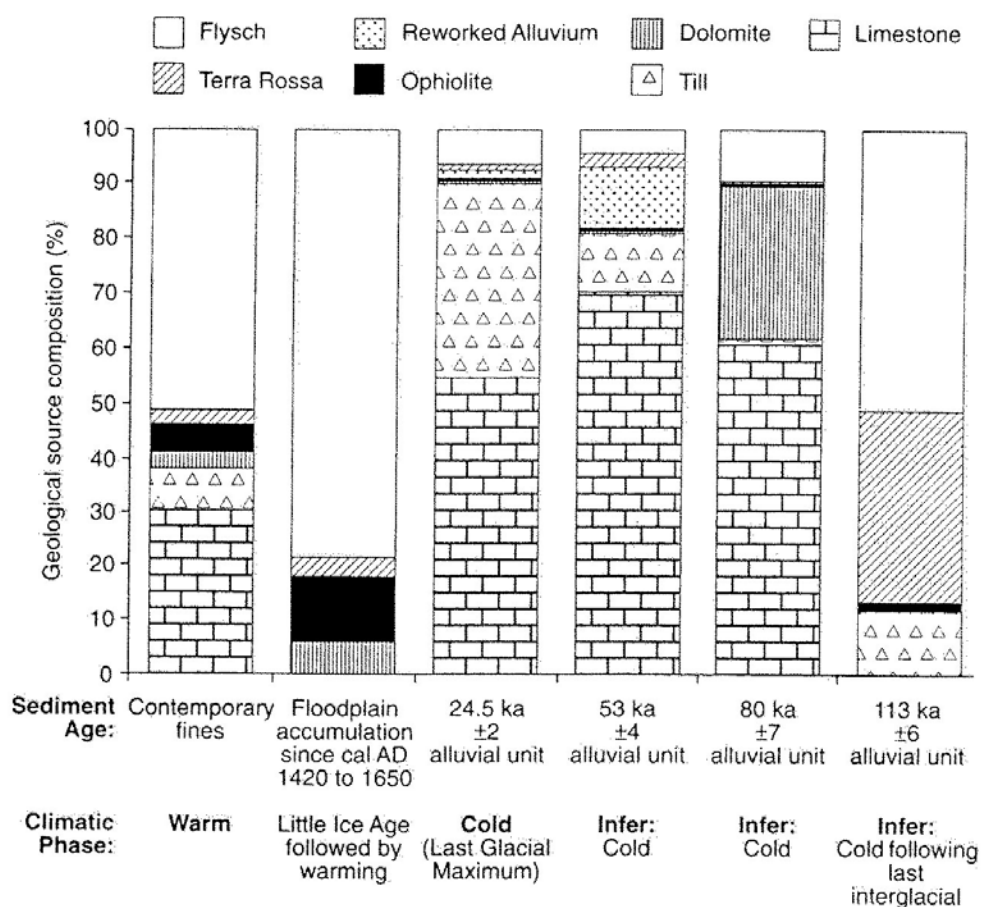


Figure 2.15 Fluvial sediment sources based on a geochemical fingerprint technique in the Voidomatis basin. At least four aggradation phases have been linked to increased sediment supply from the glaciated upper catchment on Mount Tymphi which is dominated by limestone bedrock and till (ka = 1,000 years) (from Hamlin *et al.* 2000).

Early Würmian is characterised by oscillating climate between stadials and interstadials which are recognised in numerous long terrestrial sequences, including at Ioannina (Tzedakis *et al.* 2002). Major alluviation episodes in the Mediterranean region are correlated with MIS 5d and the MIS 5a boundary (Macklin *et al.* 2001). In the Voidomatis basin on Mount Tymphi, Hamlin *et al.* (2000) suggested that an aggradational unit, cemented by calcite dated to 113,000 ± 6,000 years BP may have been the result of glaciation in the upper catchment during MIS 5d. The high presence of significant levels of *terra rossa* and flysch was suggested as indicating erosion of soils and weak flysch bedrock during the climatic deterioration of MIS 5d after the last interglacial (Hamlin *et al.* 2000). However, a more recent report based on the long pollen sequence at Ioannina suggests that interglacial conditions persisted until 111,000 years BP into the interval of MIS 5d. (Tzedakis *et al.* 2002). Nevertheless, a pronounced reduction in tree pollen is interpreted as representing stadial conditions between 111,000 years and 104,500 years BP and is recognised as Stadial 1 in Tzedakis *et al.* (2002). Whilst it is possible that conditions were

conducive to glaciation during this Early Würmian stadial, the cement dated by Hamlin is more likely to have formed in sediments which predate the last interglacial and the aggradational unit is perhaps better explained as being the result of glaciation during the late Rissian, equivalent to MIS 6. Moreover, the significant *terra rossa* component in this aggradational unit is likely to have developed under interglacial conditions and represent the *in-situ* weathering of the sediments.

The alluvial units in the Voidomatis basin, with calcite cements dated at $80,000 \pm 7,000$, $53,000 \pm 4,000$ and $25,000 \pm 2,000$ years BP, are likely to have formed during the cold intervals of the Würmian Stage. It is likely that the alluvial unit dated at $80,000 \pm 7,000$ years BP formed during Stadial 2 at Ioannina which is correlated with MIS 5b (*cf.* Tzedakis *et al.* 2002). The calcite cement is likely to have formed during the following interstadial recognised in the Ioannina sequence, Interstadial 2, which is correlated with MIS 5a (*cf.* Tzedakis *et al.* 2002). Following this interstadial, it is likely that cold stage climate persisted, perhaps intermitted by short phases of climatic warming corresponding with periods of incision at $53,000 \pm 4,000$ and $25,000 \pm 2,000$ years BP. It has never been established whether any of these cold phases were characterised by glacial activity in the upper Voidomatis catchment.

The nature of climate change after the most severe phase of the Würmian Stage (22-20,000 ^{14}C years BP) and during the Late-glacial Substage (14-10,000 ^{14}C years BP) in Greece is unclear from the geological record. The evidence is often contradictory, with no established consensus. A climatic reversal, *i.e.* a brief return to cooling during an overall climatic amelioration equivalent to the Younger Dryas Chronozone (12,900-11,500 years BP) of northwest Europe, is claimed to be recognised at Tenaghi Philippon (Wijmstra 1969), Xinias (Bottema 1978, 1979) and at Kopais (Turner and Greig 1975). It is also been recognised in rock shelter sediments at Theopetra, in Thessaly (Karkanis 2001) as well as in marine sediments in the Adriatic Sea (Rossignol-Strick 1995). However, little or no evidence has been found at Ioannina (Bottema 1974, Lawson 2001), Nisi (Lawson 2001), Khimaditis (Bottema 1974), Gramousti (Willis 1992a) or from Allen's (1986) analysis of Kopais. In a review of Late-glacial studies in the eastern Mediterranean, Bottema (1995) argues that there is no evidence for a climatic reversal in Greece equivalent to the Younger Dryas Chronozone of northwest Europe. It is apparent, therefore, that the Younger Dryas signal in Greece is by no means clear and, whilst it may have occurred, it was neither characterised by precipitation nor temperatures as low as for the interval 22-20,000 ^{14}C years BP, at the height of the last glacial stage. The poor representation in the pollen record in the Pindus Mountains may result from orographic effects reducing the

impact of aridity (Lawson 2001). Indeed, based on sequences near to and on Mount Tymphi, Willis (1992b, 1992c) suggests that higher precipitation in the Pindus Mountains may have contributed to the occurrence of arboreal refugia through the Late-glacial and earlier glacial stages.

This thesis aims to construct a glacial chronostratigraphy for Greece and apply relative-age and radiometric dating to understand the chronology of this sequence. This will enable correlation with the long pollen record and then with the marine isotope record. Similarly, a firm glacial chronology will help in understanding the link between glacial and periglacial processes and the fluvial sedimentary record in the Voidomatis basin. In addition, palaeoclimatic reconstructions based on sensitive glacier- and periglacial-climate relationships will provide important new data and help understand differences between different glacial stages in the eastern Mediterranean.

Chapter Three

Methods - geomorphology and sedimentology

3.1 Geomorphological Mapping

The glacial geomorphology of part of the northwest Pindus range, incorporating Mount Tymphi, Mount Smolikas and Mount Vasilitsa was mapped onto 1:25,000 topographic base maps. These base maps were enlarged versions of 1:50,000 topographic maps obtained from the Cambridge University Library. The accuracy of the field mapping was much improved using a Global Positioning System (*cf.* Heywood *et al.* 1999). Field mapping was aided on Mount Tymphi using evidence derived from 1:30,000 aerial photographs. The aerial photographs were helpful in planning the mapping programme, as they allowed some of the clearer features to be mapped beforehand, resulting in a more efficient field-mapping programme.

In total, an area of over 200 km² was explored. Many of the field sites were in the remote centres of each massif and were reached on foot, although some of the features formed by larger glaciers extended to areas crossed by roads at lower elevations. The mapping was undertaken over a total of twelve weeks during four separate field campaigns during July 2001, October 2001, April 2002 and May 2003.

The features mapped in the field included ice-marginal moraines, hummocky moraine, fluted moraines, drift limits, boulder limits, a range of erosional forms, glaciofluvial features and periglacial features, including rock glaciers and pronival ramparts. The nature and significance of these features are described below.

3.1.1 Ice-marginal moraines

Ice-marginal moraines are depositional features, which form, as the term suggests, at the margins of glaciers. Bennett and Glasser (1996) recognise three ice-marginal moraine types: a) glacitectonic moraines; b) dump moraines and; c) ablation moraines. These ice-marginal moraines, depending upon their position, constitute end and lateral moraines.

End moraines are formed at the glacier snout, transverse to glacier flow and can be divided into terminal moraines and recessional moraines. The former represent the maximum limit of glaciation and the latter represent a period of ice-front stability or

readvance during overall glacier retreat (Hambrey 1994). End moraines are commonly arcuate in form, reflecting the shape of the former glacier snout.

Lateral moraines are formed at the ice-margin, parallel to ice-flow and develop primarily by the dumping of glacial debris, although some debris may be derived from the valley sides (Bennett and Glasser 1996). However, in the case of larger valley glaciers, lateral moraines can be entirely glacially-derived and the glacier may be more constrained by its moraines than by the steep valley sides (Hambrey 1994). Lateral moraines always form below the equilibrium line altitude (ELA) of a glacier and thus provide important information regarding former glacier dynamics. This is because ice flows towards the glacier centre above the ELA and towards the glacier margins below (Nesje and Dahl 2000).

3.1.2 Hummocky moraine

The term 'hummocky moraine' is used to describe irregular morainic topography within former glacier limits and has been applied to a wide range of moraine types in different parts of the world (*e.g.* Hoppe 1952, Gravenor and Kupsch 1959, Sissons 1967, Aario 1977, Sharp 1985, Ciner *et al.* 1999).

Sissons (1967, 1979a, 1979b) regarded hummocky moraine in Scotland as evidence of *in situ* glacier stagnation, a view which influenced many of the British glacial geomorphological studies in the 1970s and early 1980s. However, there became unease with this interpretation, and workers such as Eyles (1983), Bennett and Glasser (1991), Bennett and Boulton (1993) and Bennett (1994) have argued that hummocky moraine topography can be formed during active glacier retreat. For example, in the Cairngorm Mountains, Scotland, Bennett and Glasser (1991) re-interpreted hummocky moraine mapped by Sissons (1979b) as closely-spaced recessional moraines. It is also possible that, in some cases, hummocky moraine is the product of the decay of detached ice-blocks from an actively retreating glacier (Eyles 1983). In addition to these theories of formation by ice-stagnation and active retreat, Hodgson (1982) concluded that hummocky moraine is formed by the subglacial deformation of coarse debris including older till deposits. A genetic link between certain occurrences of hummocky moraine and subglacial fluting had also been considered by other workers (*e.g.* Donner and West 1955, Peacock 1967, Gray and Brooks 1972). Finally, yet another mode of formation has been proposed by Bennett *et al.* (1998). They propose that some types of hummocky moraine are formed via englacial thrusting in polythermal glaciers.

Despite the problems of genetic definition, the term 'hummocky moraine' is very useful for describing the overall appearance of many areas of moraines in formerly glaciated areas. This a point clearly evident in the recent work of Ciner *et al.* (1999) in the Taurus Mountains of Turkey. As such, the morphological term 'hummocky moraine' is used throughout this thesis, with moraine genesis considered individually at different sites based on available sediment exposures and overall landform assemblage.

The recognition of 'hummocky moraine' in glaciated areas is not always straightforward. This is especially the case in limestone areas, such as Mount Tymphi, where it is important that karstic doline depressions are distinguished from true glacial 'hummocky moraine'. This is usually obvious on close inspection because, unlike depressions enclosed by hummocky moraine, dolines have regular geometries and are often circular to subcircular in planform. Nevertheless, dolines often form in formerly glaciated environments, especially suffosion dolines which are formed as a consequence of seepage through thick unconsolidated regolith such as till (Ford and Williams 1989). Care is therefore needed in karstic areas and close examination of landform structure and internal sedimentology is often required.

3.1.3 Fluted moraine

Flutes are typically low (< 3 m), narrow (< 3 m), regularly-spaced ridges which are usually less than 100 m long and are aligned parallel to the direction of ice flow. Flutes are therefore useful indicators of former glacier movement. They are also indicative of rapid ice-flow and normally occur where glaciers would have been flowing rapidly (Sissons 1980). They usually begin up-valley at a boulder bedrock obstacle and are typically composed of lodgement till, although they may also contain fluvial sands and gravels (Bennett and Glasser 1996). Unfortunately, flutings have low preservation potential because they are readily degraded by wind and water (Benn and Evans 1998). Even so, they have been noted in relict glacial landscapes (Sissons 1967, 1980, Gordon *et al.* 1992, Bennett 1995).

3.1.4 Drift limits

Drift limits are mapped at the approximate boundary between glacial deposits and non-glaciated areas down-valley. This is not always obvious morphologically and careful tracing of the furthest down-valley exposures is necessary. Drift-delimitation in the field

was aided by prior consultation of aerial photographs and Institute of Geology and Mineral Exploration (IGME) geological maps, which mark some, though not all, areas of glacial deposits. Sometimes, however, drift limits are morphologically expressed where there exists a sharp change in drift thickness at former glacier margins, especially in locally glaciated mountain areas (*cf.* Gray and Coxon 1991) (Fig. 3.2).

3.1.5 Perched boulders and boulder limits

Perched boulders are large clasts (> 25 cm width) which are situated on the surface of the landscape, well away from valley sides or higher areas of bedrock. The latter point is important since boulders near to valley sides or any locally elevated bedrock can contribute boulders by rock-fall. However, if boulders are different to the underlying lithology this precludes any possibility that they are of local origin. Perched boulders, especially 'erratic' boulders of differing lithology to the underlying bedrock, are a classic indicator of glacial transport at the land surface and initial observations of such features formed part of the basis for glacial theory in the 19th century (Fig 3.1).

Boulder limits are similar to drift limits but are clear morphological expressions and tend to be limited to areas once occupied by smaller valley or cirque glaciers, where boulder accumulations are often dense (Fig. 3.2). In the British Isles, Sissons (1980) noted that glacially-deposited boulders are often very abundant in ground formerly occupied by localised cirque glaciers during the last phase of glaciation. This probably reflects the short transport distances of boulder-sized clasts and consequently lower abrasion in comparison to large-scale valley glaciers.

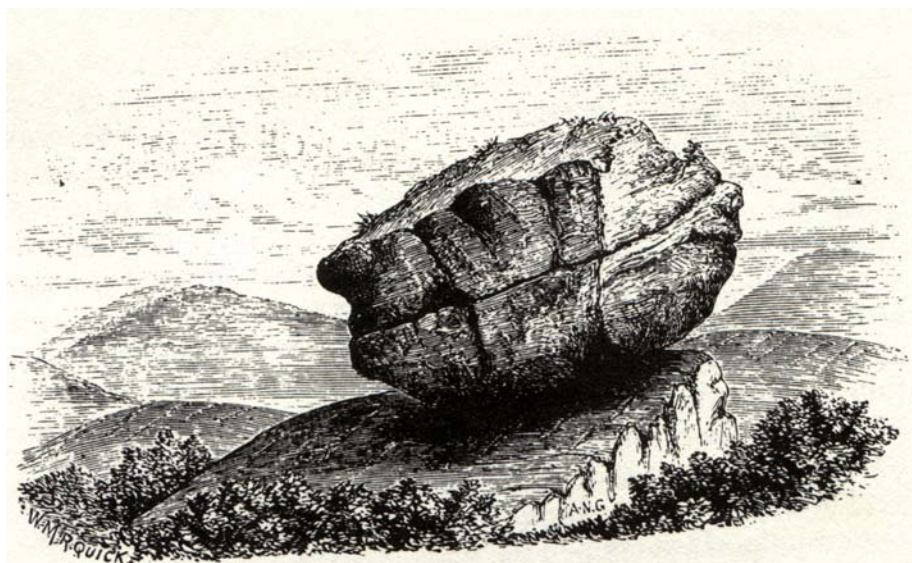


Figure 3.1 A perched rock in Scotland. This image is reproduced from Geikie (1894). Questions concerning the origin of such landforms were fundamental to the development of glacial theory.

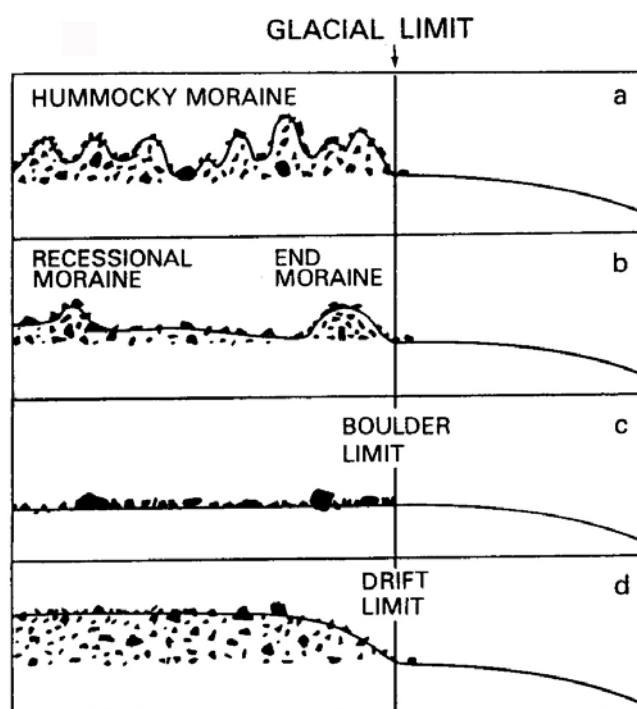


Figure 3.2 Some types of geomorphological evidence used to delimit the extent of local cirque or valley glaciers: a) limit of hummocky moraine; b) end moraine; c) boulder limit, and; d) drift limit (from Gray and Coxon 1991, Fig.37).

3.1.6 Erosional forms

Erosional forms include small-scale forms such as friction cracks and striae, larger-scale stoss and lee landforms, and glacio-karst limestone pavements. Friction cracks and striae can be used to interpret former ice-flow directions of former glaciers. The term 'friction crack' was introduced by Harris (1943) and is now used to cover a variety of erosional forms, including crescentic gouges, lunate fractures and crescentic fractures. Striae are lines or scratches on a rock surface produced by glacial abrasion and, when particularly large, they grade in to p-forms and grooves (Benn and Evans 1998). Striae have probably been used more in determining ice movement (Gray and Lowe 1982), although there are several problems in their interpretation, including (a) possible changes in ice movement over one glacier phase; (b) influence of more than one phase of glacier activity; (c) influence of local factors such as relief and rock structure and; (d) possible occurrence of striae produced by agencies other than ice (Flint 1971, p.90-93). Even so, a general picture of former ice movement can be achieved provided sufficient samples are measured.

Unfortunately, in areas of limestone bedrock, as is the case on Mount Tymphi, small-scale erosional forms such as striae and friction cracks are usually poorly preserved or absent altogether. Unless protected, striae disappear quickly from limestones as a result of solution. However, striae may be preserved on limestone surfaces if protected by a sheet

of till. For example, in 1947 till was removed from a glaciated pavement in Yorkshire, England, and by 1960 glacial striae had been removed by corrosion (Sweeting 1966). In Ireland, Williams (1966) found that calcareous till may inhibit corrosion of the underlying bedrock surface because the seepage water within the till becomes saturated with calcium carbonate. Thus, where a thin veneer of till has recently been removed, especially in areas prone to modern overgrazing and subsequent erosion, small-scale erosional features may well be preserved, especially larger p-forms such as grooves. Striae are also not so well preserved on Mount Smolikas, since the mountain is predominantly formed in ophiolite which is prone to rapid weathering and the development of an orange crust. This arises from the oxidisation of ferromagnesium oxides upon subaerial exposure of the iron- and magnesium-rich olivine minerals characteristic of the ophiolite in this area. Nevertheless, striae are in evidence locally and were noted by Boenzi *et al.* (1992, Fig. 5).

Large-scale erosional forms, such as stoss and lee landforms and limestone pavements, are particularly useful for determining patterns of glacial erosion and former ice movement. A common type of stoss and lee landform are *roche moutonnées*. These are asymmetric bedrock protrusions with abraded up-ice or stoss faces and quarried down-ice lee faces and range in size from 1 m to several hundred metres across (Benn and Evans 1998). However, in limestone areas, glacial erosion is more frequently represented in the form of limestone pavements (Sweeting 1972, p.263-269) and in Britain, nowhere outside former Devensian Stage glacial limits displays limestone pavements (Jennings 1988). Limestone pavements are flat-lying or slightly dipping areas of strata dominated by patterns of regular clints and grikes (Ford and Williams 1989). Glacial erosion on limestones is particularly selective, with weaker layers being scoured away, leaving stronger more massive layers. In this way a stepped profile of alternating ledges and cliffs may be formed and is known by the German term *Schichttreppen* karst (Sweeting 1972, Bögli 1980, Vincent 1985). Glaciated valleys in limestone areas therefore commonly display a series of pavements separated by abrupt steps or cliffs facing in a down-ice direction.

3.1.7 Glaciofluvial features

Glaciofluvial features include numerous sediments and landforms formed in the sub-glacial and ice marginal environment, such as meltwater channels, kames, kame terraces, outwash fans and eskers. In this study, only meltwater channels are marked on the geomorphological maps. Morphologically, other features were poorly preserved and often ambiguous. However, glaciofluvial deposits were noted in several sedimentary sections and played an important role in understanding the assemblage of associated glacial features.

3.1.8 Periglacial features

The term *periglacial* refers to the influence of frost action in forming or modifying the landscape (French 1996). Periglacial features, such as frost-shattered bedrock, patterned ground and tors, are mapped using a collective symbol. Rock glaciers and landslide features, although often periglacial in origin, are considered separately below. Distinct contrasts between glacially-moulded areas and distinctly frost-shattered areas can sometimes be defined by a periglacial trimline. However, periglacial trimlines are poorly preserved on limestone rocks and are best seen on hard crystalline rocks such as granite, gneiss and schists (Thorp 1981). Ophiolitic rocks are also poor in preserving trimlines because of their susceptibility to rapid weathering. Nevertheless, differentiation can sometimes be made between clearly glacially-moulded areas and areas where there is no evidence of glaciation.

3.1.9 Rock glaciers

Rock glaciers are masses of angular debris which have the appearance of small glaciers and because of their large non-ice component, retain much of their morphology long after they were active. The features often have transverse ridges on their surface, possibly the product of differential movement of discrete layers of debris (Loewenherz *et al.* 1989). Rock glaciers have been one of the most contentious issues in cold-climate geomorphological research. The traditional view is that they are periglacial forms with movement explained by a model of creeping permafrost (Barsch 1978, 1988, 1996, Haeberli 1985). This interpretation suggests that rock glaciers form in areas characterised by at least discontinuous permafrost in high mountain and polar regions. However, some workers separate rock glaciers into glacial and periglacial origins. For example, Martin and Whalley (1987) recognise ice-cored rock glaciers, which are essentially debris-covered 'normal' glaciers, and ice-cemented rock glaciers which are essentially periglacial forms.

It has been shown that some rock glaciers are debris-covered glaciers since ice exposures have been noted in rock glaciers in the Colorado Front Range, USA (Outcalt and Benedict 1965, White 1975), Yukon Territory, Canada (Johnson and Lacasse 1988) and in Iceland (Whalley *et al.* 1994). Ice-cored rock glaciers may be produced by climatic amelioration and the overloading of a retreating glacier (Morris and Olyphant 1990). However, the case supporting a permafrost model is considerable. The main evidence tends to be from geophysical investigations (*e.g.* Potter 1972, Barsch 1973, Fisch *et al.* 1977, Haeberli 1985, Barsch and King 1989, Evin and Fabre 1990) and drilling operations (Barsch *et al.* 1979, Vonder Mühll and Haeberli 1990) and seems to show the presence of

interstitial ice rather than an ice-core. The issue of formation by permafrost or a debris-mantled glacier is one which has dominated the rock glacier literature and is symptomatic of the wider problem of equifinality in geomorphology, *i.e.* two morphologically-similar features having been formed by different processes (*cf.* Haines-Young and Petch 1986).

In the case of relict rock glaciers, evidence of melt-out topography is likely to be indicative of an ice-core. However, variations in the content of interstitial ice in an ice-cemented rock glacier could also result in melt-out topography and would depend on the ratio of debris to interstitial ice content. Even so, it is probable that an ice-cored rock glacier would not leave as clear a morphological feature as an ice-cemented rock glacier. This is because the debris mantle would be lowered significantly as the ice core melted - thus creating a low-lying bouldery moraine over the cirque or valley floor. This melt-out moraine would then be mapped as hummocky moraine. In the case of ice-cemented rock glaciers, the volume of debris would be far greater relative to the ice content. The relict form would therefore resemble the active form much more closely than is the case for an ice-cored rock glacier. This theory is important as it eliminates the problem of determining relict rock glacier genesis since all relicts will be of a permafrost origin. It also supports palaeoclimatic reconstructions based on the presence of relict rock glaciers *e.g.* Kerschner (1978, 1983) and Girauldi and Frezzotti (1997). In these studies, a permafrost origin was assumed in order to determine palaeotemperatures for former cold-stage rock glaciers.

Rock glaciers can be classified following the approach of Barsch (1988, 1996) who recognised *debris* rock glaciers and *talus* rock glaciers. This approach is by no means exclusive and several different models have been proposed in explaining rock glacier formation in different localities. Indeed it is often difficult, especially with regard to relict rock glaciers, to be certain of the exact mode of formation. What is important, when reconstructing palaeoclimates on the basis of rock glacier evidence, is that climatic assumptions hold, even where different modes of formation can be envisaged.

Debris rock glaciers often form below glaciers (Figure 3.3A). According to Barsch (1988), during times of maximum glacial advance the deposited moraines act as a 'rooting zone' for a rock glacier which develops from this debris below the glacier. This type of rock glacier can be identified where the cirque basin displays erosional evidence and a distinct morainic lobe (the rock glacier) has formed on the distal side of moraines, at the lip of a cirque. A modern example of this type is the rock glacier in the Cirque de Marinette in the French Alps (Evin and Fabre 1990, Fig. 8). Debris rock glaciers can also form where a

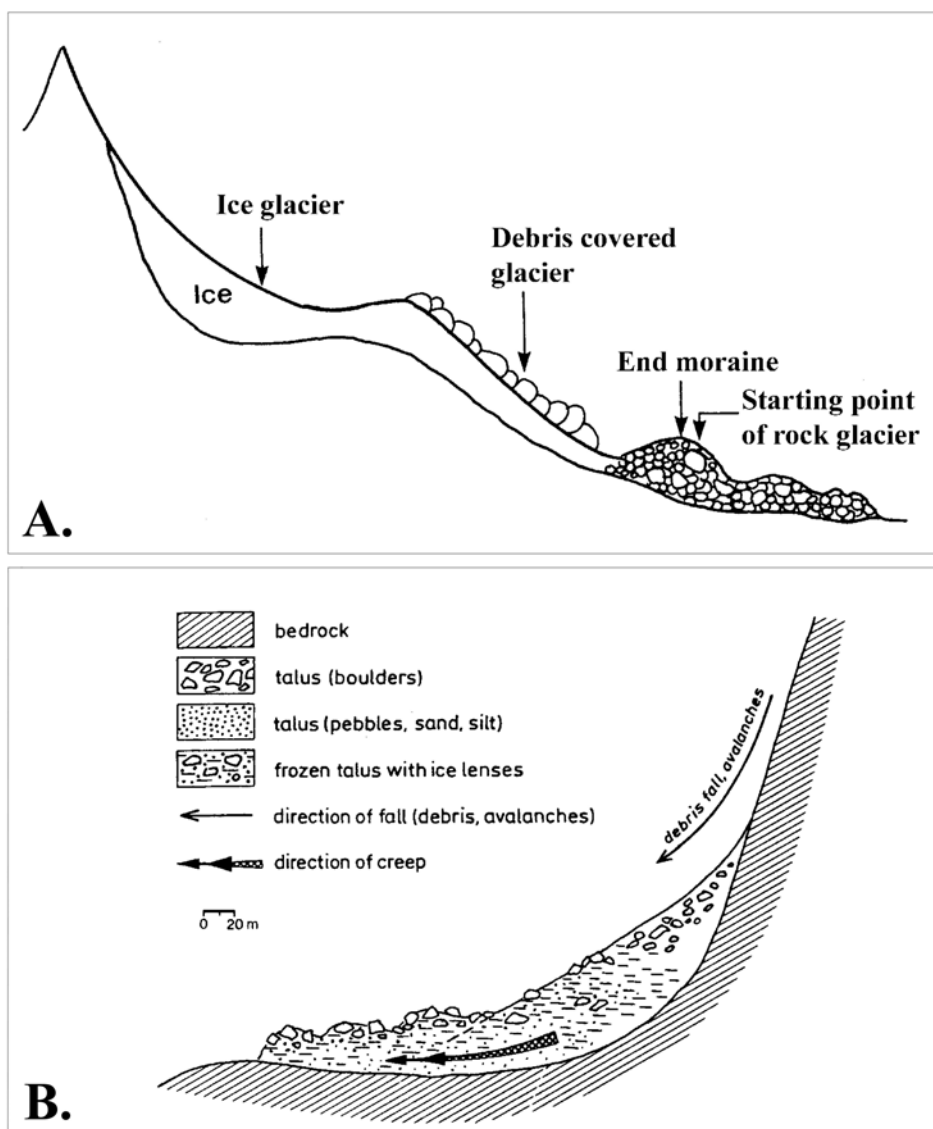


Figure 3.3 The formation of debris rockglaciers is illustrated in frame A. and the formation of talus rockglaciers in frame B. Both are periglacial forms (adapted from Barsch 1988).

glacier retreats into a high-walled cirque and becomes buried as a result of high debris supply due to frost-shattering of the surrounding rockwalls (Johnson, 1980, 1987, Morris and Olyphant 1990, Benn and Evans 1998, p.257-258). In this case, the rockglacier has evolved due to both glacial and periglacial processes, and the fossil rock glacier will not necessarily represent the most severe stage of climate. *Talus rock glaciers* form below talus slopes and are built up by layers of coarse colluvial debris. Their ice content is derived from snowmelt as well as from avalanches, which are incorporated into the rock glacier (Figure 3.3B).

3.1.10 Rock-slope failure deposits

Rock-slope failure deposits are commonly found at the base of steep rock slopes. In well-jointed limestone areas, rock-slope failure is common and often involves *fall* and *topple* mechanisms. Rock *falls* involve the breaking away of rock material due to joints and weaknesses high on a rock-face (Flageolet and Weber 1996). Rock *topples* involve the collapse of jointed blocks along points of flexure (Dikau *et al.* 1996). It is important to recognise rock-slope failure deposits since these may be closely related to glacial and/or periglacial activity. Moreover, rock-slope failure deposits can be misinterpreted as rock glaciers, especially talus rock glaciers, since these features sometimes have a similar form. On the geomorphological maps produced in this study, major rock-slope failure landforms are differentiated from rock glacier deposits with the letters 'rs' (Fig 3.4).

Rock-slope failures occur under a variety of conditions. They can form as a result of frost action widening rock joints and promoting slope instability and may, therefore, form under periglacial conditions. They can also form by slope failure following the retreat of glacier ice. In a valley situation, the retreat of glacier ice and the removal of support to newly-eroded valley sides can potentially result in slope failure if the eroded valley sides are too steep. During glacier retreat, pressure release and slope steepening enhance rock falls and erosion of convex pre-glacial surfaces, depending on block-joint orientation, can lead to an increase in points of flexure and thus block-flexure toppling. This post-glacial response represents one aspect of paraglacial activity which is defined as "nonglacial processes that are directly conditioned by glaciation" (Church and Ryder 1972). Paraglacial activity is distinct from periglacial processes which occur in all cold, non-glacial regions regardless of whether ice is or was present. However, rock-slope failure could have occurred well after glacier-retreat, as a result of processes that are independent of former glaciation. These could include joint weakening due to periglacial freeze-thaw action or seismic activity. Seismic activity and moderate periglacial activity still occur today and the landforms may have formed in recent times as well as during cold-stage climates. It is likely that all of these potential causes have promoted conditions for rock-slope failure with one particular cause, most probably seismicity, merely triggering the eventual debris release.

3.1.11 Pronival (or protalus) ramparts

A pronival rampart is a ridge of debris formed at the downslope margin of a snow-bed. Pronival ramparts range in plan-form from linear to arcuate features and are usually found below rockwalls (*e.g.* Ballantyne and Kirkbride 1986). In addition, they often consist of

coarse, angular clasts derived from bedrock cliffs rising above the supposed former snowbed (Washburn 1979, Harris 1986, Shakesby 1997). Most geomorphologists have assumed that they form through rock-fall debris accumulating by rolling, sliding or bouncing down the surfaces of static perennial snow-beds (*e.g.* Drew 1873, Russell 1933, Bryan 1934, Washburn 1979, Goudie *et al.* 1994). However, Shakesby (1997) argues that the features are formed by a whole range of different processes. He also advocates the use of the descriptor 'pronival' in preference to the widely used term 'protalus', because the latter is misleadingly restrictive in terms of the known range of possible localities.

3.1.12 Symbols used in the geomorphological maps

All the features described above were mapped using symbols distinctive to each feature. The symbols used in the maps are shown in Figure 3.4. No standardised and universally accepted geomorphological system exists in the literature and, although proposals have been advocated (Cooke and Doornkamp 1973, Gardiner and Dackombe 1983), many workers have devised their own schemes. The symbols used here are a combination of an adaptation of symbols used in earlier literature - particularly in mountain glacial geomorphology in the uplands of Britain (*e.g.* Sissons 1980, Ballantyne 1989, Anderson *et al.* 1998, Hughes 2002) - as well as symbols unique to this thesis. Some of the symbols, such as the till symbol, involve genetic interpretation of sedimentary exposures, and the approach to the description and analysis of such exposures is described in the following sections.

3.2 Sedimentological Investigation

Sediments were described and analysed in both the field and the laboratory. The methods employed are described in the following sections. Analytical methods applied to Quaternary soils are described in Chapter Six, since this chapter deals with chronology, and soils were used as a relative-age indicator.

3.2.1 Section Logging

Sections through deposits were described by systematically logging their basic sedimentary and stratigraphical characteristics. Most sections were in road/track cuttings and small quarries, although some natural sections were exposed by stream incision. Lithofacies and sedimentary structures were described using the codes and symbols of Miall (1977) and Eyles *et al.* (1983). Sections were measured from the base upwards and sedimentary units

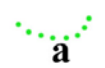











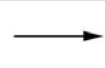
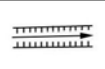




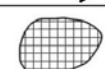

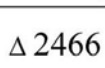
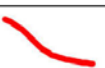
	Stratigraphical boundary
	Maximum extent of glaciation
	Area of pronounced periglacial features
	Rock glacier
	Rock-slope failure deposit
	Pronival rampart
	Perched boulders
	Till
	Moraine ridge
	Drift limit
	Boulder Limit
	Hummocky moraine
	Fluted moraine
	Meltwater channel
	Ice-moulded bedrock
	Periglacial trimline
	Steep cliffs of glacier source area
	Arête
	Lake
	Land surface contours (100 m interval)
	Major summit (height in metres)
	Paved road

Figure 3.4 Key to geomorphological maps.


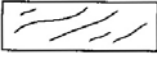
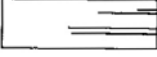
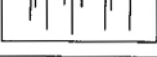
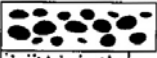
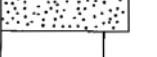
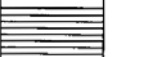

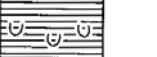

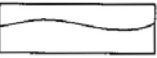
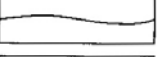
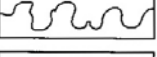
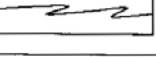
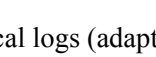

SYMBOLS	
	Diamict
	stratified
	sheared
	jointed
	Gravel
	Sand
	Fines
	Laminations
	with interclasts
	with dropstones
	with loading structures
	Contacts
	Erosional
	Conformable
	Loaded
	Interbedded

Figure 3.5 Key to lithological logs (adapted from Benn and Evans 1998, Fig. 10.3).

were identified, measured, described and sampled following established guidelines and recommendations (*cf.* Jones *et al.* 1999). All sections were sketched in the field and photographed using a visible scale reference. A key for the lithological logs is shown in Figure 3.5.

3.2.2 Clast Analysis

At least 50 clasts were sampled from individual sediment units. The clasts were used for analysis of fabric, shape, particle-size, surfaces features and lithology. Where sediment sections appeared massive, clast analysis was done at different levels in the section. However, in the case of high vertical sections (> 3 m) often only the lower parts could be accurately sampled. The methods and uses of each clast analysis are described below.

3.2.2.1 Clast-fabric

Clast-fabric was measured in the field following the guidelines of Andrews (1971). The fabric data were processed using the computer programme Stereonet by Rockware Earth Science Software and plotted as an equal-area stereographic plot using the spherical Gaussian method (Fig. 3.6). Fabric strength and shape was analysed using the eigenvalue method (Mark 1973, Woodcock 1977) and the isotropy and elongation indices of Benn (1994a).

Three eigenvalues (S_1 , S_2 and S_3), normalised between 0 and 1, provide direct information about the distribution and uniformity of the clast fabric. The strength of a fabric is essentially measured by the magnitude of the first eigenvalue (S_1). The relative magnitudes of S_1 , S_2 , and S_3 reflect the 'shape' of fabric data (Watson 1966, Benn 1994a). Basically, there are three types of point distribution:

- 2) The first eigenvalue (S_1) is much greater than the other two. This indicates a single area of point concentration on the sphere and can be described as a cluster distribution with all observations approximately parallel.
- 3) The first (S_1) and second (S_2) eigenvalues are roughly equal but much greater than the third value (S_3). This indicates a girdle distribution where points lie on a great circle trace.
- 4) All of the eigenvalues are of the same magnitude. This typically indicates an isotropic distribution with data points evenly distributed over a sphere.

Graphical methods of displaying clast fabric shape are described by Benn (1994a), and three types of point distribution can be represented on an equilateral ternary diagram (See Figure 3.7). The fabric-shape continuum is scaled using isotropy ($I = S_3/S_1$) and elongation ($E = 1 - (S_2/S_1)$) indices. This approach appears to give the best representation of clast-fabric shape and was adopted to display clast-fabric shape in this thesis.

Clast-fabric is a well established method to indicate the ice-flow directions of past glaciers (*e.g.* West and Donner 1956, Glen *et al.* 1957, Andrews 1965, Hirvas and Nenonen 1990). Elongated clasts have a tendency to lodge in till with their long-axis parallel to the direction of flow, and thus the preferred orientation of pebbles sampled from glacial deposits will give an indication of former ice-flow direction.

Clast-fabric has also been used to suggest possible processes and facies of glacial deposition (*e.g.* Boulton 1971, Lawson 1981, Dowdeswell *et al.* 1985, Johnson *et al.* 1995, Huddart and Hambrey 1996) and in the analysis of local strain patterns (*e.g.* Hart 1994,

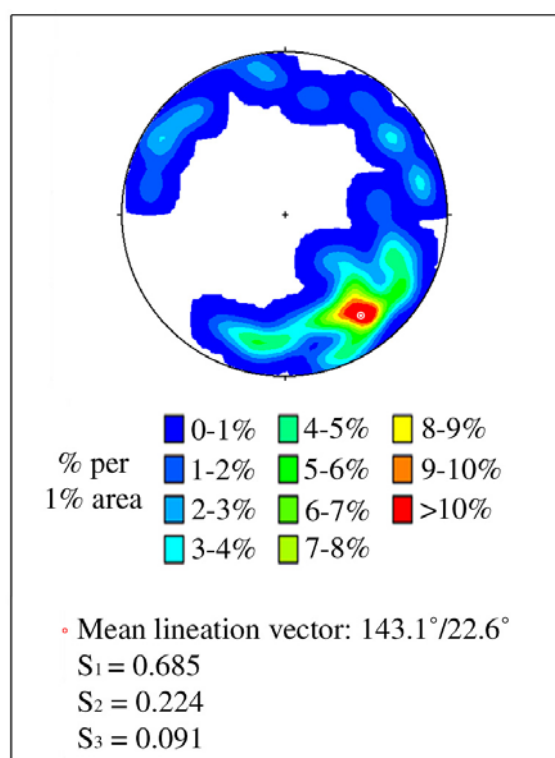


Figure 3.6 An example of an equal-area spherical Gaussian stereographic projection of clast orientation. The mean lineation vector displays two values, the first represents direction of orientation and the second represents the dip. The S_1 , S_2 and S_3 values represent the eigenvalues.

Benn 1995, Benn and Evans 1996). However, using data from modern glacial sediments, where depositional histories are well constrained, Bennett *et al.* (1999) argue that clast-fabric determinations are of little value as a genetic fingerprint. They therefore question the value of continuing to collect fabric data as part of routine sedimentary description and interpretation.

In recent years, there has been a shift towards micromorphology in order to interpret till genesis (*cf.* van der Meer 1997, Menzies and van der Meer 1998, Carr 1999, Carr *in press*). It is particularly useful where the surface geomorphology does not aid interpretation - such as in lowland regions once covered by vast ice sheets (*e.g.* Carr 1999). However, since the most extensive glacial deposits of northern Greece were predominantly deposited by valley glaciers, where the sedimentology is often coupled with well-preserved geomorphological features, micromorphological studies were not employed. Even though there are limitations in the interpretation of clast fabric statistics, clast fabric is only one criterion with which glacial diamictos should be interpreted. As such, when used critically in conjunction with other geomorphological and sedimentological data, clast

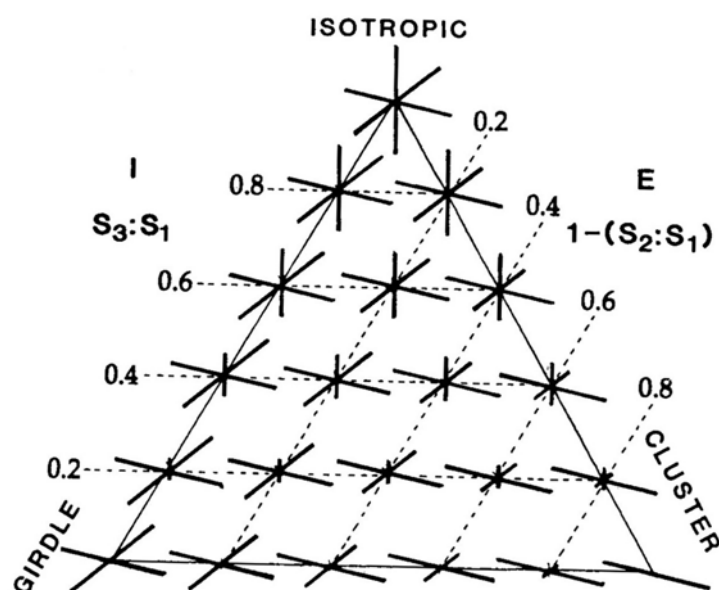


Figure 3.7 Fabric shape represented on an equilateral ternary diagram. The fabric-shape continuum is scaled using isotropy ($I = S_3/S_1$) and elongation ($E = 1 - (S_2/S_1)$) indices (after Benn 1994a).

fabric can play an important role in characterising glacial sediments. This is emphasized by Benn and Ringrose (2001) who note that the genetic identification of sediments should be based on multiple criteria, such as depositional and deformational structures, facies geometry, particle morphology and a range of fabric elements.

3.2.2.2 Clast form and clast size

The long, intermediate and short (a , b and c) axes of each clast were measured using vernier callipers. This provided information regarding clast shape and size. Clast size is described using the Wentworth scale (*cf.* Lowe and Walker 1997, Fig. 3.1). The proportion of material > 2 mm was also estimated visually using clast density charts (*cf.* Hambrey 1994). Examples of such charts are given in Flugel (1982, Fig. 40b and 40c). Deposits including a coarse clast fraction of less than 40% is usually referred to as matrix-supported, whilst a coarse fraction greater than this, where clasts touch each other, is referred to as clast-supported (Sladen and Wrigley 1983).

The morphological form of glacially-transported clasts is an important source of information for former glacial processes and environments. Systematic study of clast form enables the reconstruction of patterns of debris entrainment, transport and deposition (Boulton 1978, Benn and Ballantyne 1994). Glacial debris can be transported via two distinct modes, that of active and that of passive flow (Boulton 1978). Active flow takes place at the glacier sole or within the deforming subglacial sediment. Abrasion and

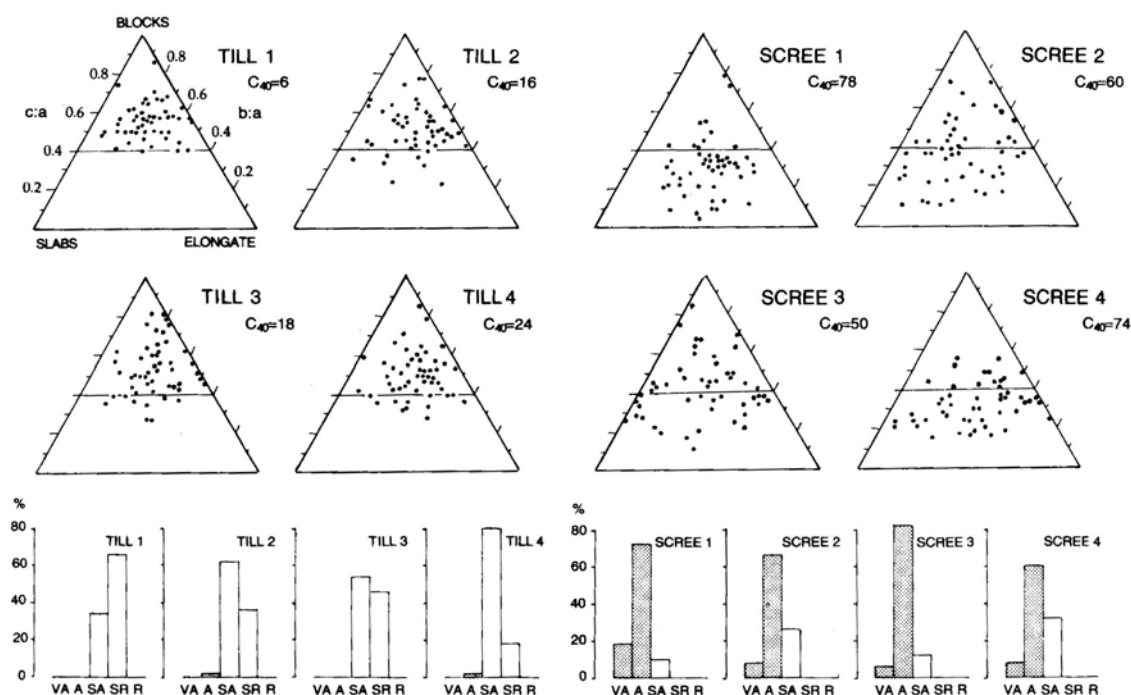


Figure 3.8 Clast shape data plotted on ternary diagrams and roundness data plotted as histograms. Note the difference between clasts in the till deposits which have undergone active transport and those of the scree which have not undergone active transport (from Benn and Ballantyne 1994).

crushing results in debris characterised by abundant edge-rounded clasts, high c/a ratios and a high incidence of faceting and striations. In contrast, passive flow takes place englacially and supraglacially. As a result, clasts often retain their original shape because of limited inter-particle contact. Passively-transported clasts therefore tend to be angular and have low c/a axial ratios (Boulton 1978, Ballantyne 1982, Matthews and Petch 1982, Sharp 1982, Benn 1989, 1992, Benn and Ballantyne 1993, Benn and Ballantyne 1994). This theory can be applied in several ways, such as in understanding till genesis and in determining changes in the relative proportions of actively and passively transported debris with increasing transport distance. For the latter application, Matthews and Petch (1982) showed that there is a tendency for clast roundness to increase down-moraine, towards the glacier snout. Also, Benn and Ballantyne (1994) showed that this increase in clast roundness is due to an increasing proportion of actively-transported debris in the moraines closer to the former glacier centre-line.

The long, intermediate and short (a , b and c) axes of clasts define three basic shapes: a) blocks (spheres) with high b/a and c/a ratios; b) slabs (discs) with a high b/a and a low c/a ratio and; c) elongate clasts (rods) with low b/a and c/a ratios (Benn and Ballantyne 1994). The shape characteristics of clasts within a particular deposit can be represented graphically by plotting the b/a and c/a ratios on a ternary diagram resulting in

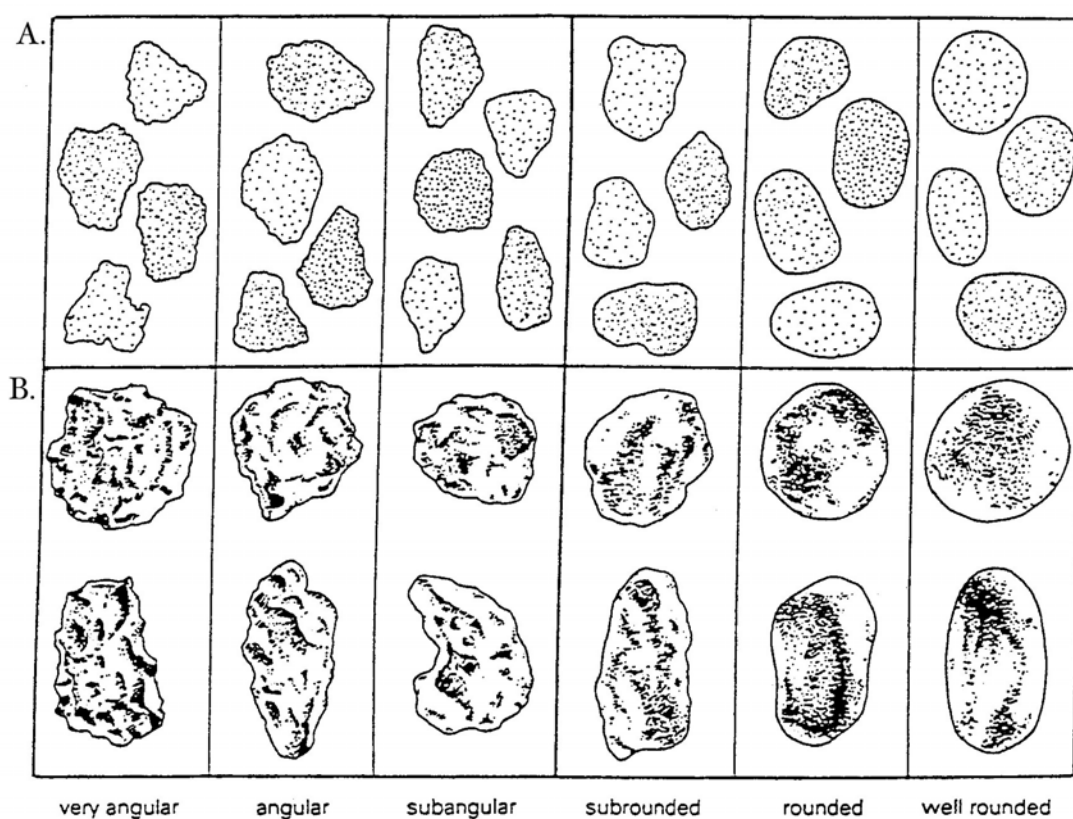


Figure 3.9 Clast images for visual determination of roundness: (A.) two-dimensional grain outlines based on Krumbein (1941); (B.) three-dimensional images after Powers (1953). The class names are based on Powers (1953). (Diagram from Lindholm 1987).

block-shaped clasts towards the top of the triangle, slab-shaped clasts towards the bottom left and elongate-shaped clasts towards the bottom right (Fig 3.8). Benn and Ballantyne (1994) suggest that a c/a ratio of 0.4 is a sensitive discriminant statistic in recognising high proportions of block-shaped clasts. The percentage of clasts within a sample with a c/a ratio of less than or equal to 0.4 is termed the C_{40} index and can help quantify shape characteristics aiding discrimination between clasts which have undergone active or passive transport. Clast populations within subglacial till tend to have a low C_{40} index, whilst clast populations within scree tend to have a high C_{40} index due to the different transport history of clasts within these deposits.

In addition to clast shape, clast roundness was also defined using a visual descriptive approach and comparison with the two and three-dimensional clast images presented in Krumbein (1941) and Powers (1953) and illustrated in Figure 3.9. Clast roundness is defined, with increasing roundness, as very angular, angular, subangular, subrounded, rounded and well rounded. This approach has been applied in numerous studies, including Dowdeswell *et al.* (1985) and Benn and Ballantyne (1994), and has been shown to be a powerful tool in discriminating between different modes of transport. Clasts

which have undergone active transport, such as in subglacial tills, tend to be more rounded than those which have undergone passive transport such as supraglacial debris.

3.2.2.3 Clast surface features

The presence or absence of surface features such as striae were recorded for each clast. Boulton (1978) has shown that clasts which travel through the basal transport zone of a glacier often have striated abrasional facets. The presence of striated clasts within diamictons is therefore taken as indication of glacial genesis. Also, the relative proportions of striated clasts within glacial sediments can be used to help differentiate between deposits derived from the sub-glacial, englacial or supraglacial environment.

3.2.2.4 Clast lithology

Clast lithology was noted for each clast after detailed examination of the surrounding bedrock lithologies. Clast lithology provides basic information regarding the provenance of the deposited material.

3.2.3 Fine-Fraction Particle-Size (< 2 mm)

Up to 1 kg samples of till matrix were collected in the field. These samples were sieved through a 2 mm mesh. The particle-size distribution of the fine sediment fraction (< 2 mm) was determined in the laboratory using a Malvern Mastersizer-X laser particle-sizer.

The sediment samples (*ca.* 5 g) were placed in 50 ml test-tubes and treated for 6 hours in hot 7% sodium pyrophosphate to encourage the break-up of aggregates. The samples were then centrifuged at 3000 revolutions per minute for 13 minutes and the supernatant decanted. The remaining samples were then fully mobilised using a whirlimixer and input to the Malvern Mastersizer-X laser particle-sizer. This instrument holds the sediment sample in suspension and passes it through a glass-windowed cell into the path of the laser. The machine then calculates the cross-sectional areas of the particles from the diffraction pattern of the laser beam.

Particle-size composition of till matrix is particularly useful in determining till genesis. This is because certain till-types have matrix particle-size distributions which fall within characteristic envelopes on a ternary diagram (Sladen and Wrigley 1983). For example, subglacial lodgement till has a greater concentration of fines in relation to supraglacial, melt-out or flow tills arising from clast crushing beneath the former glacier (Boulton *et al.* 1974).

3.2.4 Carbonate Content

Carbonate content by weight (%) and the acid insoluble residue component (%) were determined by calculating the weight loss after sample digestion in 7% hydrochloric acid (*cf.* Gross 1971, Woodward 1990). Approximately 2 g of sample was placed in a pre-weighed 50 ml test-tube (and mount) then *ca.* 40 ml of 7% hydrochloric acid was added to each sample as well as small amounts of methylated spirits (< 5 ml) to control the reaction. The test-tube was then placed in a waterbath at 90°C for 2 hours to ensure digestion of magnesium carbonate (common where the bedrock is dolomite) in addition to calcium carbonate. The samples were then centrifuged at 3000 revolutions per minute for 5 minutes, decanted, and oven dried at 100°C for 6 hours. The remaining acid insoluble residue was then weighed and the carbonate content calculated as a percentage of the original dry weight.

3.3 Morpho-lithostratigraphy

In order to systematically establish the sedimentary sequence over the study area, a formal stratigraphical approach was adopted. Lithostratigraphical units are the basic units of geological mapping that conform to the Law of Superposition. In glaciated cirque-valley systems, lithostratigraphy is usually applied in conjunction with morphostratigraphy, and the establishment of an integrated morpho-lithostratigraphy is described below.

Lithostratigraphical units are bodies of sediment or rocks that are defined and characterised on the basis of their lithological properties and their stratigraphical position. Each formal lithostratigraphical unit should have a clear and precise definition or characterisation. The proposal of a type section for a layered unit or a type locality for a non-layered unit is therefore essential. Salvador (1994) defines type sections as "a specific interval or point in a specific sequence of rock strata and constitutes the standard for the definition and characterisation of the stratigraphic unit being defined". However, in the context of localised glacial deposits in mountain areas, the sequence of rock or sediment strata is often expressed through the spatial surface morphology since sections are often limited in vertical extent. In these circumstances, the sediment can be regarded as massive and non-layered and therefore a type locality can define the deposits of the area. A type locality is "the specific geographic locality in which the type section is situated" (Salvador 1994) and provides a systematic basis for a local stratigraphy.

A particular type section or type locality may be defined by lithological characteristics of the sediment. Lithostratigraphical units should be defined on the basis of sediment properties such as dominant lithology, sorting, clast shape, size, fabric, etc. It is

important that non-genetic terms are used, such as diamicton rather than till, since some type-sections may be incorrectly interpreted, with colluvial deposits perhaps misinterpreted as till, for example. Also, soil development may characterise certain deposits and the pedostratigraphy may be useful in conjunction with the lithostratigraphy.

In mountain areas which have experienced localised valley and cirque glaciation, geomorphology is commonly a key characteristic in defining a type section or type locality. For example, sections may be cut in well-defined and possibly arcuate ridges. Ridge freshness may also be a distinctive characteristic, with 'freshness' being defined here as the morphological clarity of landforms, as expressed by ridge amplitude and sharpness - though this is a difficult quality to quantify. Rawson et al. (2002) suggest that the identification of a sediment body based on its surface form, or morphostratigraphy, is not comparable to standard lithological units. However, it is often the case in glaciated cirque-valley systems, that definition on litho- and morphological grounds is virtually identical or overlapping, and the International Commission on Stratigraphy (2004) state that both geological and geomorphological characteristics can be used to describe a type section. For example, rock glaciers may be described (in non-genetic terms) as lobes of angular, poorly-sorted boulders and this surface morphological description could equally constitute a lithological description.

In all instances, it is the combination of landform and sediment which is key to interpreting upland glaciated systems. The usual bases of stratigraphical position are often expressed in the lateral, rather than vertical plane, since it is always the case that the lowest moraines will be older than those which lie inside and up-valley. Therefore, it is the relative positions of sediment-landform assemblages within a cirque-valley system, defined in key areas by type sections or type localities, which is the basis of stratigraphy in mountain areas glaciated by localised ice. For this reason, a morpho-lithostratigraphical approach should be given formal status, as for example, has been done for the Salpausselkä moraines in southern Finland (Rawson et al. 2002).

The nature of the glacial record, especially that concerning both sediments and landforms, means that inside of the most extensive glacial phase only glaciations of lesser extent are recorded. Numerous glacial advances may be missing from the sediment-landform record and, in cases where the last glaciation was the most extensive, only recessional deposits from this phase will exist. Exceptions to this rule may occur where older till units are preserved beneath younger till units and, in these circumstances, it is

important to differentiate between the landform and the sediment sequence in deriving the morpho-lithostratigraphy.

Sediments and associated landforms can be subdivided using the established lithostratigraphical hierarchical terms of Group, Formation, Member and Bed. These basic subdivision units are arbitrary units of convenience, and the use of these words will depend on the area under consideration and the field conditions under which the area was first mapped (Matthews 1984). These terms are therefore applied according to the spatial scale of this research and their application is described briefly below.

a) Beds

Beds represent individual sediment units that are considered to have formed during the same depositional event. Bed units are applied in a broad sense so that interbedded sands and silts, for example, would be classified as one unit. In a particular locality, for example in the hypothetical Lower Valley (LV), a section may comprise the following beds:

<i>(top)</i> 100-150 cm	<i>Unit LV4:</i> diamicton.
70-100 cm	<i>Unit LV 2:</i> interbedded sand and silts
<i>(base)</i> 0-70 cm	<i>Unit LV 1:</i> diamicton

Where multiple sections are logged, then beds could be subdivided by locality *e.g.* *Unit LVa* 1,2,3....., *Unit LVb* 1,2,3....., and so on. It is important to note that the term 'unit' has no stratigraphical significance and is used merely to describe any body of related sediment such as a bed and can be applied at any level of the stratigraphical hierarchy.

b) Members

Where a number of bed units are formed by similar processes, then the beds may be grouped as part of a member. Sediments which make up a member may be defined by a type section or type locality. Several type sections may best describe a member since one exposure may not give a full representation of all the components of the sedimentary sequence. Also, numerical ordering of members is avoided since further units may be discovered in future. Members could include different landform-sediment associations at different positions in a valley and, for example, two different members at different morphostratigraphical positions in the valley could be called the *Lower Valley Member* and the *Upper Valley Member*.

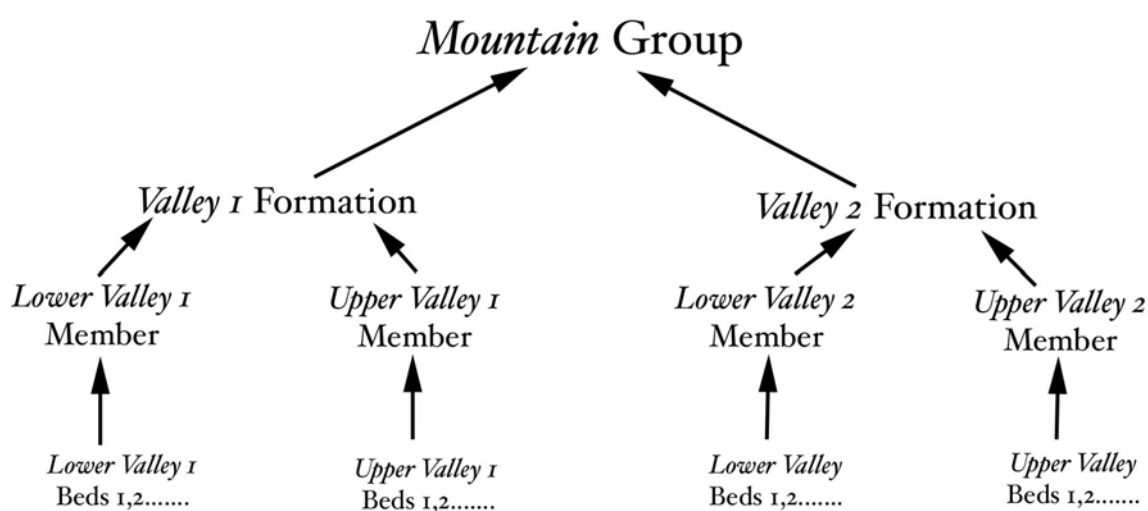


Figure 3.10 The hierarchical stratigraphical framework based on two simple valleys.

c) Formation

A Formation would include all members from a particular cirque-valley system. For example, all the members in Valley 1 could be called the *Valley 1 Formation*.

d) Group

This would include all the formations of a massif or range of mountains. So, for example, in the Pindus Mountains all the glacial deposits could form part of the *Pindus Group*.

This approach enables the glacial sequence to be systematically sub-divided and a hypothetical lithostratigraphical framework is shown in Figure 3.10. If, as is often the case, the upper valley area is characterised by multiple cirques or tributary valleys, then the approach can still be applied. In these circumstances, multiple members can be identified and grouped together in the stratigraphical sequence.

The morpho-lithostratigraphical approach described above is the most logical approach in locally glaciated areas, although it does result in the designation of numerous formations at small spatial scales, *i.e.* in every glaciated cirque-valley system. An alternative approach would be to define type sections for inter-valley formations. For example, the lowest deposits in a sequence, characterised by a particular type section, could be identified where it occurs in multiple valleys as the same formation. If three distinct stratigraphical units of deposits occur in all valley systems within a particular region, then three formations, stacked in time one above the other, would exist in this method of classification. However, in glacial systems, since the glaciers which ultimately formed these deposits are independent of each other, it is questionable as to whether deposits in

different valley systems should be viewed as part of the same formation. This creates a spatial component which is likely to lead to erroneous aggregations of units into the same formation. This is especially the case in marginal glacial environments where local controls potentially exert considerable influence on the local valley-system chronostratigraphy. Inter-valley correlations should therefore only be attempted once the stratigraphy is established independently for each separate cirque-valley system.

In the following chapters, Chapters Four and Five, the geomorphological and sedimentological evidence is described and then interpreted in each cirque-valley system. This provides the morpho-lithostratigraphical basis for a chronostratigraphical and geochronological framework for the glacial sequence in Greece. This is fundamental in any efforts towards reconstructing Quaternary glacial environments and is the focus of the subsequent chapter, Chapter Six.

Chapter Four

Geomorphological and sedimentological evidence – Mount Tymphi

Although not the highest, Mount Tymphi is by far the most complex of all three mountains investigated in this thesis. This is partly a result of the limestone lithology and the local tectonics. However, a major factor in the shaping of this mountain has been widespread glacial action - the most widespread of all three mountains. This chapter presents the evidence for glaciation on Mount Tymphi, beginning with the Tsepelovo area on the south side of the mountain.

4.1 The Tsepelovo area

The Tsepelovo area consists of a major valley system which encompasses Tsepelovo village and extends down to the Voidomatis river (Fig. 4.1). Above the village the valley is known as the Laccorponi valley and this is fed by two higher valley-cirque systems, the Laccos Tselon and Laccos Megalon Litharion (laccos (greek) = valley). This area is therefore subdivided into the three areas: the Laccorponi and lower Tsepelovo areas; the Laccos Tselon; and the Laccos Megalon Litharion.

4.1.1 The Tsepelovo village area and the Laccorponi valley

Boulder-covered ground, enclosed on either side by ridges, extends down to the modern banks of the Voidomatis river at an altitude of *ca.* 850 m a.s.l. In this area, the ridges are subdued in form and sections are provided by the numerous natural exposures on the channel margins and along a track leading from Tsepelovo village to the river. A section photograph and sedimentary log of the sequence exposed at the banks of the Voidomatis river (39°53'30"N, 20°50'01"E, 860 m a.s.l.) are given in Figures 4.2 and 4.3. The units displayed in this sequence represent part of the **Voidomatis Member** and the section is one of three sections by which this member can be defined and is named type section Va.

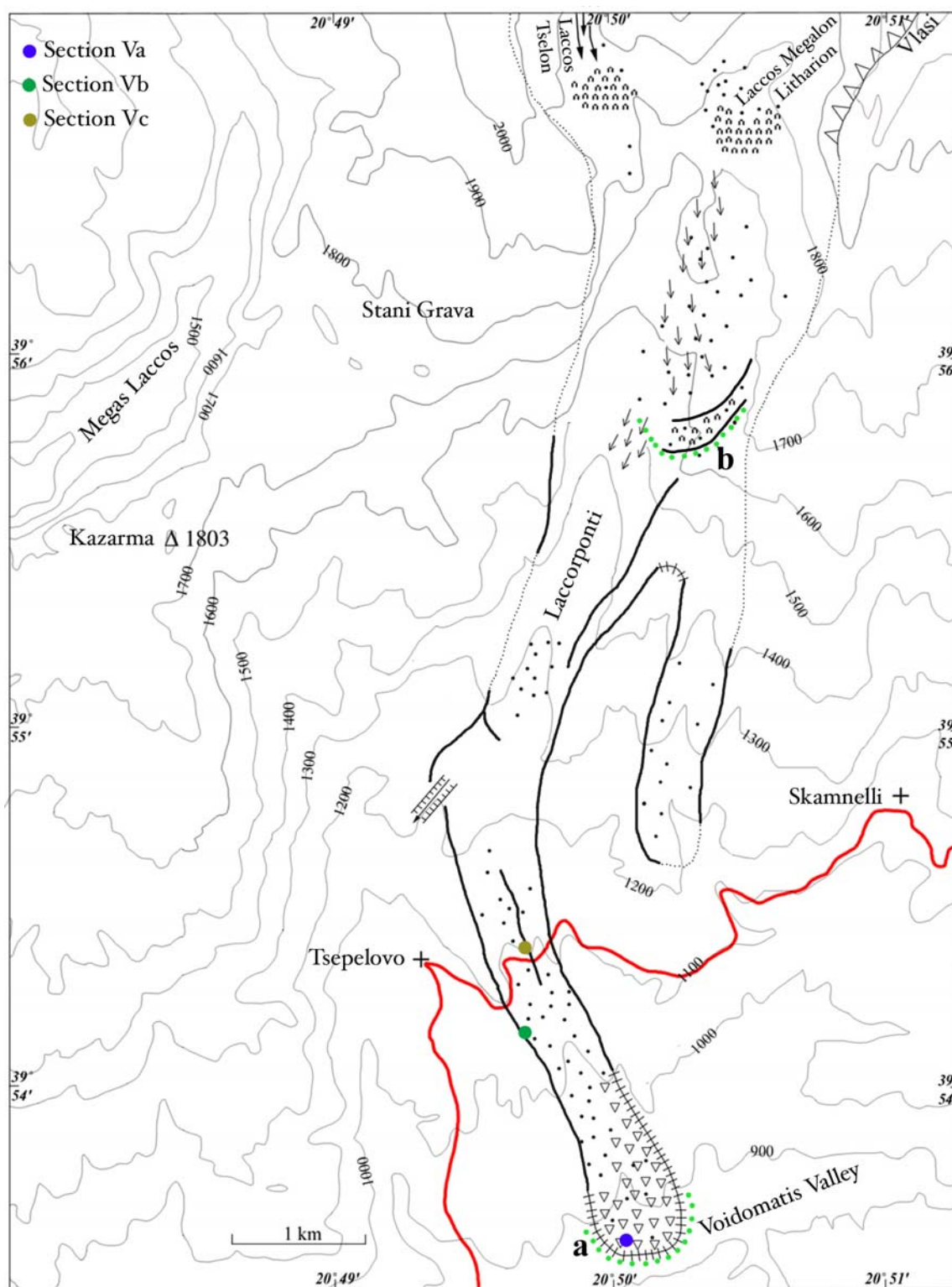


Figure 4.1 Geomorphological map of the Lower Tsepelovo area and the the Laccorponi valley. A key is provided in Figure 3.4. All deposits marked are part of the Tsepelovo Formation. Stratigraphical units: **a.** Voidomatis Member, **b.** Laccorponi Member.

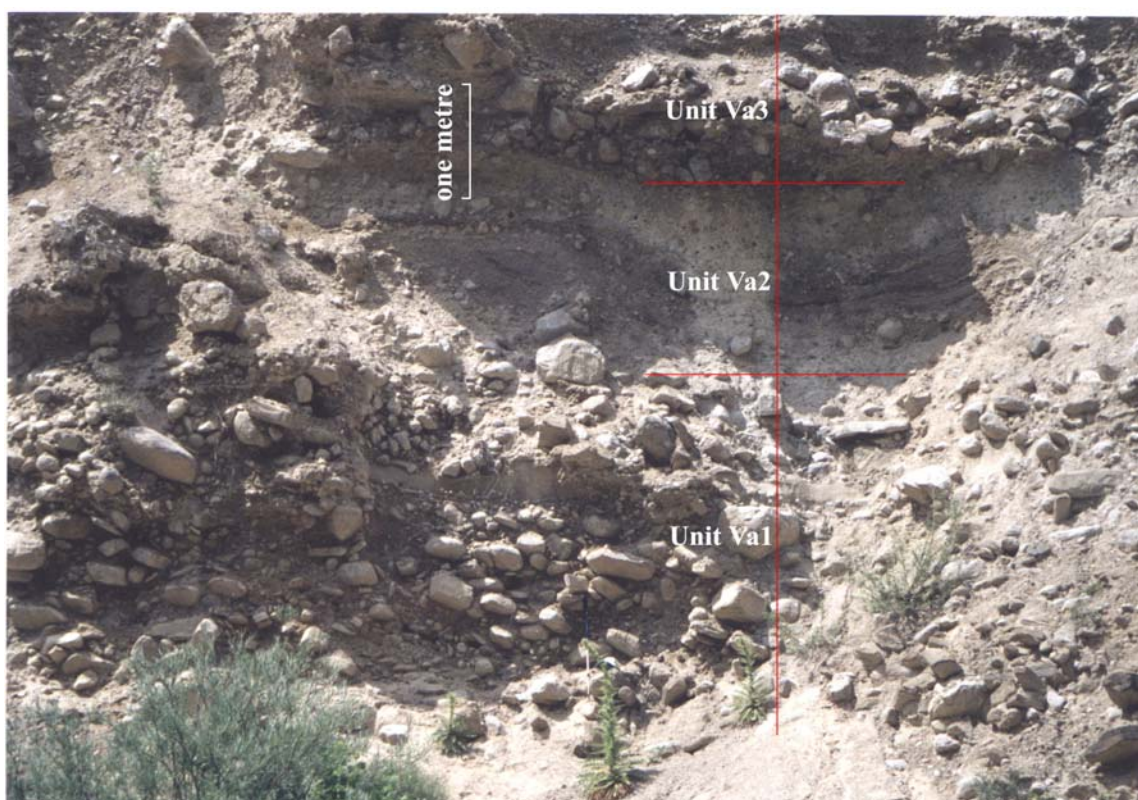


Figure 4.2 Section photograph of the Voidomatis sedimentary sequence (section Va). (39°53'30"N, 20°50'01"E, 860 m a.s.l.) (October 2001). The location of this section is shown in Figure 4.1.

Section Va

0 - 3.4 m *Unit Va1.* This unit is largely a massive clast-supported diamicton (clast density > 60%) and the results of clast analyses are shown in Fig. 4.4. The clast fabric is relatively weak (S_1 : 0.523, S_2 : 0.332, S_3 : 0.145) with a mean lination vector of 350.2°/ 6.6°. The mean a-axis of 50 clasts measured at random was 7.9 cm and the mean of the 10 largest clasts was 14.9 cm. The clasts can therefore be described as cobbles and are predominantly subrounded (rounded [R]: 20%, sub-rounded [SR]: 50%, subangular [SA]: 20%, angular [A]: 10%) with 60% showing evidence of surface striae. The bedrock in this area is flysch. However, 90% of the clasts in this diamicton were limestone and only 20% flysch. Whilst being clast-supported, it is interesting to note that the silt/clay matrix is generally thicker and more conspicuous on the upper sides of the clasts. Also, a sand lens, *ca.* 20 cm thick, occurs within this diamicton. The sand is massive and laterally discontinuous.

3.4-4.9 m *Unit Va2.* This unit is separated from Va1 by an erosional contact. From 3.4-4.1 m stratified fine/medium sands (54% sand, 18% silt, 28% clay) are

present and contain numerous dropstones. This grades into laminated silty clays (10% sand, 44% silt, 46% clay) between 4.1-4.5 m. The silty clays are composed of 60% calcium carbonate, 37% non-carbonate minerals and only 3% organic. These silty clays were analysed for pollen but were found to be barren with only a limited number of unidentifiable degraded grains. The silty clays are topped by fine/medium sands (4.5-4.9 m), similar to those described at the base of this unit, and again contain numerous dropstones.

4.9-6 m *Unit Va3*. The whole of this unit can be described as a stratified matrix-supported diamicton (clast density *ca.* 25%) and is separated from Unit Va2 by a clear erosional boundary. Clasts and matrix were not analysed in this unit because of their inaccessibility. However, clast concentrations vary laterally and vertically within crudely stratified layers of *ca.* 30-40 cm thickness.

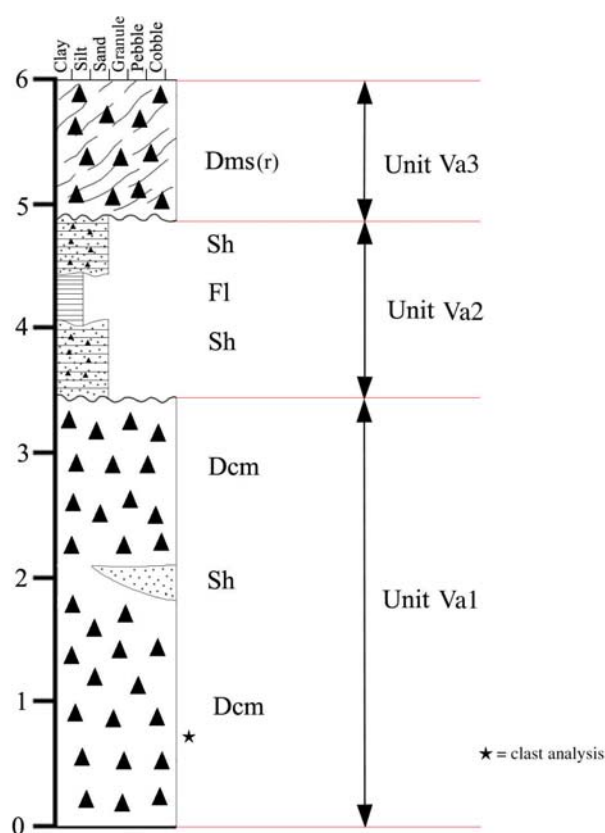


Figure 4.3 Lithological log of the sediments at section Va on the banks of the Voidomatis (39°53'30"N, 20°50'01"E, 860 m a.s.l.). A key is provided in Figure 3.5.

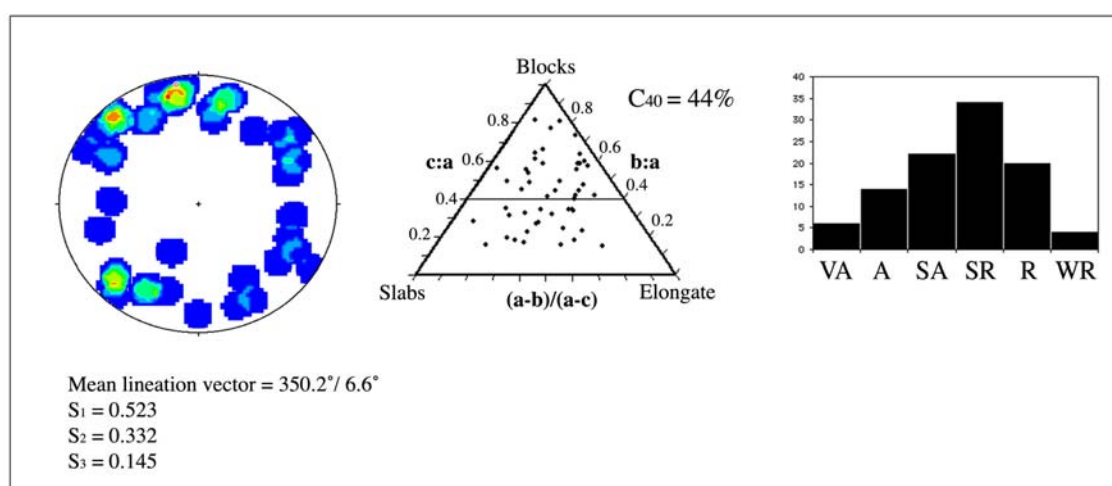


Figure 4.4 Clast analyses from the Voidomatis section (Va). A key to the fabric diagram is provided in Figure 3.6.

The boulder-covered ground and ridges in the lower Tsepelovo area have been interpreted as glacial moraines (Lewin *et al.* 1991, Woodward *et al.* 1992) and this interpretation is supported by the sediments described in section Va. Unit Va1 has the characteristics of a melt-out till in that it is coarse and contains sand lenses. The sub-rounded nature of the clasts and the high percentage of striated clasts suggest that the till is of subglacial origin and can therefore be described as subglacial melt-out till. However, the C_{40} index of 44% (Fig. 4.4) shows that a significant proportion of the clasts were slab or elongate in shape (*i.e.* disc- or rod-shaped). This is because of the presence of flysch clasts (20%) which consist of thin beds of graded sandstones (10-20 cm) intercalated with softer, fissile siltstones (Lewin *et al.* 1991) and break up to form clasts with low $b:a$ and $c:a$ ratios. The clast fabric mean lineation vector is consistent with ice movement from the north-northwest. However, the clast fabric strength is weak ($S_3 = 0.523$) and the low isotropy ($S_3:S_1 = 0.28$) and low elongation ($1 - (S_2:S_1) = 0.37$) of the fabric shape is characteristic of compaction and clast interaction during melt-out (Lawson 1979, Benn 1994a). Moreover, the lack of matrix and the presence of silt and clay, preferentially on the upper sides of clasts, possibly results from leaching by escaping porewater during melt-out (*cf.* Lawson 1979, Lundqvist 1989).

The sands and silty clays of Unit Va2 indicate deposition within slow-moving water, possibly in ponds formed by the melt-out of a stagnant ice block. The numerous dropstones within the stratified sands are probably derived from the coarser deposits on the pond margin which have rolled into the ponded basin.

Unit Va3 is interpreted as a flow till, and the lateral variation in the clast concentrations and the crude stratification within this unit are suggestive of pulsed

sediment flow into the basin containing Unit Va2 (*cf.* Benn and Evans 1998, p.409). The sediment sequence therefore represents a classic ice-marginal ablation sequence with firstly, the deposition of subglacial melt-out till, followed by the deposition of sands and silts in ponds formed by ice-block melt-out *in-situ*, and then by flow tills which flowed in pulses into the basin left by the melted ice.

An excellent exposure in diamicton (*ca.* 3 m thick) exists on the new Tsepelovo 'bypass' (39°54'07"N, 20°49'40"E, 1060 m a.s.l.) (Fig. 4.5), and has been named section Vb. The sediment can be described as a matrix-supported diamicton with a clast density of only 10%. The matrix contains predominantly clay fines (50% clay, 28 % silt, 22% sand). The results of the clast fabric, shape and roundness analyses are shown in Figure 4.6. Nearly half of the 40 clasts sampled were largely striated (46%) and the majority were block-shaped as indicated by the low C_{40} value (25%). Many of the striated clasts are bullet shaped, or *stoss-and-lee* clasts, with smoothed stoss- and fractured lee-sides. Clast roundness is evenly spread between angular and rounded. The clast fabric results indicate a reasonably strong fabric ($S_1 = 0.603$, $S_2 = 0.214$, $S_3 = 0.184$) with a mean lineation vector of 343/5.6°.



Figure 4.5 Section Vb on the Tsepelovo Bypass (39°54'07"N, 20°49'40"E, 1060 m a.s.l.) (October 2001).

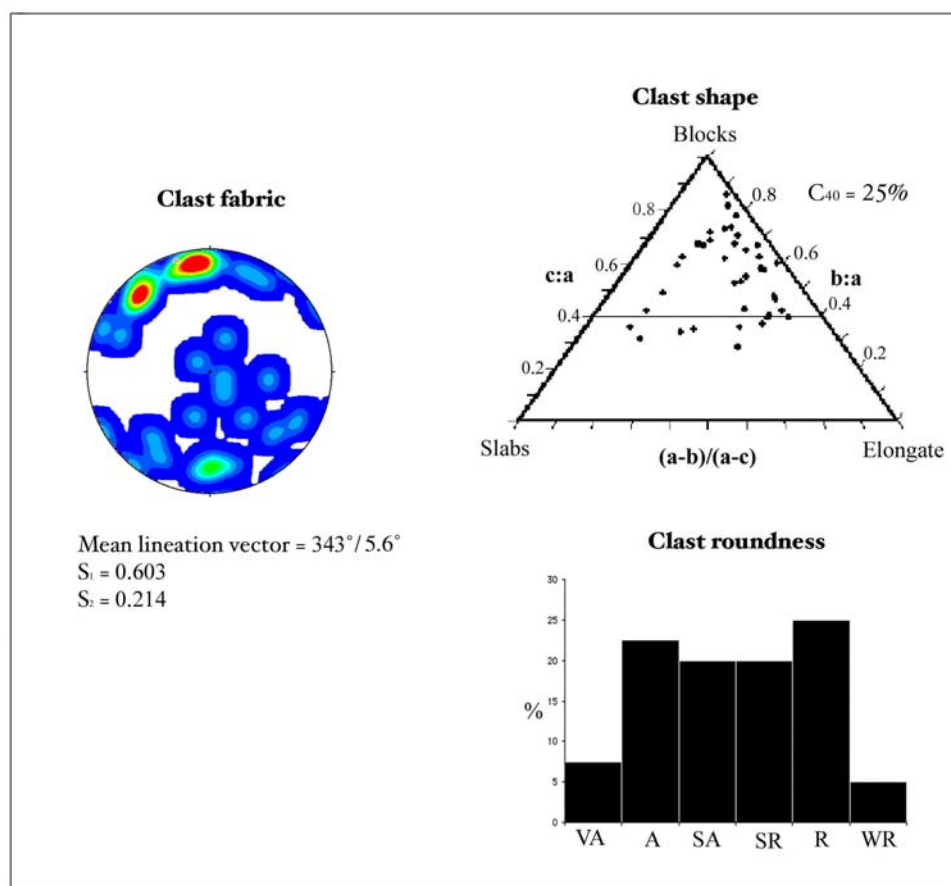


Figure 4.6 Clast analysis results for the Tsepelovo bypass till (section Vb). A key to the fabric diagram is provided in Figure 3.6.

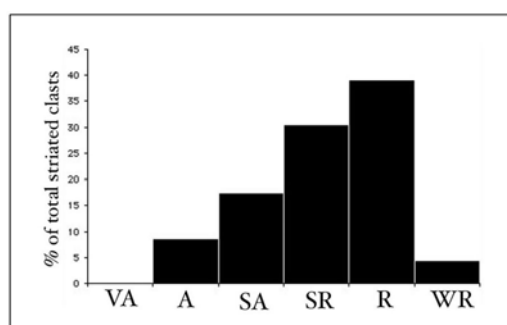


Figure 4.7 The percentage of total striated clasts in each roundness division (section Vb).

The fine matrix, as well as the striated nature of many of the clasts suggest that the sediment is a subglacial till, and the clast fabric orientation is consistent with ice-movement from the north-northwest, from the Laccorponi area. The high percentage of clay fines indicates clast crushing during subglacial transport (Boulton *et al.* 1974). The unstriated, angular clasts within this till have probably not travelled far in the subglacial zone and are likely to have been incorporated only a short distance up-valley. This is because the sediment body forms part of a lateral moraine, where it is likely that a significant proportion of clasts were transported by passive flow (*i.e.* from valley sides, or



Figure 4.8 The Tsepelovo buried soil. This soil rests above the diamicton unit Vb (interpreted as till) and is covered by an angular diamicton (interpreted as colluvial deposit). The pole is one metre long. (*ca.* 39°54'13"N, 20°49'36"E, 1092 m a.s.l.) (July 2001).

supraglacial). Figure 4.7 shows that the majority of striated clasts are subrounded or rounded, suggesting active transport for these clasts and passive transport for the subangular and angular clasts.

Around 200 m along the road towards Skamnelli, sections reveal a buried soil lying above a matrix-supported diamicton and beneath a clast-supported diamicton (*ca.* 39°54'13"N, 20°49'36"E, 1092 m a.s.l.) (Fig. 4.8). The soil is *ca.* 1 m thick and has a reddish-brown colour (Munsell: 2.5YR 3/2). It is laterally extensive, visible along the road-cutting for more than 60 m and, where it is exposed at the present land surface, appears to be subject to pedogenic processes. The magnetic susceptibility, iron oxide, clay, CaCO₃ and organic content of the soil profile, and the use of these soil characteristics in providing

a relative-age for the underlying diamicton, are discussed in Chapter Six. The lower diamicton can be traced along the roadside to section Vb, described earlier. The upper diamicton consists of clast-supported angular gravels.

Since the lower diamicton is laterally contiguous with the diamicton at section Vb, it is interpreted in the same way - as a subglacial till. The upper diamicton, above the buried soil, probably represents a colluvial deposit given the angularity of the clasts and the lack of matrix.

Due east of Tsepelovo village, three well-defined lateral moraines are evident (Fig. 4.1). The morphology of the moraine crests is clear, and the two outermost moraines extend southwards towards the Voidomatis river where their morphological clarity diminishes. These moraines are dissected by the main Tsepelovo-Skamnelli road revealing excellent till sections (Woodward *et al.* 1992, Fig. 6). The sedimentology of a quarried section just outside of Tsepelovo (39°54'20"N, 20°49'40"E, 1100 m a.s.l.) is described below (section Vc). The section is illustrated in Figures 4.9, 4.10 and 4.11 and the results of clast analyses shown in Figure 4.12.

Section Vc

- 0-2 m** *Unit Vc1.* This unit is a matrix-supported diamicton. Clast density is *ca.* 5% with a mean a-axis of the 10 largest clasts of 28 cm. The clast fabric strength is fairly strong (S_1 : 0.618, S_2 : 0.262, S_3 : 0.120) with a mean lineation vector of 310.9°/9.0°. The matrix is predominantly limestone rock flour (85% calcium carbonate) comprising 47% sand, 28% silt and 25% clay. The majority of clasts are striated (64%), display well-developed abrasional facets and are largely block-shaped (C_{40} index: 18%).
- 2-2.4 m** *Unit Vc2.* Massive sands characterise this thin unit (51% sand, 33% silt, 16% clay). The sands contain very little organic material (< 1%) and are composed primarily of calcium carbonate (79%). The upper and lower contacts are both erosional and the bedding plane of this unit has a dip angle of *ca.* 42° and dip direction of 242° SW.
- 2.4-5.2 m** *Unit Vc3.* This unit is similar to Vc1 in that it is a matrix-supported diamicton. However, clast density is greater at *ca.* 25% and the largest clasts are much bigger (mean a-axis of the 10 largest clasts: 45cm). As with Vc1, the clast fabric is fairly strong (S_1 : 0.663, S_2 : 0.195, S_3 : 0.142). The clasts

are largely subrounded (R: 12%, SR: 48%, SA: 26%, A: 14%), block-shaped (C_{40} index: 14%) and striated (78%).

- 5.2-5.6 m** *Unit Vc4.* This unit is a sand bed, similar to Vc2 and has a dip angle of *ca.* 36° and dip direction 238° SW with erosional contacts between both the upper and lower unit. This sand unit is highly variable laterally and is nearly 1 m in thick in places.
- 5.6-7.6 m** *Unit Vc5.* This unit is a matrix-supported diamicton. Details of the sedimentology are scant due to its position in the sequence. However, on visual inspection, it closely resembles Unit Vc1 and has a similar clast density of *ca.* 5%.
- 7.6-9 m** *Unit Vc6.* This unit is a clast-supported diamicton grading into Unit Vc5. Clast density is *ca.* 40-45% and fabric strength weaker than in Units Vc1 and Vc3 (S_1 : 0.510, S_2 : 0.354, S_3 : 0.136). The clasts are angular with 68% angular to very angular (SR: 32%, SA: 38%, A: 18%, VA: 2%) and largely block-shaped, 34% of which display striae.

The basal diamicton, Unit Vc1, is characterised by predominantly subrounded block-shaped clasts. This, and the fact that the majority of clasts are faceted and show evidence of striae, suggests that the diamicton is of subglacial origin and the result of largely active flow at the basal layer. The sediment, probably originally a lodgement till, has subsequently been deformed. The clast fabric results for Unit Vc1 show that the fabric is quite strong since the eigenvalue S_1 is much greater than S_2 and S_3 . The mean lineation vector of 310.9/9.0° does not necessarily reflect ice flow direction because it could reflect relative strain in a deforming layer (*cf.* Bennett *et al.* 1999). Hart (1994) suggests that strong fabrics within deformed diamictons reflects deformation within a thin basal layer. However, this is thought to be an oversimplification by Benn and Evans (1998) since fabric organisation can vary within a single deforming layer of uniform thickness. The Unit Vc1 clast fabric has low isotropy and moderate elongation (S_3/S_1 : 0.19, $1-(S_2/S_1)$: 0.58) and is characteristic of sediments which have undergone brittle rather than ductile deformation (*cf.* Hart 1994, Benn 1994b, 1995). Overall, however, cumulative strains must have been quite low since the sediment is not totally homogenised (*cf.* Benn and Evans 1998, p. 390-394).

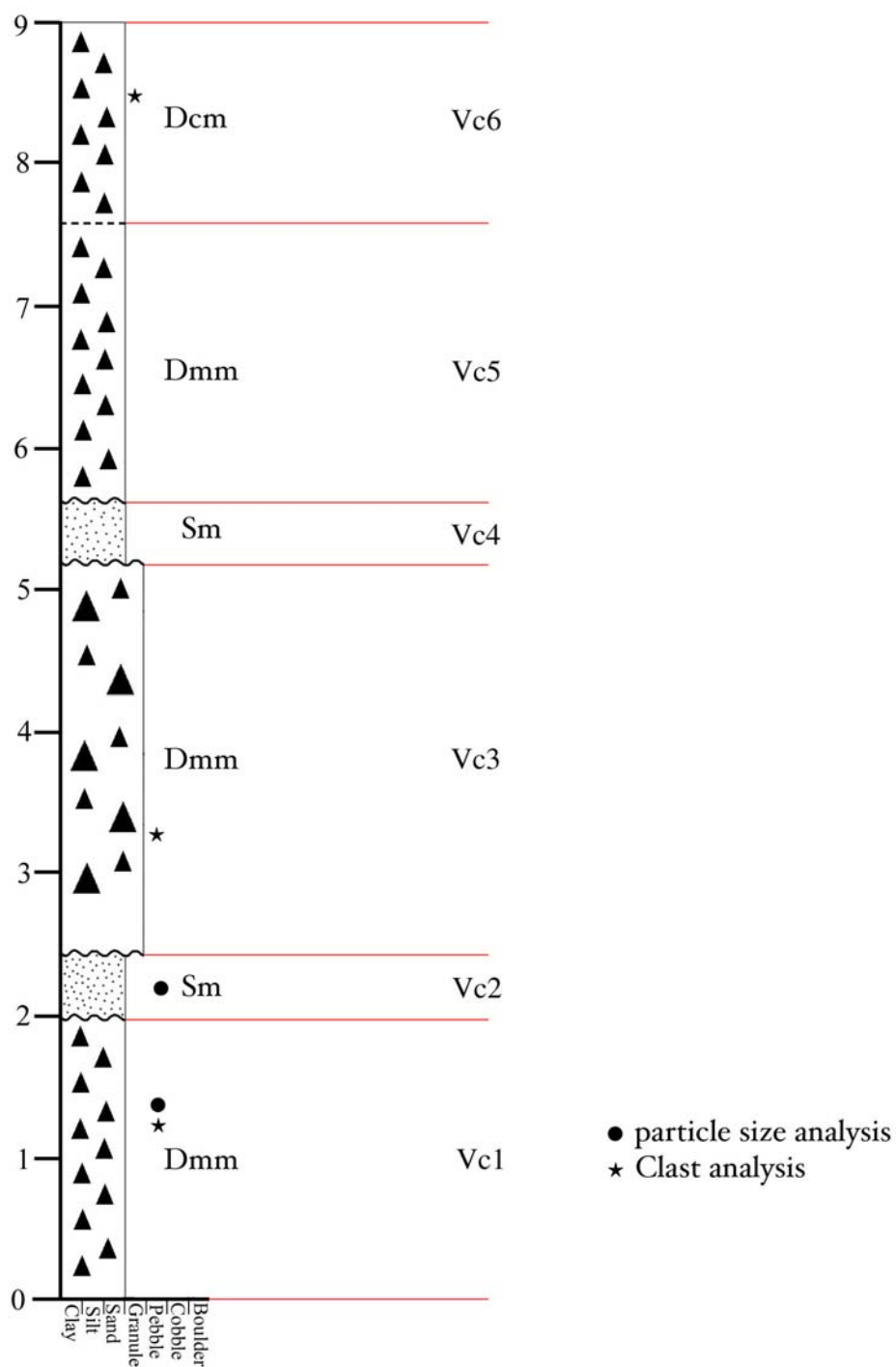


Figure 4.9 Sediment log from section Vc on the road from Skamnelli to Tsepelovo (39°54'20"N, 20°49'40"E, 1100 m a.s.l.). A key is provided in Figure 3.5.

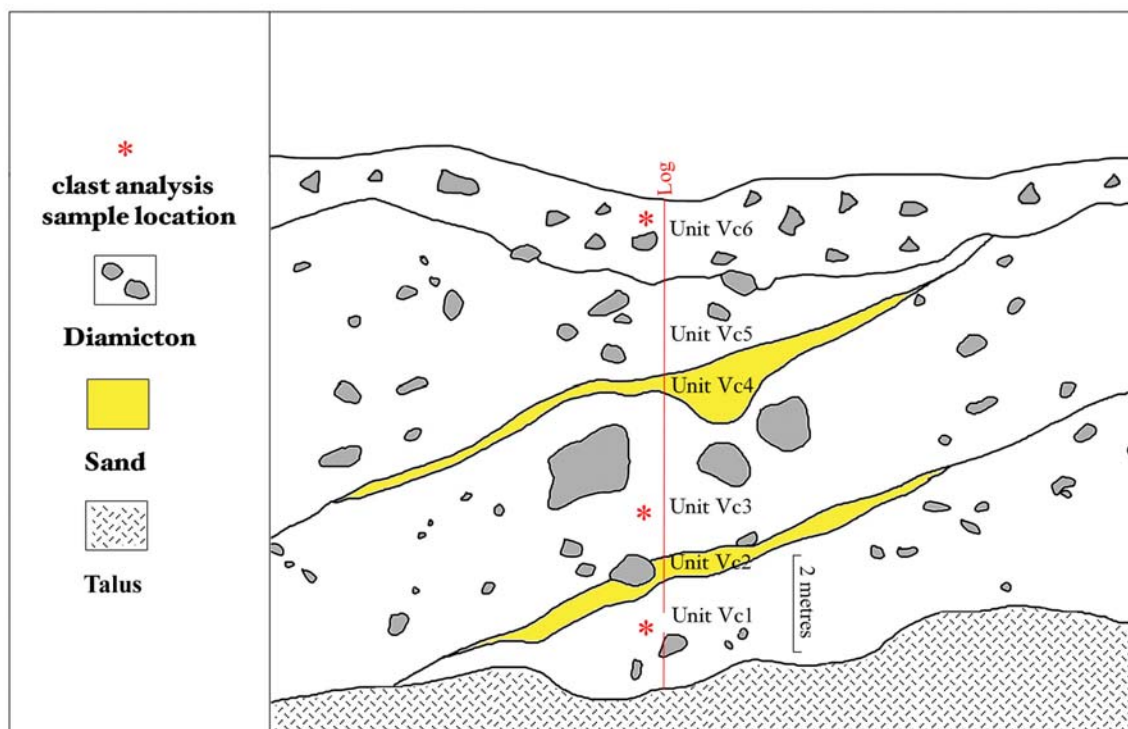


Figure 4.10 Schematic sketch of the Tsepelovo-Skamnelli road section (Vc). (39°54'20"N, 20°49'40"E, 1100 m a.s.l.).



Figure 4.11 Photograph of the Tsepelovo-Skamnelli road section (Vc). (39°54'20"N, 20°49'40"E, 1100 m a.s.l.). The was section logged vertically around the position of the yellow measuring tape. The two sand units Vc2 and Vc 4 are clearly evident above and below the large boulder clasts in the centre of the picture.

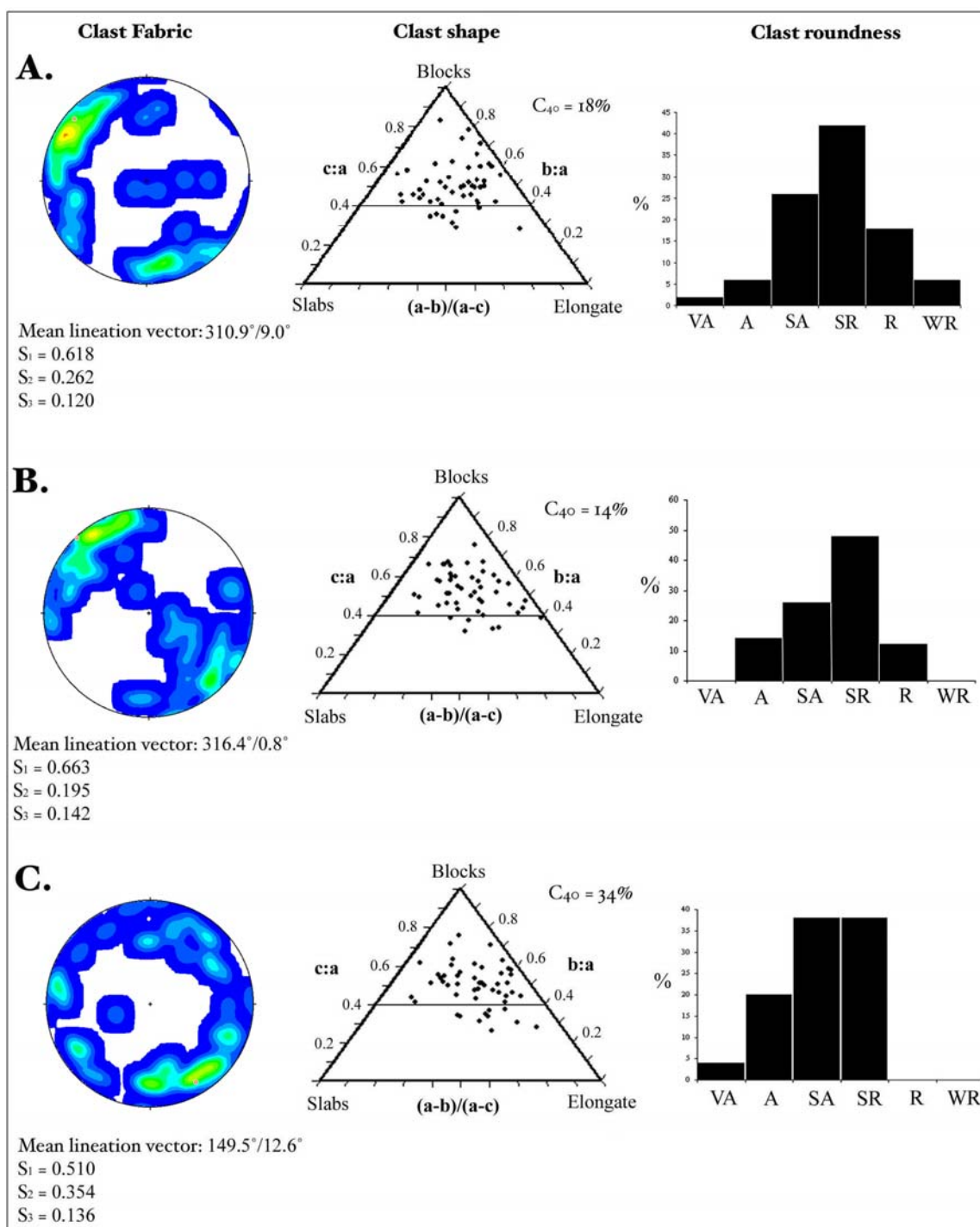


Figure 4.12 Clast analyses from units Vc 1 (A.), Vc 3 (B.) and Vc 6 (C.) in the section Vc on the road from Tsepelovo to Skammelli. A key to the fabric plots is given in Figure 3.6.

The inorganic carbonate sand bed of Unit Vc2 possibly formed in the proglacial zone, in a lacustrine or low-energy glacio-fluvial environment, as the glacier which deposited Vc1 retreated. The erosional lower and upper boundaries, as well as the angle of the bedding plane, indicate that the sand unit has been truncated and deformed.

The matrix-supported diamicton of Unit Vc3 possibly represents glacial readvance. The fairly strong clast fabric, the subrounded, block-shaped and striated clasts as well as the fact that the lower units Vc1 and Vc2 are deformed, supports this interpretation. The mean lineation vector show that the clasts dip north-northwest, up-valley, and this is consistent with ice-flow from the Laccorponi area.

Unit Vc4 is similar to Vc2 and again probably represents proglacial deposition as the glacier which deposited Unit Vc3 retreated. However, the unit could equally represent deposition in sub- or englacial cavities. This unit is truncated and deformed and would appear to be the result of glacier readvance and deposition of Unit Vc5. The latter unit is interpreted as a till, similar to Vc3, although detailed clast analysis was not possible because of the inaccessible position in the sequence.

Unit Vc6 is clast-supported diamicton. The clast fabric is relatively weak (S_1 : 0.510, S_2 : 0.354, S_3 : 0.136) and the clasts dip in a down-valley direction (149.5°) unlike the lower units Vc1 and Vc 3 which have strong fabric in the up-valley direction. The weak clast fabric and angularity of the clasts in this unit support an interpretation of this unit as a supraglacial melt-out till with fabric related to slope and not former ice direction. In addition, the fact that this unit also forms the surface profile of a large moraine ridge, aligned parallel to former ice flow in the middle of the valley (Fig. 4.1), suggests that the surface landform is a medial moraine.

In summary, a possible sequence of events could be as follows. Unit Vc1 was deposited by an extensive valley glacier which subsequently retreated resulting in the deposition of proglacial sands in Unit Vc2. Glacial readvance resulted in the deposition of Unit Vc3 and the deformation of units Vc1 and Vc2, including the partial erosion of the latter unit. Glacier retreat resulted in the deposition of proglacial sand and Unit Vc4. A third glacial phase resulted in the deposition of Unit Vc5, the partial erosion of Unit Vc3 and the deformation of the underlying sediment. The top diamicton unit Vc6 probably formed during glacier retreat and may represent melt-out of supraglacial medial debris.

Whether this sequence reflects oscillation of the ice margin during one glacial phase or renewed ice build-up during different glacial phases is difficult to establish. Whilst the sediment-landform association represents one glacial phase, the sediment sequence may record multiple phases of glaciation. However, in stratigraphical terms, whether a diamicton deformed during the deposition of overlying units, represents part of the same stratigraphical member as these overlying units is open to debate. Since the present form of the deformed unit is the result of processes active during the deposition of the overlying units, it could be argued that the collective sequence represents part of the same sediment

body. Taking this approach, the whole sedimentary sequence can be viewed as part of the Voidomatis Member and the individual units of section Vc as component beds.

The Laccorponi valley is north of Tsepelovo village. The eastern side of this valley is bounded by a boulder-covered ridge which has a very high proximal slope (over 100 m high). The proportion of this slope which is bedrock is difficult to judge in the field, although the distal slope is somewhat smaller reaching only *ca.* 50 m in height. The western side of the valley contains a smaller ridge *ca.* 1 km in length and 50 m in height and the continuation of this ridge southwards is broken by a incised channel. Higher up-valley, boulder-covered ridges also exist on top of the western valley cliffs.

The boulder-covered ridges in the Laccorponi valley are interpreted as moraine ridges formed by a valley glacier. The incised channel in the moraine above Tsepelovo is mapped as a meltwater channel in Figure 4.1. However, it may also represent post-glacial fluvial erosion - or both.

Boulder-covered ridges, *ca.* 10-20 m high, east of the main Laccorponi valley are interpreted as moraine ridges and provide evidence of a smaller former off-shoot glacier in this area. It is also possible that these moraines were formed from ice coming from the neighbouring Vourtapa valley to the east (Fig. 4.15). The former interpretation is preferred since there is little direct geomorphological or sedimentological evidence of glacial activity between the upper parts of these moraines and the Vourtapa valley.

The upper Laccorponi valley is characterised by large areas of limestone pavements and extensive, well-defined, boulder-covered ridges. In places, the sedimentology of these ridges is exposed revealing matrix-supported diamictos containing striated and polished clasts varying in size from pebble- to boulder-size. These sediments and landforms represent the type locality of the **Laccorponi Member** (39°55'50"N, 20°50'20"E, 1600 m a.s.l.). The ridges are interpreted as terminal and recessional moraines of a mid-valley glacier and the limestone pavements as products of glacial scour. These moraines appear much fresher, *i.e.* the crests are more sharper and well-defined, than the moraines further down-valley near Tsepelovo and recessional moraines are evident as far as the entrance to the Laccos Megalon Litharion valley. The area is a classic example of glacio-karst, and large boulders often rest on these pavements attesting transport by ice. These pavements are also clearly evident in satellite images (Smith *et al.* 2000). The pavements outside of the Laccorponi Member end moraines dip to the south-southwest, whereas those inside of the moraines dip in a south-southeast direction. This probably reflects slightly differing ice directions during different glaciations since the bedding planes of these rocks are similar. The grikes of the inner pavements are also narrower and less

dense, again reflecting less weathering since glaciation in comparison to the outer pavements.

4.1.2 Laccos Tselon

At least two suites of boulder ridges are evident in the Laccos Tselon valley (Fig. 4.13). The lower ridges bound the entrance to this valley and several irregular crests can be identified. These ridges are mapped as hummocky moraine and probably represent a series of recessional moraines. Further up-valley, linear ridges are evident on the valley floor. These are *ca.* 2 m in height and several hundred metres long. They are interpreted as fluted moraine and lie in the lee of a large bedrock *roche moutonnée* and their position is typical of flute formation, down-flow of a bedrock obstacle (Boulton 1976). These lower deposits appear contiguous with the sediments and landforms of the Laccorponi Member.

The upper boulder ridges of the Laccos Tselon lie above the 2000 m contour on both sides of the valley and inside of these, irregular boulder-covered hummocks are present. These deposits are considered to represent a separate and higher stratigraphical unit to those of the Laccorponi Member, lower in the valley. These sediments are recognised as the type locality of the **Tselon Member** (39°57'20"N, 20°50'00"E, 2025 m a.s.l.). The ridges are interpreted as lateral moraines formed at the margins of a cirque glacier and the hummocks as recessional glacial moraines. Immediately outside of these cirque moraines is a concentration of dolines, probably reflecting meltwater action at the snout of the former cirque glacier.

4.1.3 Laccos Megalon Litharion

A lobe of angular boulders exists on the western slopes of the mountain known as Vlasi, in the Laccos Megalon Litharion valley (Fig. 4.13). Several ridges are present and the feature extends down to *ca.* 1850 m a.s.l (39°56'40"N, 20°50'45"E, 1850 m a.s.l.). The sediments at this type locality represent the **Vlasi Member** and are interpreted as a talus rockglacier (Hughes *et al.* 2003).

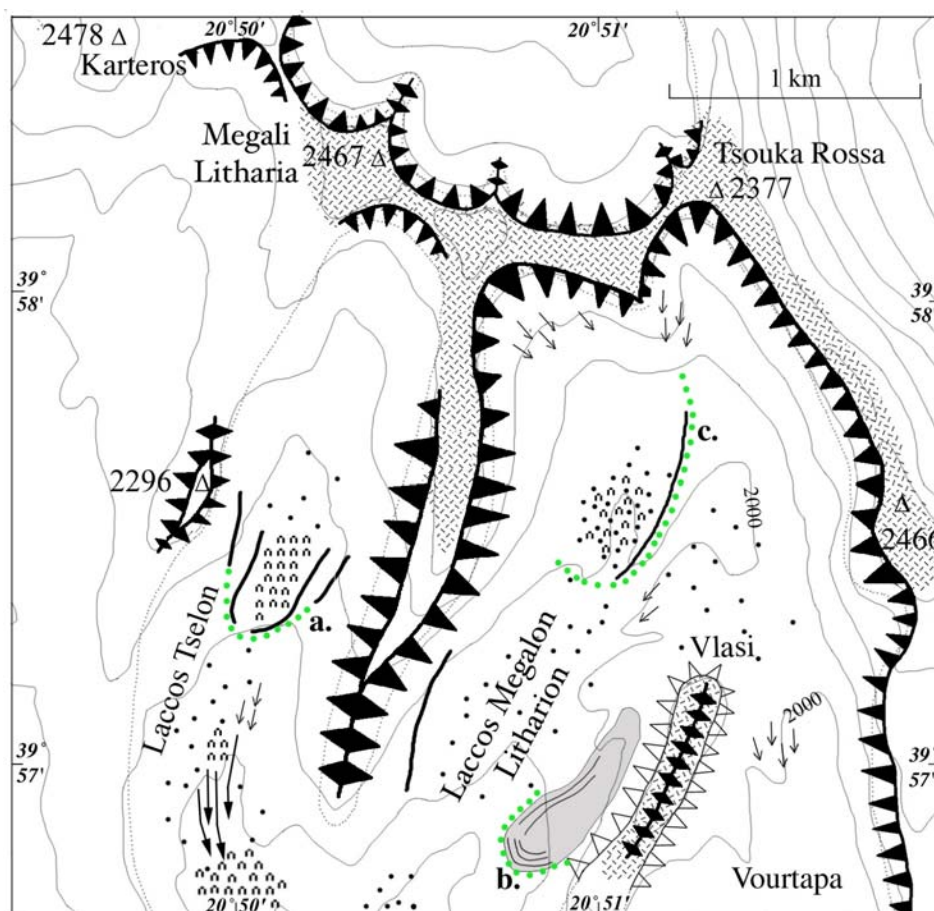


Figure 4.13 Geomorphological map of the Laccos Megalon Litharion and Laccos Tselon areas. A key is provided in Figure 3.4. All deposits marked are part of the Tsepelovo Formation. Stratigraphical units: **a.** Tselon Member, **b.** Vlasi Member, **c.** Litharion Member.

On the western valley-side, a boulder-covered ridge *ca.* 600 m long is evident. The centre of the valley floor is littered with boulders, explaining this valley name, Laccos Megalon Litharion - "Valley of the Big Stones". These boulders and the boulder-covered ridge are clearly glacial in origin and provide impressive evidence of glacial transport and in places are perched on bedrock knolls.

In the upper cirque of the Laccos Megalon Litharion valley, a boulder ridge exists at an altitude of *ca.* 2000 m a.s.l. and is *ca.* 800 m long and > 20 m high. The ridge runs from north to south and arcs slightly to the southwest in its lower parts. Subrounded boulders litter the surface of the ridge and boulder-covered hummocks are present on the cirque-floor to the west. In the upper parts of the cirque, the limestone bedrock is smooth over a wide area. These landforms represent the type locality of the **Litharion Member** (39°57'30"N, 20°51'05"E, 2000 m a.s.l.). The ridge is interpreted as an end moraine, formed in front of a glacier which occupied the cirque to the northwest, and the hummocks as

recessional moraines formed during glacier retreat. This interpretation suggests that the smoothed bedrock in the upper part of the cirque is the result of ice scour.

The upper Laccos Megalon Litharion area represents an accumulation area which fed not only the Tsepelovo glacier system but also the Skamnelli glacier system during the most extensive glacial phases. The lack of a backwall to the Vourtapa valley and the presence of ice-moulded features on the Vlasi-Goura col clearly demonstrate the flow of ice from the upper Laccos Megalon Litharion area either side of the mountain known as Vlasi. This mountain shows no evidence of having been glaciated along its ridge and the bedrock is heavily weathered showing evidence of intense frost shattering along its length (Fig. 4.14). Vlasi is therefore likely to have stood above the ice-surface, directing ice to the southwest and southeast, into the Tsepelovo and Skamnelli glacier systems respectively.

4.1.4 Morpho-lithostratigraphical summary of the Tsepelovo area

The morpho-lithostratigraphy of the Tsepelovo area is summarised below and in Table 4.1. Three stratigraphical units, each defined by a single or multiple type sections or localities, can be recognised on the basis of morpho-lithostratigraphical position.

Unit 1. The **Voidomatis Member**, identified by type sections Va, Vb and Vc, is situated in the lowest valley areas, near to the Voidomatis River and Tsepelovo village. It is characterised by diamictons, interbedded with sand units, which form poorly-defined ridges. Also, a well-developed soil is formed on these diamictons. The lower lateral boundary of this unit is *ca.* 850 m a.s.l. These sediments are interpreted as glacial moraines, till and proglacial associations formed by an extensive valley glacier with a fluctuating frontal margin.

Unit 2. The **Laccorponti Member** is situated in the upper Laccorponti valley, and is characterised by diamicton sections which form well-defined ridges. The lower lateral boundary of this unit is situated at *ca.* 1650 m a.s.l. This unit is interpreted as glacial moraines formed by a valley glacier which reached a mid-valley position.

Unit 3. The **Vlasi, Tselon and Litharion Members** are positioned in the uppermost valley and cirque areas. These members are characterised by diamictons and bouldery ridge-forms

at valley heads and cirques and are interpreted as cirque glacier moraines and a relict rock glacier.

Unit 3	Vlasi Member Litharion Member Tselon Member	TSEPELOVO FORMATION
Unit 2	Laccorponi Member	
Unit 1	Voidomatis Member	

Table 4.1 Morpho-lithostratigraphical summary of the Tsepelovo area.



Figure 4.14 The ridge of Vlasi between the Laccorponi and Vourtapa valleys on Mount Tymphi. This ridge would have stood above ice in each of these valleys during the most extensive glacial phases.

4.2 The Skamnelli area

The Skamnelli area consists of a major valley system below Skamnelli village fed by several higher valleys – the Vourtapa valley and the Vrichos and Tsioumako cirque-valley systems (Fig. 4.15).

4.2.1 The lower Skamnelli area

South of Skamnelli, in the Kato Radza valley, boulder-covered ground extends southwards towards the Voidomatis valley. Surface morphology is subdued in this area, although the ground is littered with large limestone boulders – effectively erratics atop flysch bedrock. Also, diamicton sediments have been temporarily exposed in several areas, such as in construction excavations in Skamnelli village (Fig. 4.17), and are continually exposed in stream cuttings south of the village (Fig. 4.18). Diamictons are evident right down to the banks of the modern Voidomatis river at *ca.* 850 m a.s.l., and in the lowest valley area ridges are evident. These are interpreted as lateral moraines. The former glacier terminus is marked by a drift limit (Fig. 4.15).

Two sections were logged for this area, section SKa (39°54'08"N, 20°50'40"E, 984 m a.s.l.) and section SKb (39°54'05"N, 20°50'36"E, 980 m a.s.l.). Both are described below and illustrated in Figures 4.16 and 4.19. Section SKb is also shown in Figure 4.18. These sections represent the type sections for the **Kato Radza Member**.

Section SKa

- 0-1.4 m** *Unit SKa1.* This unit consists of alternating beds of gravel and coarse sand. Six beds can be recognised, each around 20-25 cm thick. The gravel clasts show signs of imbrication in the downvalley direction. The upper contact with unit SKa2 is erosional.
- 1.4-4 m** *Unit SKa2.* This is a massive matrix-supported diamicton. The deposit has a clast density of *ca.* 15%. The largest clasts in this unit are very large, the largest measuring >150 cm along the a-axis. The mean a-axis of the ten largest clasts is 76 cm and the shape of these clasts is largely subrounded to rounded. All of the larger clasts showed evidence of striae.

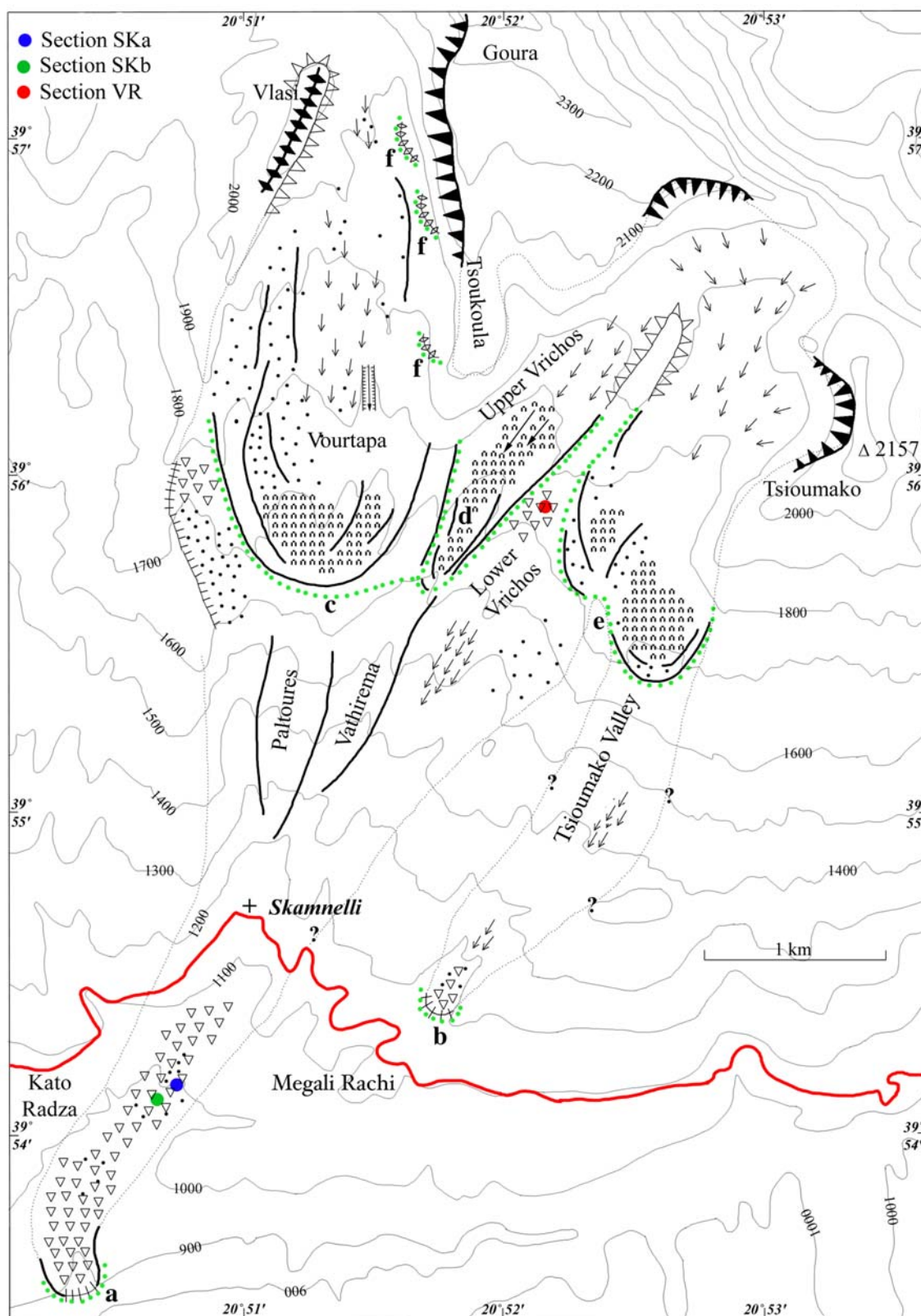


Figure 4.15 Geomorphological map of the Skamnelli area. A key is provided in Fig 3.4. All deposits marked are part of the Skamnelli Formation. Stratigraphical units: **a.** Kato Radza Member, **b.** Megali Rachi Member, **c.** Vourtapta Member, **d.** Vrichos Member, **e.** Corifula Member, **f.** Tsoukoula Member.

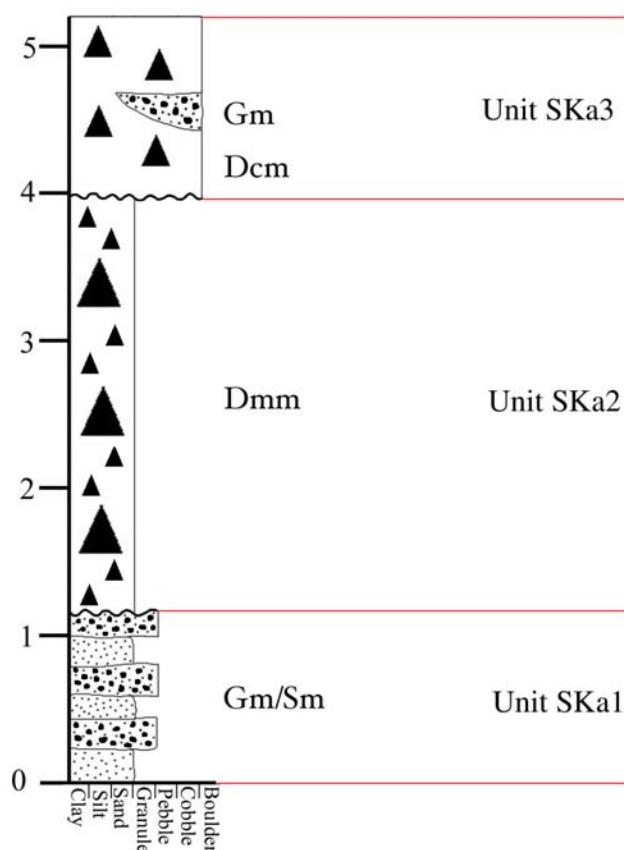


Figure 4.16 Lithological log of the sediments at section SKa, south of Skamnelli (39°54'08"N, 20°50'40E, 984 m a.s.l).

4-5.2 m *Unit SKa3*. This is a clast-supported diamicton containing gravel inclusions. The clast density is ca. 60%. The coarse gravel inclusions are laterally discontinuous and appear graded, coarsening upwards.

The sediments described above are clearly glacial and glaciofluvial in origin. The basal unit, Unit SKa1, can be interpreted as a proglacial sequence in front of a fluctuating ice margin. The proximity of the ice-front and discharge from the glacier may have resulted in different particle sizes deposited at the location of this section. In general, when the glacier front was near, gravels would have been deposited, and when the glacier was more distant, sands would be deposited, due to the contrast in energy. The erosional contact with overlying SKa2 implies the possibility of significant sediment loss from Unit SKa1. This is especially likely given that the diamicton of SKa2 is most probably glacially-derived. Unit SKa2 represents an ice advance over the proglacial gravels. However, no deformation is evident in these gravels - perhaps because they would have been permeable and well-drained, resulting in low porewater pressures and high sediment strength (*cf.* Boulton



Figure 4.17 Diamictic deposits under a house in Skamnelli village viewed from the main road. These deposits are interpreted as till and represent part of the Kato Radza Member (May 2003).



Figure 4.18 Section SKa, south of Skamnelli (ca. $39^{\circ}54'08''\text{N}$, $20^{\circ}50'40''\text{E}$, 984 m a.s.l.). Note the large boulder clasts which are in Unit SKa2 (October 2001).

1987). The topmost unit, SKa3, is most probably a melt-out till. The presence of water sorted gravel lenses within this diamicton supports this deduction.

Section SKb

- 0 - 1.2 m** *Unit SKb1.* Massive clast-supported diamicton. Clast density is > 60%. The clasts are mainly cobbles (mean a-axis of 50 clasts: 7.63 cm) and block-shaped with a C_{40} index of only 18%. Also, 60% of the clasts are striated and 52% are subrounded. The fabric strength is relatively weak (S_1 : 0.528, S_2 : 0.325, S_3 : 0.147) displaying low isotropy ($S_3/S_1 = 0.28$) and low elongation ($1 - (S_2 - S_1) = 0.38$). (Fig. 4.20).
- 1.2 – 1.6 m** *Unit SKb2.* Alternating gravels and sand with an erosional lower contact. The lower medium gravel unit is normally graded (1.2 - 1.3 m). A sand unit into which the lower gravel grades is *ca.* 10 cm thick (1.3 - 1.4 m). A coarse gravel bed lies on top of this sand (1.4 - 1.6 m). This gravel appears massive.
- 1.6 – 2.6 m** *Unit SKb3.* Massive matrix-supported diamicton. Erosional lower contact. Clast density is *ca.* 30%.
- 2.6 - 3.1 m** *Unit SKb4.* Clast supported diamicton. Gradational lower contact.
- 3.1 – 4.1 m** *Unit SKb5.* Massive matrix-supported diamicton. Erosional lower contact. Clast density is *ca.* 30%.
- 4.1 – 5.5 m** *Unit SKb6.* Clast supported diamicton with occasional sand lenses. Gradational lower contact.

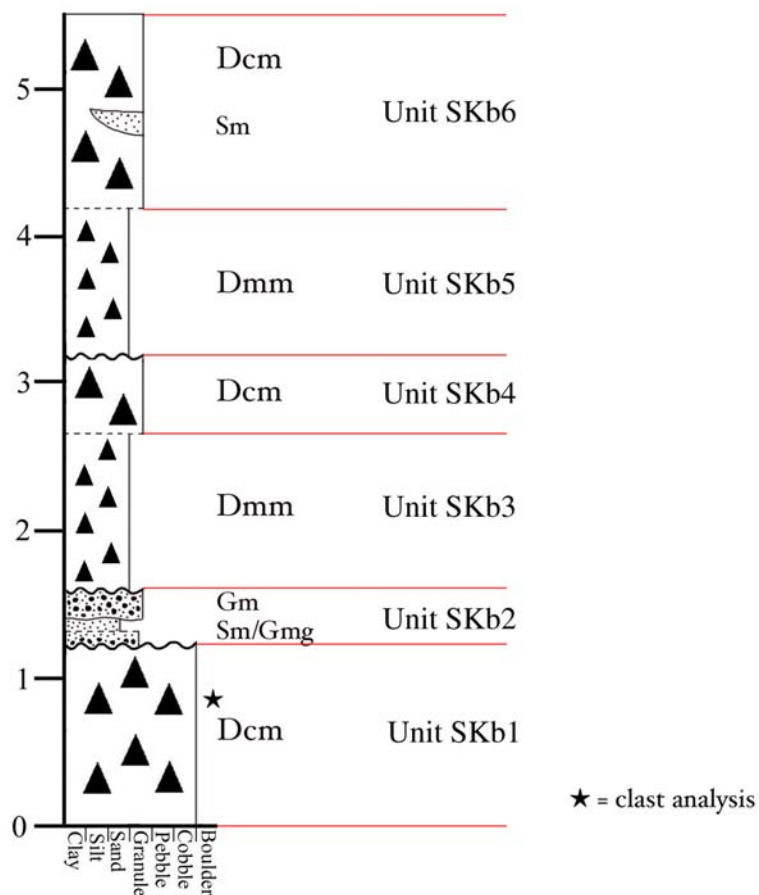


Figure 4.19 Lithological log of the sediments at section SKb, south of Skammelli (39°54'05"N, 20°50'36"E, 980 m a.s.l.).

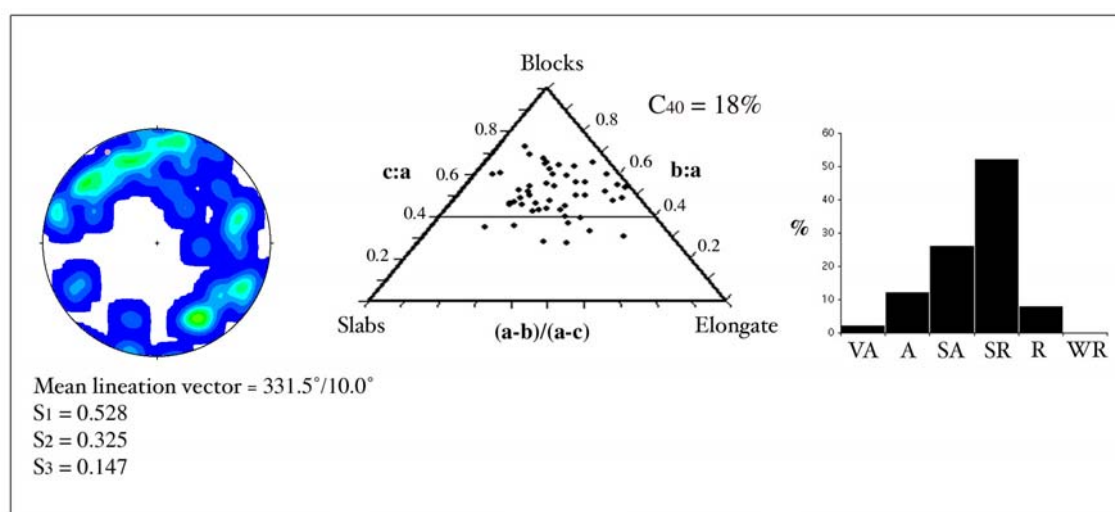


Figure 4.20 Clast analysis from Unit SKb1. A key to the fabric diagram is provided in Figure 3.6.

The subrounded and striated clasts of unit SKb1 suggest that the clasts have undergone active transport. This feature and the poor fabric strength favour an interpretation of this diamicton as a subglacial melt-out till. Compaction during the melt-out process reduces the range of dip values and 'flattens' the fabric, reducing the isotropy. Clast interactions during the melt-out process also weaken the preferred orientation and consequently reduce the elongation (Benn and Evans 1998).

The sands and gravels of unit SKb2 are very similar to those in nearby unit SKa1. It is possible that the lower diamicton unit SKb1 is not exposed in section SKa but lies hidden beneath unit SKa1. These sands and gravels were interpreted as a proglacial sequence in front of a fluctuating ice margin.

The diamicton units SKb3 and SKb4 are interpreted as lodgement tills that grade into melt-out till. These units therefore represent deposition during glacier advance and retreat. The same interpretation is given for the topmost diamictons, units SKb5 and SKb6. The erosional contact between these units and SKb4 suggests that the former glacier would have advanced over this locality, forming SKb5, then retreated forming the topmost melt-out till, SKb6.

Unlike at section SKa, where one glacier advance is recorded, there is evidence here of three glacier advances. Three till units are also recorded in section Vc of the Voidomatis Member. If these units all represent glacier fluctuation during the same glacial stage, then it would appear that the former glacier readvanced on at least three occasions. There is no evidence from the lithological record to suggest that these till units represent different glacial events, and they are regarded here as beds of the same lithostratigraphical member.

In parts of the Kato Radza valley, a reddish-brown (Munsell: 2.5YR 3/2) soil can be found on the surface of the deposits and is similar to that found atop the Voidomatis moraines. The properties of this soil were analysed and the results are described and discussed in Chapter Six.

North of Skamneli, the streams of the Paltoures and Vathirema drain through thick diamicton deposits. At least three major ridges are evident enclosing these streams. These deposits are similar to the topmost diamicton units in sections SKa and SKb and clearly represent glacial deposits. However, it is not clear whether the ridges represent lateral moraines that formed during a period of glacial retreat, or formed due to fluvial incision on both sides by the Paltoures and Vatherima streams. However, the eastern ridge, bounding the Vathirema stream, extends northeastwards towards the upper Vrichos valley and bounds the western side of the lower Vrichos valley. This feature is a very conspicuous feature and is clearly visible on aerial photographs (Figure 4.25). It is likely that this ridge



Figure 4.21 The Vourtapa valley moraines (Vourtapa Member) viewed from the southern ridge of Vlasi (July 2001).

is a lateral moraine ridge formed during glacier retreat from the Kato Radza valley.

4.2.2 Vourtapa valley

The Vourtapa valley is situated directly to the north of Skamnelli village and drains into the lower Skamnelli area. The valley is bounded at its southern end by impressive well-defined boulder-covered ridges (Fig. 4.21). These deposits begin at *ca.* 39°55'40"N, 20°51'20"E, 1650 m a.s.l and this area is defined as the type locality of the **Vourtapa Member**. The clarity of these ridges is visible in modern topographical maps, where they can be clearly recognised by the shape of the contours, and also in aerial photographs, where the glacial features of this valley can be clearly seen (Fig. 4.25). The ridges are multi-crested features measuring nearly 30 m in height on their proximal sides. The composition of these ridges is clearly exposed at trackside locations and the ridges are composed of matrix-supported diamictons containing occasional large boulder clasts. On the western side of the Vourtapa valley, boulder-covered ridges extend for over 1 km. Here, in the mid Vourtapa valley, at least two ridge crests are evident of similar freshness and clarity to those further down-valley. Unlike in the lower Kato Radza valley below Skamnelli, soils are thin and poorly developed on the Vourtapa moraines. The deposits and associated ridges are clearly end

and recessional moraines and appear to have formed at the terminus of a former glacier in the Vourtapa valley.

On the east side of the Vourtapa valley, three small arcuate ridges (3-5 m high) exist at the base of the steep Tsoukoula cliffs between 1850 and 2000 m. The ridges are slightly arcuate and are composed of angular boulders (Fig. 4.22). These deposits represent the type locality for the **Tsoukoula Member**. The ridges resemble pronival ramparts and are likely to have formed in front of a snowpatch against the cliff to the east (*cf.* Washburn 1979, Ballantyne and Kirkbride 1986, Shakesby 1997).

Ice-moulded bedrock and stoss and lee erosional forms are well-displayed throughout the Vourtapa valley. Extensive ice-planed pavement surfaces are widespread, although striae are usually absent. As with most sites on Mount Tymphi, erosional directional analysis is restricted to larger-scale features such as friction cracks and p-forms. This erosional evidence is consistent with a valley glacier flowing from north to south through the valley.

There is no headwall to the Vourtapa valley since glacier ice would have originated in the upper Laccos Megalon Litharion valley, flowing into the Vourtapa valley over the Vlasi-Goura col (Fig. 4.15). The mountain of Vlasi, bounding the western side of the Vourtapa valley, would have stood above this ice, as is evidenced by its heavily-weathered ridge which lacks any local evidence of glaciation (Fig. 4.14).

4.2.3 Vrichos valley

The Vrichos valley lies to the east of the Vourtapa valley and to the north-east of Skamnelli village. Limestone pavements are widespread in the lower parts of this valley and display the classic clint-and-grike morphology. Here, the pavements appear much older than those inside of the main moraine complexes higher up-valley since they have deeper fissures scored by well-developed *rundkarren*.

A diamicton section, section VR, is exposed at 39° 55' 58"N, 20° 52' 09"E, 1773 m a.s.l. in a *ca.* 4 m high section (Fig 4.23). It is a massive clast-supported diamicton with a clast density of *ca.* 60%. The results of clast analyses are shown in Figure 4.24. The clast fabric is weak, as indicated by the low S_1 value, and the dip direction indicated by the mean lineation vector does not correspond with former ice flow indicated by the geomorphology. The clasts are largely block-shaped and subrounded and the matrix is predominantly composed of sand-sized particles (20% clay, 25% silt, 55% sand) and is red in colour



Figure 4.22 The pronival ramparts representing the Tsoukoula Member of the Skamnelli Formation at *ca.* 39°56'50"N, 20°51'40"E, 1980 m a.s.l. (May 2003).



Figure 4.23 A weathered diamicton, section VR, in the lower Vrichos valley (39° 55' 58"N, 20° 52' 09.4"E, 1773 m a.s.l). The pole is 1.5m long (July 2001).

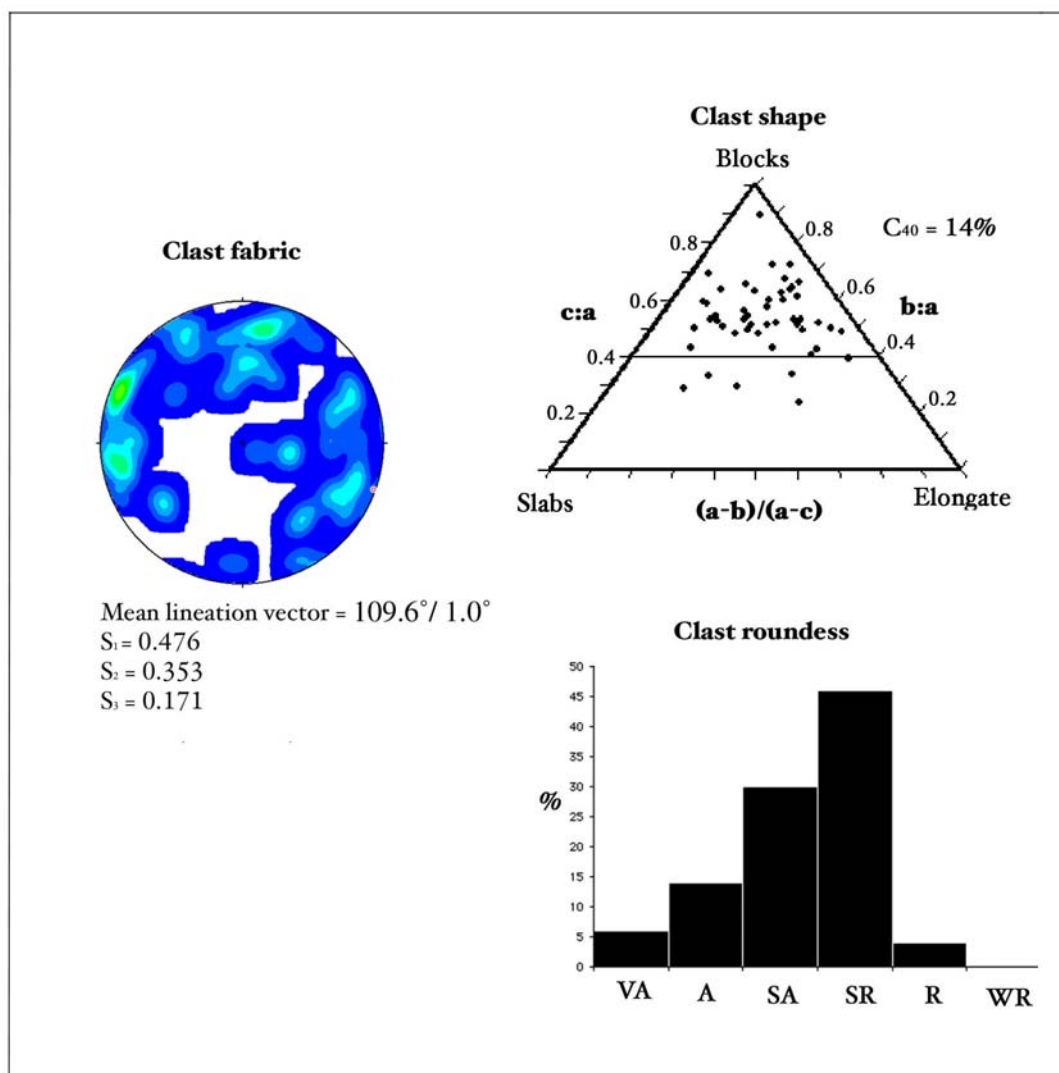


Figure 4.24 Clast analysis results from the Vrichos diamicton, section VR. A key to the fabric diagram is provided in Figure 3.6.

(Munsell: 2.5YR 7/5), contrasting markedly with diamictons noted elsewhere which tend to be white or cream coloured (Munsell: 10YR 8/2). Observation of striae was made difficult due to the calcite coatings present on most clasts and therefore no results are presented here. Secondary calcite is well-developed and covers cobbles and boulders and also fills intra-clast voids and this feature was utilised for U-series dating (Chapter Six).

The weak clast fabric suggests that the sediment is a melt-out till. This is because clast interactions during dewatering and consolidation weaken the preferred fabric orientation in melt-out tills (Benn 1994a). Also, since the majority of clasts are sub-rounded, it is likely that they have undergone active transport in the basal zone, suggesting that the till is a subglacial melt-out till. However, the high sand content of the matrix does not indicate clast-crushing in the basal zone (*cf.* Boulton *et al.* 1974), although much of the matrix may represent inwash during ice melt-out. The red colour of the matrix implies that

the till is particularly weathered and the limestone-dominated matrix has broken down into iron oxides with time. This may have been promoted by water percolation, as shown by the extensive secondary cements, since increased leaching results in the removal of bases and build-up of iron oxides (Woodward *et al.* 1994).

The lower Vrichos valley sediments appear to be contiguous with deposits further down-valley and therefore represent part of the Kato Radza Member. The evidence of till exposures, pavements and perched rocks show that, at a time of extensive glaciation, glaciers from the Vrichos valley coalesced with ice from the Vourtapa valley to form a large glacier which extended south beyond Skamnelli.

The upper Vrichos valley, separated from the Vourtapa valley by the Tsoukoula bedrock spur, is bounded to the southeast by a well-defined boulder-covered ridge. Inside of this ridge, to the northwest, several smaller-scale ridges exist on both sides of the valley with boulder-covered hummocky ground between these ridges. This area represents the type locality for the **Vrichos Member**, and the lower lateral boundary occurs at *ca.* 39°55'40"N, 20°51'50"E, 1600 m a.s.l. These ridges are interpreted as lateral and end moraines. The hummocky ground inside of these is mapped as hummocky moraine and probably formed during glacier retreat.

The interpretation of the ridge bounding the northwest side of the upper Vrichos valley is not straight-forward. The ridge could feasibly be a lateral moraine of a former Vrichos valley glacier. However, the moraine could also be an end/lateral moraine of a former glacier coming from the Vourtapa valley. On the basis that ice-marginal moraines tend to be asymmetric in cross-sectional form, with gentler proximal (ice-contact) and steeper lee slopes (*e.g.* Price 1976, Matthews *et al.* 1979, Matthews and Petch 1982, Shakesby 1989), the latter appears more likely since the moraine slope is gentler towards the position of the former Vourtapa valley glacier. Also, the moraine ridge is slightly arcuate in favour of an interpretation supporting formation by a Vourtapa valley glacier.

Irregular mounds, covered in boulders, exist up-valley of the upper Vrichos end and lateral moraines and are mapped as hummocky moraine. However, within the irregular hummocky moraine, there are at least two linear forms, 80 and 100 m long respectively. The ridges are 3-4 m in height and are aligned parallel to the probable down-valley direction of former ice flow. These are interpreted as fluted moraine and imply that the surrounding hummocks were formed during active ice-flow and not ice-stagnation as has been suggested for some types of hummocky moraine (*cf.* Sissons 1967, 1979a, 1979b). It is possible that the hummocky moraine formed after the flutes were formed, but there is no evidence of superimposition of hummocky moraine on to fluted moraine. The observation

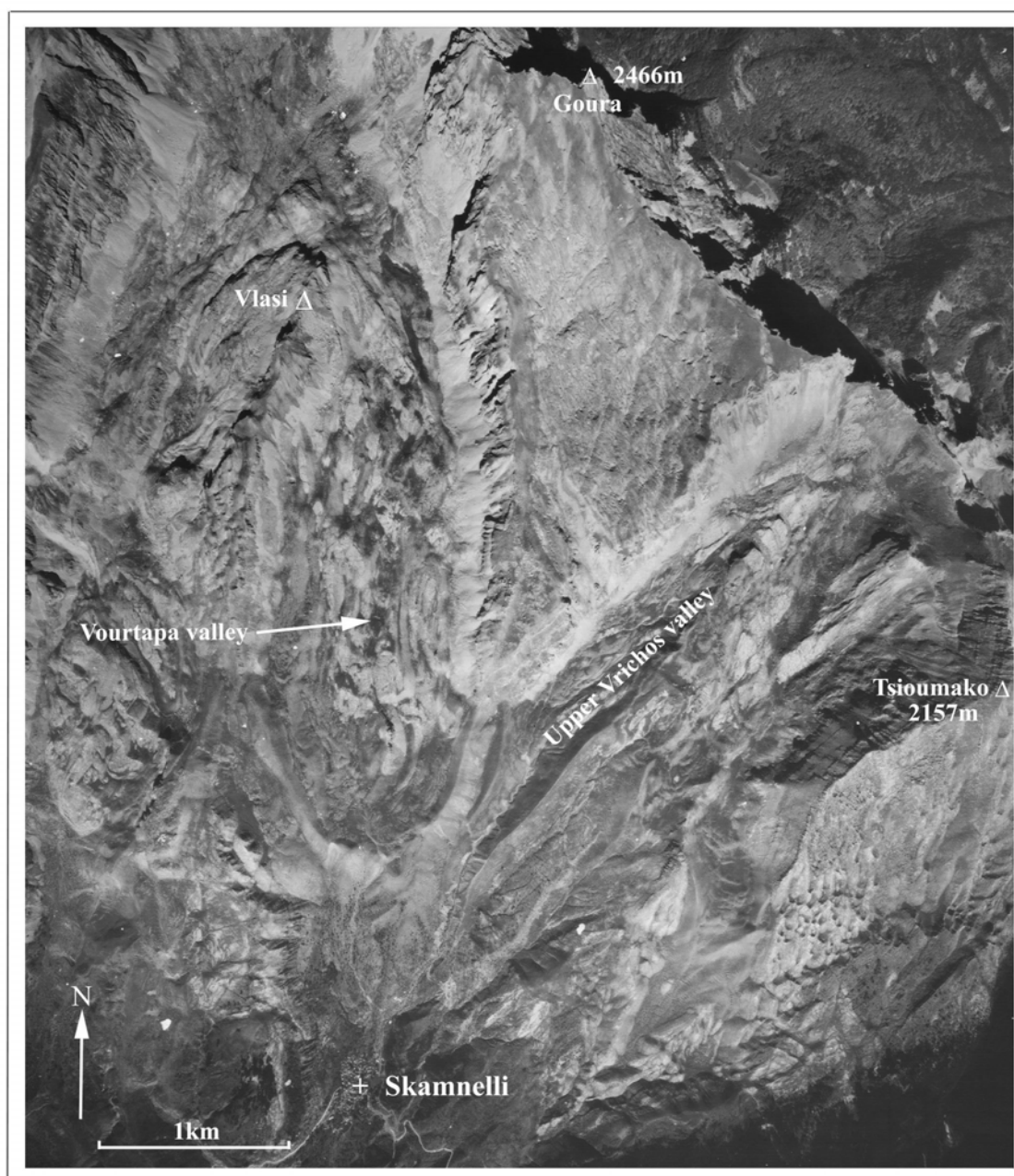


Figure 4.25 Aerial photograph of the Skamnelli area. The arcuate moraines of the Vourtapa are clearly visible as are the moraines of the lower Vrichos valley.

of apparently morphologically contemporaneous fluted and hummocky moraine supports the concepts of Hodgson (1982) who concluded that hummocky and fluted moraine are part of a single continuum between chaotic and streamlined forms.

The source of the Vrichos glacier was in the south-facing cirque at the far northeastern end of the valley. The ground in this area is clearly ice-scoured with widespread ice-moulded features.

4.2.4 Tsioumako valley

The Tsioumako valley is named after the peak (2157 m a.s.l.) at its head, and lies to the east of the Vrichos valley (Fig 4.15). Bouldery diamicton deposits are present at 39°54'29"N, 20°51'44"E, 1164 m a.s.l., northeast of an area named Megali Rachi. The diamicton is largely composed of limestone and rests on flysch bedrock. Up-valley of these diamicton deposits, limestone pavements are widespread (Fig. 4.26) and these features, as well as the diamicton deposits in the lower valley area, are interpreted as glacial in origin. The formation of these pavements by glacial action is also supported by the presence of large perched rocks. The morphostratigraphical position of the deposits in this area suggests that they probably formed contemporaneously with those of the Kato Radza Member, further down-valley, and a red soil is developed on these deposits as in the Kato Radza valley. However, since the deposits do not continue downvalley and are not contiguous with those in the Kato Radza valley, they are considered as a separate member and the sediments are named the **Megali Rachi Member**.

In the upper Tsioumako valley, two sets of clear arcuate ridges, 20-30 m high, occur at *ca.* 1680 m and 1700 m a.s.l., respectively (Fig. 4.27). Inside these ridges, irregular boulder-covered topography is widespread. The sediments and associated landforms of this area define the type locality of the **Corifula Member** (*ca.* 39°55'30"N, 20°52'40"E, 1700 m a.s.l.), so named after the alternative local name of the nearby summit of Tsioumako (2157 m a.s.l.). These features clearly represent moraines formed in front of a glacier in the upper Tsioumako valley. This glacier appears to have had two snout lobes either side of the bedrock knoll separating the moraines. The two sets of moraines are also separated up-valley of this knoll by a linear moraine *ca.* 400 m long. This moraine could represent a medial moraine, although upper basin morphometry does not support the supply of medial debris. A more likely interpretation is that the moraine is a lateral moraine of the eastern ice lobe at a time when the western lobe was inactive because of ice retreat, resulting in the existence of only a single glacier.

The Tsioumako glacier(s) emanated from a south-facing cirque, which also fed the Vrichos glacier, and from the western cirque of Tsioumako (2157 m a.s.l.) (Fig. 4.15). All of the ground in the upper areas of this former glacier is clearly ice-scoured with widespread ice-moulded features, including *roches moutonnées*. A rocky knoll separating the Vrichos and Tsioumako glaciers appears to have acted as an ice-divide in much the same way as the mountain Vlasi did with the Laccorponi and Vourtapa glaciers. The crest of this bedrock ridge is heavily weathered in comparison with the ice-moulded valley floors



Figure 4.26 Limestone pavement situated in the Tsiumako valley at *ca.* 39°54'30", 20°51'50"E, 1250 m a.s.l. (May 2002).



Figure 4.27 The moraines of the Corifula Member, in the upper Tsiumako valley looking southeast from *ca.* 39°55'40"N, 20°52'20"E, 1750 m a.s.l. (July 2001).

to the west (Vrichos) and to the east (Tsioumako), and the approximate transition is marked by a periglacial trimline in Figure 4.15. This interpretation is further supported by the presence of lateral moraines to the south of this suggested ice-free area.

4.2.5 Morpho-lithostratigraphical summary of the Skamnelli area

The Skamnelli glacier system displays some of the best preserved glacial features in Greece. The morpho-lithostratigraphy of the area is described below and summarised in Table 4.2.

Unit 1. This unit comprises the **Kato Radza and Megali Rachi Members** and is defined from type sections KRa and KRb in the Kato Radza valley below Skamnelli village and a type locality near Megali Rachi in the lower Tsioumako valley – a tributary of the Kato Radza valley. These units are characterised by diamicton sequences interbedded with sand and gravel units and subdued ridge forms. The diamictons are usually strongly weathered or have a red soil developed on them. The lower lateral boundary of this unit is *ca.* 850 m a.s.l. This unit is interpreted as till and proglacial associations with moraines preserved in places, formed by extensive valley glaciers.

Unit 2. The **Vourtapa, Vrichos and Corifula Members** are defined from type localities in the Vourtapa, upper Vrichos and upper Tsioumako valleys and have a lower lateral boundary of *ca.* 1600 m a.s.l. They are characterised by diamicton sections within well-defined arcuate boulder-strewn ridges. Soils are thin and poorly-developed in these deposits. This unit is interpreted as glacial moraines formed by valley glaciers which reached mid-valley positions.

Unit 3. The **Tsoukoula Member** is defined by a type locality in the Vourtapa valley and is characterised by bouldery ridge forms at the base of steep talus slopes which have a lower boundary between 1850 and 2000 m a.s.l. No equivalents are recorded in the Vrichos and Tsioumako valleys. The sediments and associated forms of this unit are interpreted as pronival ramparts.

Unit 3	Tsoukoula Member	SKAMNELLI FORMATION
Unit 2	Vourtapa Member Vrichos Member Corifula Member	
Unit 1	Kato Radza Member Megali Rachi Member	

Table 4.2 Morpho-lithostratigraphical summary of the Skamnelli area.

4.3 The Vrisochori area

The Vrisochori area is dominated by the Maghoula valley which stretches over 8 km from the cliffs of Goura (2466 m a.s.l.) to beyond Vrisochori village and drains into the Aaos valley.

4.3.1 Maghoula valley

Diamicton deposits are exposed in numerous road cuttings around the village of Vrisochori. The lower Maghoula valley (Fig. 4.28), in which the village of Vrisochori is situated, is enclosed on both sides by boulder-covered diamicton ridges 40-50 m high. The maximum extent of these diamicton deposits can be traced just to the north of the village at *ca.* 800 m a.s.l. To the south of the village, four ridges are evident. They are rounded forms but cover a large area and run more or less parallel to the valley floor and can even be seen on satellite photographs of this area (Fig. 4.30). The road cuttings at *ca.* 39°59'40"N, 20°53'20"E, 1100 m a.s.l. represent the type area for the **Vrisochori Member** (Fig. 4.29). The diamictons are largely matrix-supported and largely limestone-dominated with clasts that are also are predominantly block-shaped, subrounded and often striated. A reddish-brown soil (Munsell: 2.5YR 3/3) has developed on these deposits and is similar in colour to those developed in the lowest units of the Skamnelli and Tsepelovo Formations. Samples were taken for laboratory analysis and the results are presented in Chapter Six.

The deposits of this area are clearly glacial in origin and are similar to the tills found on the southern side of Mount Tymphi near Tsepelovo and Skamnelli. The deposits were laid down by a large former valley glacier which emanated from the Maghoula cirques beneath the mountain of Goura (2466 m a.s.l.) and extended to the northwest of the modern

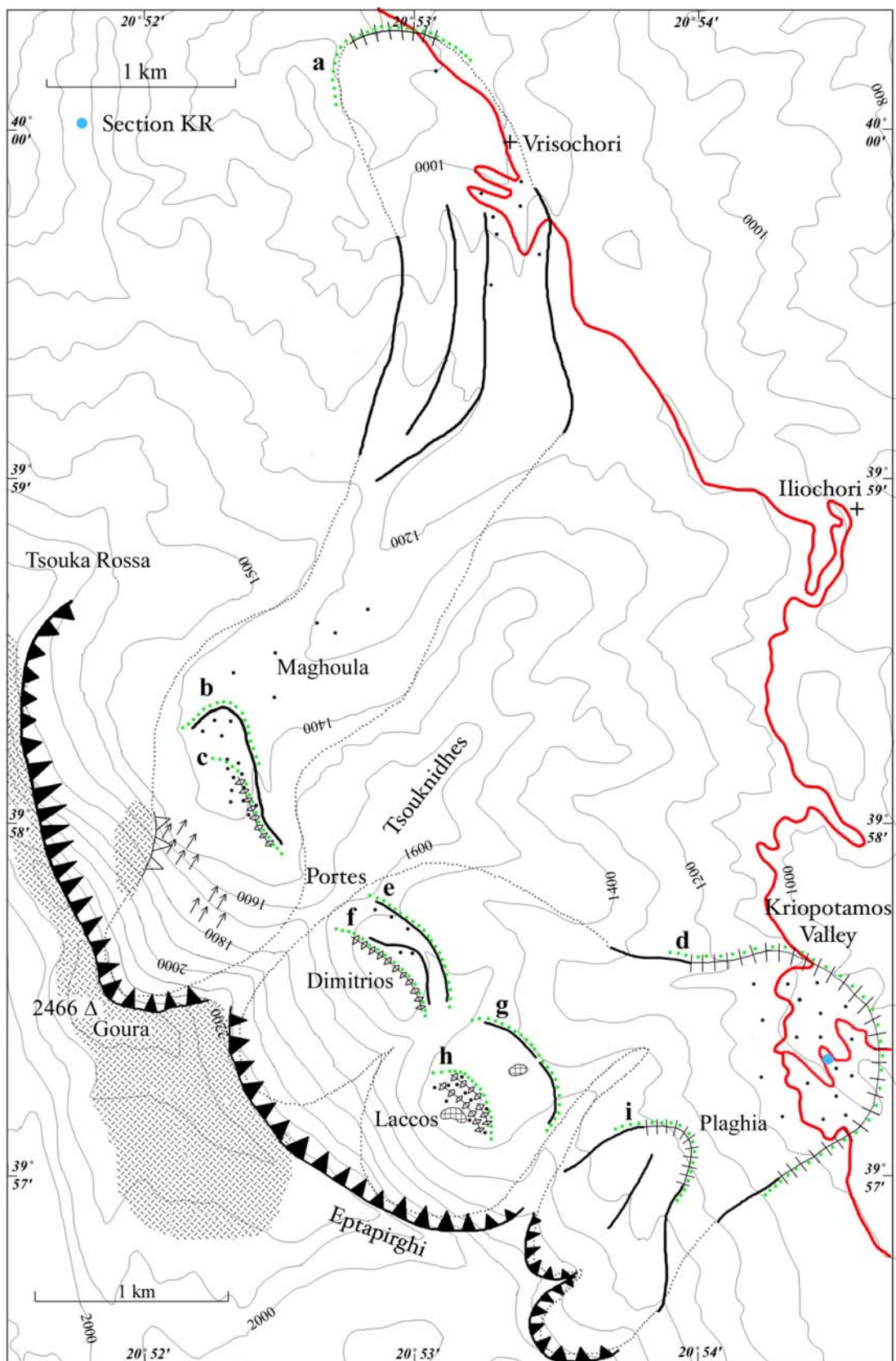


Figure 4.28 Geomorphological map of the Vrisochori and Iliochori area. See Figure 3.4 for key. The stratigraphical units marked **a-c** represent the Vrisochori Formation (**a**. Vrisochori Member, **b**. Maghoula Member, **c**. Portes Member) and the units marked **d-i** represent the Kriopotamos Formation (**d**. Kriopotamos Member, **e**. Tsouknidnes Member, **f**. Dimitrios Member, **g**. Laccos Member, **h**. Eptapirghi Member, **i**. Plaghia Member).



Figure 4.29 The type area of the Vrisochori Member at *ca.* 39°59'40"N, 20°53'20"E, 1100 m a.s.l. These deposits are interpreted as glacial in origin (October 2001).

Vrisochori village. The extent of glaciation in this area, identified above by the limit of diamicton deposits, is corroborated by the depiction of glacial deposits on geological maps by IGME (1976). The ridges to the south of Vrisochori represent lateral moraines of the former valley glacier. It is likely that the two outermost moraines represent lateral moraines formed on either side of a former glacier, although the relationship between the inner two moraines and the former glacier is unclear. It is probable, given their relation to valley morphometry, that these ridges represent recessional lateral moraines from ice retreat on the western side of the valley.

Boulder-covered mounds and ridges are evident in the upper Maghoula valley. A ridge, 10 m high and littered with very large boulders (> 3 m diameter), is evident in the woods *ca.* 500 m below the great cliffs of Goura (2466 m a.s.l.). Perched boulders of similar size are also clearly visible in meadow clearings inside this ridge. The area around these meadows is becoming densely wooded with new saplings and scrub and the position of this ridge is difficult to trace, although using a Global Positioning System it was possible to map the feature. These ridges and boulders represent the type locality for the **Maghoula Member** and are interpreted as glacial in origin (*ca.* 39°58'20"N, 20°52'21"E, 1340 m a.s.l.). The ridge is interpreted as an end moraine and appears to have been formed by a glacier sourced in the cirque to the south. On the eastern side of the valley, this moraine



Figure 4.30 Satellite image of the Vrisochori area. The glacier moraines to the south of the village (marked by the cross) are clearly visible.

ridge can be traced up-valley for *ca.* 800 m. Inside this moraine, a sharp-crested ridge is evident at the base of the towering cliffs at the head of the valley, near the area known as Portes. It is linear in form, consists of angular boulder debris and represents the type locality for the **Portes Member**. It is interpreted as a pronival rampart, formed by boulder accumulation at the base of a perennial snow-bed (*cf.* Shakesby 1997). This snow-bed would have been fed by avalanching and preserved due to low insolation. This process has been confirmed in modern environments by Pérez (1988) below Lassen Peak in California, where it was demonstrated that clasts introduced at the top of a snow-bed could reach its foot.

4.3.2 Morpho-lithostratigraphical summary of the Vrisochori area

Three distinct stratigraphical units can be identified in the Vrisochori area. These are summarised below and in Table 4.3.

Unit 1. The lowest unit is characterised by the **Vrisochori Member** around Vrisochori village. This unit is characterised by diamicton ridge forms which have a reddish-brown soil (Munsell: 2.5YR 3/4) developed on them. The lower lateral boundary of this unit is *ca.*

800 m a.s.l. This unit is interpreted as a collection of moraines formed by an extensive valley glacier.

Unit 2. This unit is characterised by the **Maghoula Member** and consists of boulder-strewn ridges and concentrated areas of perched rocks. The lower lateral boundary of this unit is *ca.* 1350 m a.s.l. This unit is interpreted as glacial moraines formed by a glacier which reached mid-valley positions.

Unit 3. This unit is represented by the **Portes Member** and is characterised by a distinct bouldery-ridge at the base of the steep Goura cliffs, at the head of Maghoula valley (*ca.* 1380-1430 m a.s.l.). The sediments and associated form of this unit are interpreted as a pronival rampart.

Unit 3	Portes Member	VRISOCHORI FORMATION
Unit 2	Maghoula Member	
Unit 1	Vrisochori Member	

Table 4.3 Morpho-lithostratigraphical summary of the Vrisochori area.

4.4 The Iliochoiri area

The Iliochoiri area includes the Kriopotamos valley and the three cirques which feed this valley – the Dimitrios, Laccos and Plaghia cirques to the south of the village (Fig. 4.28).

4.4.1 Kriopotamos valley

Boulder-covered ground occurs down to 1000 m a.s.l. in the Kriopotamos valley and roadside sections reveal thick diamicton accumulations. The northern and southern boundaries of these diamictons are clearly indicated by sections cut by the Skamnelli-Vrisochori road which runs from north to south at around the 1100 m contour, as well as in a roadside quarry on the road to Laista. In the latter locality, a massive matrix-supported diamicton is exposed with no major discernible lateral and vertical lithological variation. This section, named section KR, is proposed as the type section for the **Kriopotamos Member** (39°57'19"N, 20°54'25"E, 1076 m a.s.l.). The results of clast analysis are shown in Figure

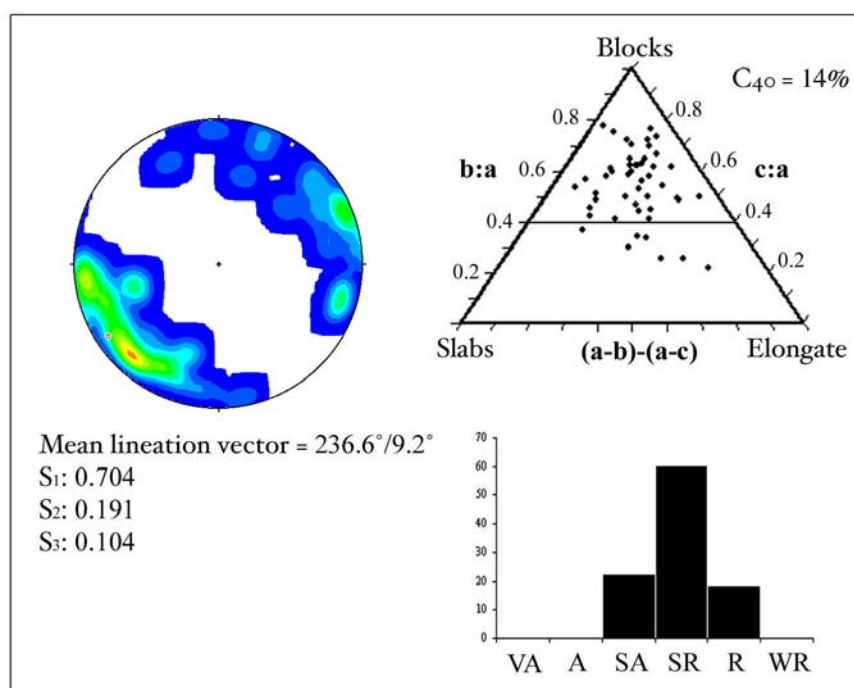


Figure 4.31 Clast analysis results from the Kriopotamos diamicton in section KR ($39^{\circ}57'19''\text{N}$, $20^{\circ}54'25''\text{E}$, 1076 m a.s.l.). A key to the fabric diagram is provided in Figure 3.6.

4.31. The clasts have a strong clast fabric ($S_1: 0.704$, $S_2: 0.191$, $S_3: 0.104$) and a mean lineation vector of $236.6^{\circ}/9.2^{\circ}$. The clasts are largely subrounded and block-shaped ($C_{40} = 14\%$) and over half were striated. These results support an interpretation as subglacial lodgement till with clast dip strongly oriented up-valley towards the former glacier source areas of the Dimitrios, Laccos and Plaghia cirques. Further up-valley, the drift limits become defined by ridges and these are mapped as lateral moraines.

4.4.2 Dimitrios cirque

In the Dimitrios cirque, two sets of diamicton ridges, up to 20 m in height, can be seen. The outermost ridge is situated at just under 1500 m a.s.l., around 500 m from the base of the steep backwall cliffs, to the south of the Tsouknidhes ridge, and represents the type locality for the **Tsouknidhes Member** ($39^{\circ}57'41''\text{N}$, $20^{\circ}52'54''\text{E}$, 1470 m a.s.l.). These ridges are interpreted as end moraines of a former cirque glacier. A short distance (< 250 m) inside these moraines, at *ca.* 1490 m a.s.l., a very well-preserved slightly arcuate boulder ridge exists, around 5-10 m high and nearly 800 m long (Fig. 4.32). This boulder ridge represents the **Dimitrios Member**. At first impression, this ridge appears classically glacial in origin. However, it is far more likely that the ridge is a pronival rampart. It is composed of angular boulder debris, showing little sign of glacial smoothing and consists of minimal fines. In contrast, the ridges of the Tsouknidhes Member are built of glacially-rounded boulders and



Figure 4.32 A pronival rampart in the Dimitrios cirque (Dimitrios Member). Part of the lower, older moraines (Tsouknidhes Member) are visible to the right (May 2002).



Figure 4.33 The pronival rampart of the Dimitrios cirque (Dimitrios Member) taken from the proximal slope of the outer moraines (Tsouknidhes Member). It is clear from this photograph that there is very little space for a glacier behind the boulder-strewn ridge (May 2002).

a significant matrix. This is indicated not only in section but by the ability of vegetation to cover these outer moraines unlike with the inner rampart of the Dimitrios Member which remains very sparsely vegetated because of the absence of sufficient fine matrix. As with the rampart in the neighbouring Maghoula valley (Portes Member), the ridge is likely to have formed at the foot of a perennial snow-bed, where boulder debris, derived from the huge backwall cliffs (>1000 m from base to cliff-top), would have accumulated due to movement of the debris down the snow-bed surface. The steepness of the backwall cliffs and the fact that the base is less than 100 m from the ridge crest indicate that glacier ice could not have formed the ridge. It is unlikely that there was sufficient space between the ridge and the backwall cliffs to accommodate dynamic glacier ice. A snow-bed, however, can be envisaged existing well below the regional snow-line, due to avalanche input and low insolation. Even today, as late as May, snowpatches exist at the base of the cliffs, and it is not difficult to envisage perennial snow-beds existing during the last major period of cold climate (Fig. 4.33).

4.4.3 Laccos cirque

In the Laccos cirque, the situation is similar to that in the Dimitrios cirque. A ridge exists at the entrance to this cirque at *ca.* 39°57'20"N, 20°53'20"E, 1450 m a.s.l. It is largely tree-covered and extends right across the cirque lip with a break in the middle which has been eroded by stream action. This ridge encloses a wide area of the cirque floor and contains a small ephemeral lake. The sediments which form this ridge represent those of the **Laccos Member** and are interpreted as glacial in origin, formed at the margin of a cirque glacier. A series of ridges also exist near to the backwall cliffs, falling from the Eptapirghi ridge at *ca.* 1450 m a.s.l. Two ridge crests can be defined. They are composed of angular boulders and constitute the **Eptapirghi Member**. Again, a small ephemeral lake exists behind the ridges and is fed by melting snow. The proximity of the ridges to the backwall suggests that these ridges are pronival ramparts, as in the Dimitrios cirque, with the different crests probably representing periods of stability during snow-bed retreat.

4.4.4 Plaghia valley

Boulder-covered ridges are present on either side of the Plaghia valley. These represent the **Plaghia Member**. The down valley limit of these deposits is marked by a boulder limit at *ca.* 39°57'06"N, 20°54'00"E, 1400 m a.s.l. (Fig. 4.28). The boulder-ridges are interpreted as lateral moraines of a former small valley glacier. The former glacier appears to have had two source-areas in the cirques above the valley. This is supported by the presence of a

boulder ridge in the centre of the valley which appears to represent a medial moraine formed by the presence of a spur separating the two cirques. Neither landforms nor sediments provide evidence of perennial snow cover in these cirques, unlike in the neighbouring cirques of Laccos, Dimitrios and Maghoula. During the most extensive phase of glaciation, ice from the Plaghia cirques appears to have coalesced with ice coming from the Laccos and Dimitrios cirques. Glacial deposits extend below the deposits of the Plaghia valley into the Kriopotamos valley and are considered part of the Kriopotamos Member.

4.4.6 Morpho-lithostratigraphical summary of the Iliochori area

Three distinct stratigraphical units can be identified in the Iliochori area. These are described below and summarised in Table 4.4.

Unit 3	Dimitrios Member Eptapirghi Member	ILIOCHORI FORMATION
Unit 2	Tsouknidhes Member Laccos Member Plaghia Member	
Unit 1	Kriopotamos Member	

Table 4.4 Morpho-lithostratigraphical summary of the Iliochori area.

Unit 1. This unit is represented by the **Kriopotamos Member**. This unit comprises diamicton deposits and the lower lateral boundary occurs at *ca.* 1000 m a.s.l. This unit is interpreted as till formed by an extensive valley glacier.

Unit 2. This unit is characterised by the **Tsouknidhes, Laccos and Plaghia Members** and consists of arcuate ridges at the entrance to the cirques. The lower lateral boundary of this unit is at 1400, 1450 and 1470 m a.s.l. respectively. This unit is interpreted as moraines that were formed by glaciers which reached mid-valley positions.

Unit 3. This unit is represented by the **Dimitrios and Eptapirghi Members** which are characterised by distinct boulder-ridges at the base of the steep cliffs at *ca.* 1490 and 1450 m a.s.l. in the Dimitrios and Laccos cirques respectively. The sediments and associated

forms of this unit are interpreted as pronival ramparts. This unit is absent in the Plaghia cirques.

4.5 Neraidhovrisi valley

Diamicton deposits are exposed in river and track sections in the Neraidhovrisi valley (39°59'31"N, 20°51'44" E, 1232 m a.s.l.) and define the **Neraidhovrisi Member** (Fig. 4.34). The diamictons are matrix-supported with occasional very large subrounded boulders. They are similar to the diamictons interpreted as till elsewhere on Mount Tymphi. The downvalley extent of these deposits is, however, unclear. Moreover, no higher deposits have been located. This is largely because of the very rough forested terrain and consequent difficulties in mapping the extent of the deposits in this area. The apparent lack of clear moraines higher up-valley may also be due to the very steep slopes and very low preservation potential in this valley.

4.6 Stani Katsanou valley

The Stani Katsanou valley drains into the Aaos valley on the northern slopes of Mount Tymphi and leads down to the Aghia Triada Monastery. In the upper parts, the valley is characterised by the Tsouka Rossa and Karteros cirques.

4.6.1 Aghia Triada and Stani Katsanou

Above the Aghia Triada monastery, boulder-covered ground extends down to nearly 1100 m a.s.l. (*ca.* 40°00'05"N, 20°50'45"E) (Fig. 4.34). The boulders are largely subrounded and constitute the **Aghia Triada Member**. These boulders are interpreted as glacially-derived and correspond with the lowest glacial units elsewhere on Mount Tymphi. Higher up-valley, near the Stani Katsanou sheepfolds and *loutsas* (small artificial pond for livestock), a boulder-covered arcuate ridge exists and represents the type locality for the **Stani Katsanou Member** (39°59'25"N, 20°50'20"E, 1690 m a.s.l.). The ridge is 5-6 m in height and *ca.* 220 m long. The ridge is interpreted as an end moraine of a former valley glacier emanating from two separate cirque complexes - the Karteros cirque to the southwest and the Tsouka Rossa cirque complex to the southeast. A boulder limit extends up-valley from the easternmost part of the end moraine towards the Tsouka Rossa cirques. Irregular boulder-covered ground, interpreted as hummocky moraine, is mapped at around 39°59'00"N, 20°50'25"E, 1900 m a.s.l. and probably represents recessional moraines. These deposits are also regarded as part of the Stani Katsanou Member.

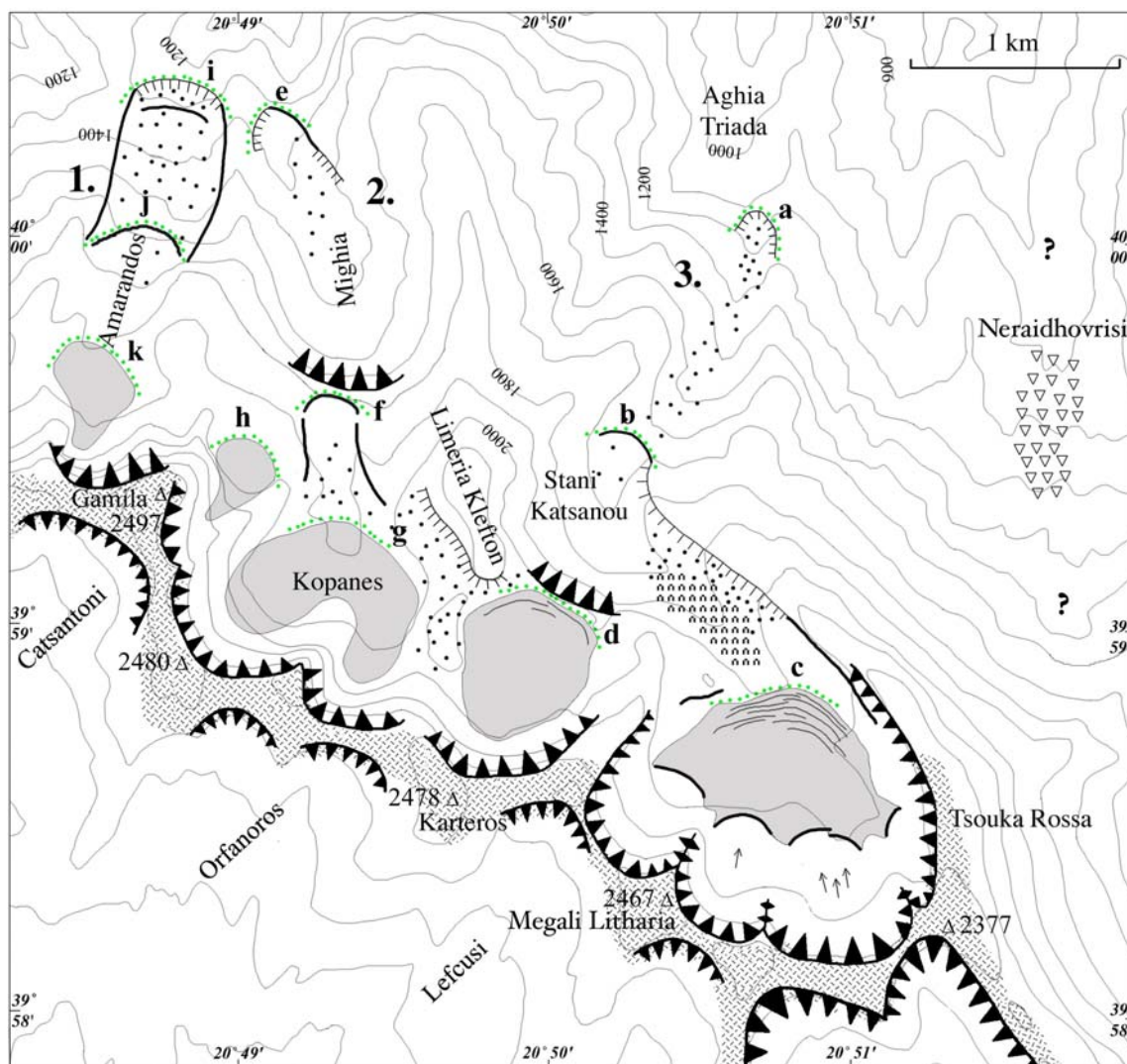


Figure 4.34 Geomorphological map of the Vrisochori area. See Figure 3.4 for key. The stratigraphical units marked **a-d** represent the Stani Katsanou Formation (**a**. Aghia Triada Member, **b**. Stani Katsanou Member, **c**. Tsouka Rossa Member, **d**. Karteros Member). The units marked **e-h** represent the Mighia Formation (**e**. Mighia Member, **f**. Limeria Klefton Member, **g**. Kopanes Member, **h**. Gamila Member) and the units **i-k** represent the Amarandos Formation (**i**. Drochaio Member, **j**. Stomio Member, **k**. Amarandos Member).

4.6.2 Tsouka Rossa cirques

In the vast amphitheatre containing the Tsouka Rossa cirques (Fig 4.34), a lobate mass of dense boulders extends down to a height of 2000 m a.s.l. (Fig. 4.35 and 4.36). The feature has a steep distal scarp and its surface is characterised by boulder-covered transverse ridges. The feature appears to emanate from boulder-covered ridges in the four inset cirques and all of these sediments are grouped into the **Tsouka Rossa Member**. The type locality for this member is situated at *ca.* 39°58'45"N, 20°50'40"E, 2025 m a.s.l. The higher ridges are interpreted as end moraines and the lower area of dense boulder ridges as a

debris rock glacier (Hughes *et al.* 2003). The moraines of the small cirque glaciers appear to have provided the 'rooting zone' of the rock glacier. In this model, the small cirque glaciers continually add debris to the rooting zone and the debris moves downslope due the action of permafrost (*cf.* Barsch 1988, 1996).

4.6.3 Karteros cirque

The Karteros cirque also contains a boulder-covered lobe with a steep distal scarp extending down to *ca.* 2020 m a.s.l. at 39°59'05"N, 20°50'00"E (Fig. 4.34). Transverse ridges are not as well-developed as in the Tsouka Rossa cirques, although they can still be discerned. Moreover, these boulders do not emanate from higher boulder ridges but from the extensive talus slopes at the head of this cirque. These deposits constitute the **Karteros Member**. As in the Tsouka Rossa cirque, this feature is interpreted as a rock glacier. However, here it is regarded as a talus rock glacier rather than a debris rock glacier (*cf.* Barsch 1988, 1996), since the feature is sourced from talus and not cirque moraines.

4.6.4 Morpho-lithostratigraphical summary of the Stani Katsanou valley

Three distinct stratigraphical units can be identified in the Stani Katsanou valley and tributary cirques. These are summarised below and in Table 4.5.

Unit 1. This unit is termed the **Aghia Triada Member** and is characterised by boulder deposits. The lower lateral boundary of this unit is *ca.* 1100 m a.s.l. This unit is interpreted as glacially-derived boulders formed by an extensive valley glacier.

Unit 2. This unit is termed the **Stani Katsanou Member** and consists of an arcuate boulder-covered ridge and hummocky boulder-covered ground. The lower lateral boundary of this unit is *ca.* 1690 m a.s.l. This unit is interpreted as moraines formed by a glacier which reached a mid-valley position.

Unit 3. This unit is represented by the **Tsouka Rossa and Karteros Members** which are characterised by dense ridged boulder-fields. The lower lateral boundary of these deposits is *ca.* 2020 m a.s.l. The sediments and associated forms of this unit are interpreted as a composite of cirque glacier and debris rock glacier deposits in the Tsouka Rossa cirque, and solely as talus rock glacier deposits in the Karteros cirque.



Figure 4.35 The Tsouka Rossa rock glacier viewed from the Tsouka Rossa col to the south near to peak 2377 m a.s.l. (Fig. 4.34). Note the transverse ridges characteristic of rockglaciers (May 2003).



Figure 4.36 The Tsouka Rossa rockglacier viewed from within the cirque. The peak in the background left is Megali Litharia. (2467 m a.s.l.) (July 2001).

Unit 3	Tsouka Rossa Member Karteros Member	STANI KATSANOU FORMATION
Unit 2	Stani Katsanou Member	
Unit 1	Aghia Triada Member	

Table 4.5 Morpho-lithostratigraphical summary of the Stani Katsanou valley.

4.7 Mighia valley

In the Mighia valley, a boulder limit and a boulder ridge extend down to *ca.* 1325 m a.s.l. (40°00'10"N, 20°49'05"E) (Fig. 4.34). The area inside of this boulder ridge and its extensional boulder limit are littered with perched boulders. The deposits of this area constitute the **Mighia Member**. These ridges, boulder accumulations and perched blocks are clearly glacial in origin and indicate the former presence of an extensive valley glacier. A thick well-developed reddish-brown soil (Munsell: 2.5YR 3/4) has formed on these sediments and bears superficial similarities to other soils on the lowest glacial deposits elsewhere on Mount Tymphi.

Glacial action is evidenced by the widespread presence of smooth, ice-moulded, bedrock in the central U-shaped valley area. A *riegel*, or rock-step, is well-developed at the top of the Mighia valley and above this rock formation exist the Kopanes cirques. Boulder-covered ridges exist in the lower parts of these cirques at *ca.* 39°59'35"N, 20°49'20"E, 1800 m a.s.l. These deposits are recognised as the **Limeria Klefton Member** and are named after the ridge to the east. These landforms are interpreted as end and lateral moraines of a former glacier. In the upper parts of the cirques, boulder lobes with steep distal slopes are evident and extend down to *ca.* 1900 m a.s.l. from the base of talus slopes. These deposits are termed the **Kopanes Member** and are interpreted as a talus rockglacier. A similar lobe of boulders is also present in the small cirque northeast of Gamila peak, with a lower limit of *ca.* 1950 m a.s.l, and is named the **Gamila Member**. This is also interpreted as a talus rock glacier. The dividing ridge between the Kopanes and the Karteros cirques is clearly ice-moulded and is littered with perched rocks. These surface boulders are likely to have been deposited during the most extensive glacial phase and probably correspond with the Mighia and Aghia Triada Members in the lower Mighia and Stani Katsanou valleys, respectively. This is an unusual situation since these surface boulders are located in the

highest parts of the glaciated valleys, up-valley of younger members – a situation possibly unique to interfluvial positions.

4.7.1 Morpho-lithostratigraphical summary of the Mighia valley

Three distinct stratigraphical units can be identified in the Mighia valley. These are described below and in Table 4.6.

Unit 1. This unit is represented by the **Mighia Member** and is characterised by boulder deposits, ridges and perched blocks. Also, a thick well-developed red soil is developed on these deposits in places. The lower lateral boundary of this unit is *ca.* 1325 m a.s.l. The deposits and landforms of this unit are interpreted as deposits of a former extensive valley glacier.

Unit 2. This unit is represented by the **Limeria Klefton Member** and consists of boulder-covered ridges. The lower lateral boundary of this unit is *ca.* 1800 m a.s.l. This unit represents moraines formed by a glacier which reached a mid-valley position.

Unit 3. This unit is represented by the **Kopanes and Gamila Members** which are characterised by dense boulder lobes. The lower lateral boundary of these deposits is between 1900 and 1950 m a.s.l. for the Kopanes and Gamila Members respectively. The sediments and associated forms of this unit are interpreted as talus rock glacier deposits.

Unit 3	Kopanes Member Gamila Member	MIGHIA FORMATION
Unit 2	Limeria Klefton Member	
Unit 1	Mighia Member	

Table 4.6 Morpho-lithostratigraphical summary of the Mighia valley.

4.8 Amarandos valley

In the Amarandos valley, a boulder limit can be defined at *ca.* 40°00'25"N, 20°48'37"E, 1250 m a.s.l., just over 1 km southwest of the Drochaio area of the Aaos valley (Fig. 4.34). Inside of this limit exist clear boulder ridges. The ridges are *ca.* 5 m high and extend nearly 800 m along both sides of the valley. These deposits constitute the **Drochaio Member** and are interpreted as glacially-transported boulders and lateral moraines formed by a glacier which filled the Amarandos valley. A moraine, transverse to former glacier flow, also exists *ca.* 300 m inside of the terminal boulder limit and the boulder limit may mark the distal foot of a broad end moraine. On these lowermost deposits, a thick (*ca.* 1.5 m depth) well-developed soil is evident, similar in colour to those found on the lowest deposits elsewhere on Mount Tymphi.

Higher up-valley, another boulder ridge occurs at *ca.* 39°59'59", 20°48'35"E, 1600 m a.s.l. This arcuate ridge represents the **Stomio Member**, so named after the nearby monastery, and again most likely represents moraines formed by a small valley glacier. The former glaciers appear to have been sourced at over 2100 m in the upper feeder cirque northwest of Gamila peak (2497 m a.s.l.) (Fig. 4.34). Soils are thin and appear poorly developed on these deposits in contrast to the lower deposits of the Drochaio Member.

In the highest part of the Amarandos valley (*ca.* 39°59'40"N, 20°48'20"E, 1800 m a.s.l.), a boulder lobe is evident and is named the **Amarandos Member**. The boulders are angular and very dense, covering the whole ground surface. The landform is similar to those that characterise the Kopanes and Gamila Members. This feature, which extends down to *ca.* 1800 m a.s.l., is therefore interpreted in the same way - as a talus rock glacier.

4.8.1 Morpho-lithostratigraphical summary of the Amarandos valley

Three distinct stratigraphical units can be identified in the Amarandos valley. They are described below and in Table 4.7.

Unit 1. This unit is termed the **Drochaio Member** and comprises boulder deposits and ridge forms. A thick reddish-brown soil (Munsell: 2.5YR 3/4) is also developed in these deposits. The lower lateral boundary of this unit is *ca.* 1250 m a.s.l. and the deposits are interpreted as moraines formed by an extensive valley glacier.

Unit 2. This unit is termed the **Stomio Member** and consists of a well-defined arcuate boulder ridge. The lower lateral boundary of this unit is *ca.* 1600 m a.s.l. and the deposits are interpreted as a moraine formed by a glacier which reached a mid-valley position.

Unit 3. This unit is represented by the **Amarandos Member**. This unit is characterised by an angular boulder lobe which extends down to *ca.* 1800 m a.s.l. The deposits and the associated landform are interpreted as a talus rock glacier.

Unit 3	Amarandos Member	AMARANDOS FORMATION
Unit 2	Stomio Member	
Unit 1	Drochaio Member	

Table 4.7 Morpho-lithostratigraphical summary of the Amarandos valley.

4.9 Megas Laccos valley

The Megas Laccos valley is a tributary of the main Vikos Gorge and the Voidomatis river (Fig. 4.37). The area covered in the following text includes all the land which drains the upper parts of the Megas Laccos valley and includes a vast area of gently sloping plateau, named here the Tymphi plateau, incorporating land between the main Tymphi ridge and the peak of Astraka (2436 m a.s.l.).

Diamictons can be found in the upper part of the Megas Laccos valley (*ca.* 39°55'58"N, 20°48'24"E, 1520 m a.s.l.). The diamicton is matrix-supported, containing occasional subrounded cobbles and boulders (clast density: *ca.* 10%) and is similar to the tills found near Skamnelli and Tsepelovo (Fig. 4.38). Subrounded perched boulders can also be found in the vicinity. These sediments constitute the **Megas Laccos Member** and are interpreted as till and glacially-transported boulders. The down-valley limit of glaciation is difficult to trace on the basis of glacial sediments but the U-shaped upper Megas Laccos valley is distinctly different to the lower and narrower V-shaped lower gorge (Fig. 4.39 and 4.40). This is arguably a reflection of the dominant geomorphological processes operative in valley formation - former glacial processes in the upper valley and fluvial processes in the lower gorge. It is likely that glaciation occurred down to *ca.* 1380 m

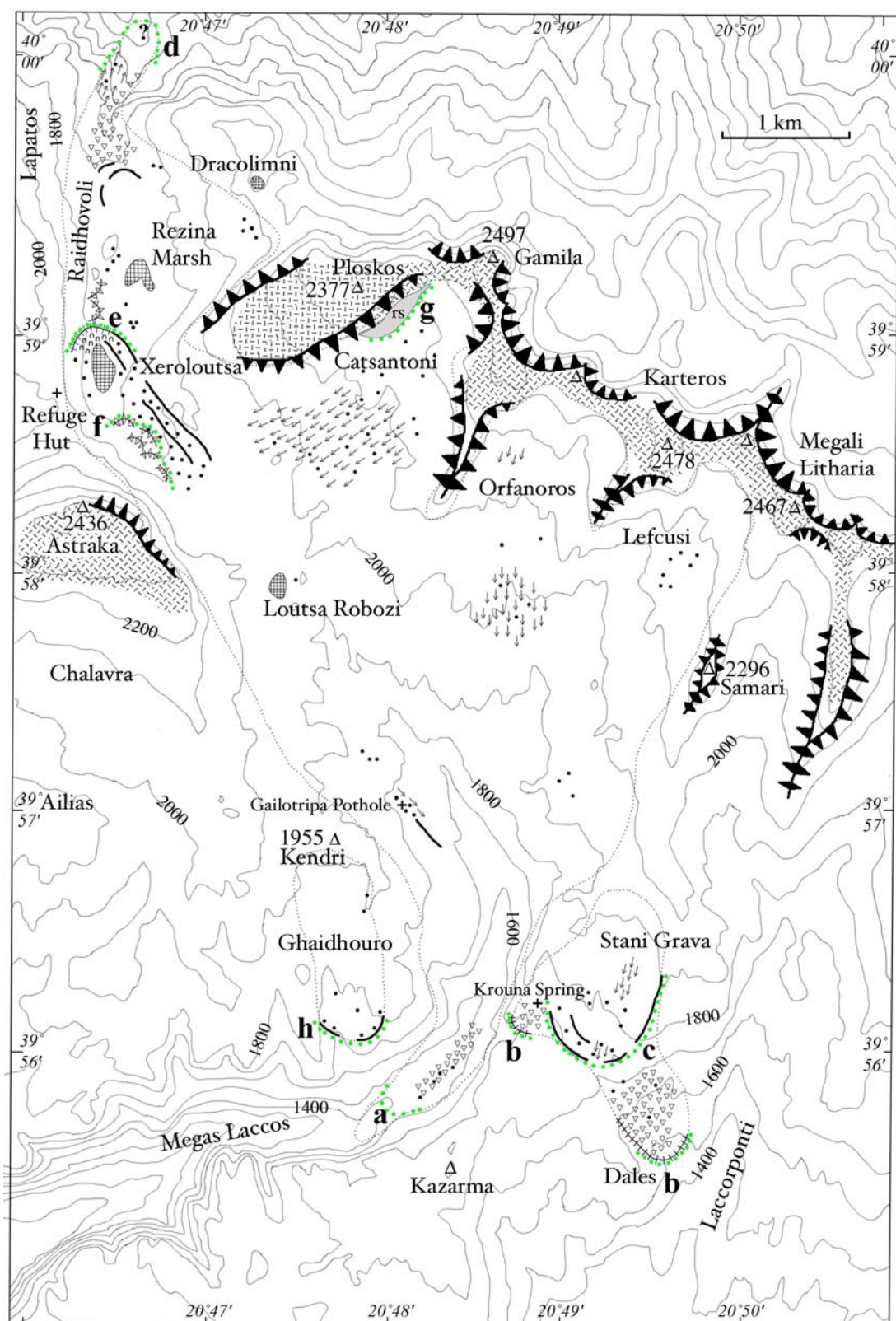


Figure 4.37 Geomorphological map of the Tymphi plateau area. A key is provided in Figure 3.4. The stratigraphical units marked **a** represent the Megas Laccos Formation, the units marked **b-c** represent the Stani Grava Formation (**b**. Dales Member, **c**. Stani Grava Member), the units **d-g** represent the Raidhovoli Formation (**d**. Raidhovoli Member, **e**. Xeroloutsa Member, **f**. Astraka Member, **g**. Ploskos Member) and the unit marked **h** represents the sole member of the Ghaidhouro Formation.



Figure 4.38 A matrix-supported diamicton containing subrounded clasts in the upper Megas Laccos valley. This section is situated at 39°55'58" N, 20°48'24"E, 1520 m a.s.l. Part of a well-developed soil horizon is shown in this picture. In areas of shallower slope, this soil is deeper and reaches a depth of nearly 1.5 m (photograph by Jamie Woodward, May 2003).

a.s.l. where the valley suddenly becomes much narrower and markedly V-shaped.

However, the lowest down-valley evidence of the diamicton deposits occurs at *ca.* 1450 m a.s.l. Below this, between 1400 m and 1450 m a.s.l., the eastern side of the valley floor is filled with cemented breccia deposits. These are interpreted as scree deposits which perhaps accumulated under a cold periglacial climate. The position of these breccia deposits, named here the **Kazarma Member**, at the base of a U-shaped valley indicates that they must be post-date glaciation, and in the higher part of the valley, sections show that they sit atop the tills of the Megas Laccos Member. The breccias and glacial deposits have been incised and reworked by fluvial action on the western side of the upper Megas Laccos valley and must have supplied considerable volumes of coarse sediment to the lower Voidomatis catchment (*cf.* Lewin *et al.* 1991, Woodward *et al.* 1992, Hamlin *et al.* 2000).

A thick, well-developed, reddish-brown soil (Munsell: 2.5YR 3/3) is present on parts of the till of the Megas Laccos Member. This soil is similar in appearance to the soils found on the lowest units elsewhere on Mount Tymphi.

In the upper catchment of the Megas Laccos valley, a linear ridge composed of subrounded boulders occurs near the Gailotripa pothole (*ca.* 39°56'55"N, 20°48'13"E, 1794 m a.s.l.) and also a few hundred metres further south. The features are interpreted as part of

a moraine which trends in a northwest-southeast direction on the western side of the upper Megas Laccos headwater basin. The moraine is particularly subdued and many of the boulders may be exhumed with the rest of the moraine having been eroded away. It is likely that the moraine formed as the Megas Laccos glacier retreated back up to its source area in the southern Tymphi cirques. The till in this area is therefore considered stratigraphically contiguous with the Megas Laccos Member and there is no strong case to suggest these deposits should be considered as a stratigraphically separate unit. Moreover, ice-moulded bedrock is preserved near the Gailotripa pothole on either side of the moraine - a further indication that this is a recessional feature. Parallel U-shaped grooves, *ca.* 1 cm wide, are visible and are clearly different to V-shaped water-formed karstic *karren* and *rinnen*. The preservation of fresh, ice-moulded bedrock is probably due to protection from solutional processes under a former thin calcareous till sheet (*cf.* Sweeting 1966, Williams 1966, Aubert 1969). This till sheet has now been largely removed by erosion and the lack of till in this area and elsewhere on the Tymphi plateau may be due to a combination of: a) the time elapsed since glaciation; and b) the fact that only a thin veneer of till was deposited over the plateau, with most deposition occurring in the narrow confines of the upper Megas Laccos valley - an area prone to rapid erosion.

The entire Tymphi plateau to the south of the main ridge consists of extensive limestone pavements and ice-scoured, streamlined surfaces. These features are clearly visible in the aerial photograph of this area shown in Figure 4.41. Also, boulders are perched on these pavements in places. They must have been transported by ice since they are often positioned well away from any steep slopes and, near Loutsa Robozi, limestone boulders rest on flysch bedrock on an interfluvial ridge. Also, two cirques are cut into the southern side of the Tymphi ridge which drain into the Megas Laccos valley. These are the Orfanoros and Lefcusi cirques. These are less well-developed compared with the other cirques on Tymphi and do not contain sediment-landforms resembling moraines or rock glaciers.

Overall, the evidence suggests glaciation by an ice-field situated over the plateau with a distributary glacier through the upper Megas Laccos valley. It is more correct to refer to the former ice mass as an 'ice-field' rather than as an 'ice-cap' since it appears to have been constrained by topography in most areas and did not submerge the highest peaks and ridges. The area near the lake of Loutsa Robozi, in the col between Astraka and Gamila, is likely to have represented the ice-shed of this ice-field since moraines and other evidence of glaciation exist to the south and to the north. No moraines exist near the lake, as would be



Figure 4.39 The upper Megas Laccos valley. Glacial deposits occur in the bottom of this valley (April 2002).



Figure 4.40 The lower Megas Laccos valley. Note the tigher valley morphometry compared with Figure 4.39. Glacial deposits are absent in this area (April 2002).

expected near a former ice-divide. Also, easily erodible flysch bedrock is preserved here and there are few signs of glacial scouring - again this is to be expected near an ice-divide where horizontal velocity and basal shear stresses are low.

4.9.1 Morpho-lithostratigraphical summary of the Megas Laccos valley

Two stratigraphical units can be identified in the Megas Laccos valley and its upper catchment. These are described below and summarised in Table 4.8.

Unit 1. This unit is characterised by the **Megas Laccos Member** and is a matrix-supported diamicton. The lower lateral boundary of this unit is *ca.* 1450 m a.s.l. This unit is interpreted as glacial deposits formed by an extensive valley glacier. A thick, well-developed soil is present on top of the deposits of this unit.

Unit 2. This unit is characterised by the **Kazarma Member** and consists of angular breccia deposits. The deposits are interpreted as periglacial talus.

Unit 2	Kazarma Member	MEGAS LACCOS FORMATION
Unit 1	Megas Laccos Member	

Table 4.8 Morpho-lithostratigraphical summary of the Megas Laccos valley.

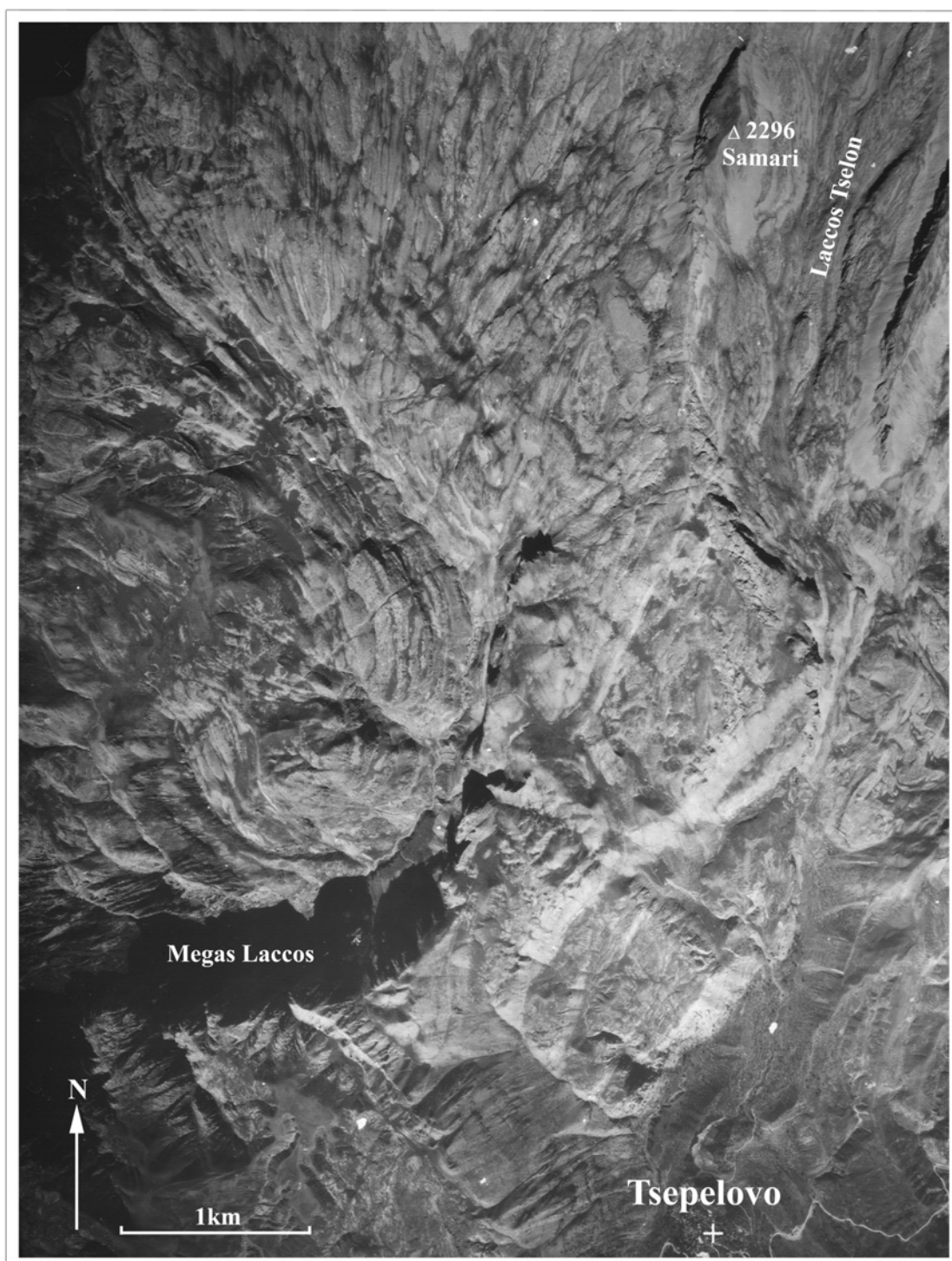


Figure 4.41 Aerial photograph showing the upper Megas Laccos valley and part of the south Tymphi Plateau. Note the streamlined and ice-scoured features on the plateau leading into the gorge, west of the peak Samari (2296 m a.s.l.). Refer to Figure 4.37 for a map of this area.



Figure 4.42 A perched rock on pavement inside of the Stani Grava moraines. Note the moraine in the background (May 2003).

4.10 Stani Grava

Stani Grava is a shepherding area on the high broad ridge between the Megas Laccos valley and the Laccorponi valley near Tsepelovo (Fig. 4.37). It is an unusual site since moraines and pavements are well-preserved within a shallow depression on an interfluvium between two major valleys. The evidence for glaciation is described below.

Diamictons and perched boulders are present down to 1480 m a.s.l. at *ca.* 39°55'35"N, 20°49'30"E in the area known as Dales. They are similar to deposits found elsewhere on Tymphi interpreted as glacial deposits. A diamicton is also exposed at 39°56'12"N, 20°48'49"E, 1763 m a.s.l., near to the Krouna spring, and deposits can be traced down to 1680 m a.s.l. in this area. The matrix-supported, subrounded and striated clasts suggest that this diamicton, as at Dales, is glacial in origin. These deposits represent the Dales Member.

The area up-valley of the Dales area and Krouna spring, around the shepherd hut of Stani Grava (39°55' 57"N, 29°49'05"E, 1800 m a.s.l.), is bounded to the south and east by a series of boulder-covered ridges. At least two ridge crests can be defined and reach *ca.* 20 m in height and represent the type locality for the **Stani Grava Member**. These sediment-landforms resemble end moraines and limestone pavements inside of these moraines

support numerous perched rocks (Figure 4.42). The area immediately in front of the moraines is characterised by a concentration of dolines. Waltham (1978) argued that these dolines have a genetic connection with the moraines, suggesting that they result from the action of meltwater at the front of the former glacier.

The relationship of the moraines of Stani Grava to the larger-scale glacial picture is somewhat puzzling. The Stani Grava area is a rather shallow, open valley and is not bounded to the north by a steep headwall. The moraines could have been formed by ice sourced in the southern cirques of Mount Tymphi, such as Lefcusi and Orfanoros. However, the morphology of the landscape, on an interfluvium, does not appear to have been able to support a glacier lobe from that area. It may therefore be more likely that the Stani Grava moraines are the product of a small local glacier which developed in a hollow on the interfluvium between the Megas Laccos and the Laccorponi valleys.

4.10.1 Morpho-lithostratigraphical summary of the Stani Grava area

Two stratigraphical units can be identified in the Stani Grava area. These are described below and summarised in Table 4.9.

Unit 1. This unit is characterised by matrix-supported diamictites of the **Dales Member**. The lower lateral boundary of this unit is *ca.* 1480 m a.s.l. in the Dales area and *ca.* 1680 m a.s.l. near the Krouna spring. This unit is interpreted as glacial deposits formed by a valley glacier with two diverging snout areas in the Dales and Krouna spring areas.

Unit 2. This unit is characterised by the **Stani Grava Member** and consists of arcuate boulder-covered ridges with a lower lateral boundary of *ca.* 1800 m a.s.l. The deposits are interpreted as moraines of a small glacier which occupied the hollow to the north.

Unit 2	Stani Grava Member	STANI GRAVA FORMATION
Unit 1	Dales Member	

Table 4.9 Morpho-lithostratigraphical summary of the Stani Grava area.

4.11 Ghaidhouro valley

Perched boulders and arcuate ridges are also preserved in the Ghaidhouro valley which hangs above the northern cliffs of the Megas Laccos valley (*ca.* 39°56'10"N, 20°47'40"E, 1720 m a.s.l.) (Fig. 4.37). These features are interpreted as glacial in origin and represent the deposits of the **Ghaidhouro Member**. It is likely that this shallow valley was glaciated by a thin glacier, separate from that on the main plateau, since it is unlikely that ice over-rode the flysch hillock of Kendri (1955 m a.s.l.) to the north. The deposits of the Ghaidhouro Member are overlain by a well-developed red soil – a situation unique to the lowest deposits of valley formations elsewhere on Mount Tymphi. No further units exist in the Ghaidhouro valley.

4.12 Raidhovoli valley

The Raidhovoli valley is located to the north of Astraka (2436 m a.s.l.) and contains Rezina Marsh and the lake of Xeroloutsas. Thick diamicton sequences are exposed in section as low as 1500 m a.s.l. where the valley steepens into a narrow ravine (Fig. 4.37). Figure 4.43 shows a section through these deposits and this area is the type locality of the **Raidhovoli Member** (*ca.* 39°59'40"N, 20°46'20"E, 1675 m a.s.l.). Whilst matrix-supported, these deposits are clast-rich with a clast density of *ca.* 35% and contain largely subangular clasts. These deposits are expressed at the surface by a series of ridges. A thick red soil is also developed on these deposits, especially in the Rezina Marsh area.

The landforms and deposits of the Raidhovoli Member are interpreted as moraines and tills. The subangular clasts and the high clast density perhaps reflect high debris supply from the steep valley-side cliffs of Lapatos (2254 m a.s.l.) and Astraka (2436 m a.s.l.) to the west. Bedrock bluffs, in the ravine at the northern end of the Raidhovoli valley, are smoothly moulded, and subrounded boulders are perched on bedrock promontories in places suggesting the former passage of ice. The steepness of the terrain in this area and the susceptibility of glacial deposits to erosion preclude the precise delimitation of glaciation. However, it is likely that a former glacier descended through this ravine and subsequently stabilised on retreat at the upper edge at *ca.* 1700 m a.s.l. forming the higher moraines (Fig. 4.37). Inside of these moraines, *ca.* 500 m up-valley, the vegetated lake, known as Rezina Marsh, most probably represents a kettle hole where ice-cored debris has melted leaving a depression. The deposits in this area are mapped as *éboulis*, or rock debris, by IGME (1970) rather than *moraines glaciaires* though it is more likely that the deposits are glacial in origin. Rezina Marsh has been cored and analysed for pollen by Willis (1992b) who



Figure 4.43 Matrix-supported diamicton in a section cut through ridges at the northern end of the Raidhovoli valley. This is the type section of the Raidhovoli Member at *ca.* 39°59'40"N, 20°46'20"E, 1675 m a.s.l (May 2003).



Figure 4.44 Moraine ridges impounding the lake of Xeroloutsa (*ca.* 39°58'50"N, 20°46'20"E, 1760 m a.s.l.) viewed from near the Astraka refuge. This photograph was taken in May 2003 and this lake is usually dry by the end of summer.

described a Holocene sequence. Willis (*personal communication*) reached impenetrable gravels at the base of the core, and the depth of sediment beneath the lake sediments is unknown.

Higher up-valley, the lake of Xeroloutsa (*ca.* 39°58'50"N, 20°46'25''E, 1760 m a.s.l.) is dammed to the northeast by clearly-defined boulder ridges (Fig. 4.44). There appears to be at least two ridge crests. These extend southeastwards for *ca.* 300 m until a faulted bedrock bluff around 80 m high. The ridges continue on the top of this bluff in a southeasterly direction for over 500 m (Fig. 4.37). The sediments and landforms of this area represent the type locality for the **Xeroloutsa Member**. Soils are absent or very thin on these moraines in contrast to the deposits of the Raidhovoli Member deposits where a thick reddish-brown soil (Munsell: 2.5YR 3/4) has developed. The boulder ridges in this area are interpreted as a continuum between end and lateral moraines, formed at the margins of a small valley glacier sourced near the northern cliffs of Astraka (2436 m a.s.l.). Moraines to the north of the lake are irregular in form, have been mapped as hummocky moraine and probably formed during glacier recession.

Boulder ridges also exist to the north, immediately outside of the Xeroloutsa moraines, at the base of the eastern slopes of Lapatos (2254 m a.s.l.). These ridges are arcuate and composed of angular boulders and are situated very near to the base of steep slopes. The ridges are interpreted as pronival ramparts and probably formed contemporaneously with the moraines at Xeroloutsa. They are not assigned separate stratigraphical status.

At the base of the northern Astraka cliffs between 1850 - 2000 m a.s.l., inside of the Xeroloutsa moraines, a series of ridges composed of angular boulders exist. At least five slightly arcuate forms can be defined, all less than 100 m from the base of the cliff. These ridges are the type locality of the **Astraka Member** (*ca.* 39°58'30"N, 20°46'30"E). The features are interpreted as pronival ramparts and represent the last major cold-climate landforms in this area.

East of Astraka, the Catsantoni cirque is cut into the southern side of the Tymphi ridge between the peaks of Ploskos (2377 m a.s.l.) and Gamila (2497 m a.s.l.) and drains into the Raidhovoli valley (Fig. 4.37). Figure 4.45 illustrates that this area is characterised by extensive limestone pavements. Numerous perched rocks rest on these pavements and the whole landscape shows evidence of former ice scour. As with the neighbouring Orfanoros and Lefcusi cirques further east, this cirque is less well-developed in comparison with other cirques on Mount Tymphi and does not contain sediment-landforms resembling moraines or rock glaciers. Thus, this erosional landscape most likely corresponds with the

most extensive phase of glaciation. However, very large and very angular boulder accumulations occur between 2100 and 2200 m (39°59'05"N, 20°48'00"E) at the base of the southeastern cliffs of Ploskos (2377 m a.s.l.). These deposits, illustrated in Figure 4.46, represent the **Ploskos Member**. These deposits are clearly sourced from the cliffs and probably represent rock-slope failure deposits. The limestone cliffs are well-jointed and large blocks are tilted on a convex slope. In places, the tilt is so great that the joints have become tens of centimetres wide and the rock-failure deposits have probably resulted from the toppling of these blocks (*cf.* Dikau *et al.* 1996). This may have been promoted by frost shattering and joint-weakening of the cliffs under a periglacial climate, or soon after glacier retreat and perhaps represent paraglacial deposits. However, other scenarios can also be invoked such as mass failure due to seismic activity, especially since Epirus is tectonically very active (King *et al.* 1993,1997). In fact, all three scenarios invoked above may have contributed to the instability of the cliff face leading to the rock-fall.

4.12.1 Morpho-lithostratigraphical summary of the Raidhovoli valley

Three distinct stratigraphical units can be identified in the Raidhovoli valley. These are outlined below and in Table 4.10.

Unit 1. This unit is represented by the **Raidhovoli Member** and comprises clast-rich matrix-supported diamicton deposits and boulder ridge forms. The lower lateral boundary of this unit is *ca.* 1500 m a.s.l. This unit is interpreted as glacial deposits formed by an extensive valley glacier. A thick soil has also developed on these deposits.

Unit 2. This unit is represented by the **Xeroloutsa Member** and consists of well-defined arcuate boulder ridges. The lower lateral boundary of this unit is *ca.* 1760 m a.s.l. The unit is interpreted as moraines formed by a glacier which reached a mid-valley position. Contiguous boulder ridges, on the distal side of the Xeroloutsa ridges, near the steep eastern slopes of Lapatos (2254 m a.s.l.), are interpreted as pronival ramparts.

Unit 3. This unit is represented by the **Astraka** and **Ploskos Members**. The deposits of this unit are characterised by large to very large angular boulder accumulations and some of these form ridges at the base of steep cliffs. The deposits are interpreted as pronival ramparts, in the case of the Astraka Member, and rock-slope failure deposits, in the case of



Figure 4.45 Limestone pavements and the Catsantoni cirque behind (May 2003).



Figure 4.46 Boulder accumulations on the southeastern slopes of Ploskos (*ca.* 39°59'05"N, 20°48'00"E) with the peak of Gamila (2497 m a.s.l.) in the background. These boulder accumulations probably represent rock-fall deposits (May 2003).

the Ploskos Member with lower lateral boundaries of 1850 m and 2100 m a.s.l., respectively.

Unit 3	Ploskos Member Astraka Member	RAIDHOVOLI FORMATION
Unit 2	Xeroloutsas Member	
Unit 1	Raidhovoli Member	

Table 4.10 Morpho-lithostratigraphical summary of the Raidhovoli valley.

4.13 Laccos Radenas

Boulder-covered ridges exist on the north and south sides of the valley draining into the Laccos Radenas gully which feeds into the Vikos gorge at *ca.* 39°56'59"N, 20°44'30"E (Fig. 4.47 and 4.48). Both sets of ridges extend for over 1 km and contain at least two crests, the inner crests being more extensive on the northern side of the valley and the outer being more extensive on the southern side. In addition, a reddish-brown soil (Munsell: 2.5YR 3/4) is well-developed on these deposits, nearly one metre thick in places. Sections are exposed through these ridges, showing that they are clearly composed of matrix-supported diamictons, and are marked on geological maps as glacial deposits (IGME 1970). The deposits of this area, representing the **Laccos Radenas Member**, are therefore interpreted as glacial deposits, and the ridges appear to represent lateral moraines of a former valley glacier emanating from the vicinity of Chalavra (Fig. 4.47). Inside the northern moraines, irregular boulder-draped mounds are present. These mounds are mapped as hummocky moraine and probably formed during glacier retreat.

Ice-moulded bedrock is evident east of the Laccos Radenas area through a glacially-moulded U-shaped valley separating the subsidiary summits of Ailias (*ca.* 2100 m a.s.l.) and Kalogheros (2112 m a.s.l.). This valley leads through to the gently sloping southern slopes of Astraka named Chalavra. Limestone pavements are abundant throughout the Chalavra area and, in many places perched rocks rest atop the pavements, well away from any steep slopes. No further units exist in the Laccos Radenas valley.

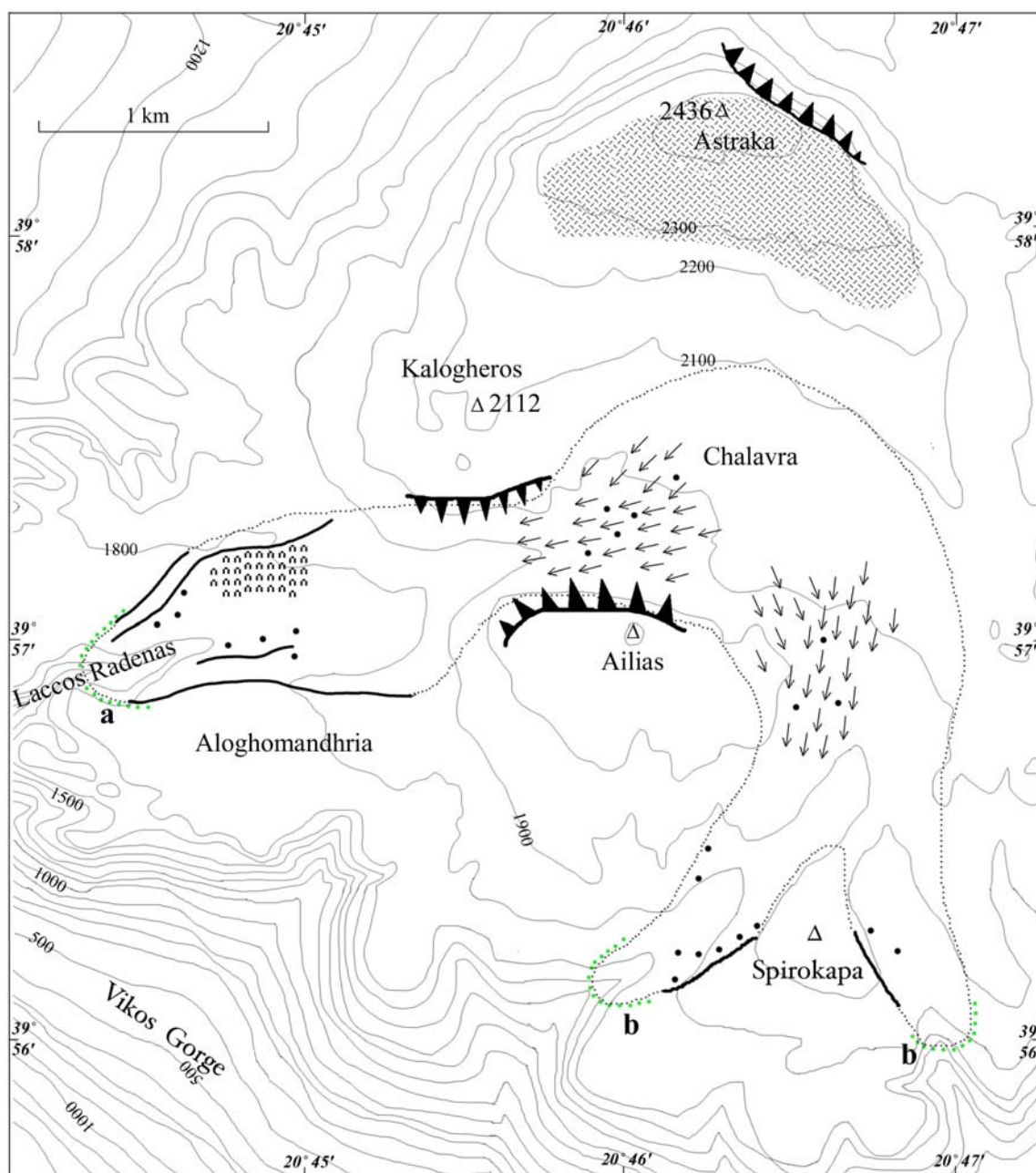


Figure 4.47 Geomorphological map of the Astraka area. A key is provided in Figure 3.4. The stratigraphical boundaries marked **a** represents the Laccos Radenas Member of the Laccos Radenas Formation. The boundaries marked **b** represent the boundaries of the Spirokapa Member of the Spirokapa Formation.

4.14 Spirokapa

Boulder-covered ridges exist in the valleys draining the area either side of the hillock known as Spirokapa and extend to the Vikos Gorge edge at *ca.* 1600 m a.s.l. (Fig. 4.47). The type locality for these contiguous deposits is situated at *ca.* 39°56'25"N, 20°46'15"E, 1850 m a.s.l. These deposits represent the **Spirokapa Member** and are interpreted as

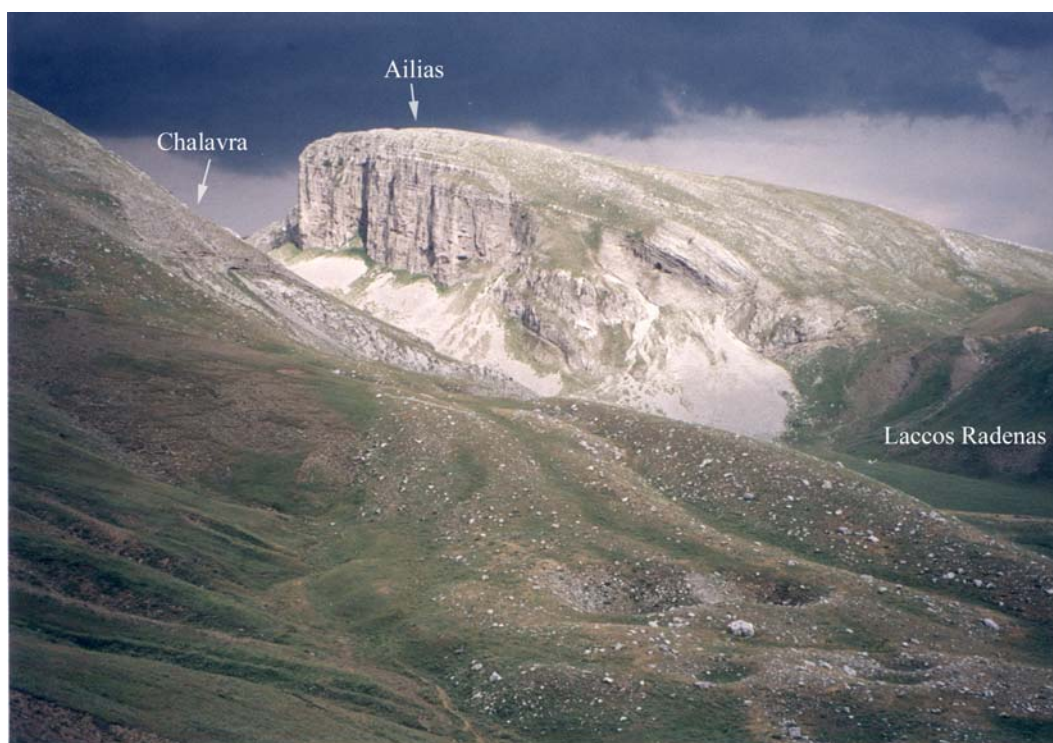


Figure 4.48 Moraines in the Laccos Radenas valley, south of Astraka (2436 m a.s.l.) (July 2001).

moraines formed by glaciers sharing their source with the Laccos Radenas glacier in the Chalavra area, south of Astraka (2436 m a.s.l.). As noted earlier, the pavements and perched boulders at Chalavra, in addition to the moraines in the Laccos Radenas, Ghaidhouro and Spirokapa valleys all indicate that the southern slopes of Astraka were glaciated.

It is likely that during the most extensive phases of glaciation ice on the southern slopes of Astraka would have dry calved into the Vikos Gorge and the lower Megas Laccos valley, since the 1000 m near-vertical cliffs in these areas could not have supported glacier ice. Also, the top of these cliffs are over 1700 m a.s.l., higher than most of the lowermost glacial units found elsewhere on Tymphi. However, given that only one glacial unit is present on the southern slopes of Astraka, and the fact that a thick reddish-brown soil (Munsell: 2.5YR 3/4) is developed in these deposits, it is possible that the unit corresponds with the lowest, most extensive deposits found elsewhere on Mount Tymphi.



Figure 4.49 Shattered rocks on the southeast ridge of Astraka (39°58'00"N, 20°46'40"E, 2340 m a.s.l.). These landforms are interpreted as the result of intense frost action (May 2003).

4.15 Mount Tymphi summits – geomorphological notes

On the main Tymphi ridge, periglacial features are very well-developed. The bedrock is very shattered and a combination of frost action on the ridge and glaciation in neighbouring cirques and valleys has produced a narrow and weathered summit spine. Widened rock fractures, which occur all over this ridge, were probably initially solutional features, *i.e.* grikes, but have been widened considerably by ice. This process is still active today whereby thick accumulations of snow, sometimes up to 2 m thick, undergo cycles of freezing and thawing during the spring and summer melt. Evidence for this process has been witnessed until at least the end of July in some localities near the summit of Goura (2466 m a.s.l.). Periglacial weathering is, therefore, still a major geomorphological agent on the highest parts of the Tymphi ridge where mean winter temperatures during the coldest month are likely to be below -7°C . This figure is based on a mean January temperature of 4.6°C at 483 m a.s.l. at Ioannina (World Meteorological Organisation 1998) and a standard atmospheric lapse rate of 0.6°C per 100 m altitude (*cf.* Whiteman 2000).

On many of the higher summits, the limestone bedrock has been so shattered that the ridge surface is characterised by over a metre thickness of very angular gravel limestone clasts. In places, this weathered substrate displays distinct clast orientation and this patterned ground is a clear sign of frost heaving (*cf.* French 1996). Periglacial action

and comminution of the surface bedrock has provided ample debris for rock glacier formation in the northern cirques, as well as thick accumulations of talus. The latter is still forming at a rapid rate today and rock falls can be frequently observed, especially during the spring melt. Thus, it is possible that in some northern cirques, protalus ramparts and small rock glaciers up-valley of the more extensive evident forms have been buried by an advancing talus front during the Holocene.

The summit ridges of the outlying peak of Astraka (2436 m a.s.l.) also display impressive periglacial rock shattering (Fig. 4.49). This contrasts with the ice-smoothed pavements of the lower Chalavra area. The periglacial features are very well-developed and it is likely that the landforms represent frost shattering throughout the Quaternary, especially during glacial phases.

4.16 Possible glacial evidence in outlying areas

In some places, possible glacial evidence exists well outside of the limits the former glaciers discussed above. For example, near the Nifis Pothole, located at *ca.* 1520 m a.s.l., 2 km southwest of Kazarma (Fig. 4.38), there are extensive pavements. The location of these pavements is anomalous to where glaciers would be expected since they are positioned on gentle slopes without any retaining valley sides. A valley glacier supported by valley sides could not have occurred here, although it is possible that a plateau ice-field existed in this area (*cf.* Rea *et al.* 1998). However, no other glacial features such as perched boulders or moraines exist. Waltham (1978) believed that ice had advanced over this area but also suggested that the pavements were older than on the Tymphi plateau since fissures between the clints are more than 3 metres deep and dissected by deep *rundkarren* with troughs around 15 cm wide.

Other mechanisms for pavement formation could be sought. For example, in the High Atlas of Morocco, Robinson and Williams (1992) considered pavements formed in sandstone to be the product of preferential erosion along bedding planes. Similar pavements have been noted in the Drakenberg Mountains of South Africa (Twidale 1980). Here, it is suggested that the pavements began forming beneath the ground surface as a result of moisture attack on the bedrock. At a later stage, the weathered debris was stripped off by erosion (Twidale 1980). A further possibility is that the limestone pavements represent cryoplanation surfaces formed by frost weathering or nivation (*cf.* Robinson and Williams 1992).

In this case, it would seem that limestone pavements are insufficient as evidence alone to conclude that glaciers scoured this area. Elsewhere on Mount Tymphi where

pavements occur, there is often other forms of glacial evidence too, either in the immediate vicinity, such as perched rocks, or down-valley, such as till and moraines. It is therefore advisable to only deduce glacial activity where multiple lines of evidence occur.

4.17 Summary of Mount Tymphi

Fourteen morpho-lithostratigraphical formations have been identified in the valley systems of Mount Tymphi. A maximum of three member units, interpreted as glacial or periglacial in origin, are present in eight of the fourteen formations. Where there are not three units, there are less and never more. Therefore, in eight cirque-valley systems, the morpho-lithostratigraphy can be interpreted as representing at least three phases of glaciation or major periglacial activity on Mount Tymphi. It is likely, given the closeness of these valleys, that these three different phases of glaciation occurred contemporaneously in each valley. However, where units are absent, such as in the Ghaidhouro Formation, it is difficult to determine relative position in the regional stratigraphy based on the morpho-lithostratigraphical evidence alone. Further, absolute and relative age dating is needed to do this confidently. The absolute and relative timing of the glacial sequence at the inter-valley scale and the designation of stage names for a common chronostratigraphy are the focus of Chapter Six.

Chapter Five

Geomorphological and sedimentological evidence - Mount Smolikas and Vasilitsa

This chapter presents the evidence for glaciation on Mount Smolikas and Mount Vasilitsa. Mount Smolikas (2637 m a.s.l.) is the highest peak of the Pindus Mountains and the second highest mountain in Greece after Mount Olympus (2917 m a.s.l.). The mountain covers a vast area with over 30 km² of land over 2000 m a.s.l. Mount Vasilitsa (2248 m a.s.l.) lies to the southeast of Mount Smolikas and is today occupied, on the northern slopes, by a ski resort. Both mountains are less complex in form compared with neighbouring Mount Tymphi. They are generally rounded mountains with only a few cirques and deep valleys cut in to them.

5.1 The Vadulakkos valley and cirques

The Vadulakkos valley is a major valley fed by multiple cirques on the northern side of Mount Smolikas and represents the heart of this mountain region. A geomorphological map of this area is shown in Figure 5.1 and the evidence for glacial and periglacial activity is presented below.

5.1.1 The lower Vadulakkos valley

Thick diamicton deposits characterise the lower Vadulakkos valley where it merges with Ellenikos valley on the northern slopes of Mount Smolikas. Near Aghia Paraskevi, west of the area mapped in Figure 5.1, a large debris cone, mapped as a landslide by IGME (1987), extends over 1.5 km from 1800 to 900 m a.s.l. (Fig. 2.5B). Landslides are common in areas of flysch, such as at Aghia Paraskevi, and probably result from slippage along the flysch bedding planes where harder siltstone is intercalated with fissile sands and silts. Today, and for quite some time, the landslip has been relatively stable (IGME Preveza, *personal communication*) although it is unknown whether these deposits formed during the Holocene or are cold-stage periglacial features. Diamicton deposits are exposed further east along the Aghia Paraskevi-Fourka road and the maximum extent of glaciation in this valley can be traced down to *ca.* 1025 m a.s.l. (40°08'30"N, 20°54'30"E) (Fig. 5.1). An extensive area of diamicton can be traced in this lower valley area and much of the evidence is displayed

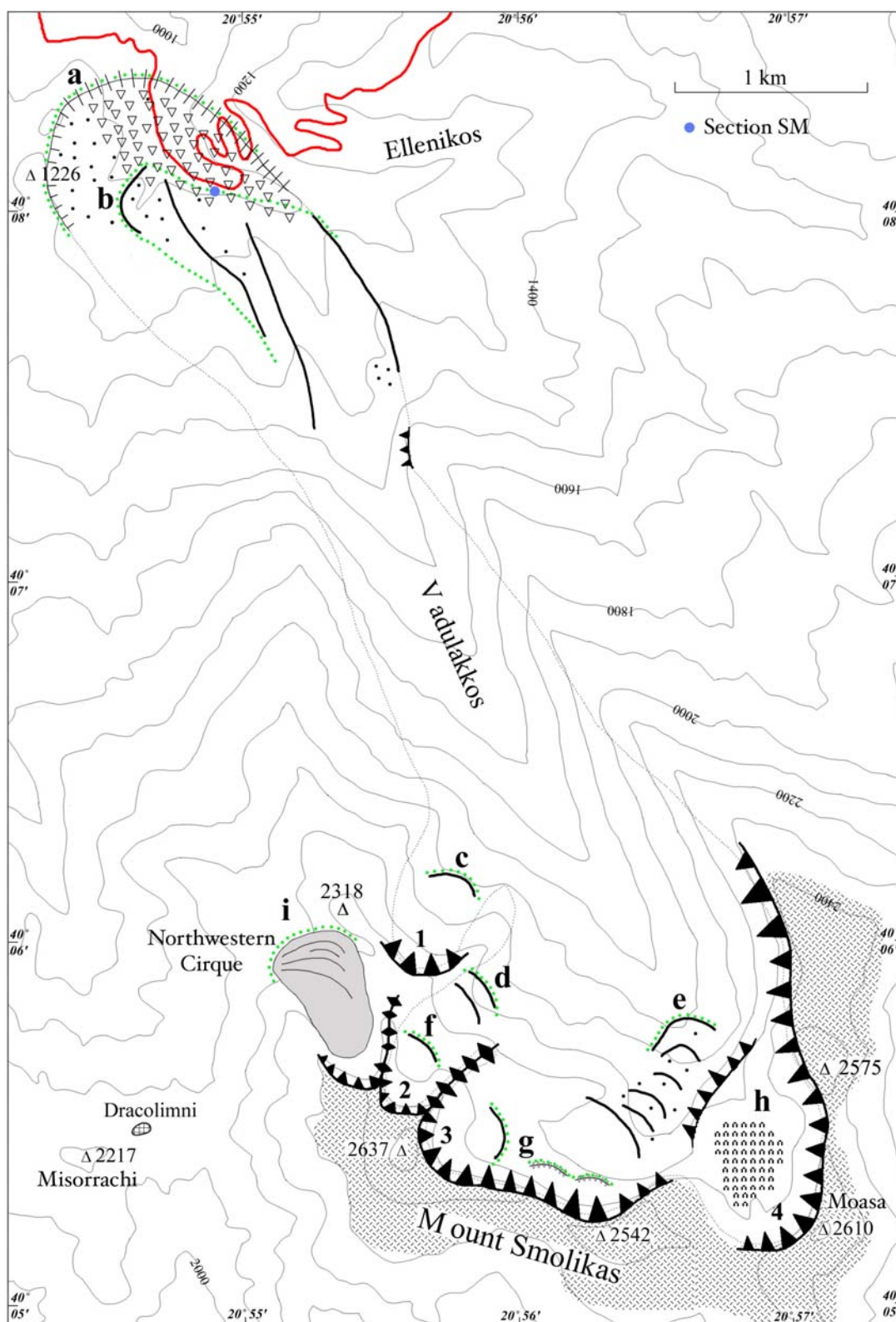


Figure 5.1 Geomorphological map of the northern Mount Smolikas area. See Figure 3.4 for key. The numbers 1-4 represent Cirques 1-4. The stratigraphical units marked **a-g** represent the Vadulakkos Formation (**a**. Aghia Paraskevi Member, **b**. Vadulakkos Member, **c**. Cirque 1 Member, **d**. Cirque 2 Member, **e**. Cirque 3 Member, **f**. Smolikas Summit North Member, **g**. Smolikas Summit East Member, **h**. Cirque 4 Member - the lower boundary of this unit is the same as for the Cirque 3 Member). The unit marked **i** represents the Northwestern Cirque Formation.



Figure 5.2 The Smolikas Vadulakkos moraines viewed from the north. The peak in the background is Mount Smolikas (2637 m a.s.l.) (April 2002).



Figure 5.3 The Vadulakkos section at *ca.* 40°08'06"N, 20°54'50"E, 1080 m a.s.l. on the Aghia Paraskevi - Fourka road (May 2002).
in sections and by surface boulders.

Around 500 m up-valley, the diamictos form more pronounced ridges (Fig. 5.2) which are generally parallel to the valley axis and are found on both sides of the valley. These ridges and associated sediments represent the **Vadulakkos Member**. Within this suite of ridges, excellent sections are exposed along the Aghia Paraskevi - Fourka road. They are very thick (> 30 m) diamicton sequences and a well-exposed section occurs at *ca.* 40°08'06"N, 20°54'50"E, 1080 m a.s.l. (Figure 5.3). This section, assigned the name section SM, is described below and illustrated in Figure 5.4. The results of clast analyses from this section are presented in Figure 5.5.

Section SM

- 0 - 3 m** *Unit SM1.* This unit is a matrix-supported diamicton. Clast density is *ca.* 10% and the matrix is largely sand-dominated (62% sand, 22% silt, 16% clay). The clasts have a mean lineation vector of 143.1°/22.6° with a moderate fabric strength (S_1 : 0.685, S_2 : 0.224, S_3 : 0.091). The clasts are largely block-shaped (C_{40} index: 14%), subrounded and over 80% of clasts are striated (Fig. 5.5). Nearly all clasts are composed of ophiolite though a small proportion (10%) are Jurassic limestone clasts. A 30 cm carbonate horizon (76% of weight soluble in acid) topped by 10 cm of non-carbonate silts is situated at the top of this unit. The carbonate horizon is friable and crystalline and can be described as a tufa. It is laterally variable in thickness and appears broken and fragmentary in places. The tufa also encloses clasts and would appear to sometimes occupy interclast voids. The silts (13% sand, 53% silt, 34% clay), overlying the tufa, are finely laminated and consist of 3% organic material, 20% calcium carbonate and 77% residue. These silts were found to contain no preserved pollen.
- 3 - 3.9 m** *Unit SM2.* This is a massive clast-supported bouldery diamicton. The lower contact with Unit SM1 appears conformable. The mean diameter (a-axis) of the 10 largest clasts is 50.4 cm, although the clasts are poorly-sorted and range in size from 18 cm to over 100 cm. The boulders are largely subrounded (R: 10%; SR: 60%; SA: 30%) and striated (striated: 90%).

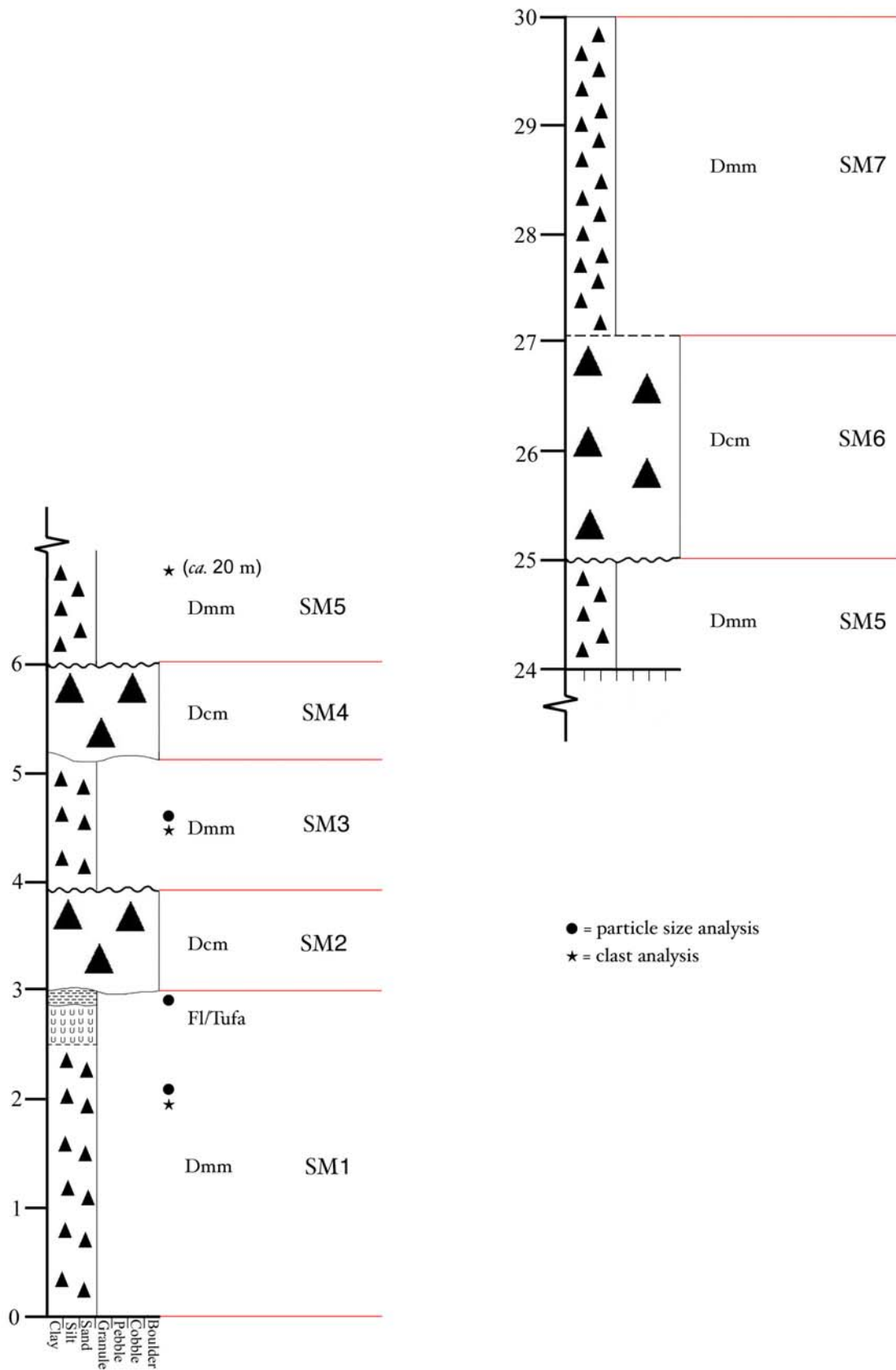


Figure 5.4 Sediment log of the Smolikas Vadulakkos sediments (section SM) at *ca.* 40°08'06"N, 20°54'50"E, 1080 m a.s.l.

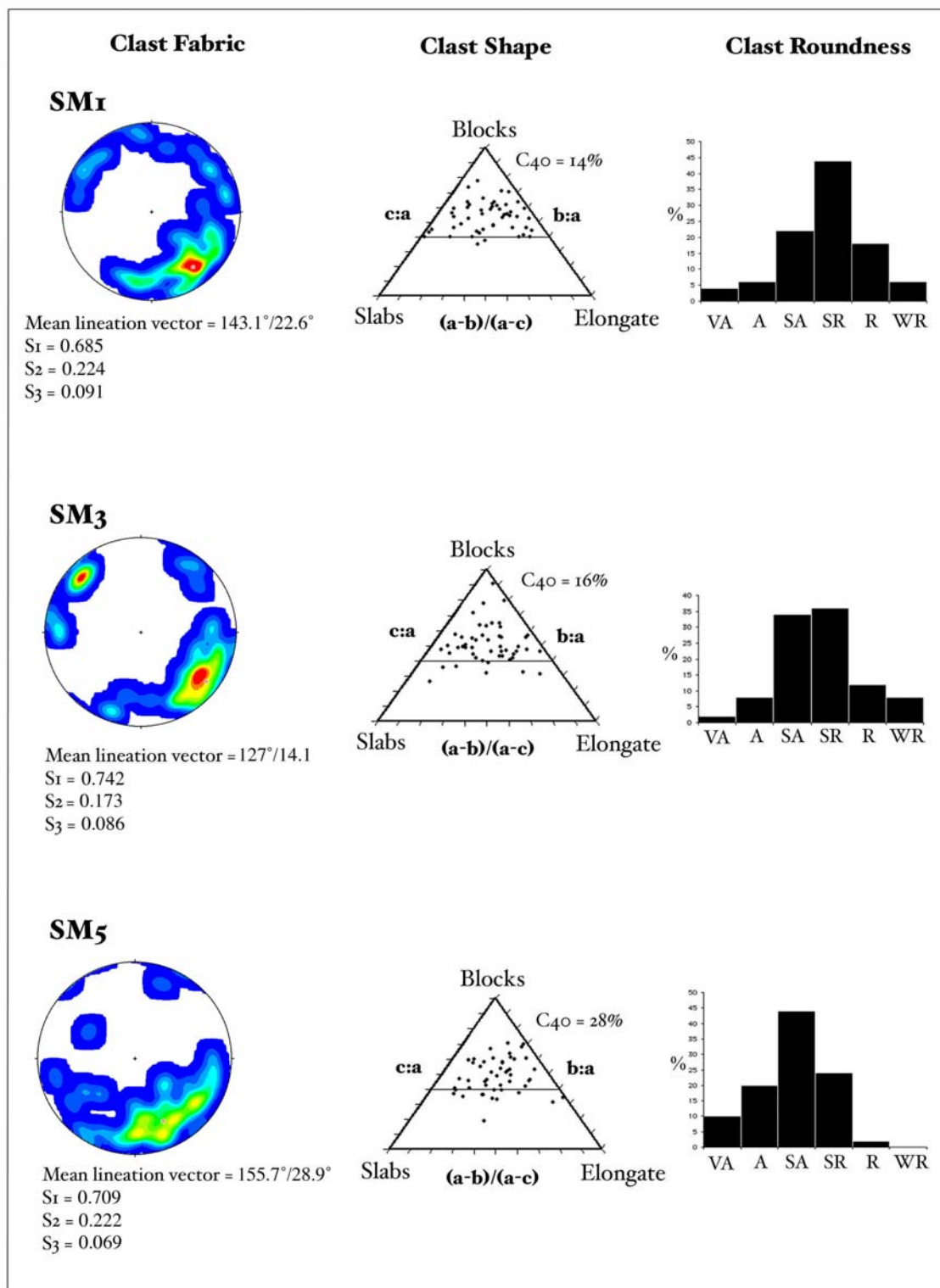


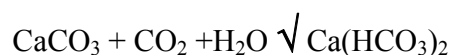
Figure 5.5 Clast analyses from the Smolikas Vadulakkos section (SM). The sample locations are illustrated in Figure 5.4. A key to the fabric diagram is provided in Figure 3.6.

- 3.9 - 5.1 m** *Unit SM3.* This unit is a matrix-supported diamicton which is separated from Unit SM2 by an erosional boundary. In places, the lateral extension of this boundary indicates that this unit dips up-valley at *ca.* 12°. The deposit is slightly more clast-rich than SM1 (clast density: 15%) though the matrix particle-size is similar in that it is sand-dominated (sand: 57%; silt: 29%; clay: 14%). The clast fabric is strong (S_1 :0.742, S_2 :0.173, S_3 : 0.086) with a mean lineation vector of 127.3°/14.1°. Clasts are largely block-shaped (C_{40} index: 16%), subangular to subrounded, and 78% of clasts are striated (Fig. 5.5). Of the unstriated clasts, 91% were subangular, angular or very angular.
- 5.1 - 6 m** *Unit SM4.* This is a massive clast supported bouldery diamicton. The lower contact with Unit SM3 is conformable. The mean size (a-axis) of the 10 largest clasts is 72.9 cm. The clasts are larger than in the lower boulder unit, Unit SM3, although are similar in shape, being largely subrounded (R: 20%, SR: 80%).
- 6 - 25 m** *Unit SM5.* This unit is vertically extensive and consists of a matrix-supported diamicton (Dmm) which is separated from SM4 by an erosional boundary. As with Unit SM3, this unit appears to be dipping up-valley at *ca.* 12°. Clast fabric and shape measurements were taken at *ca.* 20 m. The clast fabric is strong (S_1 : 0.709, S_2 : 0.222, S_3 : 0.069) with a cluster distribution (*cf.* Benn 1994a) and a mean lineation vector of 155.7°/28.9°. The clasts are more angular than in the lower units, SM1 and SM3, and the C_{40} index of 28% indicates that more than a quarter of clasts are more elongate- or slab-shaped than block shaped (Fig. 5.5). 70% of the clasts are striated.
- 25 - 27 m** *Unit SM6.* This unit is composed of poorly-sorted clast-supported boulders. The contact with Unit SM5 is erosional. The mean size (a-axis) of the 10 largest clasts is 91.2 cm. The boulders are more angular than the lower boulder units, SM4 and SM2 (SA: 50%, SR: 50%).
- 27 - 30 m** *Unit SM7.* This unit is a matrix-supported diamicton. The contact with Unit SM6 is gradational. Little work could be done on these deposits because of the exposed position in the section.

The Smolikas Vadulakkos sequence is particularly interesting because of the great thickness of the deposits as well as the evidence of multiple diamictons. Unit SM1 is interpreted as a subglacial till. This is supported by the high percentage of striated clasts, their block-shape and subrounded nature. The moderately-strong clast fabric, high elongation ($1-(S_2:S_1) = 0.673$) and low isotropy ($S_3:S_1 = 0.133$) further supports a theory of formation by subglacial deposition, *i.e.* lodgement till. The mean lineation vector is also consistent with ice movement from southeast and the alignment of clasts parallel to the direction of ice movement (*cf.* Holmes 1941).

The tufa at the top of Unit SM1 is a secondary carbonate and post-dates the diamicton in which it is found. It is best explained by the perched spring line model of Pedley (1990) whereby lines of springs, each supporting tufa deposits, coalesce to form sheet-like slope deposits. This would explain the lateral continuity of the tufa and the variable tufa thickness. The thicker areas are probably located near to former spring heads and calcium-rich waters in the Vadulakkos area are likely to be sourced from the nearby Jurassic limestones, which occur at the overthrust nappe of the ophiolitic complex. In fact, the till-matrix of Unit SM1 contains over 9% calcium carbonate and 10% of the clasts are Jurassic limestones. However, secondary carbonates are not unknown from serpentinite rocks, such as ophiolite, and have been observed in the British Isles (Flinn and Pentecost 1995), western USA (Barnes and O'Neill 1971) and in the Middle East (Clark and Fontes 1990) and often are often composed of magnesium-rich brucite and hydromagnesite or calcium-rich aragonites.

Precipitation of CaCO_3 at springs is caused by the heating and expulsion of CO_2 upon atmospheric exposure and may be aided by the biochemical activity of plants. This process, termed "outgassing" (Pentecost 1991), is illustrated by the equation below for calcite or aragonite:



Calcium bicarbonate ($\text{Ca}(\text{HCO}_3)_2$) dissociates into calcium carbonate (CaCO_3), carbon dioxide (CO_2) and water (H_2O) to compensate for the loss of carbon dioxide from the water during outgassing. Carbon dioxide is less soluble and more easily degassed at high temperatures, so that deposition is faster from warmer waters. In addition, water evaporates faster at higher temperatures which aids the formation of tufa (Pentecost 1991). The formation of tufa is therefore favoured by a warm climate where there is sufficient supply of cool water, *i.e.* cooler than the ambient air temperature.

Whether the tufa is recent, *i.e.* of Holocene age, or older, is an interesting question. The dating of the tufa was deemed unrealistic given its high content of non-carbonate detritus (24% of dry weight). A Holocene age would seem the most likely, especially given the friability of the deposit. Older tufas might be expected to be more lithified due to diagenetic carbonate precipitation adding later calcite spar to the fabric (*cf.* Pedley 1990). The thin silts which overlie the tufa probably represent the reworking of the fines in the till matrix by spring water following cessation of tufa formation. This would have occurred during a shift to cooler ambient air temperatures and/or a reduction in biological activity within the precipitating waters.

In Unit SM2, the large proportion of striated subrounded boulders indicates most of the clasts have undergone active transport in the subglacial zone. The lack of matrix and the clast-supported nature of the unit may reflect the leaching of fines during subglacial melt-out (*cf.* Lawson 1979). The unit is, therefore, interpreted as a subglacial melt-out till formed during the decay of the glacier which deposited the underlying Unit SM1. Both of the basal units, SM1 and SM2, can be traced down-valley and appear to correspond to the deposits of the Aghia Paraskevi Member.

In Unit SM3, the strong clast fabric and the high elongation ($1-(S_2:S_1) = 0.767$) and low isotropy ($S_3:S_1 = 0.116$) of the fabric shape, combined with the dominance of a sand-silt matrix, support an interpretation of this deposit as a subglacial till which has undergone high levels of strain. Moreover, the dominance of block-shaped and striated clasts suggest transport in the active subglacial zone. Therefore, this unit is likely to have been deposited during glacial advance over Unit SM2. The underlying till units show little sign of deformation. This is probably because of the coarse, porous nature of Unit SM2, which would have resulted in low porewater pressures below an advancing glacier and subsequently, a relatively rigid bed. The fact that Unit SM3 appears to dip on its contact with Unit SM2 may indicate that the erosional boundary is a thrust fault with SM3 stacked atop SM2.

The subrounded, coarse clast-supported boulders which characterise Unit SM4 may represent a melt-out till formed near the former ice margin. As with SM2, the fine matrix may have been leached by escaping porewater during melt-out (*cf.* Lawson 1979).

Unit SM5 may represent more than one genetic unit, although its thickness and access to the face prohibit any detailed interpretation. However, as with Unit SM3, the lower contact appears to dip up-valley and may represent stacking of this unit over SM4

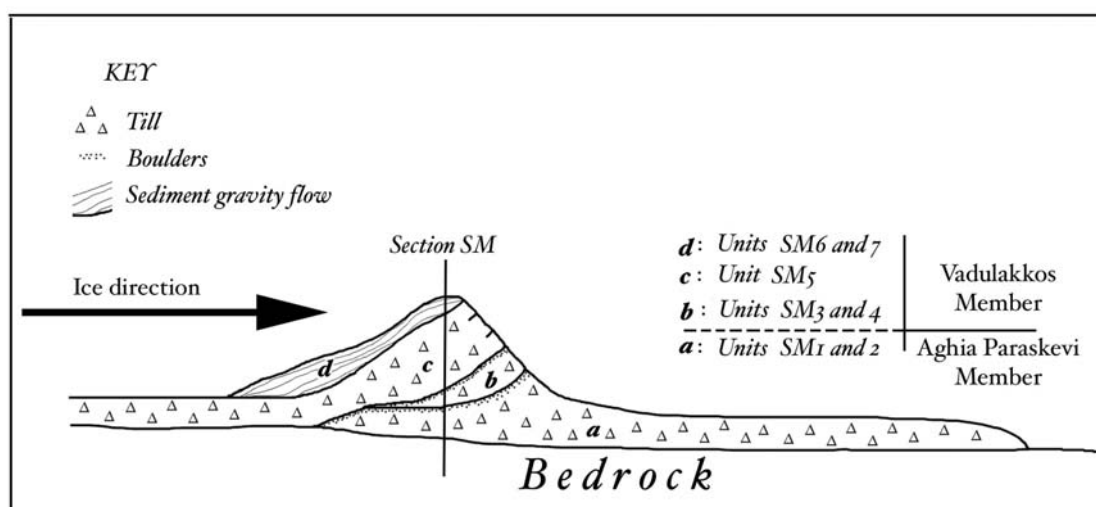


Figure 5.6 Schematic diagram showing the down-valley profile of the Vadulakkos moraines and associated units. The moraine is interpreted as a composite moraine formed by ice-thrusting in front of a former valley glacier.

due to thrusting in front of a former glacier. The strong clast fabric, orientated in the likely direction of ice flow indicated by the geomorphology, suggests that the diamicton is a subglacial till which has undergone high levels of strain. However, it appears that a significant proportion of the clasts have undergone less active transport than in the lower till units, SM1 and SM2. It may be the case that angular colluvial valley fill deposits, post-dating the glaciation which deposited Units SM3 and SM4, have been reworked during a subsequent glacial advance. This would explain the slightly more angular, elongate- and slab-shaped clasts of this unit. Unit SM5 cannot be traced down-valley.

Units SM6 and SM7 probably represent sediment mass flow deposits reworked from glacial moraines. The angular boulders of SM6 may represent accumulation at the base of a slope, whilst the gradation to the finer-grained Unit SM7 may represent a gradual reduction in slope-angle.

Overall, it is clear that the Smolikas Vadulakkos sequence represents a multiple till sequence combined with post-glacial colluvial and tufa deposits. At least two separate phases of glacier advance are recorded in these sediments. The lowest units (SM1 and SM2) represent part of the Aghia Paraskevi Member, and can be traced down-valley. The upper sediments (SM3 - SM7) and the surface ridge forms, comprise the Vadulakkos Member and represent a separate glacial phase. This upper sequence and the associated surface ridge morphology are interpreted as a composite moraine ridge (*cf.* Benn and Evans 1998, p. 463) with the surface sediments representing sediment gravity flow deposits. A schematic representation of the sediment-landform sequence in the lower Vadulakkos valley is shown in Figure 5.6.

No moraines occur higher up the Vadulakkos valley, though arcuate boulder ridges are clearly displayed in the high northern cirques and these are interpreted as moraines formed in front of former cirque glaciers. There are four cirques draining into the Vadulakkos valley and all contain moraines. Local names are unknown for these remote cirques and they are therefore named the Vadulakkos Cirques and numbered 1 to 4 from west to east. Another cirque, draining into the valley to the west of the Vadulakkos valley is named here the Northwestern Cirque (Fig. 5.1).

5.1.2 Cirque 1

Cirque 1 is the lowest of the Vadulakkos cirques and is situated on the western side of the upper Vadulakkos valley below a subsidiary summit (2318 m a.s.l.). A set of boulder ridges occur at *ca.* 40°06'08"N, 20°55'50"E, 2000 m a.s.l. and are classified as the **Cirque 1 Member**. These ridges are interpreted as cirque moraines which formed in front of a small glacier in the cirque to the south.

5.1.3 Cirque 2

Cirque 2 is separated from the Northwestern cirque (see below) by a sharp glacial arête (Fig. 5.7). The cirque contains two sets of small boulder ridges at 2175-2225 m and 2350 m a.s.l., identified here as the **Cirque 2 Member** and the **Smolikas Summit North Member** respectively. The ridges are all slightly arcuate and are between 200 and 250 m in length. These are interpreted as cirque moraines formed in front of glaciers occupying the cirque to the southwest (Fig.5.8).

5.1.4 Cirque 3

Cirque 3 is the largest and most central cirque draining into the Vadulakkos valley (Fig. 5.1) and contains two sets of ridges arcing transverse to valley orientation. The lower set of ridges are characterised by multiple boulder-covered crests between 2000 and 2250 m a.s.l. These landforms represent the **Cirque 3 Member** (*ca.* 40°05'30"N, 20°56'40"E). Higher ridges occur between 2325 and 2400 m a.s.l. and represent the **Smolikas Summit East Member** (40°05'25"N, 20°55'55"E). An arcuate boulder ridge at *ca.* 2350 m a.s.l. bounds the entrance to the highest part of the cirque on the eastern face of the highest Smolikas summit (2637 m a.s.l.). In addition, two small boulder ridges, each *ca.* 100 m long and 3-4 m high, also exist at *ca.* 2325 m a.s.l. at the base of the northern cliffs of the central Smolikas summit (2542 m a.s.l.).

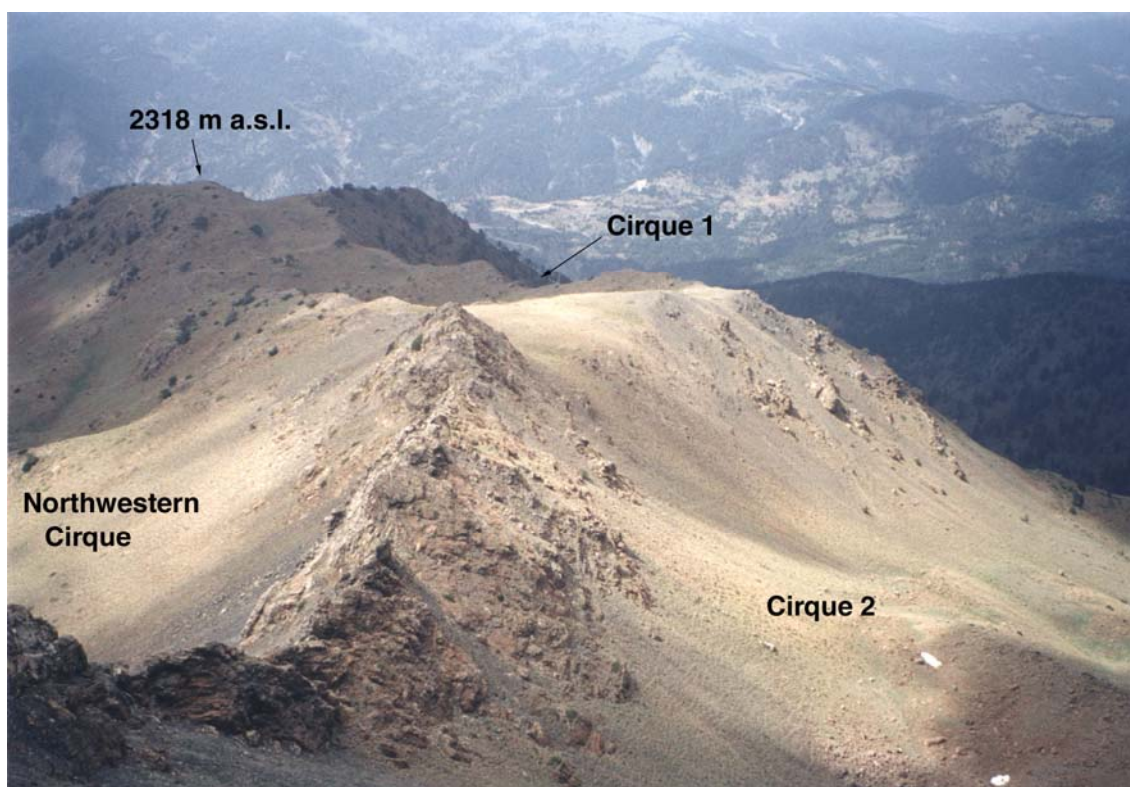


Figure 5.7 The arête dividing the Northwestern Cirque from Cirque 2 on Mount Smolikas (July 2001).



Figure 5.8 Moraines in Cirque 2 on Mount Smolikas. The inner moraines (in shade) represent the Smolikas Summit North Member and the more distant outer moraines (in sunlight) represent the Cirque 2 Member.

The sediments and landforms of the Cirque 3 Member are interpreted as a terminal moraine (the outermost ridge) and a series of recessional moraines. The ridges of the Smolikas Summit East Member are interpreted as moraines and pronival ramparts of the last glacial advance on Mount Smolikas. The moraine ridge in the cirque directly to the east of the highest Smolikas summit (2367 m a.s.l.) was formed at the margin of a small cirque glacier whilst the two boulder ridges at the base of the northern cliffs of the central summit (2542 m a.s.l.) formed at the base of perennial static snow beds (*cf.* Washburn 1979, Ballantyne and Kirkbride 1986).

5.1.5 Cirque 4

Cirque 4 is the eastermost cirque draining into the Vadulakkos valley, situated at *ca.* 2300-2400 m a.s.l. on the northwestern slopes of Moasa (2610 m a.s.l.). This cirque contains boulder-covered hummocks and represents the type locality of the **Cirque 4 Member**. These hummocks are mapped as hummocky moraine. The steep slopes at the lip of this cirque suggest that the glacier slope would have been very steep. Therefore, it is possible that an ice-fall occurred over these steep cliffs during the same glacial phase which deposited the Cirque 3 Member in the valley below. The hummocky moraines of the Cirque 4 Member are 250 m higher than the latter deposits and probably formed upon glacier retreat into the confines of the cirque lip.

The summit ridge of Mount Smolikas is shown in Figure 5.9. In this photograph, there is a clear contrast between the glaciated northern cirques (left side of the ridge) and the smooth unglaciated southern slopes (right side of the ridge). The unglaciated summit areas also display evidence of prolonged periglacial weathering. Blockfields can be found all over the summit ridges and the ophiolite bedrock is deeply weathered, often displaying thick orange weathering crusts around the black/ dark green original rock surface. The original pre-glacial plateau surface is well-displayed near one of the eastern Smolikas summits (2575 m a.s.l.). Here, glacial action has not eroded cirque headwalls sufficiently to form sharp ridges leaving deeply-weathered plateau remnants of the pre-glacial surface (Fig. 5.10). Periglacial processes probably still operate today on the highest slopes since the mean temperature during the coldest month is likely to be lower than -7°C , given that the modern mean January temperature at Ioannina (483 m a.s.l.) is 4.6°C (World Meteorological Organisation 1998) and assuming a lapse rate of 0.6°C per 100 m altitude.

5.1.6 Morpho-lithostratigraphical summary of the Vadulakkos valley

The morpho-lithostratigraphy of deposits in the Vadulakkos valley is summarised in Table 5.1. Four stratigraphical units, each defined by single or multiple type sections or localities, can be recognised in this area on the basis of morpho-lithostratigraphical position.

Unit 1. The **Aghia Paraskevi Member** is situated in the lowest part of the Vadulakkos valley and in the Ellenikos valley, east of the village of Aghia Paraskevi. It is characterised by diamicton deposits which have little surface form. The sediments are exposed in Section SM (Units SM1 and SM2), and the lower lateral boundary occurs at *ca.* 1050 m a.s.l. These sediments are interpreted as till formed by an extensive valley glacier.

Unit 2. The **Vadulakkos Member** includes Units SM3 to SM7 in Section SM and consists of diamicton deposits and ridge forms. The deposits of this member are interpreted as till units forming a composite moraine ridge, topped by sediment gravity flow deposits. The lower lateral boundary of this unit is *ca.* 1070 m a.s.l. The moraines were formed by a valley glacier which filled the Vadulakkos valley.

Unit 3. The **Cirque 1, Cirque 2, Cirque 3 and Cirque 4 Members** are positioned at the entrance to the higher cirques draining into the Vadulakkos valley. These deposits are characterised by diamictons and bouldery ridge forms and are interpreted as cirque glacier moraines.

Unit 4. This unit is characterised by the **Smolikas Summit North** and **Smolikas Summit East Members** in the highest parts of Cirques 2 and 3. The unit is characterised by arcuate boulder ridges which are interpreted as small cirque glacier moraines and pronival ramparts.

Unit 4	Smolikas Summit North Member Smolikas Summit East Member	NORTH SMOLIKAS FORMATION
Unit 3	Cirque1 Member/ Cirque 2 Member/ Cirque 3 Member/ Cirque 4 Member	
Unit 2	Vadulakkos Member	
Unit 1	Aghia Paraskevi Member	

Table 5.1 Morpho-lithostratigraphy of the Vadulakkos valley.

5.2 Northwestern Cirque

The Northwestern cirque is an isolated cirque on the northwestern slopes of the main summit of Mount Smolikas (2632 m a.s.l.) (Fig. 5.1). This cirque contains a lobate mass of bouldery sediment. This feature has several surface furrows and fills the cirque floor, descending to around 2160 m a.s.l. These deposits represent the **Northwestern Cirque Member** and, since only one unit exists in this valley, they also represent the **Northwestern Cirque Formation**. The sediment-landform is interpreted as a former rock glacier. The feature has retained a lobate morphology and is slightly elevated from the cirque margins, indicating that it was largely debris-dominated. The rock glacier debris would have been supplied by talus from the surrounding cirque walls and moved downslope by permafrost creep. For these reasons, it is interpreted as a periglacial talus rock glacier (*cf.* Barsch 1988, 1996). The rock glacier occupied a well-developed cirque bounded to the east by a sharp arête. Since no glacial moraines are found down-valley of the rock glacier, it is likely that the rock glacier formed contemporaneously with the highest, most recent, small cirque glaciers elsewhere on Mount Smolikas. During earlier, more extensive, glacial phases, it is likely that the cirque was insufficiently well-developed to accommodate glacier ice and nivation patches probably occupied this hollow. An excess of debris supply over snow accumulation during the most recent major cold phase then led to the development of a rock glacier.

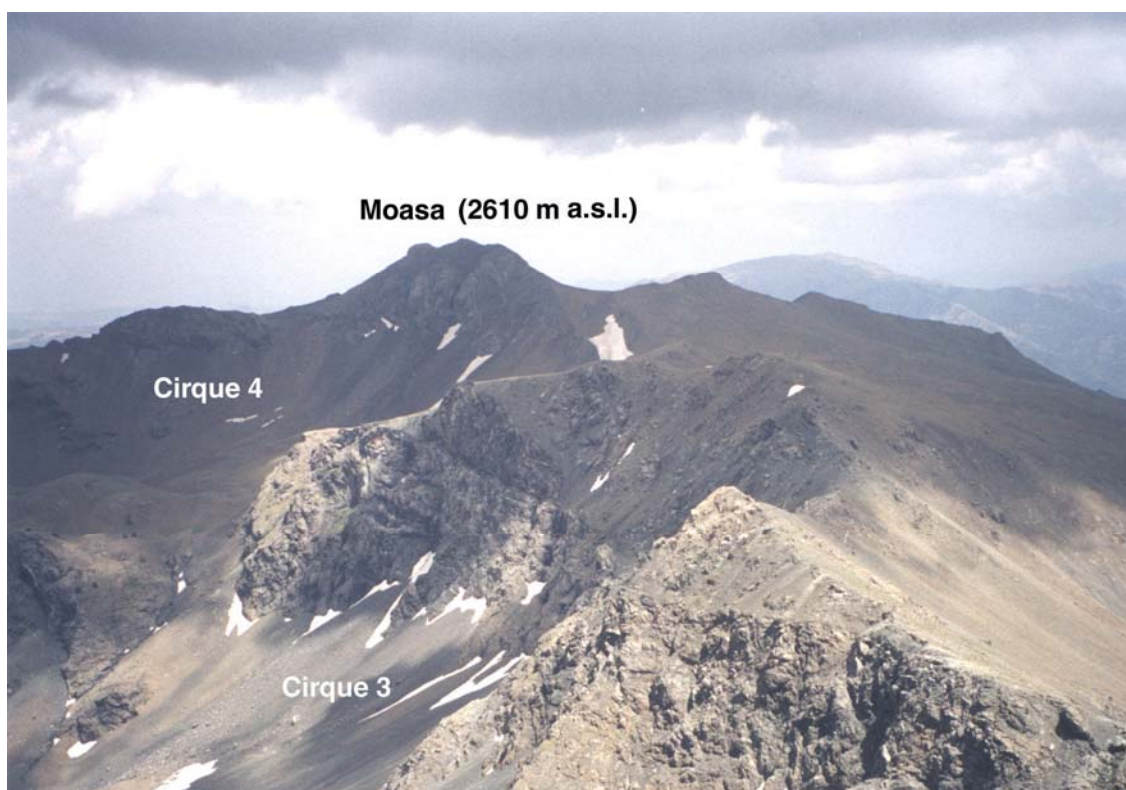


Figure 5.9 The summit ridge of Mount Smolikas looking east from the main summit (2637 m a.s.l.) (July 2001).



Figure 5.10 Remnants of the weathered pre-glacial plateau surface to the north of the eastern Smolikas peak (2575 m a.s.l.). Note the headwall cliffs of Cirque 4 and the Galanos Limni cirque on the left and right sides of this plateau (May 2003).

5.3 The Konkutino valley and cirques

The Konkutino valley is situated on the eastern slopes of Mount Smolikas, east of the subsidiary peak Moasa (2610 m a.s.l.). There are two major branches at *ca.* 1400 m a.s.l. The southern branch leads to the southeastern cirque of Moasa. The northern branch leads to the northeastern cirque of Moasa, containing the lake Galanos Limni, and the southern cirque of Bogdoni (2248 m a.s.l.) (Fig. 5.11).

5.3.1 Konkutino valley

A bulldozed track leads off the Samarina-Distrato track up the Konkutino valley at *ca.* 40°04'35"N, 20°59'45"E, 1220 m a.s.l. Where this road turns on itself at *ca.* 40°05'21"N, 020°58'46"E (1420 m a.s.l.) bouldery diamictons are evident. These deposits are now deeply incised by the Konkutino river and represent the type area for the **Konkutino Member**. On the east side of the river, a well defined ridge occurs. The base of this ridge is incised by the river and appears to be bedrock. However, the upper part consists of several metres of unconsolidated bouldery material and the feature is interpreted as a moraine. This interpretation is supported by the superficial morphology which is arcuate and littered with boulders. The former glacier limits on the western side of the river is marked by a drift limit. Higher in the Konkutino valley, ice-moulded bedrock is widespread including polished bedrock, striae and larger erosional forms, such as *roches moutonnées*.

5.3.2 Bogdoni cirque

In the southern cirque of the north peak of Bogdoni (2238 m a.s.l.), diamicton deposits are evident containing subrounded and striated clasts. These deposits represent the **Bogdoni Member**. The deposits are morphologically expressed as hummocky terrain and sections through diamicton occur in areas incised by the modern stream. Also, subrounded perched boulders can be found atop these hummocks in many areas of this cirque. The deposits are clearly glacial in origin. They are interpreted as having formed during localised cirque glaciation and extend down to the cirque lip at *ca.* 1900 m a.s.l. However, the surface morphology of the deposits is poorly expressed compared with cirque moraines found in the highest parts of the Konkutino valley near Galanos Limni (refer to North Limni and Galanos Limni Member deposits below). Moreover, the glacier which occupied this cirque would have also been much lower than the glacier which deposited the North Limni and Lower Galanos Limni Members. Thus, for these reasons, the glacial deposits in the Bogdoni cirque are considered contemporaneous with the Konkutino Member.

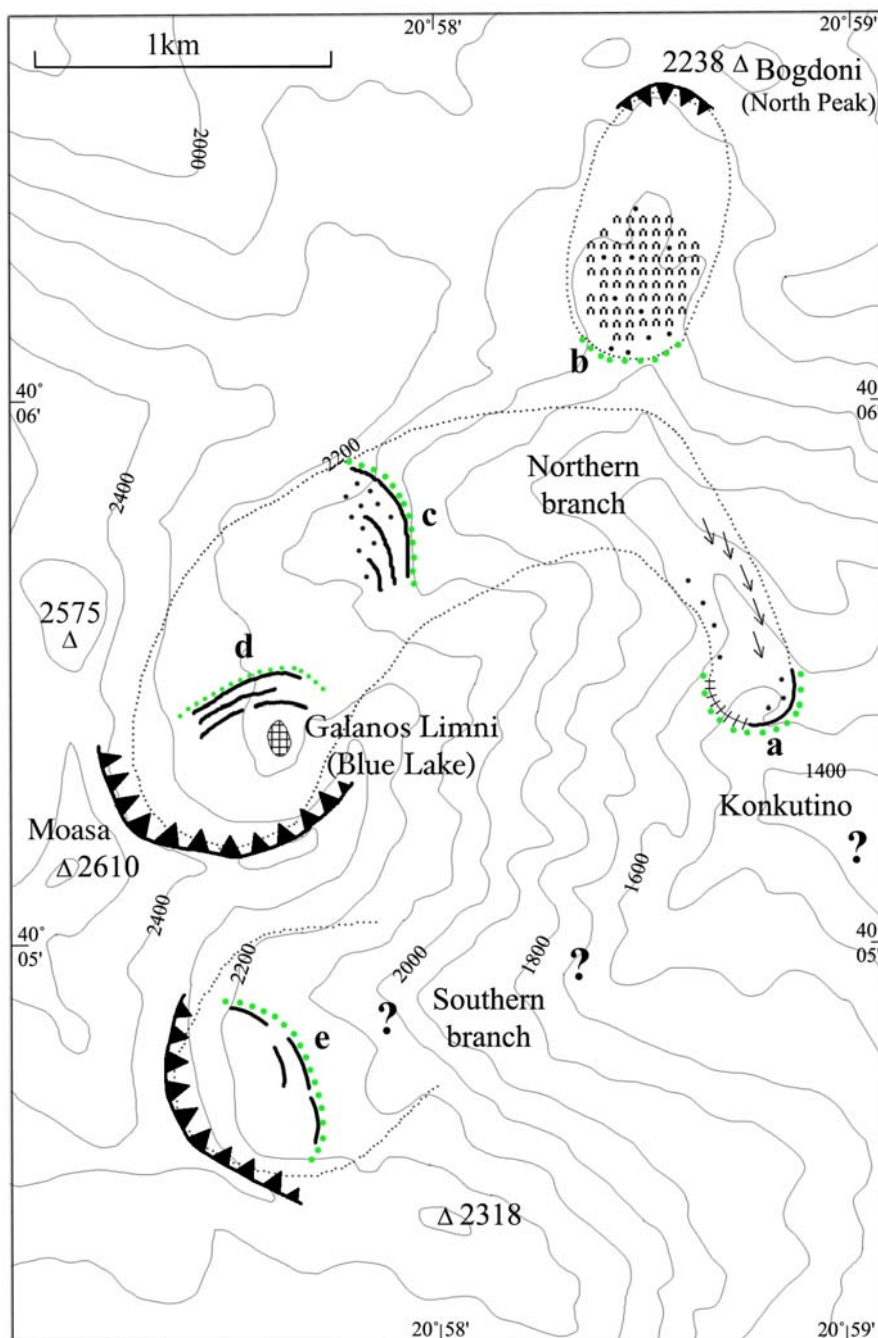


Figure 5.11 Geomorphological map of the eastern Smolikas area. See Figure 3.4 for key. Stratigraphical units marked **a-e** represent the Konkutino Formation (**a.** Konkutino Member, **b.** Bogdoni Member, **c.** North Limni Member, **d.** Galanos Limni Member, **e.** Moasa Member).

5.3.3 Moasa northeastern cirque

Arcuate bouldery ridges occur in the northeastern cirque of Moasa (2610 m a.s.l.). Two sets of ridges exist, both with multiple crests. The lowest ridges, referred to here as the **North Limni Member**, exist between 2000 and 2075 m a.s.l. at *ca.* 40°05'45"N, 20°57'55"E. At least three crests can be identified and all have boulders perched on their surfaces. These

ridges are interpreted as end and recessional moraines formed at the margins of a large cirque glacier.

A further 1 km up-valley, ridges impound a small lake known locally as Galanos Limni (Blue Lake) at *ca.* 40°05'21"N, 20°57'35"E, 2160 m a.s.l. (Fig. 5.12). Multiple ridge crests can be identified and are aligned almost parallel to the main valley floor, unlike the ridges further down-valley which are transverse to the valley floor. These ridges represent the **Galanos Limni Member** and are interpreted as cirque glacier moraines. The ridges appear to represent end and recessional moraines in front of a glacier emanating from the steepest cliffs on the southeastern side of the cirque. The sediment ridges of the Galanos Limni Member correspond with a northerly ice-flow direction. This contrasts with the earlier, more extensive, glacial phases where the glacier had a northeasterly ice-flow direction.

5.3.4 Moasa southeastern cirque

The southeastern cirque of Moasa (2610 m a.s.l.) also contains boulder ridges. Several ridges are evident at *ca.* 40°04'44"N, 20°57'38"E, 2150 m a.s.l. These deposits are named the **Moasa Member** and are interpreted as cirque moraines. These deposits are similar in form and occur at a similar altitude to the Galanos Limni Member, the highest deposits in the cirque to the north, and it is likely that they correlate. Outside of these moraines, evidence of glaciation is difficult to trace. It is probable that glaciers did extend some distance down-valley, since glacial deposits extend to altitudes over 700 m lower than the highest cirque moraines in the other areas of the Konkutino valley. The deposits have probably been eroded as a consequence of the very steep slopes of this area. Trace deposits may exist but locating these is difficult due to the dense woodland and steep terrain.

Given the approach adopted in this thesis, the Moasa Member should strictly be considered within a separate formation, since no deposits exist in the lower parts of the Konkutino valley. Even so, in this instance there is no strong reason to separate the southern branch of the Konkutino valley, containing the Moasa Member, from the northern branch containing the Konkutino, Bogdoni, North Limni and Galanos Limni Members. This is particularly justified given the likelihood of missing, eroded or undiscovered deposits in the southern branch as well as in the lower Konkutino valley below the point where both branches merge (*i.e.* below *ca.* 1500 m a.s.l.).

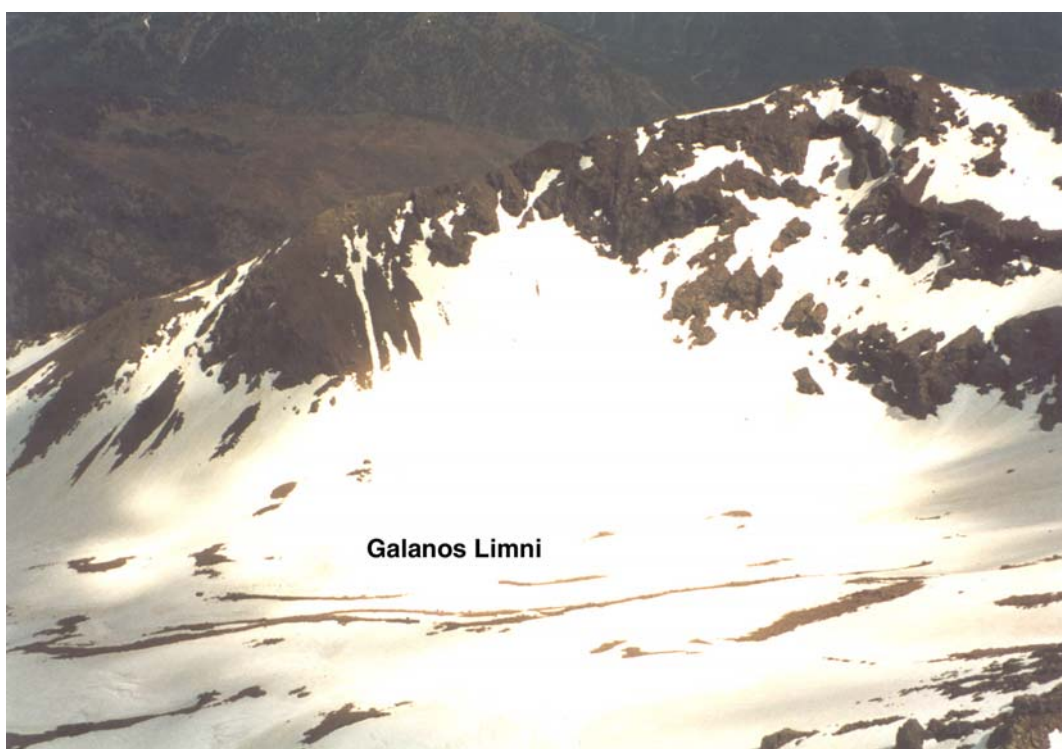


Figure 5.12 The northeastern cirque of Moasa (2610 m a.s.l.) containing the lake Galanos Limni. Although the lake is frozen and covered by snow, the moraine ridges are clearly evident in this photograph aligned parallel to the main valley axis. The glacier would have been sourced on the slopes of the peak in the background (May 2003).

5.3.5 Morpho-lithostratigraphical summary of the Konkutino valley

The stratigraphy of deposits in the Konkutino valley is summarised in Table 5.2. Three stratigraphical units can be recognised in this area on the basis of morpho-lithostratigraphical position.

Unit 1. The **Konkutino and Bogdoni Members** are situated in the middle part of the Konkutino valley and in the Bogdoni cirque. The Konkutino Member is characterised by diamicton ridges with a lower lateral boundary at *ca.* 1420 m a.s.l. The Bogdoni Member is characterised by hummocky diamicton deposits and perched boulders. The sediment-landforms are interpreted as moraines formed at the margin of a former valley glacier in the Konkutino valley and a smaller cirque glacier in the Bogdoni cirque.

Unit 2. This unit is represented by the **North Limni Member** and is characterised by arcuate bouldery ridges. These are interpreted as cirque moraines. The lower lateral boundary of this unit is situated at between 1900 and 2000 m a.s.l. in the middle reach of the Konkutino valley.

Unit 3. This unit is characterised by the **Galanos Limni Member** and the **Moasa Member** and consists of bouldery ridges at cirque heads. These deposits were formed by small cirque glaciers. The deposits of this unit occur no lower than *ca.* 2150 m a.s.l. in both the the Galanos Limni and Moasa cirques, the uppermost cirques of the northern and southern branches of the Konkutino valley.

Unit 3	Galanos Limni Member Moasa Member	KONKUTINO FORMATION
Unit 2	North Limni Member	
Unit 1	Konkutino Member Bogdoni Member	

Table 5.2 Morpho-lithostratigraphy of the Konkutino valley.

5.4 The Samarina area

Bouldery ridges occur to the northeast of the south peak of Mount Bogdoni (2253 m a.s.l.) near the village of Samarina (Fig. 5.13). The deposits are marked as glacial deposits on IGME geological maps (IGME 1987) and are named here the **Samarina Member**. They represent the sole unit of the **Samarina Formation**. These ridges are consistent with formation at the margins at a former glacier which appears to have reached down to the position of the modern Vriazi river. The maximum extent of the former glacier is marked by a clear boulder limit at *ca.* 1500 m a.s.l. (40°06'59"N, 21°00'30"E). The Fourka-Samarina road cuts through the deposits in this lower area and diamictons are clearly exposed. Several boulder ridges on the north side of the valley are interpreted as lateral recessional moraines (Fig. 5.14). These moraines are well-preserved and morphologically expressed, *ca.* 5 m high and 200 m long. They are poorly vegetated and, as a result, clasts are readily exposed (Fig. 5.15). The shape and roundness of 50 randomly sampled surface clasts were measured on one moraine at site SA (*ca.* 40°06'57"N, 21°00'10"E, 1570 m a.s.l.). The results are shown in Figure 5.16. They were sampled from the crest of the moraine ridge only, so as not to sample clasts which have accumulated via slope processes following glaciation.

The clasts have a mean size of 105 mm and are largely blocks but with a significant proportion of slabs. The latter is indicated by a high C_{40} index of 36% and the fact that only 8% of clasts had a $b:a$ ratio of ≤ 0.5 (therefore indicating that the clasts with a low $c:a$ ratio are slabs rather than elongate). The clasts are also predominantly angular (VA: 16%; A: 32%; SA: 46%; SR: 6%) and 80% were ophiolite, 10% flysch and 10% Jurassic limestone. Only 3 of the 50 sampled clasts were striated.

The clast analyses of the Samarina moraine provide interesting information regarding moraine genesis. The angularity of the clasts and the lack of striae suggest a passive transport route, *i.e.* via englacial or supraglacial transport, rather than in the subglacial basal zone (*cf.* Boulton 1978, Benn and Ballantyne 1994). It is interesting that, whilst the underlying bedrock in the lower part of the glaciated valley is flysch, 90% of the clasts sampled from the lateral moraine were ophiolite or Jurassic limestone. These lithologies are only found in the upper reaches of the valley. This, and the fact that nearly all of the clasts display no evidence of abrasion, suggests that the moraine debris is composed of from supraglacial material derived from the upper valley sides. Frost shattering and subsequent addition of this valley-side material to the glacier surface provided the main source of debris for the surface deposits of the moraine. However, the internal composition may be quite different and perhaps dominated by clasts which have travelled via active transport in the basal zone. Variable moraine composition is typical of conventional lateral moraines (Bennett and Glasser 1996, Fig 9.11). This is partly a limitation of using only surface clasts rather than sections which expose the internal sedimentology, although in this case, only the former was available.

A lateral moraine also exists on the southern side of the valley and is around 400 m long and 10 m high. The moraine is a single form and recessional features do not exist, unlike on the north side of the valley. Inside of the lateral moraines of the lower valley area, extensive spreads of unvegetated fluvial gravels exist and are probably post-glacial, formed by the reworking of till up-valley of this area.

As noted earlier, the source of the Samarina glacier is characterised by steep ophiolite cliffs on the northeastern flanks of Mount Bogdoni. The site is interesting since the incised backwall cliffs occur on the lower flanks of this mountain and not on higher areas, where snow accumulation would be more favoured. This is probably a function of the local geology and the associated inherited landscape. Indeed, the backwall area occurs at the position of the ophiolite overthrust and associated faults, which provide areas of weakness favouring hollow development.

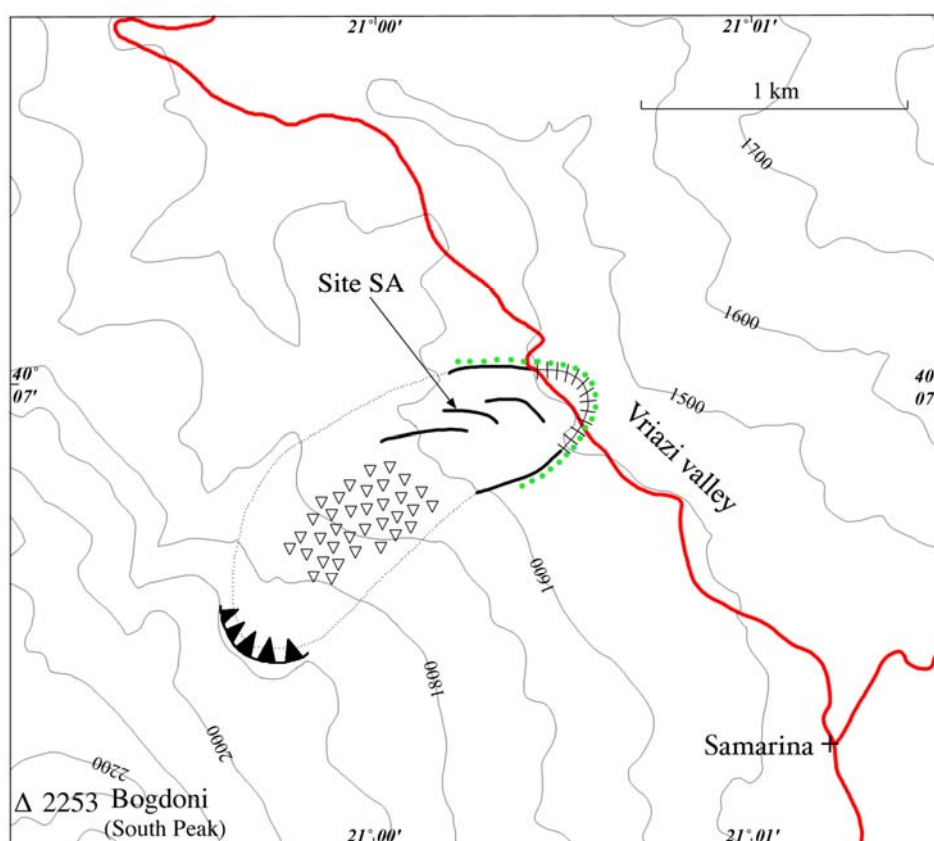


Figure 5.13 Geomorphological map of the Samarina area. A key to the geomorphological map is provided in Figure 3.4.



Figure 5.14 The Samarina moraines. Sample site SA is indicated at *ca.* 40°06'57"N, 21°00'10"E, 1570 m a.s.l.



Figure 5.15 Sample site SA on the crest of a moraine ridge at *ca.* 40°06'57"N, 21°00'10"E, 1570 m a.s.l. The former glacier would have been sourced in the up-valley area in the top left hand corner of this photograph.

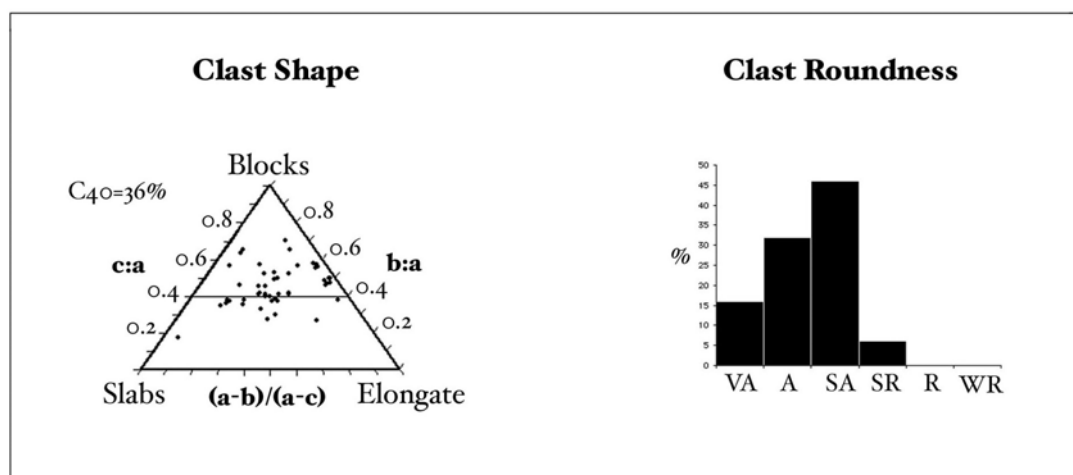


Figure 5.16 Clast analyses from a lateral moraine of the Samarina glacier (sample site SA).

5.5 Northeastern slopes of Mount Vasilitsa

Boulder-covered diamicton deposits extend to just above the village of Smixi at *ca.* 1320 m a.s.l. on the northeastern slopes of Mount Vasilitsa (2248 m a.s.l.) (Fig. 5.17 and 5.18). Sections are cut in several places by roads and tracks, and large perched rocks occur in

many areas on the surface of these deposits. The diamicton is largely matrix-supported and resembles the glacial deposits noted elsewhere such as in the Vadulakkos valley on Mount Smolikas. Moreover, glacial deposits are shown on the geological maps of this area (IGME 1983). In the lowermost areas, moraine ridges are still preserved, although these are rather subdued and the clasts are often covered in thick orange weathering crusts. These deposits are termed the **Smixi Member**.

Further up-valley, diamicton ridges impound a small lake on the north-eastern slopes of Vasilitsa (2248 m a.s.l.) at *ca.* 40°03'16"N, 021°05'23"E, 1750 m a.s.l. Two more ridges also exist to the southwest of the lake. These sediment-landforms are named the **North Vasilitsa Member** and are interpreted as end and recessional moraine ridges formed in front of a former cirque glacier.

Diamicton ridges also exist further south and impound a lake at *ca.* 40°02'52"N, 21°05'40"E, 1790 m a.s.l. (Fig. 5.19). Here, at least three ridge crests can be defined. These sediment landforms are identified as the **Central Vasilitsa Member** and are interpreted as end and recessional moraines formed in front of a small valley glacier. Hummocky, boulder-covered ground is evident up-valley of these ridges and probably formed during glacier retreat. A boulder ridge is also evident in the shallow valley to the southeast at *ca.* 1730 m a.s.l. and appears to represent the terminus of an off-shoot glacier which had the same source as the glacier which produced the lake moraines described above.

Higher up-valley, arcuate boulder-ridges dam another lake at *ca.* 2000 m a.s.l. (probably ephemeral) and is identified as the **Vasilitsa Summit Member**. These ridges are interpreted as cirque moraines and are morphologically distinct from the intervening recessional hummocky moraine. They probably represent a separate glacial advance during a later glacial phase.

5.5.1 Morpho-lithostratigraphical summary of northeastern Mount Vasilitsa

The stratigraphy of deposits on the northeastern slopes of Mount Vasilitsa is summarised in Table 5.3. Three stratigraphical units can be recognised in this area on the basis of morpho-lithostratigraphical position.

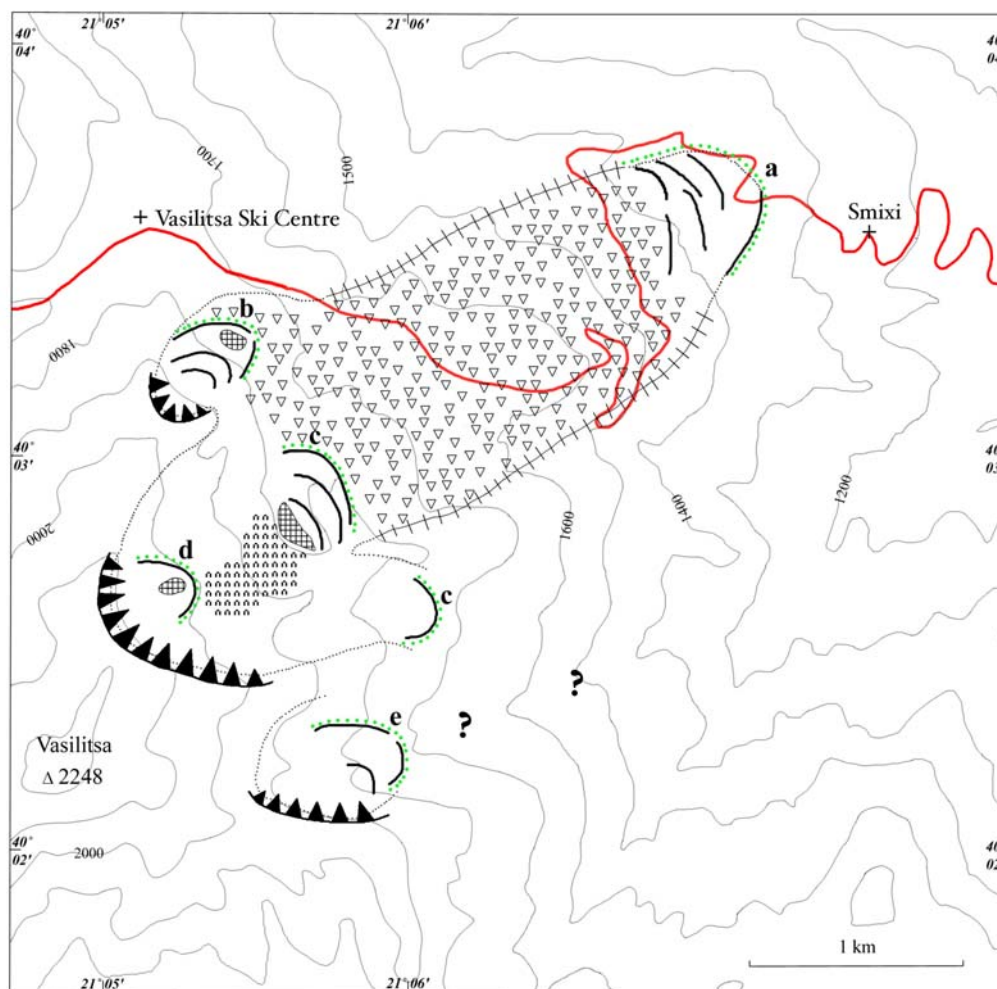


Figure 5.17 Geomorphological map of the Mount Vasilitsa area. A key is provided in Figure 3.4. The stratigraphical units marked **a-d** represent the Vasilitsa Formation (**a.** Smixi Member, **b.** North Vasilitsa Member, **c.** Central Vasilitsa Member, **d.** Vasilitsa Summit Member). The stratigraphical unit marked **e** represents the East Vasilitsa Member, the sole unit of the East Vasilitsa Formation.

Unit 1. The **Smixi Member** is situated in the valley leading northeastwards from Vasilitsa summit to the village of Smixi. It is characterised by diamicton ridges and perched boulders with a lower lateral boundary at *ca.* 1320 m a.s.l. The sediment-landforms are interpreted as glacial deposits formed by an extensive valley glacier.

Unit 2. This unit is represented by the **North and Central Vasilitsa Members** and is characterised by arcuate boulder ridges that dam small lakes. The lower lateral boundary of this unit is situated at between 1700 and 1800 m a.s.l. in the middle reach of the northeastern valley of Mount Vasilitsa. The ridges are interpreted as moraines small cirque and valley glaciers.

Unit 3. This unit is characterised by arcuate boulder ridges of the **Vasilitsa Summit Member**. These deposits were formed by a small cirque glacier. The deposits of this

member occur down to *ca.* 2000 m a.s.l. in the uppermost cirque draining into the northeastern valley of Mount Vasilitsa.

Unit 3	Vasilitsa Summit Member	VASILITSA FORMATION
Unit 2	North Vasilitsa Member Central Vasilitsa Member	
Unit 1	Smixi Member	

Table 5.3 Morpho-lithostratigraphy of the northeastern valley of Mount Vasilitsa.

5.6 Eastern slopes of Mount Vasilitsa

East of the summit of Vasilitsa, the boulder ridges exist in a small hollow at *ca.* 40°02'20"N, 21°05'50"E, 1730 m a.s.l. These deposits represent the **East Vasilitsa Member**. As this is the sole unit, these deposits also represent the **East Vasilitsa Formation**. Two main crests can be identified. The lower ridge is interpreted as a lateral-end moraine formed by a glacier which extended down to *ca.* 1730 m a.s.l., and the higher ridge, only a short distance upslope, as a recessional moraine. No diamicton deposits were located outside of these moraines. However, given that glaciers extended as low as 1320 m a.s.l. in the neighbouring Vasilitsa Formation, it is likely that ice extended beyond the lower boundary of the East Vasilitsa Formation. However, these deposits appear to have been eroded. Alternately, it is possible that the hollow in this area was not sufficiently well-developed to enable glacier formation during earlier glacial phases.

5.7 Differences between the Mount Smolik/Vasilitsa glacial deposits and those on Mount Tymphi

The glacial deposits of Mount Smolik and Mount Vasilitsa are much less well-preserved than those on Mount Tymphi. This is largely a qualitative observation based on the preservation of moraine morphology and their overall 'freshness'. On Mount Tymphi, the moraines are often very well-preserved, especially those in mid-valley positions and in higher valley areas. On Mount Smolik and Vasilitsa, however, even the highest moraines



Figure 5.18 A section through the Smixi Member at *ca.* 40°03'10"N, 21°05'50"E, 1690 m a.s.l. These diamicton deposits are interpreted as till (May 2003).



Figure 5.19 A moraine impounding a lake to the east of Mount Vasilitsa at *ca.* 40°02'52"N, 21°05'40"E, 1790 m a.s.l. (May 2003).

are subdued, with crests that are much lower and less sharp than on Mount Tymphi. Since the glacial sequence on Mount Tymphi would be expected to correlate with the sequence on Mount Smolikas and Vasilitsa, given the closeness of these mountains, the difference in moraine preservation and 'freshness' must be controlled by factors other than age. The most probable explanation lies in the composition of the moraines. On Mount Tymphi, the moraines are largely composed of limestone. Woodward *et al.* (2004) suggest that the permeability of the limestone moraines would have limited runoff and erosion by fluvial action and mass wasting. The strength of the deposits is also promoted by the widespread development of secondary carbonate cements. In addition, these cements provide evidence of widespread free-drainage through the moraines since they are often formed by the outgassing of percolating waters saturated with CaCO_3 (see Chapter Six). Conversely, on Mount Smolikas and Mount Vasilitsa, the moraines are largely composed of ophiolite which is impermeable. Whilst the unconsolidated moraines are likely to enable free-drainage, particularly where clast-supported, the impermeable lower bedrock would have concentrated flow in these surface deposits, promoting saturation and greater frequency of surface runoff. Furthermore, in matrix-supported glacial deposits on Mount Smolikas and Mount Vasilitsa, runoff is likely to have been much higher than on the limestone-dominated tills of Mount Tymphi since the insolubility of the matrix prevents the development of an efficient internal drainage. This would be particularly pronounced in highly compacted tills which are widespread on both Mount Smolikas and Mount Vasilitsa.

5.8 Summary of Mount Smolikas and Vasilitsa

Three separate morpho-lithostratigraphical formations are identified in the valley systems of Mount Smolikas and two on Mount Vasilitsa. A maximum of four member units are present in one of these formations: in the Vadulakkos valley on Mount Smolikas. Elsewhere on Mount Smolikas and Mount Vasilitsa, a maximum of three units are present. The morpho-lithostratigraphy on Mount Smolikas can be interpreted as representing at least four discrete phases of glaciation, one more than on neighbouring Mount Tymphi. The absolute and relative chronology of the glacial sequence on all mountains, and the designation of stage names for a common chronostratigraphy, is the focus of the next chapter, Chapter Six.

Chapter Six

Chronology

In the previous chapter, the geomorphology and local morpho-lithostratigraphy of the glacial and periglacial deposits in the cirque-valley systems of Mounts Tymphi, Smolikas and Vasilitsa were established. The position of these units in time is fundamental to inter-valley and wider-scale correlation. The element of stratigraphy that deals with the relative time relations and ages of rock or sediment bodies is termed **chronostratigraphy**. The science of dating and determining the time sequence of the events in the history of the Earth is termed **geochronology**. In this chapter, radiometric and relative-age dating techniques are used in conjunction with the geomorphological and morpho-lithostratigraphical evidence to derive a chronostratigraphical, and where possible, a geochronological framework for the glacial and periglacial deposits of Greece.

6.1 Geochronology

The issue of dating is one of the biggest obstacles to understanding the glacial sequence in the Mediterranean region. In many areas on Mount Tymphi, secondary carbonate cements have formed within glacial and glaciofluvial deposits. In glacial systems, subglacial transport of carbonate rock debris produces abundant fine reactive particles (rock flour) which are susceptible to dissolution and re-precipitation as secondary carbonates (Fairchild *et al.* 1994). This fact was successfully utilised by Woodward *et al.* (2004) to provide minimum ages for glacial deposits in this area using Uranium-series (U-series) dating. This approach was also applied to cemented glacial deposits in the Gran Sasso area of the Italian Apennines by Kotarba *et al.* (2001) and appears to be one of the most useful methods of dating glacial deposits in areas dominated by carbonate lithologies. This technique was therefore applied in this study.

Unfortunately, U-series dating of secondary cements was only of use on Mount Tymphi since this mountain is formed in limestone, unlike Mount Smolikas and Mount Vasilitsa which are formed in ophiolite, a non-carbonate rock. Nevertheless, since the glacial and periglacial deposits were most extensive on Mount Tymphi, U-series dating provided a powerful geochronological tool. The theory, application and method of U-series dating secondary carbonates are described below.

6.1.1 U-series dating - theory

Uranium has three naturally occurring radioactive isotopes: ^{238}U (half-life 4.4683×10^9 years); ^{235}U (half-life 7.13×10^8 years); and ^{234}U (half-life 245,250 years). These decay in two series: the ^{238}U series and the ^{235}U series. However, ^{235}U is much less abundant than ^{238}U , comprising only 0.72 atom percent of natural uranium. The most useful and versatile U-series method in Quaternary studies is the $^{230}\text{Th}/^{234}\text{U}$ method based on the ^{238}U series (Smart 1991). This method of U-series dating relies on the propensity of uranium, a very soluble element in water, to co-precipitate with calcium during carbonate formation. Its daughter isotope, ^{230}Th (half life 75,690 years), does not co-precipitate during carbonate formation due to its total immobility in the near-surface environment (Langmuir and Herman 1980). As a result, at the time of formation, a secondary carbonate deposit such as calcite cement, contains ^{234}U and no ^{230}Th , the daughter isotope. There is disequilibrium, therefore, between ^{234}U and ^{230}Th , and the subsequent ingrowth of ^{230}Th provides a chronometer with which to measure elapsed time since carbonate deposition. The practical range of U-series dating using $^{230}\text{Th}/^{234}\text{U}$ is *ca.* 350,000 years, although with the development of sensitive analytical techniques of mass spectrometry, the range of this technique is potentially <100 to 600,000 years (Ku 2000).

In most natural waters, there is also a disequilibrium between ^{238}U and ^{234}U that results from the preferential release of ^{234}U from mineral surfaces. Therefore, upon incorporation into a closed solid state, there may be an excess of ^{234}U which will decline at a rate controlled by the half-life of ^{234}U . The decay of excess ^{234}U increases the $^{230}\text{Th}/^{234}\text{U}$ slightly for any given time. Figure 6.1 illustrates the relationship between $^{230}\text{Th}/^{234}\text{U}$ and $^{234}\text{U}/^{238}\text{U}$ ratios through time for a closed system with varying initial $^{234}\text{U}/^{238}\text{U}$ and an initial $^{230}\text{Th}/^{234}\text{U}$ of zero. Age is therefore calculated from the measured $^{230}\text{Th}/^{234}\text{U}$ and $^{234}\text{U}/^{238}\text{U}$ ratios in the sample and is calculated from the equation:

$$\frac{^{230}\text{Th}}{^{234}\text{U}} = \left(\frac{1 - e^{-\lambda_{230}t}}{^{234}\text{U}/^{238}\text{U}} \right) + \left(1 - \frac{1}{^{234}\text{U}/^{238}\text{U}} \right) \left(\frac{\lambda_{230}}{\lambda_{230} - \lambda_{234}} \right) (1 - e^{-(\lambda_{230} - \lambda_{234})t})$$

where t is time and λ is the decay constant for the adjacent isotope mass. Given the $^{234}\text{U}/^{238}\text{U}$ and $^{230}\text{Th}/^{234}\text{U}$ ratios for a sample, the equation may be solved for t using an iterative procedure (Smart 1991, Ivanovich and Harmon 1992).

The dating of secondary carbonates via U-series relies on several assumptions and criteria for application (Smart 1991). Upon deposition, the carbonate should be entirely free of ^{230}Th . Most non-authigenic ^{230}Th is introduced bound to silicate or organic material. The presence of detrital ^{230}Th can be deduced from the presence of the isotope ^{232}Th . This long-

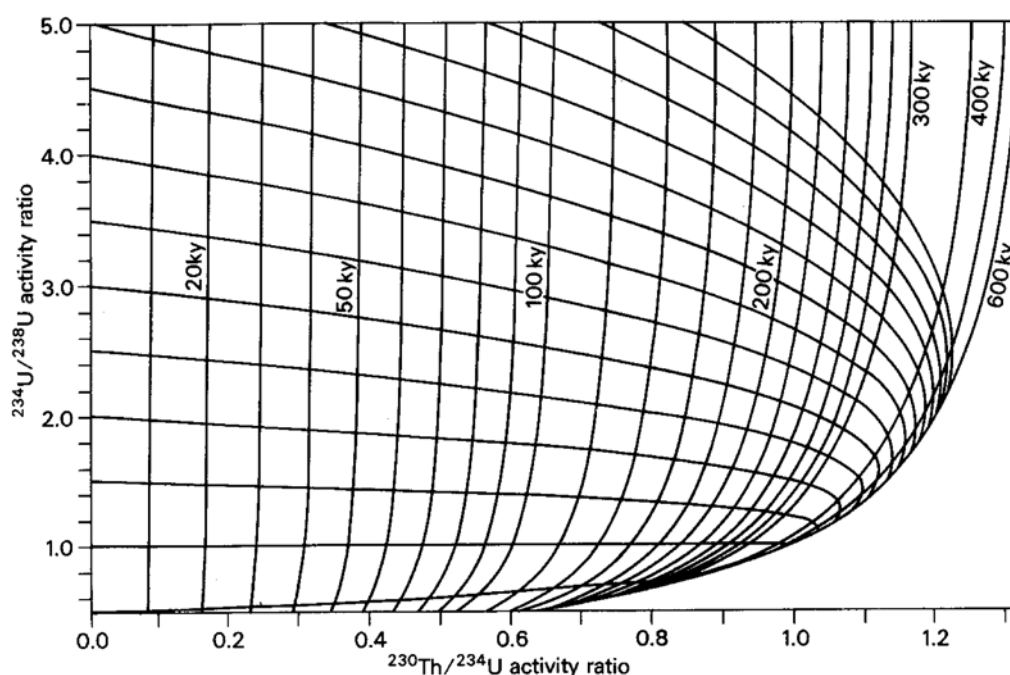


Figure 6.1 Variation of $^{234}\text{U}/^{238}\text{U}$ and $^{230}\text{Th}/^{234}\text{U}$ activity ratios with time in a closed system with no initial ^{230}Th . The near-vertical lines represent isochrons and the sub-horizontal lines are the decay paths for systems of initial $^{234}\text{U}/^{238}\text{U}$ equal to values of 0.5, 1, 1.5 *etc.* (after Smart 1991).

lived isotope occurs in water as a trace impurity adsorbed onto particles and, where present, indicates that contamination has occurred. Detrital contamination is deemed significant when the $^{230}\text{Th}/^{232}\text{Th}$ ratio of a sample is less than 20 (Smart 1991, Bischoff and Fitzpatrick 1991). In these instances, sample dates need correcting to account for the detrital component. Methods of correcting for non-authigenic ^{230}Th incorporated from detrital contamination are described in Smart (1991), Bischoff and Fitzpatrick (1991) and Kaufman (1993), and the technique applied depends of the level of contamination. Uncorrected ages will always be older than real ages since extra non-authigenic ^{230}Th suggests that a sample is nearer to secular equilibrium than is the case in reality.

Another assumption is that the system should remain closed to the migration of uranium and thorium after deposition. This will not be the case if a sample is characterised by recrystallisation, solution, secondary precipitation or high porosity (Smart 1991). It is therefore important that the physical characteristics of the sample are assessed before considering it for dating.

Uranium-series ages can be measured by alpha spectrometry or thermal ionisation mass spectrometry (TIMS). Alpha spectrometry involves the monitoring of α particles emitted during radioactive decay. TIMS, however, enables individual atoms to be counted directly. TIMS is therefore more rapid and is not restricted by the half-life of the isotope.

This fact also provides the potential to extend the dating range to beyond the conventional alpha spectrometry limit of 350,000 years. In theory, U-series dating can be used to date material as old as 600,000 years (Ku 2000). However, at present this is rarely demonstrated in practice for carbonates older than 350,000 years. In this thesis, dates obtained older than 350,000 years BP are referred to as >350,000 years BP since the precision of older dates is usually in doubt. However, a further benefit of TIMS over alpha spectrometry is that smaller samples can be measured and, since the technique is much more precise, error bars are much reduced.

6.1.2 Secondary cements

Secondary carbonate deposits which cement unconsolidated sediments, such as till, provide considerable potential for U-series dating. The age of the cement will provide a minimum age for the deposit within which it is found. As noted earlier, this fact was used to date glacial deposits by Kotarba *et al.* (2001) in the Gran Sasso area of the Italian Appenines and by Woodward *et al.* (2004) on Mount Tymphi in the same study area as in this thesis.

Woodward *et al.* (2004) refer to cements formed in tills on Mount Tymphi as calcretes. The original definition of calcrete by Lamplugh (1902) does in fact refer to cemented deposits, although calcretes are now often regarded as carbonates formed within soil profiles (Wright and Tucker 1991, Candy *et al.* 2003). Other cements, often referred to as non-pedogenic calcretes, encompass a wide range of mechanisms and modes of formation (*cf.* Carlisle 1983). However, cemented sediments have also been classified as travertines. For example, the term *cemented rudite* was used in the travertine classification of Pentecost (1993, 1995) and Pentecost and Viles (1994) to describe "surface-cemented rudites, consisting of cemented screes, alluvium, breccia and gravel, *etc.*". Here, to avoid any confusion, secondary carbonates found cementing unconsolidated sediments will be referred to as *cement* (*cf.* Fairchild *et al.* 1994), since this is a descriptive term lacking any genetic connotations.

6.1.2.1 Composition

The composition of cement was investigated by two principal means. Firstly, the percentage acid insoluble residue was determined following the procedures outlined in section 3.2.4. Secondly, the cements were analysed by X-ray diffraction (XRD) to determine their mineralogical content. This was useful for determining whether they consisted entirely of calcite or whether they were partly aragonite, as well as indicating the

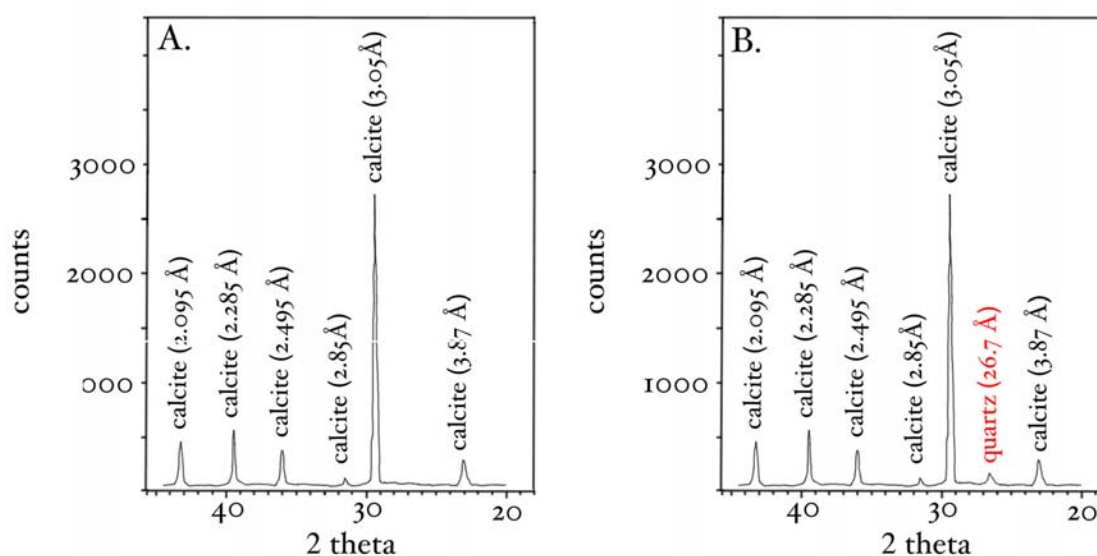


Figure 6.2 XRD traces for cement samples. Trace A is that consistently produced from 4 samples (Pindus D, Pindus H, Pindus J and Pindus K) indicating that the cements are composed of calcite. Trace B is that from one sample (Pindus R) and indicates the sample is largely calcite with a minor detrital presence of quartz.

mineralogy of the detrital component. Samples, approximately 2 g in weight, were crushed using a pestle and mortar until a fine powder was produced. The samples were then processed by Dr. C. Jeans in the Department of Earth Sciences, University of Cambridge.

All samples used for dating in this study contained < 1% acid insoluble residue. XRD results from five samples show that they are composed almost entirely of calcite and any trace detritus present was identified as quartz (Fig 6.2). The cements can therefore be referred to as *calcite cement*. Two characteristic cement types were used for dating on Mount Tymphi. They are described and interpreted separately below.

6.1.2.2 Vadose zone cements

These cements often coat large clasts, fill interclast voids and are usually localised deposits with little lateral extension. Sometimes the calcites are up to 5 cm thick and consist of multiple layers and, in places, small dripstones or stalactites, have developed within sediment voids (Fig. 6.3). This type of secondary carbonate cement is interpreted as being formed by localised water flow through the unconsolidated sediments in the vadose zone, above the water table. Since these cements coat glacially-transported clasts and boulders, as well as fill interclast voids, it is clear that they post-date the host sediment. This form of cement has been recognised in drum sands and gravels in Wisconsin, USA, by Fairchild *et al.* (1991, Fig. 13.15) and in glacial conglomerates on the Appalachian plateau of New York State, USA, by Aber (1979).



Figure 6.3 Vadose zone cement within the weathered glacial deposits of the Kato Radza Member (39° 55' 58"N, 20° 52' 09"E) on Mount Tymphi. This type of cement is likely to have formed as a result of localised percolation of calcium-rich waters in the vadose zone (Samples: Pindus F , Pindus G, Pindus H and Pindus I).

6.1.2.3 Phreatic zone cements

These cements are found in sand and gravel-sized sediments and often form horizontal benches of resistant cemented sediment (Fig. 6.4). The calcite in these cements usually contains much more detritus than in those of the vadose zone cements. This form of cement is often found in valley-floor sediments and probably formed by precipitation of calcium carbonate in the groundwater phreatic zone (*e.g.* Arakel and McConchie 1982, Nash and Smith 1998, 2003, Kelly *et al.* 2000), *i.e.* below or at the water table. The fact that cemented benches are often present near to valley bottoms, in sediments now incised by stream action (*i.e.* terraces), is consistent with cement formation close to the level of the water table. For example, Kelly *et al.* (2000) suggest that the main periods of cement formation may be narrowly temporally restricted, inhibited or halted by incision of the river

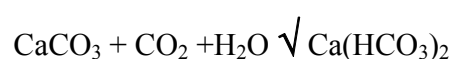


Figure 6.4 Phreatic zone cement within till of the Voidomatis Member (*ca.* 39°53'31"N, 20°50'01"E, 870 m a.s.l.). This form of cement tends to be fine-grained with a high detritus content. Since this is a groundwater cement, it is often forms rigid laterally-continuous benches near to river channels and the photographed cement is only a short distance from the Voidomatis river.

below the point at which lateral groundwater recharge and flooding occur.

6.1.2.4 Mode of formation

Cement formation in both the vadose and phreatic zone involves the solution and subsequent precipitation of calcium carbonate:



Dissolution of calcium carbonate is illustrated by the reaction shown above reading from left to right whilst precipitation occurs by reversal of this reaction.

A mode of formation can be envisaged for the cements of Mount Tymphi by applying this theoretical equation. In the case of vadose zone cements, spring water would have percolated through the glacial deposits and dissolved the calcium carbonate from the fine matrix. Calcium and bicarbonate ions are then redeposited as calcium carbonate (calcite), especially where it enters voids causing the water to lose carbon dioxide by outgassing. The latter occurs because the pressure of the carbon dioxide in the water is

greater than in the air within the void (Pentecost 1991). This process would have been promoted if percolating water had passed through a respiring soil horizon on top of the glacial deposits (A. Pentecost, *personal communication*).

Phreatic zone cements are likely to have formed by precipitation below the water-table. Groundwater saturated with calcium carbonate loses carbon dioxide due to the air in the surface area, as well as through carbon dioxide uptake in a respiring surface soil, resulting in the precipitation of calcite cement. The fact that these cements are formed in the water-saturated phreatic zone, and not by percolating water in the vadose zone, results in the cement occupying much finer voids. Cements of this type are therefore detritus-rich. For this reason, phreatic zone cements described by Hamlin *et al.* (2000), in the Voidomatis Basin, were dated using the isochron method of U-series dating (after Bischoff and Fitzpatrick 1991). However, in this thesis, only when clean calcite crystals could be separated from the surrounding detritus were phreatic cements dated. This allowed conventional dating of relatively clean calcite requiring only minor detrital correction. The problem of detritus in phreatic zone cements meant that vadose zone deposits were preferred for dating. Furthermore, vadose zone cements are much more ubiquitous in moraines, since these are often elevated above the water table whereas phreatic zone cements are more often found in alluvial deposits at the valley floor.

Precipitation of calcite is promoted by high temperatures and high evaporation rates. Carbon dioxide is less soluble and more easily degassed at high temperatures. This, as well as high rates of evaporation, increase the concentration of calcium and bicarbonate ions in the water. In addition, a respiring surface soil increases carbon dioxide outgassing from carbonate-rich waters and promotes cement precipitation. These facts suggest that cement formation would have been favoured during interglacial or interstadial climates. However, calcite cements are known to form in a wide range of environments including those that are hot and semi-arid (Nash and Smith 1998, 2003, Kelly *et al.* 2000), cool and wet (Flinn and Pentecost 1995), and cold and arid (Swett 1974, Vogt and Delvalle 1994).

Vadose zone cements require a persistent supply of percolating water and a continual supply of calcium carbonate. The latter is maintained by readily soluble rock-flour in the matrix of glacial sediments. High moisture availability and readily soluble calcium carbonate are therefore key for vadose zone cement formation. Thus, it is unlikely that conditions were semi-arid during the formation of vadose zone cements.

Phreatic zone cements can form in a variety of environments provided evaporation rates are sufficiently high. They can form under arid conditions in valley-bottom areas continually fed by groundwater recharge. However, they can also form under wet

atmospheric conditions and may form contemporaneously with vadose zone cements provided evaporation rates are high. This is the case today in the northern Pindus, an area characterised by high precipitation (1500 to > 2000 mm yr⁻¹) and hot summers with high rates of evaporation. In many localities, thin, poorly-developed secondary carbonates can be seen forming in both near-surface modern alluvium, and where percolating water flows through tills. Therefore, it appears that both vadose and phreatic zone cements are forming today in the Pindus Mountains.

Detailed understanding of the palaeoclimatic implications of the cements can be gained by applying geochemical and micromorphological analytical techniques (*e.g.* Raghavan and Courty 1987, Nash and Smith 2003). However, here, the main aim of the dating was to provide a minimum age for host deposits. Therefore, for the purpose of reliable dating, the general structure of the cements was examined using a hand lens. Large samples were sawn and then examined for multiple cement layers and re-crystallisation. Care was taken to ensure that samples used for U-series dating were from distinct crystal horizons and showed no evidence of re-crystallisation and open-system behaviour (*cf.* Smart 1991).

6.1.2.5 Interpreting glacial sequences using U-series dates on cements

Dated cements provide minimum ages for the host sediments. However, interpretations regarding the age of the host sediments are determined by the oldest date obtained from cements. For example, glacial deposits containing cement dated at 10,000 years BP may be much older than this and may contain older cements which are not exposed in section. This problem is inherent with minimum-age dating using secondary deposits such as calcite cements. Nevertheless, the problem can be reduced by dating multiple samples from a lithological unit, and by using dates from within the same and neighbouring valley formations to build a geochronology for any particular group of sediments.

6.1.4 Uranium-series dating – methods

In the field, calcite cements were detached using a hammer and chisel. In some cases, cemented blocks of sediment were sampled and sub-sampled later. In the laboratory, all cements were examined for evidence of open-system behaviour, *i.e.* recrystallisation, porosity and multiple growth layers. Where multiple growth layers occurred, samples were taken from particular crystal layers and dating of whole parts of multi-layered cements was avoided. The calcite cements were disaggregated and clean crystals were picked under a low-power light microscope. In order to reduce surface detrital contamination, the cements

were washed in dilute hydrochloric acid (7%) and air-dried. Clean calcite crystals were then crushed using a pestle and mortar. Cross contamination was avoided by ensuring acid-cleaned implements were used for each sample.

Chemical preparation and TIMS dating of the calcite cements was undertaken at the Open University Uranium-series Facility (NERC Grant Reference Number: IP/754/0302). Sixteen samples were processed and dated by the author, whilst two trial samples and a further eight samples were processed and dated by the Open University staff. Samples of powdered calcite (1-4 g) were leached in dilute HNO₃, separated from any detritus by centrifugation and split into two aliquots. One aliquot was 'spiked' with ²²⁹Th and ²³⁵U tracers and the other left 'unspiked' for U-series analysis. Uranium and thorium isotopes were separated and purified on anion exchange columns and loaded onto graphite-coated single rhenium filaments (*cf.* Edwards *et al.* 1987). The uranium and thorium isotope abundances were then measured on a Finnigan MAT262 multicollector mass spectrometer. ²³⁴U/²³⁸U ratios were measured in static mode, ²³⁴U by secondary electron multiplier (SEM) via a retarding potential quadrupole (RPQ) and ²³⁸U by Faraday cup. Abundances of ²³⁴U, ²³²Th and ²³⁰Th were measured by a dynamic peak switching routine on the SEM/RPQ. Concentrations were then determined by isotope dilution using the ²²⁹Th and ²³⁵U tracers previously calibrated against gravimetric methods.

Measures were taken to assess the background contamination using a total procedure blanks (TPBs) and to assess the degree to which isotope ratios from known standards could be reproduced. These contained no sample, only 'spike', and were run through the same procedure described above. Typical total procedure blanks were < 50 pico grammes (1 g x 10⁻¹²) for ²³⁸U and < 20 pico grammes for ²³²Th. These values were low relative to the cement samples and therefore no blank correction was applied. Repeat measurement of laboratory standards gave a 2 sigma between-run precision of 1.5 % for ²³²Th/²²⁹Th and 1.1 % for ²³⁴U/²³⁸U.

The uranium and thorium isotope content of detritus was determined separately by total dissolution. Four detritus samples were prepared from various sites around Mount Tymphi (Pindus A, Pindus G, Pindus P, Pindus R) and analysed by TIMS. All the sites on Mount Tymphi are lithologically similar and, therefore, detrital contribution at all localities would be expected to be similar. The mean ²³²Th/²³⁸U ratio of the detritus samples was 4.9 (range: 4.7 - 5.1) allowing the amounts of extra ²³⁴U and ²³⁰Th introduced by the detrital component to be deduced. This detrital contribution was then subtracted from the isotope abundance values used in the ²³⁰Th/²³⁴U and ²³⁴U/²³⁸U ratios for the dated carbonate and the dates adjusted accordingly. Since this correction is an estimate, there is no validity in

providing an error margin on a corrected age, and error margins are only shown with the uncorrected age. For this reason, where corrected ages fall between the error limits at 2 sigma error, the uncorrected ages and associated error are used in most of the following discussion. Further details of the chemical and machine procedure are provided in Appendix 1.

6.1.5 Uranium-series – results

In total, 26 samples were processed for U-series dating and 5 showed evidence of excessive contamination. The details of 21 samples deemed reliable, although containing variable amounts of detrital contamination, are presented in Table 6.2 and described below. The dates were calculated using a computer spreadsheet formulated by Open University Uranium Series Facility and the most recent isotope half-lives determined in Cheng *et al.* (2000). All dates, unless otherwise stated, are in calendar years before present.

6.1.5.1 Laccos Radenas Formation

Cement was collected from sediments of the Laccos Radenas Member on the southern slopes of Astraka (39°56'50"N, 20°44'20"E, 1750 m a.s.l.). A thin (5 mm) veneer of calcite cement covered and joined clasts and is interpreted as vadose zone cement formed by the localised percolation of calcium-rich water. A cement sample (**Pindus A**) yielded a date of $103,328 \pm 4,849$ years BP (Table 6.1). However, the sample had a $^{230}\text{Th}/^{232}\text{Th}$ ratio of 11. This ratio is somewhat lower than 20, the value considered to represent the cut-off between clean and contaminated samples (Smart 1991). The corrected age, taking into account the contribution of extra ^{230}Th from detritus, was calculated at 99,371 years BP. Even though this sample contained a relatively high level of detrital ^{230}Th , this date is consistent with a period of cement formation indicated by a similar date obtained from a clean calcite sample in the Skamnelli Formation, sample Pindus M (section 6.1.5.4).

Table 6.1 Uranium-series dates from cemented units in the Laccos Radenas Formation.

U-series dates (years BP)	Stratigraphical unit	Morpho-lithostratigraphy	
103,328 ± 4,849	1	Laccos Radenas Member	LACCOS RADENAS FORMATION

Table 6.2 Uranium-series TIMS data. Samples marked with an asterisk were processed by Open University Uranium Facility staff. All other samples were processed completely by the author. Samples are ordered in groups and the sample localities are described in the text.

	Sample				
	Pindus A*	Pindus B	Pindus C	Pindus D	Pindus E
²³⁸ U ppm	0.02563	0.02642	0.0202	0.02738	0.02762
error	0.00005802	0.00012495	0.00011736	0.00004773	0.0000501
²³⁴ U/ ²³⁸ U	1.14885	1.03442	1.18884	1.03093	1.04802
Error	0.01013	0.01367	0.03369	0.00655	0.00883
²³⁴ U ppm	1.59E-06	1.47E-06	1.30E-06	1.52E-06	1.56E-06
Error	1.37E-08	1.83E-08	3.60E-08	9.46E-09	1.30E-08
²³⁰ Th ppb	0.0003	0.000442	0.000339	0.000262	0.000484
Error	0.000008	0.000017	0.000007	0.000005	0.000012
²³² Th ppb	5.21979	1.76165	2.54432	0.15827	3.76075
error	0.76005	0.25652	0.38625	0.02304	0.54762
²³⁰ Th/ ²³² Th	11.08711	48.41295	26.11109	315.24965	24.82510
error	0.53595	2.89917	1.11782	12.84885	1.15794
²³⁰ Th/ ²³⁴ U	0.62251	0.98829	0.86164	0.56741	1.02100
error	0.01694	0.03838	0.01769	0.01112	0.02605
Age	103,328	>350,000	194,194	90,990	>350,000
+	4,849		13,998	2,918	
-	4,628		12,013	2,832	
% error (2σ)	4.69		7.21	3.21	
Corrected Age	99,371	>350,000	192,000	90,863	>350,000

	Sample					
	Pindus F	Pindus G*	Pindus H	Pindus I	Pindus J	Pindus K
²³⁸ U ppm	0.01595	0.02138	0.02866	0.02265	0.0203903	0.0242
error	0.000029	0.0000459	0.0001327	0.00005	3.99E-05	0.0000714
²³⁴ U/ ²³⁸ U	1.17913	1.15519	1.04985	1.15325	1.1721539	1.20561
Error	0.00854	0.00871	0.01896	0.00902	0.0750441	0.01869
²³⁴ U ppm	1.01E-06	1.33E-06	1.62E-06	1.41E-06	1.29E-06	1.57E-06
Error	7.20E-09	9.75E-09	2.84E-08	1.07E-08	8.25E-08	2.40E-08
²³⁰ Th ppb	0.000168	0.0002177	0.000405	2.51E-04	0.0002665	0.000311
Error	0.000004	0.0000041	0.000018	3.56E-06	7.56E-06	0.000006
²³² Th ppb	0.25688	1.54637	2.28757	0.950	1.5040458	1.45936
error	0.03766	0.22513	0.33307	0.083	0.2191005	0.21258
²³⁰ Th/ ²³² Th	133.1170	27.7361	34.25373	51.561	35.321899	42.00072
error	6.00935	1.11267	2.20811	1.127	1.7515796	1.72409
²³⁰ Th/ ²³⁴ U	0.54427	0.53856	0.82223	0.58710	0.6813159	0.65099
error	0.0129	0.01022	0.03583	0.00836	0.0221185	0.01306
Age	83,666	82,614	183,488	94,101	119,818	110,198
+	3,040	2,411	25,006	2,212	9,249	4,107
-	2,952	2,354	19,953	2,186	8,022	3,925
% error (2σ)	3.63	2.92	13.63	2.4	7.71	3.73
Corrected Age	83,365	81,222	181,790	93,298	118,450	109,116

Table 6.2 Continued.

	Sample					
	Pindus L	Pindus M	Pindus N	Pindus O*	Pindus P	Pindus Q
²³⁸ U ppm	0.02682	0.02238	0.02371	0.02676	0.02874	0.01619
error	0.000053	0.0000513	0.000045	0.00006	0.0000564	0.0000337
²³⁴ U/ ²³⁸ U	1.05606	1.16012	1.03771	1.01807	1.11529	1.08533
Error	0.00724	0.01356	0.00728	0.00963	0.00765	0.00953
²³⁴ U ppm	1.53E-06	1.40E-06	1.33E-06	1.47E-06	1.73E-06	9.48E-07
Error	1.02E-08	1.61E-08	9.08E-09	1.35E-08	1.15E-08	8.16E-09
²³⁰ Th ppb	0.000441	0.000262	0.000406	4.52E-04	0.000458	0.000297
Error	0.000009	0.000014	0.000008	6.38E-06	0.000009	0.000008
²³² Th ppb	2.7531	0.76856	0.18512	2.167	6.45259	2.31975
error	0.40106	0.11193	0.02697	0.190	0.93963	0.33854
²³⁰ Th/ ²³² Th	30.89017	66.90916	421.1273	39.925	13.78065	25.14752
error	1.31217	4.88407	17.04155	0.870	0.57208	1.18961
²³⁰ Th/ ²³⁴ U	0.95223	0.61716	1.00705	1.01347	0.87283	1.031
error	0.02028	0.03204	0.01943	0.01439	0.01776	0.02689
Age	301,159	101,711	>350,000	>350,000	208,142	>350,000
+	43,345	9,087			13,776	
-	-30792	-8367			-12188	
% error (2σ)	14.39	8.93			6.62	
Corrected Age	299064	101,062	>350,000	>350,000	203802	>350,000

	Sample			
	Pindus R	Pindus S*	Pindus T*	Pindus U*
²³⁸ U ppm	0.04471	0.02831	0.03238	0.4928
error	0.00007469	0.00007	0.00007	0.00011
²³⁴ U/ ²³⁸ U	1.11821	1.09881	1.19245	1.12088
Error	0.00641	0.00960	0.00995	0.00780
²³⁴ U ppm	2.70E-06	1.68E-06	2.08E-06	2.98E-06
Error	1.51E-08	1.43E-08	1.69E-08	1.99E-08
²³⁰ Th ppb	0.000079	5.86E-05	3.69E-04	6.28E-04
Error	0.000002	2.23E-06	5.72E-06	1.08E-05
²³² Th ppb	1.24309	1.678	0.669	9.428
error	0.18102	0.147	0.059	0.825
²³⁰ Th/ ²³² Th	13.35758	8.028	106.283	12.718
error	0.5787	0.367	2.460	0.315
²³⁰ Th/ ²³⁴ U	0.09671	0.11515	0.58430	0.69507
error	0.002142	0.00439	0.00909	0.01193
Age	11,087	13,335	92,914	125,530
+	259	535	2,350	4,202
-	259	542	2,321	4,115
% error (2σ)	2.33	4.1	2.5	3.3
Corrected Age	10,519	12,099	92,536	121,731

6.1.5.2 Megas Laccos Formation

Three cement samples were collected from sediments of the Megas Laccos Member in the upper Megas Laccos valley (39°55'58"N, 20°48'24"E, 1500 m a.s.l.) (Table 6.3). The calcite was up to 5 cm thick and covered and joined clasts. This cement is likely to have formed in the vadose zone by prolonged localised percolation and precipitation. The calcite showed evidence of multiple layers. Two different layers of calcite crystals, including the basal layer nearest to the host clast, were sampled for dating. Two samples were dated from the basal calcite layer (**Pindus B and Pindus E**) and one from the upper layer (**Pindus C**). The two samples from the basal calcite layer were both dated at >350,000 years BP, whilst the sample from the upper layer was dated at 194,194 ± 13,998 years BP.

A further sample (**Pindus D**) was collected from the cemented breccia deposits of the Kazarma Member (39°55'30"N, 20°47'50"E, 1450 m a.s.l.), and again this cement is interpreted as a vadose zone cement. Sample **Pindus D** gave a date of 90,990 ± 2918 years BP (Table 6.3).

All of these samples gave a $^{230}\text{Th}/^{232}\text{Th}$ ratio of over 20 indicating that they are relatively clean. **Pindus D** was particularly clean with a $^{230}\text{Th}/^{232}\text{Th}$ ratio of 315. The corrected ages therefore show little variation from the original dates unadjusted for non-authigenic detritus.

Table 6.3 Uranium-series dates from cemented units in the Megas Laccos Formation.

U-series dates (years BP)	Stratigraphical unit	Morpho-lithostratigraphy	
90,990 ± 2,918	2	Kazarma Member	MEGAS LACCOS FORMATION
>350,000 >350,000 194,194 ± 13,998	1	Megas Laccos Member	

6.1.5.3 Tsepelovo Formation

Calcite cement was present in the Voidomatis Member on the Tsepelovo bypass near to the section Vb (39°54'07"N, 20°49'40"E, 1060 m a.s.l.). The calcite occurred in a localised area in voids between clasts where the fine matrix had been removed, and was characteristic of a vadose zone cement. The calcite cemented clasts and also formed mini-stalactites or 'soda straws' (*cf.* Schwarz and Rink 2001) (2-3 cm long) within some interclast cavities. One of these stalactites was sampled for dating (**Pindus R**). A U-series date of $11,087 \pm 259$ years BP was derived for this sample (Table 6.4). The low $^{230}\text{Th} / ^{232}\text{Th}$ ratio of 13.4 in this sample indicates significant detrital contamination, and the corrected age was calculated at 10,519 years BP.

Cement was also sampled slightly further north at 39°54'09"N, 20°49'34"E, 1065 m a.s.l. The cement was similar in form to Pindus R, and a small stalactite (2.5 cm long) from this cement (**Pindus S**) was dated at $13,335 \pm 543$ years BP (Table 6.4). Again, the $^{230}\text{Th} / ^{232}\text{Th}$ ratio of 8.0 was relatively low for this sample, and the corrected age of 12,099 years BP is younger than that covered by the error margin for the uncorrected sample. Although there is a minor detrital component, the facts that the detritus from this sample was used in deriving the detrital isotope correction and that the $^{230}\text{Th} / ^{232}\text{Th}$ ratio remains well above a silicate ratio of 2 suggests that the corrected age is valid. This is further supported by a difference of only 1,000 years between the corrected date and the date obtained for cleaner Pindus R cement which occurs nearby.

Woodward *et al.* (2004) also dated cement from Voidomatis Member tills. They dated samples from a cemented bench, probably formed in the phreatic zone near to the Voidomatis river and obtained an age of $96,250 \pm 15,500$ years BP (Fig. 6.4). They also dated till cement - probably of vadose zone origin - in road cuttings near Tsepelovo village and in the Laccorponi valley, and obtained ages of $105,730 \pm 21,450$ years BP and $71,000 \pm 8,700$ years BP respectively (Table 6.4). All of the dates determined by Woodward *et al.* (2004) were obtained using alpha spectrometry.

Table 6.4 Uranium-series dates from cemented units in the Tsepelovo Formation. Dates marked with an asterisk are from Woodward *et al.* (2004).

U-series Dates (years BP)	Stratigraphical unit	Morpho-lithostratigraphy	
	3	Vlasi Member Litharion Member Tselon Member	TSEPELOVO FORMATION
	2	Laccorponi Member	
*105,730 ± 21,450 *96,250 ± 15,500 *71,000 ± 8,700 13,335 ± 543 11,087 ± 259	1	Voidomatis Member	

6.1.5.4 Skamnelli Formation

Numerous cements within the Kato Radza Member of the Skamnelli Formation were sampled for dating. Cement was sampled near to section SKb in the Kato Radza valley at *ca.* 39°54'08"N, 20°50'40"E, 984 m a.s.l. (**Pindus O**) from a laterally-continuous cemented till unit in the centre of the valley. Calcite crystals were fine-grained and occupied small voids within a sandy matrix, characteristic of formation in the phreatic zone, and were separable from the matrix detritus by careful picking under a light microscope. These crystals gave a U-series age of >350,000 years (Table 6.5). Furthermore, the sampled calcite crystals were relatively clean with a $^{230}\text{Th}/^{232}\text{Th}$ ratio of 39.9.

Cement within the deposits of the Kato Radza Member was also located above Skamnelli in the Vathirema valley at 39°55'18"N, 20°51'25"E, 1411 m a.s.l. Calcite covered and joined the clasts and in places reached a thickness of *ca.* 6 cm. The cement is likely to have been formed as a result of precipitation from percolating waters saturated with calcium carbonate in the vadose zone. Calcite nearest to the host clast was sampled (**Pindus N**) and dated to >350,000 years BP (Table 6.5). This sample was particularly clean, giving a $^{230}\text{Th}/^{232}\text{Th}$ ratio of 421.

Calcite cement covered and joined boulders exposed in cuttings through till, again belonging to the Kato Radza Member, on the track up to the Vourtapa valley from Skamnelli, at 39°55'32"N, 20°51'16"E, 1594 m a.s.l. As in the Vathirema valley, the cement is likely to have formed as a result of prolonged percolation of calcium-rich waters in the vadose zone. A cement sample (**Pindus Q**), with a $^{230}\text{Th}/^{232}\text{Th}$ ratio of 25, was dated at

>350,000 years BP. West of this area, at 39°55'37"N, 20°51'14"E, 1610 m a.s.l., cement was found covering and cementing boulders of the Kato Radza Member with *ca.* 5 mm of calcite. Two separate calcite layers (top: furthest from host boulder surface) were evident, each *ca.* 2.5 mm thick. Calcite from both layers was sampled and the dates obtained for the top (**Pindus M**) and bottom (**Pindus L**) layers were $101,711 \pm 9,087$ and $301,159 \pm 43,345$ years BP, respectively (Table 6.5).

Further up-valley, a track leading to the neighbouring Laccorponi valley cuts through till just outside of the Vourtapa moraines. This till is contiguous with similar deposits of the Kato Radza Member further down-valley. At 39°48'54.3"N, 20°51'03.0"E, 1670 m a.s.l., the till is cemented with vadose zone cement. A sample (**Pindus P**) was dated at $208,142 \pm 13,776$ years BP (Table 6.5). The sample had a $^{230}\text{Th} / ^{232}\text{Th}$ of 13 and the corrected age, accounting for detritus, was calculated at 203,802 years BP - within the error limits of the uncorrected sample.

An excellent cemented section occurs in the lower Vrichos valley at 39°55' 58"N, 20°52' 09"E, 1773 m a.s.l. (Fig. 4.23 and 6.3). In Chapter Four, the sediments exposed in this section are assigned to the Kato Radza Member of the Skamnelli Formation. Localised cements cover and join clasts and are interpreted as vadose zone cements. Four discrete samples were collected - **Pindus G**, **Pindus F**, **Pindus I** and **Pindus H** and were dated to $82,614 \pm 2,411$, $83,666 \pm 3,040$, $94,101 \pm 2,212$ and $183,488 \pm 25,006$ years BP, respectively. All of these samples gave $^{230}\text{Th} / ^{232}\text{Th}$ ratios of > 20 and, therefore, corrected ages differ only slightly at 81,222, 83,365, 93,298 and 181,790 years BP. Woodward *et al.* (2004) also dated cements from this section and derived dates of $121,400 \pm 21,000$, $321,500 \pm 35,650$ and $>350,000$ years BP (Table 6.5).

Cements were also sampled from a section through the innermost moraine of the lower Vourtapa valley at 39°56'21.4"N, 20°51'25.5"E, 1823 m a.s.l. in the Vourtapa Member of the Skamnelli Formation. The cement was thick (up to 3 cm), uni-layered and contiguous, and apparently represents a single phase of calcite formation. Two samples were dated to test this observation (**Pindus J** and **Pindus K**) and gave ages of $119,818 \pm 9,249$ and $110,198 \pm 4,107$ years BP, respectively. The error margins show that these dates overlap, supporting the possibility that the cement represents one phase of calcite formation. In addition, dates of $131,250 \pm 19,250$ and $81,700 \pm 12,900$ years BP were obtained from different cements in a section cut in the western moraines of the Vourtapa Member by Woodward *et al.* (2004) (Table 6.5).

Woodward *et al.* (2004) also noted cements in glacial deposits of the upper Vrichos valley and obtained a date of $80,450 \pm 15,100$ years BP. This area is termed the Vraccachi

valley in Woodward *et al.* (2004) after Palmentola *et al.* (1990a). However, on Greek topographical maps, the area is clearly defined under the name Vrichos and cemented deposits are those of the Vrichos Member in this thesis (Anavasi 2002)

Table 6.5 Uranium-series dates from cemented units in the Skamnelli Formation. Dates marked with an asterisk are from Woodward *et al.* (2004).

U-series dates (years BP)	Stratigraphical unit	Morpho-lithostratigraphy	
	3	Tsoukoula Member	SKAMNELLI FORMATION
*131,250 ± 19,250 119,818 ± 9,249 110,198 ± 4,107 *81,700 ± 12,900 *80,450 ± 15,100	2	Vourtapa Member Vrichos Member Corifula Member	
>350,000 >350,000 >350,000 *>350,000 *321,500 ± 35,650 301,159 ± 43,345 208,142 ± 13,776 183,488 ± 25,006 *121,400 ± 21,000 101,711 ± 9,087 83,666 ± 3,040 82,614 ± 2,411	1	Kato Radza Member Megali Rachi Member	

6.1.5.5 Raidhovoli Formation

Cemented deposits occur in the Xeroloutsa Member of the Raidhovoli Formation at 39°58'55"N, 20°46'10"E 1850 m a.s.l., on the slopes between the refuge hut and the lake of Xeroloutsa. Cement covered and cemented boulders and was characteristic of cements formed in the vadose zone. A sample (**Pindus T**) was dated at 92,914 ± 2350 years BP. A second sample (**Pindus U**) was collected from a nearby matrix-supported diamicton. This cement was much thinner than the cement of Pindus T although again is likely to have formed by percolation of calcium-rich waters in the vadose zone. The sample was dated at 125,530 ± 4202 years BP suggesting that this cement did not form contemporaneously with Pindus T. The two cements also differ in terms of detrital component. Pindus T gave a $^{230}\text{Th}/^{232}\text{Th}$ ratio of 106, whilst Pindus U which had a $^{230}\text{Th}/^{232}\text{Th}$ ratio of only 12.7. The

latter cement therefore had a significant detrital component ($^{230}\text{Th}/^{232}\text{Th} < 20$) and the corrected age is calculated at 121,731 years BP.

Table 6.6 Uranium-series dates from cemented units in the Raidhovoli Formation.

U-series dates (years BP)	Stratigraphical unit	Morpho-lithostratigraphy	
	3	Ploskos Member Astraka Member	RAIDHOVOLI FORMATION
92,914 ± 2,350 125,530 ± 4,202	2	Xeroloutsas Member	
	1	Raidhovoli Member	

6.1.5.6 The significance of the cement ages

The assumption that the secondary calcite cements post-date the host sediments is the key to the chronology of the glacial (and indirectly the periglacial) sequence. Several populations of dated cements from glacial deposits can be identified (Table 6.7) and these are discussed below.

The youngest sample, from the Voidomatis Member in the Tsepelovo Formation is dated at 11,087 ± 259 years BP. This cement age corresponds with the beginning of the interglacial conditions at Ioannina dated at 10,080 ± 25 ^{14}C years BP (Galanidou *et al.* 2000). Another sample from the same area has a slightly older age of 13,335 ± 543 years BP, although this sample was detritally contaminated. The corrected age of 12,099 years BP corresponds to the Late-glacial Substage. Cement formation appears to have coincided with dense mixed woodland, containing at least sixteen different tree taxa, on Mount Tymphi in the early Holocene (Willis 1992b). Although cements form under a wide range of climatic conditions, the combined evidence of vadose zone cement formation and rich vegetation perhaps indicates a warm and moist climate. This would appear to support the idea of a montane Late-glacial refugia (Willis 1992b) and also suggests that the interval equivalent to the Younger Dryas Chronozone in northwest Europe was characterised by high moisture availability. This is in opposition to suggestions that this interval was characterised by marked aridity in the eastern Mediterranean (*cf.* Rossignol-Strick 1995).

Age (x 1,000 years BP)	MIS	Ioannina 249/ 284	Dated cements
	1	Holocene	λ λ
66 - 11.5 *	2	Glacial	
	3		
	4		
83 - 66 *	5a	Vikos/ 'Interstadial 2'	λ λ μ μ μ
88.5 - 83 *	5b	Stadial 2	
104.5 - 88.5 *	5c	Perama-Thyamis/ 'Interstadial 1'	λ λ λ λ λ μ
111 - 104.5 *	5d	Stadial 1	
127 - 111 *	5e	Metsovon	λ λ λ μ μ
190 - 127	6	Glacial	
250 - 190	7a	IN-26	λ λ λ
	7c	Zitsa	
	7e	IN-23a	
300 - 250	8	Glacial	
340 - 300	9a	Katara	λ μ
	9c	IN-17	
	9e	Pamvotis	
350 - 340	10	Glacial	
430 - 350	11	Dodoni I and II	λ λ λ λ λ μ
480 - 430	12	Glacial	

Table 6.7 Cement ages from glacial deposits in relation to the pollen stratigraphical record at Ioannina and correlations with the marine isotope record (*cf.* Tzedakis *et al.* 1997, 2002). The symbol λ represents a cement dated in this thesis whilst the symbol μ represents a cement dated in Woodward *et al.* (2004). The interval dates marked with an asterisk are from the Ioannina sequence (Tzedakis *et al.* 2002) and all other dates are from Lowe and Walker (1997, Table 1.1).

The next group of cement ages from glacial deposits are clustered between 70 and 130,000 years BP. However, in alluvial sediments in the lower Voidomatis basin, phreatic zone cements have yielded dates of $25,000 \pm 2,000$ years, and $53,000 \pm 4,000$ years BP. The former date corresponds with the most severe and arid phase of the last glacial cycle as indicated in the Ioannina pollen sequence (22-20,000 ^{14}C years BP/ *ca.* 25,600-23,200 years BP). This cement is likely to have therefore formed under cold arid conditions. Conversely, in the Ioannina 284 record at 53,000 years BP, arboreal percentages are high, indicating a wetter and possibly warmer phase of climate. This emphasises the range of environments in which the phreatic zone cements form.

A date of $71,000 \pm 8,700$ years BP was obtained from a vadose zone cement in glacial deposits of the Voidomatis Member by Woodward *et al.* (2004). This age corresponds with the Vikos Interstadial at Ioannina (Tzedakis 1994) which is correlated with MIS 5a (Tzedakis *et al.* 1997). This interstadial is termed 'Interstadial 2' in Tzedakis *et al.* (2002) and dated to 66,000 - 83,000 years BP on the basis 'pollen-orbital' tuning. Cement dates of $82,614 \pm 2,411$, $83,666 \pm 3,040$ years BP, from the Kato Radza Member also correlate with the early part of this interstadial. In addition, dates of $81,700 \pm 12,900$ and $80,450 \pm 15,100$ years BP reported by Woodward *et al.* (2004), from the Vourtapa and Vrichos Members respectively, also correlate with 'Interstadial 2' in the Ioannina sequence. Although the error margins for these dates are large, the age ranges are corroborative with the more precise dates obtained in this thesis.

Three cements, in the Megas Laccos, Raidhovoli and Skamnelli Formations are dated to $90,990 \pm 2,918$, $92,914 \pm 2,350$ and $94,101 \pm 2,212$ years BP respectively and correspond with the latter part of 'Interstadial 1' in the Ioannina 284 record (Tzedakis *et al.* 2002). 'Interstadial 1' (104,500 - 88,500 years BP) is equivalent to the Perama-Thyamis Interstadial in the earlier 249 record (*cf.* Tzedakis 1994) and is correlated with MIS 5b (Tzedakis *et al.* 1997, 2002). In addition, two cement samples dated at $101,711 \pm 9,087$ and $103,328 \pm 4,849$ years BP in the Skamnelli and Laccos Radenas Formations respectively, correlate with the early part of 'Interstadial 1' at Ioannina. Similarly, a date of $105,730 \pm 21,450$ years BP from cement in the Voidomatis Member obtained by Woodward *et al.* (2004) could also imply formation during this interstadial, although this date is not very precise.

The oldest cement dates from the 70-130,000 years BP group are $125,530 \pm 19,250$, $119,818 \pm 9,249$ and $110,198 \pm 4,107$ years BP in the Xeroloutsas and Vourtapa Members of the Raidhovoli and Skamnelli Formations, respectively. Woodward *et al.* (2004) also obtained cement ages of $131,250 \pm 19,250$, and $121,400 \pm 21,000$ years BP in the Vourtapa

and Kato Radza Members of the Skamnelli Formation and all correspond with interglacial conditions at Ioannina between 127-111,000 years BP (Tzedakis *et al.* 2002, 2003a). The error margins for these dates make any inference concerning which phase of the interglacial impossible. However, the youngest date of $110,198 \pm 4,107$ years BP corresponds with the latter part of the interglacial.

A further three sets of cement ages can be identified and at least two of these correspond with interglacial intervals identified in both the terrestrial and marine isotope records. For example, dates of $183,488 \pm 25,006$, $194,194 \pm 13,998$ and $208,142 \pm 13,776$ years BP from the Megas Laccos and Kato Radza Members correspond with the Zitsa Interglacial at Ioannina which has been correlated with MIS 7 (Tzedakis *et al.* 1997). In addition, dates of $301,159 \pm 43,345$ years BP derived here, and a date of $321,000 \pm 35,650$ years BP derived by Woodward *et al.* (2004) from the Kato Radza Member, correlate with the Katara-Pamvotis Interglacial at Ioannina which is correlated with MIS 9 (Tzedakis *et al.* 1997). However, the large error margins for both of these dates make precise correlations impossible, especially given the short span of the interglacial intervals.

A final group of dates predate the maximum reliable range of U-series dating of 350,000 years BP. Here, five separate cement samples gave ages of greater than 350,000 years BP, from the Megas Laccos and Kato Radza Members - the lowest members of the Skamnelli and Megas Laccos Formations. Woodward *et al.* (2004) also obtained a date of >350,000 years BP from the Kato Radza Member of the Skamnelli Formation. Since 350,000 years BP is the minimum age of these cements, they could have formed at any time before. However, the cements (especially the vadose zone cements) may have formed during the Dodoni Interglacial which is correlated with MIS 11 (Tzedakis *et al.* 1997). This is especially likely if the host till was laid down during the preceding glacial stage, equivalent to MIS 12.

Most of the cements found on Mount Tymphi, with the exception of some alluvial phreatic zone cements, appear to have formed during intervals which coincided with high arboreal pollen percentages at Ioannina. This suggests that periods of cement formation were characterised by high moisture availability. Phreatic zone cements appear to have formed in both moist and arid phases indicated in the Ioannina pollen record. It is apparent, therefore, that as well as providing minimum ages for host deposits, calcite cements provide important information regarding warm phase climates. Moreover, cemented glacial deposits provide a composite record of Quaternary environments with five interglacials and two interstadials recorded in the cement record of Mount Tymphi. However, it is the glacial deposits and the minimum ages derived from the cements which are the focus of this work.

6.2 Soil development as a relative-age technique

Relative-age techniques rely on changes in physical or chemical properties of sediments or soils over time. Soils have been widely used as a basis for relative chronologies of glacial events and also as a means of correlation. They form during periods of geomorphological stability and, in Mediterranean environments, may continue to develop over lengthy periods allowing soils to reach advanced levels of maturity (Woodward *et al.* 1994, van Anandel 1998). For example, in Greece, soils form chronosequences that span more than 200,000 years (van Anandel 1998).

Mediterranean soils are typically alfisols with an upper dark organic A horizon grading into a pale leached E horizon (Fig. 6.5). Solutes are leached through the E horizon, then precipitate oxides and hydroxides and deposit illuvial clay in a yellow-brown to red B horizon. In some areas, especially those formed on carbonate lithologies, CaCO_3 is precipitated at the base of the B horizon forming a carbonate-rich K horizon. However, in alluvial soils on terraced surfaces of the Voidomatis basin, Woodward *et al.* (1994) did not observe any secondary carbonate deposition. They suggested that this is because of vigorous and effective leaching as a consequence of high rainfall and unconsolidated parent

Mediterranean soil profile

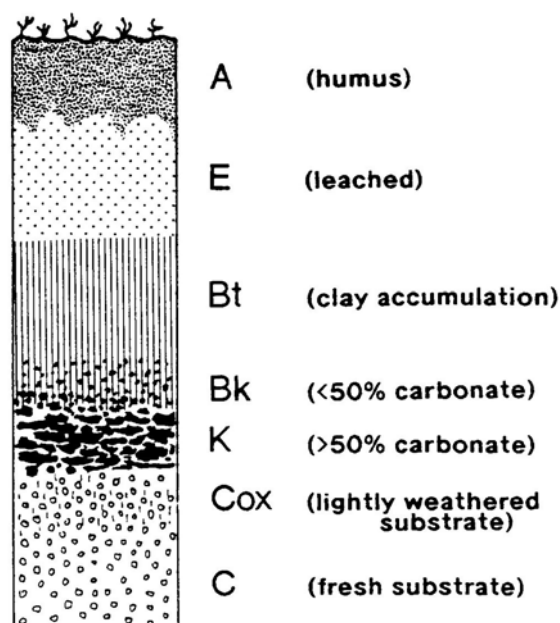


Figure 6.5 Mature profile of a Mediterranean alfisol in Greece (from van Anandel 1998). The letters on the right represent well-established soil codes (*cf.* Birkeland 1984) and the defining soil characteristics are shown in brackets.

Stage	Colour	Structure	Clay Films
>2000 yr B.P.	10YR, medium grey-yellowish brown	Granular	None
4–6000 yr B.P.	10YR-7.5 YR, yellowish to reddish brown	Subangular blocky	Thin, few
10–15000 yr B.P.	7.5YR, reddish to dark brown	Subangular blocky	Thin, common
ca. 40000 yr B.P.	5YR, yellow red to reddish brown	Angular blocky	Thin, many
ca. 80000 yr B.P.	2.5YR, reddish brown	Angular blocky to small prismatic	Thick to continuous
>110000 yr B.P.	2.5YR to 10R, reddish brown to red	Medium to large prismatic or platy	Thick, pervasive

Table 6.8 Maturity indicators for the B horizon of Quaternary soils in Greece as defined by van Andel (1998). The colour code are based on Munsell soil colour charts (Munsell 1975).

material. At the base of soils, the unweathered parent material characterises the C horizon (van Andel 1998).

In the Voidomatis basin on Mount Tymphi, Woodward *et al.* (1994) developed a simple weathering index based on the iron content of the soil and the depth of the weathered zone. The index is the product of the difference between the maximum ferric iron values and the least weathered sample at the base of each profile, and the depth of the weathered horizon. They then plotted index values for four soils against the age of radiometrically-dated alluvial units upon which the soils rest and found that a linear relationship existed. However, the oldest alluvial unit was dated at *ca.* 28,000 years BP using the thermoluminescence method, and it is not known whether the relationship between the weathering index and age is linear beyond this age range. This limits the value of the technique on older soils.

On Mount Olympus, Smith *et al.* (1997) employed Harden profile development indices (PDI) which characterise soil properties and enable statistical comparison between different soil profiles (*cf.* Harden 1982, Harden and Taylor 1983). The technique has also been widely applied in North America as a basis for relative chronologies and it has been possible to assign relative ages to moraine sequences extending back 140,000 years (Birkeland 1985, Colman and Pierce 1986). However, apart from the work on Mount Olympus, PDI's have not been used elsewhere in Greece (van Andel 1998). Based on soil studies across Greece, van Andel (1998) showed that a limited set of field characteristics including colour, structure and the presence of clay films were adequate to define six maturity stages extending to beyond 110,000 years BP (Table 6.8).

In this thesis, numerous soil properties were measured and described. This allowed comparison with other soil studies in Greece involving the various different approaches applied by Woodward *et al.* (1994), Smith *et al.* (1997) and van Andel (1998).

6.2.1 Analysis of soil properties - methods

In the field, soils were identified, described and horizon thicknesses recorded. Soils were then sampled (150-200 g air-dry weight) from the top of the profile through the B horizon to the C horizon at 10 cm intervals. The lowest sample represents the uppermost part of the C horizon whilst the rest of the samples are from the B horizon. Where soils were found in section, this was straightforward. Where they were not, pits were dug and samples were taken from the soil horizons exposed in these pits.

In both the field and laboratory, a number of soil properties were examined. In the laboratory, all the samples were air-dried at room temperature for 48 hours and then screened through a 1 mm mesh sieve. All eight parameters used in the Harden index (rubification, clay film, texture, structure, dry consistency, moist consistency, colour value and pH) were measured and scored following the methods of Harden (1982). Scores from individual horizons were then normalised and summed to provide a PDI. Actual values of clay content, organic content, iron oxide and magnetic susceptibility were also measured following Woodward *et al.* (1994). The methods of recording the soil properties are outlined below.

6.2.1.1 Rubification

The colour of the soil was described using a Munsell soil colour chart (Munsell 1975). Soil colour was taken when moist in the field and when dried in the laboratory at 60°C for 6 hours.

Soil colour changes as soil develops; colour hues become redder and chromas brighter with soil age if pigments are available in oxidising environments (Harden 1982). Change in hue and chroma is called rubification (Kubiěna 1970) and older soils will tend to be more rubified than younger soils in the same area. This is a key component in defining the six maturity stages described by van Andel (1998) in his study of soils across Greece (Table 6.8)

6.2.1.2 Structure

The structure of the soil was evaluated in the field on the basis of grade and aggregate type. Grade was classified as weak, moderate or strong and aggregate type classified as granular, platy, prismatic, columnar or blocky (*cf.* Birkeland 1984).

In unconsolidated parent material, structure types in the B horizon develop from structureless granular to blocky to prismatic. With time, the B horizon may become a prominent hard-pan due to high amounts of clay or carbonate cementation. Structure is therefore an important maturity indicator in soils (van Andel 1998).

6.2.1.3 Texture

Texture incorporates the particle size distribution described in classes on a sand-silt-clay triangular plot (Soil Survey Staff 1951) and the soil consistency. Particle size distribution for this purpose was determined using a Malvern Mastersizer-X laser particle-sizer on the < 2 mm fraction (*cf.* section 3.2.3). For wet soil, consistency was measured using the properties of stickiness and plasticity whilst moist and dry consistency was determined by noting the friability and hardness of the soil respectively (*cf.* Harden 1982).

With time, soils become harder when dry, firmer when moist and more sticky and plastic when wet. This is because, over time, soil aggregates become bound more strongly by clays, oxide compounds and organic compounds (Harden 1982).

6.2.1.4 Clay content

Clay films were described using the methods described in Birkeland (1984) and defined in terms of frequency, thickness and morphology. The percentage clay of the fine fraction (< 63 μm) of the soil was also measured. All air-dried samples screened through a 1 mm mesh sieve were screened further, through a 63 μm sieve (*cf.* Woodward *et al.* 1994). Clay content was determined using a Malvern Mastersizer-X laser particle-sizer (*cf.* section 3.2.3) and expressed as percentage of the fraction < 63 μm .

The development of a clay-rich argillic horizon is largely time-dependent since mineral breakdown and clay translocation are relatively slow processes (Birkeland 1984). As a result, soils which display clay-rich B horizons are likely to be older than those which display lesser clay content.

6.2.1.5 Organic content and melanization

Organic content was determined by weight loss after ignition for 6 hours at 550°C (*cf.* Woodward *et al.* 1994). The darkening of a soil with time due to the accumulation of

organic matter is called melanization (Buol *et al.* 1973). This was measured for use in the Harden index by comparing the difference in Munsell colour value for a particular soil horizon with the parent material (Harden 1982).

Soil organic matter is derived from sources such as surface litter, dissolved or suspended organic load from stemflow and the *in situ* decomposition of root material and soil organisms (Woodward *et al.* 1994). This results in topsoil tending to be richer in organic material than further into the profile. However, organic content in the upper profile is unrelated to soil age. It is the organic content deep in the profile which is of importance in deducing the relative age of soils. This is due to aggregate shrinkage and vertical fracturing, allowing humus and particulates to be translocated as colloidal suspensions from the upper soil, especially during periods of moisture deficiency (Woodward *et al.* 1994).

6.2.1.6 Iron oxide content

Total ferric iron was determined using the dithionite-citrate-bicarbonate procedure described in Mehra and Jackson (1960). This method is outlined in Appendix 2. The ferrous iron component in the minerals of the parent material is progressively converted to ferric iron through time. In the lower Voidomatis basin, Woodward *et al.* (1994) showed that total ferric iron and the depth and thickness of the iron-enriched illuvial horizon provides a useful measure of relative age.

6.2.1.7 Magnetic susceptibility

Measurements of low frequency mass specific magnetic susceptibility were taken using a Bartington Instruments system in 10 cm³ plastic measuring pots. Magnetic susceptibility measures the ease with which a sample can be magnetised and is proportional to the concentration of ferrimagnetic minerals in a sample. The production of magnetic minerals by pedogenic weathering is time-dependent, and a positive relationship exists between magnetic susceptibility and soil profile age (Singer *et al.* 1992, Woodward *et al.* 1994).

6.2.1.8 pH

The pH of the soil was measured in the laboratory by mixing soil samples with de-ionised water. The pH of the water-soil mix was measured using a pH meter. Soil pH is sensitive to the extent of leaching and decreases as basic cations are leached away with time. The difference between the pH of the soil and the parent material is therefore a key indicator of soil maturity (Harden 1982).

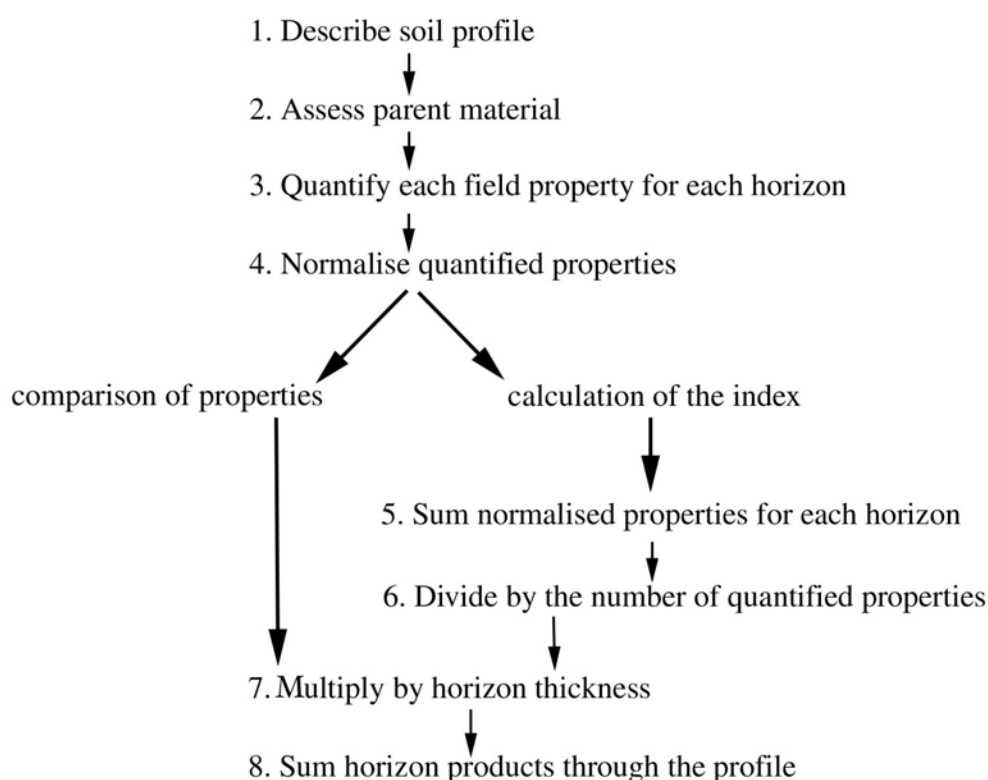


Figure 6.6 A flow diagram showing the various steps in deriving the Harden soil profile development index (after Harden 1982).

6.2.2 Analysis of soil properties - results

Soils developed on glacial deposits were sampled in several valleys of Mount Tymphi. However, well-developed soils were only found on the lowest glacial deposits in any given valley. On higher deposits, soils were usually thin and poorly developed.

The measured soil properties of rubification, clay film, texture, structure, dry consistency, moist consistency, colour value and pH were quantified using the method described in Harden (1982). The sum of the normalised properties was divided by the number of properties and multiplied by the horizon thickness to obtain a horizon index. The sum of the soil horizon indices represents the soil profile development index (for detailed procedure: Harden 1982, Table III). This index, as well as measured values of organic, clay, iron oxide content and magnetic susceptibility in the soil profile, are described below for each sampled soil. A flow diagram illustrating the various steps in the Harden method is shown in Figure 6.6.

6.2.2.1 Voidomatis Member soil

A well-developed soil is present on glacial deposits of the Voidomatis Member in the Tsepelovo Formation. At *ca.* 39°54'13"N, 20°49'36"E, 1092 m a.s.l., this soil is buried by colluvial deposits (Chapter 4, Fig. 4.8), although it can be traced laterally over a wide area. In places, the soil is exposed at the surface and is much thinner, indicating significant erosion. Where soils are buried, the maturity stage of the palaeosol represents the time elapsed before burial occurred (van Andel 1998). Whilst the buried soil is much thicker than when exposed at the surface, it would appear that, prior to burial, the soil was truncated and the A and E horizons were eroded. Therefore, only the B horizon is present and reaches a total depth of 110 cm. Two, slightly different coloured, sub-horizons were identified within this horizon at depths of 0-50 cm and 50-110 cm (0 cm = top of the soil). Unweathered parent material of the C horizon was sampled at 120 cm depth.

The upper B horizon (0-50 cm) has a weak red colour (Munsell: 2.5YR 4/2) and the lower B horizon (50-110 cm) has a reddish-brown colour (Munsell: 2.5YR 3/2). Moreover, the upper B horizon has a silty clay loam texture, whilst the lower B horizon has a finer, silt clay texture. Both of the horizons have a moderate- to well-developed subangular blocky structure. The soil of both horizons has a sticky and plastic wet consistency. Clay films are evident covering ped faces, bridging grains and lining pores. Down-profile variations in soil properties are shown in Figure 6.7. The clay content of the fine fraction ($< 63 \mu\text{m}$) fluctuates between 16 and 38% through the soil profile, with the greatest values occurring in the lower B horizon. The organic content is greatest at the top of the upper B horizon (8.1%) and decreases gradually towards the base of the lower B horizon (6%). Calcium carbonate content increases with depth from 15.4 % to 20.3 %, although not so high as to form a carbonate K horizon. Iron oxide content is highest in the lower B horizon at $25 \times 10^3 \text{ mg kg}^{-1}$ and decreases rapidly near to the base of the profile and the parent material. The magnetic susceptibility results show that the highest values are present in the upper B horizon, with values decreasing markedly in the lower B horizon. Using Harden's (1982) approach, the upper and lower B horizons have horizon indices of 21.9 and 32.7 respectively (Table 6.9). The sum of these values gives a PDI of 54.6 which most likely represents a minimum value given that the soil has been truncated. Further information regarding the description of the soil properties is given in Appendix 3.

The increase in clay content through the profile is consistent with clay illuviation with time. In the lower catchment of the Voidomatis basin, Woodward *et al.* (1994) noted that only pre-Holocene soils contained argillic horizons. The high organic content of the soil (6-8%), reflected by the strong melanization of the soil, further suggests that the soil is

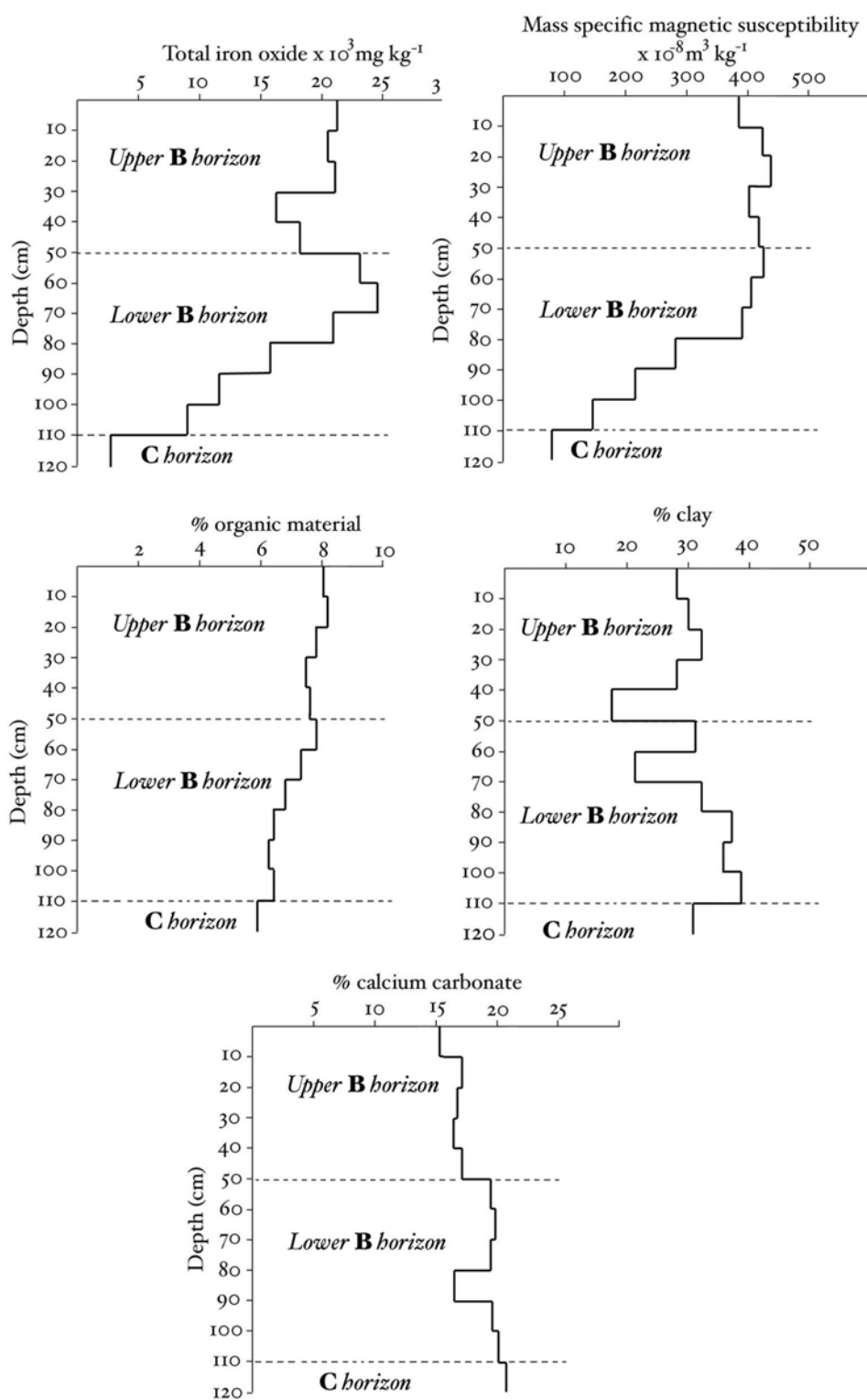


Figure 6.7 Variations in iron oxide content, magnetic susceptibility, % organic content, % clay content and % calcium carbonate content down-profile of the Voidomatis buried soil.

	Upper B horizon 0-50 cm		Lower B horizon 50-110 cm	
	Raw value	Normalised	Raw value	Normalised
Clay film	100	0.62	100	0.62
Texture	60	0.66	70	0.78
Rubification	90	0.47	90	0.47
Structure	30	0.5	40	0.67
Dry consistency	20	0.2	30	0.3
Moist consistency	20	0.2	30	0.3
Colour value	40	0.57	60	0.86
pH	1.00	0.29	1.25	0.36
Sum		3.51		4.36
Horizon Index (sum / number of properties x horizon thickness <cm>)		21.9		32.7
Profile development index (PDI) (sum of horizon indices) = 54.6				

Table 6.9 Harden index values for the Voidomatis soil profile.

of pre-Holocene age. In the lower Voidomatis, only profiles older than 25,000 years BP contained >7% organic material in the B horizon (Woodward *et al.* 1994). The soil iron oxide content confirms the antiquity of the soil. The values reach between 16 and 25 ($\times 10^3$) mg kg^{-1} . This compares with values up to 24 ($\times 10^3$) mg kg^{-1} in the Aristi-B soil formed atop alluvial sediments in the lower Voidomatis valley. Woodward *et al.* (1994) estimated the age of this soil at *ca.* 85,000 years BP using their weathering index model. Application of the weathering index gives the Voidomatis Member soil an age of 72,500 years BP. However, as noted by Woodward *et al.* (1994), it is unknown whether the relationship between soil profile age and the weathering index is linear beyond 28,000 years BP. Given that cement in the Voidomatis Member till has been dated to at least $105,730 \pm 21,450$ years BP (Table 6.4), it would appear that the model prediction underestimates the soil age in this locality. The magnetic susceptibility results mirror those of the iron oxide, with the highest values in the top half of the lower B horizon and in the upper B horizon. This is to be expected given that magnetic susceptibility measures the degree to which a sample can be magnetised – a property enhanced by the presence of iron.

The PDI value of 54.6 compares with values of between 50.8 and 81.7 obtained for soils developed on the oldest glacial deposits on Mount Olympus (Smith *et al.* 1997). The PDIs of Tymphi and Olympus are comparable, since it is likely that soils in these two areas have undergone similar rates and styles of weathering given the similar geology and relatively short distance between the sites. On Mount Olympus, all soils developed in younger, less extensive glacial deposits give values lower than 40. The soils on the most

extensive glacial deposits on Mount Olympus are correlated with a deep-red soil developed on fan remnants of the southern Olympus Piedmont, in the Larissa basin. Calcretes, formed at the base of this soil, have been U-series dated to 210,000 years BP (Demitrack 1986). This led Smith *et al.* (1997) to believe that soils, developed on the most extensive glacial deposits on Mount Olympus, formed during MIS 7 and that the underlying glacial deposits formed during the preceding cold stage equivalent to MIS 8. Since the value of 54.6 is only a minimum, it is clear that the Voidomatis Member soil shows weathering characteristics similar to those thought to be at least 210,000 years old on Mount Olympus. Similarly, in the scheme of van Andel (1998), the colour, structure and prevalence of clay films suggest that the soil can be placed in the most mature bracket with ages of greater than 110,000 years BP (Table 6.8).

6.2.2.2 Maghoula Member soil

A soil is developed on the glacial deposits of the Maghoula Member. Soil samples were collected from a section exposure at 39°59'30" N, 20°53'15"E, 1100 m a.s.l., just before the surfaced road from Iliochori descends into VrISOchori. The soil depth to the base of the B horizon was 130 cm. In total, four samples were taken, from the A, E, B and C horizons.

Table 6.10 shows that the soil exhibits the classic down-profile soil weathering characteristics. Clay content is low in the A and E horizons but reaches over 30% in the B horizon due to translocation of clay. Iron oxide levels are greatest in the B horizon and reach values similar to those found in Voidomatis Member soil, as well as those found on the Aristi unit in the lower Voidomatis basin (*cf.* Woodward *et al.* 1994).

It is clear, therefore, that the Maghoula Member soil is well-developed. The PDI of 61.0 is higher than that for the Voidomatis Member soil, although this may be because of the absence of A and E horizons in the Voidomatis Member soil. The B horizon index for the Maghoula Member soil is 50.4, similar to the truncated Voidomatis Member soil PDI of 54.6. This suggests that the Maghoula Member soil may be of similar age and it is possibly as old as those which have formed on the oldest, most extensive glacial deposits of Mount Olympus, which are estimated to be >210,000 years BP old (Smith *et al.* 1997). Moreover, the colour, structure and content of the B horizon correspond with the most mature stage defined by van Andel (1994), which are thought to be older than 110,000 years old (Table 6.8).

Depth (cm)	Horizon	Colour	Harden horizon index	% clay content	% organic content	Iron oxide content ($\times 10^3$) mg kg ⁻¹	Mag' suscept' ($\times 10^{-8}$) mg ³ kg ⁻¹
0-10	A	5YR 3/2 dark reddish brown	2.7	5%	12%	12	143
10-30	E	5YR 6/3 light reddish brown	7.9	9%	6%	12	135
30-130	B	2.5YR 3/4 dark reddish brown	50.4	34%	8%	21	159
>130	Parent material (C)	10YR 7/1 light grey	-	23%	2%	3	34
Profile development index: 61.0							

Table 6.10 Horizon characteristics from the Maghoula Member soil.

6.2.2.3 Kato Radza Member soil

A soil is developed in the glacial deposits of the Kato Radza Member below Skamnelli. The soil could not easily be sampled in section and therefore a 100 cm pit was dug through the soil reaching the parent till at 39°54'20" N, 20°50'40"E, 1040 m a.s.l. Samples were taken from the B horizon at *ca.* 25 cm and 75 cm as well as from the parent till beneath (Table 6.11).

The B horizon samples had a reddish-brown colour (Munsell colour: 2.5YR 3/2), and the upper and lower samples had a clay content of 31 and 33% respectively in the < 63 micron fraction. The preponderance of clay is illustrated by the presence of thick clay films. The two soil samples had a well-developed subangular blocky structure with a clay loam texture and a very sticky and very plastic wet consistency. The upper and lower soil samples had an organic content of 9% and 5%, respectively. The soil iron content of the upper and lower soil samples were 20×10^3 mg kg⁻¹ and 29×10^3 mg kg⁻¹, respectively, and the corresponding magnetic susceptibility values were 189 and 194×10^{-8} m³ kg⁻¹.

Using the approach of Harden (1982), the soil had a PDI of 51.8. This index is really a B horizon index since the A and E horizons were very thin, reflecting either compaction or erosion, and can be taken as representing a minimum development index for the whole profile. It may be the case that the soil horizons have been oversimplified here. However, as noted by Harden (1982), if there is a tendency to subdivide horizons, the description of numerous horizons will not have an appreciably larger index sum than a more general description with fewer horizons.

Depth (cm)	Horizon	Colour	Harden horizon index	% clay content	% organic content	Iron oxide content ($\times 10^3$) mg kg ⁻¹	Mag' suscept' ($\times 10^{-8}$) mg ³ kg ⁻¹
25	Upper B horizon	5YR 3/2 dark reddish brown	51.8	31%	9%	20	189
75	Lower B horizon	5YR 3/2 dark reddish brown		33%	5%	29	194
>100	Parent material (C)	10YR 7/1 light grey	-	24%	2%	5	54

Table 6.11 Horizon characteristics from the Kato Radza Member soil.

It is clear from the results that the Kato Radza Member soil is probably of a similar age to those on the Voidomatis and Maghoula Members. The PDI of 51.8 is similar to both of these soils (54.6 and 60.1). All three soils therefore represent prolonged weathering of the parent tills. This is an important observation, supporting the inter-valley correlation of the glacial deposits on the basis of their stratigraphical position and the cement U-series dates.

6.2.2.4 Other soils

Well-developed soils, similar to those on the Voidomatis, Maghoula and Kato Radza Members are present on the lowest and most extensive glacial deposits in several other valleys. For example deep red soils are evident on deposits of the Mighia, Amarandos, Megas Laccos, Ghaidhouro, Spirokapa and the Laccos Radenas Members, the lowest morpho-lithostratigraphical units of their respective formations. Whilst systematic analysis was not carried out on these soils, preliminary field observations of colour, clay films, structure and texture suggest that the soils are similarly well-developed.

6.2.3 Soils – summary and significance

All three of the soils analysed above are formed on the most extensive glacial deposits. The cemented Kato Radza Member deposits have been dated at >350,000 years BP, whilst the oldest date from the Voidomatis Member deposits is $105,730 \pm 21,450$ years BP. No dates have been obtained from the Maghoula Member deposits. Based on these dates alone, correlation is not obvious. However, the fact that the deposits occupy similar morpho-lithostratigraphical positions within their respective formations and display soils with similar weathering characteristics, suggests that they are of the same age. In addition, soils

similar to the Voidomatis, Maghoula and Kato Radza soils have formed on the most extensive glacial deposits elsewhere on Mount Tymphi and, in the case of the Megas Laccos Member, cements have been dated at >350,000 years BP.

The PDI values for the soils of Mount Tymphi correspond to similar values obtained from soils on Mount Olympus considered to be >210,000 years old (Smith *et al.* 1997). Moreover, the soil characteristics correspond to the maturity stage, defined by van Andel (1998), for soils older than 110,000 years. Finally, the chemistry of these soils is similar to the oldest soils on alluvial sediments in the lower Voidomatis which are thought to be greater than 80,000 years old (Woodward *et al.* 1994).

It is likely that soil formation has occurred at different rates through time and that during periods of reduced soil formation, such as during the most intense phases of glacial climate, the A and E horizons have been eroded. Nevertheless, intervals of destabilisation tend to be brief in a Mediterranean climate (van Andel 1998) and, even during glacial Mediterranean climates, it is not inconceivable that soils may have continued forming. For example, in modern-day alpine environments, soils are still actively forming in areas adjacent to the lower reaches of glaciers (Tscherko *et al.* 2003).

Whilst well-developed soils exist on the lowest, most extensive glacial deposits, soils are poorly developed on the higher morpho-lithostratigraphical units. Although this may be expected for the highest, most recent units, the absence of well-developed soils on the mid-valley units (*i.e.* the Laccorponi, Vourtapa and Portes Members in the Tsepelovo, Skamnelli and Vrisochori Formations) is unexpected, especially since cement dates show that these deposits formed before the last interglacial (>127,000 years BP). The absence of soils on these moraines may result from inhibited soil development at the higher altitude of the mid-valley units. This, combined with the younger age of the mid-valley glacial deposits, may have resulted in a sharp contrast in soil development compared with the lower more extensive glacial deposits. However, deeply-weathered soils on the most extensive glacial deposits are evident as high as 1700 m a.s.l. in the Laccos Radenas valley. Therefore, whilst it is possible that soil development is slower at higher altitudes, the soils on the oldest glacial deposits become so well-developed because of very prolonged stability in comparison to those soils formed on the younger, yet still relatively old, mid-valley deposits.

The fact that highly weathered soils are preserved on top of glacial deposits dated to at least 350,000 years BP illustrates the preservation potential of soils and sediments in tectonically active areas. Usually, rapid rates of uplift in tectonically active areas such as Epirus are commonly perceived to result in widespread landscape instability (King *et al.*

1997). Whilst rates of erosion and fluvial incision may be locally high, it does not necessarily imply that erosion is high everywhere. Erosion is usually concentrated along valleys, especially those which already existed before the Middle Pleistocene (Amato *et al.* 2003). The resulting landscape is therefore one of an ancient surface dissected locally by concentrated incision. In limestone areas, preservation of the ancient landscape between areas of concentrated incision is promoted by permeability and subsurface drainage. Soil and sediment preservation has much more potential in these areas than in areas of less-permeable flysch or ophiolite. For example, it is notable that deep soil sequences are not preserved on the most extensive glacial deposits of Mount Smolikas and Mount Vasilitsa. Local geology is therefore probably a key factor in landscape and sediment preservation in areas like Greece and can lead to markedly stable local landscapes - even in areas of regional tectonic instability.

6.3 Defining a common inter-valley chronostratigraphy

A geochronological framework has been achieved for some glacial deposits on Mount Tymphi using U-series dating, as has a relative-age framework based on soil characteristics. However, the morpho-lithostratigraphical units recognised in each cirque-valley system are so far not defined with respect to a globally applicable standard time-scale, *i.e.* chronostratigraphical units are un-defined. The conventional hierarchy for chronostratigraphical and geochronological terms is shown in Table 6.12.

The stage represents the basic unit of chronostratigraphy. A stage is defined by its boundary stratotypes; sections that contain a designated point in a stratigraphical sequence. The lower and upper boundary stratotypes of a stage represent specific moments in geological time, and the time interval between them is the time span of the stage. This concept is quite difficult to apply in the context of glaciated mountain environments, since defining the base of a unit is often not possible because the lithostratigraphical units represent only 'snapshots' in time and do not represent continuous deposition.

One area where attempts have been made to formalise the stratigraphical approach to mountain glaciation has been in the Himalaya. Here, Owen *et al.* (1998) noted that the low level of understanding of the glacial sequence was due to a poor adherence to strict stratigraphical procedures and proposed a series of measures to redress this issue. However, their measures also fail to adhere to strict stratigraphical procedure and, whilst they may be of use in separating glacial phases, they are incommensurable with formal stratigraphies established elsewhere. For example, Owen *et al.* (1998) recognise glacial 'stages' separated spatially, stratigraphically and sedimentologically. However, they do not use the term

<i>Chronostratigraphical</i>	<i>Geochronological</i>	<i>Examples</i>
Eonothem	Eon	Phanerozoic
Erathem	Era	Cenozoic
System	Period	Quaternary
Series	Epoch	Pleistocene
Stage	Age	Würmian
Chronozone	Chron	Younger Dryas

Table 6.12 Conventional hierarchy of chronostratigraphical and geochronological units in the Quaternary (after Lowe and Walker 1997).

'stage' in a formal chronostratigraphical sense since, for example, they argue that there is the possibility that two or more glacial 'stages' may occur in a single full glacial cycle. Whilst multiple advance/retreat glacial phases are possible, it is not true that more than one chronostratigraphical glacial stage can exist within a single glacial cycle. This is because in Quaternary stratigraphy, chronostratigraphical stages are usually subdivided based on climate, *i.e.* warm and cold stages (Gibbard and West 2000). The approach of Owen *et al.* (1998) is more akin to event stratigraphy, whereby geologically short-lived occurrences up to several thousand years or more leave some trace in the rock record, *i.e.* moraines, (Whittaker *et al.* 1991, Rawson *et al.* 2002), than chronostratigraphy. The result is that the 'stages' of Owen *et al.* (1998) cannot be compared with established chronostratigraphical units such as the Würmian Stage of the Alps (*cf.* Chaline and Jerz 1983, 1984). However, a precedence appears to have already been set, for the Himalaya at least (*cf.* Taylor and Mitchell 2000). If a sound stratigraphical framework is to be achieved, it is fundamental that stratigraphical nomenclature is consistent with that used in other regions. If this is not done, comparison with other terrestrial chronostratigraphies and reference to a globally applicable standard time-scale is difficult to achieve.

The stratigraphical problems encountered when dealing with the fragmentary nature of mountain glacial records, especially with respect to chronostratigraphy, can be resolved by comparing local sequences to a nearby continuous record, *i.e.* a parastratotype. In this study, a formal chronostratigraphical framework which can be compared to a globally-applicable standard timescale, developed with reference to the continuous lacustrine sequence at Ioannina, was used for this purpose (*cf.* Tzedakis 1994, Tzedakis *et al.* 2002).

Tzedakis (1994) showed that the long lacustrine pollen sequence (*ca.* 423,000 years) at Ioannina can be compared and correlated with the marine isotope record (*cf.* Ninkovich and Shackleton 1975, Shackleton and Pisias 1985). This is also the case for

other long continuous sequences such as that at Tenaghi Philippon (Wijmstra 1969, Wijmstra and Smit 1976, Wijmstra and Groenhart 1983, van der Wiel and Wijmstra 1987a, 1987b) and a number of other terrestrial sequences in southern Europe (Tzedakis *et al.* 1997). The relationship between the Ioannina and Tenaghi Philippon sequences and the marine record is shown in Table 6.13.

In both the Tenaghi Philippon and Ioannina sequences, chronostratigraphical stages are not defined. Instead, a climatostratigraphical approach was adopted, applying the terms 'interglacial' and 'interstadial' on the basis of vegetational succession and total pollen concentrations. At Ioannina, Tzedakis (1994) applies the terms 'glacial' and 'interglacial' informally to refer to periods characterised by relatively cold and/or arid and warm and/or moist climates - a situation not entirely satisfactory, even for climatostratigraphical purposes (*cf.* Turner and West 1968). Moreover, although a climatostratigraphical approach has been adopted at both Tenaghi Philippon and Ioannina, at both sites, climatic intervals such as interglacials and interstadials have been directly correlated with chronostratigraphical units in the marine isotope stratigraphy. This practice has been discouraged by West (1984, 1988), Gibbard and Turner (1990) and Gibbard and West (2000). This is because the interchanging of climatostratigraphical and chronostratigraphical units results in considerable confusion about the precise distinction between schemes of subdivision (Gibbard and West 2000). However, since the initial publication of the Ioannina and Tenaghi Philippon records, climatostratigraphical units such as 'interglacial', 'interstadial' and 'stadial' and their links with the marine chronostratigraphy have been perpetuated to the degree whereby it would be futile to redefine the pollen stratigraphy in true chronostratigraphical terms. The result is a stratigraphical approach to cold-stage definition based on a combination of formalised glacial and periglacial chronostratigraphy, and a climatostratigraphically continuous sequence. Although not ideal, it serves the purpose of establishing a quasi-chronostratigraphical sequence for Greece.

The Ioannina sequence has the advantage of being less than 40 km from the field area, on the leeward side of the main Pindus axis. Tenaghi Philippon is over 300 km to the northeast of the field area and lies in the lee of the Pindus range. The sequence at Ioannina is therefore more likely to reflect the climatic events in the mountains with greater accuracy than Tenaghi Philippon. Although Ioannina is used as the formal primary parastratotype, both sequences are referred to in the discussion. In fact, two parastratotypes are used, from adjacent cores Ioannina 249 (Tzedakis 1994) and Ioannina 284 (Galanidou *et al.* 2000,

Age (x 1,000 years BP)	MIS	Ioannina 249/ 284	Tenaghi Philippon
	1	Holocene	Holocene
66 - 11.5 *	2	<i>Glacial conditions</i>	<i>Glacial conditions</i>
	3		
	4		
83 - 66 *	5a	Vikos/ Interstadial 2	Elevtheropolis
88.5 - 83 *	5b	Stadial 2	<i>Stadial conditions</i>
104 - 88.5 *	5c	Perama-Thyamis/ Interstadial 1	Drama/ Doxaton
111 - 104 *	5d	Stadial 1	<i>Stadial conditions</i>
127 - 111 *	5e	Metsovon	Pangaion
190 - 127 *	6	<i>Glacial conditions</i>	<i>Glacial conditions</i>
250 - 190	7a	IN-26	H2-3 Symvolon
	7c	Zitsa	H1 Symvolon
	7e	IN-23a	Strymon
300 - 250	8	<i>Glacial conditions</i>	<i>Glacial conditions</i>
340 - 300	9a	Katara	Kavalla
	9c	IN-17	Krimenes
	9e	Pamvotis	Litochoris
350 - 340	10	<i>Glacial conditions</i>	<i>Glacial conditions</i>
430 - 350	11	Dodoni I and II	Lekanis
480 - 430	12	<i>Glacial conditions</i>	<i>Glacial conditions</i>
	13	Base of sequence	Alistrati II
	14		Alistrati I
	15		Falakron
	16		<i>Glacial conditions</i>
	17		Niki
	18		<i>Glacial conditions</i>

Table 6.13 The pollen stratigraphical sequences at Ioannina (cores IN 249 and 284) and Tenaghi Philippon (after Tzedakis *et al.* 1997, 2002). Interval ages marked with an asterisk are taken from Tzedakis *et al.* (2002). All other interval ages are taken from Lowe and Walker (1997, Table 1.1).

Tzedakis *et al.* 2002). However, before a regional chronostratigraphy can be established, the first step towards this goal is the correlation of inter-valley morpho-lithostratigraphical units and the establishment of a common inter-valley stratigraphical sequence.

6.3.1 Inter-valley correlations

The relative sequence of sediment units in each cirque-valley system on Mounts Tymphi, Smolikas and Vasilitsa has already been established (Chapters Four and Five). Based on this stratigraphical framework, correlation was made between stratigraphical units using the

results of soil analysis and U-series dating. Correlation tables for each mountain are shown in Figures 6.8 and 6.9.

It was shown in Chapters Four and Five that the maximum number of morpho-lithostratigraphical units that can be defined in the valleys of Mount Tymphi and Mount Vasilitsa is three, whilst on Mount Smolikas a fourth upper morpho-lithostratigraphical unit can be identified. It is very likely that the chronostratigraphy of these units is the same for each valley formation with the lowest, most extensive glacial deposits representing the same glacial phase. The absence of deposits equivalent to the highest unit on Mount Smolikas, Mount Tymphi and Mount Vasilitsa, is because these deposits occur at an altitude above the highest cirque floors of the latter mountains.

Problems arise where there are less units recorded in some valleys than others, such as in the Ghaidhouro, Laccos Radenas and Spirokapa Formations, on Mount Tymphi, and in the Samarina Formation, on Mount Smolikas, which contain only one stratigraphical unit. In these circumstances, correlation was made based using characteristics such as altitude, morphological freshness, the presence, absence and degree of weathering of soils or by absolute dating where possible. Even when inter-valley correlations proved difficult or tenuous, only cirque-valley formations where there is the fullest stratigraphical sequence were used to provide the basis for any formal chronostratigraphical framework.

On Mount Tymphi, the inter-valley correlations are based on a whole range of morphological, lithological, pedological and geochronological criteria. However, the bases of correlation between Mount Tymphi and neighbouring Mount Smolikas and Mount Vasilitsa are obviously based on little more than morphostratigraphy. There is little way around this. In formations where the sequence appears to have units comparable to the full Mount Tymphi sequence, then it is likely that morphostratigraphical correlations are valid - especially given the proximity of these mountains. However, there will always be questions as to the exact position of some of these units - especially in areas such as the Konkutino valley, on Mount Smolikas, where the sequence is very fragmented. The following chapters regarding glacier reconstruction and palaeoclimatic reconstructions provide information enabling the correlations to be tested. If the requirements of these tests are met, then these correlations will be substantiated.

Figure 6.10 shows the proposed correlations between fully represented formations on Mount Tymphi, Mount Vasilitsa and Mount Smolikas. The formations shown in Figure 6.10 are for illustrative purposes only and all numbered units in each formation, on each mountain (Fig. 6.8 and 6.9), are correlated.

	Tsepelovo Formation	Skamnelli Formation	Vrisochori Formation	Iliochoiri Formation	Stani Katsanou Formation	Mighia Formation	Neraidhovrisi Formation
3	{ Vlasi Member Litharion Member Tselon Member	Tsoukoula Member	Portes Member	{ Dimitrios Member Eptapirghi Member	Tsouka Rossa Member	{ Kopanes Member Gamila Member	
2	Laccorponi Member	{ Your tapa Member Vrichos Member Corifula Member	Maghoula Member	{ Tsouknidhes Member Laccos Member Plaghia Member	Stani Katsanou Member	Limeria Klefton Member	
1	<i>Voidomatis soil</i> Voidomatis Member *	{ Kato Radza soil Kato Radza Member Megali Rachi Member	<i>Maghoula soil</i> Vrisochori Member	Kriopotamos Member	Aghia Triada Member	<i>Mighia soil</i> Mighia Member	+ Neraidhovrisi Member
	Amarandos Formation	Stani Grava Formation	Megas Laccos Formation	Ghaidohouro Formation	Raidhovoli Formation	Spirokapa Formation	Laccos Radenas Formation
3	Amarandos Member				{ Astraka Member Ploskos Member		
2	Stomio Member	+ Stani Grava Member	Kazarma Member *		Xeroloutsa Member *		
1	<i>Drochatio soil</i> Drochatio Member	+ Dales Member	<i>Megas Laccos soil</i> Megas Laccos Member *	<i>Ghaidohouro soil</i> Ghaidohouro Member	<i>Raidhovoli soil</i> Raidhovoli Member	<i>Spirokapa soil</i> Spirokapa Member	<i>Laccos Radenas soil</i> Laccos Radenas Member *

Key

{ Member units of equivalent stratigraphical position in upper tributary valleys/cirques

* Cemented unit dated using U-series

+ Correlated on the basis of altitudinal position only

Figure 6.8 Inter-valley correlation of morpho-lithostratigraphical units on Mount Tymphi.

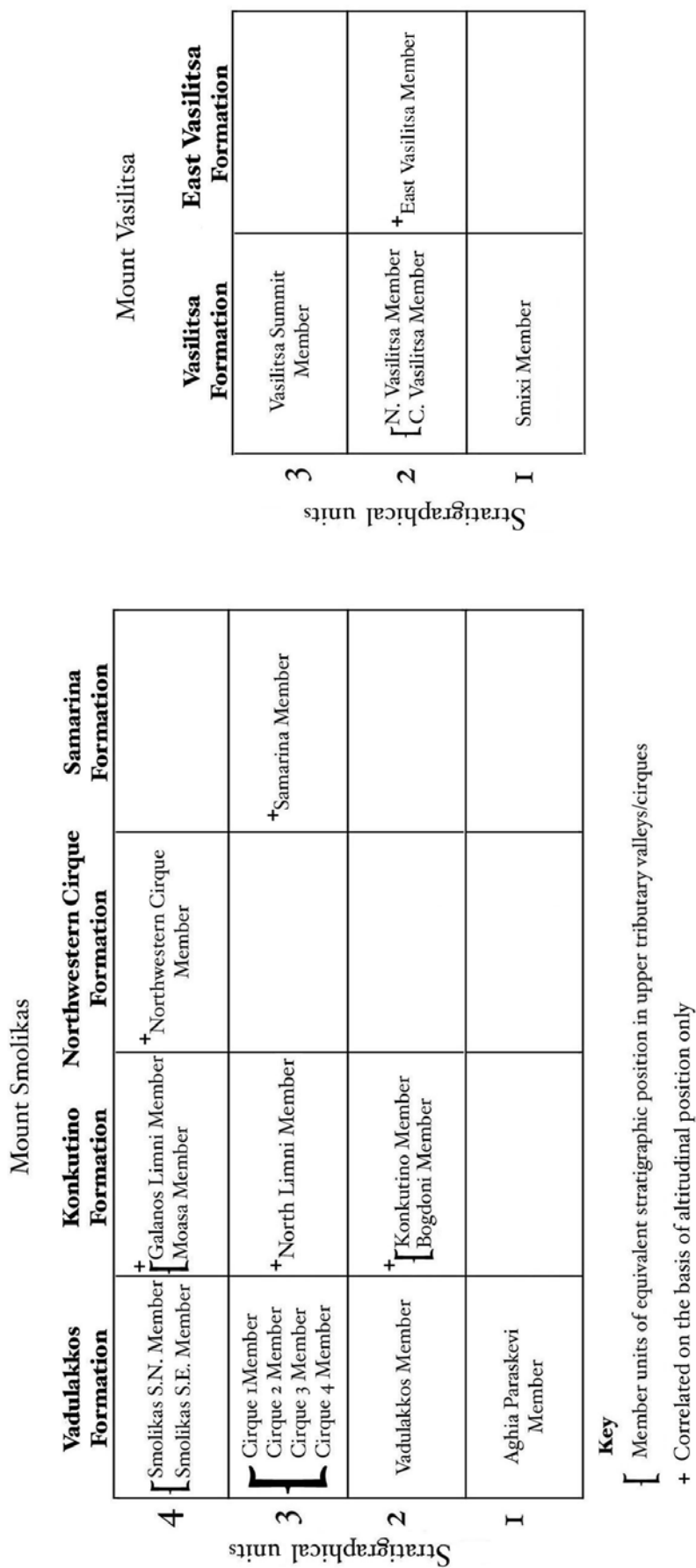


Figure 6.9 Inter-valley correlation of morpho-lithostratigraphical units on Mount Smolikas and Mount Vasilitsa.

Pindus Group				
		Vadulakkos Formation	Vasilitsa Formation	Tsepelovo Formation
Stratigraphical units	4	{ Smolikas S.N. Member Smolikas S.E. Member		
	3		{ Cirque 1 Member Cirque 2 Member Cirque 3 Member Cirque 4 Member	{ Vasilitsa Summit Member Vlasi Member Litharion Member Tselon Member
	2	Vadulakkos Member	{ N. Vasilitsa Member C. Vasilitsa Member	Laccorponi Member
	I	Aghia Paraskevi Member	Smixi Member	<i>Voidomatis soil</i> Voidomatis Member
		Mount Smolikas	Mount Vasilitsa	Mount Tymphi

Key

{ Member units of equivalent stratigraphical position in upper tributary valleys/cirques

Figure 6.10 Correlations between formations on Mount Smolikas, Mount Vasilitsa and Mount Tymphi. The formations shown here are for example purposes. All formations on all three mountains collectively constitute the Pindus Group.

Collectively, all of the Quaternary deposits in all of the formations described in this study are grouped into the **Pindus Group**. The sediments which represent the morpho-lithostratigraphical units are largely of glacial origin. However, some of the sediments are periglacial, especially the uppermost stratigraphical units. Therefore, the Pindus Group represents both glacial and periglacial deposits. An exception is the Ploskos Member of the Raidhovoli Formation, which is a rock-slope failure deposit and may not necessarily be of periglacial origin. Deposits of the Pindus Group should be traceable throughout the Pindus Mountains and across Greece as a whole. The next step is to define a globally-comparable chronostratigraphical framework into which these units can be placed.

6.3.2 Defining the chronostratigraphy with reference to a parastratotype

According to Salvador (1984), the name of a chronostratigraphical stage should be derived from a geographical feature in the vicinity of its stratotype or type area. In English, the adjectival form of the geographical term is used ending in "ian" or "an". Stage units are defined by well-represented type sections or type localities, especially those where geochronology is available.

The earliest stage is termed the **Skamnellian Stage** after the village of Skamnelli near to where both the Kato Radza and Megali Rachi Members are located. The type section for the Skamnellian Stage is section SKa in the deposits of the Kato Radza Member south of Skamnelli village at *ca.* 39°54'08"N, 20°50'40"E, 984 m a.s.l. (Chapter Four). The next stage is termed the **Vlasian Stage** after the mountain of Vlasi (*ca.* 2200 m a.s.l.) separating Vourtapa and upper Laccorponi valleys where deposits of this stage are very well represented. The type locality for this stage is situated on the eastern side of Vlasi, in the Vourtapa valley and is characterised by deposits of the Vourtapa Member (Chapter Four) and situated at *ca.* 39°55'40"N, 20°50'30"E, 1650 m a.s.l. The most recent stage on Mount Tymphi and Vasilitsa, although present also on Mount Smolikas, is named the **Tymphian Stage** after Mount Tymphi where the deposits are well represented in its highest cirques. The type locality is characterised by the deposits of the Tsouka Rossa Member (Chapter Four), at *ca.* 39°58'45"N, 20°50'40"E, 2025 m a.s.l. The most recent unit on Mount Smolikas, a higher still, morpho-lithostratigraphical unit which is absent on Mount Tymphi and Mount Vasilitsa, is assigned to the **Smolikasian Substage**. The type locality for the Smolikasian Substage is represented by the deposits of the Smolikas Summit East (Smolikas S.E.) Member at *ca.* 40°05'25"N, 20°55'55"E, 2375 m a.s.l. (Chapter Five).

The position of these stages in time has been determined geochronologically using U-series dating, and relatively by soil analysis. This allows chronostratigraphical boundaries in the Ioannina parasequence to be identified (Table. 6.14). The Skamnellian Stage clearly pre-dates 350,000 years BP and many of the deposits are topped by soils with high profile development indices suggesting they are of considerable antiquity. At Ioannina, this stage must correspond to cold intervals prior to the Dodoni Interglacial (basal boundary: 162.75 m in Ioannina core 249) which has been correlated to MIS 11. Unfortunately, the sequence at Ioannina does not extend further back than the cold phase immediately preceding the Dodoni Interglacial. Therefore, the base of the lowest stage cannot be defined lower than the lowest part of the Ioannina 249 sequence at 185.50 m (*cf.* Tzedakis 1994). However, it is possible that the Skamnellian Stage correlates with the cold

Age (x 1,000 years BP)	MIS	Ioannina (IN 249/ 284)	Para- stratotype boundary (IN 249)	Pindus Chrono- stratigraphy	Local Stratotype		
11.5 -	1	Holocene	17.25 m				
66 - 11.5 *	2			Smolikasian Substage	Smolikas S.E. Member 40°05'25"N, 20°55'55"E. 2375 m a.s.l		
	3			Tymphian Stage	Tsouka Rossa Member 39°58'45"N, 20°50'40"E. 2025 m a.s.l		
	4						
83 - 66 *	5a	Interstadial 2 [§]		Vlasian Stage	Vourtapa Member 39°55'40"N, 20°50'30"E. 1650 m a.s.l		
88.5 - 83 *	5b	Stadial 2 [§]					
104 - 88.5 *	5c	Interstadial 1 [§]					
111 - 104.5 *		Stadial 1 [§]	45.88 m				
127 - 111 *	5e	Metsovon					
190 - 126.6 *	6		76.00 m				
250 - 190	7a	Zitsa		?			
	7c						
	7e						
300 - 250	8						
340 - 300	9a	Katara					
	9c						
	9e	Pamvotis					
350 - 340	10						
430 - 350	11	Dodoni I and II					
480 - 430	12		162.75 m			Skamnellian Stage	Kato Radza Member 39°54'08"N, 20°50'40"E. 984 m a.s.l

[§] Names based on Tzedakis *et al.* (2002). All other names from Tzedakis (1994).

* Interval dates from Tzedakis *et al.* (2002). All other interval dates from Lowe and Walker (1997, Fig. 1.1).

Table 6.14 Chronostratigraphical table showing the relationship between the fragmentary glacial sequence in the Pindus Mountains and the continuous parasequence in the Ioannina 249 and 284 cores (Tzedakis 1994, Tzedakis *et al.* 2002).

interval immediately preceding the Dodoni Interglacial and MIS 12.

At Tenaghi Philippon, the Dodoni Interglacial is locally termed the Lekanis Interglacial (van der Wiel and Wijmstra 1987b). The preceding cold interval, between the Lekanis and Alistrati II interglacials is thought to have spanned the period 445,000 to 400,000 years BP and is also correlated with MIS 12 (van der Wiel and Wijmstra 1987). This is equivalent to the Elsterian Stage in northern Europe. Although the deposits of the Skamnellian Stage may be older, since the Elsterian Stage was characterised by the most

extensive ice cover of the Middle-Late Pleistocene in northern and eastern Europe (Sibrava *et al.* 1986), it would seem a preferable correlation compared with the earlier cold intervals. For example, the next major 'glacial' phase on the basis of the pollen stratigraphy (van der Wiel and Wijmstra 1987b) occurs much earlier, between 621,000 and 562,000 years BP in the interval between the Niki and Falakron interglacials and is correlated with MIS 16. If the Skamnelliian deposits do belong to this glacial phase or even earlier phases such as between the Polistilos and Niki interglacials at Tenaghi Philippon, correlated with MIS 18 between 701,000 and 649,000 years BP, then this would imply remarkable widespread preservation of the deposits. Therefore, until further evidence is presented, the Skamnelliian Stage is correlated with the pre-Dodoni cold phase at Ioannina and the equivalent interval between the Lekanis and Alistrati II interglacials at Tenaghi Philippon, which is correlated with MIS 12, equivalent to the Elsterian Stage in northern Europe. However, it is possible, and perhaps probable, that whilst the Skamnelliian and Elsterian Stages generally correlate, the timing of their glacial maximum events may not.

The deposits of the Vlasian Stage pre-date the Metsovon Interglacial (127-111,000 years BP). However, the oldest U-series dates from these deposits show that none of the sampled cements are older than this interglacial. The oldest U-series date obtained from Vlasian Stage deposits is $121,400 \pm 21,000$ years BP (Woodward *et al.* 2004) and the oldest date obtained in this thesis is $119,818 \pm 9,249$ years BP - both from the Vourtopa Member of the Skamnelli Formation. In addition, soils on Vlasian Stage deposits are much less well-developed than soils on Skamnelliian Stage deposits, suggesting a large difference in time elapsed since deposition. Therefore, it is probable that the Vlasian Stage correlates with the 'cold' stage between the base of the Metsovon and Zitsa interglacials in Ioannina core 249 (*cf.* Tzedakis 1994). This interval has been correlated with MIS 6 and is equivalent to the Saalian Stage in northern Europe. The most severe phase of climate during this stage and the penultimate local last glacial maximum at Ioannina is thought to have occurred between 133,000 and 129,300 years BP when arboreal pollen percentages reached just below 20% in the Ioannina 284 core (Tzedakis *et al.* 2002). The deposits of the Vlasian Stage may have been deposited around this time or during an intermediate period of cold yet wetter conditions.

The Tymphanian Stage deposits are undated. However, they are younger than those of the Vlasian Stage on the basis of stratigraphical position. The deposits of this stage represent the deposits of the last major 'cold' event in Greece and it is likely that they are equivalent to the interval between the top of the Metsovon Interglacial and the base of the Holocene, corresponding to a basal boundary at 45.88 m in the Ioannina 249 core (Tzedakis

1994). This interval is comparable to the Würmian, Weichselian and Devensian Stages of the Alps, northern Europe and Britain, respectively. The climax of this glacial stage may correlate with the lowest frequencies of arboreal pollen at Ioannina during the last glacial cycle between *ca.* 22 and 20,000 years BP (Galanidou *et al.* 2000, Tzedakis *et al.* 2002), or as with other glacial stages, during an intermediate period of cold and wetter conditions.

It is possible that the Tymphian Stage deposits were laid down during an earlier part of this stage, such as between the Perama-Thyamis and Vikos Interstadials (Interstadials 1 and 2) which are correlated with MIS 5c and 5a (Tzedakis *et al.* 1997, Tzedakis *et al.* 2002). They also may have formed during the Late-glacial Substage. However, these possibilities are unlikely. If the Tymphian Stage deposits in the Pindus were deposited during the early part of this stage then this would leave a major hiatus in the glacial/periglacial record and an absence of deposits for the most severe phase of climate recorded in the Ioannina pollen record (Hughes *et al.* 2003). A Late-glacial age is also unlikely, since that would imply that the Late-glacial glaciers and rock glaciers were more extensive than those of the most severe phase of climate during the Tymphian Stage.

The Smolikasian Substage post-dates the Tymphian Stage glacial maximum on Mount Smolikas. In the Ioannina parastratotype, the Tymphian Stage covers the interval from the end of the Metsovon Interglacial (*ca.* 111,000 years BP) to the beginning of the Holocene (*ca.* 11,500 years BP/ 10,000 ¹⁴C years BP). Glacial readvance following the Tymphian Stage glacial maximum is likely to have occurred during the Late-glacial Substage (14-10,000 ¹⁴C years BP) and possibly during the Younger Dryas Chronozone. At Ioannina, evidence of a climatic oscillation during the Late-glacial is often contradictory with some records recording an oscillation, *i.e.* increased aridity and cooling during the Younger Dryas (*e.g.* Rossignol-Strick 1995, Karkanis 2001), and some not (*e.g.* Willis 1992a, Bottema 1994, Lawson 2000) (refer to section 2.5). A further possibility is that the highest, most recent deposits are of Holocene neoglacial age but again there is no dating control supporting such a conclusion. Thus, the highest deposits on Mount Smolikas are defined as a substage at the top of the Tymphian Stage with its base corresponding to pollen zone 41 at a depth of 19.75 m in the Ioannina 249 sequence (Tzedakis 1994).

6.3.3 Missing Glacial Stages

Whilst three glacial stages are recorded in the glacial and periglacial deposits of Mounts Tymphi and Vasilitsa, and an additional, more recent, substage recorded on Mount Smolikas, it is possible that glacial phases are missing from the depositional record between the Skammellian and the Tymphian Stages. For instance, at least two further glacial

cycles are recorded in the pollen stratigraphy in the Ioannina 249 core between the Skamnellian and the Tymphian Stages and are correlated with MIS 8 and 10 (Tzedakis 1994, Tzedakis *et al.* 1997). If glaciation did occur during these stages, then they must have been lesser in extent than the more recent glaciers of the Vlasian Stage. Nevertheless, although there is the possibility of missing glacial deposits, the extent and breadth of the glacial sequence in the Pindus is quite remarkable. The characteristics of the glaciers during the different glacial stages are the subject of the next chapter, Chapter Seven.

Chapter Seven

Glacier Reconstruction

7.1 Methods of glacier reconstruction

The former glaciers of Mounts Tymphi, Smolikas and Vasilitsa were reconstructed using the geomorphological and sedimentological evidence mapped in the field. Glaciers of different ages were reconstructed on the basis of the morpho-lithostratigraphy, U-series dating, and soil evidence discussed in Chapter Six. The methods adopted for the reconstructions are discussed below.

7.1.1 Glacier shape

Former glacier shape was deduced from the geomorphological evidence, in particular ice-marginal features such as lateral and end moraines, ice-marginal meltwater channels, boulder and drift limits, and periglacial trimlines. Shape reconstruction was often most accurately achieved for the lower parts of the former glaciers where moraine limits are widespread. In the upper parts of the former glaciers, shape was more subjective and was often based on valley/cirque morphometry in addition to trimline evidence. The upper extent of the former glaciers was estimated at 20-30 m below the top of cirque scarps, on the basis of the likely depth for snow-ice transformation. This parameter has been applied in the reconstruction of cirque and valley glaciers in many British studies (*e.g.* Gray 1982, Shakesby and Matthews 1993, Wilson and Clark 1998, Carr 2001) and seems reasonable where there is no other way of determining upper ice extent.

7.1.2 Glacier surface contours

The former glacier surfaces were contoured at 50 m intervals onto 1:25,000 base maps. Contours were plotted based on the position of the former ice margin and follow the general pattern seen on modern glaciers whereby the contour curvature closely corresponds to snout curvature in the snout area but diminishes up-glacier to become reversed in upper parts (Sissons 1974, Lowe and Walker 1997, p.43). Ice-surface contours should be plotted normal to ice-movement direction. This is because of the direct relationship between glacier slope and ice-flow at the base of a glacier (Benn and Evans 1998, ch.4). Contour plotting was, therefore, also aided by mapped ice-directional indicators such as fluted moraine, erosional forms and sub-glacial meltwater channels.

7.1.3 Glacier area

Glacier area was calculated using the computer programme NIH Image. This programme enables the rapid calculation of shape areas using user-defined calibrated scales. Firstly, base maps were scanned into the computer programme Adobe Photoshop where the outlines and contours of the former glaciers were traced. The contoured glacier outlines were then saved as TIFF files and opened in NIH Image.

7.1.4 Ice-divides

In cases where several former glaciers over-spill the drainage divide and flow down more than one valley, the accumulation area was divided by reconstructing ice-divides perpendicular to the glacier-surface contours. This was important since glaciers with separate snouts must logically be considered as separate glaciers. These forms of glaciers are often referred to as transection glaciers (Benn and Evans 1998). Conversely, valley glaciers, which have multiple accumulation basins but a single snout, can be considered as a single glacier - providing the accumulation basins are joined above the ELA.

Glaciers where multiple accumulation areas coalesce above the ELA to form a single snout, are characterised by a continuum of flow from the accumulation areas to a single ablation area that regulates mass balance for the whole glacier. For transection glaciers, this is not the case, since multiple ablation areas combine with discrete portions of the accumulation area to form independent glaciers. As a result, ELAs may differ on each outlet glacier in the case of transection glaciers. This is especially likely if outlet glaciers descend in different directions, such as glaciers 4 and 5 in the hypothetical examples in Figure 7.1, which descend north and south from a central ice field. In this example, the north-facing glacier, glacier 5, may have a significantly lower ELA than that facing south, glacier 4, due to lower insolation. If the glaciers were considered as one ice mass, the reconstructed ELA would be an average of the two and local differences in the glacier ELAs would not be separated.

Further problems exist where glaciers coalesce in the lower, ablation area and have separated accumulation areas (*e.g.* glacier 6, Fig 7.1). These glaciers, whilst sharing ablation areas, essentially have independent mass balance regimes because of independent accumulation areas. On smaller glaciers, the difference in ELAs will be insignificant. However, larger glaciers, which coalesce in the lower areas, may have widely varying accumulation input as a result of local factors. Therefore, in the case of valley glaciers, with shared ablation areas, ELAs were calculated for the separate glacier parts. This was achieved by splitting the lower (shared) area of the glaciers on the basis of relative

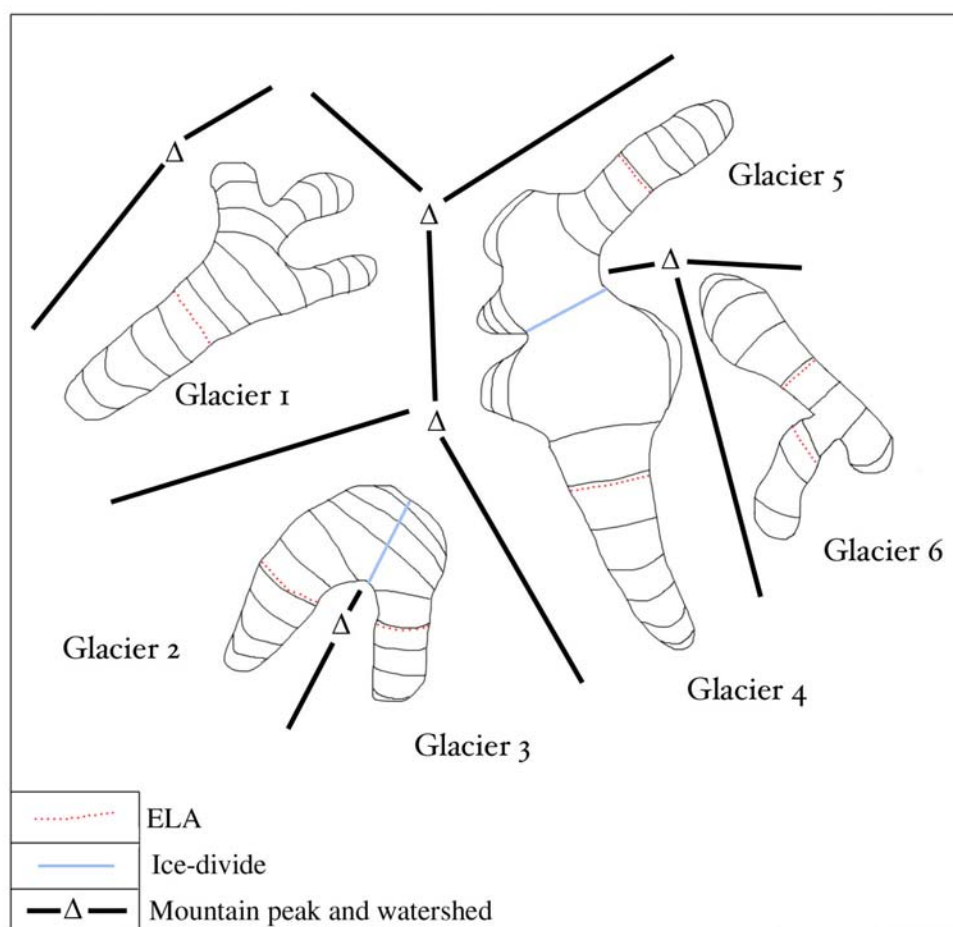


Figure 7.1 Hypothetical glacier reconstruction showing different shaped glaciers and ice-divides. Glacier 1 represents a valley glacier fed by multiple cirque glaciers. Glaciers 2 to 5 represent transection glaciers whereby ice-flow splits over drainage divides and sends branches into more than one valley (*cf.* Benn and Evans 1998). Glacier 6 illustrates two glaciers that coalesce below the ELA. In the latter situation, the ELA was derived separately for each glacier portion.

up-valley contributory area. For example, if one glacier had an upper area equal to that of a coalescing glacier, then the shared lower glacier was split into two equal portions.

7.1.5 Equilibrium Line Altitude (ELA)

The equilibrium line altitude (ELA) of a glacier is the altitude at which accumulation and ablation are equal. It is a critical concept in the understanding of glacier dynamics and there is a very close relationship between the ELA and local climate (Sutherland 1984, Ohmura *et al.* 1992, Benn and Lehmkuhl 2000). Several methods have been applied to calculate the ELA on former glaciers. Some of these are discussed below.

7.1.5.1 Maximum elevation of lateral moraines

The maximum altitude of lateral moraines provides an approximate estimate of the former ELA. This results from the flow of ice towards the glacier centre above the ELA and

towards the glacier margin below, resulting in lateral moraines only being deposited below the ELA (Andrews 1975). However, it is difficult to know whether or not a lateral moraine is preserved entirely in its upper part or whether moraine formation occurred immediately down-glacier of the ELA. Moreover, subsequent glacier retreat after reaching its maximum extent results in the incremental deposition of lateral moraines in an up-slope direction. The use of this method in deriving the former ELA is therefore limited and potentially rather inaccurate.

7.1.5.2 Toe-to-headwall altitude ratio (THAR)

This method is based on a set ratio between the maximum and minimum altitude of a glacier. Ratios of 0.35-0.4 normally provide the most reliable estimates of ELA (Meierding 1982). However, the technique is rather crude and takes no account of glacier hypsometry or climatic considerations.

7.1.5.3 Toe-to-summit altitude method (TSAM)

Former snowlines have been calculated by taking the average of the maximum height of the peaks around the cirque and the minimum height of each frontal moraine. This method, described by Louis (1955), is referred to as the Louis method by Benn and Lehmkuhl (2000). It has been used in the morphological studies of glacial features in Greece, Albania and Italy by Boenzi and Palmentola (1997). As with the THAR method, the TSAM is very crude and takes no account of glacier hypsometry. In the Alps, Gross *et al.* (1976) showed that this method overestimated ELAs by 100 m. However, in Tibet, Lehmkuhl (1998) has shown that calculated values are similar to the observed ELAs seen in aerial photographs and in the field. Benn and Lehmkuhl (2000) suggest that values for this method, as well as for the THAR method, should be determined empirically for each region. However, this is impossible in areas where glaciers no longer exist. For this reason, in this study alternative methods were sought for northwest Greece.

7.1.5.4 Area-weighted mean altitude

The area-weighted mean altitude method, also known as the Kurowski method, depends on weighting the area of each altitude contour band of the glacier surface by its altitude above or below the ELA. It was originally introduced by Kurowski (1891), neglected for over half a century and then rediscovered in the 1960s when it was applied by Osmaston (1965) working in East Africa and later by Sissons in Great Britain (Sissons 1974). This method employs the following equation:

$$ELA = \frac{\sum A_i \cdot h_i}{\sum A_i}$$

Where A_i are the areas between particular contour intervals and h_i are the corresponding mid-point altitudes for those contour intervals. This procedure is based on two assumptions: (a) during the glacial maxima the glacier was in equilibrium; and (b) both the accumulation and ablation gradients have a linear relationship with altitude. The first assumption is reasonable given that during maximum glacier extent, a glacier has neither positive nor negative mass balance. However, the second assumption is questionable and Sutherland (1984) noted that a linear mass balance curve is unlikely in practice. In order to establish the extent to which the assumption of a linear mass balance curve biases the results, Sutherland (1984) calculated the steady-state ELAs for 25 glaciers from a wide variety of climatic regimes using original mass balance data, allowing for the non-linearity of mass balance curves. These results were compared with the results gained using the area-weighted mean altitude method. A close relationship was found, although the calculated ELA values tended to overestimate the real ELA. This method has been applied to former cirque and valley glaciers and even small ice-caps in the British Isles (*e.g.* Sissons 1974, Ballantyne 1989, Hughes 2002) although it is thought to be most appropriate for small cirque glaciers with even area/altitude distributions (Rune 1996).

7.1.5.5 Accumulation area ratio

The accumulation area ratio (AAR) method applies a set value to the ratio of the accumulation area to the total glacier area. The ELA of a former glacier is determined by dividing the hypsometric curve appropriately using this ratio. For modern mid- and high-latitude glaciers, steady state AARs generally lie in the range 0.5-0.8 (Meier and Post 1962, Hawkins 1985), with typical values lying in the range 0.6 ± 0.05 (Porter 1975). However, glaciers with debris-covered ablation areas will have lower AARs than clean glaciers because of the effect of thick debris on lowering ablation, increasing the size of the ablation area required to balance accumulation (Müller 1980, Clark *et al.* 1994). In these circumstances, AAR values may be between 0.1 and 0.5 (Benn and Evans 1998).

A problem with both the accumulation area ratio and the area-weighted mean altitude methods is that they take little account of variations in glacier shape, particularly the distribution of glacier area over its altitudinal range, or hypsometry (Benn and Evans 1998, Nesje and Dahl 2000). For example, a glacier with a wide accumulation area and a narrow snout will have a different AAR to one where the snout is wide and the accumulation area is narrow, even if the ELA is the same (Furbish and Andrews 1984). Therefore, the use of a

standard AAR for determination of the ELA of former glaciers will be open to significant error if there was a wide range of glacier shapes.

7.1.5.6 Balance ratio

To overcome the problems with the AAR and area-weighted mean altitude method discussed above, Furbish and Andrews (1984) developed the balance ratio method (BR). This approach, also referred to as the accumulation area balance ratio method (AABR) (Osmaston 2002) and the accumulation balance ratio method (ABR) (Ballantyne 2002a), takes into account both glacier hypsometry and the shape of the mass balance curve. It is based on the fact that, for glaciers in equilibrium, the total annual accumulation above the ELA must balance the total annual ablation below. This can be expressed by the equation:

$$d_b A_b = d_c A_c$$

Where d_b is the average net annual ablation in the ablation area, d_c is the average net annual accumulation in the accumulation area, A_b is the area of the ablation area, and A_c is the area of the accumulation area.

Assuming that the ablation and accumulation gradients are linear, d_b and d_c are equal to ablation and accumulation at the area-weighted mean altitudes of the ablation area (z_b) and the accumulation area (z_c), respectively. These are effectively the elevations on the hypsometric curve associated with $1/2 A_b$ and $1/2 A_c$ (Benn and Evans 1998). For equilibrium conditions, the altitudes of z_b and z_c are determined by the balance ratio according to the relationship:

$$b_{nb}/b_{nc} = z_c A_c / z_b A_b$$

Where b_{nb} and b_{nc} are the mass balance gradients in the ablation and accumulation area respectively, and the ratio between these two gradients represents the balance ratio. The steady-state ELA is then defined as the altitude that satisfies the above equation for the balance ratio thought to be representative of the area under study. The ELA can be found by drawing the hypsometric curve for the former glacier and choosing trial values of the ELA. From these trial ELA values, the associated values of z_c , z_b , A_c and A_b can be measured, enabling the calculation of the balance ratio associated with these ELA positions. This can be done until a suitable balance ratio value is achieved (Benn and Evans

1998). If balance ratios are known, or can be assumed, then the ELA can be calculated using the balance ratio method using a spreadsheet provided in Benn and Gemmell (1997).

A major problem in using this method is obviously choosing a suitable balance ratio. For a rectangular slab-shaped glacier, $(b_{nb}/b_{nc}) = 1 / \text{AAR}$, so for an AAR of 0.6 the balance ratio is 1.67. For a sample of 22 glaciers in Alaska, Furbish and Andrews (1984) found that balance ratios averaged at about 1.8, with an overall value of 2 thought to be representative of maritime glaciers in general. This indicates that the vertical change in mass balance is twice as large in the ablation area than in the accumulation area. Furthermore, Ballantyne (2002a) applied a range of balance ratios for reconstructing former glaciers on the Isle of Mull in Scotland and found that there was little difference for reconstructions using balance ratios of 1.67 to 2, and a value of 1.8 was selected as the 'best' estimate of the former ELA.

However, an assumption of a balance ratio around 2 only holds when considering maritime mid-latitude glaciers. For example, the balance ratios of tropical glaciers are much higher, reaching values as high as 25, because of intense year-round ablation and very poor dependence of accumulation with altitude (Benn and Evans 1998). Neither a maritime mid-latitude nor a tropical analogy are suitable for the former glaciers of Greece. Finding a suitable balance ratio for former Pleistocene glaciers in Greece is therefore exceedingly difficult and prescribed values are always going to be questionable. The balance ratio, although probably the best and most sensitive measure of the former ELA, was also not used because of the difficulty in deriving balance ratios for former glaciers in Greece.

7.1.6 The method of ELA reconstruction applied here

Herein, a variation of the AAR method was applied. It was refined using the methods outlined by Osmaston (2002) for the Rwenzori Mountains of Uganda. This involves taking the altitudes corresponding to 11 evenly-spaced accumulation area ratios of between 0 and 1 (0, 0.1, 0.2, 0.3, 0.4, 0.5, 0.6, 0.7, 0.8, 0.9, 1.0). The standard deviation at each AAR for groups of glaciers was calculated and the AAR with the lowest standard deviation was chosen. The altitude of the snout area within a group of glaciers is likely to vary considerably depending on the hypsometry of the former glaciers. This is why moraine altitude is a poor comparative measure of glacier altitude. Glacier source areas will also vary, though to a lesser degree, and will be a function of the altitude of the mountain watershed - which is often controlled by tectonic and structural geology. As a result, groups of glaciers will tend to produce an asymmetrical U-shaped curve when standard deviation

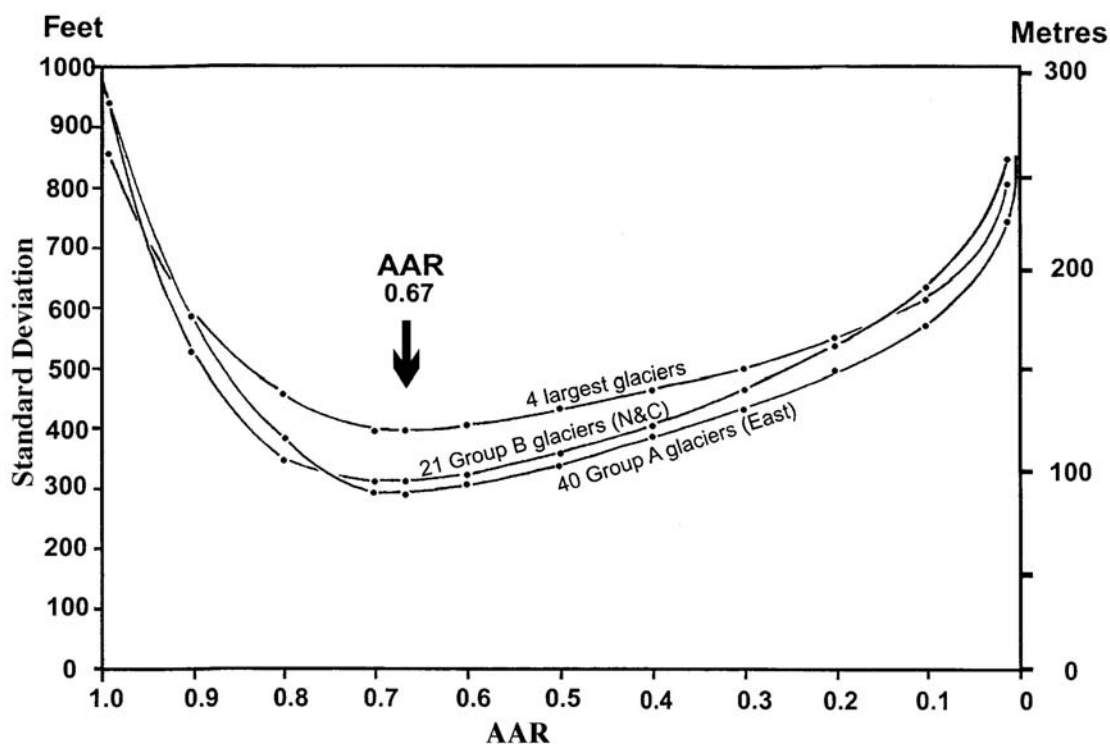


Figure 7.2 Graphical test for the accumulation area ratios (AAR) on three groups of reconstructed glaciers in the Rwenzori Mountains of Central Africa (Osmaston 2002). This technique can be applied on any reconstructed glaciers and was used here to derive suitable AAR values to determine former equilibrium line altitudes.

of altitude is plotted against AAR (Fig. 7.2). This method appears to be one of the best approaches to solving an old problem, especially in areas where former balance ratios are unknown (D. Benn, *personal communication*).

7.1.7 Testing the glacier reconstructions using glaciological theory

Once a glacier has been reconstructed, with information regarding the ELA and ice-depths (deduced from ice-surface contours) over the glacier known, then the basal shear stress at selected points within the glacier can be calculated using:

$$\tau = \rho g h \sin \alpha$$

where τ is the shear stress (kPa), ρ is the density of ice (900 kg m^{-3}), g is the acceleration due to gravity (9.81 m s^{-2}), h is the thickness of the glacier (m) and α is the surface slope of the glacier in degrees.

W	F
1	0.45
2	0.65
3	0.75
4	0.81
6	0.87
8	0.9
16	0.95
∞	1.00

Table 7.1 Shape factor (F) for parabolic valley profiles derived from the ratio between the half width of the glacier to its maximum thickness (W) (after Nye 1965).

A shape factor **F** modifies the equation for basal shear stress when glacier flow is affected by drag against valley walls (Nye 1965):

$$\tau = F\rho gh \sin\alpha$$

This shape factor depends primarily on **W**, the ratio between the half width of the glacier to its maximum thickness, and to a lesser extent on the shape of the valley cross section. Glaciated valleys usually have a roughly parabolic cross section and the shape factor (F) for parabolic valley profiles is given in Table 7.1. Basal shear stress measurements were calculated at regularly-spaced intervals based on glacier thickness and surface slope reconstructions along the centre line of the former glaciers, in both the accumulation and ablation zones.

Empirical observations suggest that the vast majority of modern glaciers, flowing over deformable substrates, have basal shear stresses between 50 and 150 kpa (Paterson 1981, Bennett and Glasser 1996). The reasons for this narrow range of basal shear stress is because at low shear stresses (< 50 kpa), glacier movement would virtually cease until accumulation of more ice increased thickness or slope, or both, and these in turn increased the basal shear stress. At high shear stresses (> 150 kpa), which would be brought about if glacier ice became too thick or steep, the basal ice could be deformed so easily that the glacier would move very rapidly until its thickness or slope were reduced. Glaciers therefore maintain an equilibrium stress between 50 and 150 kpa.

High values of shear stress tend to occur in areas which are likely to have experienced extending flow, while lower values are typical of areas of compressive or

decelerating flow. Analysis of theoretical basal shear stress values over the reconstructed glaciers should show a pattern of high values in the accumulation zone, reaching a maximum around the ELA, and lower values in the ablation zone. Such theoretical analysis of extending and compressive flow areas should be supported by field evidence, *i.e.* erosional evidence in extending zones and faulted sedimentary structures in compressive zones (Bennett and Glasser 1996).

All glacier reconstructions were adjusted to form glaciers with realistic slope and depth relationships. However, in the case of the oldest glaciers this was not always straightforward since the landscape is likely to have been much altered (see below). This was a particular problem for reconstructing accurate glacier depths. Therefore, this approach to test glacier reconstructions was applied more rigorously on younger glaciers, particularly those of the Vlasian and Tymphian Stages (Chapter Six).

7.1.8 Problems and limitations in glacier reconstruction

Paraglacial processes including talus accumulation, debris flows and mass failure of valley sides (Church and Ryder 1972, Ballantyne 2002b) as well as post-glacial erosion all act to disguise evidence of glaciation in the geomorphological record. This problem becomes more acute the older the glaciation. Where attempts are made to reconstruct the oldest glaciers, which perhaps date from the Middle Pleistocene, it must be realised that reconstructions are subject to significant error. In some instances, glacier-surface contours may not link up precisely with modern land surface contours, especially where depositional landforms resulting from later glaciations and later fluvial incision obscure the former valley shape at the small to medium scale. However, given that the oldest preserved glacial landforms were formed by the largest glaciers, errors in reconstructing ELAs are often smoothed by the large surface area.

A further problem is that of tectonic uplift and sea-level change. Reconstructed ELAs will be relative to modern sea level. It is well established that the mountains of Epirus have been undergoing uplift throughout the Quaternary. However, during glacial periods glacioeustatic global sea-level lowering is to be expected. Correcting for uplift and sea-level change is very difficult. However, since uplift in Epirus is estimated at *ca.* 40 - 80 m per 100,000 years (King and Bailey 1985), then tentative corrections can be made for uplift. Sea-levels, on the other hand, would have been variable depending on the glaciation under consideration. At the height of the last glaciation, during the Tymphian Stage (MIS 2), sea-levels are known to have been *ca.* 120 m lower around Greece (Lambeck 1995), with some estimates ranging to 165 m (van Andel and Shackleton 1982). In fact, the whole

northern section of the Adriatic Sea would have been land *ca.* 20,000 years ago. Lower eustatic sea-levels during glacial stages implies that ELAs would have been higher than those reconstructed using modern sea-levels. This is counter to the effects of uplift which result in real ELAs being lower than those reconstructed in the modern environment.

During the most severe phase of climate during the Tymphian Stage, indicated in the pollen record at *ca.* 22-20,000 ¹⁴C years BP (Galanidou *et al.* 2000), sea-levels 120 m lower than today and uplift at rates of 40 - 80 m per 100,000 years suggest that reconstructed ELAs will underestimate the 'real' ELA by 104 - 112 m. Therefore, tentatively, a reconstructed ELA of 1500 m corresponds with a 'real' ELA of 1604 - 1612 m for the height of the last glaciation. Adjustments for older glaciations are likely to be even more tentative, since rates of uplift and sea-level lowering are likely to have varied through time. Nevertheless, applying a minimum glacioeustatic sea-level depression of 120 m and uplift rates of 40 - 80 m per 100,000 years enables the application of approximate correction factors.

For the Vlasian Stage (Table 6.14), reconstructed ELAs will underestimate the real ELA by 8 - 64 m if the maximum glaciation occurred at *ca.* 140,000. Beyond 300,000 years BP, uplift outstrips a minimum sea level depression of 120 m and therefore reconstructed ELAs are likely to be overestimated rather than underestimated. For example, during the Skamnellian Stage (*ca.* 450,000 years BP, Chapter Six - Table 6.14) reconstructed ELAs may be 60 - 240 m greater than the 'real' ELAs. However, given that global ice volumes were greater during MIS 12 than during any subsequent glacial stage, then it is possible that the figure is less than this because of lower glacioeustatic sea levels. The corrections for uplift and sea level change suggested here are very rough estimates. Nevertheless, they illustrate the major differences which potentially exist between reconstructed ELAs and 'real' ELAs during the different glacial events. This is not attempted in the palaeoclimatic reconstructions outlined in Chapter Eight. There, temperature reconstructions for different glacial stages reflect those at fixed points and are independent of sea-level change.

7.2 Skamnellian Stage glaciers

The most extensive glacial deposits are older than 350,000 years BP and formed during the Skamnellian Stage (Chapter Six, Table 6.14). The glacial deposits belonging to this glacial stage occur in nearly all valleys of Mount Tymphi, Mount Smolikas and Mount Vasilitsa. However, the limits of the former glaciers are more difficult to define than for more recent glacier phases because the deposits do not always have a morphological expression. In addition, later landscape modification has probably been considerable in places, especially

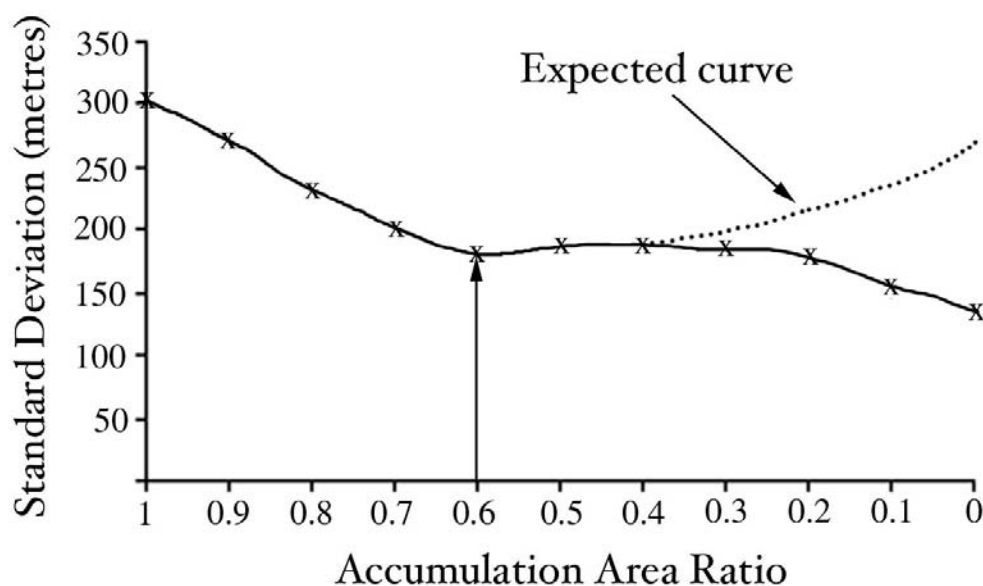


Figure 7.3 Standard deviation of the glacier surface altitudes at varying accumulation area ratios. An AAR of 0.6 would seem to represent the most suitable value for ELAs during glaciation of the Skamnellian Stage (see text for details).

since in many areas at least two subsequent glacial advances have occurred up-valley. Estimates of glacier depth are probably the parameter most prone to error as a consequence of erosion, and in some places, deposition. For this reason glacier reconstructions were not tested by reconstructing glaciological parameters, such as basal shear stress, since they often depend on determining ice depth.

In total, 19 glaciers covering a total area of 72.6 km² were reconstructed on the three mountains. Figure 7.3 shows the altitudinal variation, at AAR 0 to 1 for all 19 of the former glaciers during the Skamnellian Stage. An AAR of 1 will always be situated at the snout of a former glacier and an AAR of 0 always at the highest part. Therefore, Figure 7.3 shows that the glaciers during the Skamnellian had most altitudinal variation in the snout area and least variation in their uppermost parts. High variation in the altitude of the snout area is to be expected. However, the shape of the curve, with lowest variation in the upper parts, is contrary to the theoretical model of Osmaston (2002) where an asymmetrical U-shaped curve, with lowest variation in the highest parts, is expected when plotting altitude against AAR (Fig 7.2). The low standard deviation in the altitude of the upper parts of the former glaciers partly results from the fact that many individual glaciers were sourced from portions of an accumulation area on the same drainage divide. In fact, 10 out of the 19 glaciers have accumulation areas separated by ice divides, not topographic divides, and can therefore be defined as transection glaciers. This is a key limitation of the method and

suggests that it is best applied on cirque and valley glaciers such as the hypothetical glacier 1 in Figure 7.1 rather than transection glaciers. However, where a significant number of transection glaciers with adjacent accumulation areas separated by ice divides exist (such as the hypothetical glaciers 2 - 5 in Figure 7.1), the problem can be circumvented by choosing the AAR corresponding with the lowest standard deviation before the fall in variation at low AAR values. In the case of the Skamnelliian Stage glaciers, this corresponds to an AAR of 0.6 which lies within the 0.5 - 0.8 AAR range found on modern mid- and high- altitude glaciers (Meier and Post 1962, Hawkins 1985).

7.2.1 Mount Tymphi

On Mount Tymphi, ice covered nearly 60 km². Ice fields existed in many areas, often supplying numerous outlet glaciers. The ELA of the Skamnelliian Stage glaciers, derived using an AAR of 0.6 are shown in Table 7.2, as are the former glacier areas.

The glaciers were divided into four groups on the basis of location. The mean ELA from each glacier group was used to derive an overall mean ELA. This was preferable to taking all glaciers individually and deriving an overall mean because numerous glaciers within a group of glaciers, significantly lower or higher than other glaciers in other areas,

<i>Glacier</i>	<i>Group</i>	<i>Area (km²)</i>	<i>ELA (m a.s.l.)</i>	<i>Group mean ELA (metres a.s.l.)</i>
Amarandos	A	0.94	1670	1863
Mighia		1.80	1970	
Stani Katsanou		2.99	1950	
Neraidhovrisi		?	?	
Maghoula	B	4.59	1285	1410
Kriopotamos		2.64	1535	
Skamnelli	C	8.33	1720	1765
Tsioumako		2.98	1760	
Stani Grava		1.48	1780	
Tsepelovo		9.04	1800	
South Plateau	D	12.03	1990	1928
North Plateau		7.48	1940	
Ghaidhouro		0.79	1840	
Astraka Laccos Radenas		2.09	1890	
Astraka Spirokapa West		1.10	1960	
Astraka Spirokapa East		0.96	1950	
Total area (km²):		59.24	overall group mean ELA:	1741

Table 7.2 Areas and equilibrium line altitudes of the 16 glaciers of the Skamnelliian Stage.

will tend to distort the overall ELA giving a false impression of the spatial mean. This is especially so for later glaciations, where numerous smaller glaciers may have occurred in a valley previously occupied by one larger glacier, thereby having greater influence on the overall mean. Therefore, by grouping the glaciers, a much more representative spatial and temporal comparison of overall mean ELA values can be achieved.

Using the method described above, the mean reconstructed ELA of the four groups of former Skamnelliian Stage glaciers was 1741 m a.s.l. Adjusted for sea-level depression and uplift the 'real' ELA was *ca.* 1591 m a.s.l., *i.e.* approximately 150 m lower than the present altitude of the preserved glacial features (section 7.1.8). All ELAs in the following discussion represent reconstructed (*i.e.* above modern sea level) rather than 'real' ELAs, unless otherwise stated. The individual reconstructed ELAs ranged from 1285 m to 1990 m a.s.l. The characteristics of the glaciers within each glacier group are discussed below.

7.2.1.1 Group A glaciers

The glaciers of this group are situated on the northern slopes of Mount Tymphi which drain into the Aoos valley (Fig. 7.4). In total, four glaciers existed, the Stani Katsanou, Mighia, Amarandos and Neraidhovrisi glaciers, with a mean ELA of 1863 m a.s.l. This mean does not include the Neraidhovrisi glacier which was not reconstructed because of difficulties in delimiting the former extent of this glacier (Chapter Four, section 4.5).

The glaciers of Stani Katsanou and Mighia were sourced in the northern cirques of Tsouka Rossa, Kopanes and Karteros. The two glaciers joined over the drainage divide of the Kopanes and Karteros cirques and can therefore be defined as transection glaciers. The Stani Katsanou glacier, the more easterly of the two, covered an area of 2.99 km² and had an ELA of 1950 m a.s.l. The ice surface would have been particularly steep at the lip of Karteros cirque and it is likely that an ice-fall would have existed here. The Mighia glacier covered an area of 1.80 km² and had an ELA of 1970 m a.s.l., similar to that of the Stani Katsanou glacier. This glacier would also have been very steep in places, such as at the lip of the Kopanes cirque, and it is likely that an ice-fall occurred here.

To the east of the Mighia and Stani Katsanou glaciers, the Amarandos glacier existed on the northern slope of Gamila. This glacier was a simple valley glacier, covering an area of 0.94 km² with an ELA of 1670 m a.s.l.

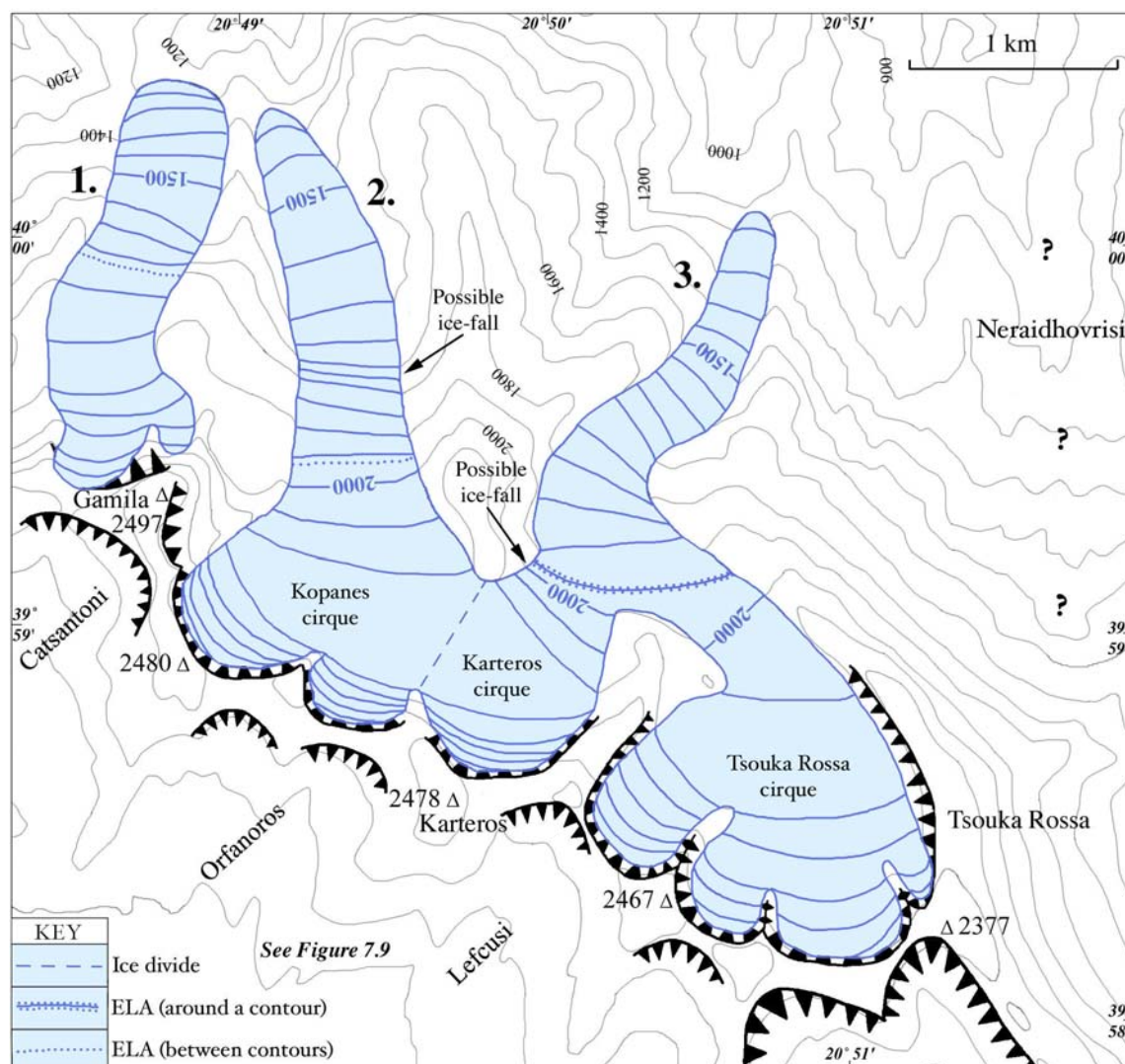


Figure 7.4 The Group A glaciers of Mount Tymphi during the Skamnellian Stage. 1: Amarandos glacier. 2: Mighia glacier. 3: Stani Katsanou glacier. The Neraidhovrisi glacier is not reconstructed due to difficulties in defining the former glacier limits. Glaciers are contoured at 50 m intervals (land contours at 100 m intervals). The key to the base map is the same for the geomorphological maps (Fig. 3.4).

7.2.1.2 Group B glaciers

This group of glaciers occurred on the northeastern slopes of Mount Tymphi at the foot of the cliffs of Goura (2466 m a.s.l.). Two glaciers were present, the Maghoula and Kriopotamos glaciers, with a mean ELA of 1410 m a.s.l. (Fig. 7.5).

The Kriopotamos glacier was sourced in the Plaghia, Laccos and Dimitrios cirques and would have coalesced to form a single glacier in the Kriopotamos valley. The glacier covered an area of *ca.* 2.64 km² and had an ELA of 1535 m a.s.l.

The Maghoula glacier was situated in the neighbouring valley to the north. This was an extensive valley glacier which filled the Maghoula valley and extended *ca.* 5.6 km from source to snout, to beyond the modern position of Vrisochori village. It had an ELA of 1285 m a.s.l. and covered an area of 4.59 km².

7.2.1.3 Group C Glaciers

The glaciers of this group occupied the south-facing southern slopes of Mount Tymphi draining into the upper Voidomatis basin near Tsepelovo and Skamnelli (Fig. 7.6, 7.7, 7.8). In total, four glaciers occurred here, the Stani Grava, Tsepelovo, Skamnelli and Tsioumako glaciers with a group ELA mean of 1765 m a.s.l.

The Stani Grava glacier was the smallest and most westerly of the Group C glaciers. It covered an area of 1.48 km² and had an ELA of 1780 m a.s.l.

Further east, near Tsepelovo and Skamnelli, valley glaciers descended to *ca.* 850 m a.s.l. These glaciers were sourced in the high southern cirques of Laccos Tselon, Laccos Megalon Litharion and in the Vrichos and Tsioumako cirques to the east. In the Laccos Megalon Litharion area, ice would have spilled over the drainage divide and flowed down towards Tsepelovo and Skamnelli either side of the mountain known as Vlasi.

The Tsepelovo glacier covered an area of 9.04 km² with an ELA of 1800 m a.s.l., and was by far the longest glacier on Mount Tymphi extending *ca.* 12.3 km from source to snout. The geomorphological evidence suggests that an off-shoot, or distributary glacier occurred in the lower parts of this glacier (Fig. 7.6). Since the ice-divide between the main Tsepelovo glacier and the distributary glacier occurred in the lower ablation area, it is difficult to separate contributing accumulation areas. For this reason, the glaciers were considered as one when reconstructing the former ELA.

The Skamnelli glacier originated in both the Laccos Megalon Litharion and Vrichos areas and flowed down into the Vourtapa and Vrichos valleys, respectively. Glaciers in these valleys, either side of the Tsoukoula ridge, would have coalesced to form a single valley glacier which extended into the Kato Radza valley beyond Skamnelli. The area of this glacier was 8.33 km² with a reconstructed ELA of 1720 m a.s.l., and a length from source to snout of *ca.* 7.3 km.

A further glacier, with its snout in the lower Tsioumako valley, had an area of 2.98 km² and an ELA of 1760 m a.s.l. The Tsioumako, Skamnelli and Tsepelovo glaciers were connected across drainage divides and they therefore represent a series of transection glaciers. In addition, ice in the Vrichos and Tsioumako valleys would have been separated by a small hillock that would have protruded above the ice as a minor nunatak (Fig. 7.7).

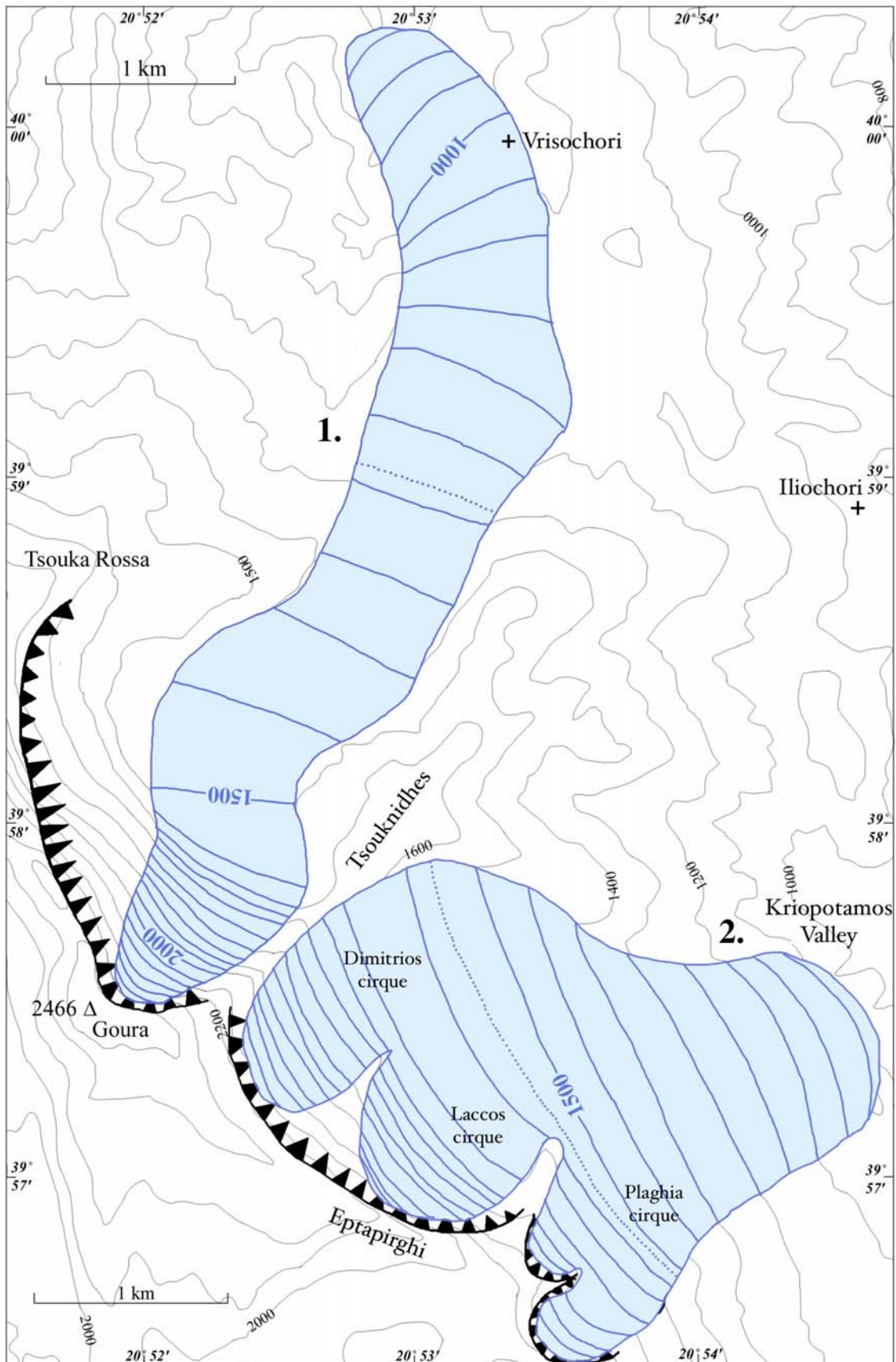


Figure 7.5 The Group B glaciers of Mount Tymphi during the Skamnellian Stage. 1: Maghoula glacier. 2: Kriopotamos glacier. Glaciers are contoured at 50 m intervals (land contours at 100 m

intervals). The key to the map is provided in Fig. 7.4 and symbols used in the basemap are the same for the geomorphological maps (Fig. 3.4).

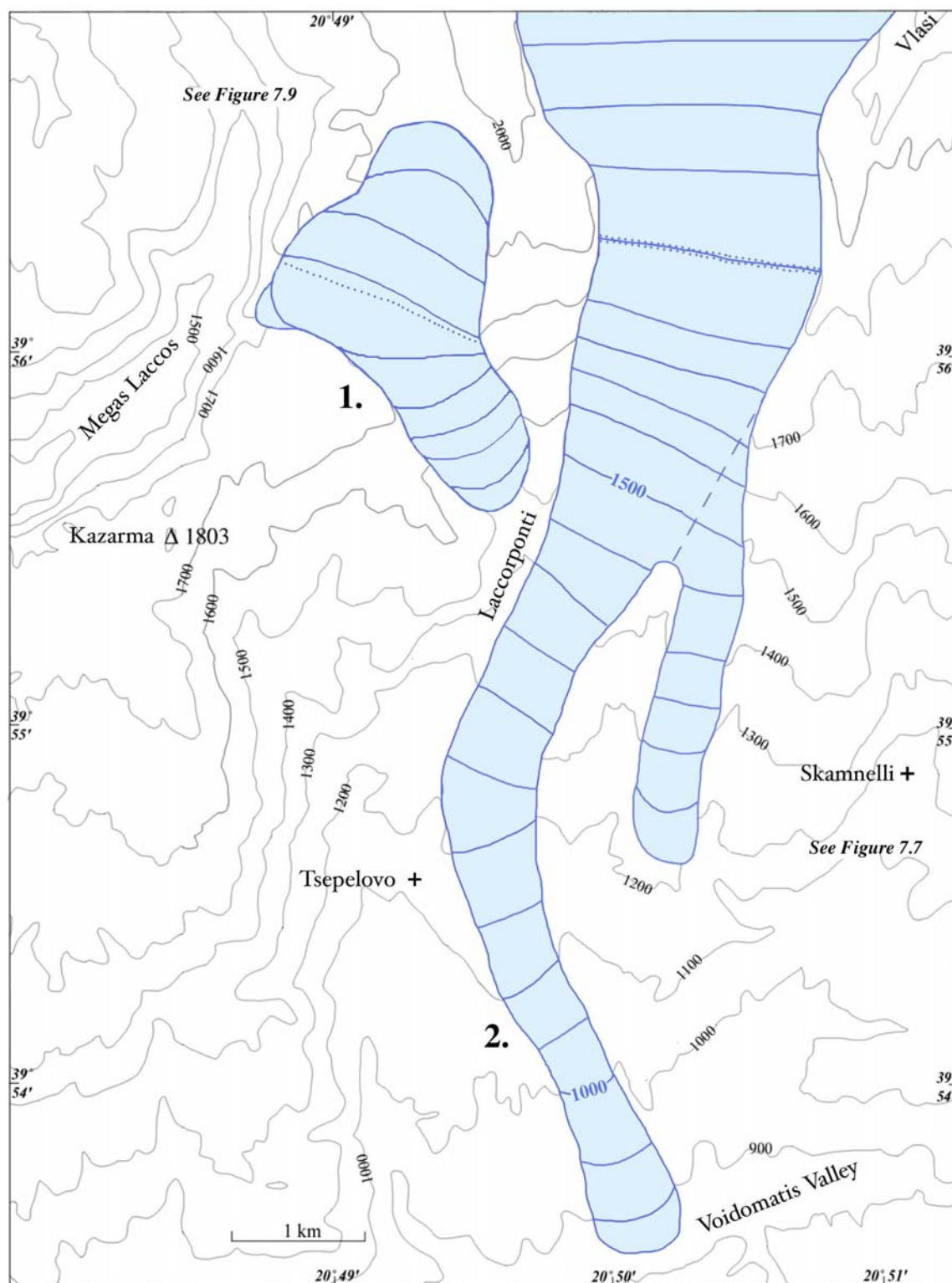


Figure 7.6 The Stani Grava (1.) and Tsepelovo (2.) glaciers of Mount Tymphi during the Skamnellian Stage. These glaciers represent some of the Group C glaciers. Glaciers are contoured at 50 m intervals (land contours at 100 m intervals). The key to the map is provided in Fig. 7.4 and symbols used in the base map are the same for the geomorphological maps (Fig. 3.4).

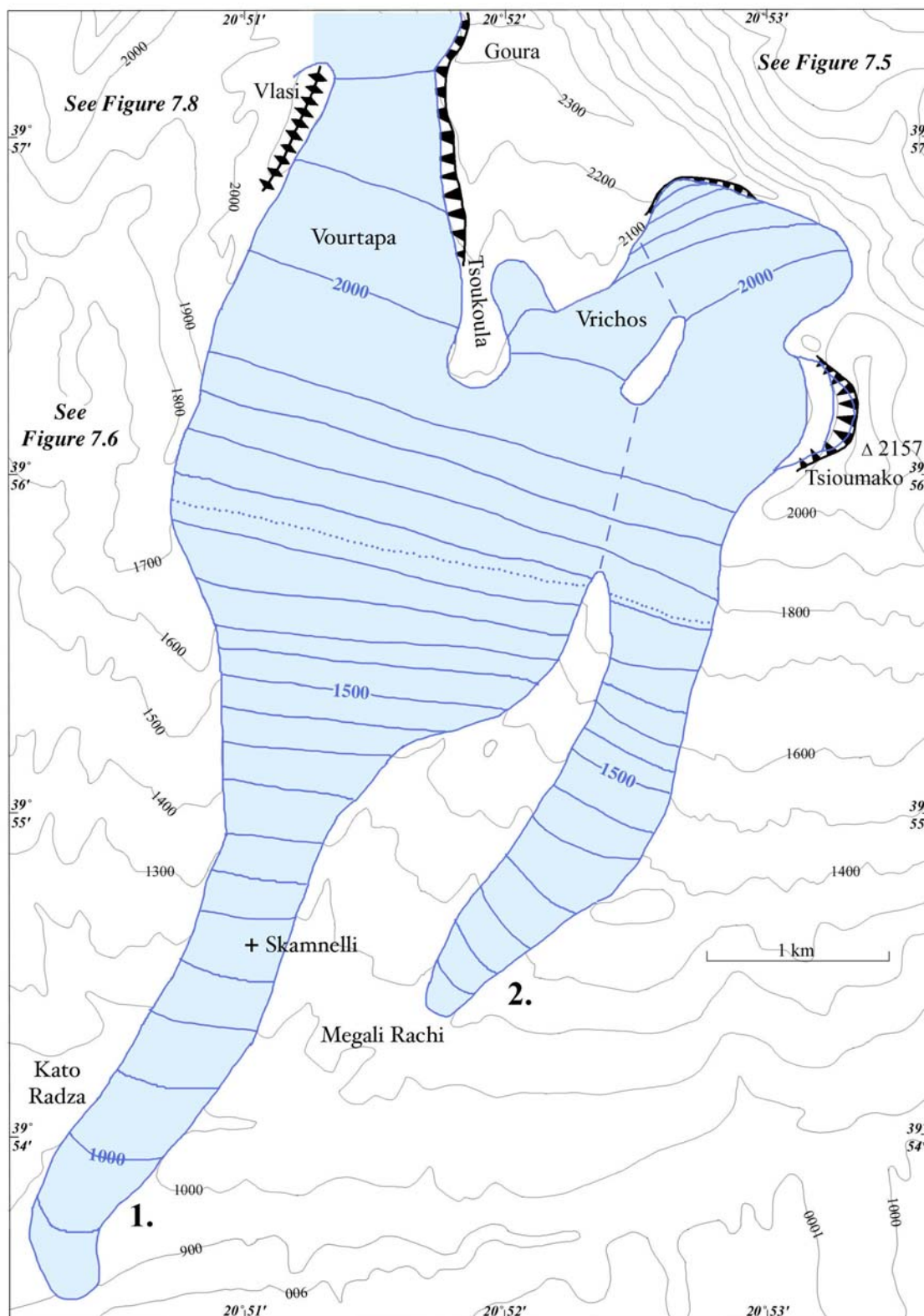


Figure 7.7 The Skamnelli (1.) and Tsioumako (2.) glaciers of Mount Tymphi during the Skamnellian Stage. These glaciers represent part of the Group C glaciers. Glaciers are contoured at 50 m intervals (land contours at 100 m intervals). The key to the map is provided in Fig. 7.4 and symbols used in the base map are the same for the geomorphological maps (Fig. 3.4).

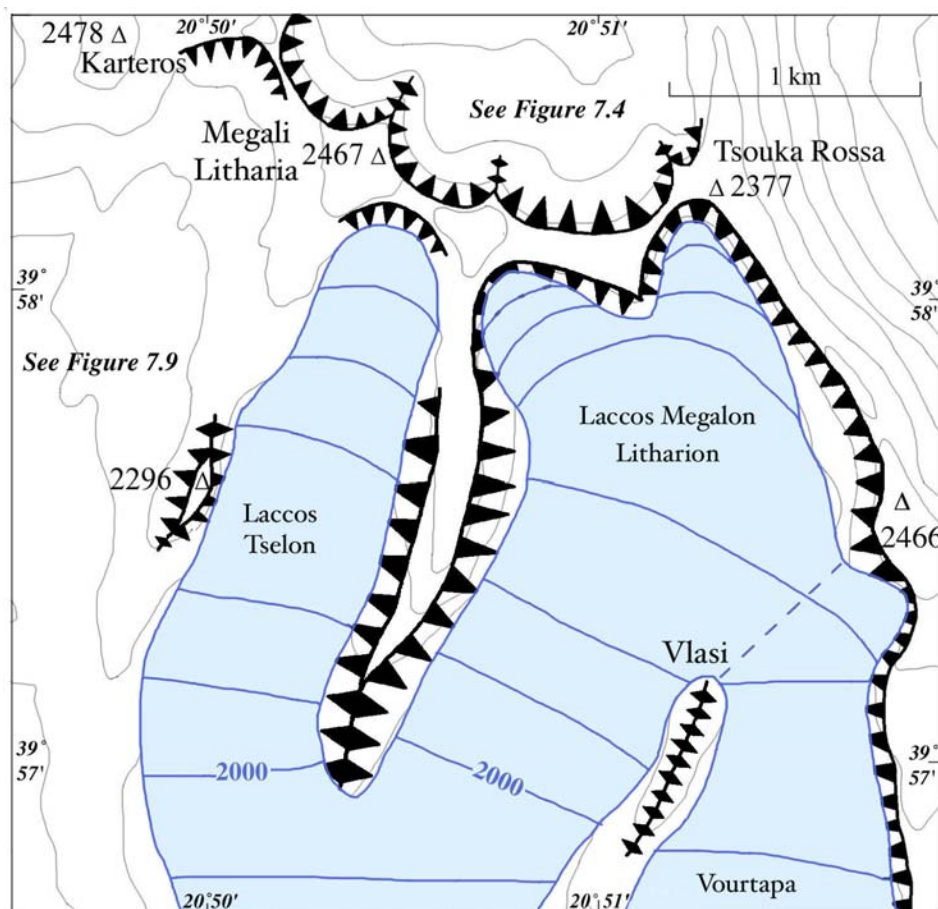


Figure 7.8 The source areas of the Tsepelovo and Skamnelli glaciers in the Laccos Tselon and Megalon Litharion cirques during the Skamnelliian Stage. Glaciers are contoured at 50 m intervals (land contours at 100 m intervals). The key to the map is provided in Fig. 7.4 and symbols used in the base map are the same for the geomorphological maps and a key is provided in Figure 3.4.

7.2.1.4 Group D glaciers

The glaciers of this group originated on the gently sloping plateau surfaces on the south side of Astraka (2436 m a.s.l.) and on the plateau between this peak and the main ridge of Tymphi, which reaches its highest point at Gamila (2497 m a.s.l.). Six glaciers have been reconstructed here: the South plateau, North plateau, Ghaidohouro, Astraka Laccos Radenas, Astraka Spirokapa West and Astraka Spirokapa East glaciers (Fig. 7.9 and 7.10). Their mean ELA was 1928 m a.s.l.

A large ice-field developed on the plateau between the peaks of Astraka (2436 m a.s.l.) and Gamila (2497 m a.s.l.) with a surface area of *ca.* 19.5 km². The ice-field centre was situated near the lake of Loutsa Robozi, with outlet glaciers descending to the north and south into the Aaos and Voidomatis basins, respectively. The north plateau glacier had a lower ELA (1940 m a.s.l.) than the south plateau glacier (1990 m a.s.l.). Maximum ice depths reached just over 200 metres at the ELA of the south glacier and 150 m around the area of the ELA on the north glacier. Greater glacier depths near the ELA are to be

expected because of the greatest glacier discharge at this position (Benn and Evans 1998). However, reconstructed depths can only be viewed as approximate since precise depths of the former glaciers are difficult to determine because of later landscape modification.

In the Ghaidhouro area, a small glacier existed separate from the main plateau ice in a hollow above the northern cliffs of the Megas Laccos gorge (Fig. 7.9). It covered an area of only 0.79 km², and was less than 50 m thick. The ELA of this glacier was *ca.* 1840 m a.s.l.

West of the main plateau ice field and south of Astraka (2436 m a.s.l.), a large transection glacier covering an area of 4.15 km² was sourced in the vicinity of Chalavra (Fig. 7.10). Three outlet glaciers dispersed from this ice-covered drainage divide; one into the Laccos Radenas valley and two into valleys either side of the Spirokapa hill that drained into the Vikos and Megas Laccos gorges. The ELAs of these three outlet glaciers were 1890, 1960, 1950 m a.s.l., respectively

A problem with the glaciers in this area, as well as others on Mount Tymphi, is that the glaciers often had asymmetric area-to-altitude distributions. This was especially so with the plateau ice-field and the largest transection glaciers. Meier and Post (1962) cautioned that glaciers with asymmetric area-to-altitude distributions may have AARs which differ greatly from simple valley glaciers. Therefore, whilst an AAR of 0.6, used here to derive the ELA for all glaciers, is within the range noted for modern mid- and high-altitude glaciers of 0.55-0.65 (Porter 1975) and 0.5-0.8 (Meier and Post 1962, Hawkins 1985), there may be some discrepancy between glaciers. This problem is difficult to resolve given the wide variety of glacier shapes on Mount Tymphi during the Skamnellian Stage. Nevertheless, an AAR value of 0.6 overall would seem likely to produce a representative mean given the lowest variance observed in reconstructed ELAs using this value (Figure 7.3).

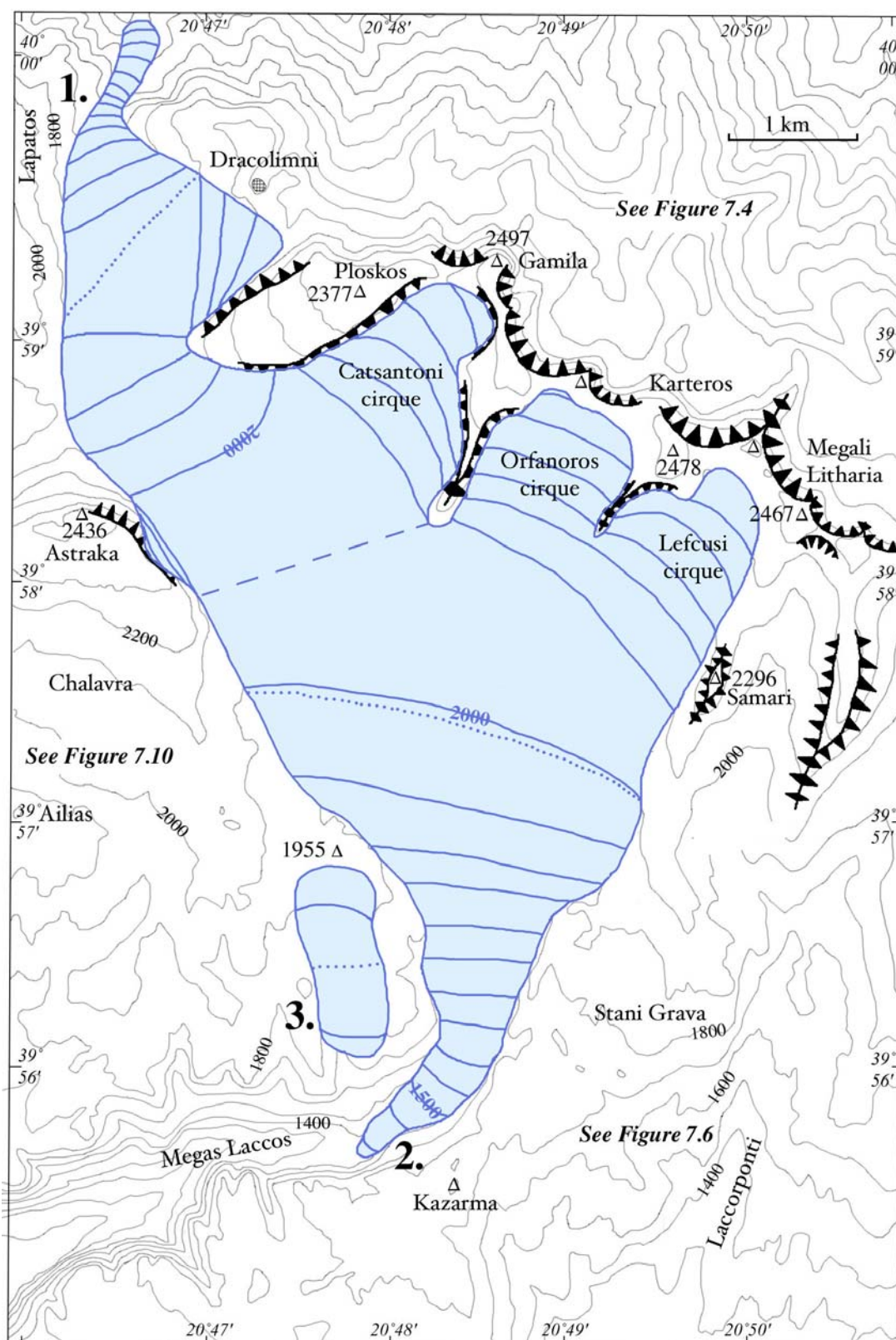


Figure 7.9 The easternmost Group D glaciers of Mount Tymphi during the Skamnellian Stage. 1: North Plateau glacier. 2: South Plateau glacier. 3: Ghaidouro glacier. Glaciers are contoured at 50 m intervals (land contours at 100 m intervals). The key to the map is provided in Fig. 7.4 and symbols used in the base map are the same for the geomorphological maps (Fig 3.4).

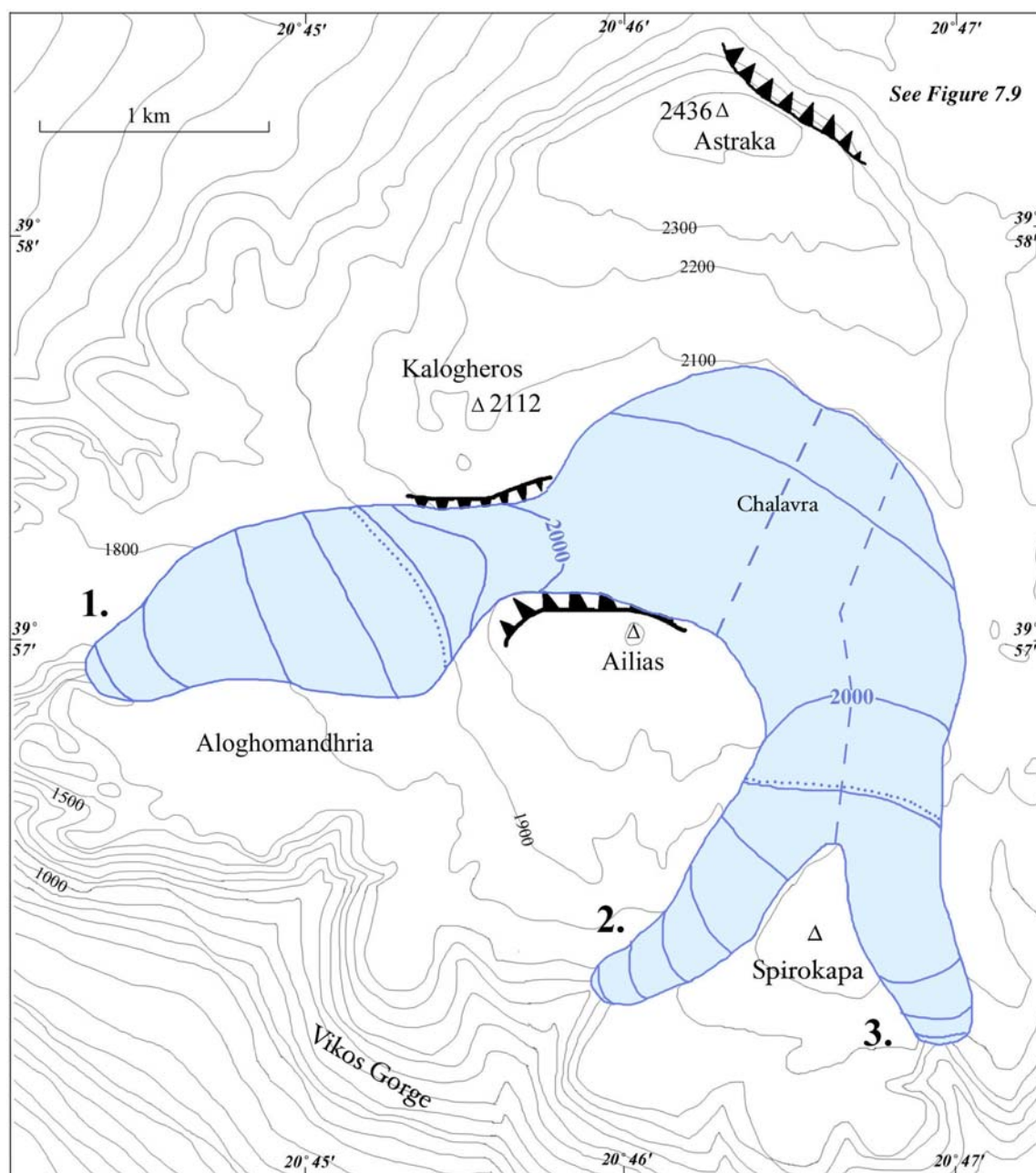


Figure 7.10 The westernmost Group D glaciers of Mount Tymphi during the Skamnellian Stage. 1: Laccos Radenas. 2: Spirokapa West glacier. 3: Spirokapa East glacier. Glaciers are contoured at 50 m intervals (land contours at 100 m intervals). The key to the map is provided in Fig. 7.4 and symbols used in the base map are the same for the geomorphological maps (Fig. 3.4).

7.2.2 Mount Smolikas

Ice covered an area of at least 8 km² on Mount Smolikas during the Skamnellian Stage. The glaciers were not grouped because of the limited number but are considered individually (Table 7.3). The mean ELA of the Smolikas glaciers was 1680 m a.s.l. - about 60 m lower than the overall mean of 1741 m a.s.l. for the glacier groups on Mount Tymphi. Whilst the mean ELA on Mount Smolikas was *ca.* 60 m lower than on Mount Tymphi, the coverage of ice was much less extensive. However, total glacier area is underestimated because of the difficulties in establishing former glacier limits in the Konkutino valley, although this is likely to contribute no more than *ca.* 5 km². The relatively limited ice cover on Mount Smolikas is surprising given that the mountain is 140 m higher than Mount Tymphi. Possible reasons for this difference are explored in the next chapter.

The largest glacier on Mount Smolikas was that in the Vadulakkos valley which covered 7.32 km². This valley glacier was north-facing, *ca.* 7 km long and fed by cirque glaciers on the northern side of the main Smolikas summit ridge (Fig 7.11). Ice would have been channelled from these cirques down the Vadulakkos valley, which is less than a kilometre wide at *ca.* 1400-1500 m a.s.l. The glacier would have narrowed at this point, before broadening into a piedmont-style glacier where the Vadulakkos valley merges with the Ellenikos valley 2 km east of Aghia Paraskevi village. A small glacier also existed near Samarina. The latter glacier covered an area of only 0.74 km² and had an ELA of 1660 m a.s.l. (Fig. 7.12).

It is likely that valley glaciers also developed on the eastern slopes of Mount Smolikas, in the Konkutino valley. Here, they would have been fed by cirque glaciers in the northeast cirques of the subsidiary peak Moasa (2610 m a.s.l.) and in the southern cirque of Bogdoni (2238 m a.s.l.). However, the lowest moraines of this valley are at an altitude corresponding to those of the mid-valley glaciation found elsewhere, and it is likely that much of the evidence for glaciation in the lower part of this valley has been eroded and reworked (Chapter Five, section 5.3).

<i>Glacier</i>	<i>Area (km²)</i>	<i>ELA (metres a.s.l.)</i>
Vadulakkos	7.32	1700
Samarina	0.74	1660
Konkutino	?	?
Total area/ mean ELA	8.06	1680

Table 7.3 The glacier characteristics during the Skamnellian Stage on Mount Smolikas.

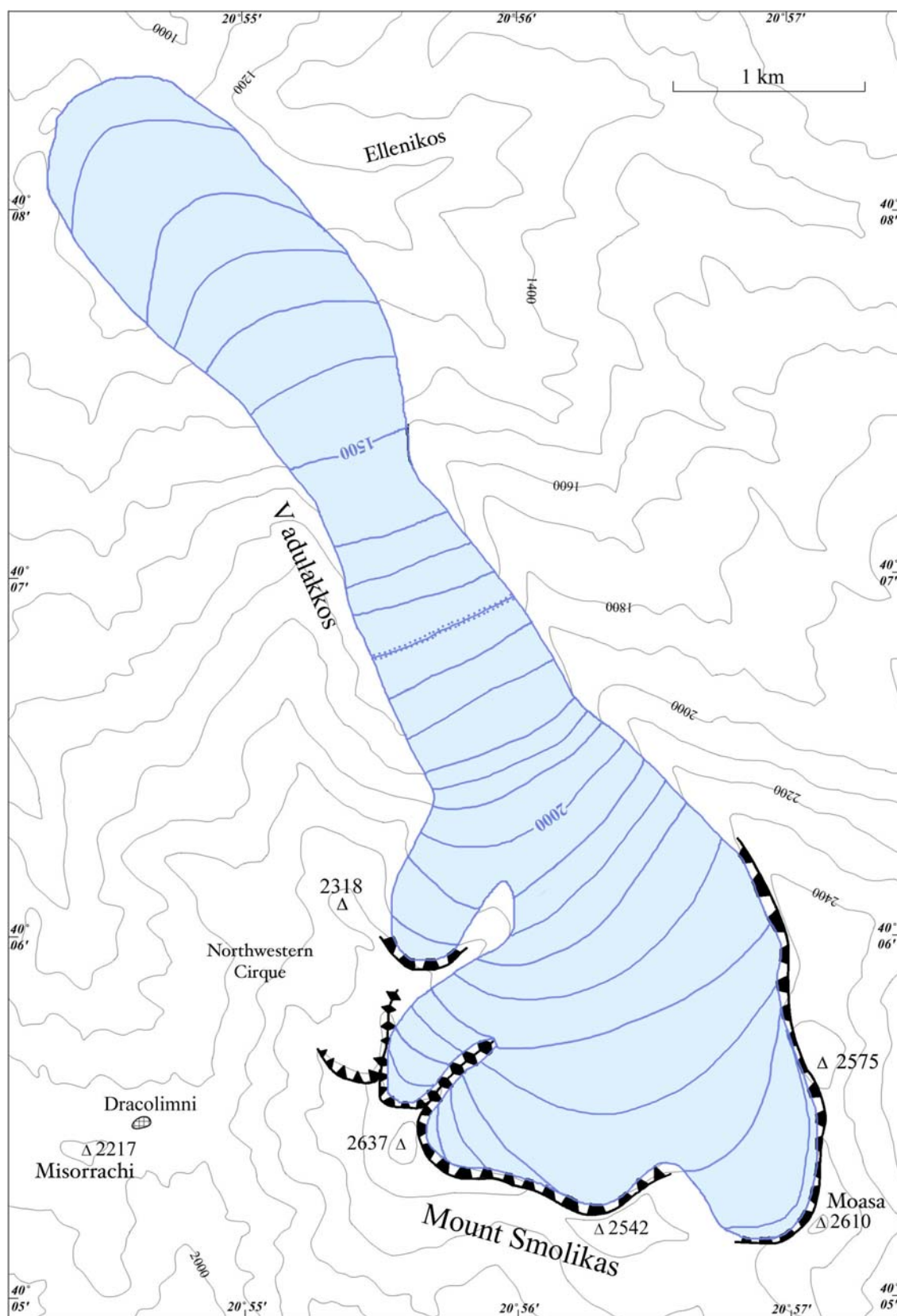


Figure 7.11 The Vadulakkos glacier of Mount Smolikas during the Skamnellian Stage. Glaciers are contoured at 50 m intervals (land contours at 100 m intervals). The key to the map is provided in Fig. 7.4 and symbols used in the base map are the same for the geomorphological maps (Fig 3.4).

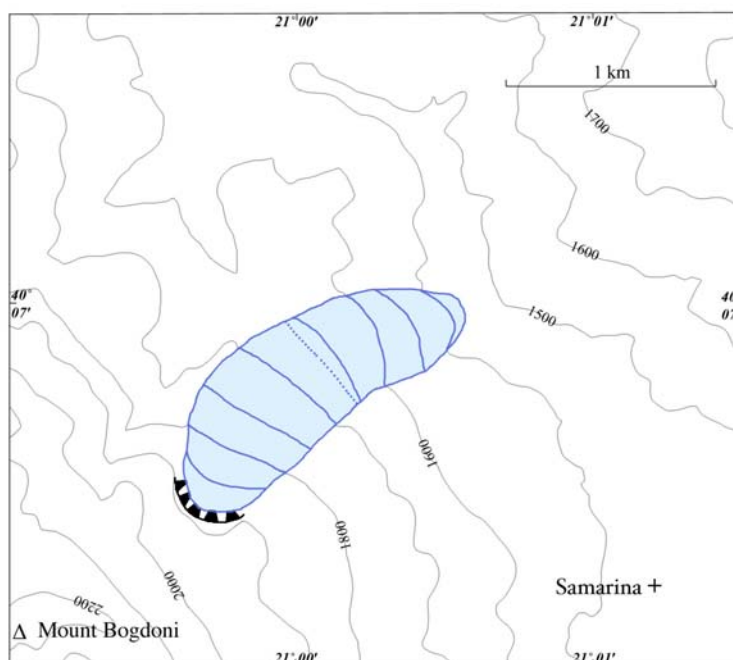


Figure 7.12 The Samarina glacier of Mount Smolikas during the Skamnelliian Stage. The glaciers is contoured at 50 m intervals (land contours at 100 m intervals). The key to the map is provided in Fig. 7.4 and symbols used in the base map are the same for the geomorphological maps (Fig. 3.4).

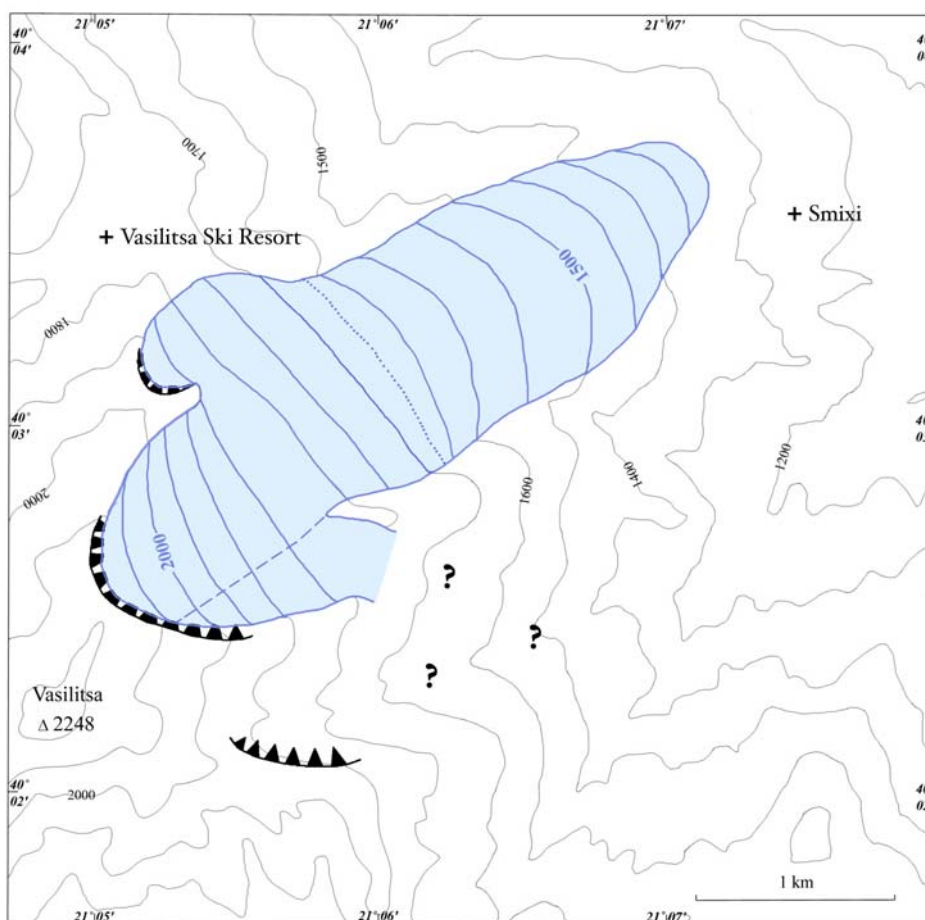


Figure 7.13 The Smixi glacier of Mount Vasilitsa during the Skamnelliian Stage. Glaciers are contoured at 50 m intervals (land contours at 100 m intervals). The key to the map is provided in Fig. 7.4 and symbols used in the base map are the same for the geomorphological maps (Fig. 3.4).

7.2.3 Mount Vasilitsa

It was argued in the previous chapter that the most extensive glacial deposits on Mount Vasilitsa correlate with those dated to >350,000 years BP on Mount Tymphi and formed during the Skamnellian Stage. The glaciers of Mount Vasilitsa during this stage are shown in Figure 7.13.

The reconstruction of Skamnellian Stage glaciers on Vasilitsa proved to be very difficult because of significant subsequent landscape change. Although the glacial limits could be traced with reasonable accuracy for the Smixi glacier, reconstruction of the surface contours did not fit with the modern land surface. For example, in many areas the modern land surface 'bulges' in the centre of the reconstructed glacial limits, forming a rounded and subdued ridge, and the glacial deposits are not confined by clear valley walls. This results in land surface altitude being greater than reconstructed ice surface altitudes in some areas which is clearly impossible. Possible explanations could include: a) substantial supraglacial deposition following glacier retreat; b) periglacial mass movement of large areas of unconsolidated glacial deposits in later cold phases or; c) erosion at the former glacier margins reducing land surface altitudes at the valley sides and thereby causing the land surface at the centre of the former glacier to be greater than that at the former edge. The latter possibility is supported by the presence of modern stream channels at the margins of the former glacier and, given the assumed age of the deposits, this is not difficult to envisage.

A further problem is the lack of deposits in valleys that have higher cirque moraines, such as in the eastern cirques of Vasilitsa. These cirque moraines may have only formed during later glacial phases when a hollow of sufficient size had been generated, perhaps by nivation during the Skamnellian Stage. Alternately, the deposits in the lower valley areas may have been eroded.

Although many problems and inconsistencies were encountered on Mount Vasilitsa, the main glacier for which there is clear evidence, the Smixi glacier, was reconstructed using the mapped drift limits. Glacier contours were estimated based on the modern land surface but taking into account erosion at the former glacier limits. Using this approach the reconstructed Smixi glacier had a surface area of at least 3.44 km² and an ELA of 1675 m a.s.l. This reconstruction is clearly more tentative than that achieved elsewhere, although the ELA value is similar to the mean ELA for the glaciers on Mount Smolikas (ELA: 1680 m a.s.l.).

7.3 Vlasian Stage glaciers

In many of the glaciated valleys of the field area, mid-valley moraines can be found. These are higher than the most extensive deposits, yet lower than the highest cirque moraines and rock glaciers. The oldest calcite cements in these moraines have been dated to the last interglacial, and it was argued in the previous chapter that these moraines were formed during the preceding cold stage. This glacial stage, given the local name Vlasian Stage, is equivalent to the Rissian Stage and the Warthe Stadial of the Saalian Stage in the Alpine and Northern Europe stratigraphy respectively and MIS 6 (*cf.* Sibrava *et al.* 1986).

The glacial landforms which formed during this stage are very well-preserved, and the reconstructions of the glaciers are likely to be much more accurate than for the Skamnelliian Stage. In total, 20 glaciers have been reconstructed on Mount Tymphi, Mount Smolikas and Mount Vasilitsa, covering a total area of 30.9 km².

Figure 7.14 shows the variation in altitudinal distribution of all 20 former glaciers during the Vlasian Stage on all mountains. The asymmetrical U-shaped curve is as expected and the lowest variation corresponds to an accumulation area of 0.6. This value is the same as that used for the Skamnelliian Stage glaciers and lies within the AAR range found on modern mid- and high-latitude glaciers of 0.5 - 0.8 (Meier and Post 1962, Hawkins 1985). This value was therefore used to reconstruct ELAs for glaciers of this stage.

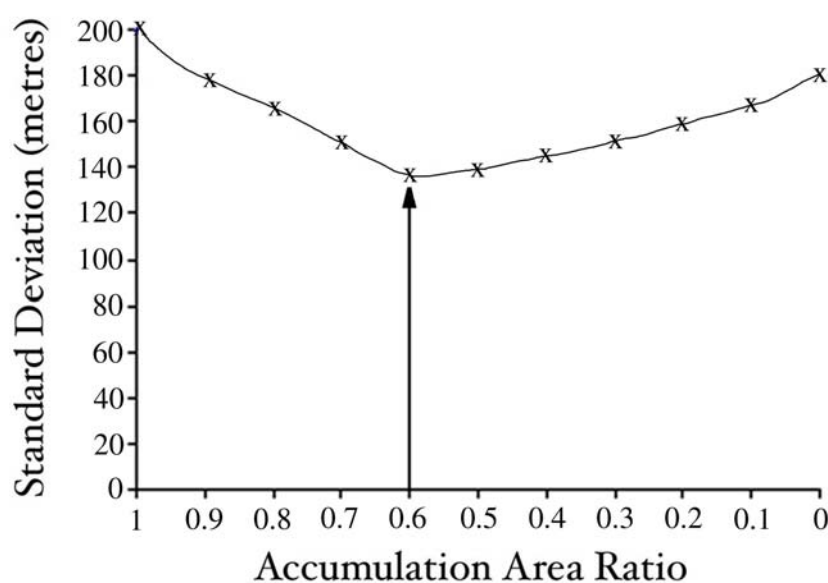


Figure 7.14 Standard deviation of the Vlasian Stage glacier surface altitudes at varying accumulation area ratios. An AAR of 0.6 would seem to represent the most suitable value for ELAs during glaciation of the Vlasian Stage.

It is notable that the standard deviation at all AARs is much lower for the mid-valley Vlasian glaciers than for the older, more extensive Skamnelliian glaciers (*cf.* Fig. 7.3). This probably results from the greater accuracy of the reconstructions for the Vlasian Stage glaciers, brought about by well-preserved moraines, tight valley morphometry and, therefore, more accurate glacier delimitation. As noted by Osmaston (2002), it is medium and smaller glaciers that give the most precise estimate of their own ELA. This is because there are larger uncertainties in deriving the shape and dimensions of larger glaciers.

7.3.1 Mount Tymphi

Fourteen glaciers covered a total area of 21.33 km² on Mount Tymphi during the Vlasian Stage - about 36% of the area covered by ice during the most extensive glacial phase during the Skamnelliian Stage. In most areas, the Vlasian Stage glaciers occupied higher mid-valley positions. However, in some areas, such as on the the south slopes of Astraka and over large parts of the Tymphi plateau, no deposits relating to this glacial phase can be found. This may be the result of higher ELAs during the Vlasian Stage. The details of the individual glaciers are presented in Table 7.4. The glacier groups are the same as those described above for the Skamnelliian Stage. However, in some cases, the glacier names have been changed where more than one glacier formed in cirques where, during the earlier Skamnelliian Stage, ice formed part of a larger, single valley glacier.

The mean ELA of the glacier groups was 1862 m a.s.l., some 121 m higher than that for the Skamnelliian Stage (1741 m a.s.l.). However, when adjusted for sea level and uplift interactions the mean ELA of the glacier groups during the Vlasian Stage was 1747 m a.s.l., *i.e.* 110 m lower than the modern altitude (Section 7.1.8). If correct, this implies that the 'real' ELAs on Mount Tymphi during the Vlasian Stage were 156 m higher above sea-level than that for the Skamnelliian Stage (1591 m a.s.l.).

7.3.1.1 Group A glaciers

On the northern slopes of Mount Tymphi, valley glaciers reached mid-valley positions in the Stani Katsanou, Mighia and Amarandos valleys (Fig. 7.15). In contrast to the Skamnelliian Stage, the Stani Katsanou and Mighia glaciers were true valley glaciers and did not overspill the drainage divide and become transection glaciers.

The Stani Katsanou glacier was by far the largest of this glacier group, covering an area of 2.57 km². This glacier had two distinct accumulation areas, in the Karteros and Tsouka Rossa cirques, and could therefore be considered as two separate glaciers which

<i>Glacier</i>	<i>Group</i>	<i>Area (km²)</i>	<i>ELA (m a.s.l.)</i>	<i>Group mean ELA (metres a.s.l)</i>
Amarandos	A	0.54	1850	2005
Mighia		0.98	2050	
Stani Katsanou (East)		2.57	2050	
Stani Katsanou (West)			2070	
Maghoula	B	0.84	1640	1628
Dimitrios		0.67	1690	
Laccos		0.71	1600	
Plaghia		0.65	1580	
Vourtapa	C	3.10	1900	1894
Vrichos		0.88	1840	
Tsioumako		2.20	1900	
Tselon/Litharion		6.01	1970	
Stani Grava		0.89	1860	
Xeroloutsa	D	1.29	1920	1920
Total area		21.33	overall group mean ELA	1862

Table 7.4 Glacier areas and ELAs for the Vlasian glaciers of Mount Tymphi.

coalesced in the ablation area. In order to calculate the different ELAs of these two glacier parts, the ablation area was divided into two, with the area of each portion related to the contributory areas of the up-valley glacier portions. The western and the eastern glaciers had ELAs of 2070 and 2050 m a.s.l. respectively. Although the ELAs were 100 m higher than during the Skamnellian Stage, the glacier area was only 14% smaller.

The Mighia glacier, covered an area of 0.98 km² and had an ELA of 2050 m a.s.l. This glacier occupied the Kopanes cirque at the head of the Mighia valley and had its limits just above the well-defined rock step in this valley.

The Amarandos glacier below the peak of Gamila (2497 m a.s.l.) was the smallest glacier of this group and covered an area of 0.54 km². It was also the lowest with an ELA of 1850 m a.s.l.

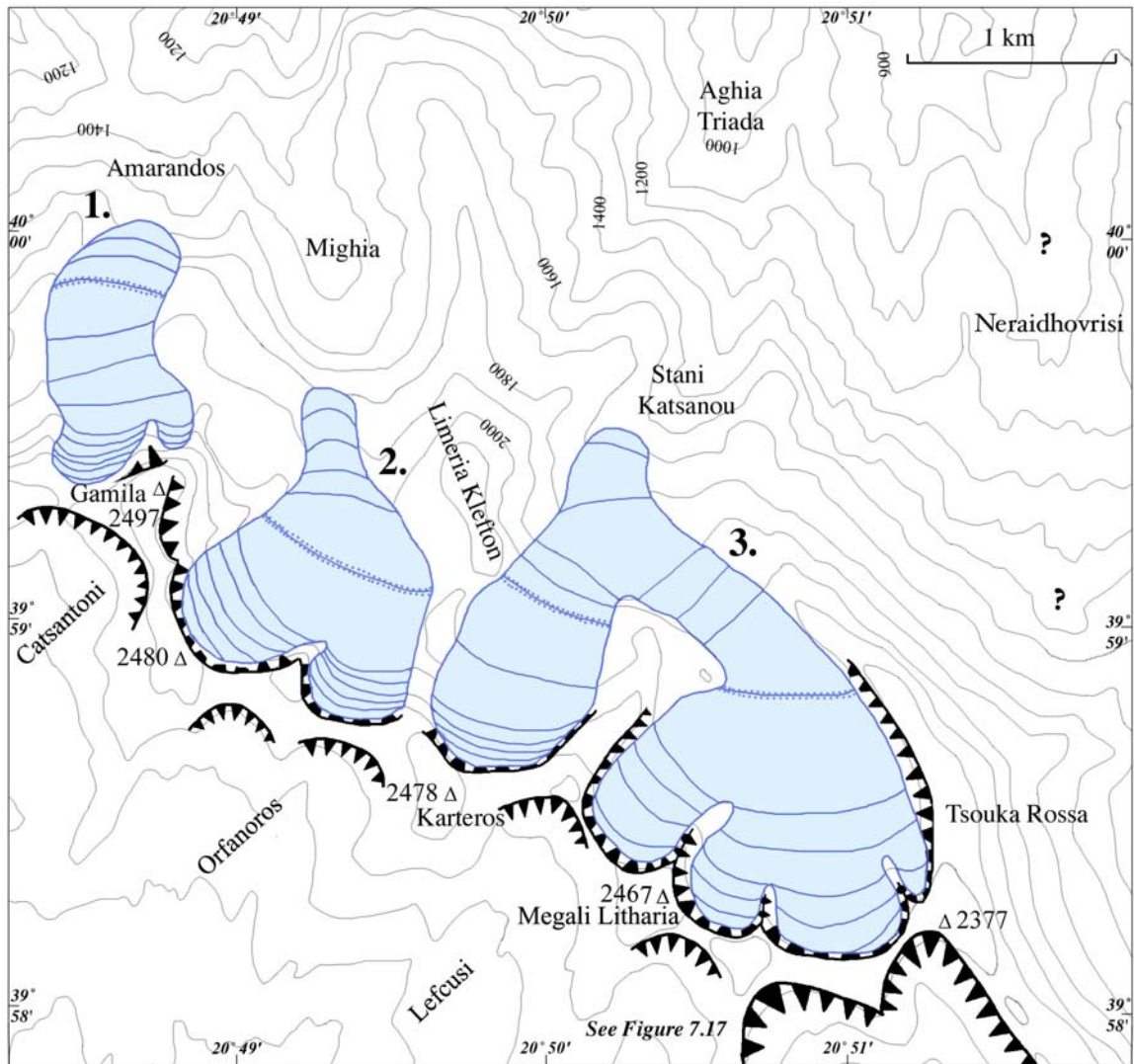


Figure 7.15 The Group A glaciers during the glacial maximum of the Vlasian Stage. 1: Amarandos glacier. 2: Mighia glacier. 3: Stani Katsanou glacier(s). Glaciers are contoured at 50 m intervals (land contours at 100 m intervals). The key to the map is provided in Fig. 7.4 and symbols used in the base map are the same for the geomorphological maps (Fig. 3.4).

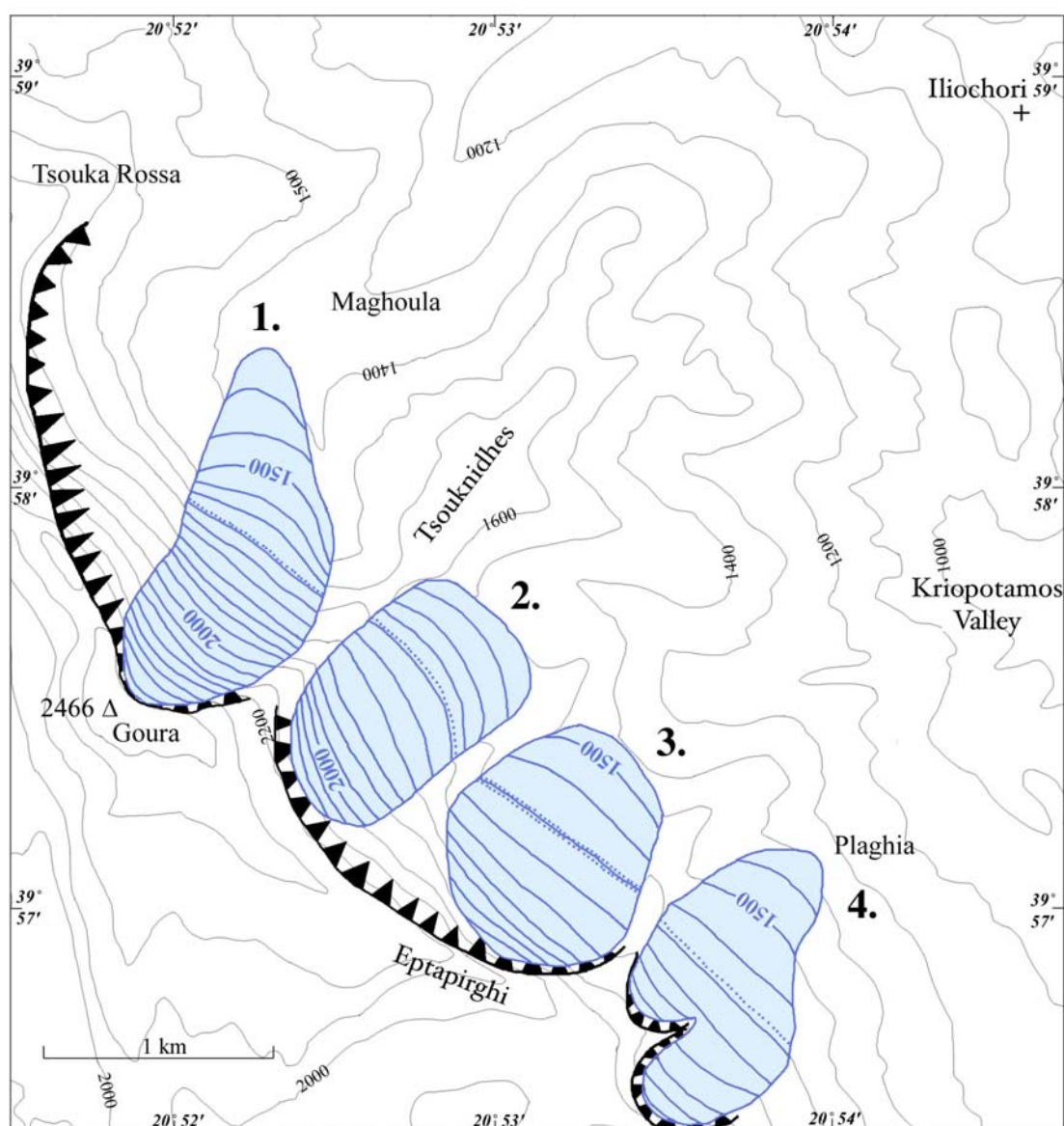


Figure 7.16 The Group B glaciers during the glacial maximum of the Vlasian Stage. 1: Maghoula glacier. 2: Dimitrios glacier. 3: Laccos glacier. 4: Plaghia glacier. Glaciers are contoured at 50 m intervals (land contours at 100 m intervals). The key to the map is provided in Fig. 7.4 and symbols used in the basemap are the same for the geomorphological maps (Fig. 3.4).

7.3.1.2 Group B glaciers

At the base of the northern escarpment of Goura (2466 m a.s.l.), small glaciers formed in the cirques at the heads of the Kriopotamos and Maghoula valleys (Fig. 7.16). At the head of the former valley, three glaciers occurred in the Dimitrios, Laccos and Plaghia cirques. These covered areas of *ca.* 0.67, 0.71 and 0.65 km² and had ELAs of 1690, 1600 and 1590 m a.s.l. respectively. At the head of the Maghoula valley, only one glacier existed and covered an area of *ca.* 0.84 km² with an ELA of 1640 m a.s.l.

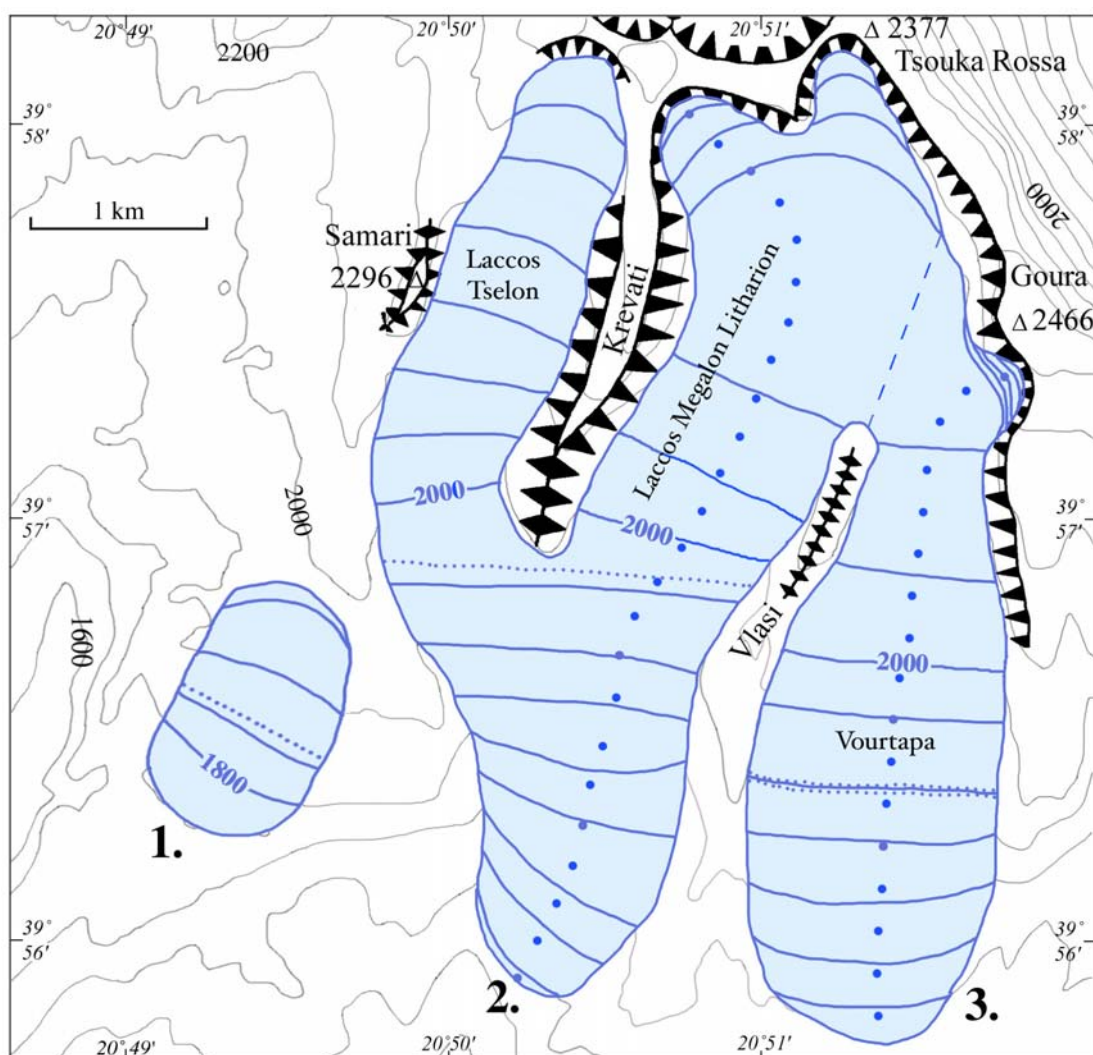


Figure 7.17 The western Group C glaciers during the glacial maximum of the Vlasian Stage. 1: Stani Grava glacier, 2: Tselon/Litharion glacier. 3: Vourtapa glacier. Glaciers are contoured at 50 m intervals (land contours at 100 m intervals). The blue dots represent stations along a shear stress transect. The key to the map is provided in Fig. 7.4 and symbols used in the basemap are the same for the geomorphological maps (Fig. 3.4).

7.3.1.3 Group C glaciers

Above Tsepelovo, a small glacier formed on the eastern edge of the Tymphi plateau, at Stani Grava. This glacier covered an area of 0.89 km^2 and had an ELA of 1860 m a.s.l. (Fig. 7.17).

Further east, ice reaching mid-valley positions extended from the Laccos Tselon and Laccos Megalon Litharion cirques. The Tselon/Litharion glacier was by far the largest of all the Vlasian Stage glaciers and covered an area of 6.01 km^2 with an ELA of 1970 m a.s.l. and extended 5.3 km from source to snout. This compares with a glacier area of 9.04 km^2 , ELA of 1800 m a.s.l. and length of 12.3 km in this valley during the earlier Skamnellian Stage. As was the case during the Skamnellian Stage, ice in the Laccos

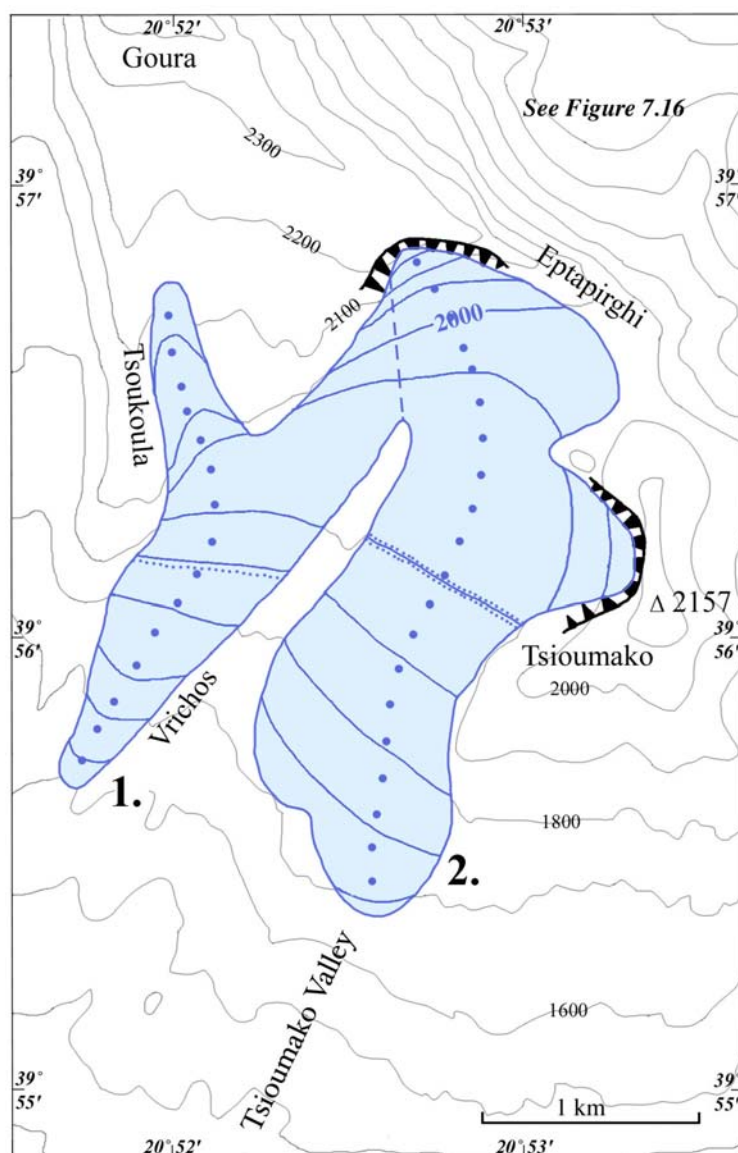


Figure 7.18 The easternmost Group C glaciers during the glacial maximum of the Vlasian Stage. 1: Vrichos glacier. 2: Tsioumako glacier. Glaciers are contoured at 50 m intervals (land contours at 100 m intervals). The blue dots represent stations along a shear stress transect. The key to the map is provided in Fig. 7.4 and symbols used in the base map are the same for the geomorphological maps and a key is provided in Figure 3.4.

Megalon Litharion cirque would have spilled over into the Vourtapa valley during the Vlasian Stage. The glaciers above Tsepelovo and Skamnelli therefore represent transection glaciers, separated by the peak of Vlasi. The Vourtapa glacier above Skamnelli covered an area of 3.1 km² and had an ELA of 1900 m, 100 m higher than the Tselon/Litharion glacier above Tsepelovo.

The easternmost Group C glacier occurred in the Tsioumako and Vrichos cirques where ice spilled over a local ice divide and formed two outlet glaciers. The Tsioumako glacier was the larger of the two, covering an area of 2.20 km² with an ELA of 1900

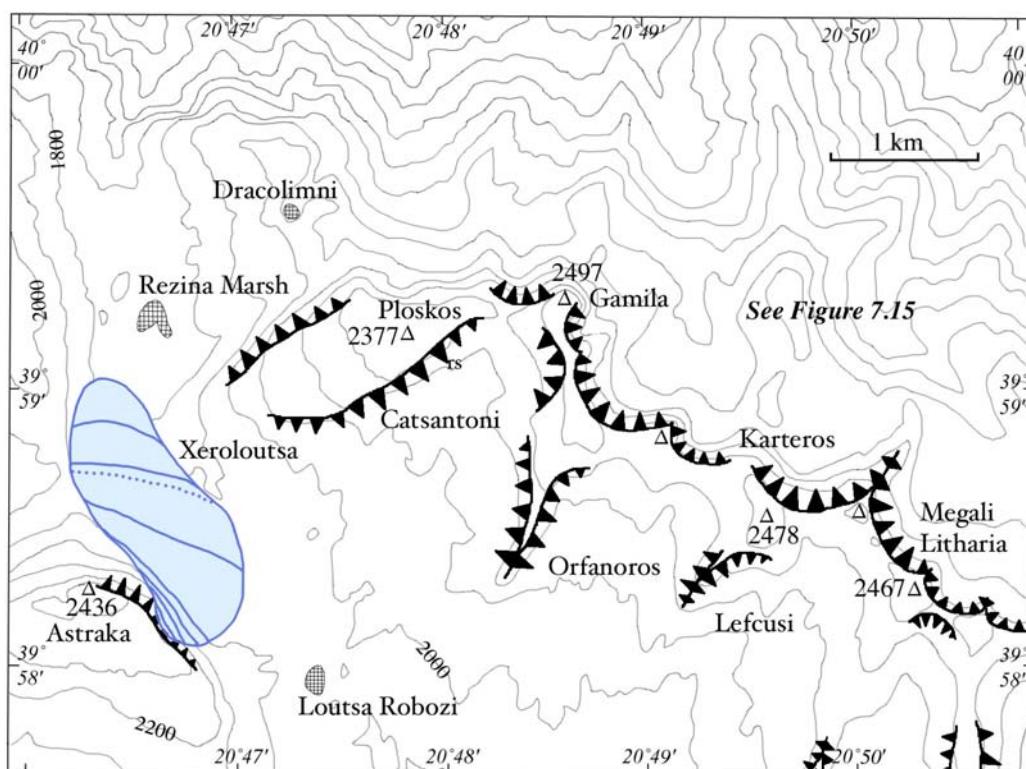


Figure 7.19 The Xeroloutsa glacier (Group D). Glaciers are contoured at 50 m intervals (land contours at 100 m intervals). The key to the map is provided in Fig. 7.4 and symbols used in the base map are the same for the geomorphological maps (Fig. 3.4).

m a.s.l. The Vrichos glacier was lower with an ELA at 1840 m a.s.l., although it was much smaller, covering only 0.88 km².

7.3.1.4 Group D glaciers

Only one small glacier existed on the Tymphi plateau between the peaks of Gamila (2497 m a.s.l.) and Astraka (2436 m a.s.l.), and none existed on the southern slopes of Astraka during the Vlasian Stage (Fig 7.19). This contrasts with the large ice-field and outlet glaciers which existed during the earlier Skamnellian Stage. The glacier formed at the foot of the 600 m high northern cliffs of Astraka. This glacier, named here the Xeroloutsa glacier after the moraine-dammed lake in this vicinity, covered an area of 1.29 km² and had an ELA of 1920 m a.s.l. (Fig. 7.19).

7.3.1.5 Testing the glacier reconstructions

The excellent preservation of the Vlasian Stage moraines, as well as the tight closure of many of the glaciated valleys, suggests that the reconstruction of these glaciers is particularly accurate, much more so than for the older Skamnellian Stage glaciers. All of the reconstructions were tested to determine whether the glaciers were physically plausible.

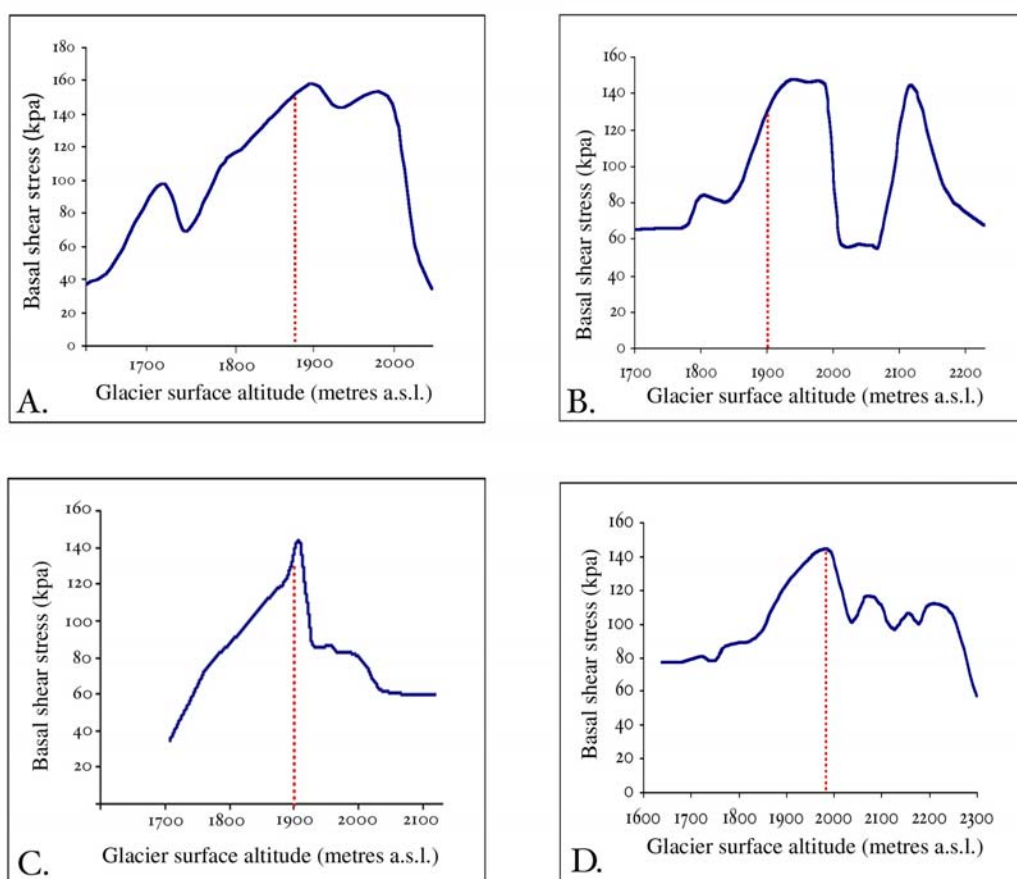


Figure 7.20 Basal shear stress plotted against glacier surface altitude along glacier centre-line profiles. The red dotted line represents the ELA. A: Vrichos glacier. B: Vourtapa glacier. C: Tsioumako glacier. D: Litharion glacier.

The glaciological reconstructions of the some of the largest of the glaciers are presented here with the down-glacier basal shear stress profiles shown in Figure 7.20. The examples include the Vrichos, Vourtapa, Tsioumako and Litharion glaciers, which existed above Tsepelovo and Skamneli.

Overall, the glaciers display wide range of values and down-glacier patterns of basal shear stress. However, they all have realistic values, rarely exceeding the range of 50-150 kpa expected for glacier ice. The highest values always occur in the mid-glacier area, at or around the ELA, whilst the lowest occur at the former glacier margins where ice thicknesses were lowest. In the accumulation area, lower basal shear stresses only occur in the uppermost area because of the reduced glacier depths near the backwall margins. This pattern is especially true for the Vrichos and Litharion glaciers (Fig. 7.23A and 7.23D). However, the reconstructed Vourtapa glacier displays widely variable basal shear stress values for the accumulation area (Fig 7.23B). This results from the highest part of this glacier being sourced in the Laccos Megalon Litharion cirque which primarily fed the Litharion glacier. Ice feeding the Vourtapa glacier had to breach the Vlasi-Goura col in

order to leave this cirque resulting in reduced ice thickness, reduced ice surface slope and, as a result, lower shear at the drainage divide at *ca.* 2000 m a.s.l (Fig. 7.17).

The fact that the basal shear stress often peaks near the ELA supports the use of an AAR of 0.6 to derive the ELA and gives confidence in the accuracy of the glacier reconstruction. The down-profile variation in shear stress is nearly always reflected in the geomorphology and sedimentology. Around the ELA and in the accumulation area, extending glacier flow and high basal stress is reflected in the strong erosional forms in these areas (cirque basins, *riegels*, pavements). Below the ELA, in the ablation area, compressive glacier flow and low basal shear stress are reflected in the depositional landforms of this area.

7.3.2 Mount Smolikas

The mid-valley Vlasian Stage glaciers on Mount Smolikas comprised of only two glaciers covering only 6.61 km² compared with over 21.32 km² on Mount Tymphi (Table 7.5). Moreover, unlike during the Skamnellian Stage, the Mount Smolikas glaciers (mean ELA: 1997 m a.s.l.) had higher ELAs than those on Mount Tymphi (mean group ELA: 1862 m a.s.l.).

The Vadulakkos glacier was the largest and lowest glacier, covering an area of 4.86 km² with an ELA of 1890 m a.s.l. and extended 6.6 km from source to snout (Fig 7.21). This glacier was only 34% smaller and 6% shorter than the Skamnellian Stage glacier in the same valley, although the ELA was 190 m higher and similar to the Vlasian Stage glacier group mean for Mount Tymphi.

A valley glacier in the Konkutino valley covered a total area of 1.39 km² and had an ELA of 2060 m a.s.l. (Fig. 7.22). This glacier faced northeast in the accumulation area and veered to the south in the ablation area. In the nearby Bogdoni cirque, a small south-facing glacier existed covering an area of only 0.36 km² with an ELA of 2040 m a.s.l. A further glacier may have occurred in the southeastern cirque of Moasa, although geomorphological evidence supporting any reconstruction is lacking.

<i>Glacier</i>	<i>Area (km²)</i>	<i>ELA (metres a.s.l.)</i>
Vadulakkos	4.86	1890
Konkutino	1.39	2060
Bogdoni	0.36	2040
Total area/ mean ELA	6.61	1997

Table 7.5 Glacier areas and ELAs for the 3 Vlasian glaciers of Mount Smolikas.

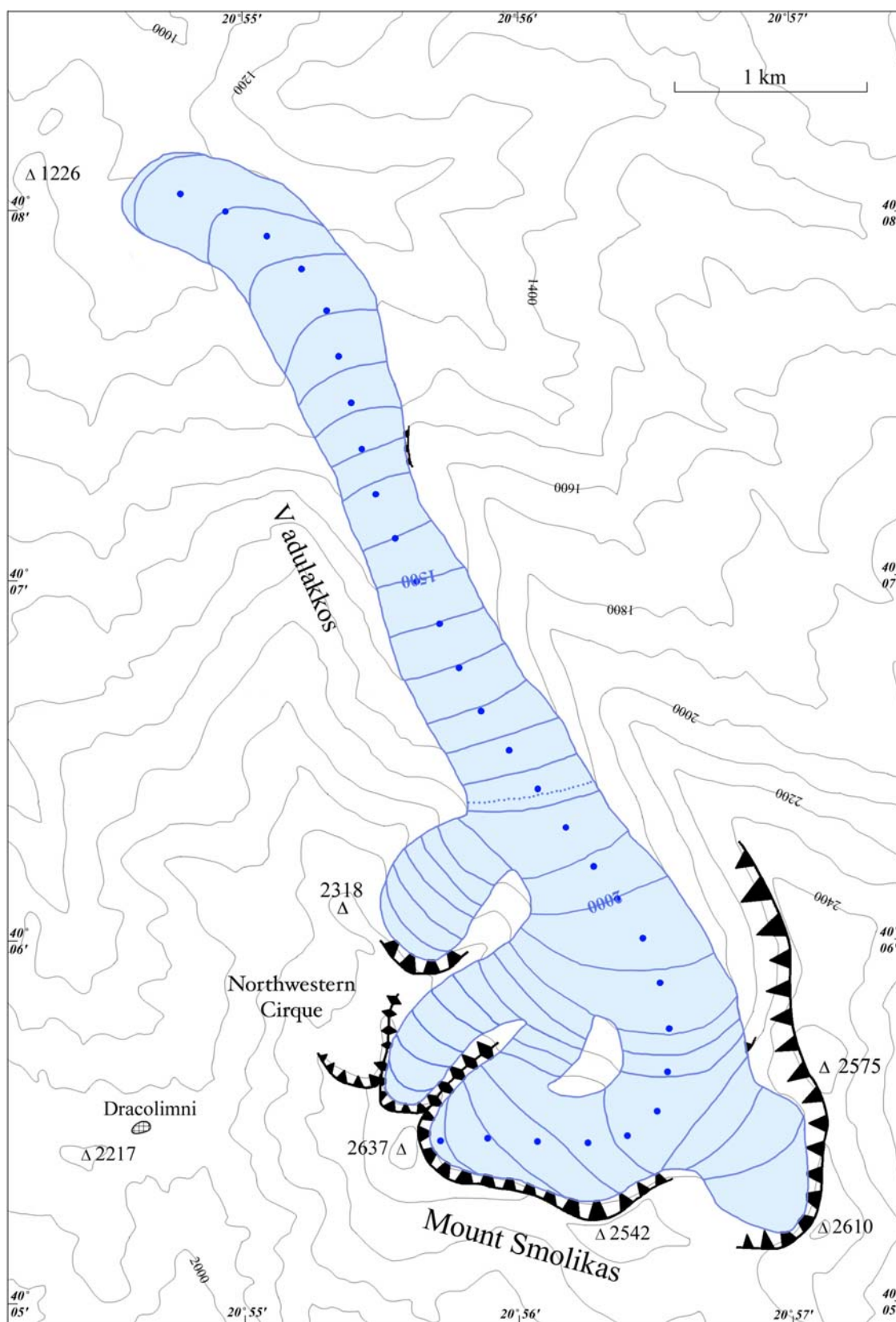


Figure 7.21 The Vadulakkos glacier during the glacial maximum of the Vlasian Stage. Glaciers are contoured at 50 m intervals (land contours at 100 m intervals). The blue dots represent stations along a shear stress transect. The key to the map is provided in Fig. 7.4 and symbols used in the base map are the same for the geomorphological maps (Fig. 3.4).

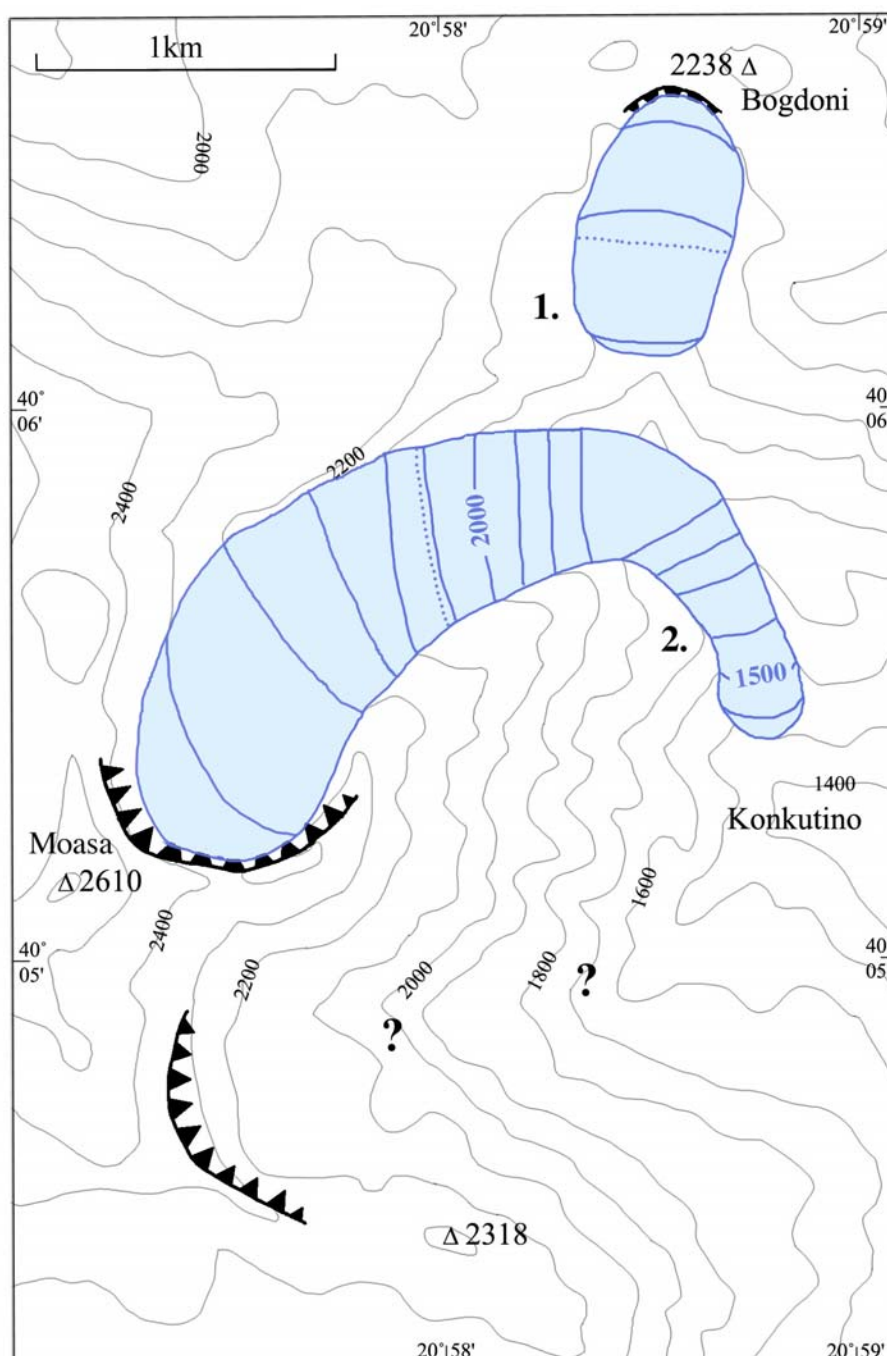


Figure 7.22 The Konkutino (1.) and the Bogdoni (2.) glaciers during the Vlasian Stage glacial maximum. Glaciers are contoured at 50 m intervals (land contours at 100 m intervals). The key to the map is provided in Fig. 7.4 and symbols used in the base map are the same for the geomorphological maps (Fig.3.4).

There is no evidence to suggest that a glacier was present near Samarina during the Vlasian glaciation. This is probably because the hollow occurred below the altitude possible for glacier formation, even under the influence of local controls.

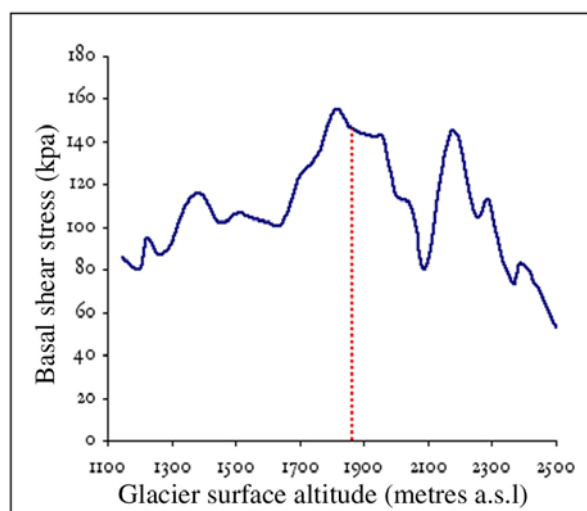


Figure 7.23 Basal shear stress plotted against glacier surface altitude along the centre-glacier profile of the Vadulakkos glacier.

The Smolikas glacier reconstructions were tested by determining basal shear stress profiles. The profile for the Vadulakkos glacier, the largest glacier on Mount Smolikas during the Vlasian Stage is shown in Figure 7.23. Again, basal shear stress reaches a maximum near to the reconstructed ELA, as would be expected due to greatest ice discharge in this area. This fact also supports the ELA reconstruction using an AAR of 0.6. In the accumulation area, shear stress values fluctuate but reach higher values than in the ablation area. This reflects variable topography, greater ice depths and steeper ice gradients. The peak in basal shear stress values at *ca.* 2200 m a.s.l. reflects steep ice gradients as ice discharged from a cirque over a *riegel* into a single valley channel. Conversely, the trough at 2100 m a.s.l. reflects reduced gradient below the *riegel* within a single valley channel (Fig. 7.21). Basal shear stress decreases steadily down the glacier profile into the ablation area, though a small peak occurs at 1400 m a.s.l. This results from localised ice steepening and thickening because ice would have been forced through a constriction in the valley at this point, caused by an outcrop of resistant Jurassic limestone in this area, which is commonly found at the overthrust nappe of the ophiolitic complex (IGME 1987).

7.3.3 Mount Vasilitsa

At least four glaciers occupied mid-valley positions on Mount Vasilitsa and correlate with Vlasian Stage glaciers identified on Mount Tymphi and Mount Smolikas (Fig. 7.24). They all had a northeasterly aspect and covered an area of only 1.21 km² with a mean ELA of 1865 m a.s.l. (Table 7.6).

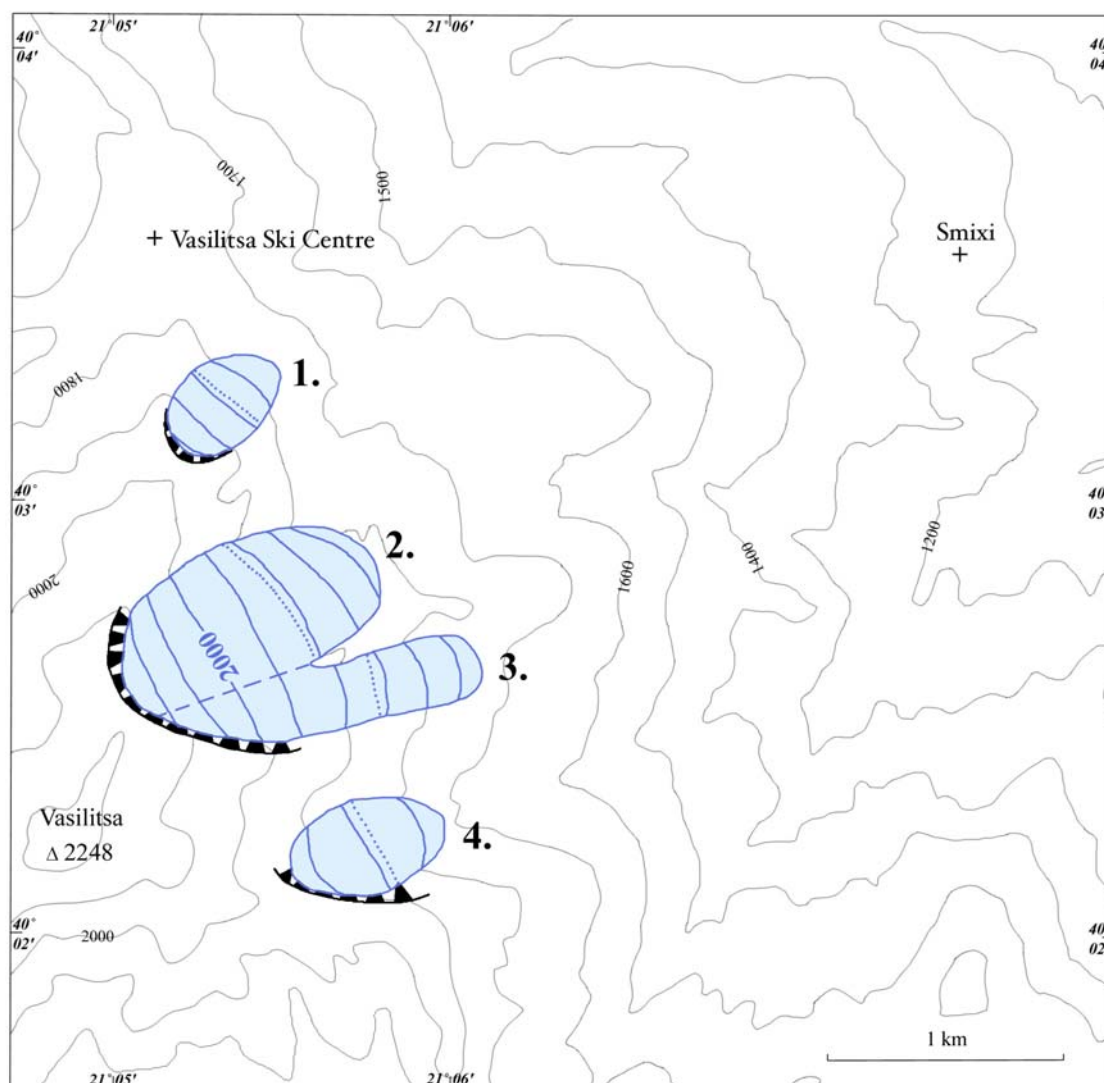


Figure 7.24 The Vasilitsa glaciers during the Vlasian Stage glacial maximum. 1: Vasilitsa North glacier. 2: Vasilitsa Central glacier. 3: Vasilitsa Central South glacier. 4: Vasilitsa South glacier. Glaciers are contoured at 50 m intervals (land contours at 100 m intervals). The key to the map is provided in Figure 7.4 and symbols used in the base map are the same for the geomorphological maps (Fig. 3.4).

<i>Glacier</i>	<i>Area (km²)</i>	<i>ELA (metres a.s.l.)</i>
Vasilitsa North	0.14	1840
Vasilitsa Central North	0.55	1920
Vasilitsa Central South	0.31	1860
Vasilitsa South	0.21	1840
Total area/ mean ELA	1.21	1865

Table 7.6 Glacier areas and ELAs for the 4 Vlasian glaciers of Mount Vasilitsa.

The Vasilitsa North glacier was the smallest glacier covering only 0.14 km² with an ELA of 1840 m a.s.l. In the neighbouring cirque, a short distance to the south, two glaciers occurred, the Vasilitsa Central North and Central South glaciers, covering 0.55 and 0.31 km², respectively. They were both derived from the same cirque and shared accumulation areas but had snouts separated by a low bedrock ridge. However, their ELAs were slightly different, with the more northerly glacier having an ELA of 1920 m a.s.l. and the southerly glacier having an ELA of 1860 m a.s.l. All of these glaciers occupied cirques formerly occupied by the Smixi valley glacier during the Skamnellian Stage, and covered only 35% of the latter glacier area. Further south in the next valley, a small cirque glacier, named here the Vasilitsa South glacier, covered an area of 0.21 km² with an ELA of 1840 m a.s.l.

7.4 Tymphian Stage glaciers and rock glaciers

During the last major cold stage, small glaciers and rock glaciers occupied the cirques of the northern Pindus (Hughes *et al.* 2003). The last glacial stage in Greece is named the Tymphian Stage after the glacier moraines and rock glaciers found on Mount Tymphi (Chapter Six). Cirque moraines are also present on Mount Smolikas and Mount Vasilitsa, and on the former mountain, two sets of moraines are evident in 3 out of 5 cirques containing deposits assigned to the last glacial stage. The lower moraines most likely correlate with the Tymphian Stage glaciers of Mount Tymphi, whilst the highest moraines may represent glacial readvance during the Late-glacial Substage and possibly during the Younger Dryas Chronozone (11-10,000 ¹⁴C years BP) (Chapter Six). On Mount Tymphi and Mount Vasilitsa these later glaciers did not form because of the lower altitude of these mountains.

Figure 7.25 shows the variation in altitudinal distribution between all of the former glaciers during the Tymphian Stage on Mount Tymphi, Mount Smolikas and Mount Vasilitsa. The standard deviations are low compared to other glacial stages and there is little difference in standard deviation at all AARs. The standard deviation consistently ranges between 68 and 83 m. The low standard deviations result from all of these glaciers being small in area and occurring at the limit of glaciation in the highest cirques with a small altitudinal range. The low inter-glacier variability, with no trends towards lower standard deviation at the ELA, again reflects the small size of the former glaciers and their sensitivity to local effects such as avalanche and snowblow input. However, An AAR of 0.6 was chosen since this is the value found to be most suitable for the older glaciations.

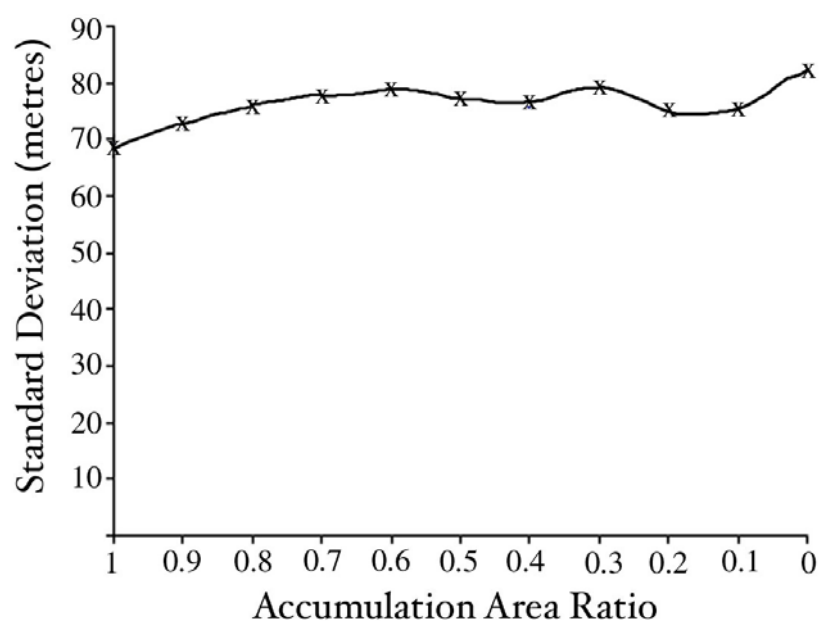


Figure 7.25 Standard deviation of the Tymphian Stage glacier surface altitudes at varying accumulation area ratios. There is little variation in the standard deviation between different AARs.

7.4.1 Mount Tymphi

The last glaciers of Mount Tymphi covered an area of 3.90 km² and had a mean ELA of 2174 m a.s.l. (Table 7.7 and Fig. 7.26). Only two of the glaciers, the Laccos Tselon and the Laccos Megalon Litharion glaciers, had areas greater than 1 km². Six rock glaciers formed below the Tsouka Rossa cirque glaciers and in several cirques not occupied by glaciers. These rock glaciers had a lower limit of 1800 m a.s.l. (Table 7.8). The longest rock glacier was the Karteros rock glacier at *ca.* 725 m a.s.l., whilst the largest was the Tsouka Rossa debris rock glacier which covered an area of just over 0.5 km². Perennial snow patches would also have existed in favourable localities, as evidenced by pronival ramparts in the Vourtpa valley.

<i>Glacier</i>	<i>Area (km²)</i>	<i>ELA (metres a.s.l.)</i>
Laccos Megalon Litharion	1.11	2100
Laccos Tselon	1.55	2175
Tsouka Rossa 1	0.21	2180
Tsouka Rossa 2	0.35	2200
Tsouka Rossa 3	0.55	2215
Tsouka Rossa 4	0.13	2175
Total area/ mean ELA	3.90	2174

Table 7.7 The Tymphian Stage glaciers of Mount Tymphi

<i>Rock glacier</i>	<i>Area (km²)</i>	<i>Length (metres)</i>	<i>Front altitude (metres a.s.l.)</i>
Tsouka Rossa	0.53	690	2000
Karteros	0.35	725	2000
Kopanes	0.39	650	1900
Gamila	0.08	400	1950
Amarandos	0.12	480	1800
Vlasi	0.14	300	1850
Total area/ mean length/ lowest glacier front	1.61	541	1800

Table 7.8 The Tymphian Stage rock glaciers of Mount Tymphi.

7.4.2 Mount Smolikas

Five glaciers covering an area of 2.55 km² with a mean ELA of 2241 m a.s.l. formed on Mount Smolikas during the Tymphian Stage. These glaciers occupied the northern cirques of the main ridge and the eastern cirques of Moasa (Fig. 7.26 and 7.27). The mean ELA was only 67 m higher than the mean of the Mount Tymphi glaciers supporting the correlation of these cirque moraines. However, the range of ELAs was greater on Mount Smolikas compared to those on Mount Tymphi (Table 7.9).

<i>Glacier</i>	<i>Area (km²)</i>	<i>ELA (metres a.s.l.)</i>
Cirque 1	0.25	2125
Cirque 2	0.21	2340
Cirque 3/4	1.12	2340
Galanos Limni	0.69	2180
Southeast Moasa	0.28	2220
Total area/ mean ELA	2.55	2241

Table 7.9 The Tymphian Stage glaciers of Mount Smolikas.

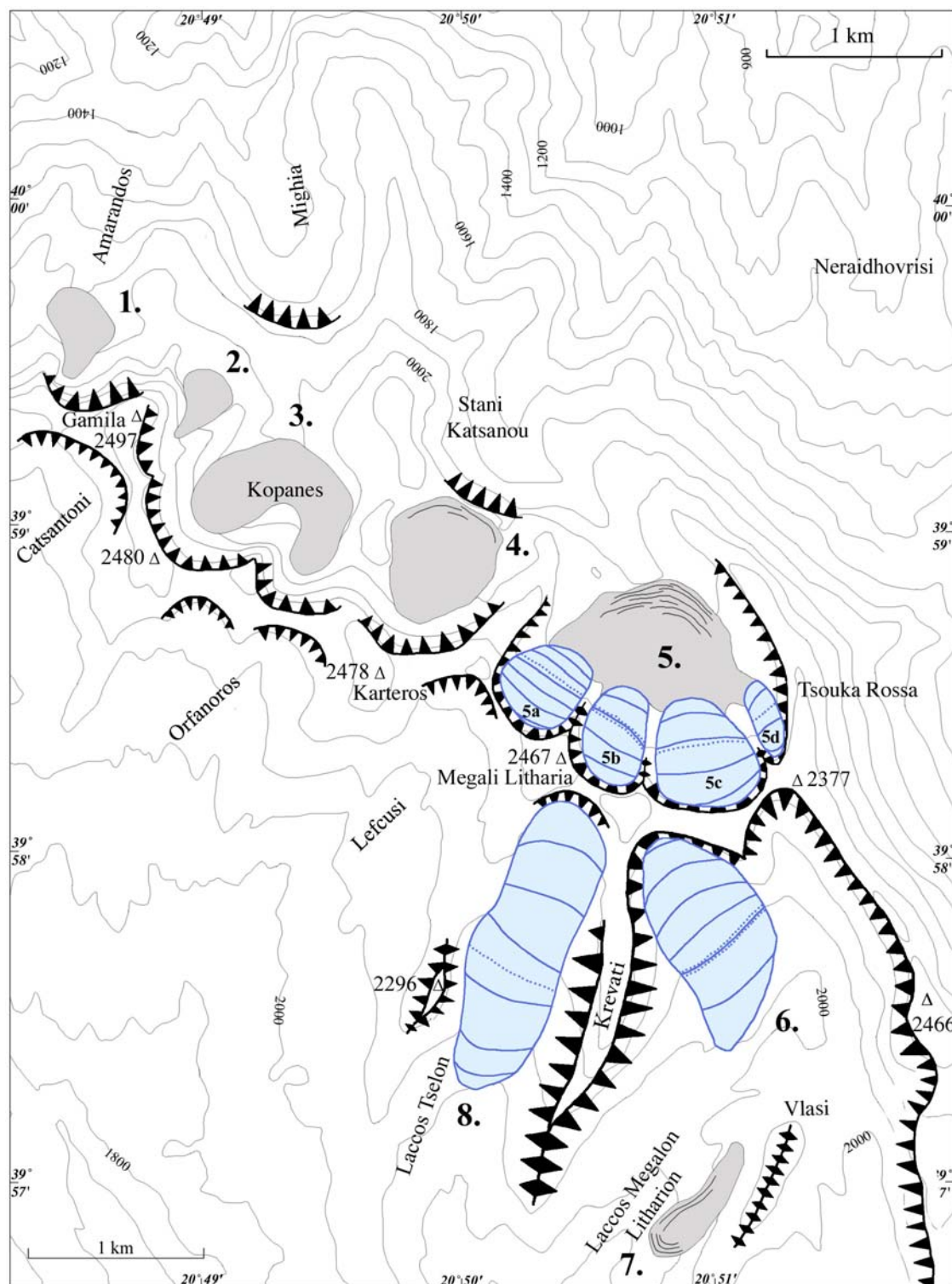


Figure 7.26 The Mount Tymphi glaciers and rock glaciers during the maximum Tympthian Stage glacial maximum. 1: Amarandos rock glacier. 2: Gamila rock glacier. 3: Kopanes rock glacier. 4: Karteros rock glacier. 5: Tsouka Rossa rock glacier (5a-d: Tsouka Rossa glaciers 1-4 respectively). 6: Laccos Megalon Litharion glacier 7: Vlasi rock glacier. 8: Laccos Tselon glacier. Glaciers are contoured at 50 m intervals (land contours at 100 m intervals). The key to the map is provided in Fig. 7.4 and symbols used in the base map are the same for the geomorphological maps (Fig. 3.4).

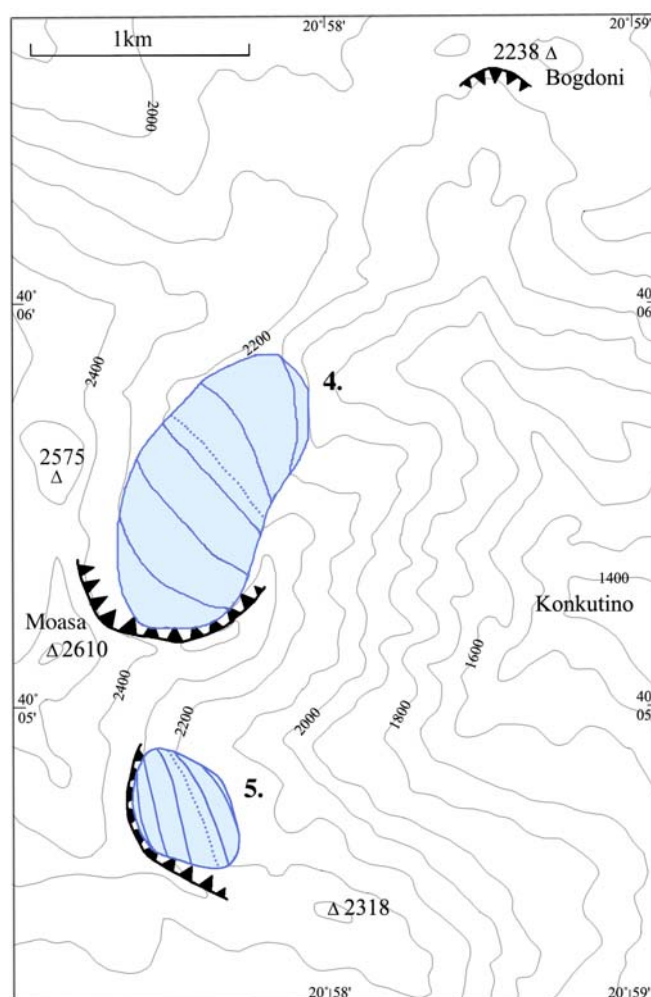
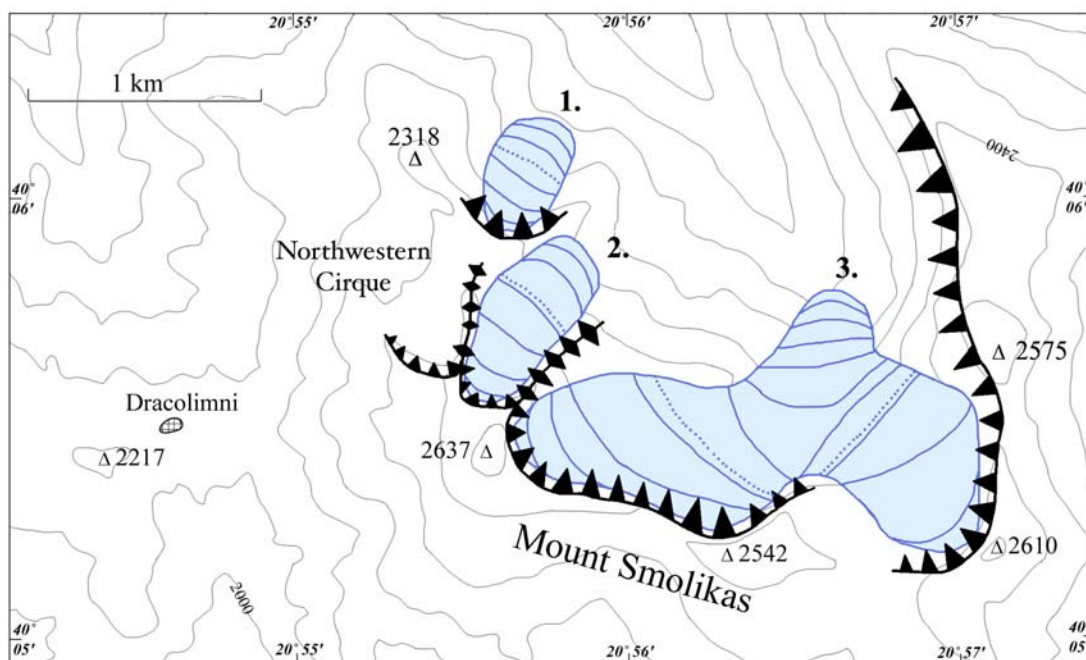


Figure 7.27 The Smolikas glaciers during the Tymphian Stage glacial maximum. 1: Cirque 1 glacier. 2: Cirque 2 glacier. 3: Cirque 3/4 glacier. 4: Galanos Limni glacier. 5: Southeast Moasa glacier. Glaciers are contoured at 50 m intervals (land contours at 100 m intervals). The key to the map is provided in Fig. 7.4 and symbols used in the base map are the same for the geomorphological maps (Figure 3.4).

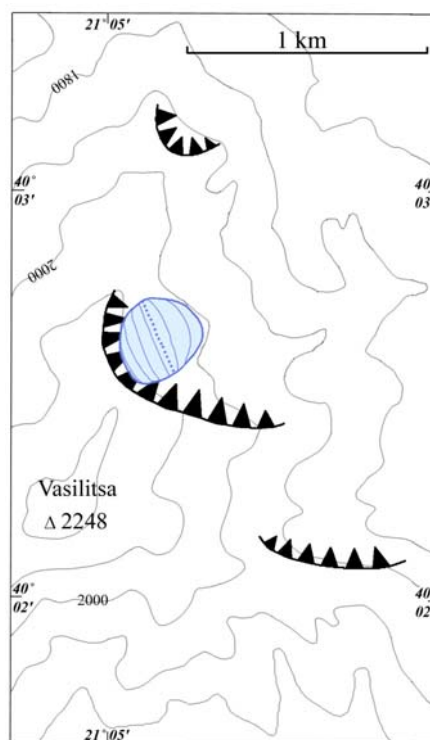


Figure 7.28 The single Vasilitsa cirque glacier during the glacial maximum of the Tymphian Stage. The glacier is contoured at 20 m intervals (land contours at 100 m intervals). The key to the map is provided in Fig. 7.4 and symbols used in the base map are the same for the geomorphological maps (Fig. 3.4).

7.4.3 Mount Vasilitsa

A small cirque glacier also formed on the northeastern slopes of Mount Vasilitsa during the Tymphian Stage glacial maximum. It covered only 0.122 km² and had an ELA of 2050 m a.s.l., lower than any of the glaciers on Mount Smolikas and Mount Tymphi (Fig. 7.28).

7.5 Smolikasian Substage glaciers and rock glaciers

A set of moraines above *ca.* 2200 m a.s.l. exists on Mount Smolikas and these are likely to have formed during the Smolikasian Substage (Chapter Six), during a readvance or a separate advance of glaciers (Figure 7.29). There is no evidence to suggest that equivalent glaciers existed on Mount Tymphi because of the lower altitude of this mountain and the fact that the highest cirque floors are only *ca.* 2100 m a.s.l. In total, three glaciers existed in the highest cirques and covered an area of only 0.43 km² with a mean ELA of 2372 m a.s.l. (Table 7.10). Two glaciers in Cirques 2 and 3 covered areas of 0.12 km² and 0.1 km² and had ELAs of 2415 and 2425 m a.s.l. respectively. A glacier in the Galanos Limni cirque was larger and lower, covering an area of 0.21 km² with an ELA of 2275 m a.s.l. The ELAs

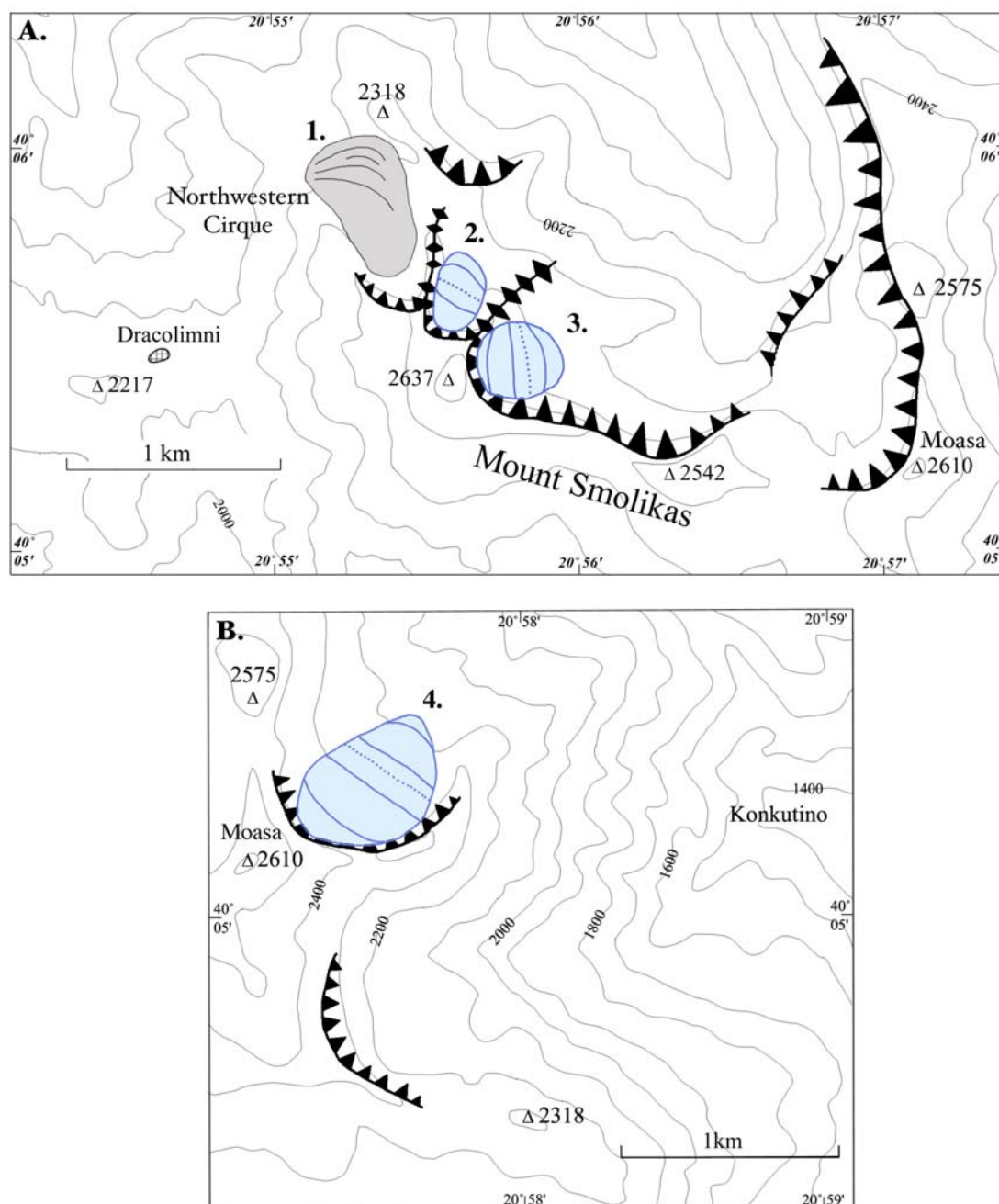


Figure 7.29 The glaciers and rock glacier of Mount Smolikas during the Smolikasian Substage (Late-glacial Substage) in the upper Vadulakkos cirques (A) and upper Konkutino cirques (B). 1: Northwestern Cirque rock glacier. 2: Cirque 2 glacier. 3: Cirque 3 glacier. 4: Galanos Limni glacier. Glaciers are contoured at 50 m intervals (land contours at 100 m intervals). The key to the map is provided in Fig. 7.4 and symbols used in the basemap are the same for the geomorphological maps and a key is provided in Figure 3.4.

of the glaciers were determined using an AAR of 0.6, the same as for the earlier Tymphian Stage glacial maximum glaciers.

A rock glacier also formed in the Northwestern Cirque (Fig. 7.29). This rock glacier is considered to have formed contemporaneously with the highest cirque glaciers (Chapter 5, section 5.2). The front of the feature is 160 m higher than the highest rock glacier fronts

on Mount Tymphi, which is likely to have formed during an earlier cooler phase of climate at the climax of the last glacial cycle.

<i>Glacier</i>	<i>Area (km²)</i>	<i>ELA (metres a.s.l.)</i>
Cirque 2	0.12	2415
Cirque 3	0.10	2425
Galanos Limni	0.21	2275
Total area/ mean ELA	0.43	2372

Table 7.10 The last glaciers of Mount Smolikas. These represent readvance glaciers during the Smolikasian Substage and most likely correlate with the Late-glacial Substage elsewhere in Europe.

<i>Rock glacier</i>	<i>Area (km²)</i>	<i>Length (metres)</i>	<i>Glacier Front (metres a.s.l.)</i>
Northwestern cirque	0.2	500	2160

Table 7.11 The rock glacier in the Northwestern Cirque of Mount Smolikas. This rock glacier is likely to have formed contemporaneously with the Smolikasian Substage glaciers.

Tymphian Stage. The rock glacier covered an area of 0.2 km² and was *ca.* 500 m in length (Table 7.11). In addition to the glaciers and rock glacier, perennial snow patches would have existed in Cirque 3, forming pronival ramparts to the west of the glacier which occupied part of this cirque.

7.6 Glacier reconstruction - summary

Glacier summaries for the four phases of glaciation in the northern Pindus Mountains are shown in Figures 7.30, 7.31 and 7.32. The lowest, most extensive glaciers of the Skamnellian Stage covered over 70 km² on the mountains of Tymphi, Smolikas and Vasilitsa and had a mean ELA of 1700 m a.s.l. This glaciation is correlated with extensive glacier formation elsewhere in Europe during the Middle Pleistocene such as the Elsterian Stage in northern Europe, the Mindelian Stage in the Alps and MIS 12. Glacier ELAs were higher and less extensive during later cold stages. For example, during the Vlasian Stage, equivalent to the later Rissian and Late Saalian Stages, of northern Europe and the Alps (MIS 6), glaciers reached mid-valley positions with a mean ELA of 1910 m a.s.l. and covered a total area of *ca.* 29 km². During the Tymphian Stage, equivalent to the Weichselian and Würmian Stages of northern Europe and the Alps (MIS 5d-2), glaciers were higher and smaller with a mean ELA of 2155 m a.s.l. and a total area of only *ca.* 5 km². In addition, on Mount Tymphi, six rock glaciers formed and reached down to 1800 m a.s.l. Finally, during the Smolikasian Substage, equivalent to the Late-glacial Substage, small glaciers and rock glaciers formed in the highest cirques of Mount Smolikas. The

glaciers had a mean ELA of 2370 m a.s.l. and covered a total area of only 0.43 km². The palaeoclimatic significance of the glacier and rock glacier reconstructions and distributions, at both the local and regional scales, is the focus of the following chapter.

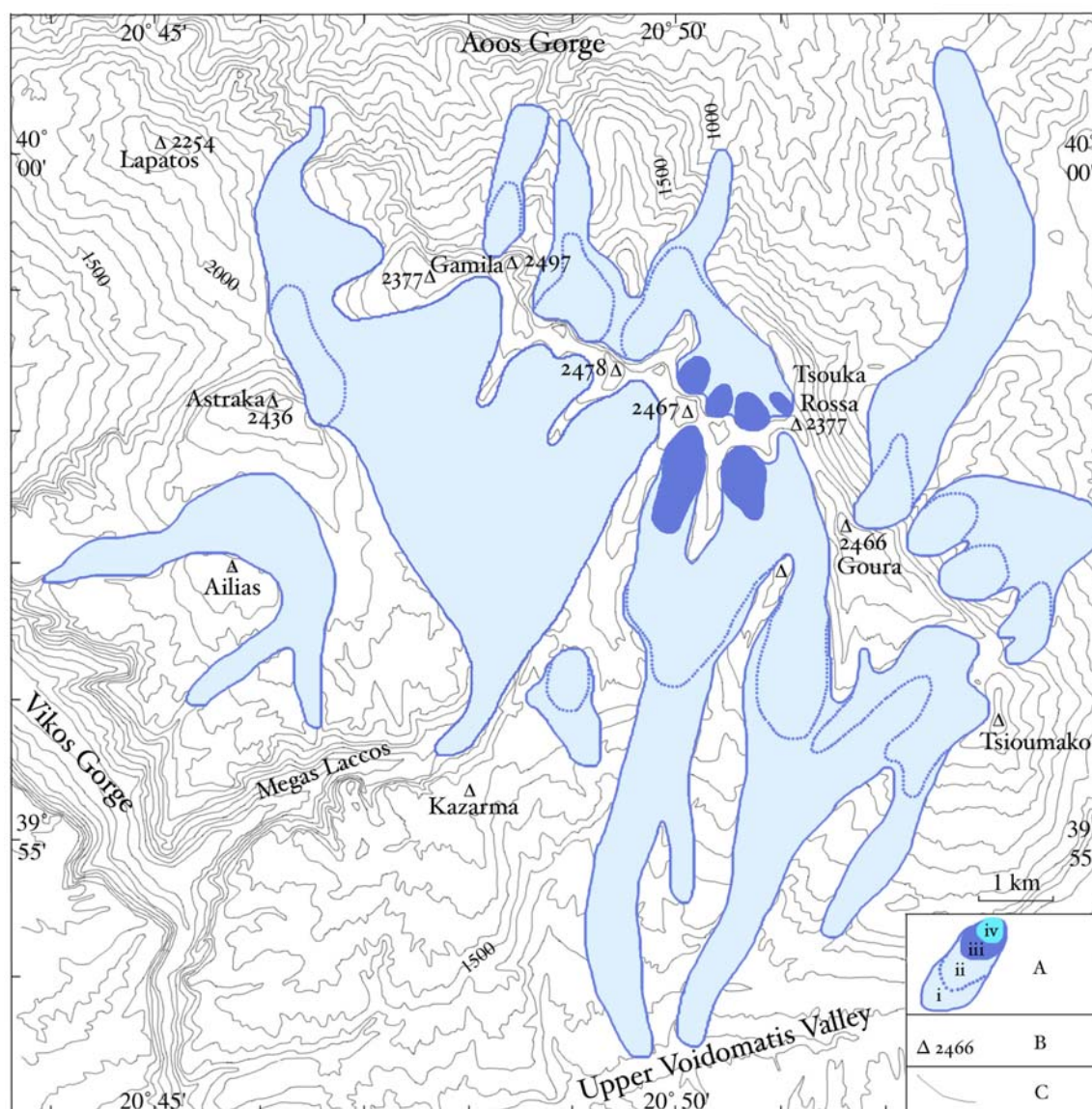


Figure 7.30 Summary of the glacier extent on Mount Tymphi during the Middle to Late Pleistocene. Legend to key: A) i. Skamnellian Stage glacier limits, ii. Vlasian Stage glacier limits, iii. Tymphian Stage glacier limits, iv. Smolikasian Substage glacier limits; B) mountain peak and altitude in metres a.s.l.; C) land surface contour (100 m interval). Rock glaciers are omitted from this map.

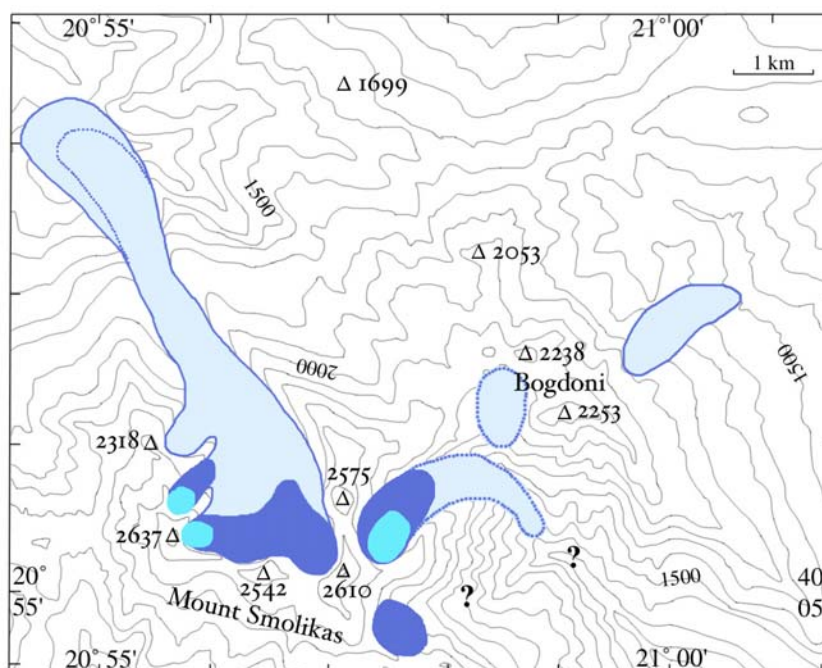


Figure 7.31 Summary of the glacier extent on Mount Smolikas during the Middle to Late Pleistocene. The key is the same as for Figure 7.30. Rock glaciers are omitted from this map.

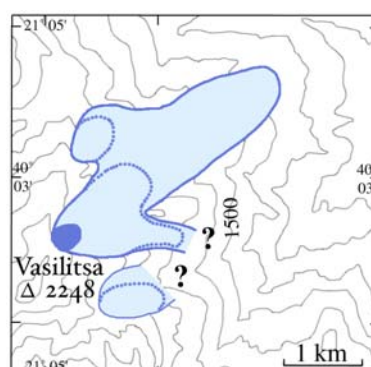


Figure 7.32 Summary of the glacier extent on Mount Vasilitsa during the Middle to Late Pleistocene. The key is the same as for Figure 7.30.

Chapter Eight

Palaeoclimatic Reconstruction and Discussion

In this chapter, glacial climates in Greece are reconstructed using the glacial and periglacial evidence presented in the previous chapters. Glaciers and rock glaciers are powerful tools in palaeoclimatology and this fact is used to provide a new approach to palaeoclimatic study in Greece. Some of the results of this chapter have been published in Hughes *et al.* (2003), and a copy of this paper can be found in Appendix 4.

8.1 Glaciers and climate

Glaciers have a sensitive relationship with climate. The two most important climatic variables are temperature and precipitation. In modern glacial environments, it is well established that a positive relationship exists between temperature and precipitation. This is because higher levels of mass turnover at the ELA require higher ablation, and thus higher summer temperatures to balance the mass budget (Ahlmann 1948, Loewe 1971, Ballantyne 1989, Ohmura *et al.* 1992). The form of this relationship has global application (Nesje and Dahl 2000). The version of Ohmura *et al.* (1992), derived from 70 glaciers worldwide, is used in this study (Fig. 8.1). The relationship between annual precipitation and mean summer temperature at the ELA corresponds to the following polynomial regression curve (Ohmura *et al.* 1992):

$$P = a + bT + cT^2$$

Where **a** = 645, **b** = 296 and **c** = 9, and **P** and **T** are mean annual precipitation (mm) and mean summer temperatures (°C) respectively. The standard error of estimate for this curve is relatively narrow at 200 mm and can be explained as being largely due to different radiation conditions (Ohmura *et al.* 1992).

The Ohmura *et al.* (1992) equation represents the relationship between mean annual precipitation and temperature rather than winter accumulation and temperature. After comparing precipitation and accumulation at glacier ELAs around the world, Ohmura *et al.* (1992) concluded that the winter mass balance (accumulation) comes very close to the mean annual meteorological precipitation on a number of glaciers. They therefore argued that this justified the approximation of the annual precipitation using the winter mass balance. Obviously, discrepancies arise where local inputs, such as wind blown snow and

avalanche accumulation, exert dominance over the mass balance. In such circumstances, the precipitation value derived will be higher than the true meteorological annual precipitation. However, for any reconstructed glacier within a sample, major local inputs will be recognised due to a lower ELA relative to the mean.

Using the Ohmura *et al.* (1992) equation, for any reconstructed former glacier the possible combinations of temperature and precipitation, at the time of maximal extent, can be deduced. However, in order to determine which of these combinations applied to the Pleistocene glaciers in Greece, values for palaeoprecipitation or palaeotemperature are needed in order to determine the other. Either of these inputs can be derived from other contemporaneous evidence, such as that from climatic models based on pollen evidence (*e.g.* Peyron *et al.* 1997, Tzedakis *et al.* 2002) or from associated evidence in the periglacial record, such as rock glaciers (*e.g.* Hughes *et al.* 2003).

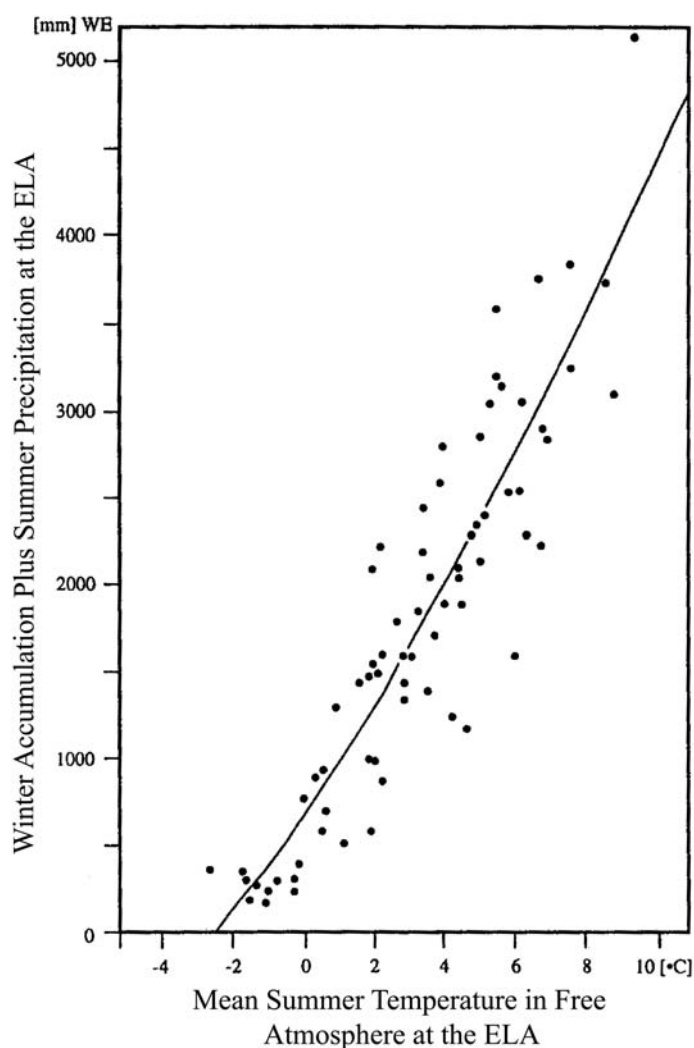


Figure 8.1 Annual total precipitation and the free-atmospheric temperature observed at the ELAs for 70 glaciers worldwide (redrawn from Ohmura *et al.* 1992).

8.2 Rock glaciers and climate

As with glaciers, periglacial rock glaciers are highly sensitive to climate. It is well established that rock glaciers form in areas of discontinuous permafrost, where mean annual temperatures are no higher than *ca.* -2°C . This has been demonstrated in a wide range of mountain environments, including the Swiss and Italian Alps (Barsch 1978, Fisch *et al.* 1977, Belloni *et al.* 1988, Carton *et al.* 1988), as well as in the New Zealand Alps (Brazier *et al.* 1998). Rock glaciers will form at temperatures much lower than -2°C but only where precipitation is sufficiently low to inhibit glacier formation (Haeberli 1982, 1985) (Fig. 8.2). Therefore, rock glaciers would be expected to form below the regional glacier ELA. However, they sometimes form above the regional glacier ELA because rock glacier formation also depends on debris supply exceeding snow accumulation (Humlum 1999). This means that, even where precipitation is adequate for glacier formation, if debris supply is sufficiently large, a rock glacier will form. Nevertheless, in any given region it is likely that the lowest occurrence of rock glaciers will lie close to the limit of permafrost. In areas where this is much lower than the highest mountains, a wide range of rock glacier altitudes may exist contemporaneously. Where the lower limit of discontinuous permafrost lies close to the highest parts of a mountain, rock glacier fronts will often have low altitudinal variation since there is simply not the space to accommodate rock glaciers in

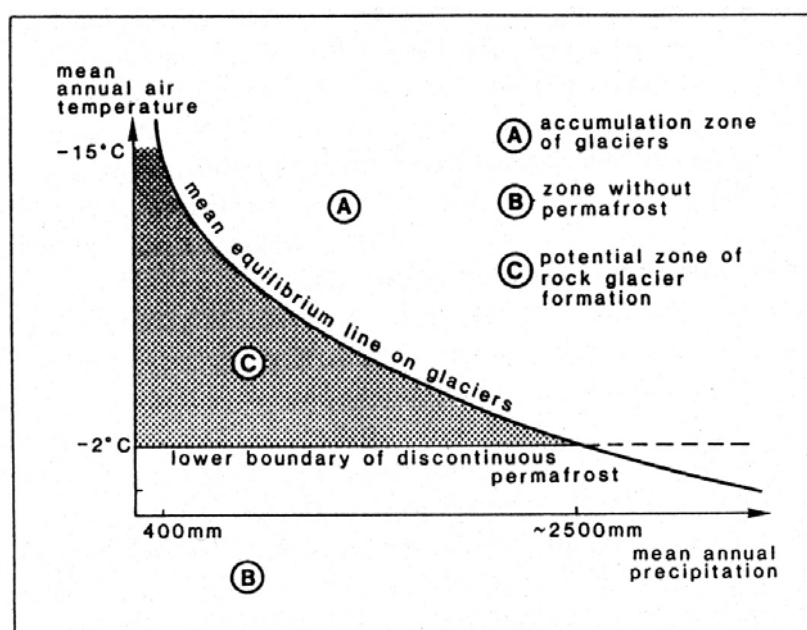


Figure 8.2 Rock glacier - permafrost relationship based on modern rock glaciers in the Alps. The diagram illustrates the fact that rock glaciers tend to form no lower than the lower boundary of discontinuous permafrost and when mean annual precipitation levels are < 2500 mm (after Haeberli 1982, 1985).

areas above the -2°C isotherm. In some cases, rock glaciers may not always occur at the lower limit of the permafrost boundary and may not form at all. Their formation will depend on local debris supply and topographic conditions. However, where there is a strong concentration of rock glaciers at a particular altitude, it is likely that this altitudinal preference is related to the lower limit of the permafrost boundary and the -2°C isotherm.

8.3 Palaeoclimate during the Tymphian Stage

The Tymphian Stage glaciers and rock glaciers are considered first, since the deposits of this stage are well-preserved, and the glacier and rock glacier limits are well-constrained. The Tymphian Stage is equivalent to the Würmian Stage of the Alps and the glacial maximum may have occurred during an interval equivalent to MIS 2 (Chapter Six, Table 6.14).

8.3.1 Local controls on glacier development

The small size of the Tymphian Stage glaciers shows that the climate in Greece at this time was marginal for glacier development. In such conditions, glacier development is often the result of particular local controls, in combination with the prevailing climate. Dominant local controls would have included wind-blown snow, avalanching snow, direct insolation and debris cover. Wind-blown snow and avalanching snow represent accumulative controls whilst insolation and debris cover represent ablative controls. Larger-scale differences between massifs are also likely to influence glacier formation. For example, mountain altitude, distance from the sea, as well as lithological controls, can influence differences in glacier ELAs between neighbouring massifs. All of these factors must be considered when accounting for the variation in glacier characteristics on Mount Tymphi, Mount Smolikas and Mount Vasilitsa.

On Mount Tymphi, six glaciers with a mean ELA of 2174 m a.s.l. occurred together with five groups of rock glaciers, the latter with a lowermost altitude of 1800 m a.s.l. (Tables 7.7 and 7.8). The standard deviation from the mean ELA of the six glaciers was only 43 m and the range of glacier ELAs was only 100 m. Aspect appears to have had little influence on glacier ELAs. As a result, few patterns of local variability are apparent - not even between north- and south-facing glaciers. However, the lowermost glacier, the Megalon Litharion glacier (ELA: 2100 m a.s.l.), is a southeast-facing glacier and would have been shaded from afternoon sunshine by the Krevati cliffs, a ridge on its western side

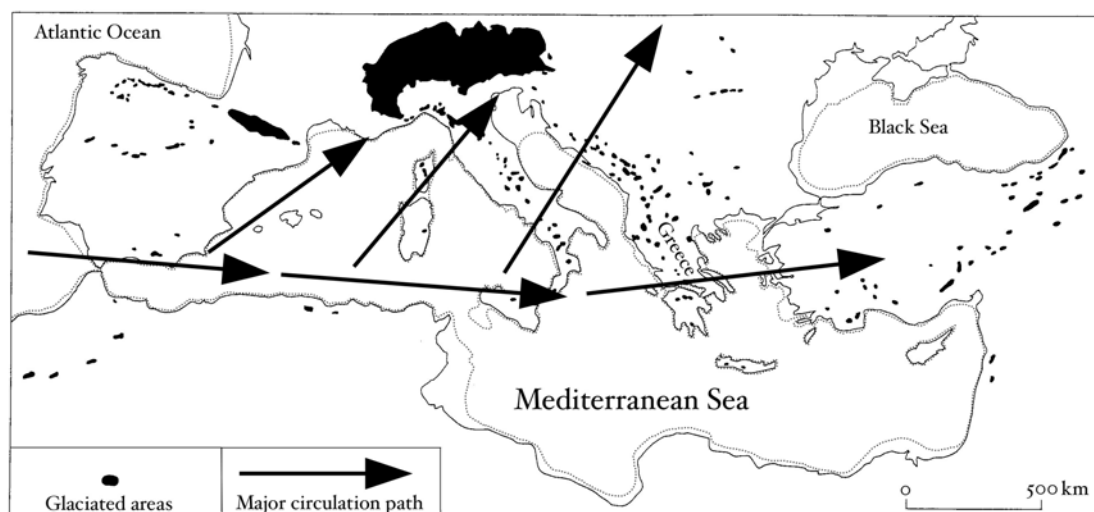


Figure 8.3 Map of the Mediterranean showing the dominant air circulation paths during the last glacial period. Airflow and the passage of depressions would have been west to east through the Mediterranean basin, diverting northeastwards over the Alps and eastern central Europe. In Greece, the dominant track of depressions would have been from the west to south west. Lower glacial sea levels are depicted by a broken line (from Florineth and Schlüchter 2000).

(Fig. 7.26). In addition, assuming prevailing winds were westerlies (*cf.* Florineth and Schlüchter 2000) (Fig. 8.3), this broad ridge would have also been the source of significant wind-blown snow.

The distribution of snow patches indicated by pronival ramparts further illustrates the influence of local factors, especially avalanche (Shakesby *et al.* 1999). In the Vourtopa valley, perennial snow patches existed at *ca.* 1800-1850 m a.s.l. at the base of the steep cliffs of the Tsoukoula ridge (Fig. 4.15 and 4.22). Avalanche input is likely to have contributed to these snow patches, enabling their formation over 300 m below the mean ELA of the cirque glaciers. Perennial snow patches also occurred at much lower altitudes at the base of the 1000 m-high northeast-facing cliffs of Goura (2466 m a.s.l.). These snow patches formed at elevations as low as 1350 m a.s.l., over 800 m lower than the ELA of cirque glaciers at this time. Here, avalanche is again likely to have been important, although shading would have also been a major contributory factor in the formation of these snow patches (Fig 8.4).

On Mount Smolikas, the five Tymphian Stage glaciers had a mean ELA of 2241 m a.s.l. The standard deviation from this mean was 97 m and the range of ELA values was 215 m, much higher than on Mount Tymphi. Three of the glaciers were north-facing and two east-facing (Fig. 7.27). Surprisingly, two of the north-facing glaciers were the highest on Mount Smolikas. It can therefore be concluded that, as was the case on Mount Tymphi, aspect and insolation were not major controls on glacier distribution. It is probable that accumulative inputs, such as avalanche and wind-blown snow, were more important than

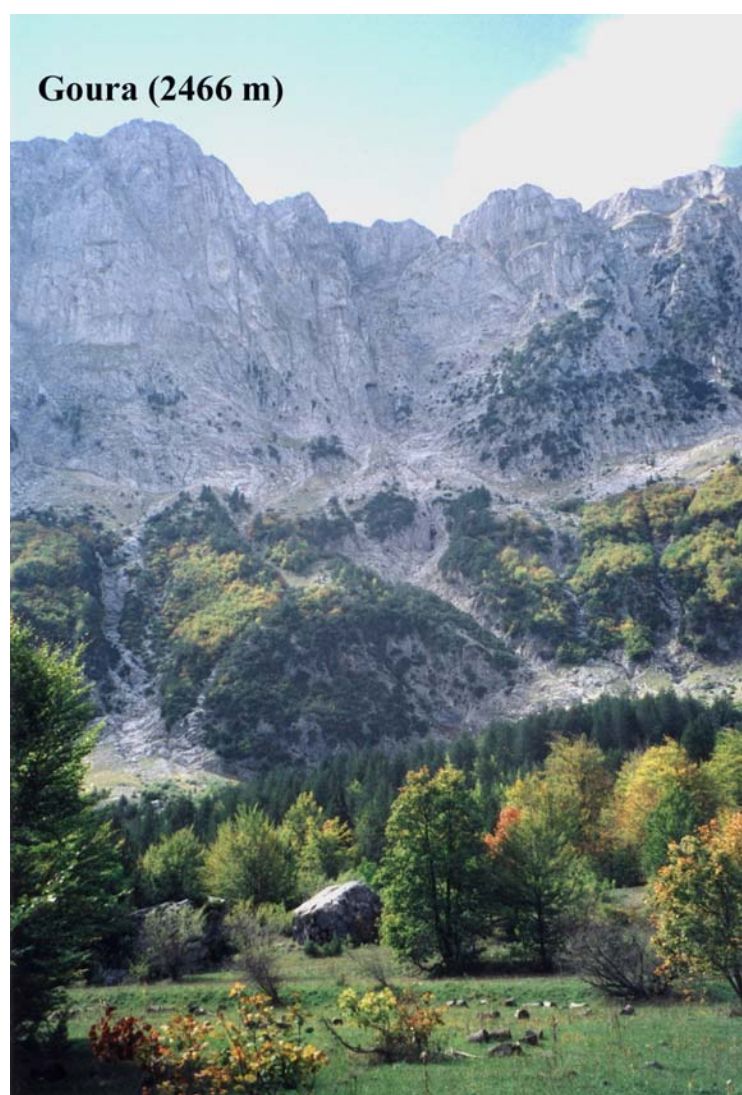


Figure 8.4 The northeast-facing cliffs of Goura (2466 m a.s.l.) at the head of the Maghoula valley. Avalanche and shading would have promoted the development of pronival ramparts at the base of these cliffs during the Tymphian Stage, and low-lying glaciers during earlier glacial stages.

local ablative controls. Indeed, on Mount Smolikas, the lowest northern glacier and the eastern glaciers were bounded to the west by broad, rounded ridges which were potential sources of wind-blown snow by prevailing westerlies.

On Mount Vasilitsa, only one glacier formed during the Tymphian Stage (Fig. 7.28). This glacier had an ELA of 2050 m a.s.l., nearly 200 m lower than the mean of the glaciers on Mount Smolikas and over 100 m lower than the mean for the glaciers on Mount Tymphi. The Vasilitsa glacier lay in the lee of prevailing winds on the northeastern slopes of the rounded summit of Mount Vasilitsa. Both low insolation and wind-blown snow accumulation probably contributed to the formation of this glacier at an altitude lower than any other glacier on Mount Smolikas and Mount Tymphi.

In terms of inter-mountain variability, the Mount Smolikas glaciers were slightly higher than those on Mount Tymphi. The main reason for this was probably the lower

precipitation during the maximum extent of the Tymphian Stage glaciation on Mount Smolikas, compared to Mount Tymphi. This is the case today where mean annual precipitation at Pades (1170 m a.s.l.) at the foot of Mount Smolikas is 1247 mm, whilst at Skamnelli (1180 m a.s.l.) on Mount Tymphi, on a similar slope with respect to prevailing westerlies, mean annual precipitation is 1721 mm. This difference can be attributed to the more easterly, inland position of Mount Smolikas. Moreover, lithology may have some control during marginal phases of glaciation. On Mount Tymphi, karstic hollows (dolines) favour snow accumulation in comparison to the generally smooth surface morphology on ophiolitic rocks. The bright colour of the limestone on Mount Tymphi is likely to have enhanced the albedo of debris cover on the former glaciers compared with the very dark, ophiolite lithology on Mount Smolikas. Lithology is also likely to be a major factor in the development of rock glaciers, since the well-jointed limestones of Mount Tymphi are far more susceptible to frost shattering than the massive ophiolites of Mount Smolikas and Mount Vasilitsa. This may explain the absence of rock glaciers on the latter two mountains at a time when six rock glaciers formed on Mount Tymphi. The lowest Tymphian Stage glacier occurred on Mount Vasilitsa, even though this area was likely to have received the least precipitation of all three mountains. Thus, the effects of wind-blown snow accumulation combined with low insolation are likely to have enabled a low glacier altitude. This emphasises the importance of local factors at individual sites and, in marginal conditions, local factors may be more important than regional trends.

8.3.2 Palaeotemperature reconstruction

On Mount Tymphi, six rock glaciers were mapped and assigned to the Tymphian Stage (Chapter Four). The rock glaciers of Tymphi all occurred no lower than 1800 m a.s.l. In the Tsouka Rossa cirque, they formed below cirque glacier moraines, and it is likely that all of the rock glaciers were coeval with the most recent small cirque glaciers on Mount Tymphi (Fig 7.26). The altitudes of the Mount Tymphi rock glaciers are similar to others identified in Greece on Mount Parnassus, *ca.* 200 km to the southeast, which has its terminus just beneath the 2000 m contour (Pechoux 1970). If these rock glaciers are contemporaneous, they imply that similar climatic conditions prevailed throughout the Pindus range at this time.

The reconstructed temperature at the lowest altitude of the relict rock glaciers (*ca.* 1800 m a.s.l.) can be compared to modern-day mean annual temperatures. At nearby Ioannina, at an altitude of 484 m a.s.l., the modern mean annual temperature is 14.3°C with mean January and July temperatures of 4.6°C and 24.8°C, respectively (World

Meteorological Organisation 1998). During the Tymphian Stage, if the mean annual temperature at 1800 m was *ca.* -2°C , at 484 m a.s.l. (the altitude of the Ioannina meteorological station) the mean annual temperature would have been *ca.* 5.9°C , assuming a lapse rate of 0.6°C per 100 m altitude. This implies an 8.4°C depression of mean annual temperature compared with the present, at the time of rock glacier formation. However, this is derived using a standard lapse rate for the troposphere (Barry and Chorley 1996, Whiteman 2000), and a range of environmental lapse rates are possible under periglacial conditions. As a result, temperature reconstructions can only be viewed as approximate.

8.3.3 Palaeoprecipitation

As well as providing information on palaeotemperatures, the presence of rock glaciers indicates a continental climate where precipitation values do not exceed 2500 mm (Haeberli 1985, Belloni *et al.* 1988). If precipitation levels were too high, glaciers would form. Glaciers often form at higher altitudes than rock glaciers, where temperatures are lower, offsetting low rates of accumulation. This is the reason why glaciers on Mount Tymphi provided the moraine 'root' from which the rock glacier in the Tsouka Rossa cirque formed (Fig 7.26). The fact that small cirque glaciers existed above the Tsouka Rossa rock glacier and in the uppermost reaches of the Laccos Tselon and Laccos Megalon Litharion valleys indicates that, whilst precipitation must have been low enough to preclude glacier extension down to lower altitudes, it was not so low as to inhibit ice build-up entirely. This is illustrated by the fact that tree pollen is preserved in sediments spanning the entire last glacial stage at Ioannina (Tzedakis 1993).

The palaeotemperature reconstruction derived from the relict rock glaciers can be used to determine palaeoprecipitation values by applying the 8.4°C temperature depression to the modern mean summer temperature. This can then be extrapolated to the ELA of contemporaneous glaciers during the Tymphian Stage, enabling the calculation of the corresponding precipitation value, as defined by the Ohmura *et al.* (1992) equation. The Mount Tymphi cirque glaciers had a mean ELA of 2174 m a.s.l. The mean summer temperature (June/July/August) at Ioannina (484 m a.s.l.) is 23.6°C (Chapter 2, Table 2.1). Therefore, at the mean ELA of the Tymphian Stage cirque glaciers, the modern mean annual temperature would be *ca.* 13.5°C , assuming a standard lapse rate of 0.6°C per 100 m. A depression of 8.4°C during the Tymphian Stage implies that the mean summer temperature at the ELA of the former cirque glaciers would have been *ca.* 5.1°C . Using the Ohmura *et al.* (1992) equation, a mean summer temperature of 5.1°C corresponds with an annual precipitation of *ca.* $2387 \text{ mm} \pm 200 \text{ mm}$. Given that the range of ELAs on Mount

Tymphi was narrow, it is likely that local accumulative inputs by avalanche and wind-blown snow would have been small, and glaciers are likely to have been close to the meteorological ELA, *i.e.* the altitude where annual precipitation input is balanced by summer temperatures. To allow this precipitation reconstruction to be compared with modern values, an estimate of precipitation at 2174 m a.s.l., the ELA of the former cirque glaciers, is required.

The modern precipitation gradient can be calculated on Mount Tymphi, where two meteorological stations at Skamnelli (39°55', 20°51', 1180 m a.s.l.) and Kipi (39°51', 20°48', 790 m a.s.l.) are only 6.5 km apart. The modern mean annual precipitation at Skamnelli is 1721 mm, whilst at Kipi it is 1508 mm (Fotiadi *et al.* 1999). The precipitation gradient is therefore *ca.* 55 mm per 100 m altitude - a gradient also recorded between other neighbouring meteorological stations in Epirus, such as between those at Fourka and Pournia on Mount Smolikas (*cf.* Fotiadi *et al.* 1999).

Using a precipitation gradient of 55 mm per 100 m altitude, the modern precipitation at the ELA of the former glaciers on Mount Tymphi (2174 m a.s.l), is probably *ca.* 2263 mm, given that at Skamnelli (1180 m a.s.l) modern precipitation is 1721 m a.s.l. Therefore, if the modern precipitation value at 2174 m a.s.l. is *ca.* 2263 mm, the reconstructed precipitation value for the Tymphian Stage glacial maximum (2387 mm \pm 200 mm) was similar to that of the present-day.

The palaeoprecipitation reconstruction presented here is based on the assumption that the mean annual temperature depression is mirrored equally in the mean monthly temperatures across the year. This would not have been the case if the modern amplitude of the mean annual temperature curve was different to that which occurred during the Tymphian Stage. This possibility, and the effects on the palaeoprecipitation reconstruction, is investigated in the next section.

8.3.4 Palaeoprecipitation - the importance of annual palaeotemperature range

A more sophisticated approach to that described above is to allow for winter temperature depressions to be lower than summer depressions relative to modern values and *vice-versa*. In order to do this, the mean annual temperature was distributed over the months of the year using different amplitude sinusoidal curves. Figure 8.5 shows the modern mean monthly temperature distribution at Ioannina beside a sinusoidal curve with the same range and tied to the same minimum temperature. Whilst there is a slight discrepancy in the spring and early summer months, a sinusoidal distribution best describes the Ioannina monthly

temperature distribution, as do the records at most other sites around the world. This approach permits more detailed insight into not just temperature-precipitation relationships, but also temperature ranges between the coldest and warmest months.

The temperature at the foot of the lowest rock glaciers was extrapolated to the altitude of the highest contemporaneous glaciers. The mean annual temperature of -2°C , at the foot of the former rock glaciers (*ca.* 1800 m a.s.l.), corresponds to a temperature of -4.2°C at the ELA of the highest glaciers ELA at 2174 m a.s.l. using the standard atmospheric lapse rate of $0.6^{\circ}/100$ m. This mean annual temperature was distributed over mean annual ranges of 10 to 30°C on a sinusoidal mean monthly temperature curve. The derived mean summer temperature (June/July/August) and associated annual precipitation combination based on the relationship defined in Ohmura *et al.* (1992) are shown in Table 8.1.

A mean annual temperature of -4.2°C at the mean ELA of the former cirque glaciers (2174 m a.s.l.), distributed over an annual mean monthly temperature range of 20°C , results in precipitation of >2500 mm. This would have been the case even at the lowest altitude of the former rock glaciers (1800 m a.s.l.) assuming a precipitation gradient similar to today of 55 mm per 100 m. Therefore, given that rock glaciers rarely form in areas where precipitation exceeds 2500 mm (Haeberli 1985) (Fig. 8.3), the actual annual mean monthly temperature range must have been no higher than *ca.* 20°C . If the temperature range was similar to the modern temperature range of 20°C , then a reconstructed precipitation value of 2300 ± 200 mm is derived for the Tymphian Stage glacial maximum. This is similar to the value of 2387 ± 200 mm derived in section 8.3.3 because the modern Ioannina temperature record closely approximates the sinusoidal curve used here (Fig. 8.5). A lower temperature range than today is unrealistic, especially since a more continental climate was likely with sea levels *ca.* 120 m lower (*cf.* Lambeck 1995) resulting in Mount Tymphi being *ca.* 30 km further inland during the last cold stage.

In Chapter Seven (section 7.1.8), it was argued that lower sea levels at *ca.* 21,000, and subsequent uplift, result in reconstructed ELAs underestimating the real ELA by 104 - 112 m. Nevertheless, this does not affect the temperature calculation at the lowest point of the former rock glaciers. It also does not affect any extrapolation of temperature to different altitudes, assuming that uplift between extrapolated points has been uniform. Only when extrapolations are to modern sea level, will comparisons with modern-day values be flawed. This has not been attempted here.

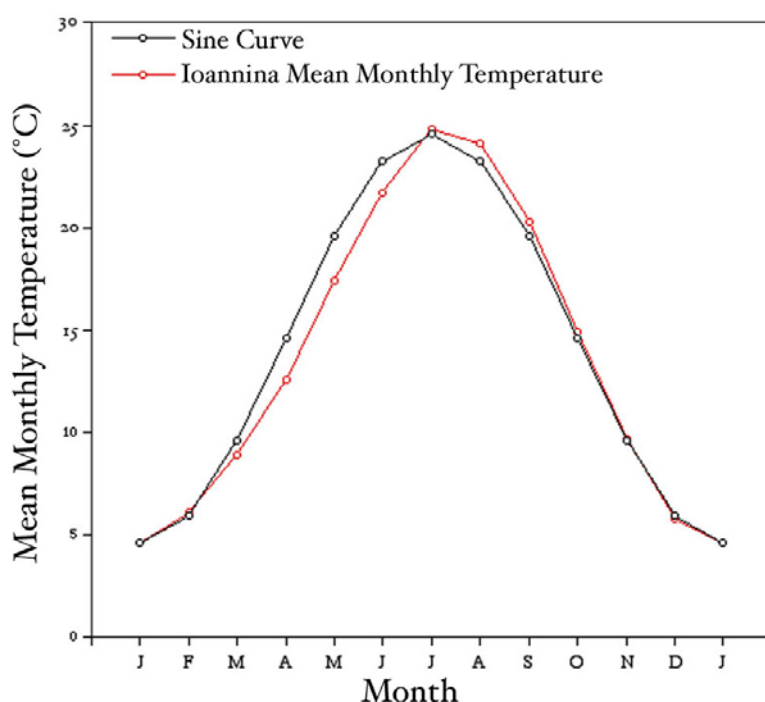


Figure 8.5 Mean monthly temperatures distributed over the year using the modern mean monthly temperatures at Ioannina (World Meteorological Organisation 1998) and a sinusoidal curve with the same range tied to the same minimum temperature. It is clear that the modern Ioannina temperature distribution closely approaches a sinusoidal curve, with only a slight discrepancy in the spring and early summer months.

<i>Mean annual temperature</i>	<i>Annual range</i>	<i>Mean summer temperature</i>	<i>Coldest month mean</i>	<i>Warmest month mean</i>	<i>Annual precipitation</i>
-4.2°C	30°C	9.46°C	-19.20°C	10.80°C	4251 mm
-4.2°C	27.5°C	8.29°C	-17.98°C	9.52°C	3717 mm
-4.2°C	25°C	7.18°C	-16.70°C	8.30°C	3234 mm
-4.2°C	22.5°C	6.00°C	-15.5°C	7.00°C	2745 mm
-4.2°C	20°C	4.87°C	-14.24°C	5.76°C	2300 mm
-4.2°C	17.5°C	3.77°C	-12.95°C	4.55°C	1889 mm
-4.2°C	15°C	2.63°C	-11.70°C	3.30°C	1486 mm
-4.2°C	12.5°C	1.49°C	-10.45°C	2.05°C	1106 mm
-4.2°C	10°C	0.35°C	-9.20°C	-0.80°C	750 mm

Table 8.1 Palaeoclimatic combinations reconstructed at the mean ELA of the last cirque glaciers on Mount Tymphi (2174 m a.s.l.). The values in bold represent the most likely combination for the glacial maximum of the Tymphian Stage (see text for details). Annual precipitation was reconstructed using the equation of Ohmura *et al.* (1992).

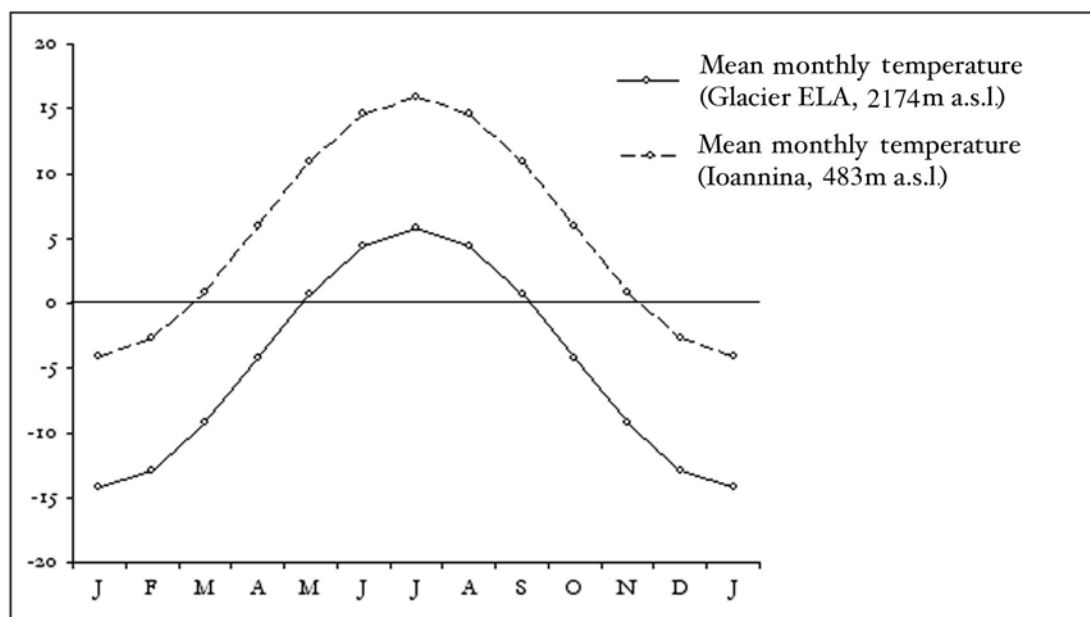


Figure 8.6 Mean monthly temperature distribution at 2174 m a.s.l. on Mount Tymphi during the Tymphian Stage based on a 2300 mm annual precipitation. The top curve shows the temperature distribution extrapolated to the altitude of Ioannina (484 m a.s.l.) for the same period.

In summary, precipitation at 2174 m a.s.l. during the LGM would have been *ca.* 2300 ± 200 mm, derived by applying a range of 20°C to a mean annual temperature of minus 4.2°C . This suggests that mean annual precipitation was similar to that of today. Higher temperature ranges result in precipitation values well above that considered maximum for rock glacier formation, even at altitudes as low as 1800 m a.s.l., the minimum altitude of the rock glaciers on Mount Tymphi. The only possible situation that would result in lower precipitation values than those of today is if the annual temperature range was less than 20°C . This is unlikely given that the modern range is 20°C and that a more continental climate would have existed at this locality during glacial phases. The best compromise is, therefore, a palaeoprecipitation reconstruction derived under an annual temperature range of 20°C . A summary of the climate at the ELA of the former glaciers of Mount Tymphi (2174 m a.s.l.) and Ioannina (483 m a.s.l.) during the LGM is illustrated in Figure 8.6.

8.3.5 The Smolikasian Substage

The highest glacial and periglacial deposits on Mount Smolikas post-date the Tymphian Stage glacial maximum and are assigned substage status under the name Smolikasian Substage. These deposits are found in four localities and are interpreted as small cirque glacier deposits and a rock glacier (Fig. 7.29).

The mean ELA of the three Smolikasian Substage glaciers was 2372 m a.s.l. The lowest glacier, with an ELA of 2275 m a.s.l., occurred in the Galanos Limni cirque, on the northeast of Moasa (2610 m a.s.l.). It is likely that the ELA of this glacier was depressed by leeward wind-blown snow accumulation from prevailing westerly winds and low insolation due to the easterly aspect. The next lowest glacier, the Cirque 2 glacier, in the upper Vadulakkos valley, also formed in the lee of a broad western ridge (Mount Smolikas summit). The ELA of this east-facing glacier is also likely to have been depressed due to wind-blown snow and low insolation. Conversely, the highest glacier, formed in a position open to prevailing westerlies in the northwestern cirque of Moasa (2610 m a.s.l.) and was probably prone to wind deflation.

The sole rock glacier of Mount Smolikas formed in the Northwestern Cirque and reached down to 2160 m a.s.l., 160 m higher than the highest rock glaciers on Mount Tymphi during the Tymphian Stage. In this cirque, debris accumulation is likely to have been greater than snow accumulation, resulting in the downslope movement of debris by permafrost creep. The formation of a rock glacier during the Smolikasian Substage is of major significance. It shows that the lower limit of discontinuous permafrost and the -2°C isotherm occurred down to at least 2160 m a.s.l. Whether or not the position of this isotherm and the limit of discontinuous permafrost was lower than 2160 m a.s.l. is difficult to ascertain given the small sample of relict rock glaciers. However, the absence of equivalent features in the stratigraphical record on Mount Tymphi suggests that the lower limit of discontinuous permafrost was above cirque floor altitudes, the highest of which occur at *ca.* 2100 m a.s.l.

Assuming that the lowest part of the Mount Smolikas rock glacier (2160 m a.s.l.) corresponds with the lower limit of discontinuous permafrost and the -2°C isotherm, then it implies that temperatures were *ca.* 2.2°C warmer than during the coldest part of the Tymphian Stage. It also implies a temperature depression of 6.2°C compared with today when extrapolated to Ioannina (484 m a.s.l., mean annual temperature: 14.3°C) using a lapse rate of 0.6°C per 100 m. However, since there is a possibility that the limit of discontinuous permafrost was lower than the lowest part of the Northwestern Cirque rock glacier, this is a minimum value.

The ELAs of the three cirque glaciers were all higher than the lowest part of the rock glacier in the Northwestern Cirque, and two of the glaciers had ELAs higher than the highest parts of the rock glacier. This is consistent with greater accumulation at higher altitudes as a result of lower temperatures. Assuming that the rock glacier formed contemporaneously with the glaciers, a minimum mean annual temperature of -2°C at 2160

m a.s.l. can be used to reconstruct precipitation values at the ELAs of the former glaciers. This was done in much the same way as for the Tymphian Stage glaciers. However, given the wide variation in glacier ELAs during the Smolikasian Substage, the temperature of -2°C was extrapolated to the altitude of the highest glacier, the Cirque 3 glacier (2425 m a.s.l.), using a lapse rate of 0.6°C per 100 m. This glacier was used because the relationship between accumulation and temperature most likely reflects that between meteorological precipitation and temperature. The extrapolated mean annual temperature of -3.6°C at 2425 m a.s.l. was then distributed over a sinusoidal curve with mean maxima and minima monthly temperature ranging from 10 to 30°C . The results are shown in Table 8.2.

In common with the Tymphian Stage reconstruction, temperature ranges greater than 20°C result in high summer temperatures and precipitation values much greater than 2500 mm at 2425 m a.s.l. Therefore, given that rock glaciers rarely form where precipitation exceeds 2500 mm (Haeberli 1983, 1985), it is unlikely that the annual temperature range was greater than *ca.* 20°C . However, precipitation levels were probably slightly lower at the altitude of the rock glacier in the Northwestern Cirque (2160 - 2400 m a.s.l.). This suggests that the rock glacier occurred close to the threshold conditions, in terms of both moisture supply and temperature, for rock glacier formation.

The modern mean annual temperature range at Ioannina is 20°C , and as argued for the Tymphian Stage, lower temperature ranges than today are unlikely given that sea levels

<i>Mean annual temperature</i>	<i>Annual range</i>	<i>Mean summer temperature</i>	<i>Coldest month mean</i>	<i>Warmest month mean</i>	<i>Annual precipitation</i>
-3.6°C	30°C	10.06°C	-18.60°C	11.40°C	4534 mm
-3.6°C	27.5°C	8.92°C	-17.35°C	10.15°C	4001 mm
-3.6°C	25°C	7.76°C	-16.12°C	8.88°C	3484 mm
-3.6°C	22.5°C	6.65°C	-14.10°C	7.65°C	3011 mm
-3.6°C	20°C	5.49°C	-13.62°C	6.38°C	2541 mm
-3.6°C	17.5°C	4.37°C	-12.35°C	5.15°C	2110 mm
-3.6°C	15°C	3.21°C	-10.62°C	3.88°C	1688 mm
-3.6°C	12.5°C	2.29°C	-9.69°C	2.87°C	1370 mm
-3.6°C	10°C	0.91°C	-8.30°C	1.36°C	922 mm

Table 8.2 Palaeoclimatic combinations reconstructed at the highest ELA of the last cirque glaciers on Mount Smolikas (2475 m a.s.l.). The values in bold represent the most likely combination for the glacial maximum of the Smolikasian Substage (see text for details). Annual precipitation was reconstructed using the equation of Ohmura *et al.* (1992).

would have been lower at this time. Therefore, given the discussion in the previous paragraph, the temperature range during the Smolikasian Substage is likely to have been similar to that of today, *i.e.* 20°C. This also implies precipitation levels *ca.* 2541 mm at 2475 m a.s.l. (Table 8.2). Based on a modern precipitation gradient of 55 mm per 100 m altitude (section 8.3.3) and mean annual precipitation of 1391 mm at Fourka (1350 m a.s.l.) (Fig. 2.4), the modern precipitation at 2475 m a.s.l. is estimated at *ca.* 1950-2000 mm. Therefore, during the Smolikasian Substage, precipitation values would have been slightly higher than the estimated modern value. However, given the uncertainties involved in these reconstructions, it is best to take a broad interpretation, *i.e.* that precipitation values were over 2000 mm and perhaps similar to, if not a little higher, than modern extrapolated values during the Smolikasian Substage.

8.3.6 Limitations of the palaeoclimate reconstructions

Potential limitations in the palaeotemperature and palaeoprecipitation reconstructions and the comparison with modern climate include:

- 5) altitudinal temperature gradients may be different to 0.6°C per 100 m altitude since a wide range of gradients (0.5-0.8°C per 100 m) are known under periglacial climates (Ballantyne, *personal communication*);
- 6) the modern precipitation gradient may increase exponentially with altitude;
- 7) the mean annual temperature distribution may have not been sinusoidal and;
- 8) the rock glaciers used to derive the palaeotemperatures may not have been contemporaneous with the glaciers used to derive the palaeoprecipitation.

The problem of lapse rates cannot be easily resolved. Therefore temperature and associated precipitation reconstructions should be considered as approximations, even where seemingly precise values are given.

The problem of modern precipitation gradients cannot be resolved until meteorological measurements are taken at high altitudes. However, this does not alter the reconstruction, only the difference in precipitation relative to modern values.

The assumption of a sinusoidal mean monthly temperature distribution is supported by sinusoidal distributions for most climatic stations around the world, in both maritime and continental localities. Moreover, as noted in the earlier palaeotemperature discussion, modern mean monthly temperature distributions at Ioannina closely match a sinusoidal distribution (Fig. 8.5).

Finally, the possibility that the rock glaciers did not form contemporaneously with the glaciers should not affect the temperature assumptions. If the rock glaciers formed

during glacier retreat, it is likely that this was associated with increased aridity and not increased temperatures. Since the relict rock glaciers are found outside of, and lower than, the Tymphian Stage glacial deposits, their lower boundary represents the lowest limit of discontinuous permafrost and the -2°C isotherm during the last cold stage. Therefore, even if the rock glaciers do post-date the glaciers, it is very unlikely that conditions were colder during the maximum extent of the cirque glaciers.

8.4 Palaeoclimate during the Vlasian Stage

The Vlasian Stage spans the period between the Zitsa and Metsovon Interglacials in the Ioannina sequence and correlates with MIS 6 (*cf.* Tzedakis 1994) corresponding with the interval between *ca.* 190-127,000 calendar years BP (Lowe and Walker 1997, Fig. 1.1., Tzedakis *et al.* 2002). This interval was characterised by a period of extensive glaciation in Northern Europe during the Drenthe Stadial of the Saalian glacial Stage (Ehlers 1996).

8.4.1 Local controls on glacier development

On Mount Tymphi, fourteen glaciers existed during the Vlasian Stage. Four glacier groups were identified and the mean group ELA was 1862 m a.s.l. at the glacial maximum (Table 7.4). These glacier groups had widely differing ELAs, ranging from 1628 m to 2005 m a.s.l., and this range can largely be attributed to spatial variation in local factors.

The lowest glaciers were those which formed at the base of the 1000 m northeast-facing cliffs of Goura (2466 m a.s.l.) (Group B). These had a particularly low group mean of 1628 m a.s.l., and no glaciers are found at comparable altitudes anywhere else on Mount Tymphi. The Goura cliffs would have provided glaciers with ample shade and also considerable avalanche input, and this is evidenced today where snow patches exist at the base of these cliffs until June; long after snow has melted on higher slopes.

The glaciers on the north side of the main Mount Tymphi watershed (Group A) were the highest of the Vlasian Stage. This is unusual given that north-facing glaciers would be expected to be lower than those which faced south. This suggests that aspect had little effect on glacier distribution apart from when combined with other local inputs such as avalanche input such as below the cliffs of Goura (see above). Aspect also did not appear to influence glacier distribution on Mount Tymphi during the Tymphian Stage. This may have been due to: a) the effects of snow accumulation in karstic hollows on windward slopes and; b) structural controls on topography. The second point is particularly important since the northern slopes of Mount Tymphi are characterised by a steep, faulted escarpment, whilst the southern slopes are relatively gentle in comparison, resulting in

ample accommodation space. More importantly, these relatively gentle southern slopes promote the first point, *i.e.* karstic hollows for snow accumulation. It is likely, therefore, that a karstic landscape played a key role in glacier development and has been noted elsewhere such as in the Picos de Europa of Spain (Smart 1986) and the Algerian Djurdjura (Barbier and Cailleux 1950).

Elsewhere on Mount Tymphi, an interesting paradox occurs at the Xeroloutsa glacier. This glacier had a lower ELA during the Vlasian Stage than that reconstructed for the more extensive Skamnellian Stage ice-field (Table 7.4). The Vlasian Stage Xeroloutsa glacier probably existed as a result of preferential local conditions such as avalanche and shading at the base of the steep north facing cliffs of Astraka. The earlier Skamnellian stage ice-field covered the plateau between the peaks of Astraka (2436 m a.s.l.) and Gamila (2497 m a.s.l.) and would have had few local benefits (*i.e.* shade, avalanching/ wind-blown snow catchment) in proportion to its size. Apart from in favoured localities such as at Xeroloutsa, much of the snow that fell on this plateau would have been redistributed by wind, thus limiting accumulation to depths insufficient to form glacier ice. This case further highlights the importance of local factors in glacier development in this area.

On Mount Smolikas, there is evidence for only three glaciers during the Vlasian Stage with a mean ELA of 1997 m a.s.l. (Table 7.5). The two glaciers on the eastern side of Mount Smolikas, the Konkutino and Bogdoni glaciers, had similar ELAs (2060 and 2040 m a.s.l. respectively), higher than for the Vadulakkos glacier on the northern slopes (ELA: 1890 m a.s.l.). The Bogdoni glacier faced south over the whole of its area, yet was lower than the Konkutino glacier which faced northeast in the accumulation area and veered to the south only in the lower part of the ablation area (Fig. 7.22). The lower altitude of the Bogdoni glacier was probably due to the presence of an extensive plateau to the west, and prevailing westerly winds would have potentially blown large amounts of snow onto the glacier. This was not the case to the west of the Konkutino glacier which was bordered by sharper topography. The lowest glacier, the Vadulakkos glacier faced north (Fig. 7.21). It is therefore tempting to invoke an aspect control on the low ELA. However, as evidenced with the Bogdoni glacier, the role of aspect is sometimes outweighed by wind-blown snow input. The Vadulakkos glacier would have also had a large potential wind-blown snow and avalanche catchment from the highest parts of Mount Smolikas where precipitation would have been greatest.

On Mount Vasilitsa, three glaciers with a mean ELA of 1865 m a.s.l. existed during the Vlasian Stage and formed in the lee of prevailing winds on the northeastern slopes (Fig. 7.24). These glaciers occurred at a similar altitude to the Mount Tymphi glaciers and were

lower than all of those on Mount Smolikas. Since precipitation on Mount Vasilitsa was unlikely to have greater than on Mount Smolikas, it is probable that low insolation and wind-blown snow accumulation were key to the formation of these glaciers.

Inter-mountain comparisons reveal other interesting differences. For example, on Mount Smolikas at this time, glaciers were much smaller and *ca.* 130 m higher than on Mount Tymphi. The higher ELAs and smaller glacier areas probably reflect lower precipitation on Mount Smolikas, as well as topographic controls on accommodation space. Precipitation is presently lower on Mount Smolikas than on Mount Tymphi due to its more inland position. Moreover, it is likely that precipitation gradients were stronger during glacial climates since, unlike during warm interglacial conditions, a cold glacial landmass would not sustain strong convective tropospheric airflow. In addition, the ophiolite landscape of Mount Smolikas would have provided less locally-complex topography than the karstic limestone terrain of Mount Tymphi, therefore inhibiting accumulation. The limestone bedrock of Mount Tymphi is also well-jointed and more prone to shattering than the massive ophiolite of Mount Smolikas, and would have supplied greater amounts of debris to former glacier surfaces, thus inhibiting ablation and allowing lower ELAs (*cf.* Clark *et al.* 1994).

8.4.2 Palaeotemperature and palaeoprecipitation reconstruction

Equilibrium line altitudes were lower during the Vlasian Stage glacial maximum compared to those during the equivalent phase of the Tymphian Stage. This implies that either precipitation was higher or summer temperatures lower, or both, during the Vlasian Stage glacial maximum.

The former glaciers of Mount Tymphi were used for climatic reconstruction to enable direct comparison with climatic reconstructions for the Tymphian Stage. The mean group ELA of the Vlasian Stage glacier groups was taken as representing the closest representation of the regional climatological ELA. Lower glaciers were likely to have received considerable extra accumulation from wind-blown snow and avalanches, well above that provided by precipitation, whilst the highest glaciers are likely to have suffered losses from wind deflation.

The mean ELA of the Vlasian Stage glaciers on Mount Tymphi was 1862 m a.s.l., 312 m lower than the mean ELA of the Tymphian Stage glaciers. If precipitation is assumed to have been the same during these stages, a 312 m reduction in ELA implies a temperature depression of 1.87°C for the Vlasian Stage compared to the Tymphian Stage, assuming a standard lapse rate of 0.6°C per 100 m. Given that the mean annual temperature

at the mean ELA of the Tymphian Stage glaciers (2174 m a.s.l.) was -4.2°C , then the mean annual temperature at the mean ELA (1862 m a.s.l.) of the Vlasian Stage glaciers would have been *ca.* -6.1°C . However, this temperature depression more accurately reflects the depression in mean summer temperature, since it is the relationship between mean summer temperature and annual precipitation which best describes the climate at the ELA (Ohmura *et al.* 1992). Nevertheless, if mean summer temperatures were more than 1.87°C lower during the Vlasian Stage glacial maximum compared with the Tymphian Stage glacial maximum, then precipitation would have been also been lower (*i.e.* <2300 mm). In fact for every 1°C depression, precipitation would also have been depressed by 300-500 mm (*cf.* Ohmura *et al.* 1992). This relationship is important since it illustrates the temperature threshold at which precipitation was wetter or drier than the Tymphian Stage (Fig. 8.7).

The temperature-precipitation reconstruction outlined above for the Vlasian Stage is limited by the fact that it only provides information on summer temperatures and mean annual precipitation relative to the Tymphian Stage. Other information relating to mean

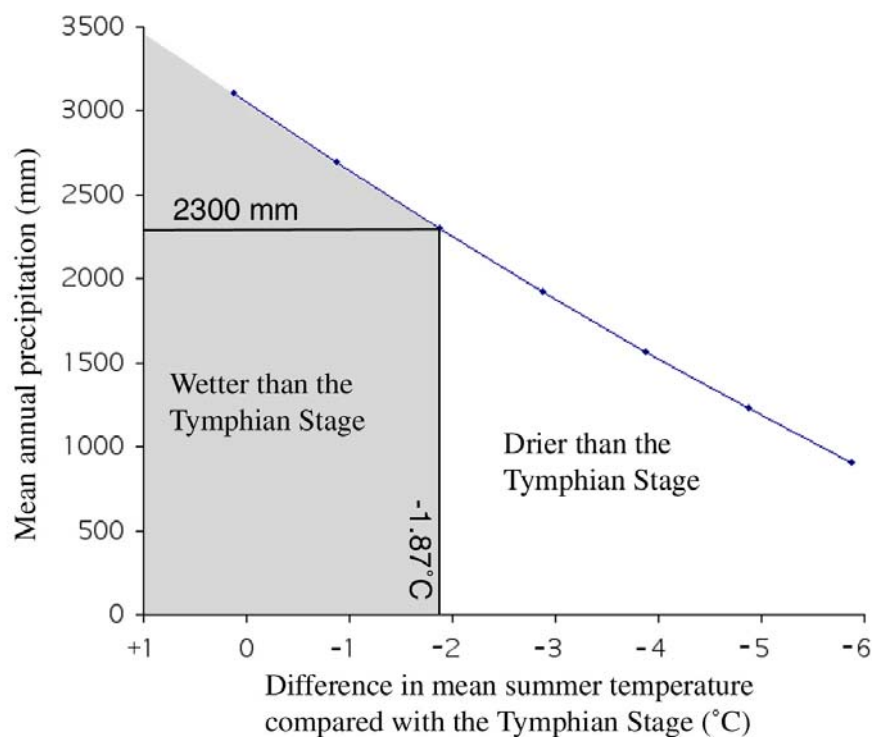


Figure 8.7 The relationship between mean summer temperatures and precipitation during the glacial maximum of the Vlasian Stage relative to Tymphian Stage values (see text for details).

annual temperature, temperature range and winter temperatures are difficult to assess due to the vast number of potential combinations. Unlike for the Tymphian Stage, these combinations cannot be constrained by limiting evidence, such as rock glaciers. Nevertheless, this approach provides a powerful comparison of the main accumulation and ablation controls during the different glacial stages.

8.5 Palaeoclimate during the Skamnellian Stage

The Skamnellian Stage is defined as the glacial interval before the Dodoni Interglacial in the Ioannina pollen sequence, which is correlated with MIS 12 (Tzedakis 1994, Tzedakis *et al.* 1997), which occurred between *ca.* 430-480,000 years BP (Lowe and Walker 1997, Table 1.1). The glaciers of the Skamnellian Stage were the most extensive recorded in the Pindus Mountains and may correlate with extensive glaciations in northern Europe during the Elsterian Stage.

8.5.1 Local controls on glacier development

On Mount Tymphi, sixteen glaciers formed during the Skamnellian Stage. The mean ELA of four glacier groups was 1741 m a.s.l., 116 m lower than during the Vlasian Stage and 433 m lower than during the Tymphian Stage. The glacier groups of Mount Tymphi had widely differing ELAs, ranging from 1285 m to 1990 m a.s.l. This range can largely be attributed to spatial variation in local factors. The lowest glaciers were those which formed at the base of the 1000 m northeast-facing cliffs of Goura (2466 m) (Group B). These had a group mean of 1410 m a.s.l. As was the case during later glacial stages, these cliffs would have provided glaciers with ample shade and also considerable avalanche input.

The glaciers and ice-fields on the south side of Mount Tymphi (Group D) were the highest of the Skamnellian Stage with a group ELA of 1928 m a.s.l. Higher ELAs are the result of the area around the ice-divides of transection glaciers having particularly gentle gradients resulting in large areas of the glacier surface at the highest altitudes. Conversely, in lower areas the glaciers were narrowly confined within steep valley walls and were relatively steep (Fig 7.9 and 7.10). If the ELA had been as low as in other glacier groups, then the outlet glaciers would have descended to much lower altitudes. Lower ELAs may have been prevented due to the large surface area of the upper ice-fields where wind-scouring may have been a major factor in reducing snow accumulation. In addition, the exposed ice-field surface is also likely to have provided limited shading inhibiting accumulation and promoting ablation.

On the northern slopes of the main Tymphi ridge (Group A), glaciers had a mean

reconstructed ELA of 1863 m a.s.l. Within this glacier group, the Amarandos glacier was significantly lower than the neighbouring Mighia and Stani Katsanou glaciers (Table 7.2). This may have been due to avalanche accumulation from the extremely steep northern slopes of Gamila (Figure 8.8). These slopes would also have afforded ample shade, enabling depression of the local ELA.

The south-facing Tsepelovo, Skamnelli, Tsioumako and Stani Grava glaciers (Group C) had a reconstructed mean ELA of 1765 m a.s.l. (Table 7.2). These glaciers were much lower than the northern and plateau glacier groups (Groups A and D), although not as low as the very low Maghoula and Kriopotamos glaciers (Group B). The relatively low ELAs of the Group C glaciers were perhaps because these glaciers were situated on the relatively gentle southern slopes of Mount Tymphi, in areas which were likely to have been characterised by extensive karstification. A combination of complex and sheltered topography may have aided other local effects. For example, dolines may have acted as traps for wind-blown snow and provided shade, a situation which was likely to have been important in all glacial stages and evident today on both glaciated and unglaciated slopes (Fig. 8.9).

As with other glacial stages, on Mount Tymphi, it appears that the role of aspect-controlled shade had little bearing on the overall distribution of the Skamnellian Stage glaciers. Whilst it may have been important in individual cases, it is likely that local controls such as avalanche, wind-blown snow and wind deflation were the dominant factors in determining spatial variation of ELAs. It is therefore apparent that not only small glaciers, confined to their own cirques, were liable to be affected by local climatic factors, but also larger scale valley and ice-field glaciers.

On Mount Smolikas, at least two glaciers existed with a mean ELA of 1680 m a.s.l., over 60 m lower than the mean on Mount Tymphi. In the Vadulakkos valley, a glacier covered 7.32 km², had an ELA of 1700 m a.s.l., and formed in a north-facing valley in the lee of the highest ridges of Mount Smolikas. Therefore, here it is likely that a combination of aspect and wind-blown snow were the dominant local controls promoting glacier development.

Another glacier, near Samarina, had an ELA of 1660 m a.s.l., similar to that for the Vadulakkos glacier. It is likely that this glacier formed because of snow accumulation from wind-blown snow off the slopes of Bogdoni (2253 m a.s.l.) to the southeast. This occurs

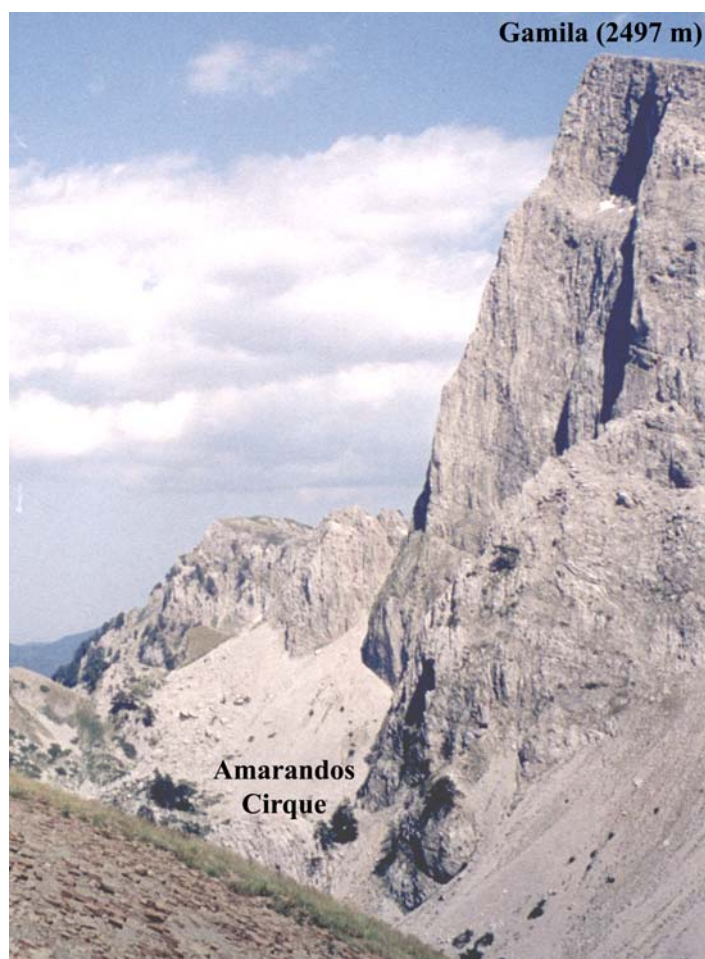


Figure 8.8 Gamila peak (2497 m a.s.l.) and the upper parts of the Amarandos valley. Avalanching snow is likely to have been a major source of accumulation in this area (July 2001).



Figure 8.9 Snow patches during July 2001 at *ca.* 39° 56' 40"N, 20° 52' 00" E, 2100 m a.s.l. in a doline field on the unglaciated southern slopes of Goura (2466 m a.s.l.).

today and snow remains in this hollow until late April - much later than in other areas nearby at a similar altitude. As with the Vadulakkos glacier, aspect and low insolation are likely to have contributed to the formation of a glacier in this hollow.

On Mount Vasilitsa, a large valley glacier formed on the northeastern slopes during the Skamnellian Stage with an ELA of 1675 m a.s.l., similar to the glaciers on Mount Smolikas. As on Mount Smolikas, the northeasterly aspect and wind-blown snow are likely to have been important factors in glacier development.

The extent of glaciation on Mount Smolikas and Mount Vasilitsa may be underestimated since it is likely that some deposits have been eroded. This is especially likely in the Konkutino valley on Mount Smolikas where glaciers were extensive during later glacial stages, such as during the Vlasian Stage. However, the missing glaciers are unlikely to have added significantly to the overall glacier area on this mountain, and total glacier area was much less than on neighbouring Mount Tymphi, even though ELAs were lower. The difference in glacier area, during this stage and later stages, is probably a result of accommodation space and bedrock geology. As noted earlier, on Mount Tymphi, karstic hollows (dolines) are widespread (Fig. 8.9) and are likely to have been favourable for snow accumulation and glacier development. On Mount Smolikas, a predominantly ophiolite mountain, the topography is locally much less complex and accommodation space is likely to be promoted by nivation processes in the first instance, rather than by karstic mechanisms. Therefore, karstic processes and landforms are probably a key control on glacier distribution throughout the Pindus Mountains and have been invoked to explain glacier development and distribution during all the glacial stages.

Whilst glacier areas were smaller on Mount Smolikas during the Skamnellian Stage, ELAs were lower - a situation unique to the Skamnellian Stage. In all later glacial stages, the Mount Smolikas glaciers were higher. This may be because later glacial stages were more marginal, favouring glacier development on limestone Mount Tymphi, where local controls would have been more dominant. This is the most likely situation since higher precipitation on Mount Smolikas compared with Mount Tymphi is opposite to that invoked for later stages and opposite to the modern situation.

8.5.2 Palaeotemperature and palaeoprecipitation reconstruction

On all mountains, glacier ELAs were lower during the Skamnellian Stage glacial maximum than during any subsequent glacial stage. This implies that either precipitation was higher or summer temperatures lower, or both.

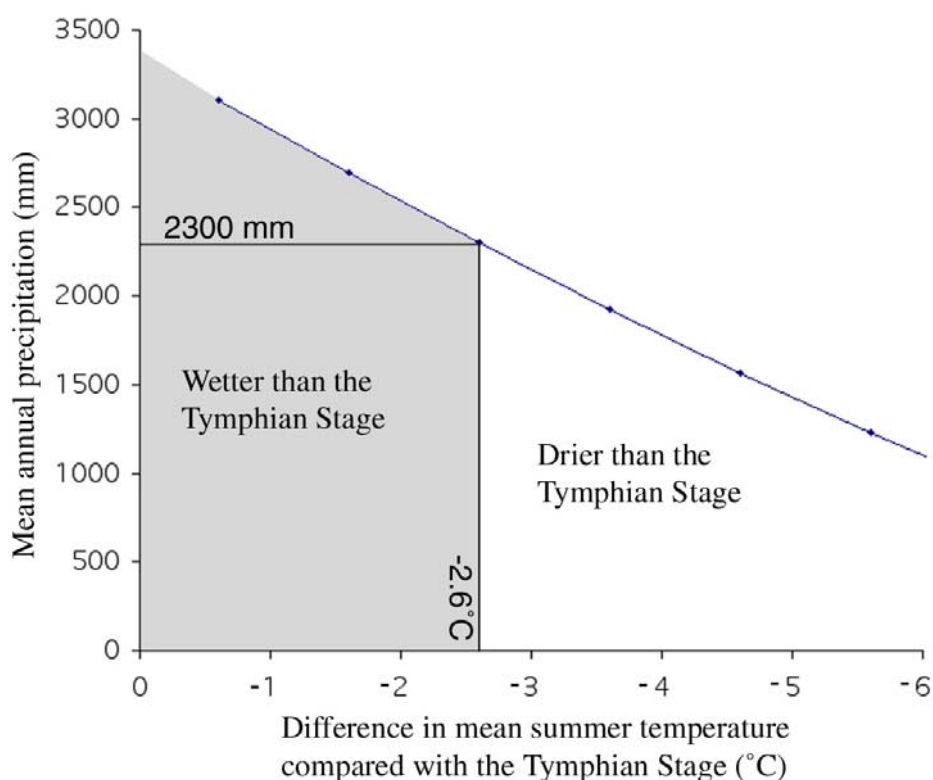


Figure 8.10 The relationship between mean summer temperatures and precipitation during the glacial maximum of the Skamnellian Stage relative to Tymphian Stage values.

The former glaciers of Mount Tymphi were used for climatic reconstruction since these were used for climatic reconstructions for both the Vlasian and Tymphian Stages. The mean ELA of the Skamnellian Stage glaciers on Mount Tymphi was 1741 m a.s.l. This is 433 m lower than during the Tymphian Stage and 121 m lower than during the Vlasian Stage. If precipitation levels are fixed, this implies a depression of mean summer temperature of 2.6°C compared to the Tymphian Stage. A depression of more than 2.6°C would mean that precipitation was also lower during the Skamnellian Stage compared with the Tymphian Stage. This relationship applies irrespective of the annual temperature range and is illustrated in Figure 8.10.

8.6 Climate during 'missing' glacial stages

It is important to appreciate the fragmentary nature of the glacial record and realise that glaciations are likely to have occurred between the various glacial stages recognised in this study. For example, between the Skamnellian and Vlasian Stages it is possible that one or more sets of glacial deposits have been over-ridden by the more recent Vlasian Stage glaciers. The glaciers of the latter stage did, after all, reach mid-valley positions. At

Ioannina, at least two 'glacial' intervals, *i.e.* where arboreal pollen percentages reach values as low as during the Skamnellian, Vlasian and Tymphian Stages, occur between the Skamnellian and Vlasian Stages. These phases in the pollen stratigraphical record have been correlated with MIS 10 and 8 at both Ioannina and Tenaghi Philippon (Tzedakis *et al.* 1997). At Tenaghi Philippon, the interval corresponding with MIS 10 was the most severe in terms of low arboreal pollen abundance (Tzedakis *et al.* 2003b). However, cold but moist conditions during MIS 8 (and therefore higher arboreal pollen abundance) could have been equally conducive to glacier formation and it is difficult, based on the pollen record, to determine the most likely periods favourable to glacier formation.

Figure 8.11 illustrates the likely climatic scenarios under which 'missing' glaciers between the Skamnellian and the Vlasian Stages could have formed. Curves are not extended for precipitation values below 1000 mm since this is very unlikely given that arboreal pollen has been identified at much lower altitudes throughout the 423,000-year Ioannina sequence (Tzedakis 1993, Tzedakis 1994). The climatic curve for the Skamnellian Stage glaciers occupies the outermost curve. Higher glaciers during subsequent stages must have occupied curves inside and to the left of this curve. This is because at any given precipitation-temperature combination, during less extensive glacial phases, either one of these parameters, or both, would have been less than during the Skamnellian Stage. If glaciers developed during a glacial stage between the Skamnellian Stage and the Vlasian Stage, *i.e.* during a cold interval indicated in the pollen record at Ioannina and correlated with MIS 10 and 8, then they most likely formed under climatic combinations indicated in the area shaded in blue. If they were smaller and higher than the very small and high Tymphian Stage glaciers, they would have formed under climatic combinations indicated inside and to the left of the blue area. However, this is unlikely since the Tymphian Stage glaciers existed at the threshold of glaciation on Mount Tymphi and there is simply a lack of space for higher glaciers.

Despite the possibilities explored above, the fact remains that glacial sediments and landforms are not present for two major cold stages equivalent to MIS 8 and 10, and there is no evidence to suggest that they occurred apart from indirect evidence in the pollen record. It is possible that, in some areas, deposits that have been assigned to the Skamnellian or Vlasian Stages may in fact represent deposits that belong to the interval between these stages. This is particularly possible if glaciations in this interval were similar in size to the glaciers of the Vlasian Stage. This possibility should always be left open and, on the basis of negative evidence, it is possible to deduce that glaciers during these cold stages were smaller and higher than those for the Vlasian Stage, or did not exist at all.

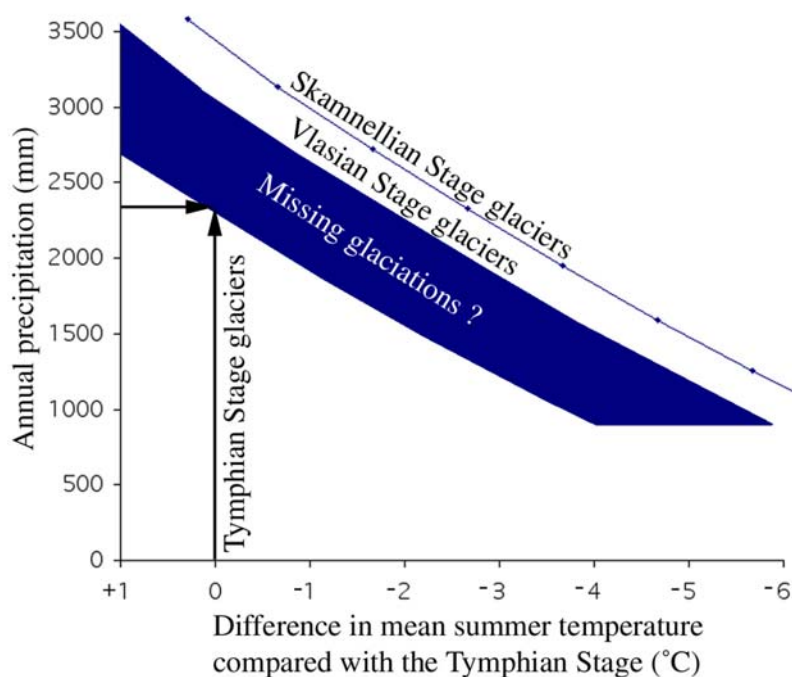


Figure 8.11 The relationship between mean summer temperatures and precipitation during the different glacial stages relative to the Tymphian Stage glacial maximum. A zero temperature difference corresponds with a mean summer temperature of 4.86°C and annual precipitation of 2300 mm. The possible climatic combinations during the maximum extent of the Skamnelliian and Vlasian Stage glaciers correspond with the curves beneath their respective names on the graph.

8.7 Glacial Greece - discussion

The palaeoclimatic reconstructions for the four phases of glacial and periglacial activity recorded in the Pindus Mountains provide new information regarding glacial stage climates, of significance for both Greece and the wider Mediterranean. The following sections examine key similarities and differences between these reconstructions and those derived from other records in this region.

8.7.1 Tymphian Stage

The Tymphian Stage represents the last glacial stage in Greece and is comparable with the Würmian and Weichselian Stages of the Alps and northern Europe. The small size of the glaciers of the northern Pindus Mountains during this stage was mirrored on Mount Olympus, in northeastern Greece, where glaciers were restricted to valley heads (Smith *et al.* 1997). ELAs were also similar (Olympus: 2200m a.s.l., northern Pindus: 2174-2241 m a.s.l.) although, given that the climate of northeastern Greece is currently much more continental (Furlan 1977), it is likely that climate was colder and drier on Mount Olympus.

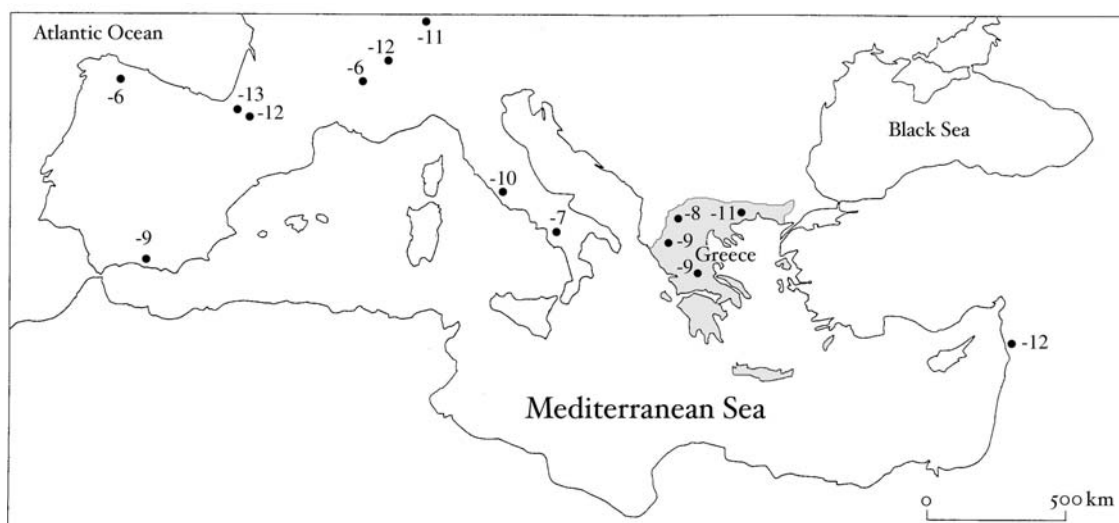


Figure 8.12 Reconstructed mean annual temperature depression ($^{\circ}\text{C}$) for southern Europe during the LGM as deduced from pollen modelling (from Peyron *et al.* 1998). In western and central Greece, mean annual temperature depressions range from 8-9 $^{\circ}\text{C}$.

In northwest Greece, at the Tymphanian Stage glacial maximum, mean annual temperatures would have been *ca.* 8-9 $^{\circ}\text{C}$ lower than, and precipitation similar to, modern values. The temperature reconstruction is within the 6.8-10 $^{\circ}\text{C}$ depression (for the warmest and coldest months respectively) during the most severe part of the last glacial stage, determined using a nested climatic model by Tzedakis *et al.* (2002). It is also very similar to the 8-9 $^{\circ}\text{C}$ depression of mean annual temperatures determined by climatic modelling based on pollen evidence in Peyron *et al.* (1998) (Fig. 8.12). Furthermore, the temperature reconstruction is similar to that calculated for the Italian Appenines for the climax of the last glacial stage. Here, Girauldi and Frezzotti (1997) used rock glacier evidence to derive palaeotemperature depressions of 7.3-8.3 $^{\circ}\text{C}$ relative to the present-day.

Whilst the mean annual temperature reconstruction obtained in this study matches that from pollen studies in Greece, the palaeoprecipitation and associated temperature distribution reconstructions do not. For example, Tzedakis *et al.* (2002) suggest that precipitation was 545 mm less than today with an equable distribution throughout the year. This is equivalent to a 51% reduction in precipitation. A similar reduction was suggested in the pollen model of Peyron *et al.* (1998). Moreover, arid conditions are also suggested from ostracod evidence of lower lake-levels at Lake Xinias (Digerfeldt *et al.* 2000) and lithological evidence from Kopais (Okuda *et al.* 2001, Griffiths *et al.* 2002). However, using glacier and rock glacier evidence, reconstructed precipitation is similar to extrapolated modern values. Whilst these extrapolations from mid-altitude meteorological stations may underestimate the real value of modern precipitation, a similar finding was derived for the Italian Appenines. Here, Giraudi and Frezzotti (1997) reconstructed

snowfall values for the equivalent of the Tymphian Stage glacial maximum which were similar to those which occur today. Based on the glacial record in the Pindus Mountains, the only way to derive lower precipitation values during the Tymphian Stage glacial maximum is to have summer temperatures depressed by much more than 8-9°C or reduce the annual temperature range to less than 20°C (Table 8.1). Both of these situations are unlikely. This is because no other modelling results suggest temperature depressions greater than this for the summer months (*cf.* Peyron *et al.* 1997, Tzedakis *et al.* 2002). In addition, the modern mean annual range is 20°C under less continental conditions than would have occurred during the Tymphian Stage.

Local inputs of snow, such as wind-blown and avalanching snow, no doubt contributed to glacier development on Mount Tymphi, as discussed in section 8.3.1. However, all the glaciers had an ELA within 100 m of the mean, with a group standard deviation of 43 m. If local inputs were a major factor, ELAs would have had greater variability, especially given the wide-ranging aspects and topographical positions of the Tymphian Stage glaciers. In addition, since the climate at the ELA is defined in Ohmura *et al.* (1992) by the relationship between summer temperatures and annual meteorological precipitation, any local accumulative inputs are likely to be partly accounted for by summer precipitation.

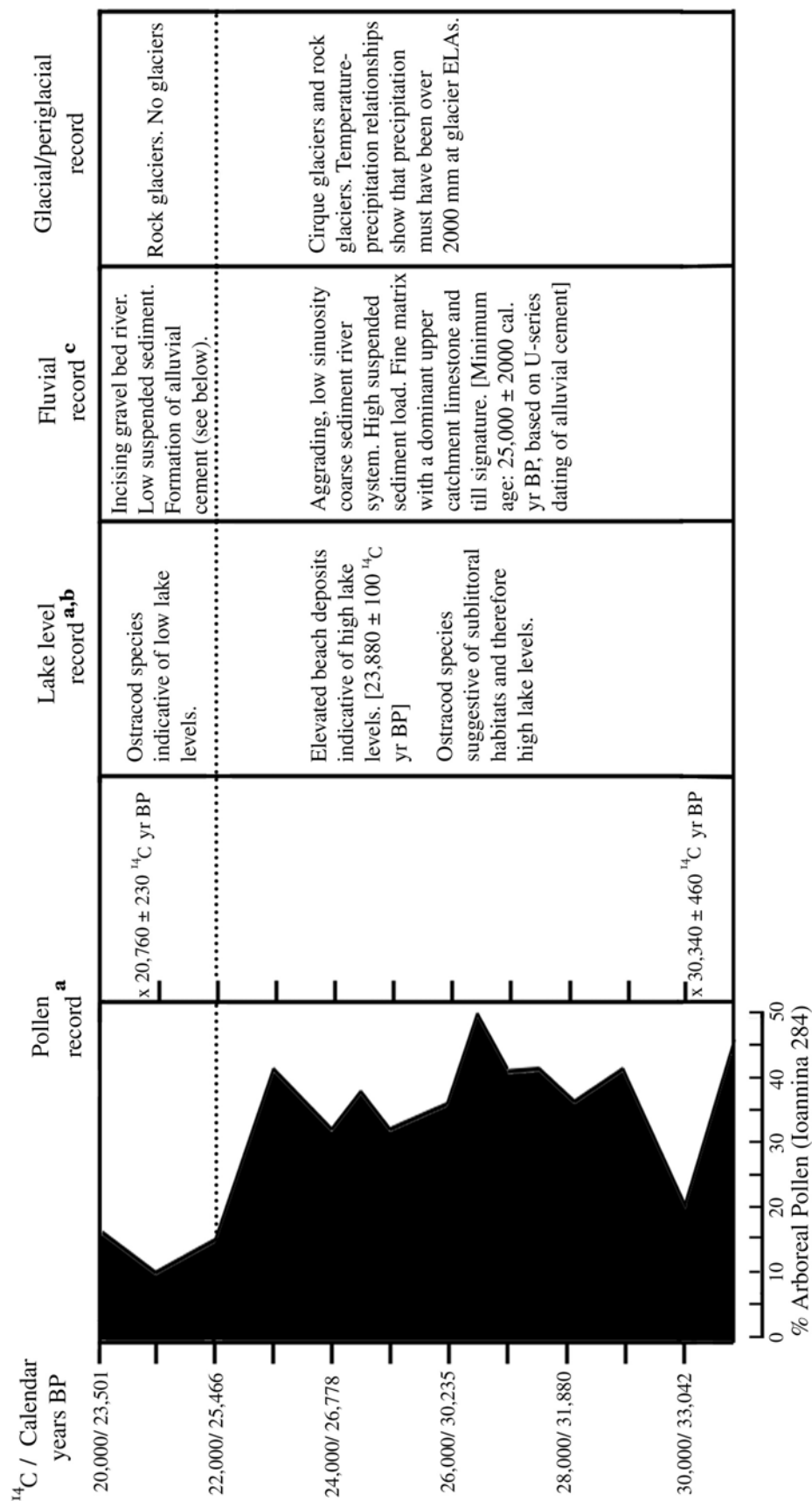
The apparent paradox between the glacier/ rock glacier evidence, which suggests precipitation comparable to modern values, and the pollen and lake-level evidence which imply more arid conditions, could potentially be resolved by a seasonal precipitation model. Such a model was proposed by Prentice *et al.* (1992) for the last cold stage. They suggested that the climate in the Mediterranean was characterised by cold winters, intense winter precipitation and summer drought. This results in a dominance of a steppic pollen assemblage resulting from a lack of moisture availability during the growing season. However, this model was designed with rainfall in mind, and if precipitation fell primarily during the winter months, it would have fallen largely as snow. This is illustrated by Figure 8.7, which shows that November to March mean temperatures would have been less than 2°C at the altitude of Ioannina and only above 0°C from May to September at over 2000 m a.s.l. during the coldest part of the Tymphian Stage. Melting during the late spring and summer months would have supplied moisture to plants throughout the summer months. A seasonal precipitation model would not, therefore, inhibit the development of high moisture level vegetation and another explanation must be sought.

The origin of the 'wet *versus* dry' climate problem is best explained by invoking asynchronicity between the most severe phases of climate in the pollen and glacial records.

Galanidou *et al.* (2000) suggest that the height of the last glacial stage, as defined by the lowest frequencies of tree pollen, occurred between 22 and 20,000 ^{14}C years (*ca.* 25,466 - 23,501 years BP). They argue that the pollen and ostracod evidence imply relatively low lake levels and arid conditions during this interval. However, Galanidou *et al.* (2000) accept that lake levels at Ioannina may have been higher at $23,880 \pm 100$ ^{14}C years BP (*ca.* 26,643 years BP). Indeed, arboreal pollen, as a percentage of the total pollen count, consistently exceeded 30% during the period 22,000 to 29,000 ^{14}C years BP (*ca.* 25,466 - 33,042 years BP) and reach 45% at 27,000 ^{14}C years BP (Galanidou *et al.* 2000). This shows that moisture must have been relatively abundant. Therefore, it is possible that the glacier evidence, which suggests precipitation values were over 2000 mm and as high as modern values, corresponds to this earlier period in the pollen record.

The possibility of maximum glacial extension at a time prior to the lowest arboreal pollen abundances is supported by fluvial deposits in the Voidomatis basin on the southern slopes of Mount Tymphi. A major aggradational element, termed the Aristi Unit, contains groundwater calcretes (phreatic zone cement) which were dated by Hamlin *et al.* (2000) to $25,000 \pm 2,000$ years BP. The host alluvium must predate the calcretes and, given that these cements formed in the groundwater zone, they must have formed soon after deposition of the host alluvium, prior to significant incision. It is therefore likely that the major phase of aggradation occurred during the moist interval between 22,000 and 29,000 ^{14}C years BP (*ca.* 25,466 - 33,042 years BP). Moreover, the fine and gravel matrix of the Aristi Unit is dominated by upper catchment limestone- and till-derived fines, which are derived from glacial erosion (Lewin *et al.* 1991, Woodward *et al.* 1992, Hamlin *et al.* 2000). In fact, the glaciers of the upper Voidomatis catchment, the Laccos Tselon and Megalon Litharion glaciers, were the largest glaciers of the Tymphian Stage and would have provided significant amounts of debris to the Voidomatis river. Meltwater erosion of older, lower glacial deposits around Tsepelovo and Skamnelli would have also added significant sediment load to the aggrading river system. Thus, there is therefore a strong link between the dated fluvial record and the glacial/ periglacial records for a glacial maximum which preceded the most severe phase of climate indicated in the pollen record.

A tentative model of events in the Pindus Mountains of northwest Greece during the height of the last glacial stage is illustrated in Figure 8.13. Glacier retreat and reduced down-stream fluvial aggradation is likely to have begun by *ca.* 22,000 ^{14}C years BP (*ca.* 25,466 calendar years BP). A transition to more steppic conditions at 22,000 ^{14}C years BP (*ca.* 25,466 calendar years BP), as indicated in the Ioannina pollen record, was probably marked by increased aridity, leading to glacier retreat, reduced fluvial discharge



- ^a Galanidou *et al.* (2000)
- ^b Frogley (1997), Galanidou *et al.* (2000)
- ^c Lewin *et al.* (1991), Hamlin *et al.* (2000)

Figure 8.13 Events between 30,000 and 20,000 ¹⁴C years BP in the Pindus Mountains of northwest Greece as deduced from a variety of geological and geomorphological records.

down-stream and the development of alluvial cement as the rivers began to incise. However, persisting cold conditions would have enabled continued rock glacier maturation and movement of debris by permafrost creep. Although rock glaciers may have begun forming, temperatures are unlikely to have been lower than at the time of the glacial maximum. The latter must have been characterised by higher precipitation but not higher temperatures. This is because higher temperatures at the former glacier ELAs would imply precipitation far greater than modern values in order to sustain the cirque glaciers.

However, the proposal of a glacial maximum between 29-22,000 ^{14}C years BP is not fully supported by the evidence of Galanidou *et al.* (2000) since they suggest that this interval was an interstadial. They argue that small abundances of Mediterranean trees such as olive (*Olea*), evergreen oak (*Quercus ilex*) and pistachio (*Pistacia*) indicate relatively warm conditions and cite evidence of warmer temperatures elsewhere in the Mediterranean (*e.g.* Allen *et al.* 2000) and in the GISP2 ice core record (*e.g.* Grootes and Stuiver 1997). Even so, Mediterranean trees such as olive can tolerate frequent frost and only injure when temperatures fall below -10°C (Larcher 1981, Martin *et al.* 1994). Similarly, pistachio trees will grow and survive under a wide range of conditions, and are tolerant of temperatures down to -14°C (Larcher 1995). Moreover, *Pistacia* pollen is found in sediments at 1800 m a.s.l. at Rezina marsh on Mount Tymphi during the Holocene (Willis 1992b), a site where modern mean temperatures during the coldest month are probably *ca.* -3°C . However, special-pleading is not really necessary since Mediterranean tree species only represent less than *ca.* 3% of the total pollen during the interval 29,000 - 22,000 ^{14}C years BP. In addition, Tzedakis (*personal communication*) has since revised his view expressed in Galanidou *et al.* (2000) and no longer considers Mediterranean taxa to be significant during this interval (*cf.* Tzedakis *et al.* 2002). Therefore, in the pollen record sequence at Ioannina, as well as elsewhere in the Mediterranean (*e.g.* Allen *et al.* 1999), increased arboreal taxa at low altitudes most likely implies wetter conditions but not higher temperatures compared with 22-20,000 ^{14}C years BP.

The climatic reconstruction presented above for the Tymphian Stage glacial maximum is supported by glacial evidence in the Italian Appenines. Here, maximum glacier extension during the last glacial stage occurred before $22,680 \pm 630$ ^{14}C years BP ($26,239 \pm 789$ years BP) (Giraudi and Frezzotti 1997). As in Greece, this glacial maximum appears to pre-date the most severe phase of climate represented in the pollen record since, at Monticchio, a long lacustrine sequence in Italy, the lowest arboreal pollen abundances occurred between 25,900 and 14,300 years BP ($22,350 - 12,500$ ^{14}C years BP) (Allen *et al.* 2000). There is therefore consistent evidence in the glacial and fluvial records from both

Greece and Italy for a glacial maximum which preceded the most severe phase of climate in the pollen records (22-20,000¹⁴C years BP) and the global glacial maximum at *ca.* 18,000 years BP (*cf.* CLIMAP 1981, COHMAP 1988).

8.7.1.1 Smolikasian Substage

The last major cold-climate landforms in the Pindus Mountains formed during the Smolikasian Substage, equivalent to the Late-glacial Substage in Northern Europe (section 6.3.2). On Mount Olympus the most recent cirque moraines were considered Neoglacial by Smith *et al.* (1997), although no definition of this term was provided. It is unlikely that conditions during the Holocene were ever severe enough for glacier formation anywhere in Greece, especially given that modern mean annual temperatures at 2000 m are *ca.* 6.4°C (Table 2.2). It is more likely that the highest moraines on both Mount Olympus and in the Pindus Mountains correlate with one of a series of readvance moraines and rock glaciers in the Italian Apennines. These formed during the Fontari and Mount Aquila Stadials between *ca.* 16 and 10,000 ¹⁴C years BP (Giraudi and Frezzotti 1997).

The Mount Aquila Stadal in the Italian Apennines is dated to *ca.* 11,000 ¹⁴C years BP and is correlated with the Younger Dryas Chronozone (11-10,000 ¹⁴C years BP). Glacier ELAs were *ca.* 2300 m a.s.l. during this readvance (Giraudi and Frezzotti 1997), similar to the mean ELA of the Smolikasian Substage glaciers in Greece (ELA: 2325 m a.s.l.). Furthermore, the temperature depression compared to the present day during the Mount Aquila Stadal in Italy is estimated at 5.6 - 6.7°C, which is similar to the depression of 6.24°C estimated for the Pindus Mountains. It is therefore possible that the Smolikasian Substage moraines correlate with the Mount Aquila Stadal and were formed during the Younger Dryas Chronozone, supporting the suggestions made in Chapter Six (section 6.3.2). However, in the Italian Apennines, climate was reconstructed as cold and very dry during this interval (Giraudi and Frezzotti 1997), unlike those made here for the Pindus Mountains which indicate cold and moist conditions (section 8.3.5).

Evidence of ample moisture availability during an interval equivalent to the Younger Dryas interval in the Pindus Mountains is supported in the pollen records at both Ioannina and Nisi (Lawson 2001). However, other pollen records in the Eastern Mediterranean suggest that the Younger Dryas is reflected by an increase in taxa indicative of arid conditions (*e.g.* Rossignol-Strick 1995). Lawson (2001) suggests that the persistence of tree taxa throughout the Late-glacial in the Pindus Mountains resulted from high orographic rainfall, a suggestion also proposed by Willis (1992a, 1992b, 1992c) based on pollen evidence from other Pindus sites. It is therefore likely that the Younger Dryas

Chronozone was characterised by cold yet moist conditions in the Pindus Mountains, possibly resulting in glacier readvance.

Unfortunately, until absolute dating is available for the glacial and periglacial deposits assigned to the Smolikasian Substage, firm correlations will remain uncertain. Indeed, the deposits could have formed before the Younger Dryas Chronozone, at any time after the preceding Tymphian Stage glacial maximum. For example, dated slackwater deposits in rock shelter sediments in the lower Voidomatis basin indicate that a series of major flood events occurred between *ca.* $14,310 \pm 200$ and $13,960 \pm 200$ ^{14}C years BP, during global cooling associated with Heinrich Event 1 (Woodward *et al.* 2001). Clearly, moisture was abundant during this interval and it may be the case that the readvance glaciers of Mount Smolikas formed at this time. The problem of chronological precision was a major reason for assigning the deposits Substage and not Chronozone status in Chapter Six. This approach allows future subdivision if more evidence becomes available.

8.7.2 Vlasian Stage

The Vlasian Stage represents the cold phase prior to the Metsovon and Pangaion Interglacials at Ioannina and Tenaghi Philippon respectively. This cold interval is correlated at both sites with MIS 6 (Tzedakis *et al.* 1997), equivalent to the interval 190 - 127,000 years BP and the later Rissian Stage and the Late Saalian Substage in the Alps and northern Europe, respectively (Lowe and Walker 1997, Fig 1.1, Sibrava *et al.* 1986).

On Mount Olympus, Smith *et al.* (1997) suggested that upland ice and valley glaciers formed during an interval equivalent to MIS 6. Similarly, in Italy cements within extensive valley glacier deposits have been U-series dated to $135,000 \pm 10,000$ years BP and the host deposits assigned to the Rissian Stage (Kotarba *et al.* 2001). In addition, in the Voidomatis basin on Mount Tymphi, cemented alluvial deposits, formed during a major phase of fluvial aggradation, are dated to before $113,000$ years BP $\pm 6,000$ years BP. The deposits were considered to have formed under a cold-stage climate after the last interglacial, during an interval equivalent to MIS 5d (Hamlin *et al.* 2000). However, as noted in Chapter 2, section 2.5, the dated cement probably formed during the last interglacial and the host sediments during the preceding cold stage corresponding to a major phase of glaciation during the Vlasian Stage (MIS 6).

The climate during the Vlasian Stage glacial maximum is likely to have been colder and/or wetter than during the equivalent event of the Tymphian Stage. If precipitation was lower than during the Tymphian glacial maximum, mean summer temperatures must have been colder by more than 1.87°C . Conversely, if precipitation was greater during the

Vlasian glacial maximum, compared with the equivalent event of the Tymphian Stage then mean summer temperatures could not have been more than 1.87°C colder (Fig. 8.7).

Few records can further resolve the combinations which best describe climate during the Vlasian Stage. In the pollen record at Ioannina, this period is characterised by steppe vegetation dominated by Gramineae, *Artemisia* and Chenopodiaceae (Tzedakis 1994). However, the sampling resolution of the Ioannina 249 core is insufficient to fully understand the dynamics of climate-related vegetation during this stage. This is the subject of current investigation of the adjacent Ioannina 284 core (Tzedakis, *personal communication*). However, even when this is achieved, it will be difficult to pinpoint the precise timing of the glacial maximum because of the wide range of climatic conditions under which the glaciers could have formed (Fig. 8.7). If the glacial maximum was coeval with the most arid phase of climate indicated in the pollen record, then temperatures must have been more than 1.87°C lower than at the equivalent event of the Tymphian. As was likely during the latter stage, the glaciers may have reached their maximum extent during a wetter, more transitional climate phase, and determining when exactly this was will, for the time being, remain elusive.

8.7.3 Skamnellian Stage

The most extensive glacial deposits in the northern Pindus Mountains are assigned to the Skamnellian Stage which represents the cold phase prior to the Dodoni and Lekanis Interglacials at Ioannina and Tenaghi Philippon, respectively. This cold phase is correlated with MIS 12 (Tzedakis *et al.* 1997), equivalent to the Elsterian Stage of northern Europe and possibly the Mindelian Stage of the Alps (Sibrava *et al.* 1986).

On Mount Olympus, Smith *et al.* (1997) suggested that the most extensive glacial deposits probably pre-date 210,000 years BP on the basis of soils correlated with dated soil sequences in the Larissa basin. They speculated that the deposits formed during MIS 8, possibly equivalent to the Early Saalian in northern Europe. However, it is more likely that they correlate with the Skamnellian Stage deposits of the northern Pindus. Glacial deposits which pre-date the Rissian Stage may also be present in the Italian Apennines. For example, Jaurand (1994) reported moraines which may represent glaciation older than the Rissian Stage. However, the Skamnellian deposits of the Pindus represent the oldest dated glacial deposits in the Mediterranean region and nowhere else have deposits been dated to >350,000 years BP.

The climate during the Skamnellian glacial maximum would have been even colder and/or wetter than was the case during both the Tymphian and Vlasian Stages. If

precipitation was greater than at the Tymphian glacial maximum, then mean summer temperatures are unlikely to have been more than 2.6°C lower. Conversely, if precipitation at the Skamnellian glacial maximum was lower than at the Tymphian maximum, then mean summer temperatures must have been more than 2.6°C lower. Mean annual temperatures were depressed by 8.4°C during the Tymphian compared with today. Therefore, assuming an even depression of monthly temperatures, lower precipitation during the Skamnellian compared with the Tymphian (*i.e.* < 2300 mm) implies a depression of monthly temperatures by at least 11°C compared with modern values.

Attempts to verify the climate reconstructions by comparison with the pollen record and pinpoint the likely timing are fraught with difficulty. This is largely because of the range of temperature-precipitation combinations possible for glaciation, a situation compounded by the poor resolution of the Ioannina pollen sequence, as well as that at Tenaghi Philippon during this period. Only when this is achieved, will it be possible to constrain the timing of glaciation. At Tenaghi Philippon, the interval equivalent to the Skamnellian Stage is dominated by aquatic plant communities associated with high lake levels (van der Wiel and Wijnstra 1987). The apparent contradiction of the occurrence of extreme steppic environments with high lake levels is suggested by van der Wiel and Wijnstra (1987a) to result from low evapotranspiration and cold-climate conditions. However, the co-occurrence of regional steppic conditions with high lake levels must imply cold, yet relatively moist conditions. It may be that precipitation was restricted to the winter months, a situation noted earlier (section 8.7.1) and proposed for the last glacial stage by Prentice *et al.* (1991). This would be conducive to extensive glacier development in the uplands.

Finally, if glaciations occurred between the Skamnellian and Vlasian Stages, they must have been less extensive than during the latter stage. Indeed, the Ioannina pollen record suggests conditions may have been severe enough for glaciation in the Pindus Mountains. If glaciation did occur, it is likely to have done so under climatic conditions intermediate to those which characterised the Skamnellian and Vlasian Stages.

8.8 Glacial climates in the Mediterranean

The glacial record in Greece suggests cold stage climates were characterised, at least in part, by cold and wet climates. This is consistent with the southerly shift of mid-latitude storm tracks during glacial phases (*cf.* Florineth and Schlüchter 2000). The west to east movement of storm tracks would have been particularly conducive to maintaining a moist climate in mountain areas, such as the Pindus Mountains, bounded to the west by large

tracts of sea. However, as the large ice sheets of the Alps and northern Europe increased in size, it is likely that anti-cyclonic conditions over these areas would have intensified. This would have caused aridity over the northern Mediterranean region, a situation widely recognised in palaeobotanical records, and pushed storm tracks even further south over the central Mediterranean Sea.

The small glaciers in the Mediterranean mountains probably responded rapidly to climate change, unlike the extensive ice sheets which covered the Alps and northern Europe. The small mountain glaciers of the Mediterranean are likely, therefore, to have grown and decayed much faster, and reached their maxima prior to the large ice sheets. The rapid response of mountain glaciers to climate change and increased aridity in southern Europe around the time of global glacial maxima, may explain evidence for an early glacial maximum in areas characterised by mountain glaciation during the last glacial stage. This has been documented in many mountain areas of southern Europe such as in the Pyrenees (García-Ruiz *et al.* 2003, Jalut *et al.* 1992), the Vosges (Seret *et al.* 1990), the Italian Apennines (Giraudi and Frezzotti 1997) and here in Greece and illustrates the sensitivity of these former glaciers to climate.

It is possible that the glacial records in different areas of the Mediterranean are unique and reflect small-scale response to climate change. Alternatively, they reflect a response which is recorded across the Mediterranean. Further work is required to understand the timing of glaciation across this region, but the present study provides the first fully mapped and dated sequence for Greece and thereby provides a basis for comparative study elsewhere. However, any future work requires a sound chronostratigraphical and geochronological framework, a situation currently lacking in most areas. Only when this is achieved, will the glacial history of the Mediterranean be more fully understood and its implications fully assessed.

Chapter Nine

Conclusions

- 9) Detailed field survey and geomorphological mapping in the northern Pindus Mountains, Greece, has revealed evidence of extensive glaciation and periglacial activity. The glacial and periglacial sequence was subdivided following formal stratigraphical procedure. On Mount Smolikas (2637 m a.s.l.), a maximum of four morpho-lithostratigraphical units were identified in any one cirque-valley formation, whilst on Mount Tymphi (2497 m a.s.l.) and Mount Vasilitsa (2248 m a.s.l.), a maximum of three units were identified in a cirque-valley formation. This evidence was interpreted as representing at least four glacial/periglacial phases on Mount Smolikas and three on Mount Tymphi and Mount Vasilitsa.

- 10) The chronology of the glacial and periglacial sequence was determined using radiometric and relative-age techniques. Cemented glacial deposits were dated using U-series. Cements in the most extensive glacial deposits on Mount Tymphi were dated at >350,000 years BP. In higher mid-valley deposits cements were dated at no older than the last interglacial in Greece (127-111,000 years BP). In addition, soils on the most extensive glacial deposits were well-developed and displayed characteristics comparable with soils elsewhere in Greece which have known to have undergone prolonged development. The combination of cemented moraines and preserved soils from the Middle Pleistocene indicates localised stability in an area characterised by intense regional tectonic activity. The combination of a geo- and relative- chronological framework with the morpho-lithostratigraphy enabled the positioning of the glacial and periglacial units within a globally comparable chronostratigraphy. The oldest most extensive glacial deposits were assigned to the Skamnellian Stage which is comparable with the Mindelian Stage in the Alps, the Elsterian Stage in northern Europe and MIS 12. Mid-valley deposits were assigned to the Vlasian Stage, which is equivalent to the late Rissian Stage in the Alps, the Late Saalian Stage in northern Europe and MIS 6. The highest deposits of Mount Tymphi and Vasilitsa were assigned to the Tymphian Stage, equivalent to the Würmian Stage in the Alps, the Weichselian Stage in northern

Europe and the interval MIS 5d-2. The highest deposits of Mount Smolikas, the highest in the Pindus Mountains, were assigned to the Smolikasian Substage and represent glacial and periglacial activity during an interval equivalent to the Late-glacial Substage (14-10,000 ^{14}C years BP).

- 11) During the most extensive glaciation of the Skamnelliian Stage glaciers covered an area of over 70 km² in the northern Pindus Mountains with a mean ELA of 1700 m a.s.l. The most extensive ice was on Mount Tymphi where glaciers covered an area of 59.2 km² whilst on Mount Smolikas and Mount Vasilitsa glaciers covered areas of only 8.0 km² and 3.4 km², respectively. Extensive valley glaciers formed on all mountains and, in addition, an extensive ice-field formed on Mount Tymphi. Glaciers were much smaller, reaching no more than mid -valley positions, during the Vlasian Stage and covered an area of 21.3 km² on Mount Tymphi, 6.6 km² on Mount Smolikas and 1.2 km² on Mount Vasilitsa. The glaciers were also much higher than during the Skamnelliian Stage and had a mean ELA of 1910 m a.s.l. During the Tymphian Stage, glaciers were limited to cirques with a mean ELA of 2155 m a.s.l. Six cirque glaciers covered an area of 3.9 km² on Mount Tymphi; five glaciers covered an area of 2.6 km² on Mount Smolikas; and only one very small glacier, covering an area of 0.12 km², formed on Mount Vasilitsa. On Mount Tymphi six rock glaciers also formed and reached down to 1800 m a.s.l. The last glaciers of the northern Pindus formed during the Smolikasian Substage in the highest cirques of Mount Smolikas, the highest mountain of the Pindus range. Here, three glaciers had a mean ELA of 2370 m a.s.l. and covered an area of 0.43 km² and a small rock glacier also formed with its front at 2160 m a.s.l.
- 12) On all mountains local factors were important in controlling glacier distribution. However, accumulative inputs (*i.e.* avalanche and wind-blown snow) were more important than local ablative controls (*i.e.* aspect and isolation). The influence of lithology was also a factor in determining the altitude and size of glaciers on each mountain. For example, a complex karstic landscape on limestone Mount Tymphi is likely to have favoured glacier development and been a major influence controlling lower ELAs on this mountain compared with others that are formed in ophiolite.
- 13) The climate during all the glacial maxima would have been characterised by cold mean annual and summer temperatures and high precipitation. Mean annual temperatures during the glacial maximum of the Tymphian Stage were *ca.* 8.4°C lower than modern

values and mean annual precipitation would have been over 2000 mm. Combined with dated fluvial sediments in the Voidomatis basin on Mount Tymphi, it is likely that the glacial maximum preceded the most severe arid phase of the last glacial stage indicated in the pollen record of 22-20,000 ^{14}C years BP. The glacial maximum in the northern Pindus Mountains also preceded the global glacial maximum - a characteristic common to many locally glaciated mountains in southern Europe. It is proposed that these glaciers reached a maximum earlier than the large ice sheets of northern Europe, most probably between 29 and 22,000 ^{14}C years BP, as a result of their much smaller size and their consequent rapid expansion and contraction. Moreover, mountain glaciers in southern Europe are likely to have retreated prior to the global glacial maximum because of increasing aridity forced by extensive anticyclonic conditions over the large expanding ice sheets of the Alps and northern Europe. This pattern is likely to have occurred during all glacial stages since palaeoclimatic reconstructions suggest cold and moist conditions prevailed, unlike the pollen records, which suggest arid steppic conditions at the height of glacial stages.

- 14) The glacial and periglacial sequence in the northern Pindus Mountains represents the most complete of its kind to be recognised in the Mediterranean region. Moreover, it is the best-dated sequence in this region. The establishment of a formal stratigraphical framework, in conjunction with the geochronology and a nearby pollen parasequence has enabled, for the first time, the development of a chronostratigraphy for Greece. This approach will provide the platform for further investigations in both Greece and the wider Mediterranean. Furthermore, since a formal stratigraphical approach was adopted, the findings and proposals presented here should facilitate any changes and revisions new evidence may bring and thus contribute to a lasting stratigraphical framework for the Quaternary of Greece.

References

- Aario, R. (1977)** Classification and terminology of morainic landforms in Finland. *Boreas* **6**, 87-100.
- Aber, J.S. (1979)** Glacial conglomerates of the Appalachian Plateau, New York. *Quaternary Research* **11**, 185-196.
- Agassiz, L. (1840)** *Études sur les glaciers*. Jent and Gaßmann: Neuchâtel. 346 pp.
- Ahlmann, H.W. (1948)** Glaciological Research on the North Atlantic Coasts. *Royal Geographical Society, London*, (Research Series 1).
- Ainsworth, W.F. (1842)** *Travels and researches in Asia Minor, Mesopotamia, Chaldea and Armenia*. J.W. Parker: London. 2 volumes, 364 pp. and 399 pp.
- Allen, J.R.M., Watts, W.A. and Huntley, B. (2000)** Weichselian palynostratigraphy, palaeovegetation and palaeoenvironment; the record from Lago Grande di Monticchio, southern Italy. *Quaternary International* **73/74**, 91-110.
- Allen, J.R.M., Brandt, U. and Brauer, A., Hubberten, H.W., Huntly, B., Keller, J., Kraml, M., Mackensen, A., Mingram, J., Negendank, J.F.W., Nowaczyk, N.R., Oberhansli, H., Watts, W.A., Wulf, S., Zolitschka, B. (1999)** Rapid environmental changes in southern Europe during the last glacial period. *Nature* **400**, 740-743.
- Allen, H.D. (1987)** Late Quaternary of the Kopais Basin, Greece: sedimentary and environmental history. Ph.D. thesis, University of Cambridge.
- Amato, A., Aucelli, P.P.C. and Cinque, A. (2003)** The long-term denudation rate in the Southern Apennines Chain (Italy): a GIS-aided estimation of the rock volumes eroded since middle Pleistocene time. *Quaternary International* **101/102**, 3-11.
- Anavasi (2002)** *Map of Pindus: Zagori (Scale 1:50,000)*. Anavasi: Athens.
- Anderson, E., Harrison, S., Passmore, D.G. and Mighall, M. (1998)** Geomorphic evidence of Younger Dryas Glaciation in the Macgillycuddy's Reeks, South West Ireland. *Quaternary Proceedings* **6**, 75-90.
- Andrews, J.T. (1965)** Surface boulder orientation studies around north-western margin of Barnes ice cap, Baffin Island, Canada. *Journal of Sedimentary Petrology* **35**, 753-758.
- Andrews, J.T. (1971)** Techniques of till fabric analysis. *British Geomorphological Research Group, Technical Bulletin No. 6*.
- Andrews, J.T. (1975)** *Glacial Systems: An Approach to Glaciers and their Environments*. Duxbury Press: North Scituate, Massachusetts.
- Arakel, A.V. and McConchie, D. (1982)** Classification and genesis of calcrete and gypsum lithofacies in palaeo-drainage basins of inland Australia and their relationship to carnotite mineralisation. *Journal of Sedimentary Petrology* **52**, 1149-1170.
- Aubert, D. (1969)** Phénomènes et formes du karst jurassien. *Eclogae Geologiae Helveticae* **62**, 325-399.

- Awad, H. (1963)** Some aspects of the geomorphology of Morocco related to the Quaternary climate. *The Geographical Journal* **129**, 129-139.
- Bailey, G.N. (ed) (1997)** *Klithi: Palaeolithic settlement and Quaternary landscapes in northwest Greece*. McDonald Institute for Archaeological Research: Cambridge. 2 volumes.
- Bailey, G.N., Carter, P.L., Gamble, C.S. and Higgs, H.P. (1983)** Asprochaliko and Kastritsa: further investigations of Palaeolithic settlement and economy in Epirus (North-west Greece). *Proceedings of the Prehistoric Society* **49**, 15-42.
- Bailey, G.N., Carter, P.L., Gamble, C.S., Higgs, H.P. and Roubet, C. (1984)** Palaeolithic investigations in Epirus: The results of the first season's excavations at Klithi, 1983. *Annals of the British School of Archaeology at Athens* **79**, 7-22.
- Bailey, G.N. and Gamble, C.S. (1990)** The Balkans at 18,000 BP: the view from Epirus. In Soffer, O. and Gamble, C.S. (eds) *The world at 18,000 BP. Volume One: High Latitudes*. Unwin Hyman: London. p. 149-167.
- Bailey, G.N., Turner, C., Woodward, J.C., Macklin, M.G. and Lewin, J. (1997)** The Voidomatis Basin: An Introduction. In Bailey, G.N. (ed) *Klithi: Palaeolithic settlement and Quaternary Landscapes in northwest Greece. Volume 2: Klithi in its local and regional setting*. McDonald Institute for Archaeological Research: Cambridge. p. 321-345.
- Bakalowicz, M., Sorriaux, P. and Ford, D.C. (1984)** Quaternary glacial events in the Pyrenees from U-series dating of speleothems in the Niaux-Lombrives-Sabart Caves, Ariège, France. *Norsk Geografisk Tidsskrift* **38**, 193-197.
- Ballais, J-L. (1983)** Moraines et glaciers quaternaires des Aurès (Algerie). *108ème Congrès national de Sociétés savantes, Grenoble, 1983, Géographie*, 291-303.
- Ballantyne, C.K. (1982)** Aggregate clast form characteristics of deposits near the margins of four glaciers in the Jotunheimen Massif, Norway. *Nordisk Geografisk Tidsskrift* **36**, 103-113.
- Ballantyne, C.K. (1989)** The Loch Lomond Readvance on the Isle of Skye, Scotland: glacier reconstruction and palaeoclimatic implications. *Journal of Quaternary Science* **4**, 95-108.
- Ballantyne, C.K. (2002a)** The Loch Lomond Readvance on the Isle of Mull, Scotland: glacier reconstruction and palaeoclimatic reconstructions. *Journal of Quaternary Science* **17**, 759-771.
- Ballantyne, C.K. (2002b)** Paraglacial geomorphology. *Quaternary Science Reviews* **21**, 1935-2017
- Ballantyne, C.K. and Kirkbride, M.P. (1986)** The characteristics and significance of some Late-glacial proglacial ramparts in upland Britain. *Earth Surface Landforms and Processes* **11**, 659-671.
- Barbier, A. and Cailleux, A. (1950)** Glaciaire et périglaciaire dans le Djurdjura occidental (Algérie). *Comptes Rendus des Séances de l'Académie des Sciences, Paris. Juillet-Décembre 1950*, 365-366.
- Barnes, I. and O'Neil, J.R. (1971)** Calcium-magnesium carbonate solid solutions from Holocene conglomerate cements in the Coast Range of California. *Geochimica Cosmochimica Acta* **35**, 699-718.
- Barry, R.G. and Chorley, R.J. (1992)** *Atmosphere, weather and climate*. 6th Edition. Routledge: London.

- Barsch, D. (1973)** Refraktionsseismische Bestimmung der Obergrenze des gefrorenen Schuttkörpers in verschiedenen Blockgletschern Graubündens, Schweizer Alpen. *Zeitschrift für Gletscherkunde und Glazialgeologie* **9**, 143-167.
- Barsch, D. (1978)** Rock glaciers as indicators for discontinuous alpine permafrost: an example from the Swiss Alps. *Proceedings of the Third International Conference on Permafrost, National Research Council of Canada, Ottawa* **1**, 349-52.
- Barsch, D. (1988)** Rock glaciers. In Clark, M.J. (ed), *Advances in periglacial geomorphology*. Wiley: Chichester. p. 69-90.
- Barsch, D. (1996)** *Rockglaciers: Indicators for the Present and Former Geocology in High Mountain Environments*. Springer Verlag: Berlin.
- Barsch, D. and King, L. (1989)** Origin and geoelectrical resistivity of rockglaciers in semi-arid subtropical mountains (Andes of Mendoza, Argentina) *Zeitschrift für Geomorphologie* **33**, 151-163.
- 1**
- Barsch, D., Fierz, H. and Haerberli, W. (1979)** Shallow core drilling and bore-hole measurements in the permafrost of an active rock glacier near Grubengletscher, Wallis, Swiss Alps. *Arctic and Alpine Research* **11**, 215-228.
- Bavec, M. and Verbic, T. (2004)** The extent of Quaternary glaciations in Slovenia. In Ehlers, J. and Gibbard, P.L. (eds) *Quaternary Glaciations - Extent and Chronology. Part I: Europe*. Elsevier: Amsterdam.
- Beaudet, G. (1971)** Le Quaternaire Marocain: état des études. *Revue de Géographie du Maroc* **20**, 3-56.
- Belloni, S., Pelfini, M. and Smiraglia, C. (1988)** Morphological features of the active rock glaciers in the Italian Alps and climatic correlations. *Permafrost, Fifth International Conference, Proceedings, Trondheim* **1**, 678-682.
- Benn, D.I. (1989)** Debris transport by Loch Lomond Readvance glaciers in Northern Scotland: basin form and the within valley asymmetry of lateral moraines. *Journal of Quaternary Science* **4**, 243-254.
- Benn, D.I. (1992)** The genesis and significance of "hummocky moraine": evience from the Isle of Skye, Scotland. *Quaternary Science Reviews* **11**, 781-799.
- Benn, D.I. (1994a)** Fabric Shape and the Interpretation of Sedimentary Fabric Data. *Journal of Sedimentary Research* **A64**, 4.
- Benn, D.I. (1994b)** Fluted moraine formation and till genesis below a temperate glacier: Slettmarkbreen, Jotunheimen, Norway. *Sedimentology* **41**, 279-292.
- Benn, D.I. (1995)** Fabric signature of till deformation, Breidamerkurjökull, Iceland. *Sedimentology* **41**, 279-292.
- Benn, D.I. and Ballantyne, C.K. (1993)** The description and representation of particle shape. *Earth Surface Processes and Landforms* **18**, 665-672.
- Benn, D.I. and Ballantyne, C.K. (1994)** Reconstructing the transport history of glacialigenic sediments: a new approach based on the co-variance of clast form indices. *Sedimentary Geology* **91**, 215-227.
- Benn, D.I. and Evans, D.J.A. (1996)** The interpretation and classification of subglacially-deformed materials. *Quaternary Science Reviews* **15**, 23-52.

- Benn, D.I. and Evans, D.J.A. (1998)** *Glaciers and Glaciation*. Arnold.
- Benn, D.I. and Gemmell, A.M.D. (1997)** Calculating equilibrium line altitudes of former glaciers: a new computer spreadsheet. *Glacial Geology and Geomorphology*.
<http://ggg.qub.ac.uk/papers/frame.htm>.
- Benn, D.I. and Lehmkuhl, F. (2000)** Mass balance and equilibrium-line altitudes of glaciers in high mountain environments. *Quaternary International* **65/66**, 15-29.
- Benn, D.I. and Ringrose, T.J. (2001)** Random variation of fabric eigenvalues: implications for the use of A-axis fabric data to differentiate till facies. *Earth Surface Processes and Landforms* **26**, 295-306.
- Bennett, M.R. (1994)** Morphological evidence as a guide to deglaciation following the Loch Lomond Stadial: a review of research approaches and models. *Scottish Geographical Magazine* **110**, 24-32.
- Bennett, M.R. (1995)** The morphology of glacially fluted terrain: examples from the Northwest Highlands of Scotland. *Proceedings of the Geologists' Association* **106**, 27-38.
- Bennett, M.R. and Boulton, G.S. (1993)** A reinterpretation of Scottish "hummocky moraine" and its significance for the deglaciation of the Scottish Highlands during the Younger Dryas or Loch Lomond Stadial. *Geological Magazine* **130**, 301-318.
- Bennett, M.R. and Glasser, N.F. (1991)** The glacial landforms of Glen Geusachan, Cairngorms: a reinterpretation. *Scottish Geographical Magazine* **107**, 116-123.
- Bennett, M.R. and Glasser, N.F. (1996)** *Glacial Geology. Ice Sheets and Landforms*. Wiley: Chichester. 364 pp.
- Bennett, M.R., Hambrey, M.J., Huddart, D. and Glasser, N.F. (1998)** Glacial Thrusting and Moraine-Mound Formation in Svalbard and Britain: the example of Coire a'Cheud-chnoic (Valley of the Hundred Hills), Torridon, Scotland. *Quaternary Proceedings* **6**, 17-34.
- Bennett, M.R., Waller, R.I., Glasser, N.F., Hambrey, M.J. and Huddart, D. (1999)** Glacigenic clast fabrics: genetic fingerprint or wishful thinking? *Journal of Quaternary Science* **14**, 125-135.
- Birkeland, P.W. (1984)** *Soils and Geomorphology*. Oxford University Press: New York.
- Birkeland, P.W. (1985)** Quaternary soil sequences in the western United States. In Boardman, J. (ed) *Soils and Geomorphology*. Wiley: Chichester & New York. p. 303-324.
- Bischoff, J.L. and Fitzpatrick, J.A. (1991)** U-series dating of impure carbonates: an evaluation of the isochron technique using total sample dissolution. *Geochimica et Cosmochimica Acta* **55**, 543-554.
- Blumenthal, M.M. (1958)** Vom Agri Dag (Ararat) zum Kaçkar Dag. Bergfahrten in nordostanatolischen Glanzlanden. *Die Alpen* **34**, 125-137.
- Boenzi, F., Palmentola, G., Sanso, P. and Tromba, F. (1992)** Le Tracce Glaciali Del Massiccio Dello Smolikas (Catena Del Pindo – Grecia). *Rivista Geografica Italiana* **99**, 379-393.
- Boenzi, F. and Palmentola, G. (1997)** Glacial features and snow-line trend during the last glacial age in the southern Apennines (Italy) and on Albanian and Greek mountains. *Zeitschrift für Geomorphologie* **41**, 21-29.

- Bögli, A. (1980)** *Karst Hydrology and Physical Speleology*. Springer-Verlag: Berlin. 284 pp.
- Bordonnau, J. (1992)** *Els complexos glacios-lacustres relacionats amb el darrer cicle glacial als pirineus*. Geoforma Ediciones: Logroño. 251 pp.
- Bottema, S. (1974)** *Late Quaternary Vegetation History of Northwestern Greece*. Ph.D. thesis. Rijksuniversiteit te Groningen.
- Bottema, S. (1978)** The late glacial in the Eastern Mediterranean and the Near East. In Brice, W.C. (ed) *The Environmental History of the Near and Middle East Since the Last Ice Age*. Academic Press: London. p. 15-28.
- Bottema, S. (1979)** Pollen investigations in Thessaly (Greece). *Palaeohistoria* **21**, 19-40.
- Bottema, S. (1995)** The Younger Dryas in the Eastern Mediterranean. *Quaternary Science Reviews* **14**, 883-891.
- Boulton, G.S. (1971)** Till genesis and fabric in Svalbard, Spitsbergen. In Goldthwait, R.P. (ed) *Till: A Symposium*. Ohio State University Press. p. 41-72.
- Boulton, G.S. (1976)** The origin of glacially-fluted surfaces: observations and theory. *Journal of Glaciology* **17**, 289-309.
- Boulton, G.S. (1978)** Boulder shapes and grain-size distributions of debris as indicators of transport paths through a glacier and till genesis. *Sedimentology* **25**, 773-799.
- Boulton, G.S. (1987)** A theory of drumlin formation by sub-glacial sediment deformation. In Menzies, J. and Rose, J. (eds) *Drumlin Symposium*. Balkema: Rotterdam. p. 25-80.
- Boulton, G.S., Dent, D.L. and Morris, E.M. (1974)** Subglacial shear formation and crushing in lodgement tills from south-east Iceland. *Geografiska Annaler* **56A**, 135-145.
- Brazier, V., Kirkbride, M.P. and Owens, I.F. (1998)** The relationship between climate and rock glacier distribution in the Ben Ohau Range, New Zealand. *Geografiska Annaler* **80A**, 193-207.
- Bryan, K. (1934)** Geomorphic processes at high altitudes. *Geographical Review* **24**, 655-656.
- Buckland, W. (1823)** *Reliquiae Diluvianae*. Murray: London. 303 pp.
- Büdel, J. (1952)** Bericht über klimamorphologische und Eiszeitforschungen in Niederafrika. *Erdkunde* **H. 2/3**.
- Buol, S.W., Hole, F.D. and McCracken, R.J. (1973)** *Soil Genesis and Classification*. Iowa State University Press. 2nd Edition.
- Calvet, M. (2004)** Le Glaciaire Quaternaire des Pyrénées Esquisse de Synthèse. In Ehlers, J. and Gibbard, P.L. (eds) *Quaternary Glaciations - Extent and Chronology. Part I: Europe*. Elsevier: Amsterdam.
- Candy, I., Black, S., Sellwood, B.W. and Rowan, J.S. (2003)** Calcrete profile development in quaternary alluvial sequences, southeast Spain: Implications for using calcretes as a basis for landform chronologies. *Earth Surface Processes and Landforms* **28**, 169-185.
- Carr, S. (1999)** The micromorphology of Last Glacial Maximum sediments in the Southern North Sea. *Catena* **35**, 123-145.

- Carr, S. (2001)** A glaciological approach for the discrimination of Loch Lomond Stadial landforms in the Brecon Beacons, South Wales. *Proceedings of the Geologists' Association* **112**, 253-262.
- Carr, S. (in press)** Micro-scale structures. In Evans, D.J.A. and Benn, D.I. (eds) *A field guide to Quaternary glacial sediments*. Arnold: London.
- Carlisle, D. (1983)** Concentration of uranium and vanadium in calcretes and gypcrettes. In Wilson, R.C.L. (ed) *Residual deposits*. Geological Society of London, Special Publication **11**. Blackwell: Oxford. p. 185-195.
- Carton, A., Dramis, F. and Smiraglia, C. (1988)** A first approach to the systematic study of rock glaciers in the Italian Alps. *Permafrost, Fifth Annual International Conference, Proceedings* **1**, 712-717.
- Cassoli, A., Corda, L., Lodoli, C., Malatesta, A., Molaroni, M.V. and Ruggeri, A. (1986)** Il glacialismo quaternario del gruppo Velino-Ocre-sirente. *Memoire Società Geologica Italiana* **35**, 855-867.
- Chaline, J. and Jerz, H. (1983)** Proposition de création d'un étage würmien par la sous-commission de Stratigraphie du Quaternaire européen de l'INQUA. *Bulletin de l'Association française pour l'étude du Quaternaire* **16**, 149-152.
- Chaline, J. and Jerz, H. (1984)** Arbeitsergebnisse der Subkommission für Europäische Quartärstratigraphie: Stratotypen des Würm-Glazials (Berichte der SEQS 6). *Eiszeitalter und Gegenwart* **35**, 185-206.
- Cheng, H., Edwards, R.L., Hoff, J., Gallup, C.D., Richards, D.A. and Asmerom, Y. (2000)** The half-lives of uranium-234 and thorium-230. *Chemical Geology* **169**, 17-33.
- Church, M. and Ryder, J.M. (1972)** Paraglacial sedimentation, a consideration of fluvial processes conditioned by glaciation. *Geological Society of America Bulletin* **83**, 3059-3072.
- Ciner, A. (2004)** Turkish Glaciers and Glacial Deposits. In Ehlers, J. and Gibbard, P.L. (eds) *Quaternary Glaciations - Extent and Chronology. Part I: Europe*. Elsevier: Amsterdam.
- Ciner, A., Deynoux, M. and Çörekcioglu, E. (1999)** Hummocky moraines in the Namaras and Susam Valleys, Central Taurids, SW Turkey. *Quaternary Science Reviews* **18**, 659-669.
- Cinque, A., Liccardo, C., Palma, B., Pappalardo, L., Rosskopf, C. and Sepe, C. (1990)** Le tracce glaciali nel Parco Nazionale d'Abruzzo (Appennino Centrale): nota preliminare. *Geografia Fisica e Dinamica Quaternaria* **13**, 121-133.
- Civjic, J. (1898)** Das Rilagebirge und seine ehemalige Vergletscherung. *Zeitschrift der Gesellschaft für Erdkunde zu Berlin* **33**, 200-253.
- Civjic, J. (1900)** L'Époque Glaciaire dans la Péninsule des Balkans. *Annales de Géographie* **9**, 359-372.
- Clark, I.D. and Fontes, J-C. (1990)** Paleoclimatic reconstruction in northern Oman based on carbonates from hyperalkaline ground waters. *Quaternary Research* **33**, 320-336.
- Clark, D.H., Clark, M.M., Gillespie, A.R. (1994)** Debris-covered glaciers in the Sierra Nevada, California, and their implications for snowline reconstructions. *Quaternary Research* **41**, 139-153.
- Clews, J.E. (1989)** Structural controls on basin evolution: Neogene to Quaternary of the Ionian zone, western Greece. *Journal of the Geological Society of London* **146**, 447-457.

- CLIMAP Project Members (1981)** Seasonal reconstructions of the Earth's surface at the last glacial maximum. *Geological Society of America Memoirs* **145**.
- COHMAP Members (1988)** Climatic changes of the last 18,000 years: observations and model simulations. *Science* **241** 1043-1052.
- Colman, S.M. and Pierce, K.L. (1986)** Glacial sequence near McCall, Idaho: weathering rinds, soil development, morphology and other relative age criteria. *Quaternary Research* **25**, 25-42.
- Conchon, O (1989)** Quaternary Glaciations in Corsica. *Quaternary Science Reviews* **5**, 429-432.
- Cooke, R.U. and Doornkamp, J.C. (1974)** *Geomorphology in environmental management : an introduction*. Clarendon Press: Oxford. 413 pp.
- Couvreur, G. (1966)** Les formations périglaciaires du Haut Atlas central Marocaine. *Revue de Géographie du Maroc* **10**, 47-50.
- Dana, J.D. (1863)** *Manual of geology*. Theodore Bliss & Co: Philadelphia. 798 pp.
- Daveau, S. (1971)** La Glaciation de la Serra de Estrela. *Finisterra, Revista portuguesa de geografia* (Centro de Estudos Geográficos, Faculdade de Letras, Universidade de Lisboa) **6**, 5-40.
- De Charpentier, J. (1834)** Sur la cause probable du transport des blocs érratiques de la Suisse. *Annales des Mines, 3e série*, **8**, 219-236.
- Diener, C. (1886)** *Libanon. Grundlinien der physischen Geographie und Geologie von Mittel-Syrien*. Wien. 412 pp.
- Demitrack, A. (1986)** *The late Quaternary geologic history of the Larissa Plain, Thessaly, Greece: tectonic, climatic, and human impact on the landscape*. Ph.D. thesis. Stanford University, California.
- Dikau, R., Schrott, L. and Dehn, M. (1996)** Topple. In Dikau, R., Brunsten, D., Schrott, L. and Ibsen, M.L. (eds) *Landslide recognition*. Wiley: Chichester. p. 29-42.
- Digerfeldt, G., Olson, S. and Sandgren, P. (2000)** Reconstruction of lake-level changes in lake Xinias, central Greece, during the last 40,000 years. *Palaeogeography, Palaeoclimatology, Palaeoecology* **158**, 65-82.
- Donner, J.J. and West, R.G. (1955)** Ett drumlinsfält på ön Skye, Skottland. *Eripainos Terrasta* **2**, 45-48.
- Dowdeswell, J.A., Hambrey, M.J. and Wu, R. (1985)** A comparison of clast fabric and shape data in Late Precambrian and modern glacial sediments. *Journal of Sedimentary Petrology* **55**, 691-704.
- Dramis, F. and Kotarba, A. (1994)** Geomorphological evidences of high mountain permafrost in Central Apennines. *Geografia Fisica e Dinamica Quaternaria* **17**, 29-36.
- Dresch, J. (1941)** Recherches sur l' évolution du relief dans le massif central du Grand Atlas: le Haouz et le Sous. *Publications de l'Institut des Haute-Etudes Marocaines: Tours* **26**. 156 pp.
- Dresch, J. (1949)** Sur des formations de remblaiement continental et la présence de formes glaciaires dans le Haut Atlas calcaire. *Comptes Rendus Sommaires des Séances de la Société Géologique de France* 1949, 169-171.

- Dresch, J. and Raynal, R. (1953)** Les formes glaciaires et périglaciaires dans le Moyen Atlas. *Comptes Rendus Sommaires des Séances de la Société Géologique de France* 1953, 195-197.
- Drew, F. (1873)** Alluvial and lacustrine deposits of the Upper-Indus Basin. *Quarterly Journal of the Geological Society of London* **29**, 441-471.
- Edwards, R.L., Chen, H. and Wasserburg, G.J. (1987)** ^{238}U - ^{234}U - ^{230}Th - ^{232}Th systematics and the precise measurement of time over the past 500,000 years. *Earth and Planetary Science Letters* **81**, 175-192.
- Ehlers, J. (1996)** *Quaternary and Glacial Geology*. Wiley: Chichester. 578 pp.
- Esmark, J. (1824)** Bidrag till vor jordklodes historie. *Magazin for Naturvidenskaberne* **3**, 29-54.
- Evin, M. and Fabre, D. (1990)** The distribution of permafrost in rock glaciers of the southern Alps (France). *Geomorphology* **3**, 57-71.
- Eyles, N. (1983)** Modern Icelandic glaciers as depositional models for "hummocky moraine" in the Scottish Highlands. In Evenson, E.B., Schlüchter, C. and Rabassa, J. (eds) *Tills and Related Deposits*. Balkema. p. 47-60.
- Eyles, N., Eyles, C.H. and Miall, A.D. (1983)** Lithofacies types and vertical profiles; an alternative approach to the description and environmental interpretation of glacial diamict and diamictite sequences. *Sedimentology* **30**, 393-410.
- Fairchild, I.J., Bradby, L. and Spiro, B. (1994)** Reactive carbonate in glacial systems: a preliminary synthesis of its creation, dissolution and reincarnation. In Deynoux, M., Miller, J.M.G., Domack, E.W., Eyles, N., Fairchild, I.J. and Young, G.M. (eds) *Earth's Glacial Record*. International Geological Correlation Project 260. Cambridge University Press. p. 176-192.
- Faugères, L. (1969)** Problems created by the geomorphology of Olympus, Greece: Relief, formation, and traces of Quaternary cold periods (with discussion). *Association Française pour l'Etude du Quaternaire Bulletin* **6**, 105-127.
- Federici, P.R. (1977)** Tracce di glacialismo prewürmiana nell'Appennino parmense. *Rivista Geografica Italiana* **84**, 205-216.
- Fisch, W., Sr., Fisch, W., Jr. and Haeblerli, W. (1977)** Electrical DC resistivity soundings with long profiles on rock glaciers and moraines in the Alps of Switzerland. *Zeitschrift für Gletscherkunde und Glazialgeologie* **13**, 239-260.
- Fisinger, W. and Ribolini, A. (2001)** Late glacial to Holocene deglaciation of the Colle Del Vei Bouc-Colle Del Sabbione Area (Argentera massif, Maritime Alps, Italy - France). *Geografia Fisica e Dinamica Quaternaria* **24**, 141-156.
- Flageollet, J.C. and Weber, D. (1996)** Fall. In Dikau, R., Brunnsden, D., Schrott, L. and Ibsen, M.L. (eds) *Landslide recognition*. Wiley: Chichester. p. 13-28.
- Flinn, D. and Pentecost, A. (1995)** Travertine-cemented screes on serpentinite seacliffs of Unst and Fetlar, Shetland. *Mineralogical Magazine* **59**, 259-265.
- Flint, R.F. (1971)** *Glacial and Quaternary Geology*. Wiley: New York. p. 90-93.
- Fliri, F. (1989)** Eine Bestimmung des Beginnes der Hupt-Würmvereisung im Zentralraum der Alpen (Albeins bei Brixen). *Der Schlern*, 62-65.

- Florineth, D. and Schlüchter, C. (2000)** Alpine evidence for Atmospheric Circulation Patterns in Europe during the Last Glacial Maximum. *Quaternary Research* **54**, 295-308.
- Flügel, E. (1982)** *Microfacies Analysis of Limestones*. Springer-Verlag: Berlin. Figures 40b and 40c.
- Forbes, E. (1846)** On the connexion between the distribution of existing fauna and flora of the British Isles, and the geological changes which have affected their area, especially during the Epoch of the northern drift. *Great Britain Geological Survey, Memoir* **1**, 336-432.
- Ford, D. and Williams, P. (1989)** *Karst geomorphology and Hydrology*. Unwin Hyman: London. 601 pp.
- Fotiadi, A.K., Metaxas, D.A. and Bartzokas, A. (1999)** A statistical study of precipitation in northwest Greece. *International Journal of Climatology* **19**, 1221-1232.
- French, H.M. (1996)** *The Periglacial Environment*. 2nd Edition. Longman: Harlow.
- Frogley, M.R. (1997)** *The biostratigraphy, palaeoecology and geochemistry of a long lacustrine sequence from NW Greece*. Ph.D. thesis, University of Cambridge.
- Frogley, M.R., Griffiths, H.I. and Heaton, T.H.E. (2001)** Historical biogeography and Late Quaternary environmental change of Lake Pamvotis, Ioannina (north-west Greece): evidence from ostracods. *Journal of Biogeography* **28**, 745-756.
- Furbish, D.J. and Andrews, J.T. (1984)** The use of hypsometry to indicate long-term stability and response of valley glaciers to changes in mass transfer. *Journal of Glaciology* **30**, 199-211.
- Furlan, D. (1977)** The Climate of Southeast Europe. In Wallen, C.C. (ed) *Climates of Central and Southern Europe*. Elsevier: Amsterdam. p. 185-223.
- Galanidou, N., Tzedakis, P.C., Lawson, I.T. and Frogley, M.R. (2000)** A revised chronological and palaeoenvironmental framework for the Kastritsa rockshelter, northwest Greece. *Antiquity* **74**, 349-355.
- Gale, S.J. and Hoare, P.G. (1997)** The glacial history of the northwest Picos de Europa of northern Spain. *Zeitschrift für Geomorphologie* **NF 41**, 81-96.
- Gams, I. (2004)** *Changes of the Triglav glacier in the 1955-94 period in the light of climatic indicators*. <http://ai.ijs.si/mezi/personal/triglav/index.htm>.
- García-Ruiz, J.M., Ortigosa, L., Gómez-Villar, A. and Martí-Bono, C. (2000)** Morphometry of glacial cirques in the Spanish Pyrenees. *Geographiska Annaler* **82A**, 433-442.
- García-Ruiz, J.M., Valero-Garcés, B.L., Martí-Bono, C. and González-Sampériz, P. (2003)** Asynchronicity of maximum glacier advances in the central Spanish Pyrenees. *Journal of Quaternary Science* **18**, 61-72.
- Gardiner, V and Dackombe, R.V. (1983)** *Geomorphological Field Manual*. George Allen and Unwin: London.
- Geikie, J. (1894)** *The Great Ice Age*. 3rd Edition. Edward Stanford: London.
- Gellatly, A.F., Smiraglia, C., Grove, J.M. and Latham, R. (1994)** Recent variations of Ghiacciaio del Calderone, Abruzzi, Italy. *Journal of Glaciology* **40**, 486-490.

- Gibbard, P.L. and Turner, C. (1990)** Cold stage type sections: some thoughts on a difficult problem. *Quaternaire* **1**, 33-40.
- Gibbard, P.L. and West, R.G. (2000)** Quaternary chronostratigraphy: the nomenclature of terrestrial sequences. *Boreas* **29**, 329-336.
- Giraudi, C. (1998)** The Late Quaternary geologic evolution of Campo Felice (Abruzzo – Central Italy). *Giornale di Geologia* **60**, 67-82.
- Giraudi, C. (2002)** Le oscillazioni oloceniche del Ghiacciaio del Calderone (Gran Sasso d'Italia Centrale) e le variazioni climatiche degli ultimi 3000 anni. *Il Quaternario* **15**, 145-150.
- Giraudi, C. (2003)** Middle Pleistocene to Holocene Apennine Glaciation (Italy). *Il Quaternario* **16**, 37-48.
- Giraudi, C. (2004)** The Apennine Glaciations in Italy. In Ehlers, J. and Gibbard, P.L. (eds) *Quaternary Glaciations - Extent and Chronology. Part I: Europe*. Elsevier.
- Giraudi, C. and Frezzotti, M. (1997)** Late Pleistocene glacial events in the Central Apennines, Italy. *Quaternary Research* **48**, 280-290.
- Glen, J.W., Donner, J.J. and West, R.G. (1957)** On the mechanism by which stones become orientated. *American Journal of Science* **255**, 194-205.
- Gordon, J.E., Whalley, W.B., Gellatly, A.F. and Vere, D.M. (1992)** The formation of glacial flutes: assessment of models with evidence from Lyngsdalen, north Norway. *Quaternary Science Reviews* **11**, 709-731.
- Goudie, A., Atkinson, B.W., Gregory, K.J., Simmons, I.G., Stoddart, D.R. and Sugden, D. (1994)** *The encyclopedic dictionary of physical geography*. Blackwell, Oxford. 2nd edition.
- Gravenor, C.P. and Kupsch, W.O. (1959)** Ice disintegration features in western Canada. *Journal of Geology* **12**, 48-64.
- Gray, J.M. (1982)** The last glaciers (Loch Lomond Advance) in Snowdonia, North Wales. *Geological Journal* **17**, 111-133.
- Gray, J.M. and Brooks, C.L. (1972)** The Loch Lomond Readvance moraines of Mull and Meinteith. *Scottish Journal of Geology* **8**, 95-103.
- Gray, J.M. and Coxon, P. (1991)** The Loch Lomond Stadial glaciation in Britain and Ireland. In Ehlers, J., Gibbard, P.L. and Rose, J. (eds) *Glacial Deposits in Great Britain and Ireland*. Balkema: Rotterdam. p. 89-105.
- Gray, J.M. and Lowe, J.J. (1982)** Problems in the interpretation of small scale erosional forms on glaciated bedrock surfaces: examples from Snowdonia, North Wales. *Proceedings of the Geologists' Association* **93**, 403-414.
- Griffiths, S.J., Street-Perrott, F.A., Holmes, J.A., Leng, M.J. and Tzedakis, P.C. (2002)** Chemical and isotopic composition of modern water bodies in the Lake Kopais Basin, central Greece: analogues for the interpretation of the lacustrine sedimentary sequence. *Sedimentary Geology* **148**, 79-103.
- Grootes, P.M. and Stuiver, M. (1997)** Oxygen 18/16 variability in Greenland snow and ice with 10⁽³⁾- and 10⁽⁵⁾- year time resolution. *Journal of Geophysical Research - Oceans* **102 (C12)**, 26455-26470.

- Gross, M.G. (1971)** Carbon determination. In Carver, R.E. (ed) *Procedures in Sedimentary Petrology*. Wiley: New York. p. 573-596.
- Gross, G., Kerschner, H. and Patzelt, G. (1976)** Methodische Untersuchungen über die Schneegrenze in alpinen Gletschergebieten. *Zeitschrift für Gletscherkunde und Glazialgeologie* **12**, 223-251.
- Haerberli, W. (1982)** Klimarekonstruktionen mit Gletscher-Permafrost-Beziehungen. *Baseler Beiträge zur Physiogeographie* **4**, 9-17.
- Haerberli, W. (1985)** Creep of mountain permafrost: internal structure and flow of alpine rock glaciers. *Mitteilungen der Versuchsanstalt für Wasserbau, Hydrologie und Glaziologie* **77**, Zürich.
- Haines-Young, R.H. and Petch, J.R. (1986)** *Physical Geography: its nature and methods*. Harper Row: London.
- Hambrey, M.J. (1994)** *Glacial Environments*. UCL Press.
- Hamlin, R.H.B. (2000)** *Environmental Change and Catastrophic Flooding in the Voidomatis and Aaos Basins, Northwest Greece*. Ph.D. thesis, University of Leeds.
- Hamlin, R.H.B., Woodward, J.C., Black, S. and Macklin, M.G. (2000)** Sediment fingerprinting as a tool for interpreting long-term river activity: the Voidomatis basin, Northwest Greece. In Foster, I.D.L. (ed) *Tracers in Geomorphology*. Wiley: Chichester. p. 473-501.
- Harden, J.W. (1982)** A Quantitative Index of Soil Development From Field Descriptions: Examples from a Chronosequence in Central California. *Geoderma* **28**, 1-28.
- Harden, J.W. and Taylor, E.M. (1983)** A Quantitative Comparison of Soil Development in Four Climatic Regimes. *Quaternary Research* **20**, 342-359.
- Harris, S.E. (1943)** Friction cracks and the direction of glacial movement. *Journal of Geology* **51**, 244-258.
- Harris, C. (1986)** Some observations concerning the morphology and sedimentology of a proglacial rampart, Oskindan, Norway. *Earth Surface Processes and Landforms* **11**, 673-676.
- Hart, J. (1994)** Till fabric associated with deformable beds. *Earth Surface Processes and Landforms* **19**, 15-32.
- Hawkins, F. (1985)** Equilibrium-line altitudes and palaeoenvironments in the Merchants Bay area, Baffin Island, NWT, Canada. *Journal of Glaciology* **31**, 205-213.
- Hérail, G. Hubschman, J. and Jalut, G. (1986)** Quaternary Glaciation in the French Pyrenees. *Quaternary Science Reviews* **5**, 397-402.
- Hewitt, S. (2001)** Pleistocene River Behaviour and Sediment Transfer in Glaciated Catchments of the Mediterranean. Ph.D. thesis, University of Leeds.
- Heybrock, W. (1953)** Eiszeitliche Gletscherspuren und heutige Schneeverhältnisse im Zentralgebiet des Hohen Atlas. *Zeitschrift für Gletscherkunde und Glazialgeologie* **2**, 317-321.
- Heybrock, W. (1954)** Firnverhältnisse auf Korsika. *Zeitschrift für Gletscherkunde und Glazialgeologie* **3**, 75-78.

- Heywood, D.I., Smith, G.R., Carlisle, B.H. and Jordon, G.H. (1999)** Global Positioning Systems as a Practical Field Work Tool: Applications in Mountain Environments. In Pacione, M. (ed) *Applied Geography*. Routledge. p. 593-604
- Higgs, E.S., Vita-finzi, C., Harris, D.R. and Fagg, A.E. (1967)** The climate, environment and industries of Stone Age Greece: part III. *Proceedings of the Prehistoric Society* **33**, 1-29.
- Hirvas, H. and Nehonen, K. (1990)** Field methods for former glacier indicator tracing. In Kujansuu, R. and Saarnisto, M. (eds) *Glacial indicator tracing*. Balkema. p. 217-247.
- Hodgson, D.M. (1982)** *Hummocky and fluted moraines in parts of northwest Scotland*. Ph.D. thesis, University of Edinburgh.
- Holmes., C.D. (1941)** Till fabric. *Bulletin of the Geological Society of America* **52**, 1299-1354.
- Hoppe, G. (1952)** Hummocky moraine regions with special reference to the interior of Norbotten. *Geografiska Annaler* **34**, 1-26.
- Huddart, D. and Hambrey, M.J. (1996)** Sedimentary and tectonic development of a high-arctic thrust moraine complex, Comfortlessbreen, Svalbard. *Boreas* **25**, 227-243.
- Hughes, P.D. (2002)** Loch Lomond Stadial glaciers in the Aran and Arenig Mountains, North Wales. *Geological Journal* **37**, 9-15.
- Hughes, P.D., Gibbard, P.L. and Woodward, J.C. (2003)** Relict rock glaciers as indicators of Mediterranean palaeoclimate during the Last Glacial Maximum (Late Würmian) of northwest Greece. *Journal of Quaternary Science* **18**, 431-440.
- Hughes, P.D., Gibbard, P.L. and Woodward, J.C. (2004)** Quaternary glaciation in the Atlas Mountains, North Africa. In Ehlers, J. and Gibbard, P.L. (eds) *Quaternary Glaciation- Extent and Chronology. Volume 3: Asia, Latin America, Africa, Australia, Antarctica*. Elsevier: Amsterdam. p. 255-260.
- Humlum, O. (1998)** Rock glaciers on the Faeroe Islands, the North Atlantic. *Journal of Quaternary Science* **13**, 293-307.
- Hutton, J. (1795)** *Theory of the Earth, Volume 2*. Creech: Edinburgh. 567 pp.
- IGME. (1970)** *1:50,000 Geological map of Greece. Tsepelovon Sheet*. Institute of Geological and Mineral Exploration: Athens.
- IGME. (1983)** *Geological map of Greece, northern part*. Institute of Geological and Mineral Exploration: Athens. 2nd Edition
- IGME. (1987)** *1:50,000 Geological map of Greece. Konitsa Sheet*. Athens: Institute of Geological and Mineral Exploration.
- Imbrie, J., Hays, J.D., Martinson, D.G., MacIntyre, A., Mix, A.C., Morlet, J.J., Pisias, N.G., Prell, W.L. and Shackleton, N.J. (1984)** The orbital theory of Pleistocene climate : support from a revised chronology of the marine $\delta^{18}\text{O}$ record. In Berger, A. Imbrie, J. Hays, J., Kukla, G. and Saltzman, B. (eds) *Milankovitch and Climate*. Reidel: Dordrecht. p. 269-305.
- International Commission on Stratigraphy (2004)** *International Stratigraphic Guide*. <http://www.stratigraphy.org/>
- Ivanovich, M. and Harmon, R.S. (1992)** *Uranium Series Disequilibrium: Applications to Earth, Marine and Environmental Sciences*. Clarendon Press: Oxford. 2nd Edition.

- Ivy-Ochs, S. (1996)** *The dating of rock surfaces using in-situ produced ^{10}Be , ^{26}Al and ^{36}Cl , with examples from Antarctica and the Swiss Alps*. Ph.D. thesis, ETH-Zurich, No. 11763.
- Jalut, G., Montserrat, J., Fontunge, M., Delibrias, G., Vilaplana, J. and Juliá, R. (1992)** Glacial to interglacial vegetation changes in the northern and southern Pyrenees: deglaciation, vegetation cover and chronology. *Quaternary Science Reviews* **11**, 449-480.
- Jaurand, E. (1994)** *Les heritages glaciaire de l'Appenin*. Thèse pour le Doctorat dès Lettres de l'Université de Paris I Panthéon-Sorbonne. 600 pp.
- Jaurand, E. (1998)** Glaciers disparu de l'Appenin: géomorphologie et paléoenvironnement glaciaires de l'Italie péninsulaire. *Monographie de l'Université de la Sorbonne, Géographie* **10**, 382 pp.
- Jennings, J.N. (1987)** *Karst Geomorphology*. Basil Blackwell: Oxford.
- Johnson, P.G. (1980)** Glacier-rock glacier transition in the southwest Yukon Territory Canada. *Arctic and Alpine Research* **12**, 195-204.
- Johnson, P.G. (1987)** Rock glaciers: glacial debris systems or high-magnitude low frequency flows. In Giardino, J.R., Schroder, F. and Vitek, J.D. (eds) *Rock glaciers*. George Allen and Unwin: London. p. 175-192.
- Johnson, P.G. and Lacasse, D. (1988)** Rock glaciers of the Dalton Range, Kluane Ranges, southwest Yukon Territory, Canada. *Journal of Glaciology* **34**, 327-332.
- Johnson, M.D., Mickleson, D.M., Clayton, L. and Attig, J.W. (1995)** Composition and genesis of glacial hummocks, western Wisconsin, USA. *Boreas* **24**, 97-116.
- Jones, A.P., Tucker, M.E. and Hart, J.K. (1999)** Chapter 3. Guidelines and Recommendations. In Jones, A.P., Tucker, M.E. and Hart, J.K. (eds), *The Description and Analysis of Quaternary Stratigraphic Field Sections. Technical Guide No. 7*. Quaternary Research Association.
- Karkanas, P. (2001)** Site formation processes in Theopetra cave: a record of climatic change during the Late Pleistocene and early Holocene in Thessaly, Greece. *Geoarchaeology: An International Journal* **16**, 373-399.
- Kaufman, A. (1993)** An evaluation of several methods for determining $^{230}\text{Th}/\text{U}$ ages in impure carbonates. *Geochimica et Cosmochimica Acta* **35**, 1269-1281.
- Kelly, M., Black, S. and Rowan, J.S. (2000)** A calcrete-based U/Th chronology for landform evolution in the Sorbas basin, southeast Spain. *Quaternary Science Reviews* **19**, 995-1010.
- Kerschner, H. (1978)** Palaeoclimatic inferences from Late Würm rock glaciers, Eastern Central Alps, Western Tyrol, Austria. *Arctic and Alpine Research* **10**, 635-644.
- Kerschner, H. (1983)** Late glacial paleotemperatures and paleoprecipitation as derived from permafrost:glacier relationships in the Tyrolean Alps, Austria. *Proceedings of the Fourth International Conference on Permafrost, Fairbanks* 589-594.
- King, G. and Bailey, G. (1985)** The palaeoenvironment of Some Archaeological Sites in Greece: The influence of Accumulated Uplift in a Seismically Active Region. *Proceedings of the Prehistoric Society* **51**, 273-282.
- King, G., Sturdy, D. and Whitney, J. (1993)** The landscape geometry and active tectonics of northwest Greece. *Geological Society of America Bulletin* **105**, 137-161.

- King, G., Sturdy, D. and Bailey, G. (1997)** The tectonic background to the Epirus Landscape. In Bailey, G.N. (ed) *Klithi: Palaeolithic settlement and Quaternary landscapes in northwest Greece, Volume 2: Klithi in its local and regional setting*. MacDonald Institute for Archaeological Research: Cambridge. p. 541-558.
- Kliment, K, Zoran, M. and Sofija, G. (2004)** *Natural Beauty of Macedonia*.
<http://www.soros.org.mk/konkurs/080/MPB.htm>.
- Kotarba, A., Hercman, H. and Dramis, F. (2001)** On the age of Campo Imperatore glaciations, Gran Sasso Massif, Central Italy. *Geografia Fisica e Dinamica Quaternaria* **24**, 65-69.
- Krumbein, W.C. (1941)** Measurement and geological significance of shape and roundness of sedimentary particles. *Journal of Sedimentary Petrology* **11**, 64-72.
- Ku, T.L. (2000)** Uranium-Series Methods. In Noller, J.S., Sowers, J.M. and Lettis, W.R. (eds) *Quaternary Geochronology: Methods and Applications*. American Geophysical Union: Washington DC. p. 101-114.
- Kubiëna, W.L. (1970)** *Micromorphological Features of Soil Geography*. Rutgers University Press: New Brunswick.
- Kurowski, L. (1891)** Die Höhe der Schneegrenze. *Geographischen Abhandlungen* **5**, 119-160.
- Kurter, A. and Sungur, K (1980)** Present glaciation in Turkey. *International Association of Hydrological Sciences* **126**, 155-160.
- Lambeck, K. (1995)** Late Pleistocene and Holocene sea-level change in Greece and south-western Turkey: a separation of eustatic, isostatic and tectonic contributions. *Geophysical Journal International* **122**, 1022-1044.
- Lamplugh, G.W. (1902)** Calcrete. *Geological Magazine* **9**, 575.
- Langmuir, D. and Herman, J.S. (1980)** The mobility of Thorium in natural waters at low temperatures. *Geochimica et Cosmochimica Acta* **44**, 1753-1766.
- Larcher, W. (1981)** Low temperature effects on Mediterranean Sclerophylls: An unconventional viewpoint. In Margaritis, N.S. and Mooney, H.A. (eds) *Components of Productivity of Mediterranean Climate Regions: Basic and Applied Aspects*. Dr. W. Junk Publishers: New York.
- Lawson, D.E. (1979)** Sedimentological analysis of the western terminus region of the Matanuska Glacier, Alaska. *United States Army Cold Regions Research and Engineering Laboratory, Research Report 79/9*. Hanover, NH.
- Lawson, D.E. (1981)** Distinguishing characteristics of diamictons at the margin of the Matanuska glacier, Alaska. *Annals of Glaciology* **2**, 78-84.
- Lawson, I.T. (2001)** The late glacial and holocene environmental history of Greece. Ph.D. thesis, University of Cambridge.
- Lawson, I.T. (2004)** The Lateglacial and Holocene environmental history of the Ioannina basin, north-west Greece. *Quaternary Science Reviews* **23**, 1599-1625.
- Lehmkuhl, F. (1998)** Quaternary Glaciations in Central and Western Mongolia. *Quaternary Proceedings* **6**, 153-167.

- Letsch, K. (1956)** Firnverhältnisse auf Korsika. *Zeitschrift für Gletscherkunde und Glazialgeologie* **3**, p. 268.
- Lewin, J., Macklin, M.G. and Woodward, J.C. (1991)** Late Quaternary fluvial sedimentation in the Voidomatis Basin, Epirus, northwest Greece. *Quaternary Research* **35**, 103-115.
- Lindholm, R. (1987)** *A Practical Approach to Sedimentology*. Allen and Unwin: London.
- Litt, T. and Turner, C. (1993)** Arbeitsergebnisse der Subkommission für Europäische Quartärstratigraphie: Die Saalesequenz in der Typusregion (Berichte der SEQS 10). *Eiszeitalter und Gegenwart* **43**, 125-128.
- Loewe, F. (1971)** Considerations of the origin of the Quaternary ice-sheet in North America. *Arctic and Alpine Research* **3**, 331-344.
- Loewenherz, D.S., Lawrence, C.J. and Weaver, R.L. (1989)** On the development of transverse ridges on rock glaciers. *Journal of Glaciology* **35**, 383-91.
- Louis, H. (1926)** Glazialmorphologische Beobachtungen im albanischen Epirus. *Zeitschrift der Gesellschaft für Erdkunde*. 398- 409.
- Louis, H. (1955)** Schneegrenze und Schneegrenzbestimmung. *Geographisches Taschenbuch* 1954/55, 414-418.
- Lowe, J. J. (1994)** Lateglacial and early Holocene lake sediments from the northern Apennines, Italy – pollen stratigraphy and radiocarbon dating. *Boreas* **21**, 193-208.
- Lowe, J.J. and Walker, M.J.C. (1997)** *Reconstructing Quaternary Environments*. 2nd Edition. Longman.
- Lundqvist, J. (1989)** Till and glacial deposits in a dry, polar region. *Zeitschrift für Geomorphologie* **33**, 27-41.
- Lyell, C. (1840)** On the Boulder Formation, or drift and associated freshwater deposits composing the mud-cliffs of eastern Norfolk. *The London and Edinburgh Philosophical Magazine and Journal of Science, Third Series* **16**, 345-380.
- Lyell, C. (1863)** *The Geological Evidences of the Antiquity of Man with Remarks on Theories of the Origin of the Species by Variation*. John Murray: London. 520 pp.
- Macklin, M., Lewin, J. and Woodward, J. (1997)** Quaternary River Sediment Sequences of the Voïdomatis Basin. In Bailey, G. (ed) *Klithi: Palaeolithic settlement and Quaternary landscapes in northwest Greece. Volume 2: Klithi in its local and regional setting*. McDonald Institute for Archaeological Research: Cambridge. 347-359.
- Macklin, M.G., Fuller, I.C., Lewin, J., Maas, G.S., Passmore, D.G., Rose, J., Woodward, J.C., Black, S., Hamlin, R.H.B. and Rowan, J.S. (2002)** Correlation of fluvial sequences in the Mediterranean basin over the last 200 ka and their relationship to climate change. *Quaternary Science Reviews* **21**, 1633-1641.
- Mark, D.M. (1973)** Analysis of axial orientation data, including till fabrics. *Geological Society of America Bulletin* **84**, 1369-1374.
- Marjanac, L. and Marjanac, T. (2004)** Glacial history of the Croatian Adriatic and Coastal Dinarides. In Ehlers, J. and Gibbard, P.L. (eds) *Quaternary Glaciations - Extent and Chronology. Part I: Europe*. Elsevier: Amsterdam.

- Martin, H.E. and Whalley, W.B. (1987)** Rock glaciers: a review. Part 1. *Progress in Physical Geography* **11**, 260 - 282.
- Martin, G.C., Ferguson, L. and V.S. Polito. 1994.** Flowering, pollination, fruiting, alternate bearing, and abscission. In Ferguson, L., Sibbett, G.S. and Martin, G.C. (eds.) *Olive production manual*. University of California: Division of Agriculture and Natural Resources. Publication 3353. p. 51-56.
- Mastronuzzi, G., Sanso, P. and Stamatopoulous, L. (1994)** Glacial landforms of the Peloponnisos (Greece). *Rivista Geografica Italiana* **101**, 77-86.
- Matthews, R.K. (1984)** *Dynamic stratigraphy : an introduction to sedimentation and stratigraphy*. 2nd Edition. Prentice-Hall: London.
- Matthews, J.A., Cornish, R. and Shakesby, R.A. (1979)** 'Saw-tooth' moraines in front of Bodalsbreen, southern Norway. *Journal of Glaciology* **22**, 535-546.
- Matthews, J.A. and Petch, J.R. (1982)** Within-valley assymetry and related problems of Neoglacial lateral moraine development at certain Jotunheimen glaciers, southern Norway. *Boreas* **11**, 225-247.
- Mehra, O.P. and Jackson, M.L. (1960)** Iron oxide removal from soils and clays by a dithionite-citrate system buffered with sodium bicarbonate. *Proceedings of the 7th National Conference on Clays and Minerals*. Pergamon: New York. p. 317-327.
- Meier, M.F. and Post, A.S. (1962)** Recent variations in mass net budgets of glaciers in western North America. *International Association of Hydrological Sciences Publication* **58**, 63-77.
- Meierding, T.C. (1982)** Late Pleistocene glacial equilibrium-line in the the Colorado Front Range: a comparison of methods. *Quaternary Research* **18**, 289-310.
- Menkovic, L. and Markovic, M. (2004)** Glacial Morphology of Serbia (Yugoslavia), with comments on the Pleistocene Glaciation of Montenegro, Macedonia and Albania. In Ehlers, J. and Gibbard, P.L. (eds) *Quaternary Glaciations - Extent and Chronology. Part I: Europe*. Elsevier: Amsterdam.
- Mensching, H. (1953)** Morphologische Studien im Hohen Atlas von Marokko. *Würzburger Geographische Arbeiten*, **Heft 1**. 104 pp.
- Mensching, H. (1960)** Bericht und Gedanken zur Tagung der Kommission für Periglazialforschung in der IGU in Marokko vom 19. bis 31. Oktober 1959. *Zeitschrift für Geomorphologie NF* **4**, 159-170.
- Menzies, J. and van der Meer, J.J.M. (1998)** Sedimentological and micromorphological examination of a Late Devensian multiple diamicton sequence near Moneydie, Perthshire, east-central Scotland. *Scottish Journal of Geology* **34**, 15-22.
- Mercer, D.C. (1963)** Cambridge expedition to the Pindus Mountains, Greece, 1962. *Cave Research Group of Great Britain Newsletter* **87**, 1-5.
- Messerli, B. (1967)** Die eiszeitliche und die gegenwartige Vertgletscherung im Mittelemeeraum. *Geographica Helvetica* **22**, 105-228.
- Miall, A.D. (1977)** A review of the braided river depositional environment. *Earth Science Reviews* **13**, 1-62.

- Mistardis, G. (1952)** Recherches glaciologiques dans les parties supérieures des Monts Oeta et Oxya (Grèce Centrale). *Zeitschrift für Gletscherkunde und Glazialgeologie* **2**, 72-79.
- Morris, S.E. and Olyphant, G.A. (1990)** Alpine lithofacies variation: working towards a physically-based model. *Geomorphology* **3**, 73-90.
- Müller, F. (1980)** Present and late Pleistocene equilibrium line altitudes in the Mt Everest region - an application of the glacier inventory. *International Association of Hydrological Sciences Publication* **126**, 75-94.
- Munsell (1975)** *Soil Color Charts*. Kollmorgen Corporation: Baltimore.
- Nash, D.J. and Smith, R.F. (1998)** Multiple calcrete profiles in the Tabernas Basin, Southeast Spain: their origins and geomorphic implications. *Earth Surface Processes and Landforms* **23**, 1009-1029.
- Nash, D.J. and Smith, R.F. (2003)** Properties and development of channel calcretes in a mountain catchment, Tabernas Basin, southeast Spain. *Geomorphology* **50**, 227-250.
- Nesje, A. and Dahl, S.O. (2000)** *Glaciers and Environmental Change: Key Issues in Environmental Change Series*. Arnold.
- Niculescu, C. (1915)** Sur les traces de glaciation dans le massif Smolica (chaîne du Pinde méridional). *Bulletin de la Section Scientifique de l'Academie Roumaine* **3**, 146-151.
- Ninkovich, D. and Shackleton, N.J. (1975)** Distribution, stratigraphic position and age of ash "L", in the Panama Basin region. *Earth and Planetary Science Letters* **27**, 20-34.
- Nye, N.F. (1965)** The flow of a glacier in a channel of rectangular, elliptic or parabolic cross-section. *Journal of Glaciology* **5**, 661-690.
- Ohmura, A., Kasser, P. and Funk, M. (1992)** Climate at the equilibrium line of glaciers. *Journal of Glaciology* **38**, 397-411.
- Okuda, M., Yasuda, Y. and Setoguchi, T. (2001)** Latest Pleistocene and Holocene records from Lake Kopais, Southeast Greece. *Geological Society of Japan* **105**, 450-455.
- Okuda, M., Yasuda, Y., Setoguchi, T. (2001)** Middle to Late Pleistocene vegetation history and environmental changes at Lake Kopais, Southeast Greece. *Boreas* **30**, 73-82.
- Orombelli, G. (1974)** Alcune date 14C per il Quaternario lombardo. *Studi Trentini di Scienze Naturali* **51**, 125-127.
- Osmaston, H. (1965)** The Past and Present Climate and Vegetation of Ruwenzori and its neighbourhood. D.Phil thesis, University of Oxford.
- Osmaston, H. (2002)** Chapter 9. The nature, extents and climates of former Quaternary tropical glaciers, with reference to the East African Mountains. In Kaser, G. and Osmaston, H. (eds) *Tropical Glaciers*. Cambridge University Press: Cambridge. p. 149-192.
- Outcalt, S.E. and Benedict, J.B. (1965)** Photo interpretation of two types of rock glaciers in the Colorado Front Range, USA. *Journal of Glaciology* **5**, 849-846.
- Owen, L.A., Derbyshire, E. and Fort, M. (1998)** The Quaternary Glacial History of the Himalaya. *Quaternary Proceedings* **6**, 91-120.
- Palgrave, W.G. (1872)** Vestiges of the glacial period in northeastern Anatolia. *Nature* **5**, 444-445.

- Palmentola, G. and Acquafredda, P. (1983)** Gli effetti dei ghiacciai quaternari sulla Montagna del Matese, al confine Molisano-Campao. *Geografia Fisica e Dinamica Quaternaria* **6**, 117-130.
- Palmentola, G., Boenzi, F., Mastronuzzi, G., and Tromba, F. (1990a)** Osservazioni sulle tracce glaciali del M. Timfi, catena del Pindo (Grecia). *Geografia Fisica e Dinamica Quaternaria* **13**, 165-170.
- Palmentola, G., Acquafredda, P. and Fiore, S. (1990b)** A new correlation of the glacial moraines in the southern Apennines, Italy. *Geomorphologie* **3**, 1-8.
- Palmentola, G., Baboci, K., Gruda, G. and Zito, G. (1995)** A note on rock glaciers in the Albanian Alps. *Permafrost and Periglacial Processes* **6**, 251-257.
- Paterson, W.S.B. (1981)** *The Physics of Glaciers*. Pergamon: Oxford. 2nd edition.
- Peacock, J.D. (1967)** West Highland morainic features aligned in the direction of ice flow. *Scottish Journal of Geology* **3**, 372-373.
- Pechoux, P.Y. (1970)** Traces of glacial action in the Mountains of Central Greece. *Revue de Géographie Alpine* **58**, 211-224.
- Pedley, H.M. (1990)** Classification and environmental models of cool freshwater tufas. *Sedimentary Geology* **68**, 143-154.
- Penck, A. (1885)** La Période glaciaire dans les Pyrénées. *Bulletin de la Societe d'Histoire Naturelle de Toulouse* **19**, 105-200.
- Penck, A. and Brückner, E. (1909)** *Die Alpen im Eiszeitalter*. Tauchnitz: Leipzig: 3 volumes, 1199 pp.
- Pentecost, A. (1991)** Springs that turn life to stone. *New Scientist* **132**, 42-44.
- Pentecost, A. (1993)** British Travertines: a review. *Proceedings of the Geologists' Association* **104**, 23-39.
- Pentecost, A. (1995)** The Quaternary Travertine deposits of Europe and Asia Minor. *Quaternary Science Reviews* **14**, 1005-1028.
- Pentecost, A. and Viles, H. (1994)** A review and reassessment of travertine classification. *Géographie Physique et Quaternaire* **48**, 305 – 314.
- Pérez, F.L. (1988)** Debris Transport over snow surfaces: a field experiment. *Revue de Géomorphologie Dynamique* **37**, 357-368.
- Peyron, O., Guiot, J., Cheddadi, R., Tarasov, P., Reille, M., de Beaulieu, J-L., Bottema, S. and Andrieu, V. (1998)** Climatic reconstruction in Europe for 18,000 YR B.P. from Pollen Data. *Quaternary Research* **49**, 183-196.
- Polunin, O. (1980)** *Flowers of Greece and the Balkans – a Field Guide*. Oxford University Press: Oxford. 389 pp.
- Porter, S.C. (1975)** Equilibrium-line altitudes of late Quaternary glaciers in the Southern Alps, New Zealand. *Quaternary Research* **5**, 27-47.
- Porter, S.C. and Orombelli, G. (1982)** Late-glacial ice advances in the western Italian Alps. *Boreas* **11**, 125-140.

- Potter, N. (1972)** Ice-cored rock glacier, Galena Creek, northern Absaroka Mountains, Wyoming. *Geological Society of America Bulletin* **83**, 3025-3057.
- Powers, M.C. (1953)** A new roundness scale for sedimentary particles. *Journal of Sedimentary Petrology* **23**, 117-119.
- Prentice, I.C., Guiot, J. and Harrison, S.P. (1992)** Mediterranean vegetation, lake levels and palaeoclimate at the Last Glacial Maximum. *Nature* **360**, 658-660.
- Price, R.J. (1976)** *Glacial and Fluvio-glacial Landforms*. Longman: London.
- Pumpelly, R. (1859)** Sur quelques glaciers dans l'île de Corse. *Bulletin de la Société Géologique de France* **17**, p.78.
- Raghavan, H. and Courty, M.A. (1987)** Holocene and Pleistocene environments in the Thar Desert (Didwana, India). In Fedoroff, N. and Courty, M.A. (eds) *Micromorphologie des Sols*. Association Française pour l'Etude du Sol. p. 371-375.
- Rawson, P.F., Allen, P.M., Brencley, P.J., Cope, J.C.W., Gale, A.S., Evans, J.A., Gibbard, P.L., Gregory, F.J., Hailwood, E.A., Hesselbo, S.P., Knox, R.W.O'B., Marshall, J.E.A., Oates, M., Riley, N.J., Smith, A.G., Trewin, N., Zalasiewicz, J.A. (2002)** *Stratigraphical Procedure*. The Geological Society: London.
- Raynal, R. (1952)** Quelques exemples de l'action du froid et le neige sur les formes du relief au Maroc. *Notes Marocaines* **2**, 14-18.
- Raynal, R., Dresch, J. and Joly, F. (1953)** Deux exemples régionaux de glaciation quaternaire au Maroc: Haut Atlas Oriental, Moyen Atlas Septentrional. *IV Congrès INQUA, Rome-Pisa, 1953*. p. 65.
- Rea, B.R., Whalley, W.B., Evans, D.J.A., Gordon, J.E. and McDougall, D.A. 1998** Plateau icefields: geomorphology and dynamics. *Quaternary Proceedings* **6**, 35-54.
- Reille, M. (1975)** *Contribution pollenanalytique à l'histoire tardiglaciaire et holocène de la végétation de la montagne corse*. Thèse Doctorat, Etat, Marseilles.
- Ribolini, A. (1996)** Note geomorfologiche sull'alta Valle del Sabbione e sulla Val'd'Ischietto (Gruppo dell'Argentera, Alpi Marittime). *Geografia Fisica e Dinamica Quaternaria* **19**, 79-91.
- Ribolini, A. (2001)** Active and fossil rock glaciers in the Argentera Massif (Maritime Alps): surface ground temperatures and paleoclimatic significance. *Zeitschrift für Gletscherkunde und Glazialgeologie* **37**, 125-140.
- Robinson, D.A. and Williams, R.B.G. (1992)** Sandstone weathering in the High Atlas, Morocco. *Zeitschrift für Geomorphologie* **36**, 413-429.
- Rossignol-Strick, M. (1995)** Sea-land correlation of pollen records in the eastern Mediterranean for the glacial-interglacial transition: biostratigraphy versus radiometric timescale. *Quaternary Science Reviews* **14**, 893-915.
- Rune, A. (1996)** Topographic control of equilibrium-line altitude depression. *The Holocene* **6**, 82-88.
- Russell, R.J. (1933)** Alpine landforms of the western United States. *Bulletin of the Geological Society of America* **44**, 927-950.

- Salvador, A. (ed) (1994)** *International Stratigraphic Guide: A Guide to Stratigraphic Classification, Terminology and Procedure*. 2nd Edition. International Subcommission on Stratigraphy, Geological Society of America.
- Schneer, C.J. (1969)** Introduction. In Schneer, C.J. (ed) *Towards a history of Geology*. The Massachusetts Institute of Technology Press: Cambridge and London. p. 1-18.
- Schwarz, H.P. and Rink, W.J. (2001)** Dating Methods for Sediments of Caves and Rockshelters with Examples from the Mediterranean Region. *Geoarchaeology: An International Journal* **16**, 355-371.
- Serrat, D. (1979)** Rock glaciers and moraine deposits in the eastern Pyrenees. In Schlüchter, C. (ed) *Moraines and Varves*. Balkema: Rotterdam. 93-100.
- Seret, G., Dricot, J. and Wansard, G. (1990)** Evidence for an early glacial maximum in the French Vosges during the last glacial cycle. *Nature* **346**, 453-456.
- Sestini, A. (1933)** Tracce glaciali sul Pindo epirota. *Bollettino della Reale Società Geografica Italiano* **10**, 136-156.
- Shackleton, N.J. and Opdyke, N.D (1976)** Oxygen isotope and palaeomagnetic stratigraphy of equatorial Pacific core V28-239, late Pliocene to latest Pleistocene. In Cline, R.M. and Hays, R.D. (eds) *Investigation of Late Quaternary Palaeoceanography and Palaeoclimatology*. *Memoirs of the Geological Society of America* **145**, 449-464.
- Shackleton, N.J. and Pisias, N.G. (1985)** Atmospheric carbon dioxide, orbital forcing, and climate. In Sundquist, E.T. and Broecker, W.S. (eds) *The carbon cycle and atmospheric CO₂: natural variations archaean to the present*. Geophysical Monograph 32. American Geophysical Union: Washington. p. 303-317.
- Shackleton, N.J., Berger, A. and Peltier, W.R. (1990)** An alternative astronomical calibration of the lower Pleistocene timescale based on ODP Site 677. *Transactions of the Royal Society of Edinburgh: Earth Sciences* **81**, 251-261.
- Shakesby, R.A. (1989)** Variability in Neoglacial moraine morphology and composition, Storbreen, Jotunheimen, Norway: within-moraine patterns and their implications. *Geografiska Annaler* **71A**, 17-29.
- Shakesby, R.A. (1997)** Pronival (protalus) ramparts: a review of forms, processes, diagnostic criteria and palaeoenvironmental implications. *Progress in Physical Geography* **21**, 394-418.
- Shakesby, R.A., Matthews, J.A., McEwen, L.J. and Berrisford, M.S. (1999)** Snow-push processes in pronival (protalus) rampart formation: Geomorphological evidence from Smorbotn, Romsdalsalpane, southern Norway. *Geografiska Annaler* **81A**, 31-45.
- Shakesby, R.A. and Matthews, J.A. (1993)** Loch Lomond Stadial glacier at Fan Hir, Mynydd Du (Brecon Beacons), South Wales: critical evidence and palaeoclimatic implications. *Geological Journal* **28**, 69-79.
- Shakesby, R.A., Matthews, J.A., McEwen, L.J. and Berrisford, M.S. (1999)** Snow-push processes in pronival (protalus) rampart formation: Geomorphological evidence from Smorbotn, Romsdalsalpane, southern Norway. *Geografiska Annaler*, **81A**, 31-45.
- Sharp, M. (1982)** Modification of clasts in lodgement tills by glacial erosion. *Journal of Glaciology* **28**, 475-481.

- Sharp, M.J. (1985)** Sedimentation and stratigraphy at Eyjabakkajökull: an icelandic surging glacier. *Quaternary Research* **24**, 268-284.
- Sibrava, V., Bowen, D.Q. and Richmond, G.M. (eds) (1986)** Quaternary Glaciations in the Northern Hemisphere. *Quaternary Science Reviews* **5**.
- Sifrer, M. (1963)** New findings about the glaciation of Triglav. *Geografiski Zbornik* **8**. Ljubljana.
- Singer, M.J., Fine, P., Verosub, K.L. and Chadick, O.A. (1992)** Time dependence of magnetic susceptibility of soil chronosequences on the Californian coast. *Quaternary Research* **37**, 323-332.
- Sissons, J.B. (1967)** *The evolution of Scotland's scenery*. Oliver and Boyd: Edinburgh & London. 259 pp.
- Sissons, J.B. (1974)** A Lateglacial ice-cap in the central Grampians, Scotland. *Transactions of the Institute of British Geographers* **62**, 95-114.
- Sissons, J.B. (1979a)** The Loch Lomond Stadial in the British Isles. *Nature* **280**, 199-203.
- Sissons, J.B. (1979b)** The Loch Lomond Readvance in the Cairngorm mountains. *Scottish Geographical Magazine* **96**, 18-19.
- Sissons, J.B. (1980)** The Loch Lomond Advance in the Lake District, northern England. *Transactions of the Royal Society of Edinburgh: Earth Science* **71**, 13-27.
- Sladen, J.A. and Wrigley, W. (1983)** Geotechnical Properties of Lodgement Till – A Review. In Evenson, E.B., Schlüchter, C. and Rabassa, J. (eds), *Tills and Related Deposits*. Balkema. p. 184-186.
- Smart, P.L. (1986)** Origin and development of glacio-karst closed depressions in the Picos de Europa, Spain. *Zeitschrift für Geomorphologie NF* **30**, 423-443.
- Smart, P.L. (1991)** Uranium Series Dating. In Smart, P.L. and Frances, P.D. (eds) *Quaternary dating methods - a users guide. Technical Guide No. 4*. Quaternary Research Association. p. 45-83.
- Smith, A.G. and Moores, E.M. (1974)** Hellenides. In Spencer, R.A. (ed) *Mesozoic and Cenozoic Orogenic Belts. Special Publication of the Geological Society of London* **4**, 159-185.
- Smith, G.W., Nance, R.D. and Genes, A.N. (1997)** Quaternary Glacial History of Mount Olympus. *Geological Society of America Bulletin* **109**, 809-824.
- Smith, G.R., Woodward, J.C., Heywood, D.I. and Gibbard, P.L. (2000)** Interpreting glacial features from SPOT HRV data using fuzzy techniques. *Computers and Geosciences* **26**, 479-490.
- Soil Survey Staff (1951)** *Soil Survey Manual*. United States Department of Agriculture Handbook **18**.
- Stefanova, I. and Ammann, B. (2003)** Lateglacial and Holocene vegetation belts in the Pirin Mountains (southwestern Bulgaria). *The Holocene* **13**, 97-107.
- Sutherland, D.G. (1984)** Modern glacier characteristics as a basis for inferring former climates with particular reference to the Loch Lomond Stadial. *Quaternary Science Reviews* **3**, 291-309.
- Sweeting, M. (1966)** The weathering of limestones, with particular reference to the Carboniferous Limestones of northern England. In Dury, G.H. (ed) *Essays in Geomorphology*. Heineman. p. 177-210.

- Sweeting, M. (1972)** *Karst Landforms*. Macmillan Press. p. 263- 269
- Swett, K. (1974)** Calcrete crusts in an Arctic permafrost environment. *American Journal of Science* **274**, 1059-1063.
- Taylor, P.J. and Mitchell, W.A. (2000)** The Quaternary glacial history of the Zaskar Range, north-west Indian Himalaya. *Quaternary International* **65/66**, 81-99.
- Thorp, P. (1981)** A trimline method for defining the upper limit of Loch Lomond Advance glaciers: examples from the Loch Leven and Glen Coe areas. *Scottish Journal of Geology* **17**, 49-64.
- Tihay, J-P. (1972)** Modelés cryonival et glaciaire dans la haute montagne Algérienne: l'exemple de la chaîne du Djurdjura (Grande Kabylie). *Revue de Géographie de Montréal* **26**, 447-463.
- Tihay, J-P. (1973)** Note sur quelques paléoformes <périglaciaires> observées en Algérie orientale. Méditerranée **13**, 2, 37-47.
- Turner, J. and Greig, J.R.A. (1975)** Some Holocene pollen diagrams from Greece. *Review of Palaeobotany and Palynology* **20**, 171-204.
- Turner, C. and West. R.G. (1968)** The sub-division and zonation of interglacial periods. *Eiszeitalter und Gegenwart* **19**, 93-101.
- Twidale, C.R. (1980)** Origin of some minor sandstone landforms. *Erdkunde* **34**, 219-224.
- Tzedakis, P.C. (1993)** Long-term tree populations in northwest Greece through multiple Quaternary climatic cycles. *Nature* **364**, 437-440.
- Tzedakis, P.C. (1994)** Vegetation change through glacial-interglacial cycles: a long pollen sequence perspective. *Philosophical Transactions of the Royal Society of London* **B345**, 403-432.
- Tzedakis, P.C. (1999)** The last climatic cycle at Kopais, central Greece. *Journal of the Geological Society* **156**, 425-434.
- Tzedakis, P.C., Andrieu, V., de Beaulieu, J.L., Crowhurst, S., Follieri, M., Hooghiemstra, H., Magri, D., Reille, M., Sadori, L., Shackleton, N.J. and Wijmstra, T.A. (1997)** Comparison of terrestrial and marine records of changing climate of the last 500,000 years. *Earth and Planetary Science Letters* **150**, 171-176.
- Tzedakis P.C., Lawson I.T., Frogley M.R., Hewitt G.M., Preece R.C. (2002)** Buffered Tree Population Changes in a Quaternary Refugium: Evolutionary Implications. *Science* **297**, 2044-2047.
- Tzedakis, P.C. (2003)** Timing and duration of Last Interglacial conditions in Europe: a chronicle of a changing chronology. *Quaternary Science Reviews* **22**, 763-768.
- Tzedakis, P.C., Frogley, M.R. and Heaton, T.H.E. (2003a)** Last interglacial conditions in southern Europe: evidence from Ioannina, northwest Greece. *Global and Planetary Change* **36**, 157-170.
- Tzedakis, P.C., McManus, J.F., Hooghiemstra, H., Oppo, D.W., Wijmstra, T.A. (2003b)** Comparison of changes in vegetation in northeast Greece with records of climate variability on orbital and suborbital frequencies over the last 450,000 years. *Earth and Planetary Science Letters* **212**, 197-212.

- Tscherko, D., Rustemeier, J., Richter, A., Wanek, W., Kandeler, E. (2003)** Functional diversity of the soil microflora in primary succession across two glacier forelands in the Central Alps. *European Journal of Soil Science* **54**, 685-696.
- van Andel, T.H. (1998)** Paleosols, Red Sediments, and the Old Stone Age in Greece. *Geoarchaeology: An International Journal* **13**, 361-390.
- van Andel, T.H. and Shackleton, J.C. (1982)** Late Paleolithic and mesolithic coastlines of Greece and the Aegean. *Journal of Field Archaeology* **9**, 445-454.
- van Andel, T. H., Zangger, E. and Demitrack, A. (1990)** Land use and soil erosion in prehistoric Greece. *Journal of Field Archaeology* **17**, 379-396.
- van der Meer, J.J.M. (1997)** Subglacial processes revealed by the microscope: particle and aggregate mobility in till. *Quaternary Science Reviews* **16**, 827-831.
- van der Wiel, A.M. and Wijmstra, T.A. (1987a)** Palynology of the lower part (78-120 m) of the core Tenaghi Philippon II, Middle Pleistocene of Macedonia, Greece. *Review of Palaeobotany and Palynology* **52**, 73-88.
- van der Wiel, A.M. and Wijmstra, T.A. (1987b)** Palynology of 112.8-197.8 m interval of the core Tenaghi Philippon III, Middle Pleistocene of Macedonia, Greece. *Review of Palaeobotany and Palynology* **52**, 89-117.
- van Zeist, W. and Bottema, S. (1991)** *Late Quaternary Vegetation of the Near East*. Beihefte zum Tübinger Atlas des Vorderen Orients. Reihe A, Naturwissenschaften. Nr. 18. Wiesbaden. 156 pp.
- Vincent, P. (1985)** Chapter 9. Quaternary geomorphology of the southern Lake District and Morecambe Bay area. In Johnson, R.H. (ed) *The geomorphology of North-west England*. Manchester University Press.
- Vogt, T. and Delvalle, H.F. (1994)** Cryogenic structures in the area of Puerto-Madrin (Chubut, Patagonia, Argentina) *Geografiska Annaler A* **76**, 57-75.
- von Buch, L. (1815)** Über die Verbreitung großer Alpengeschiebe. *Abhandlungen der Physikalischen Classe der Akademie der Wissenschaften Berlin* **1804-1811**, 161-186.
- von Humboldt, A. (1845)** *Kosmos – Entwurf einer physischen Weltbeschreibung*, Band 1. Cotta: Stuttgart & Augsburg. 507 pp.
- Vonder Mühll, D. and Haerberli, W. (1990)** Thermal characteristics of the permafrost within an active rock glacier (Murtèl/Corvatsch, Grisons, Swiss Alps). *Journal of Glaciology* **36**, 151-158
- Waltham, A.C. (1978)** The Caves and Karst of Astraka, Greece. *Transactions of the British Cave Research Association* **5**, 1-12.
- Washburn, A.L. (1979)** *Geocryology: a survey of periglacial processes and environments*. Edward Arnold: London.
- Watson, G.S. (1966)** The statistics of fabric orientation data. *Journal of Geology* **74**, 786-797.
- West, R.G. (1984)** Interglacial, interstadial and oxygen isotope stages. *Dissertationes Botanicae* **72**, 345-357.
- West, R.G. (1988)** The record of cold stages. *Philosophical Transactions of the Royal Society, London B* **318**, 505-522.

- West, R.G. and Donner, J.J. (1956)** The glaciations of East Anglia and the East Midlands: a differentiation based on stone-orientation measurements of the tills. *Quarterly Journal of the Geological Society of London* **112**, 69-91.
- Whalley, W.B., Palmer, C., Hamilton, S. and Gordon, J. (1994)** Ice exposures in rock glaciers. *Journal of Glaciology* **40**, 427-429.
- Whittaker, A., Cope, J.C.W., Cowie, J.W., Gibbons, W., Hailwood, E.A., House, M.R., Jenkins, D.G., Rawson, P.F., Rushton, A.W.A, Smith, D.G., Thomas, A.T. and Wimbledon, W.A. (1992)** A guide to stratigraphical procedure. *Journal of the Geological Society, London* **148**, 813-824.
- Whiteman, C.D. (2000)** *Mountain Meteorology: fundamentals and applications*. Oxford University Press: Oxford.
- White, S.E. (1975)** Additional data on Arapaho rock glacier in the Colorado Front Range, USA. *Journal of Glaciology* **14**, 529-530.
- Wiche, K. (1953)** Klimamorphologische und talgeschichtliche Studien im M'Gounggebiet. *Mitteilungen Der Geographischen Gesellschaft Wien* **95**, 4-41.
- Wijmstra, T.A. (1969)** Palynology of the first 30 metres of a 120 m deep section in Northern Greece. *Acta Botanica Neerlandica* **18**, 511-527.
- Wijmstra, T.A. and Groenhart, M.C. (1983)** record of 700 000 years vegetational history in Eastern Macedonia (Greece). *Revsita de la Academia Colombiana de Ciencias Exactas, fisicias y naturales/ Ministerio de education Nacional* **15**, 87-98.
- Wijmstra, T.A. and Smit, A. (1976)** Palynology of the middle part (30-78 metres) of the 120 m deep section in Northern Greece (Macedonia). *Acta Botanica Neerlandica* **25**, 297-312.
- Williams, P.W. (1966)** Limestone pavements with special reference to western Ireland. *Transactions of the Institute of British Geographers* **40**, 155-172.
- Willis, K. J. (1994)** The vegetational history of the Balkans. *Quaternary Science Reviews* **13**, 769-788.
- Willis, K.J. (1992a)** The late Quaternary vegetational history of northwest Greece. I. Lake Gramousti. *New Phytologist* **121**, 101-117.
- Willis, K.J. (1992b)** The late Quaternary vegetational history of northwest Greece. II. Rezina Marsh. *New Phytologist* **121**, 119-138.
- Willis, K.J. (1992c)** The late Quaternary vegetational history of northwest Greece. III. A comparative study of two contrasting sites. *New Phytologist* **121**, 139-155.
- Wilson, P. and Clark, R. (1998)** Characteristics and implications of some Loch Lomond Stadial moraine ridges and later landforms, eastern Lake District, northern England. *Geological Journal* **33**, 73-87.
- Woodcock, N.H. (1977)** Specification of fabric shapes using an eigenvalue method. *Geological Society of America Bulletin* **88**, 1231-1236.
- Woodward, J.C. (1990)** *Late Quaternary Sedimentary Environments in the Voidomatis Basin, Northwest Greece*. Ph.D. thesis, University of Cambridge.

- Woodward, J.C. (1997a)** Late Pleistocene rockshelter sedimentation at Klithi. In Bailey, G.N. (ed) *Klithi: Palaeolithic settlement and Quaternary landscapes in northwest Greece, Volume 2: Klithi in its local and regional setting*. MacDonald Institute for Archaeological Research: Cambridge. p. 361-376.
- Woodward, J.C. (1997b)** Late Pleistocene rockshelter sedimentation at Megalakkos. In Bailey, G.N. (ed) *Klithi: Palaeolithic settlement and Quaternary landscapes in northwest Greece, Volume 2: Klithi in its local and regional setting*. MacDonald Institute for Archaeological Research: Cambridge. p. 377-393.
- Woodward, J.C. and Bailey, G.N. (2000)** Sediment sources and terminal Pleistocene geomorphological processes recorded in rockshelter sequences in Northwest Greece. In Foster, I.D.L. (ed) *Tracers in geomorphology*. Wiley. p. 521-551.
- Woodward, J.C. and Goldberg, P. (2001)** The sedimentary records in Mediterranean rockshelters and caves: Archives of environmental change. *Geoarchaeology. An International Journal* **16**, 327-354.
- Woodward, J.C., Lewin, J. and Macklin, M.G. (1992)** Alluvial sediment sources in a glaciated catchment: the Voidomatis basin, northwest Greece. *Earth Surface Processes and Landforms* **16**, 205-216.
- Woodward, J.C., Macklin, M.G. and Lewin, J. (1994)** Pedogenic weathering and relative-age dating of Quaternary alluvial sediments in the Pindus Mountains of northwest Greece. In Robinson, D.A. and Williams, R.B.G. (eds) *Rock Weathering and Landform Evolution*. Wiley.
- Woodward, J.C., Lewin, J. and Macklin, M.G. (1995)** Glaciation, river behaviour and the Palaeolithic settlement of upland northwest Greece. In Lewin, J., Macklin, M.G. and Woodward (eds) *Mediterranean Quaternary River Environments*. Balkema. 115-129.
- Woodward, J.C., Macklin, M.G. and Smith, G.R. (2004)** Pleistocene Glaciation in the Mountains of Greece. In Ehlers, J. and Gibbard, P.L. (eds) *Quaternary Glaciations - Extent and Chronology. Part I: Europe*. Elsevier.
- Woodward, J.C., Hamlin, R.H.B., Macklin, M.G., Karkanias, P. and Kotjabopoulou, E. (2001)** Quantitative Sourcing of Slackwater Deposits at Boila Rockshelter: A Record of Lateglacial Flooding and Palaeolithic settlement in the Pindus Mountains, Northwest Greece. *Geoarchaeology: An International Journal* **16**, 501-536.
- World Meteorological Organisation (1998)** *1961-1990 global climate normals*. Electronic resource. National Climatic Data Center, US: Asheville, NC. (CD-ROM)
- World Wildlife Fund (2003)** *Nature and Culture in Zagori. Exhibition of the information centre at Papingo*.
- Wright, H.E. (1962)** Pleistocene glaciation in Kurdistan. *Eiszeitalter und Gegenwart* **12**, 131-164.
- Wright, V.P. and Tucker, M.E. (1991)** Calcretes: Introduction. *International Association of Sedimentologists Reprint Series* **2**, 1-22.

Appendix 1

U-series method for Thermal Ionisation Mass Spectrometry

The methods outlined here are those carried out by the author based on protocol guidelines issued by the Uranium Series Facility in the Department of Earth Sciences, Open University, Milton Keynes, UK.

A. Laboratory policy

It is laboratory policy to totally dissolve all samples rather than leach them with HNO₃. The reasons for this are below:

1. In leaching speleothems/flowstones/cements, with even small amounts of detrital material, it is very difficult to dissolve the calcite totally, without leaching any detrital thorium from any silicate material that may be in the sample. The U-series dating technique is based on the fact that uranium is mobile in aqueous solutions and that thorium is not. Resultant deposited uranium then decays to ²³⁰Th which gives us the age of the sample. Extra Th from a detrital silicate source however pushes up the amount of ²³⁰Th that is measured to give an older age than actuality. (Although natural Th is mainly ²³²Th a very small proportion is also present as ²³⁰Th.) It is possible to correct for this detrital component provided several assumptions are made.

2. It is necessary to keep the acidity of the leaching acid high, so that thorium is kept in solution. Unfortunately the higher acidities mean that leaching of detrital thorium is more likely. If the acidity is reduced, to minimise or stop detrital component leaching, the thorium falls out of solution back onto the detrital residue. In order to ensure all thorium is in solution, even small amounts of silicate detrital thorium, total dissolutions are undertaken.

Age calculation thus requires the concentrations of ²³⁴U, ²³⁸U, and ²³⁰Th in the sample using standard isotope dilution techniques. In addition, to assess the detrital thorium component the concentration of ²³²Th is measured.

B. Radiation protection

All the U and Th spike solutions are alpha-emitters and so must be handled with care. Always wear a lab-coat and vinyl gloves when working in the U-series lab. Everyone who handles the spikes must be registered as radiation workers and have attended a radiological protection course. All dilute working spike solutions are kept in the balance room and the tops must be sealed with parafilm when not in use. Spike dispensing must be done in one of the instrument trays so as not to contaminate bench surfaces and each time a spike is dispensed it must be logged.

C. Analysis of carbonates

1.1 The analysis of carbonates requires the following steps:

1. Preparation of equipment required for U-series

1.2 a) Beaker cleaning

- b) Column preparation
- c) Filament preparation

2. Sample preparation

- a) Sample pre-clean
- b) Weighing sample
- c) Sample dissolution and spiking of sample

- d) Column chemistry
- e) Clean-up columns
- f) Loading samples onto filaments

3. Mass spectrometric analysis of U and Th

C1. Preparation of equipment required for U-series

a) Beaker Cleaning

In the laboratory Savillex PFA (Perfluoroalkoxy) beakers were used. In order to get low blanks, beaker cleaning is the most important aspect of laboratory technique. The cleaning procedure may appear tedious and longwinded, although results can not be trusted if there is a significant “blank” component. To monitor contamination levels it is important to measure “total procedure blanks”. This is carried out by weighing a known amount of “spike” into a beaker and taking it through all the procedures as if it were a sample, collecting the element of interest and analysing it by mass spectrometry. A “spike” is a solution of an element with known isotopic composition and concentration. The mass spectrometer possesses this information in the computer software for many spikes so that it can calculate how much extra element is present, *i.e.* how much contamination (“blank”). In the case of U-series analyses, the relevant isotopic ratio is fed into an excel spreadsheet to get the results.

Cleaning method:

1. Rinse beakers with Reverse Osmosis (RO) H₂O.
2. Pour 5-10 millilitres (ml) of Quartz Distilled (QD) 6M HCl into the beakers and leave standing on a tray in the fume cupboard overnight. This essentially dissolves any residue from the previous sample and puts it into solution.
3. Rinse beakers with RO H₂O.
4. Transfer beakers into your concentrated HNO₃ beakers (on the hotplate) in the fume cupboard. When putting beakers into this acid, do not put them so that they stack into each other - this will produce a stagnant layer of HNO₃ at the bottom of the beaker which is not accessible to the main HNO₃ volume. Ensure that the beakers are covered (extra Analar conc. HNO₃ is kept in the cupboard below the fume hood, main acid store near rock store), they do not clean well in atmosphere. The beakers should be left in this hot acid for at least 24 hours. The process may be accelerated by boiling, but this not recommended for anyone just starting in the laboratory, and should only be used as a last resort.
5. Remove beakers from conc. HNO₃ into a clean tray and rinse with RO H₂O. There are tongs provided but beware the beakers tend to be very slippery.
6. Transfer the beakers into RO H₂O (large beakers on the hotplate near the window). Boil beakers at least once in RO water.
7. Remove beakers from water and rinse thoroughly with RO H₂O.
8. Add 10-15 ml of QD 6M HCl to the beakers and warm them under the evaporating hoods for up to 1 hour. Do not let the acid evaporate to dryness. Teflon oven bombs should have several millilitres of 6M HCl put in them, the bombs sealed in the metal cases, and “bombed” overnight.
9. Discard the acid and rinse the beakers with RO H₂O. Dry upside down on a clean Kimwipe in a tray. The beakers are now ready for use.

Always ensure when handling a beaker that you do not put your hands over the mouth of a beaker - bits of skin, hair or dust may drop in. Always keep beakers covered in-between additions of reagents either by using the lids provided or covering with Parafilm. Any acid additions should be carried out in the fume cupboard, avoid carrying open beakers across the lab, this is dangerous and increases the chance of contamination.

b) Column preparation

Ion exchange columns for the separation of U and Th from carbonates are composed of 2ml of Biorad anionic resin (AG1 X8, mesh 200-400) contained within a polypropylene column also purchased from Biorad. Prior to use, the resin is cleaned with a sequence of QD 6M HCl and RO water (6 washes each) to remove both 'fines' from the resin and unwanted ions left over from the resin preparation. Washed resin is always stored in RO water, so after the washing sequence a couple of additional water washes are carried out to ensure all traces of acid have been removed. New batches of washed resin are checked for U and Th yields in case there are slight differences in the elution characteristics of the batches and the resin is also checked for U and Th column 'blanks' to ensure the cleaning procedure has been successful. (Methods for yields and column blanks given at the end of this section).

The polypropylene columns are soaked in QD 6M HCl in a sealed 500ml Savillex PFA beaker on the food warming hotplate for a minimum of 12 hours before use. The columns are then rinsed copiously with RO water before drying and placing in a column rack. The racks typically hold 6 columns and thus this is a good batch size for chemistry. Once columns are in the rack the empty columns are washed through with QD 6M HCl and RO water twice. Two ml of anionic resin (2ml settled resin volume in water – use a centrifuge tube for measuring the resin against the marks on the centrifuge tube racks provided) are carefully added to the column. The resin must be added gently ensuring that no air bubbles are incorporated into the resin-bed as this would alter the elution characteristics of the column; dropping the resin through RO water in the column minimises air bubbles. Once the resin is *in situ*, and all the remaining water has dripped through, the resin is then washed with 4ml TD 6M HCl followed by 4ml TD water, twice, ensuring that the top of the resin bed is dry before each addition. Setting up of columns can be done the day before they are to be used, provided the resin is left in water overnight. Just prior to sample addition the resin is pre-conditioned with 3ml of TD 7M HNO₃ – this acid should not be added to the columns until the samples are ready for the column procedure, as the resin-bed deteriorates with the nitric acid over a period of time.

c) Filament preparation for TIMS.

1. Choose the number and type of filaments holders that you require (see the list below for info on which filament to use for the most commonly analysed elements using TIMS), ensuring that they are reasonably clean and undamaged. Holders with bent contact posts are unsuitable as they can dislodge the contact plates in the mass spectrometer.
 - Th for peak hopping on SEM (carbonates) single rhenium
 - U for peak hopping on SEM (carbonates) single rhenium
2. Check the glass insulation around the posts for metal deposits or damage and remove any old filament wire left on the holder.
3. Place the filament holder onto the teflon block connected to the MEGGER multi-tester (the short posts fit into the sockets provided) and turn the dial on the MEGGER to 1kV. Keeping your fingers away from the filament holder, hold down the test button and watch the meter. A reading of >999 means the holder is fine and there is no 'shorting' across the glass insulator. If the MEGGER reads less the holders need to be sandblasted around the glass insulator. (The most common cause of 'shorting' is the deposition of a thin coating of Re across the insulator glass, when filaments are taken up to some 5-6 amps in the mass spectrometer.
4. Use of sandblaster – make sure the sandblaster is attached to the compressed air supply and that the sandblaster and extraction box are both switched on. The foot switch for the sandblaster is located under the extraction hood. Simply use the sandblaster to clean the green glass insulator and re-test using the MEGGER. If sand-blasting does not improve the 'shorting' after 2 sand-blastings - throw the holder in the bin.
5. Wearing safety spectacles, use the dentists drill (remember to change the compressed air

supply to feed the drill if you have been using the sandblaster) to remove any dirt and filament wire left on the holder posts. Do not over do it - pointed posts are harder to weld onto.

6. Boil the holders in a beaker containing RO H₂O and a few drops of the detergent Decon 90 for 10-15 minutes. Repeat the boiling process with 2 more changes of RO water only. Decant off as much water as possible and place beaker plus holders in the vacuum oven for at least 20 mins. Remember to label the beaker. If a vacuum oven is not available, place the beaker on one of the food warming hotplates.

The holder is now ready for application of the filament wire. Handle the holders and wire with white cloth gloves from now on to avoid contamination.

Welding the filaments

1. Choose the correct jig configuration for the type of filament holder you are preparing.
 - Carefully place the filament holder onto the jig ensuring that it sits square against the positioning pegs. Tighten the knob to secure the holder, there is no need to over-tighten.
 - Cut a piece of filament wire about 1 inch in length and place in the clamp. On tightening the clamp, the ends of the filament wire will move inwards towards the holder posts. Always check you have selected the correct wire.
 - Wearing safety spectacles, open the jaws of the welder, insert the holder post and close the jaws to keep the holder secure. Weld the wire onto the posts.
 - Loosen both the knob and clamp and remove the filament holder taking care not to damage the filament. An irregular shaped filament will give irregular results. The filaments are now ready to be outgassed.

MAT262 Slit and Blank Plate Cleaning

Both slit and blank plates need to be thoroughly cleaned before use in the mass spectrometer.

1. Gently remove dirt from the slit plate using a fibreglass pencil.
2. Boil the plates in a beaker containing RO H₂O and a few drops of Decon 90 for 10-15 mins. Repeat the boiling process with two further changes of RO H₂O. Decant off the water and cover the slits and blank plates with 30% H₂O₂, leave for several hours or overnight to get rid of any residual organics. Discard the H₂O₂ and rinse with at least 2 changes of RO water.
3. Decant off the H₂O and place the beaker with filaments in the vacuum oven for at least 20 mins.
4. Store clean plates in the vacuum oven or in clean boxes.

IMPORTANT: Handle clean plates with gloves only!

C2. Sample preparation – Total dissolution

3 clean Savillex beakers are needed for each carbonate sample analysis, a large 60ml beaker for sample dissolution and two 7ml beakers for U and Th collection from the ion exchange columns.

Transfer dry clean 60ml Savillex beakers into the balance room with sample powders and allow to equilibrate to the room temperature for *ca.* 30 mins before starting to weigh samples. Place beakers under the anti-static device. Unfortunately the drier the beakers the more likely they will suffer from static problems and make weighing problematic. An anti-static gun helps.

Access is needed to a fume hood with evaporating hoods hooked up to a compressed air supply. The hoods **must** be cleaned with QD 6M HCl before and after use to minimise cross contamination – solutions of calcite are extremely gluey and tend to ‘spit’ when taken to high temperatures - so only use one sample per hood.

a) Sample pre-clean

It is important to wash the sample to ensure there are no surface contaminants. Wash the sample in a very dilute solution of TD HCl (mainly TD H₂O + a few drops of HCl), so that there is very gentle fizzing from the surface of the sample. Only keep the sample in the HCl for a few seconds and wash off immediately with TD H₂O. Wash at least 2-3 times more in TD H₂O with sonication. Remove the sample and place on a pre-cleaned petri dish under IR lamps until dry.

b) Weighing sample.

Remember to allow the sample to cool to room temperature before attempting to weigh it.

c) Sample dissolution and spiking of sample

All the following steps must be carried out quantitatively

1. Weigh the calcite accurately to 5-figures into a clean 60 ml Savillex beaker.
2. Using TD H₂O, make the powder into a slurry. Make sure you add plenty of H₂O as this prevents the escape of sample powder when acid is added.
3. Add TD 7M HNO₃ drop-wise to the sample, allowing the sample to fizz and stop reacting before the next acid addition. Once there is a reasonably large volume of liquid, TD 15M HNO₃ can be added, again drop-wise.
4. Keep adding acid carefully until the calcite is dissolved. If silicate detritus is present just add acid until no reaction is observed. Add a little more TD 15M HNO₃ to ensure that the pH remains low that helps to keep the Th in solution.
5. At this point establish whether there is any cloudiness or silicate particles in the base of the beaker. If there is, or if you are at all doubtful, centrifuge the sample.
6. To centrifuge, transfer **all** the sample quantitatively into a rinsed 50ml centrifuge tube. Using more TD 7M HNO₃ to rinse the beaker and transfer any residual sample to the tube, repeating this as many times as necessary to remove all of the sample to the centrifuge tube.
7. Centrifuging at 4000 rpm for 5 mins is usually adequate, although some samples need this step repeated, especially if organic rich.
8. If there is **NO visible detrital component** in the base of the centrifuge - Transfer the whole lot back into the original beaker and "spike" with the ²²⁹Th/²³⁶U mixed spike (weighing to 5-fig). The current code name of the mixed spike is currently 'BB', however this code changes as spikes are used up and new are prepared to replace them. For most speleothems 20-30 drops of spike is sufficient but the volume added is dependent on the U concentration and age of the sample as well as the concentration of ²²⁹Th and ²³⁶U in the spike. Go straight to step 14.
9. If there **IS visible detrital component** in the base of the centrifuge – Transfer the supernatant into a clean rinsed centrifuge and wash the residual detritus with 7M HNO₃ at least twice. This is done by suspending the residue in a small volume of the acid, mixing well, centrifuging as before and pooling the supernatants. Carry out a further wash with TD water and transfer the washing to the pooled supernatants. Reserve the pooled supernatants.
10. Re-suspend the residue in a very small volume of TD 15M HNO₃ and transfer to the original dissolution beaker, using more HNO₃ as necessary to transfer **all** the residue back to the beaker. Add a very small volume of TD HF (volume is pretty much dependent on how much residue is present but 0.5ml would be adequate for most dirty calcites). Seal the beaker and leave overnight on the food-warmer hotplate. Check that the silicate material has dissolved. Organic

material that did not oxidise with the HNO_3 may still be present at this point.

11. Evaporate the solution to dryness and re-dissolve in TD 15M HNO_3 . Seal the beaker and leave overnight on the hotplate. Evaporate to dryness.
12. Add TD 6M HCl to the dried residue. Seal the beaker and leave overnight on the hotplate. Check for total dissolution. The solution should be crystal clear at this point. If not it may be that there are still organics in the sample that have not been totally oxidised. If organics are persistent add 1 drop of TD HClO_4 (perchloric acid), seal the beaker and leave on the hotplate overnight or longer if needed. Evaporate the solution to dryness. This step will take a long time and the HClO_4 does need to get to around 150°C to fume off the acid. (HClO_4 work and evaporations **must** only be done in the designated fumehood.). Occasionally recycling with another volume of HCl helps to drive off the perchloric and 'dissolve' the organics. The solution has to be crystal clear at this stage on the addition of more HCl, however a fine graphite suspension often persists in the beaker after this treatment if the samples are particularly organic rich. The graphite tends to cling to the side of the beaker and floats on the surface – very unlike mineral grains so it should be easy to distinguish the two. Often it is impossible to get rid of this residual graphite. If samples are particularly organic rich it may be advisable to do this stage of the dissolution in the CEM microwave system.
13. Take the clear HCl solution from step 12 and "spike" with the $^{229}\text{Th}/^{236}\text{U}$ mixed spike (weighing to 5-figures). The current code name of the mixed spike is currently 'BB', however this code changes as spikes are used up and new are prepared to replace them. For most speleothems 20-30 drops of spike is sufficient but the volume added is dependent on the U concentration and age of the sample as well as the concentration of ^{229}Th and ^{236}Th in the spike.
14. Allow the sample and spike to equilibrate overnight.
15. Evaporate the sample to dryness and redissolve in 7M HNO_3 for the ion exchange column.

d) Column chemistry

The Th and U are purified on a anionic resin column using 7M HNO_3 to load the sample onto the column and elute through unwanted ions. Th is then eluted off and collected in one of the clean 7ml vials with TD HCl and U (in a second beaker) with TD 1M HBr. Evaporate the Th and U fractions to dryness.

e) Clean-up columns

The resultant Th and U fractions should form very small residues (sometimes barely visible) in the base of the beaker. If there has been a resin leak in the column, or the residue just looks too big to be comfortably loaded in $2\mu\text{l}$ of 0.1M HNO_3 , the fractions will need to go through 'clean-up' columns. These are 1ml pipette tips fitted with frit material. These mini columns are cleaned as for the 2ml columns and the elution procedure is a scaled down version of the 2ml column. See the current elution sheets for volumes of acid to use. Elute Th and U as described and evaporate to dryness.

f) Loading samples onto filaments

Both Th and U fractions are loaded onto single graphite coated ($1\mu\text{l}$ graphite suspension evaporated at 0.6A, then cooled) Re filaments using $2\mu\text{l}$ 0.1M HNO_3 , evaporated to 0.7A then turned up to 1.2A for few seconds before turning down to zero.

C3. Mass spectrometric analysis of U and Th

Both Th and U are run on the MAT 262 mass spectrometer equipped with a retarding potential quadrupole and secondary electron multiplier (described by van Calsteren and Schwieters 1995). A dynamic peak switching routine is employed measuring $^{234}\text{U}/^{236}\text{U}$ and $^{235}\text{U}/^{236}\text{U}$ (a proxy for ^{238}U , assuming a $^{238}\text{U}/^{235}\text{U}$ natural ratio of 137.88) and $^{230}\text{Th}/^{229}\text{Th}$ and $^{232}\text{Th}/^{229}\text{Th}$. Although ^{232}Th abundance is not required for the age calculation it is always measured so that we can monitor detrital Th input and consequently correct for its presence if necessary.

Reference:

van Calsteren, P. and Schwieters, J.B. (1995) Performance of a thermal ionisation mass spectrometer with a deceleration lense and post-deceleration detector selection. *International Journal of Mass Spectrometry and Ionisation Processes* **146/147**, 119-129.

D. Analysing the detrital component

1. Break down dirty calcite using a pestle and mortar or scrape detritus from the surface of a calcite.
2. Place in a 50ml centrifuge tube.
3. Cover with MilliQ water.
4. Add HCl dropwise (QD 6M).
5. Take off the supernatant immediately so as not to leach Th from the silicate fraction
6. Shake.
7. Repeat until no further reaction and all Calcium Carbonate is dissolved and removed.
8. Wash detritus with MilliQ water.
9. Transfer to a clean petri dish (large samples) or to a pre-weighed small clean Teflon beaker.
10. If a large sample, dry on the petri dish under a light and then weigh 50-100mg into a small clean pre-weighed Teflon beaker. If a small sample just dry sample in the pre-weighed beaker and take the dry weight. Again 50-100mg is adequate.
11. Add 15-20 drops of the spike BB. Add some MilliQ before hand if there is fine powder.
12. If too much water exists after the last step, dry off. You don't want to dilute the HF and HNO₃ in the next stage too much.
13. Dissolve in HF following the steps outlined in the usual procedure. (150-200mg of silicate will be dissolve by 1-2ml of HF). Dry as usual.
14. Follow through to columns, collect and load.
15. Run as U456single and Th2nd single (1st run only).
Correct the original date using the detritus sample and spike weights and derived detritus $^{235}\text{U}/^{236}\text{U}$ and $^{232}\text{Th}/^{229}\text{Th}$ ratios.

Appendix 2

Iron oxide extraction from soils

Method

1. Sample *ca.* 2 g of soil. There is a need to know the density of this soil. This can be measured by weighing the sample and also taking the volume by water displacement in a small measuring cylinder (10 ml). Density = weight/volume (g/cm^3)
2. Place the sample into a 50 ml test tube
3. Add 20 ml of 0.3 M Sodium-citrate solution
4. Add 2.5 ml of 1M NaHCO_3
5. Place in waterbath and bring solution to 80°C
6. When 80°C is reached add 0.5 g of solid $\text{Na}_2\text{S}_2\text{O}_4$
7. Stir continuously for 1 minute, then occasionally for 15 minutes
8. Add 5ml of saturated NaCl (Sodium Chloride) solution and 10 ml of acetone
9. Stir to ensure mixing and warm solution back to 80°C in the waterbath
10. Centrifuge for 5 minutes at 1600 - 2200 rev/min and decant supernatant (which contains the extracted iron) OR sieve through filter paper using a Buchner funnel and collect the filtered liquid.
11. Determine Fe content of the supernatant or filtered liquid using an atomic absorption spectrophotometer (AAS). It is likely that the supernatant will need to be diluted in order to be measured by the AAS.

The amount of iron determined using the AAS will be expressed as milligrams per litre of supernatant (m/l). This needs to be altered so as to read milligrams per kilograms of soil.

The method described here is based on that of **Mehra, O.P. and Jackson, M.L. (1960)** Iron oxide removal from soils and clays by a dithionite-citrate system buffered with sodium bicarbonate. *Proceedings of the 7th National Conference on Clays and Clay Minerals*. Pergamon: New York. p. 317-327.

Appendix 3

Soil data

a) Voidomatis Member soil (39°54'13"N, 20°49'36"E, 1092 m a.s.l.)

Depth	Moist colour	Dry colour	Texture	Structure grade/size/type	Consistence dry/moist/wet	Clay films abundance/thickness/location	pH
0-50 cm	2.5YR 4/2	2.5YR 4/4	CL	2/m/sbk	h/fi/vs,vp	2/mk/pf 2/mk/br 2/mk/po	8.27
50-110 cm	2.5YR 3/2	2.5YR 3/4	SiCL	3/m/sbk	vh/vfi/vs,vp	2/mk/pf 2/mk/br 2/mk/po	8.02
Parent material	10YR 7/1	10YR 5/6	SiCL	massive	so/vfr/so,po	none	9.27

b) Maghoula Member soil (39°59'30" N, 20°53'15"E, 1100 m a.s.l.)

Horizon and depth	Moist colour	Dry colour	Texture	Structure grade/size/type	Consistence dry/moist/wet	Clay films abundance/thickness/location	pH
A 0-10 cm	5YR 3/2	5YR 3/4	SL	1/m/gr	so/fr/so,po	v1/n/pf	8.3
E 10-30 cm	5YR 6/4	5YR 6/3	SL	2/m/sbk	sh/fi/s/p	1/n/pf 1/n/br 1/n/po	8.2
B 30-100 cm	2.5YR 4/4	2.5YR 3/4	SiCL	3/m/sbk	vh/vfi/vs,vp	3/mk/pf 2/mk/br 2/mk/po	8.1
Parent material	10YR 7/1	10 YR 8/1	SiL	massive	so/vfr/so,po	none	9.4

c) Kato Radza Member soil (39°54'20" N, 20°50'40"E, 1040 m a.s.l.)

Horizon and depth	Moist colour	Dry colour	Texture	Structure grade/size/type	Consistence dry/moist/wet	Clay films abundance/thickness/location	pH
B 0-100 cm	2.5YR 3/2	2.5YR 3/4	CL	3/m/sbk	vh/vfi/ss,vp	3/k/pf 3/k/br 3/k/po	8.0
Parent material	10YR 7/1	10 YR 8/1	SiL	massive	so/vfr/so,po	none	9.4

Key:Texture

S – sand	SCL – sandy clay loam
LS – loamy sand	CL – clay loam
SL – sandy loam	Si CL – silty clay loam
L – loam	SC – sandy clay
SiL – silt loam	C - clay
Si – silt	SiC – silty clay

Structure

<i>Grade</i>	<i>Size</i>	<i>Type</i>
m – massive	vf – very fine	gr – granular
sg – single grained	f – fine	pl – platy
1 – weak	m – medium	pr – prismatic
2 – moderate	c – coarse	cpr – columnar
3 – strong	vc – very coarse	abk – angular blocky
		sbk – subangular blocky

Consistence

<i>Dry</i>	<i>moist</i>	<i>wet</i>	
lo – loose	lo – loose	so – non-sticky	po – non-plastic
so – soft	vfr – very friable	ss – slightly sticky	ps – slightly plastic
sh – slightly hard	fr – friable	s – sticky	p – plastic
h – hard	fi – firm	vs – sticky	vp – very plastic
vh – very hard	vfi – very firm		
eh – extremely hard	efi – extremely firm		

Clay films

<i>Frequency</i>	<i>Thickness</i>	<i>Morphology</i>
v1 – very few	n – thin	pf – ped face coatings
1 – few	mk – moderately thick	br – bridging grains
2 – common	k – thick	po – pore linings
3 – many		co – coats on clasts
4 – continuous		